UNIVERSITY OF THE WITWATERSRAND

MASTER'S DISSERTATION

Friction Compensation in the Swing-up Control of Viscously Damped Underactuated Robotics

Author:
Ricardo DE ALMEIDA

Supervisor:
Dr Otis NYANDORO

A dissertation submitted to the Faculty of Engineering and the Built Environment, University of the Witwatersrand, Johannesburg, in fulfilment of the requirements for the degree of Master of Science in Engineering in the

Control Research Group
School of Electrical and Information Engineering

Johannesburg, 2017

Declaration of Authorship

I, Ricardo DE ALMEIDA, declare that this dissertation is my own unaided work. It is being submitted to the Degree of Master of Science in Engineering at the University of the Witwatersrand, Johannesburg. It has not been submitted before for any degree of examination to any other university.

Signed: _____

Date: _____

UNIVERSITY OF THE WITWATERSRAND

Abstract

Faculty of Engineering and the Built Environment
School of Electrical and Information Engineering

Master of Science in Engineering

Friction Compensation in the Swing-up Control of Viscously Damped Underactuated Robotics

by Ricardo DE ALMEIDA

In this research, we observed a torque-related limitation in the swing-up control of underactuated mechanical systems which had been integrated with viscous damping in the unactuated joint. The objective of this research project was thus to develop a practical work-around solution to this limitation.

The nth order underactuated robotic system is represented in this research as a collection of compounded pendulums with $n-1$ actuators placed at each joint with the exception of the first joint. This system is referred to as the $\mathbf{PA}_{n-1}$ robot (**P**assive first joint, followed by $n-1$ **A**ctive joints), with the Acrobot (PA_1 robot) and the PAA robot (or PA_2 robot) being among the most well-known examples. A number of friction models exist in literature, which include, and are not exclusive to, the Coulomb and the Stribeck effect models, but the viscous damping model was selected for this research since it is more extensively covered in existing literature. The effectiveness of swing-up control using Lyapunov's direct method when applied on the undamped PA_{n-1} robot has been vigorously demonstrated in existing literature, but there is no literature that discusses the swing-up control of viscously damped systems. We show, however, that the application of satisfactory swing-up control using Lyapunov's direct method is constrained to underactuated systems that are either undamped or actively damped (viscous damping integrated into the actuated joints only). The violation of this constraint results in the derivation of a torque expression that cannot be solved for (*invertibility problem*, for systems described by $n > 2$) or a torque expression which contains a conditional singularity (*singularity problem*, for systems with $n = 2$). This constraint is formally summarised as the *matched damping condition*, and highlights a clear limitation in the Lyapunov-related swing-up control of underactuated mechanical systems. This condition has significant implications on the practical realisation of the swing-up control of underactuated mechanical systems, which justifies the investigation into the possibility of a work-around. We thus show that the limitation highlighted by the *matched damping condition* can be overcome through the implementation of the partial feedback linearisation (PFL) technique. Two key contributions are generated from this research as a result, which

include the *gain selection criterion* (for Traditional Collocated PFL), and the *convergence algorithm* (for noncollocated PFL).

The gain selection criterion is an analytical solution that is composed of a set of inequalities that map out a geometric *region of appropriate gains* in the swing-up gain space. Selecting a gain combination within this region will ensure that the fully-pendent equilibrium point (FPEP) is unstable, which is a necessary condition for swing-up control when the system is initialised near the FPEP. The convergence algorithm is an experimental solution that, once executed, will provide information about the distal pendulum's angular initial condition that is required to swing-up a robot with a particular angular initial condition for the proximal pendulum, along with the minimum gain that is required to execute the swing-up control in this particular configuration. Significant future contributions on this topic may result from the inclusion of more complex friction models. Additionally, the degree of actuation of the system may be reduced through the implementation of energy storing components, such as torsional springs, at the joint.

In summary, we present two contributions in the form of the *gain selection criterion* and the *convergence algorithm* which accommodate the circumnavigation of the limitation formalised as the *matched damping condition*. This condition pertains to the Lyapunov-related swing-up control of underactuated mechanical systems that have been integrated with viscous damping in the unactuated joint.

Acknowledgements

"All that is gold does not glitter. Not all those who wander are lost."

— J.R.R. Tolkien

I am deeply grateful for the support and guidance the following special people and organisations have offered me through the process of producing this research:

The National Research Fund. The financial assistance offered by the NRF towards this research is acknowledged. Opinions expressed in this dissertation and the conclusions arrived at are those of the author, and are not necessarily to be attributed to the National Research Fund.

My supervisor, Dr Otis Nyandoro, for all of his guidance.

Prof. Van Wyk, Tinashe Chingozha, Prof. Hofsajer, Prof. Wigdorowitz, Prof. Oriolo, and Jacques Naude; thank you for your contributions and advice.

Nazime and Mirriam, thank you for welcoming me into the EOH family. The Parktown residences will always hold a special place in my heart.

The Hurwitz, Gonzalez, Vallabhapurapu, Dos Santos and Ortlepp families; thank you for offering me a helping hand when I needed it most.

Dean, thank you for involving me in your amazing project, and for offering me the opportunity to make a significant difference in this world.

Kevin, thank you for your tireless support and care. You provided me a sanctuary in times of distress, and helped me build my own.

Valerie and Rabin, thank you for your hospitality, love, and patience.

And lastly, to Diksha, you are fearless and gentle, wise beyond measure, patient and selfless. I am incredibly blessed that our paths crossed. Thank you.

Contents

List of Figures

List of Abbreviations

ACS	**A**bsolute **C**oordinate **S**ystem
BVP	**B**oundary **V**alue **P**roblem
COG	**C**entre **O**f **G**ravity
COM	**C**entre **O**f **M**ass
CPFL	**C**ollocated **P**artial **F**eedback **L**inearisation
DARPA	**D**efense **A**dvanced **R**esearch **P**rojects **A**gency
DDA	**D**irect-**D**rive **A**crobot
DIP	**D**ouble **I**nverted **P**endulum
DIPC	**D**ouble **I**nverted **P**endulum on a **C**art
DOF	**D**egree **O**f **F**reedom
EBC	**E**xplanation-**B**ased **L**earning
ELFBL	**E**xact **L**inearisation via **F**eed**B**ack **L**inearisation
FBL	**F**eed**B**ack **L**inearisation
FPEP	**F**ully-**P**endant **E**quilibrium **P**oint
IOFBL	**I**nput-**O**utput **F**eed**B**ack **L**inearisation
LDM	**L**yapunov's **D**irect **M**ethod
LHD	**L**oad **H**aul **D**ump
LLNF	**L**ocally **L**inear **N**euro-**F**uzzy
LQR	**L**inear-**Q**uadratic **R**egulator
LTI	**L**inear **T**ime **I**nvariant
MC-ROPA	**M**odified **C**ollocated-**R**educed **O**rder **P**assive-**A**ctive
MCPFL	**M**odified **C**ollocated **P**artial **F**eedback **L**inearisation
MIMO	**M**ultiple-**I**nput **M**ultiple-**O**utput
MLP	**M**ulti-**L**ayered **P**erceptron
NC-ROPA	**N**on**C**ollocated-**R**educed **O**rder **P**assive-**A**ctive
NCPFL	**N**on**C**ollocated **P**artial **F**eedback **L**inearisation
NN	**N**eural **N**etwork
PA	**P**assive-**A**ctive
PAA	**P**assive-**A**ctive-**A**ctive
PA$_{n-1}$	A **P**assive joint followed by $n-1$ **A**ctive joints
PFL	**P**artial **F**eedback **L**inearisation
PIEP	**P**artially-**I**nverted **E**quilibrium **P**oint
PMP	**P**ontryagin's **M**inimum **P**rinciple
PPEP	**P**artially-**P**endant **E**quilibrium **P**oint
RAG	**R**egion of **A**ppropriate **G**ains
RCS	**R**elative **C**oordinate **S**ystem
RL	**R**einforced **L**earning

ROPA	**R**educed-**O**rder **P**assive-**A**ctive
ROV	**R**emotely **O**perated **V**ehicle
SDRE	**S**tate-**D**ependent **R**iccati **E**quation
SIP	**S**ingle **I**nverted **P**endulum
SIPC	**S**ingle **I**nverted **P**endulum on a **C**art
TC-ROPA	**T**raditional **C**ollocated-**R**educed **O**rder **P**assive-**A**ctive
TCPFL	**T**raditional **C**ollocated **P**artial **F**eedback **L**inearisation
TIPC	**T**riple **I**nverted **P**endulum on a **C**art
TITech	**T**okyo **I**nstitute of **T**echnology
UAV	**U**nmanned **A**ir **V**ehicle
UEP	**U**pright **E**quilibrium **P**oint
UGV	**U**nmanned **G**round **V**ehicle
UMS	**U**nderactuated **M**echanical **S**ystem
VCL	**V**irtual **C**omposite **L**ink

Ad Dei gloriam.
Scientia et fides sunt in harmonia.

"We do not receive wisdom; we must discover it for ourselves after a journey that no one can take for us or spare us."

— Marcel Proust

Chapter 1

Introduction

Humans have been interacting with underactuated systems ever since they possessed the desire to manipulate the world around them [7]. The field of robotic applications began in teleoperations, where specific operations were performed at a certain distance by a manipulator [7,8]. For primitive man, this could include the instance when one was required to control a fire using a tool [7]. In a more modern context, these manipulators were first applied by R. Goertz and his team at the Argonne National Laboratory, where mechanical pantographs were used to control radioactive substances within the cores of nuclear reactors during the 1940s [7,8]. These manipulators were completely mechanical, with the progress of electronically integrated robotics being hindered by substantial computational requirements, and scarcity of literature on robotic dynamics [9]. The effects of these constraints quickly dissipated with the formation of communities that sought to amalgamate automated control and robotics [9]. Additionally, the increased interest in electronics and computing saw the rapid decrease in the cost of computation and an increase in the computation speed of programmable systems [9]. The implementation of electrical components in robotic manipulators was first seen in 1957, where the pantographs developed by R. Goertz were integrated with servomotors that were used to control movement [7].

The ability for these manipulators to navigate inhospitable territories attracted interest from researchers who desired a low-risk alternative for retrieving information about unknown landscapes [7]. This initiated the development of Remotely Operated Vehicles (ROVs) which were able to manipulate objects and store samples for research testing, specifically for oceanic expeditions [7]. These robots were refined in later years and applied to space exploration (the Voyager, NASA), in military operations (Unmanned Air Vehicles (UAVs) and Unmanned Ground Vehicles (UGVs)), and in mining, where the first examples of automation in underground mining were officially deployed in the 1960s in the form of unmanned rail carriages and Load Haul Dump (LHD) machines [7,10]. Programmed automation saw the rise of industrial process control in the 1960s due to an ever increasing desire to perform tasks that were deemed impossible or impractical to complete using human labour [11–13]. The first programmable robotic manipulator to be applied

in an industrial role was the Unimate, which was first implemented in 1961 [9]. The Unimate was used for automated movement and welding operations in the car manufacturing industry, where the manufacturers sought to take advantage of the robot's ability to perform precise operations for long periods of time without experiencing fatigue [9]. This resulted in the production of a higher quality product as compared to the deliverables produced by their human counterparts [9]. This eventually led to the Unimate's involvement in full-scale operations by 1966 [9]. Whilst these developments were significant, fully flexible autonomous procedures began to appear only during the 1980s, where the involvement of robotic manipulators in automated processes became the standard [9, 11]. The potential of robotic manipulators in applications across many different fields has yet to reach its full potential, with innovations occurring in biomedical related fields such as prosthetic development [14], humanoid robotics, security, and even surgery [7].

1.1 Background

Underactuated Mechanical Systems (UMS) are described as systems that contain more Degrees Of Freedom (DOFs) than actuators [13, 15]. These systems are frequently found across the engineering applications spectrum where robotic manipulation is required [15]. UMSs are also used to model complex systems found in nature using the *template-anchor schema* [16, 17]. Robotic manipulators are generally modelled as n-link pendulum systems, with the number of links being dependent on the environment of operation and the objective of the control [6, 15, 18].

The most common control objective applied to UMSs is swing-up control, whereby the system is *swung-up* from a particular trajectory and is regulated about the unstable and completely inverted equilibrium point (also known as the Upright Equilibrium Point, or UEP), demonstrating that stability can be achieved despite the unstable nature of the system dynamics [15]. In this dissertation, we define swing-up control as the action of directing the trajectory of the system to the UEP, but not necessarily regulating the system within an approximate neighbourhood of the UEP.

A number of projects in underactuated robotics have produced significant contributions at research institutions globally. These include the numerous projects investigated at Boston Dynamics (BigDog project [19], see figure 1.1), Mazor Robotics (surgical robots [20]), the ASIMO project [21] (seen in figure 1.2), and SpaceX (grappling arm of Dragon [22]). A number of worldwide competitions have been held to stimulate the advancement of the robotics community, including the Defense Advanced Research Projects Agency (DARPA) robotics challenge [23, 24].

FIGURE 1.1: BigDog. Used with Permission [1]

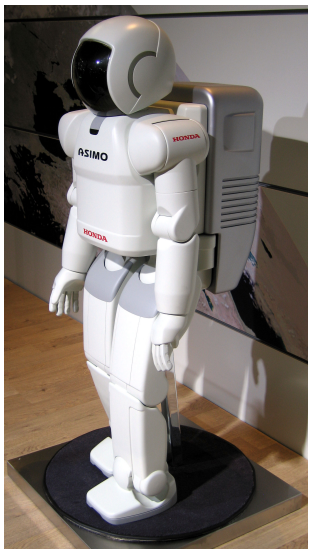

FIGURE 1.2: The ASIMO Robot (2000). Used with Permission [2]

[1] By DARPA - This file was derived from:DARPA Strategic Plan (2007).pdf, Public Domain, https://commons.wikimedia.org/w/index.php?curid=20798332.

[2] CC BY-SA 2.0 de, https://commons.wikimedia.org/w/index.php?curid=2783098

1.2 Research Objective and Methodology

The main objective of this research is to develop a work-around for a significant limitation in the swing-up control of robotic manipulators. To do this, we shall execute the methodology demonstrated in figure 1.3. The methodology contains four steps which are numbered according to the sequential order of execution. Each of these steps are summarised as follows:

(1) Identify an appropriate **system model, control objective** and **control technique** from existing literature.

(2) **Replicate the results** found in literature concerning the items in the previous point.

(3) **Alter** the model's parameters until the limitations of the selected control technique can be established.

(4) Develop a **work-around** for this limitation.

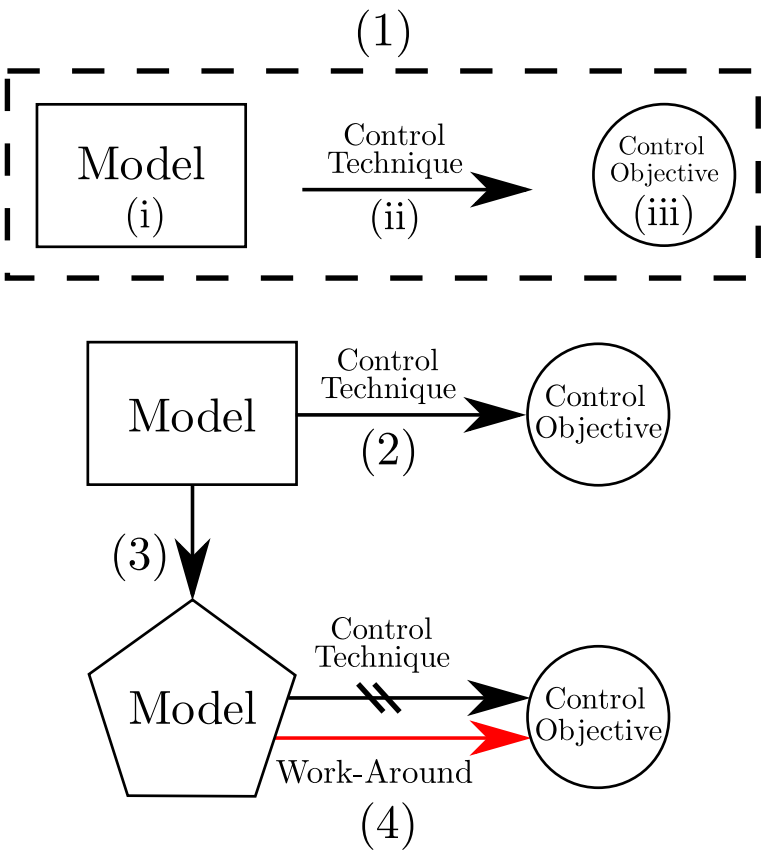

FIGURE 1.3: The research methodology implemented in this project.

The following system model, control objective, and control technique (itemised with Roman numerals in figure 1.3) were selected following an extensive literature review (included in chapter 2) according to step (1) of the research methodology:

(i) System model → PA_{n-1} robot (see section 2.2.2).

(ii) Control technique → Lyapunov's direct method (LDM) (see section 2.4.3).

(iii) Control objective → Swing-up control (see section 2.4.3).

Additionally, the system model was integrated with a simple viscous damping friction model as part of the alteration highlighted in item (3) above (see section 2.5). We hypothesise that the integration of this friction model into the PA_{n-1} robot will result in the derivation of a swing-up control torque that will not be able to satisfy the control objective.

1.3 Research Question, Scope, and Contributions

The following research question was formulated upon the results of the preliminary investigation of this research (highlighted in chapter 8), and is thus formally presented in chapter 9:

RQ: Using partial feedback linearisation (PFL) as a work-around for the key limitation in LDM highlighted by the *matched damping condition*, what are the specific conditions (if any) that need to be satisfied to accommodate the satisfactory swing-up control of a passively damped PA_{n-1} robot?

The scope of the project will be restricted to the swing-up control of an underactuated n-link pendulum system, specifically the PA_{n-1} robot. The research will be of a theoretical nature only, with the proofs, lemmas, and conditions required to perform a particular swing-up control included as required. Experimental results will only be provided in the form of simulations as the limited time-frame prevents the construction and testing of physical prototypes.

The key contributions, which are used to address the limitation highlighted in this research are summarised as follows:

(1) A set of analytical inequalities that are collectively referred to as the ***gain selection criterion*** derived specifically for the Traditional Collocated form of the PFL swing-up control formulation. This set of inequalities maps out a *region of appropriate gains*, which represents all possible gain combinations that will ensure that the fully-pendant equilibrium point (FPEP) is unstable. This increases the probability of, but does not guarantee, satisfactory swing-up control.

(2) A ***convergence algorithm*** developed for the noncollocated form of partial feedback linearisation that, once executed, will provide information about

the exact angular initial condition pairing and minimum gain that must be selected to ensure satisfactory Noncollocated PFL-related swing-up control.

1.4 Dissertation Outline

The remainder of the dissertation is organised as follows. Chapters 2-7 are included specifically to present the necessary literature that forms the foundation of this research project. Chapter 2 includes a general literature review on UMSs, system modelling, linear and nonlinear control methods used in the swing-up control of underactuated manipulators, friction models, and friction compensation; this review is performed to satisfy step (1) of the research methodology. Chapter 3 includes a discussion on the relevant modelling techniques used to represent physical systems in mathematical form. Chapter 4 includes a brief discussion on the topic of stability, specifically with reference to system equilibrium points. Chapter 5 introduces the foundational concepts of control methods that are relevant to this investigation. A brief discussion on the viscous damping model and its effect on specific physical systems are included in Chapter 6. The mathematical models of the PA_{n-1} robot, the Acrobot and the PAA robot are derived in chapter 7. Chapter 8 serves to address items (2) and (3) of the research methodology discussion in section 1.2, where we sought to identify a limitation in the LDM-related swing-up control formulation. Item (4) of the research methodology is addressed in chapter 9, whereby the contributions of the research project are presented. The concluding remarks are presented in chapter 10.

1.5 Summary of Research

The literature review performed in this research lead to the selection of the PA_{n-1} robot, the swing-up control objective, and Lyapunov's Direct Method as the most appropriate control model, control objective, and control technique respectively. We were able to replicate the LDM-related swing-up control results for the undamped PA_{n-1} robot demonstrated in [5] (including experimental results for the Acrobot and the PAA robot), but the integration of viscous damping into the unactuated joint caused the derivation of an unsuitable LDM-related swing-up control torque (formally recognised as the *invertibility* and *singularity* problems). The derivation of this unsuitable control represents a limitation in the LDM-related swing-up control, which is described by the *matched damping condition* (see criterion 8.1). The circumnavigation of this limitation involves the application of the partial feedback linearisation control technique, which results in the presentation of two specific contributions, namely the *gain selection criterion* (section 9.4) and the *convergence algorithm* (section 9.5). It has been shown that each contribution may be used as a work-around to circumnavigate the limitation highlighted by the *matched damping condition*, but it is important to note that each of these contributions are associated with a number of advantages and disadvantages that must be considered.

"To learn which questions are unanswerable, and not to answer them: this skill is most needful in times of stress and darkness."

— Ursula K. Le Guin

Chapter 2

General Literature Review

2.1 Chapter Overview

In this chapter, we present a general review on literature that is pertinent to the field of underactuated mechanical systems. The objective of this review was to accommodate the **appropriate selection** of a **system model**, **control objective**, **control technique** and **system alteration** for this research project as highlighted by the research methodology. The key areas of interest included underactuated robotics, n-link pendulum models and modelling techniques, robotic manipulator control methods, and friction modelling and compensation. Chapters 3-7 will cover specific literature in greater detail.

2.2 Underactuated Robotics

2.2.1 Relevance and Applications of Underactuated Robotic Systems

The application potential of UMSs has attracted much research interest in fields such as robotics and automated control [13]. Research into UMSs began in the early 1990s with the development of the theoretical framework for the control of nonholonomic systems [25, 26]. This was done to solve control problems on systems with constraints on velocity parameters that could not be derived from positional constraints [27]. This framework is particularly applicable to robotics as these constraints arise frequently in mechanical systems that experience rolling or sliding contacts as seen in the example of the parallel parking problem [28–30]. Since then, a number of nonholonomic systems have been modelled and controlled based on this framework, including aircraft, satellites, manipulators, precision medical instruments, and micro-robots [13]. One of the most well recognised UMSs is the ASIMO robot, which became the first underactuated bipedal robotic system to be showcased globally in 1996 [15]. Current research is aimed at understanding and solving controllability and stabilisation issues relating to nonholonomic UMSs, manipulating the dynamics of nonlinear systems to produce desired results, and finding alternative system configurations that will make control problems easier to solve [13, 15].

2.2.2 Selection of Appropriate Model

With the importance and relevance of UMSs clearly established, we need to answer the following question posed by the research methodology:

Which model should we select to represent the generalised UMS in this research project?

It is evident from literature that the UMS is typically modelled as a generalised compound pendulum system, also known as the n-link pendulum system, which has fewer actuators as compared to the DOFs [6, 15, 18]. The number of actuators that the system uses may vary, but it is logical that, since the project is subject to a stringent time constraint, an underactuated system with the highest possible ratio of number of actuators to DOFs should be chosen to reduce the complexity of the research problem. It is for this reason that the PA_{n-1} robot, a uniquely coined term used to describe the n-link pendulum system which has an actuator at each joint aside from the first joint, is chosen for this research (this model is characterised by a **P**assive most proximal joint followed by $n-1$ **A**ctive joints). With this choice in mind, it is important to research into modelling techniques that are used to mathematically model the n-link pendulum system and its variants (this review of modelling techniques is discussed in the next section).

2.3 n-link Pendulum Models and Modelling Techniques

The generalised model of the n-link pendulum system was derived using the Lagrangian method in [5]. Additionally, the generalised model of the n-link pendulum on a cart has been derived in [31, 32] by evaluating the dynamics of a single [33] and double [34, 35] inverted pendulum and ascertaining the dynamics of a generalised n-link pendulum system through induction. The mathematical model for the n-link pendulum is also derived in [36] for both the Absolute Coordinate System (ACS) and the Relative Coordinate System (RCS). This research suggests that the RCS may be preferred when generalising a system with a large number of links since the ACS modelling method introduces a number of additional terms in the equations of motion despite being the most popular method due to the ease of computation [36]. The fully-actuated n-link pendulum system is strictly holonomic, with the centre of gravity (COG) of each limb being constrained to a circular trajectory around the corresponding joint [37]. Underactuated robotic systems are classified as second-order nonholonomic systems as seen in [38].

2.4 Control Methods for Pendulum Systems

The review that is included in this section was performed to identify an appropriate *control objective* and *control technique*, as highlighted in the research methodology. The control methods applied to robotic manipulator systems can be grouped up into linear and nonlinear control methods.

2.4.1 Linear Control Methods

The inherent nonlinear dynamics of a generalised pendulum system prevents the development of a linear control method that can perform effectively across the global domain of operation. It is possible, however, to apply linear control methods when the system is linearised around a certain operating point. It has been made evident, upon compilation of the literature review, that all of the available material focusses on the balancing of a specific pendulum system about the UEP. Additionally, the literature only covers pendulum-cart systems because single-input multiple-output systems provide a more challenging balancing control problem as compared to multiple-input multiple-output (MIMO) systems. These linear control problems for various pendulum-cart systems are discussed below.

A Linear Quadratic Regulator (LQR) controller was designed for the linearised Single Inverted Pendulum on a Cart (SIPC) once it has been swung-up using an energy-shaping method in [39]. Similarly, a LQR controller was designed to balance the single inverted pendulum (SIP) on a rotating direct-drive motor (known as a TITech pendulum [40]) after swing-up using bang-bang control in [41]. A State-Dependent Riccati Equation (SDRE) controller is designed to both swing-up and balance a SIPC about the UEP in [42]. The controller is non-linear but operates in the linearised region of the SIPC during the stabilisation process [42]. This controller demonstrated more robust properties as compared to the general LQR controller when the experimental results were evaluated by inspection [42]. An adaptive Ada-line controller that operated on a linear switching surface was designed in [43, 44] to balance an SIPC and to further improve the robustness of the linear regulators. The switching surface was created with the use of both the position states and velocities of the cart and pendulum [43, 44]. This controller was termed the "Net Broom-Balancer controller" [43, 44].

Grossman and Gmiterko demonstrated in [31] that a LQR controller used to balance a double inverted pendulum on a cart (DIPC) can be trivially designed with the help of simulation packages. A more complex PID controller was designed using the pole placement technique to stabilise a DIPC around the UEP in [45]. The PID controller was shown to stabilise the DIPC significantly faster than the generic LQR controller, reducing the settling time in the cart-position by 16.4% [45]. H-∞ and μ controllers were designed to regulate a DIPC in [35], where an optimal Hankel norm approximation was used to reduce the 19th order controller to a 6th order controller with little change in the controller's performance and robustness. The optimal control of a DIPC around the UEP is performed in [46] using LQR, SDRE and optimal Neural Network (NN) controllers. Combining NN and LQR or SDRE controllers produced better results than separate methodologies by providing larger recovery regions and smaller response times [46]. A BAT algorithm is used to improve the performance of a LQR controller used to stabilise a DIPC in [47]. The controller gains were altered according to a square error fitness function [47]. The algorithm was modelled on the frequency-tuning behaviour of micro-bats which were used specifically to increase

the diversity of echolocation techniques [48]. This improved on the results produced by a LQR controller even when a time delay was applied [47]. Similarly, a NN system was used to automatically tune the gain parameters of a PID controller used to stabilise a DIPC in [49].

The stabilisation of the Triple Inverted Pendulum on a Cart (TIPC) using a linear feedback controller was first demonstrated in the discrete domain in [50]. This approach was employed using the KEDDC computer simulation package [50]. A discrete-time H-∞ controller is designed to stabilise a TIPC about the UEP using a reduced order robust dynamic observer in [51,52]. This controller is an improvement on the design demonstrated in [53,54] whereby the maximum distance moved off the desired cart trajectory is reduced from $\pm 30cm$ to $\pm 4cm$ [51,52]. A continuous-time LQR controller, used to stabilise a TIPC with linear constraints, was improved with time-multiplied quadratic indices and was cascaded with a DIPC controller in [55]. A more recent investigation into the development of a LQR controller for the TIPC can be found in [56].

This survey does not contain any literature highlighting linear control methods of a generalised n-link pendulum. It has, however, been proven in [57] that the linearised n-link pendulum system with a single actuator found in the first joint is controllable around the UEP for $n \geq 1$. It was also found that there is an inverse relationship between the stabilisability radius of the system and the number of links [57]. The pendulum system, therefore, becomes increasingly difficult to stabilise as the number of links in the system increases [57].

2.4.2 Nonlinear Control Methods

The literature covered in the nonlinear control of underactuated robotic systems is extensive. The review included in this section covers the relevant literature, but does not claim to be exhaustive. The majority of the literature covers the nonlinear control of a pendulum system with a predefined number of links and actuators. Work on the generalised n-link pendulum system is also covered in published work and is included in the review presented below.

A nonlinear fuzzy controller was designed to improve on the balancing performance of a linear proportional controller on a SIPC in [58]. The linear controller included in this research was incapable of swinging the pendulum up to the UEP if the initial angle $x_1(0)$ is found to be $> |\pi/4|$ rad [58]. The nonlinear fuzzy controller was able to swing-up the pendulum from an initial angular state of $x_1(0) \in$ [-88 88], which was a significant improvement on the linear controller [58]. A NN nonlinear adaptive controller was designed to learn how to balance a SIPC with no *a priori* knowledge of the system dynamics in [59]. Instead, the controller predicted the input required by evaluating the behaviour of the failure signal, an indicator that informed the system when balance control had not been satisfied [59]. This work was done to improve on the research performed in [43,44]. The work demonstrated

in [60] aimed to tackle the experimental travel constraint of a SIPC through the development of a nonlinear controller that balanced a SIPC with optimal cart displacement. Tests demonstrated that the controller had an operational blind spot at trajectories found approximately around the UEP; despite this drawback the controller reduced the maximum displacement of the cart significantly [60].

The swing-up control of the SIPC using a Lyapunov function was demonstrated in [61,62]. A control input was selected to ensure that this time-derivative remained negative semi-definite, producing the desired swing-up [61,62]. The TITech pendulum was swung-up to the UEP using a feedforward and feedback bang-bang control strategy in [41]. Experimental results were easier to produce with the proposed TITech pendulum as it took up less space and provided less parametric uncertainties as compared to the pendulum-cart system [41]. Additionally, Bang-Bang feedback and feedforward swing-up control was demonstrated on the TITech pendulum through the construction of pseudo-states in [40]. The pseudo-states were formed to improve the robustness of the nonlinear controller, especially in the presence of uncertainties in the values of the system parameters [40]. LDM was used as an energy shaping technique to demonstrate a simple swing-up control strategy for the SIP in [63]. The goal of this research was to swing the pendulum up to the UEP using only one swing-cycle [63]. This was done by switching between swing-up and balancing controllers and ensuring that the control input $u > {}^{4g}/_{3}$ [63].

The nonlinear control of the many configurations of the double inverted pendulum (DIP) has been extensively researched. This review, therefore, will only focus on one particular configuration of the DIP, namely the Acrobot. The first significant contributions involving the Acrobot were presented by Mark Spong in [6,34], where he utilised the combination of partial-feedback linearisation (PFL) and linear control methods to swing the Acrobot up to the UEP. The Acrobot has an active distal joint and a passive proximal joint which could be linearised in separate control scenarios, termed collocated and non-collocated PFL respectively [6,34]. Spong demonstrated that each linearisation technique requires a unique swing-up control strategy [6,34]. An inverse-trigonometric (ATAN) function acting on the angular velocity of the proximal joint was chosen as the reference trajectory for the collocated linearised Acrobot to indirectly introduce the dynamics of the proximal limb into the control input and to pump energy into the system [6,34]. The dynamics of the proximal limb would be unobserved otherwise and the control input would, therefore, cause the states of the Acrobot to tend towards the stable pendant equilibrium states [6,34]. The chosen reference trajectory lead to unstable internal dynamics, allowing the Acrobot to tend towards the unstable inverted trajectory [6,34]. The opposite was true in the non-collocated case, where the dynamics of the distal limb were evidently excluded from the control input. The correct trajectory was, therefore, only achieved if the correct outer-loop gains and initial angular states were chosen [6,34].

Swing-up control through the implementation of LDM was demonstrated on the

Acrobot by Xin and Kaneda in [64]. A Lyapunov function was specifically constructed to observe the mechanical energy, the angular velocities, and states of the Acrobot [64]. The control input was chosen to keep the time-derivative of the Lyapunov function negative semi-definite, thus ensuring that the Acrobot tended toward the UEP [64]. Minimum-time optimal control was used to directly search for swing-up trajectories for the Acrobot using a window search in [65], combining LDM and Pontryagin's Minimum Principle (PMP) in [66] and using a combination of PFL and PMP in [67]. Adaptive swing-up control was demonstrated on an Acrobot through the implementation of an adaptive fuzzy-logic controller in [68] and provided a comparative analysis between conventional techniques and adaptive control. Stable control could be achieved through the switching of multiple incomplete controllers that operated around a linearised domain as seen in [69]. The control of switching in this case was found through Reinforced Learning (RL) [69]. The Acrobot was transformed into an approximation of a single pendulum, with swing-up control being subsequently performed in [70]. The behaviour of the swing-up controller was dependent on a Lyapunov function [70]. The controller was subsequently switched to a LQR controller once the Acrobot was found to be approximately upright [70]. Explanation-based control (EBC) was used to determine the exact necessary parameters required to swing-up an Acrobot in [71]. The EBC method evaluates the swing-up of the Acrobot as two distinct movements which were linked causally, allowing for the optimisation and scheduling of each motion separately [71]. This resulted in improved results as compared to the Heuristic Control method and ATAN control method (seen in [34]) [71]. Pulse-torques and rest-to-rest manoeuvres were used to swing-up an Acrobot in [72]. The pulse torques were applied to instantaneously change the angular velocities of the limbs [72]. The torque was then released, allowing the Acrobot to swing freely toward the UEP [72]. Rest-to-rest manoeuvres were used to introduce braking torques at the links, stopping the limbs from swinging past the UEP [72]. A linear controller was then implemented to regulate the Acrobot about the UEP [72].

The majority of the literature pertaining to the nonlinear control of the TIPC involved the cascading of robust controllers on linear regulators. This includes the work of Medrano-Cerda [53,54] and Tsachouridis [51,52] (mentioned in the linear control section). The swing-up control of the TIPC using a 2 DOF control structure and a feedforward controller was demonstrated in [73]. The first instance of both theoretical and experimental results for this particular system was demonstrated in this paper. The feedforward controller was designed through the evaluation of the system's internal dynamics and the solved constrained two-point boundary value problem (BVP) [73]. A linear Ricatti feedback controller was designed to balance the TIPC once it was found to be approximately upright [73]. The work demonstrated in [73] was extended through the development of a novel feedforward controller in [74]. This approach allowed for the inclusion of the constraints provided by the saturation functions into the BVP, which could be trivially solved using the Matlab BVP solver [74].

The most extensive research into the nonlinear control of the n-link pendulum was performed by Spong, and Xin and Liu. Their research focussed on the generalisation of control for a pendulum system with any number of links. The analytical results were confirmed with simulations performed on systems with a predefined number of links, with Spong focussing on the Acrobot, Pendubot and TIP, and Xin and Liu focussing on a number of configurations, ranging from the Direct-Drive Acrobot (DDA) to the Passive-Active-Active (PAA) robot. Spong demonstrated the implementation of PFL on a generalised underactuated system with n-DOFs using ATAN (collocated) or linear swing-up control (non-collocated) in [6,75,76]. This linearisation technique resulted in a characterisation of the internal and zero dynamics of the system which, once evaluated, could be used to determine the stability and the trajectory of all the pendulums in the system [6,75]. Simulations were performed for the TIP with 2 actuators in [76]. Xin's work focussed on the application of LDM for the swing-up control of an underactuated n-link pendulum as demonstrated in [5,77,78] through the implementation of a coordinate transformation using virtual composite links (VCLs). The n-link pendulum is defined in this case to have one passive joint (i.e. $n-1$ actuators), whereby a solution to the swing-up control problem was first derived for an n-link pendulum with a passive first joint [5,77,78]. The solution was expanded to include the possibility of an unactuated joint being located anywhere in the system [5,79]. It is popular practise, however, to leave the first joint unactuated, as seen with the DDA and the PAA robot [5]. The generalised n-link form of this robot is given the name PA_{n-1} robot.

2.4.3 Selection of Appropriate Control Objective and Technique

It is evident that, upon analysis of the aforementioned literature, that the most commonly chosen control objectives in underactuated robotics involves **balancing** (linear control methods) and **swing-up control** (nonlinear control methods). Balancing control refers to the regulation of an underactuated system about some equilibrium point whereas swing-up control involves the "swinging-up" of an underactuated system from a lower energy state towards the equilibrium point which is associated with the highest possible potential energy (UEP). Whilst the regulation of a system about an equilibrium point is a relevant control objective, we decided to select the swing-up control objective instead simply because the realisation of this objective requires the implementation of more interesting control techniques. The most popular swing-up control techniques, as made evident in the aforementioned literature, are the LDM and PFL methods. The PFL method is rather trivial to implement but does not actively track the UEP. The LDM method, on the other hand, provides a more mathematically rigorous solution which results in a control torque that tracks the UEP. It is for this reason that the LDM technique is chosen to perform swing-up control on the PA_{n-1} robot in this investigation.

2.5 Altering the PA_{n-1} Model: Friction in Pendulum Systems

With the model, control objective, and control technique chosen, the appropriate selection of model alteration is the only requirement that remains outstanding according to the research methodology of this project. The PA_{n-1} robot is an ideal model that does not consider the effects of nonconservative physical phenomena such as friction. If we had to evaluate the aforementioned literature retrospectively, it is evident that there is no existing literature that discusses the swing-up control of UMSs that have been integrated with friction. This was unexpected, especially since the effects of friction cannot be ignored in any real-world scenarios. It seems that the integration of friction is a viable, novel, and trivial alteration that can be made to the PA_{n-1} robot when considering swing-up control. This section will thus include a thorough investigation into the existing friction models as well as a discussion on the selection of an appropriate friction model and methods of friction compensation respectively.

2.5.1 Friction Models

The different types of mechanical friction and their effects on robotic manipulators have been well documented. The most commonly used models of friction and their implications in the control engineering field were discussed in [80]. These included the Coulomb, viscous, Stribeck and Dahl friction models [80]. Furthermore, a second-order Dahl model was formulated [80] to estimate the elastic and plastic deformation of surfaces that are in contact with one another during stiction [80]. The research concludes that asymptotic stabilisation can be achieved under simple velocity feedback if the Stribeck model is ignored [80]. The mathematical derivation of the effects of both dry and viscous damping on a simple pendulum was demonstrated in [81]. Dry friction damping is defined as a constant torque $\pm|\tau_d|$ that acts against the movement of the pendulum [81]. Coulomb friction is an approximation of dry friction [81]. Viscous damping friction is defined as a damping torque that is dependent on the angular velocity of the pendulum, and is extensively used in literature, as seen in [81, 82]. Both torques remove energy from the system, causing the pendulum to tend toward the stable pendant equilibrium state [81].

2.5.2 Selection of Appropriate Friction Model

It is evident that the viscous damping friction model is the most extensively discussed friction model in the literature included in this review since it is the most trivial to implement, thus resulting in its selection for the project as the element that, once integrated, introduces a sufficiently significant alteration to the PA_{n-1} robot model.

It is unknown at this point whether the integration of viscous damping will have any effect on the swing-up control of the PA_{n-1} robot using the LDM technique.

An investigation into the existing methods of dealing with the effects of friction (termed friction compensation) should be performed so that we have a general idea of how to achieve the control objective in the event that the LDM technique fails under this alteration. The following section is included specifically to discuss the existing methods of friction compensation.

2.5.3 Friction Compensation

There is, to the knowledge of the author, no literature that discusses friction compensation pertaining to the generalised n-link pendulum system. The following examples do, however, include instances of friction compensation which are performed on the SIPC and the DIPC. Additionally, the friction models included in this review are not restricted to the viscous damping model or swing-up control since it is unknown at this stage what type of solution would be appropriate or required.

An H-∞ controller is designed to stabilise a dry damped SIPC about the UEP in [83]. The dry friction is located at the connecting link between the cart and the pendulum [83]. The results of this research demonstrate that the effects of dry friction cannot be ignored, even if the control strategy is simply required to balance the pendulum-cart system [83]. Ignoring the dry friction caused the pendulum to oscillate, producing limit cycles. Instead, a balanced trade-off is made between friction insensitivity and objective tracking to produce a controller that is robust enough to achieve satisfactory results [83]. This is done by incorporating the nonlinear friction model into the linearised model of the SIPC [83]. Limit cycles were also observed in [84], whereby a LQR controller was developed to balance a SIPC that was subject to both dry and viscous forces (in static and dynamic form). The oscillations are, once again, attenuated by incorporating the frictional models in the LQR controller formulation [84]. This control produces minor oscillations about the UEP, which have been attributed to the quantisation error in the digital encoders that were implemented for measurement purposes [84]. A similar approach was taken by Park, Chwa, and Hong in [85], and Jubo, Anwar, and Tomizuka in [86], with the exception that the viscous friction was ignored. Another method of tackling the effects of limit cycles caused by the presence of friction involves the implementation of a friction compensator as seen in [87, 88].

In [87], the frictional force applied to the cart in the DIPC system during the experiment was *estimated* using a modified version of the Dahl model which included the Stribeck effect. The objective was to feed the actuator the estimation in the hopes that it would completely negate the effects of friction [87]. This could only occur, however, if the estimate exactly profiled the true frictional force [87]. Experimental results demonstrate an attenuation of the limit cycle affect in the DIPC system [87]. In [88], the friction model is coupled with the dynamics of the motor whilst a locally linear neuro-fuzzy (LLNF) controller is used to inversely model the motor and friction dynamics [88]. The LLNF network is based on the divide-and-conquer strategy and has been used to model nonlinear networks and for estimation purposes [88].

The results of the control are compared to the multi-layer perceptron (MLP) method of inverse modelling [88], whereby the LLNF method demonstrates a greater attenuation of the limit cycles of the DIPC as compared to the MLP method [88].

2.6 Conclusion

The review of existing literature that is pertinent to the field of underactuated robotics resulted in the selection of an appropriate system model (PA_{n-1} robot), control objective (swing-up control), control technique (Lyapunov's Direct Method), and system alteration (integration of viscous damping model) as highlighted by the research methodology of this project. UMSs have traditionally been modelled as n-link pendulum systems according to literature, and the highest possible number of actuators to DOFs ratio makes the PA_{n-1} robot the perfect candidate to mathematically represent a generalised UMS. The most extensively selected control objectives in literature involve balancing and swing-up control, with the latter being chosen for this investigation since its fulfilment involves the implementation of more interesting control techniques. The LDM technique is selected to achieve this control objective since it produces a more mathematically rigorous solution as compared to the PFL alternative. The swing-up control solutions that currently exist in literature are only applicable to ideal frictionless systems. We, thus, identified a simple alteration to the PA_{n-1} robot that is novel when considering swing-up control, namely the integration of a simple friction model. The viscous damping friction model was selected in this instance since it is most extensively covered in literature and it can be trivially implemented. A review of the most relevant friction compensation techniques was included in this chapter to form the foundation of a work-around in the event that the integration of the viscous damping model results in the failure to achieve LDM-related swing-up control.

"He who is best prepared can best serve his moment of inspiration."
— Samuel Taylor Coleridge

Chapter 3

Introduction to System Modelling

3.1 Chapter Overview

An understanding of the dynamical behaviour of any system is required if a control technique is to be implemented. The behaviour of a system is described by its equations of motion, a set of differential equations that dictate the movement of each DOF [89]. It is relatively trivial to model simple systems based on Newtonian mechanics; a more complex system, such as a system with a transformed generalised coordinate system, may require more robust modelling methods [89]. The foundations of two modelling techniques, namely the Classical Lagrangian and the Energy modelling methods, are discussed in this chapter. Each technique is applied to a DIP to demonstrate each method's efficacy in modelling a multi-body pendulum system. Conclusions about each modelling technique are summarised thereafter.

3.2 Classic System Modelling

To understand the fundamentals of Lagrangian mechanics, the principles of Calculus of Variations must first be discussed.

3.2.1 Calculus of Variations, the Principle of Least Action, and the Euler-Lagrange Differential Equation

Calculus of variations involves the minimisation of a functional, a mapping between a collection of functions to a set of real numbers $\mathbb{R}$ [90]. The most common functional involves integration, whereby

$$I = \int_{t_1}^{t_2} \mathbf{L}(\mathbf{q}, \dot{\mathbf{q}}, \mathrm{t})\mathrm{dt} \tag{3.1}$$

[90]. The path of $\mathbf{L}(\mathbf{q}, \dot{\mathbf{q}}, \mathrm{t})$, known as the Lagrangian, can be varied by adding a *perturbation*. As defined, the function $\mathbf{L}(\mathbf{q}, \dot{\mathbf{q}}, \mathrm{t})$ is composed of the function $\mathbf{q}(t)$. This function, once perturbed by a noise function $\epsilon\eta(t)$, can produce a single path between the boundary points t_1 and t_2 for every value of ϵ (where $\epsilon \in \mathbb{R}$ and

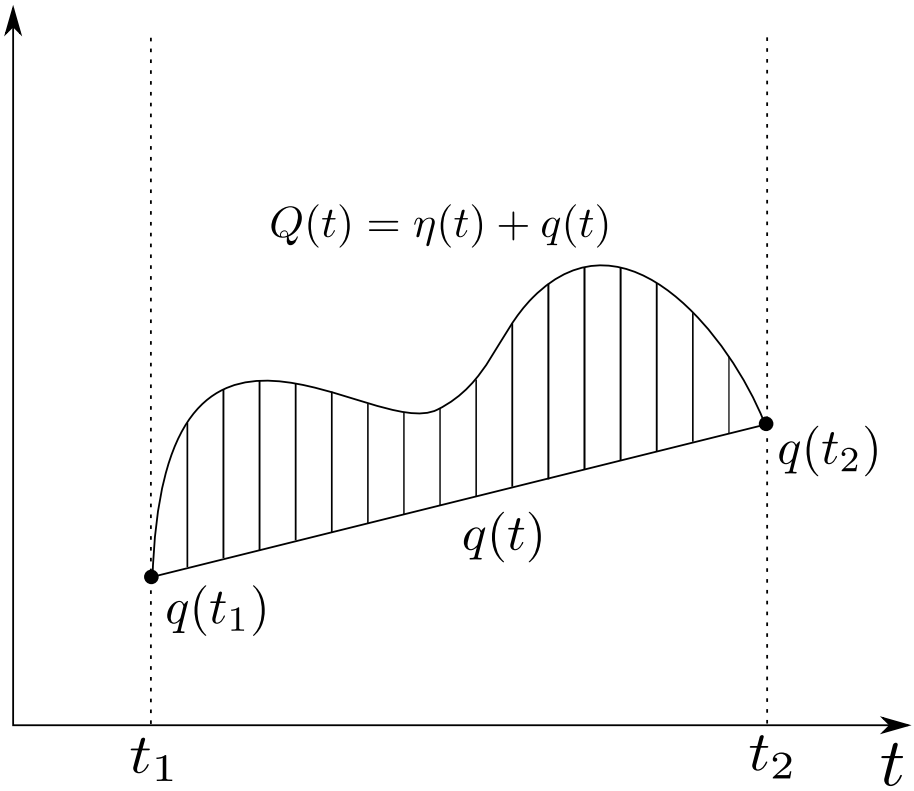

FIGURE 3.1: The perturbation of the shortest-distance function $q(t)$. Image adapted from [1]

$\eta(t_1) = \eta(t_2) = 0$). This perturbed function in figure 3.1 is described as

$$\mathbf{Q}(t) = \mathbf{q}(t) + \epsilon\eta(t) \tag{3.2}$$

where $\mathbf{Q}(t_1) = \mathbf{q}(t_1)$ and $\mathbf{Q}(t_2) = \mathbf{q}(t_2)$.

The integral is now dependent on ϵ and is not, therefore, constrained to map to one specific real number, but instead represents the integral of all the possible paths formed by $\mathbf{L}(\mathbf{q}, \dot{\mathbf{q}}, \mathrm{t})$, where

$$I(\epsilon) = \int_{t_1}^{t_2} \mathbf{L}(\mathbf{q}, \dot{\mathbf{q}}, \epsilon, \mathrm{t})\mathrm{dt} \tag{3.3}$$

[90]. In most cases there exists at least one path that, once integrated over the entire range between the bounded t-values, produces the lowest valued integral. This represents the extrenum of the functional, the shortest path between two bounded points [90].

This property proved to be useful in understanding the movement of physical

bodies [91]. Newtonian physics provided the first method of calculating the trajectory of physical bodies in space, but did not adequately describe the reasoning behind the choice of these trajectories [92]. It was discovered that physical bodies travelled along a trajectory that would always *minimise* the difference between the kinetic and potential energies (known as the *action*, $\mathbf{S}(\tilde{\mathbf{x}})$), where

$$\mathbf{S}(\tilde{\mathbf{x}}) = \int_{t_1}^{t_2} \left(\frac{1}{2} m \dot{\tilde{\mathbf{x}}}^{\mathbf{2}} - \mathbf{P}(\tilde{\mathbf{x}}) \right) \mathrm{dt} \tag{3.4}$$

and where $\mathbf{P}(\tilde{\mathbf{x}})$ represents the potential energy in the system [92]. This is known as the *Principle of Least Action*. Solving for the extrenum of the action with respect to time results in the Newtonian second law of motion described by

$$\frac{\mathrm{d}}{\mathrm{dt}} \mathbf{S}(\tilde{\mathbf{x}}) \bigg|_{\min} := 0 = -m\ddot{\tilde{\mathbf{x}}} - \nabla \mathbf{P}(\tilde{\mathbf{x}}), \tag{3.5}$$

$$\therefore m\ddot{\tilde{\mathbf{x}}} = -\nabla \mathbf{P}(\tilde{\mathbf{x}}) \tag{3.6}$$

where $\nabla \mathbf{P}(\tilde{\mathbf{x}})$ represents a potential force. The full proof can be seen in [92]. This is a remarkably elegant approach to solving for the dynamical behaviour of a system as it provides the opportunity to include coordinate systems that may not be Cartesian (which may be more difficult to derive using the Newtonian counterpart). Solving from first principles is cumbersome; a simple analysis of the structure of functionals leads to a general expression that is proven to be true for variational problems.

It is clear that $\mathbf{q}(\mathbf{t})$ in figure 3.1 was chosen to represent the shortest path between boundary points $\mathbf{t_1}$ and $\mathbf{t_2}$. It is evident that the extrenum (minimum) of the functional will exist at $\epsilon = 0$ since it is known that the shortest path exists at this value of perturbation. Therefore

$$\frac{\mathrm{d}}{\mathrm{d}\epsilon} I(\epsilon) \bigg|_{\epsilon=0} = 0 \tag{3.7}$$

[90]. Solving for this formula produces an expression known as the *Euler-Lagrange differential equation*, where

$$\frac{\mathrm{d}}{\mathrm{dt}} \frac{\partial \mathbf{L}}{\partial \dot{\mathbf{q}}}(\mathbf{q}, \dot{\mathbf{q}}, \mathrm{t}) - \frac{\partial \mathbf{L}}{\partial \mathbf{q}}(\mathbf{q}, \dot{\mathbf{q}}, \mathrm{t}) = 0. \tag{3.8}$$

The proof is not included in this dissertation, but may be viewed in [90, 91]. This expression, when used to evaluate the dynamics of a mechanical system with any generalised coordinate system $\mathbf{q}$, exploits the Principle of Least Action when the action of the system is chosen as the Lagrangian. The coordinate system will be angular in the case of a rotational system, like the multi-body pendulum system. The resulting expressions represent the equations of motion for the system, which can be represented in the *prototypical form*, representing the set of nonlinear, autonomous equations of motion. The prototypical system is described here similarly to that

found in [93], where

$$\mathbf{M}(\mathbf{q})\ddot{\mathbf{q}} + \mathbf{D}(\mathbf{q},\dot{\mathbf{q}}) + \mathbf{K}(\mathbf{q}) = \mathbf{G}(\mathbf{q})\mathbf{u} \tag{3.9}$$

with

$q \in \mathbb{R}^N$ = the generalised coordinates of the n-link pendulum system,
$\mathbf{M}(\mathbf{q})$ = the *Mass matrix*, which is positive semi-definite and symmetrical [93],
$\mathbf{D}(\mathbf{q},\dot{\mathbf{q}})$ = the collective representation of conservative torques (coriolis, centripetal, and configurational changes), and nonconservative torques (friction, mass, and pendulum length changes) acting on the system,
$\mathbf{K}(\mathbf{q})$ = the potential torques exerted on the pendulum masses possibly by gravity or springs, and
$\mathbf{G}(\mathbf{q})\mathbf{u}$ = the input torque τ introduced by actuators at the pendulum joints.

The equations of motion can be found by taking the inverse of the Mass matrix, which will be always be non-zero since the Mass matrix is positive definite and uniformly symmetric [15]. Therefore,

$$\ddot{\mathbf{q}} = \mathbf{M}^{-1}(\mathbf{q})\left(-\mathbf{D}(\mathbf{q},\dot{\mathbf{q}}) - \mathbf{K}(\mathbf{q}) + \mathbf{G}(\mathbf{q})\mathbf{u}\right)$$

represents a set of nonlinear, autonomous (time-invariant) equations of motion for the case of the n-link pendulum.

3.2.2 Symmetry and Conservation Laws

It is sometimes a challenge to obtain insightful information about a physical system by evaluating the action and dynamical equations alone. This brings the discussion to the idea of mathematical symmetry, which is covered in this section to provide some context to the derivation of some important properties of specifically structured Lagrangian functions. The most recognised theory concerning differentiable symmetry is credited to the mathematician Emmy Noether, whose theorem concerning the Lagrangian function states the following [94]:

Theorem 3.1. *(**Noether's Theorem**) A conserved law corresponds to the action of a physical system that experiences no first-order change in a specific variable once it has undergone some transformation.*

In other words, if one of the variables that the Lagrangian depends on is perturbed by a small value ϵ, the Lagrangian will remain invariant to this perturbation if there is a related conservation of some quantity [94]. This invariance to transformation is known as a *symmetry*. Two important conditions in symmetry lead to the case of *conserved angular momentum* and *conserved energy* regarding rotational systems.

Cyclic Coordinates and the Conservation of Angular Momentum

The following result was proposed by Noether for rotational systems regarding the conservation of angular momentum:

The angular momentum (p_k) of the kth DOF of a rotational system is conserved so long as the system along the aforementioned DOF remains rotationally symmetrical, i.e. the Lagrangian must remain invariant to changes in the angular coordinate of the kth DOF, i.e..

$$\dot{p}_k = 0 \quad \text{iff} \quad \frac{\mathrm{d}\mathbf{L}(\mathbf{q}, \dot{\mathbf{q}}, \mathrm{t})}{\mathrm{d}q_k} = 0. \tag{3.10}$$

This is proven in [94]. The conservation of the angular momentum for coordinate q_k implies that the angular velocity $\dot{q}_k$ is not expected to change so long as the inertial components (m_k and I_k) remain constant [94]. It is easy to imagine the conditions that will lead to this type of behaviour. One such example includes a pendulum located in space or on a plane that is perpendicular to the gravitational acceleration plane. If the pendulum is given an initial velocity, this velocity is not expected to change since gravity is unable to accelerate/decelerate the pendulum. In this case, the coordinate q_k is known as a *cyclic coordinate* [94].

Time-Translational Symmetry and the Conservation of Energy

The following result is proposed for mechanical systems regarding the conservation of energy principle:

The total mechanical energy of a system will be conserved so long as the system is time-translationally symmetrical, i.e. the Lagrangian is not explicitly dependent on time. This is demonstrated when the Hamiltonian of the system (described by $\mathcal{H}$) is constant and its constituents are not time-varying. This can only occur if

$$\frac{\partial \mathbf{L}(\mathbf{q}, \dot{\mathbf{q}}, \mathrm{t})}{\partial \mathrm{t}} = 0.$$

This is proven in appendix A (Proof A.1) since the behaviour of the states of a damped or actuated system is the result of the constituents of the Hamiltonian, which is not evident without this derivation. It is apparent that one can expect that the mechanical energy of a particular system should be conserved for all time if there is no actuation or damping. It is difficult to observe the effect of adding an actuator or friction factor to the prototypical form on the Lagrangian equation itself, but the proof suggests that *these factors will introduce a function which is explicitly time-dependent into the Hamiltonian*. This will cause the expected change of energy since the Hamiltonian must be kept constant.

3.2.3 Methodology: Modelling the Dynamics of a system using the Lagrangian

The following points summarise the Classical modelling technique using Lagrangian mechanics:

(1) Identify the generalised coordinates of the system.

(2) Construct the Lagrangian. The Lagrangian is chosen to be the difference between the total system kinetic and potential energies to exploit the Principle of Least Action for mechanical systems, where

$$\mathbf{L}(\mathbf{q}, \dot{\mathbf{q}}, \mathrm{t}) = \mathbf{T}(\mathbf{q}, \dot{\mathbf{q}}, \mathrm{t}) - \mathbf{P}(\mathbf{q},\mathrm{t}). \tag{3.11}$$

The expressions for $\mathbf{T}(\mathbf{q}, \dot{\mathbf{q}}, \mathrm{t})$ and $\mathbf{P}(\mathbf{q},\mathrm{t})$ must, therefore, be found. Friction and actuation are ignored here.

(3) Apply the Euler-Lagrange differential equation on the Lagrangian.

(4) Characterise the result in terms of the prototypical form. Add frictional terms and actuation as required.

(5) Transform the model into the state-space.

Examples of derivations for the model of the DIP can be seen in [6], [34], and [64] in the form of the Acrobot.

3.3 System Modelling using Energy

Modelling methods based on the conservation of energy principle have been used on many occasions to describe the dynamical behaviour of a system [82]. This method was first described for the generalised mechanical prototypical system in [93] by Naude. Certain definitions are adapted to include the effects of the modified friction model described in [80]. The system energy is first derived through the use of the integral transform.

3.3.1 The Integral Transform

The dynamics of a rotational system are dependent upon the torques that act on it. These torques, which include conservative and nonconservative forms, as seen in eq. (3.9). The definition of the $\mathbf{D}(\mathbf{q},\dot{\mathbf{q}})$ matrix is modified to include damping effects; this matrix will be distinctly decomposed in section 3.3.3.

The energy in the system is represented as

$$W = \int_{x_1}^{x_2} \sum \mathbf{F}\mathrm{d}\mathbf{x} = \int_{q_1}^{q_2} \sum \tau \mathrm{d}\mathbf{q} \tag{3.12}$$

[82]. A more useful formulation for energy system modelling is presented in the form of the energy integral transform, where

$$W = \mathscr{E}\{\mathbf{y}\} = \int \dot{\mathbf{q}}^{\mathrm{T}}\mathbf{y}\mathrm{dt} \tag{3.13}$$

and where

$$y := \mathbf{M}(\mathbf{q})\ddot{\mathbf{q}} + \mathbf{D}(\mathbf{q},\dot{\mathbf{q}}) + \mathbf{K}(\mathbf{q}) - \mathbf{G}(\mathbf{q})\mathbf{u} \tag{3.14}$$

[93]. The integral assists in separating the contributors of the system energy according to their forces. These contributors can thus be identified and labelled for convenience. The total mechanical energy of the system can be found using the energy integral transform seen in eq. (3.13). The result of this transformation is demonstrated by

$$\begin{aligned}\mathscr{E}\{\mathbf{y}\} = \frac{1}{2}\dot{\mathbf{q}}^{\mathbf{T}}\mathbf{M}(\mathbf{q})\dot{\mathbf{q}} - \frac{1}{2}\int \dot{\mathbf{q}}^{\mathbf{T}}\dot{\mathbf{M}}(\mathbf{q})\dot{\mathbf{q}}\ \mathrm{dt} + \int \dot{\mathbf{q}}^{\mathbf{T}}\mathbf{D}(\mathbf{q},\dot{\mathbf{q}})\ \mathrm{dt} + \\ \int \dot{\mathbf{q}}^{\mathbf{T}}\mathbf{K}(\mathbf{q})\ \mathrm{dt} - \int \dot{\mathbf{q}}^{\mathbf{T}}\mathbf{G}(\mathbf{q})\mathbf{u}\ \mathrm{dt} + E_0\end{aligned} \tag{3.15}$$

which is adapted from [93], where the easily identifiable energies are described as

$$\begin{aligned}\frac{1}{2}\dot{\mathbf{q}}^{\mathbf{T}}\mathbf{M}(\mathbf{q})\dot{\mathbf{q}} &= \text{the energy stored in the motion of the pendulum masses and} \\ &\quad \text{moments of inertia (Kinetic Energy),} \\ \int \dot{\mathbf{q}}^{\mathbf{T}}\mathbf{K}(\mathbf{q})\ \mathrm{dt} &= \int \mathbf{K}(\mathbf{q})^{\mathbf{T}}\mathrm{d}\mathbf{q} = \mathbf{P}(\mathbf{q}) = \text{the potential "spring-like" energy stored in the} \\ &\quad \text{displacement of the pendulum masses,} \\ \int \dot{\mathbf{q}}^{\mathbf{T}}\mathbf{G}(\mathbf{q})\mathbf{u}\ \mathrm{dt} &= \text{the energy introduced or removed by the actuators, and} \\ E_0 &= \text{the initial mechanical energy of the system.}\end{aligned}$$

The nature of the energies contributed by both the $\mathbf{D}(\mathbf{q},\dot{\mathbf{q}})$ and $\dot{\mathbf{M}}(\mathbf{q})$ matrices, however, cannot be easily discerned upon such a high-level inspection. The matrices are evaluated and decomposed in the following sections to determine whether the energy contributions seen in the adapted integral transform are conservative, similar to the procedure seen in [93].

3.3.2 Mass Matrix and the Multi-body Pendulum System

It is evident that the time derivative of the mass matrix $\dot{\mathbf{M}}(\mathbf{q})$ is present in the energy equation demonstrated in eq. (3.15). Intuitively, this change in the entries of the mass matrix can represent an energy input (mass gain) or a dissipation (mass loss, typically due to the burning of fuel, as seen in propelled vehicles during thrust) over time [93]. It is important to note, however, that rotational systems are dependent upon an inertial property known as the *moment of inertia* ($\mathrm{kg/m^2}$). The moment

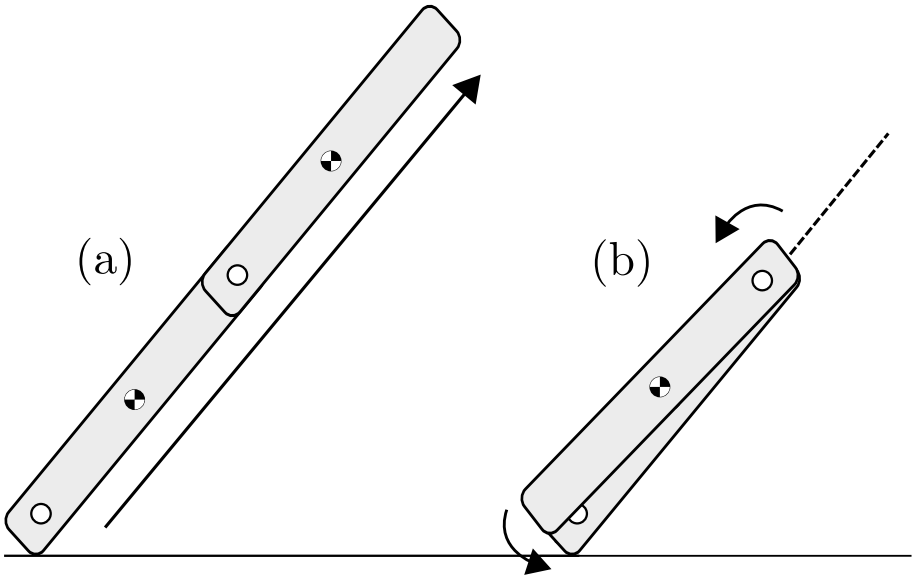

FIGURE 3.2: Two Configurations of the DIP including (a) Full-extension (b) Inverse Extension

of inertia of a rigid body differs from mass as it is not an intrinsic property of an object [82]. Instead, the moment of inertia of a rigid body is also dependent on its rotational trajectory [82]. A change in the system configuration, therefore, may result in the change of the entries in the mass matrix. This produces the illusion of a changing mass in the system, even if the system is conservative. This may not be obviously evident in the SIPC example provided in [93], but the influence of the configuration of a rotational system on the mass matrix becomes more evident in compounded pendulum system examples. This will be illustrated on the simplest multi-body pendulum system, the DIP.

Consider the two configurations of the DIP, with each pendulum in figure 3.2 having equivalent masses, lengths, and moments of inertia. The DIP has two angular DOFs described by q_1 and q_2. The first DIP is configured in a fully extended manner with $q_2 = 2k\pi$, $k \in \mathbb{Z}$. The second DIP is configured in such a way that the two pendulums are aligned on top of one another with $q_2 = \pi + 2k\pi$, $k \in \mathbb{Z}$. The Mass matrix of the generalised DIP has been derived in [78], with an adapted expressed as

$$\mathbf{M}(\mathbf{q}) = \begin{bmatrix} \frac{1}{2}mL^2\left[3 + \cos q_2\right] + 2I & \frac{1}{4}mL^2\left[1 + 2\cos q_2\right] + I \\ \frac{1}{4}mL^2\left[1 + 2\cos q_2\right] + I & \frac{1}{4}mL^2 + I \end{bmatrix}. \tag{3.16}$$

The kinetic energy of the system

$$\mathbf{T} = \frac{1}{2}\dot{\mathbf{q}}^{\mathbf{T}}\mathbf{M}(\mathbf{q})\dot{\mathbf{q}} \tag{3.17}$$

is extracted from the system energy equation seen in eq. (3.15). The DIP is generally allowed to vary in its angular positions, but the two configurations will be fixed at the joint between the two pendulums for illustration purposes (i.e. $\dot{q}_2 = 0$). The mass matrix for configuration (a) & (b) described by

$$\mathbf{M_a} = \begin{bmatrix} 2\left[mL^2 + I\right] & \frac{3}{4}mL^2 + I \\ \frac{3}{4}mL^2 + I & \frac{1}{4}mL^2 + I \end{bmatrix}, \quad \mathbf{M_b} = \begin{bmatrix} \frac{3}{2}mL^2 + 2I & \frac{1}{4}mL^2 + I \\ \frac{1}{4}mL^2 + \mathrm{I} & \frac{1}{4}mL^2 + I \end{bmatrix} \tag{3.18}$$

can be calculated since the value of q_2 is known for each case. There is a clear difference between the mass matrices in the two configurations despite there being no change in the mass in each system. Instead, the different configurations have produced differing values of moments of inertia as the pendulums travel in different rotational trajectories. This is the result of the *parallel axis theorem* [82]. The mass matrix in this case is, therefore, intended to accommodate the relationship between the angular velocity vector $\dot{q}$ and the kinetic energy (T_R) for rotational systems, where

$$T_R = \frac{1}{2}\dot{\mathbf{q}}^{\mathbf{T}}\mathbf{M}(\mathbf{q})\dot{\mathbf{q}} \tag{3.19}$$

[82]. The change of energy associated with the change in the configuration of the pendulum system is conservative as these effects can be directly observed in the formulation of the kinetic and potential energies of the system using the Energy method [82]. The distribution of the energy between the kinetic and potential form, however, differs with varying configurations.

The kinetic energies in each configuration with $\dot{q}_2 = 0$ are described by

$$T_a = \left[mL^2 + I\right]\dot{q}_1^2, \qquad T_b = \left[\frac{1}{2}mL^2 + I\right]\dot{q}_1^2. \tag{3.20}$$

These results demonstrate that if a finite and equivalent amount of mechanical energy is found in each system, E_0, the pendulums in (a) will rotate collectively at a lower angular velocity ($\dot{q}_1$). This configuration causes the system to skew more of the energy distribution toward the system's potential energy ($\mathbf{P}$), therefore explaining the change in the magnitude of some of the entries in the mass matrix. The energy is conserved in both of these systems, with the distribution of mechanical energy differing in each case due to the system configuration. This confirms that the mass matrix differential $\dot{\mathbf{M}}(\mathbf{q})$ can represent both an internal reshuffling of energy (conservative) or a change in energy due to mass gain/loss or pendulum length change (nonconservative) [93]. This conservative reshuffling of energy due to system

configuration must be expected with the generalised n-link pendulum system. The time differential of the mass matrix $\dot{\mathbf{M}}(\mathbf{q})$ is therefore defined as

$$\dot{\mathbf{M}}(\mathbf{q}) = \dot{\mathbf{M}}_{\mathbf{c}}(\mathbf{q}) + \dot{\mathbf{M}}_{\mathbf{n}}(\mathbf{q}) \tag{3.21}$$

to prevent confusion, where $\dot{\mathbf{M}}_{\mathbf{c}}(\mathbf{q})$ represents the *conservative* change in moment of inertia due to the system's configuration and $\dot{\mathbf{M}}_{\mathbf{n}}(\mathbf{q})$ represents the *nonconservative* moment of inertia change due to a gain/loss in mass or sudden changes in the length of any of the pendulums in the system. This leads to the definition of the energy contributions to the system due to the change of moment of inertia, where

$$\frac{1}{2}\int \dot{\mathbf{q}}^{\mathbf{T}}\dot{\mathbf{M}}(\mathbf{q})\dot{\mathbf{q}}\,\mathrm{dt} = \frac{1}{2}\int \dot{\mathbf{q}}^{\mathbf{T}}\dot{\mathbf{M}}_c(\mathbf{q})\dot{\mathbf{q}}\,\mathrm{dt} + \frac{1}{2}\int \dot{\mathbf{q}}^{\mathbf{T}}\dot{\mathbf{M}}_n(\mathbf{q})\dot{\mathbf{q}}\,\mathrm{dt} \tag{3.22}$$

and where

$\frac{1}{2}\int \dot{\mathbf{q}}^{\mathbf{T}}\dot{\mathbf{M}}_c(\mathbf{q})\dot{\mathbf{q}}\,\mathrm{dt} =$ the conservative energy shuffle in system due to change in system configuration, and

$\frac{1}{2}\int \dot{\mathbf{q}}^{\mathbf{T}}\dot{\mathbf{M}}_n(\mathbf{q})\dot{\mathbf{q}}\,\mathrm{dt} =$ the energy that is gained/lost due to a change in the mass or lengths of the pendulums.

3.3.3 Decomposition of the $\mathbf{D}(\mathbf{q}, \dot{\mathbf{q}})$ Matrix

The effect of the $\mathbf{D}(\mathbf{q}, \dot{\mathbf{q}})$ matrix on the energy of the system has yet to be discussed. This is done through decomposition, which will reveal every torque that has been collectively represented by this matrix. The method of decomposition is taken from [93].

The change of the system's energy can be found through the manipulation of the integral transformation seen in eq. (3.13) using

$$\frac{\mathrm{d}}{\mathrm{dt}}\mathscr{E}\{\mathbf{y}\} = \frac{\mathrm{d}}{\mathrm{dt}}\int \dot{\mathbf{q}}^{\mathbf{T}}\mathbf{y}\mathrm{dt} = \dot{\mathbf{q}}^{\mathbf{T}}\mathbf{y} \tag{3.23}$$

$$= \frac{\mathrm{d}}{\mathrm{dt}}\left(\frac{1}{2}\dot{\mathbf{q}}^{\mathrm{T}}\mathbf{M}(\mathbf{q})\dot{\mathbf{q}} + \int \mathbf{K}(\mathbf{q})\mathrm{d}\mathbf{q}\right) \tag{3.24}$$

which was derived from the fundamental theorem of calculus [93]. The change of the system's energy can, therefore, be represented using the prototypical form. The change in system energy can also be calculated by taking the direct time-differential of the total kinetic and potential energy of the system (as seen in eq. (3.24)). The energy in the system is not expected to change, however, unless an external nonconservative torque acts upon it. These torques can manifest in different forms, but are mostly introduced through *lossy friction*, *actuation* and *change of physical*

system properties, which is represented mathematically by

$$\frac{\mathrm{d}}{\mathrm{dt}}E_s = -\dot{\mathbf{q}}^{\mathbf{T}}\mathbf{R}(\mathbf{q},\dot{\mathbf{q}}) + \dot{\mathbf{q}}^{\mathbf{T}}\mathbf{G}(\mathbf{q})\mathbf{u} - \dot{\mathbf{q}}^{\mathbf{T}}\mathbf{J}(\mathbf{q},\dot{\mathbf{q}})\dot{\mathbf{q}} \tag{3.25}$$

where

$\mathbf{R}(\mathbf{q},\dot{\mathbf{q}}) =$ the lossy torques introduced by damping, air friction or stiction, and
$\mathbf{J}(\mathbf{q},\dot{\mathbf{q}})\dot{\mathbf{q}} =$ the energy shuffling matrix which represents a set of conservative torques that allow energy to be shuffled in the system [93].

The $\mathbf{J}(\mathbf{q},\dot{\mathbf{q}})$ matrix is skew-symmetrical, and will thus not produce a change in energy ($\dot{\mathbf{q}}^{\mathbf{T}}\mathbf{J}(\mathbf{q},\dot{\mathbf{q}})\dot{\mathbf{q}} = 0$). Instead, these torques accommodate energy transformation within the system and is, therefore, included in the formulation.

Eq. (3.25) is equivalent to the change of energy seen as the time derivative of the mechanical energy. Therefore,

$$\begin{aligned}\frac{\mathrm{d}}{\mathrm{dt}}\mathscr{E}\{\mathbf{y}\} &= \frac{\mathrm{d}}{\mathrm{dt}}\left(\frac{1}{2}\dot{\mathbf{q}}^{\mathbf{T}}\mathbf{M}(\mathbf{q})\dot{\mathbf{q}} + \int \mathbf{K}(\mathbf{q})\mathbf{dq}\right)\\ &= \dot{\mathbf{q}}^{\mathbf{T}}\mathbf{M}(\mathbf{q})\ddot{\mathbf{q}} + \frac{1}{2}\dot{\mathbf{q}}^{\mathbf{T}}\dot{\mathbf{M}}(\mathbf{q},\dot{\mathbf{q}})\dot{\mathbf{q}} + \dot{\mathbf{q}}^{\mathbf{T}}\mathbf{K}(\mathbf{q}).\end{aligned} \tag{3.26}$$

Making $\mathbf{M}(\mathbf{q})\ddot{\mathbf{q}}$ the subject of the prototypical form and substituting the expression into eq. (3.26) results in

$$\begin{aligned}\frac{\mathrm{d}}{\mathrm{dt}}\mathscr{E}\{\mathbf{y}\} &= \dot{\mathbf{q}}^{\mathbf{T}}\left(-\mathbf{D}(\mathbf{q},\dot{\mathbf{q}}) - \mathbf{K}(\mathbf{q}) + \mathbf{G}(\mathbf{q})\mathbf{u}\right) + \frac{1}{2}\dot{\mathbf{q}}^{\mathbf{T}}\dot{\mathbf{M}}(\mathbf{q},\dot{\mathbf{q}})\dot{\mathbf{q}} + \dot{\mathbf{q}}^{\mathbf{T}}\mathbf{K}(\mathbf{q})\\ &= -\dot{\mathbf{q}}^{\mathbf{T}}\mathbf{D}(\mathbf{q},\dot{\mathbf{q}}) + \dot{\mathbf{q}}^{\mathbf{T}}\mathbf{G}(\mathbf{q})\mathbf{u} + \frac{1}{2}\dot{\mathbf{q}}^{\mathbf{T}}\dot{\mathbf{M}}(\mathbf{q},\dot{\mathbf{q}})\dot{\mathbf{q}}.\end{aligned} \tag{3.27}$$

This expression is equal to eq. (3.25). Therefore,

$$-\dot{\mathbf{q}}^{\mathbf{T}}\mathbf{R}(\mathbf{q},\dot{\mathbf{q}}) + \dot{\mathbf{q}}^{\mathbf{T}}\mathbf{G}(\mathbf{q})\mathbf{u} - \dot{\mathbf{q}}^{\mathbf{T}}\mathbf{J}(\mathbf{q},\dot{\mathbf{q}})\dot{\mathbf{q}} = -\dot{\mathbf{q}}^{\mathbf{T}}\mathbf{D}(\mathbf{q},\dot{\mathbf{q}}) + \dot{\mathbf{q}}^{\mathbf{T}}\mathbf{G}(\mathbf{q})\mathbf{u} + \frac{1}{2}\dot{\mathbf{q}}^{\mathbf{T}}\dot{\mathbf{M}}(\mathbf{q},\dot{\mathbf{q}})\dot{\mathbf{q}}$$

which simplifies to

$$\mathbf{D}(\mathbf{q},\dot{\mathbf{q}}) = \mathbf{R}(\mathbf{q},\dot{\mathbf{q}}) + \mathbf{J}(\mathbf{q},\dot{\mathbf{q}})\dot{\mathbf{q}} + \frac{1}{2}\dot{\mathbf{M}}(\mathbf{q},\dot{\mathbf{q}})\dot{\mathbf{q}}. \tag{3.28}$$

This expression can be expanded to include the definition of the conservative and nonconservative changes in the moments of inertia in the system described in eq. (3.21), whereby

$$\mathbf{D}(\mathbf{q},\dot{\mathbf{q}}) = \underbrace{\mathbf{R}(\mathbf{q},\dot{\mathbf{q}}) + \frac{1}{2}\dot{\mathbf{M}}_{\mathbf{n}}(\mathbf{q},\dot{\mathbf{q}})\dot{\mathbf{q}}}_{\text{Nonconservative}} + \underbrace{\mathbf{J}(\mathbf{q},\dot{\mathbf{q}})\dot{\mathbf{q}} + \frac{1}{2}\dot{\mathbf{M}}_{\mathbf{c}}(\mathbf{q},\dot{\mathbf{q}})\dot{\mathbf{q}}}_{\text{Conservative}}. \tag{3.29}$$

The conservative torques in the $\mathbf{D}(\mathbf{q}, \dot{\mathbf{q}})$ matrix are labelled collectively as the $\mathbf{C}(\mathbf{q},\dot{\mathbf{q}})$ matrix for convenience. In addition to this change, the decomposed $\mathbf{D}(\mathbf{q},\dot{\mathbf{q}})$ matrix differs slightly from the one described by Naude as the $\mathbf{R}(\mathbf{q}, \dot{\mathbf{q}})$ matrix in [93] was chosen to only include viscous damping as a lossy friction. In this form, other forms of damping may be considered and encompassed within the $\mathbf{R}(\mathbf{q}, \dot{\mathbf{q}})$ matrix.

All of the matrices, except for the $\mathbf{J}(\mathbf{q}, \dot{\mathbf{q}})\dot{\mathbf{q}}$ vector, may be solved for trivially given that the mass matrix $\dot{\mathbf{M}}_{\mathbf{n}}(\mathbf{q}, \dot{\mathbf{q}})$ may be explicitly defined as required. It is important to note, however, that the $\mathbf{J}(\mathbf{q}, \dot{\mathbf{q}})\dot{\mathbf{q}}$ vector is not observable in the energy domain, thus making it difficult to identify explicit elements in the $\mathbf{J}(\mathbf{q}, \dot{\mathbf{q}})$ matrix. It seems intuitive that the conservative torques produced by the natural energy shuffling in the system must somehow be attributed to the moments of inertia in the system, as seen with the conservative torques produced by gravitational forces. This is proven through the evaluation of the Euler-Lagrange equation in matrix form. The following derivation is an addition to the method developed by Naude in [93] and is included specifically to demonstrate the generalised method of characterising the $\mathbf{J}(\mathbf{q}, \dot{\mathbf{q}})$ matrix.

The Lagrangian may be defined as

$$\begin{aligned}\mathbf{L}(\mathbf{q}, \dot{\mathbf{q}}, t) &= \mathbf{T} - \mathbf{P} \\ &= \frac{1}{2}\dot{\mathbf{q}}^{\mathrm{T}}\mathbf{M}_{\mathbf{c}}(\mathbf{q}, \dot{\mathbf{q}}) - \int \mathbf{K}(\mathbf{q})^{\mathrm{T}}\mathrm{d}\mathbf{q}.\end{aligned}$$

Substituting this expression of the Lagrangian into eq. (3.8) and simplifying the resultant expression results in

$$\begin{aligned}&\frac{\mathrm{d}}{\mathrm{dt}}\left[\frac{\partial}{\partial\dot{\mathbf{q}}}\left(\frac{1}{2}\dot{\mathbf{q}}^{\mathbf{T}}\mathbf{M}_{\mathbf{c}}(\mathbf{q})\dot{\mathbf{q}} - \int \mathbf{K}(\mathbf{q})^{\mathbf{T}}\mathrm{d}\mathbf{q}\right)\right]^{\mathbf{T}} - \left[\frac{\partial}{\partial\mathbf{q}}\left(\frac{1}{2}\dot{\mathbf{q}}^{\mathbf{T}}\mathbf{M}_{\mathbf{c}}(\mathbf{q})\dot{\mathbf{q}} - \int \mathbf{K}(\mathbf{q})^{\mathbf{T}}\mathrm{d}\mathbf{q}\right)\right]^{\mathbf{T}} \\ &= 0 \\ &= \frac{\mathrm{d}}{\mathrm{dt}}\left[\mathbf{M}_{\mathbf{c}}(\mathbf{q})\dot{\mathbf{q}} - \left(\frac{\partial}{\partial\dot{\mathbf{q}}}\int \mathbf{K}(\mathbf{q})^{\mathrm{T}}\mathrm{d}\mathbf{q}\right)^{\mathbf{T}}\right] - \left[\frac{\partial}{\partial\mathbf{q}}\left(\frac{1}{2}\dot{\mathbf{q}}^{\mathbf{T}}\mathbf{M}_{\mathbf{c}}(\mathbf{q})\dot{\mathbf{q}}\right)\right]^{\mathbf{T}} + \\ &\quad\left(\frac{\partial}{\partial\mathbf{q}}\int \mathbf{K}(\mathbf{q})^{\mathbf{T}}\mathrm{d}\mathbf{q}\right)^{\mathbf{T}} \\ &= \dot{\mathbf{M}}_{\mathbf{c}}(\mathbf{q}, \dot{\mathbf{q}})\dot{\mathbf{q}} + \mathbf{M}_{\mathbf{c}}(\mathbf{q})\ddot{\mathbf{q}} - \underbrace{\frac{\mathrm{d}}{\mathrm{dt}}\left(\frac{\partial}{\partial\dot{\mathbf{q}}}\int \mathbf{K}(\mathbf{q})^{\mathbf{T}}\mathrm{d}\mathbf{q}\right)^{\mathbf{T}}}_{=0} - \left[\frac{\partial}{\partial\mathbf{q}}\left(\frac{1}{2}\dot{\mathbf{q}}^{\mathbf{T}}\mathbf{M}_{\mathbf{c}}(\mathbf{q})\dot{\mathbf{q}}\right)\right]^{\mathbf{T}} + \\ &\quad\mathbf{K}(\mathbf{q}).\end{aligned}$$

The term $\frac{\mathrm{d}}{\mathrm{dt}}\left(\frac{\partial}{\partial \dot{\mathbf{q}}}\int \mathbf{K}(\mathbf{q})^{\mathbf{T}}\mathrm{d}\mathbf{q}\right)^{\mathbf{T}}$ is equal to zero as $\mathbf{K}(\mathbf{q})$ is not dependent on any velocity vector $\dot{\mathbf{q}}$. Therefore,

$$\mathbf{M_c}(\mathbf{q})\ddot{\mathbf{q}} + \underbrace{\dot{\mathbf{M}}_\mathbf{c}(\mathbf{q},\dot{\mathbf{q}})\dot{\mathbf{q}} - \left[\frac{\partial}{\partial \mathbf{q}}\left(\frac{1}{2}\dot{\mathbf{q}}^{\mathbf{T}}\mathbf{M_c}(\mathbf{q})\dot{\mathbf{q}}\right)\right]^{\mathbf{T}}}_{\mathbf{C}(\mathbf{q},\dot{\mathbf{q}})} + \mathbf{K}(\mathbf{q}) = 0.$$

In its current structure, the expression seen above is clearly in the prototypical form. It is evident, therefore, that if the lossy matrix $\mathbf{R}(\mathbf{q},\dot{\mathbf{q}}) = 0$, then $\mathbf{C}(\mathbf{q},\dot{\mathbf{q}})$ can be expressed as

$$\mathbf{C}(\mathbf{q},\dot{\mathbf{q}}) = \dot{\mathbf{M}}_\mathbf{c}(\mathbf{q},\dot{\mathbf{q}})\dot{\mathbf{q}} - \left[\frac{\partial}{\partial \mathbf{q}}\left(\frac{1}{2}\dot{\mathbf{q}}^{\mathbf{T}}\mathbf{M_c}(\mathbf{q})\dot{\mathbf{q}}\right)\right]^{\mathbf{T}} \tag{3.30}$$

[38]. Equating eqs. (3.30) and (3.29) allows for the representation of the $\mathbf{J}(\mathbf{q},\dot{\mathbf{q}})\dot{\mathbf{q}}$ vector in terms of the mass matrix $\mathbf{M_c}(\mathbf{q})$, where

$$\begin{aligned}\mathbf{J}(\mathbf{q},\dot{\mathbf{q}})\dot{\mathbf{q}} + \frac{1}{2}\dot{\mathbf{M}}_\mathbf{c}(\mathbf{q},\dot{\mathbf{q}})\dot{\mathbf{q}} &= \dot{\mathbf{M}}_\mathbf{c}(\mathbf{q},\dot{\mathbf{q}})\dot{\mathbf{q}} - \left[\frac{\partial}{\partial \mathbf{q}}\left(\frac{1}{2}\dot{\mathbf{q}}^{\mathbf{T}}\mathbf{M_c}(\mathbf{q})\dot{\mathbf{q}}\right)\right]^{\mathbf{T}} \\ \therefore\ \mathbf{J}(\mathbf{q},\dot{\mathbf{q}})\dot{\mathbf{q}} &= \frac{1}{2}\dot{\mathbf{M}}_\mathbf{c}(\mathbf{q},\dot{\mathbf{q}})\dot{\mathbf{q}} - \left[\frac{\partial}{\partial \mathbf{q}}\left(\frac{1}{2}\dot{\mathbf{q}}^{\mathbf{T}}\mathbf{M_c}(\mathbf{q})\dot{\mathbf{q}}\right)\right]^{\mathbf{T}}.\end{aligned} \tag{3.31}$$

The $\dot{\mathbf{q}}$ matrix is not invertible, but the individual entries may be represented with the knowledge that the $\mathbf{J}(\mathbf{q},\dot{\mathbf{q}})$ matrix is skew-symmetric (with the total number of individual elements in each $\mathbf{J}(\mathbf{q},\dot{\mathbf{q}})$ matrix $= {}^{n(n-1)}/_{2}$ for a nth order system). Therefore,

$$\mathbf{J}(\mathbf{q},\dot{\mathbf{q}}) = \begin{bmatrix} 0 & J_1(\mathbf{q},\dot{\mathbf{q}}) & J_2(\mathbf{q},\dot{\mathbf{q}}) & \cdots & J_{n-1}(\mathbf{q},\dot{\mathbf{q}}) \\ -J_1(\mathbf{q},\dot{\mathbf{q}}) & 0 & J_n(\mathbf{q},\dot{\mathbf{q}}) & \cdots & J_{2(n-1)-1}(\mathbf{q},\dot{\mathbf{q}}) \\ -J_2(\mathbf{q},\dot{\mathbf{q}}) & -J_n(\mathbf{q},\dot{\mathbf{q}}) & \ddots & \ddots & \vdots \\ \vdots & \vdots & \ddots & \ddots & \vdots \\ -J_{n-1}(\mathbf{q},\dot{\mathbf{q}}) & -J_{2(n-1)-1}(\mathbf{q},\dot{\mathbf{q}}) & \cdots & \cdots & 0 \end{bmatrix}. \tag{3.32}$$

It may be tedious to calculate each entry, but it is not required if one just wishes to characterise the behaviour of the system in terms of torques. Finding the $\mathbf{J}(\mathbf{q},\dot{\mathbf{q}})\dot{\mathbf{q}}$ vector in this case would be sufficient.

3.3.4 Modelling Methodology

The method highlighted below presents an independent system modelling alternative to the classical Lagrangian method as first presented in [93]. This method is modified here to include the explicit modelling of the energy that is shuffled within

the system (represented by the $\mathbf{J}(\mathbf{x}, \mathbf{v})\mathbf{v}$ vector). The procedure is outlined similarly to what is seen in [93]:

(1) Identify the relevant generalised coordinates of the system.

(2) Define E_s, the mechanical energy of the system by determining the kinetic and potential energies in terms of the generalised coordinates, and derive the mass matrix $\mathbf{M}(\mathbf{x})$ and the potential torque matrix $\mathbf{K}(\mathbf{x})$ from these energy expressions.

(3) Calculate the system's net change in energy by taking $\frac{\mathrm{d}}{\mathrm{dt}} E_s$.

(4) Describe the factors that add and dissipate energy, namely the power-loss component $-\mathbf{v}^{\mathrm{T}}\mathbf{R}(\mathbf{x}, \mathbf{v})$ and the actuation matrix $\mathbf{v}^{\mathrm{T}}\mathbf{G}(\mathbf{x})\mathbf{u}$. Equate these factors to the change in energy described by $\frac{\mathrm{d}}{\mathrm{dt}} E_s$. This is known as the *system power equation*.

(5) Calculate the entries of the energy-shuffling component $\mathbf{J}(\mathbf{x}, \mathbf{v})\mathbf{v}$ using eq. (3.31) that was derived in the last section.

(6) Substitute in all the relevant components into the *system power equation* and manipulate it into the generalised prototypical form, where the equations of motion may be solved for.

(7) Transform the equations of motion into the state-space representation using a relevant set of transformations.

This energy method is used for the modelling obligations of this investigation since the Lagrangian method is covered significantly in literature. The general modelling of the n-link pendulum system is demonstrated in section 7.3.1, but a more conceptual example of the application of the modelling methodology shown above can be seen in section 7.4, whereby the Acrobot is modelled for experimental purposes.

3.4 Conclusion

The foundations of two robust modelling techniques, namely the Classical Lagrangian and the Energy modelling methods, were discussed in this chapter. Each technique was implemented on a model of the DIP (energy modelling example shown in later chapter) with the objective of developing equations of motion that describe the movements of each pendulum. The classical Lagrangian modelling method involves the implementation of the Euler-Lagrange equation to derive the equations of motion of a system, whereby calculus of variations is used to exploit the *principle of least action*. Whilst the method is effective and easy to implement, the procedural nature of this technique makes it difficult to identify underlying causes to the torques represented in the prototypical form. The *energy method* involves the

classification of the torques in the system according to the effect that each torque has on the energy of the system. The structure of each component in the prototypical form is scrutinised to determine its influence on the system's energy. This leads to the decomposition of the unclassified $\mathbf{D}(\mathbf{q}, \dot{\mathbf{q}})$ matrix into conservative and non-conservative torques. The equations of motion are then determined through the evaluation of the power equation, which is found by evaluating the energy that is added or dissipated from the system due to friction and actuation. The technique highlighted by Naude has one major constraint when applied to compounded pendulum systems; the torques responsible for energy-shuffling within the system (represented by $\mathbf{J}(\mathbf{q}, \dot{\mathbf{q}})\dot{\mathbf{q}}$) are unobservable in the energy domain (the torques contribute no energy to the system, and are also not responsible for any change of energy in the system). This chapter highlights a method of determining the entries of the internal shuffling vector $\mathbf{J}(\mathbf{q}, \dot{\mathbf{q}})\dot{\mathbf{q}}$ through the matrix evaluation of the Lagrangian. This is a modification to the method highlighted by Naude. Both methods allow for the satisfactory identification of the dynamics of a multi-body pendulum system. The energy method, however, has the added benefit of identifying the particular components of the dynamics and their effects on the total energy change in the system, and is therefore selected as the preferred modelling method in this investigation.

"Chaos is merely order waiting to be deciphered."
— José Saramago

Chapter 4

Stability Concepts

4.1 Chapter Overview

This chapter serves to introduce basic concepts of system stability that are relevant to this research project. A section in this chapter is dedicated to the formal definition of stability principles with regards to system equilibrium points, including the concepts of local and global stability, the varying forms of stability (marginal, exponential, asymptotic etc.) and the characteristics of an unstable system. Short discussions are included to provide fundamental knowledge about the implementation of pole-zero diagrams to graphically demonstrate the stability of a linear system, and the Routh-Hurwitz stability criterion, which is a technique that is integral to this research project. Whilst this chapter presents a superficial level of information on certain topics, sources are provided to the reader for the purpose of supplementation if required.

4.2 Equilibrium Points and Stability

The stability of a system describes how the system behaves around a specifically chosen operating point [2]. This operating point is usually represented by an equilibrium point, whereby the states of the system do not change for the remainder of the experiment. This is formally summarised as follows [2]:

Definition 4.1. A state $\mathbf{x}^*$ is an equilibrium point of the system if, once $\mathbf{x}(\mathbf{t}) = \mathbf{x}^*$, $\mathbf{x}(\mathbf{t})$ remains equal to $\mathbf{x}^*$ as $t \to \infty$.

The number of equilibrium points found on an n-link pendulum system is equal to 2^n, as demonstrated for the case of the DIP in figure 4.1. It is evident, however, that reaching certain equilibrium points produces particular configurations that cannot sustain the equilibrium once the system is disturbed, therefore indicating that different operating points can demonstrate different stability characteristics, even within one particular system. These concepts of stability are discussed in [2], but are summarised below.

The local stability around an operating point is subject to the region of operation

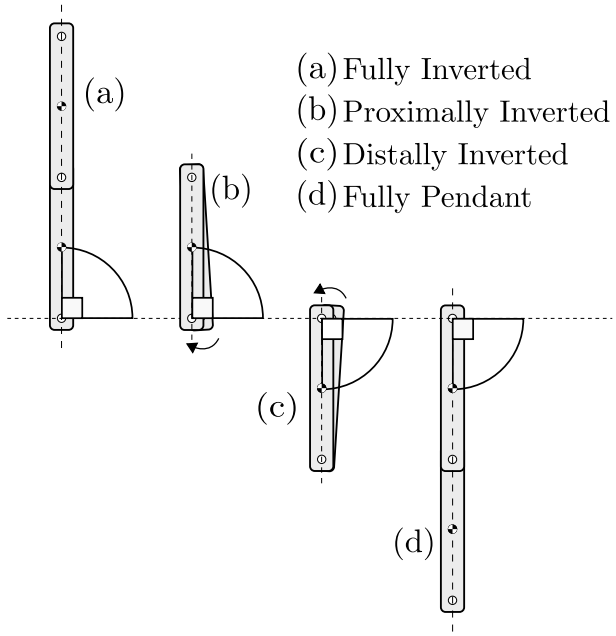

FIGURE 4.1: The equilibrium points of the unactuated DIP.

in question, which is defined arbitrarily. If the possible states are defined on a real state-space $\mathbb{R}^n$, a ball (an operational region defined as $\mathbf{B_R}$) is constructed to enclose the states located arbitrarily near to the operating point $\mathbf{x}^*$ (i.e. $\mathbf{B_R}$ is found within the range $||\mathbf{x} - \mathbf{x}^*|| < \mathbf{R}$, where $\mathbf{R}$ represents the radius of $\mathbf{B_R}$). The ball represents an open set of real numbers and therefore does not include the states found at the boundary (a closed set is referred to as a sphere ($\mathbf{S}_R$)). The concepts of stability and instability may now be defined with the use of this arbitrarily placed ball.

Let us construct a scenario where an operating point is located in the centre of an arbitrarily defined ball of operation $\mathbf{B_R}$, with the initial states of the experiment occurring within a smaller ball (i.e. $x(0) \in \mathbf{B_r}$) and is found on the 2D plane $\mathbb{R}^2$ in figure 4.2. Lyapunov stability in this scenario is defined as follows [2]:

Definition 4.2. The operating point $\mathbf{x}^*$ is said to be *Lyapunov stable* if the trajectory of $\mathbf{x(t)}$ stays within the operating region defined by the ball $\mathbf{B_R}$ whereby $||\mathbf{x(t)} - \mathbf{x}^*|| > \mathbf{R}$ for all time in the experiment $\mathbf{t} \geq \mathbf{0}$ if the initial states occurred arbitrarily close to operating point ($||\mathbf{x(0)} - \mathbf{x}^*|| < \mathbf{r}$). The operating point is *unstable* otherwise.

Lyapunov stability is defined for a ball $\mathbf{B_R}$ where

$$\forall\, \mathbf{R} > \mathbf{0},\ \exists\, \mathbf{r} > \mathbf{0},\ ||\mathbf{x(0)}|| < \mathbf{r}\ \Rightarrow \forall\, \mathbf{t} \geq \mathbf{0},\ ||\mathbf{x(t)}|| < \mathbf{R}$$

[2]. A common unstable response, known as *blowing up*, is seen in first-order

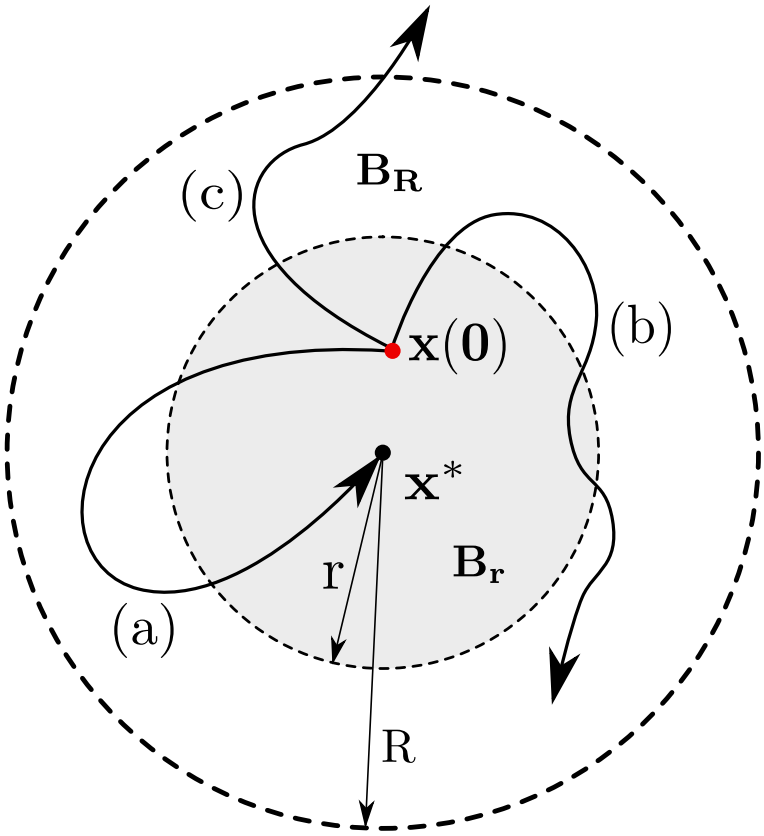

FIGURE 4.2: Concepts of Stability with (a) Asymptotic Stability (b) Marginal Stability (c) Instability. Adapted from [2].

systems of the form

$$\dot{\mathbf{L}}(\mathbf{t}) = \alpha \mathbf{L}(\mathbf{t}) \tag{4.1}$$

where $\mathbf{L}(\mathbf{t})$ represents a particular state, and $\alpha \in \mathbb{R}^+$ represents the rate of growth. Solving for this equation using the Laplace transform produces the time-domain response

$$\mathbf{L}(\mathbf{t}) = \mathbf{L}(\mathbf{0})\mathrm{e}^{\alpha \mathbf{t}}. \tag{4.2}$$

This behaviour of the function in figure 4.3 demonstrates the ideal uncontrollable growth of a population. It is clear that the population would never be able to fall within an approximate operational domain around an operating point for all time. This isn't, however, the only form of unstable behaviour demonstrated by nonlinear systems as the definition of instability is dependent on the size and placement of the ball $\mathbf{B_R}$ [2]. A perfect example is provided by the Van der Pol Oscillator, whose dynamics are described as

$$\begin{aligned}
\dot{\mathbf{x}}_1 &= \mathbf{x}_2, \\
\dot{\mathbf{x}}_2 &= -\mathbf{x}_1 + (1 + \mathbf{x}_1^2)\mathbf{x}_2
\end{aligned}$$

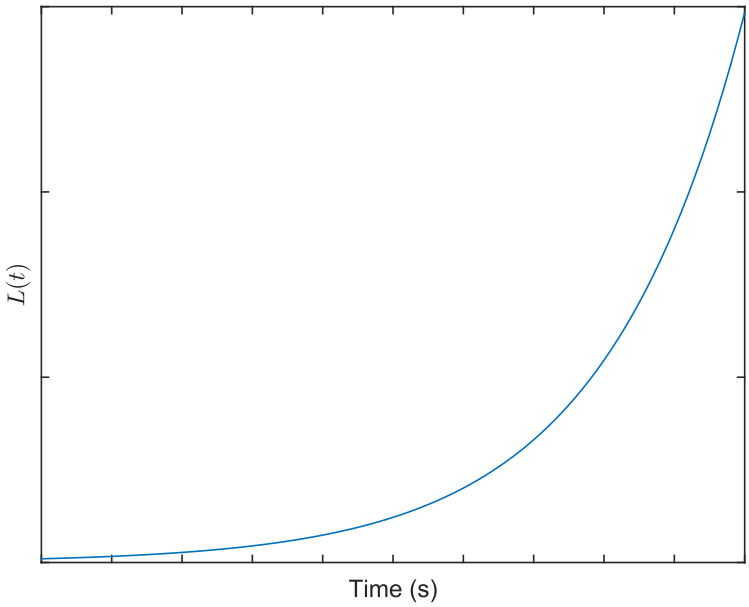

FIGURE 4.3: The blowing-up form of instability.

[2]. These dynamics tend towards a limit cycle that, if found outside the region of operation defined by $\mathbf{B_R}$, would lead to an unstable response, despite the fact that the response is bounded within the limit cycle as seen in figure 4.4. Similarly, the response would be seen as unstable even if the trajectory exits and then returns to the region of operation. This is known as *state convergence*. This phenomenon is understandably labelled as unstable since the behaviour of the trajectory outside of the region of operation may be different, as seen when an aircraft returns to subsonic operation after breaching the sound barrier [2].

The different forms of Lyapunov stability are defined by the behaviour of the trajectory within the explicit domain of operation. Operational points that are Lyapunov stable may be described as *marginally, asymptotically* or *exponentially stable* [2]. Marginally and asymptotically stable trajectories are defined as follows:

Definition 4.3. Marginally stable trajectories are Lyapunov stable, i.e. remain within the operational domain represented by the ball $\mathbf{B_R}$ for all time, but do not remain approximately near to the operational point (in the area defined by $\mathbf{B_r}$) for all time. In mathematical terms,

$$\forall \mathbf{R} > \mathbf{0}\ ,\ \exists\, \mathbf{r} > \mathbf{0}\ ,\ \mathbf{x(0)} \in \mathbf{B_r} \Rightarrow \begin{cases} \forall \mathbf{t} \geq \mathbf{0}\ ,\ \mathbf{x(t)} \in \mathbf{B_R} \\ \mathbf{t} \in \tau\ ,\ \mathbf{x(t)} \notin \mathbf{B_r} \\ \mathbf{t} \to \infty,\ \mathbf{x(t)} \nrightarrow \mathbf{x}^* \end{cases}$$

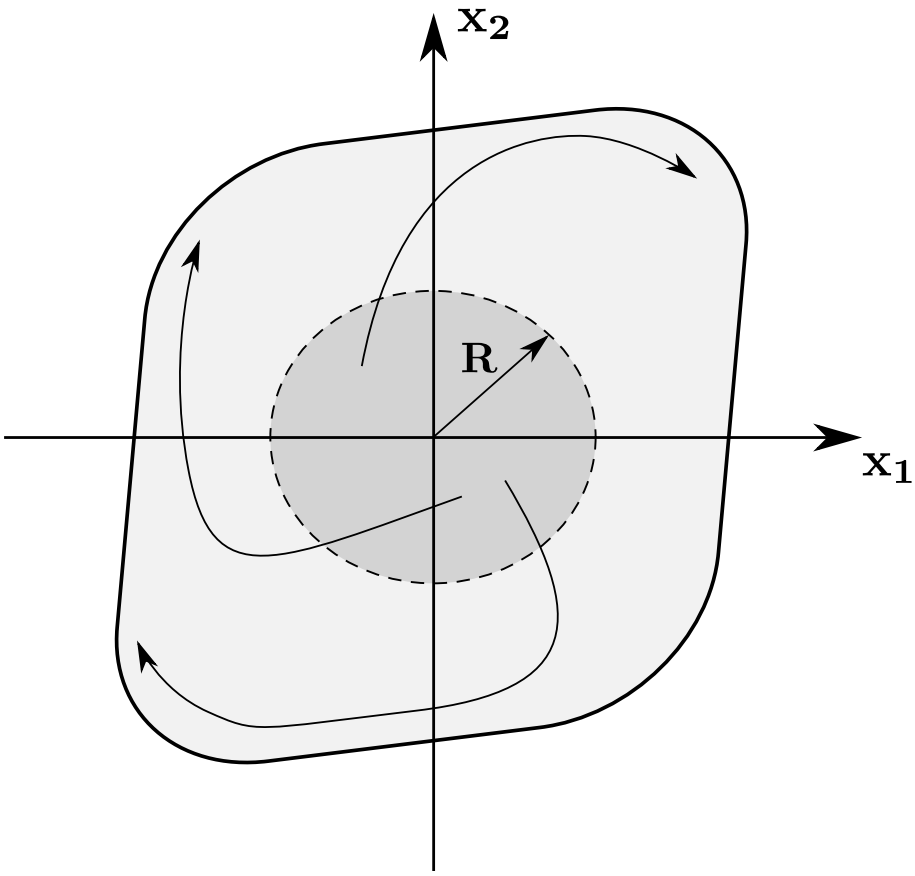

FIGURE 4.4: The phase portrait of the Van Der Pol Oscillator, with Trajectories originating in a ball with $\mathbf{R} = 1$ and tending toward the limit cycle. Adapted from [2].

where, in this case, $\tau \in \mathbb{R}$ is a set that contains the values of time when $\mathbf{x(t)}$ exits the ball $\mathbf{B_r}$.

Definition 4.4. Asymptotically stable trajectories are Lyapunov stable, remain within the ball $\mathbf{B_R}$ and will eventually converge on the operating point as time tends towards infinity, where

$$\forall \mathbf{R} > \mathbf{0}\ ,\ \exists\, \mathbf{r} > \mathbf{0}\ ,\ \mathbf{x(0)} \in \mathbf{B_r} => \begin{cases} \forall \mathbf{t} \geq \mathbf{0}\ ,\ \mathbf{x(t)} \in \mathbf{B_R} \\ \mathbf{t} \to \infty,\ \mathbf{x(t)} \to \mathbf{x}^* \end{cases}$$

[2].

Asymptotic stability infers that the trajectory will remain close to and converge onto the operating point, but gives no description of the amount of time it would take for the trajectory to converge. This estimation on the time it takes to approximately reach the desired state allows for the description of *exponential stability* [2]:

Definition 4.5. An operating point is *exponentially stable* if there exists two strictly positive numbers λ and α whereby

$$\forall \mathbf{t} > \mathbf{0}\ ,\ ||\mathbf{x}(\mathbf{t}) - \mathbf{x}^*|| \leq\ \alpha||\mathbf{x}(\mathbf{0}) - \mathbf{x}^*||\mathrm{e}^{-\lambda \mathbf{t}}$$

within close range of the operating point $\mathbf{x}^*$ (i.e. within the ball $\mathbf{B_r}$).

The trajectory will technically only reach the operating point if it is exponentially stable and the initial states are sufficiently close to the operating point. An approximate convergence can, however, be defined to describe the instance where the trajectory is sufficiently close to operating point. The construction of a control law that utilises exponential convergence can be chosen according to the desired time of convergence, knowing that $\lambda = 1/\tau$ [2].

The aforementioned concepts of stability depend upon a *local* analysis of the dynamics around the operating point. The stability of an operating point cannot be guaranteed if the initial condition of the system is not sufficiently close to the operating point. If a system hypothetically contains dynamics that allow the states to tend towards the desired operating point from any initial condition, the operating point is said to be *globally stable* [2]. More formally [2]:

Definition 4.6. An operating point is said to be *globally stable* if the operating point is asymptotically stable for any set of initial conditions, or

$$\mathbf{x}(\mathbf{0}) \in \mathbb{R}^{\mathbf{n}}\ =>\ \mathbf{x}(\mathbf{t}) \rightarrow \mathbf{x}^* \text{ as } \mathbf{t} \rightarrow \infty.$$

Linear Time-Invariant (LTI) systems are always globally stable when found to be asymptotically stable around an operating point. Additionally, unstable LTI systems demonstrate instability in the form of blowing-up, as seen in figure 4.3 [2]. Nonlinear systems are less predictable, but do demonstrate linear dynamics when evaluated in a domain that is sufficiently close to the operating point [2]. The approximate behaviour of a system found within this domain can be determined through the implementation of Lyapunov's linearisation method, which is discussed in section 5.2.1 [2].

4.3 Poles and Zeros

It may not always be convenient to determine the stability of a LTI system, or the linearised approximation around some equilibrium point of a nonlinear system, solely by evaluating the time-dependent response of each rate equation [95]. Luckily, the stability of such a system can be more easily determined through the evaluation of the system's *transfer function* [95]. This function represents the system's time-dependent response (where $0 \leq t < \infty$) in terms of a frequency response. This function is produced with the use of the *Laplace transformation* [95]. The fundamental principles behind the Laplace transform are not included in this dissertation, but the following source provides a robust background on the topic [96].

Consider the time-dependent representation of a LTI system described by

$$\dot{\mathbf{x}}(t) = \mathbf{A}\mathbf{x}(t) + \mathbf{B}\mathbf{u}(t), \tag{4.3}$$
$$\mathbf{y}(t) = \mathbf{C}\mathbf{x}(t) + \mathbf{D}\mathbf{u}(t). \tag{4.4}$$

The transfer function of this system can be found through the implementation of

$$H(s) = \mathbf{C}(sI - \mathbf{A})^{-1} + \mathbf{D} \tag{4.5}$$

where

$s = \sigma + j\omega$ (the complex Laplace variable), and
$I =$ The identity matrix.

The derivation of this equation can be found in [95]. The application of this equation results in

$$\begin{aligned} H(s) &= \frac{b_0 s^m + b_1 s^{m-1} + \cdots + b_{m-1}s + b_m}{a_0 s^n + a_1 s^{n-1} + \cdots + a_{n-1}s + a_n}, \\ &= \frac{\mathbf{Z}(s)}{\mathbf{P}(s)} \end{aligned} \tag{4.6}$$

[3]. Each expression in both the numerator and the denominator may be factorised into components that represent each intercept of the respective polynomial, where

$$H(s) = K\frac{(s - z_1)(s - z_2)\ldots(s - z_{m-1})(s - z_m)}{(s - p_1)(s - p_2)\ldots(s - p_{n-1})(s - p_n)}. \tag{4.7}$$

These factorised constituents are known as *zeros* (numerator) and *poles* (denominator) [3] and are a direct consequence of the system's characteristics. The polynomial in the denominator of the expression is also known as the *characteristic equation* [3]. The positions of these intercepts may be graphically demonstrated on the complex s-plane known as a *pole-zero plot*, an example of which is shown in figure 4.5. The position of the poles are of greatest concern, as they are responsible for the system stability [3]. If the poles are found to have an imaginary component, the response will have some oscillatory behaviour [3]. Conversely, if the pole contains a real component the response will contain some exponential behaviour, whereby the response will be an exponentially decaying function if found on the left-hand side of the pole-zero plot, and an exponentially increasing function if the pole is found on the right-hand side of the pole-zero plot [3]. Therefore, the response of a LTI system, or the linearised approximation of a nonlinear system around some equilibrium point, will be unstable if a pole is found on the right-hand side of the pole-zero plot. A marginally stable response is demonstrated by a system if the poles of its characteristic equation are found precisely on the imaginary axis of the complex pole-zero plot. The system in this case produces an indefinite oscillation when

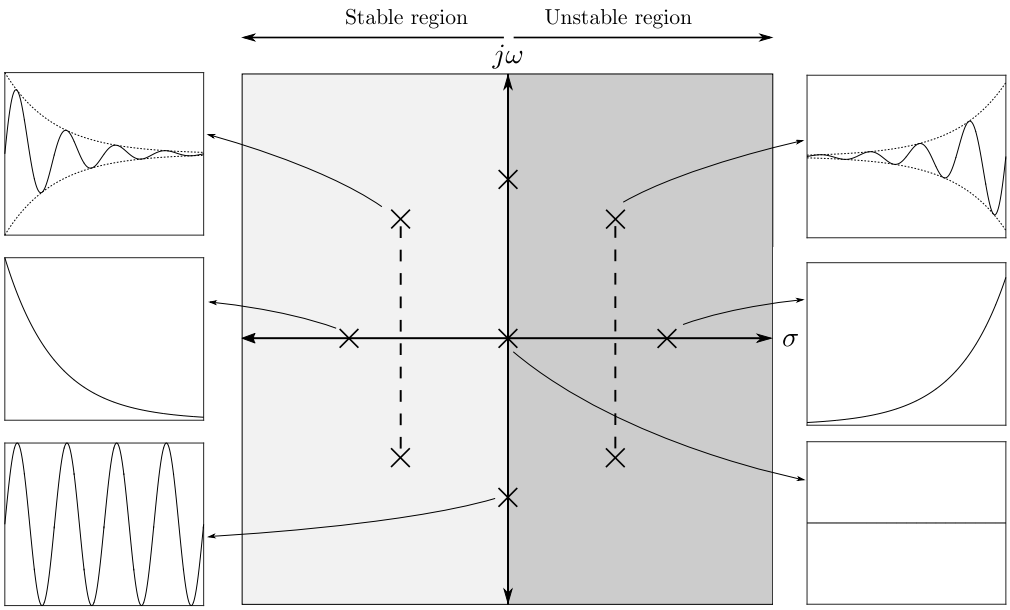

FIGURE 4.5: Generalised Pole-Zero plot. Adapted from [3].

stimulated with an impulse [3]. More information on the fundamental principles of pole-zero plots and transfer functions can be found in [3].

4.4 The Routh-Hurwitz Stability Criterion

It is difficult, in cases where the characteristic equation has a high order, to identify whether a polynomial expression is composed solely of stable roots. It is in these scenarios that it would be more convenient to apply the *Routh-Hurwitz stability criterion* to determine the stability of the system.

The Routh-Hurwitz criterion is a set of necessary and sufficient conditions that must be satisfied for the roots of a particular polynomial to be found in the left-hand side of the pole-zero complex plane [97]. A simple algorithm involving what is known as the *Routh array* can be followed to test the criterion against the characteristics of the polynomial. The algorithm is demonstrated in [98] but is included here as this technique is integral to the core investigations in this research project:

(1) Extract the characteristic equation from the transfer function described as

$$a_0 s^n + a_1 s^{n-1} + \cdots + a_{n-1} s + a_n = 0. \tag{4.8}$$

(2) Construct the following Routh-Array by organising the coefficients of the characteristic polynomial in the order

s^n	a_0	a_2	a_4	a_6	$\dots$
s^{n-1}	a_1	a_3	a_5	a_7	$\dots$
s^{n-2}	b_1	b_2	b_3	b_4	$\dots$
s^{n-3}	c_1	c_2	c_3	c_4	$\dots$
s^{n-4}	d_1	d_2	d_3	d_4	$\dots$
$\vdots$	$\vdots$	$\vdots$	$\vdots$	$\vdots$	$\vdots$
s^2	e_1	e_2			
s^1	f_1				
s_0	g_0				

where the additional coefficients are defined as

$$
\begin{aligned}
b_i &= \frac{a_1 a_{2i} - a_0 a_{2i+1}}{a_1}, \\
c_i &= \frac{b_1 a_{2i+1} - a_1 b_{i+1}}{b_1}, \\
d_i &= \frac{c_1 b_{i+1} - b_1 c_{i+1}}{c_1}, \\
&\vdots \\
g_0 &= f_1.
\end{aligned}
$$

The number of conditions that need to be satisfied to insure that all the poles of the system are found on the left-hand side of the complex plane is equal to $n+1$, where n represents the order of the system. The criterion is stated as follows:

Criterion 4.1. ***(The Routh-Hurwitz Stability Criterion)*** All of the poles of a characteristic equation are found in the left-hand plane of the pole-zero plot if all of the coefficients found on the far-left column of the Routh array seen in step (2) of the Routh array algorithm (termed the *Critical Routh Coefficients*) are found to be identical in sign. If this is not satisfied, then a pole is found in the right-hand plane of the pole-zero plot for every sign change that occurs between consecutive coefficients in the far-left column of the Routh array.

As an example, the system, whose coefficients are contained within the Routh array seen in (2) of the definition of the Routh-Hurwitz algorithm, will have all of its poles found in the left-hand plane of the pole-zero plot if and only if

$$
\begin{aligned}
a_0 &> 0, \\
a_1 &> 0, \\
b_1 &= \frac{a_1 a_2 - a_0 a_3}{a_1} > 0, \\
c_1 &= \frac{b_1 a_3 - a_1 b_2}{b_1} > 0, \\
d_1 &= \frac{c_1 b_2 - b_1 c_2}{c_1} > 0,
\end{aligned}
$$

$$\vdots$$
$$e_1 > 0,$$
$$f_1 = g_0 > 0.$$

If, for instance, $e_1 < 0$ and $f_1 = g_1 < 0$, then there is one pole in the right-hand plane, since there was one sign change between coefficients. Conversely, if $e_1 < 0$ but $f_1 = g_1 > 0$, then there are two poles in the right-hand plane of the pole-zero plot, because the signs of the coefficients changed twice during the procedure. Numerous examples of this procedure can be seen in [98].

The proof of Criterion 4.1 is not included in this dissertation, but the reader is encouraged to read [99] to supplement this work if necessary.

4.5 Conclusion

This chapter was included in this dissertation to provide the reader with a basic background on stability concepts involving system equilibrium points, pole-zero plots, and the Routh-Hurwitz stability criterion. It is difficult to estimate the stability of a nonlinear system on a global domain. If one were to restrict the domain to be localised around a particular equilibrium point, however, important information about the stability and behaviour of the equilibrium point in question may be revealed with the use of linear stability analysis techniques such as the Routh-Hurwitz stability criterion and the pole-zero plot. This concept of local stability analysis was used in this research project to generate the aforementioned key contributions.

"If you can't control your peanut butter, you can't expect to control your life."

— Bill Watterson

Chapter 5

Introduction to Control Methods

5.1 Chapter Overview

This chapter is dedicated to discussing the control techniques and concepts that are pertinent to this investigation. This discussion is aimed at introducing the reader to these control methods before they are implemented for experimental purposes in later chapters. The first section outlines Lyapunov's theory of stability, which include both his linearisation method and his direct method, whilst the second section includes a discussion on the technique of feedback linearisation (FBL). Both sections include examples that serve to assist the reader in developing a further intuition into these control methods.

5.2 Lyapunov Theory and Control

This section gives a brief outline of the application of Lyapunov's theories on stability to the control environment. The theory is covered extensively in [2, pp. 40-99]. The natural dynamics of the n-link pendulum produces a set of nonlinear, time-invariant equations of motion (whereby the rates are explicitly described only by the system states). The control theory will, therefore, only focus on applications to systems containing these properties. Time-varying systems require the inclusion of the value of the initial time of the experiment in the formulation of the stability concepts, as described in [2, pp. 100-156].

5.2.1 Lyapunov's Linearisation Method

The determination of the stability for a nonlinear system described with dynamics $\dot{\mathbf{x}}$ about an equilibrium point $\mathbf{0}$ is described in [2, pp. 53-57]. This method is adapted here to tackle the problem of determining the stability of a system around any generalised operating point $\mathbf{x}^*$, as equilibrium points may occur at states located outside of the origin (as seen with the SIP). The system in this case is generalised as an unactuated autonomous system, with dynamics

$$\dot{\mathbf{x}} = \mathbf{f}(\tilde{\mathbf{x}}) \tag{5.1}$$

where $\mathbf{f}(\mathbf{x})$ is continuously differentiable, $\tilde{\mathbf{x}} = \mathbf{x} - \mathbf{x}^*$, and $\dot{\tilde{\mathbf{x}}} = \dot{\mathbf{x}}$. The dynamics can be expanded in the form of a Taylor expansion [2], whereby

$$\mathbf{f}(\tilde{\mathbf{x}}) = \mathbf{f}(\tilde{\mathbf{x}})\Big|_{\mathbf{x}=\mathbf{x}^*} + \left(\frac{\partial \mathbf{f}}{\partial \tilde{\mathbf{x}}}\right)\Big|_{\mathbf{x}=\mathbf{x}^*} \tilde{\mathbf{x}} + \mathcal{O}_{h.o.t}(\tilde{\mathbf{x}}).$$

The dynamics at the operating point $\mathbf{f}(\tilde{\mathbf{x}})|_{\mathbf{x}=\mathbf{x}^*}$ are equal to zero if the operating point is an equilibrium point. Furthermore, the terms that have orders that are larger than first-order are grouped together as the term $\mathcal{O}_{h.o.t}(\tilde{\mathbf{x}})$. A linear approximation leads to the exclusion of the higher order terms, with

$$\dot{\mathbf{x}} \approx \left(\frac{\partial \mathbf{f}}{\partial \tilde{\mathbf{x}}}\right)\Big|_{\mathbf{x}^*} \tilde{\mathbf{x}}.$$

The linearised unactuated system can therefore be described as

$$\dot{\mathbf{x}} = \mathbf{A}\tilde{\mathbf{x}}$$

with $\mathbf{A}$ representing the Jacobian matrix $\left(\frac{\partial \mathbf{f}}{\partial \tilde{\mathbf{x}}}\right)\Big|_{\mathbf{x}=\mathbf{0}}$. The stability of the system may now be determined by first performing a Laplace Transform on the system, assuming that the system begins at $t = 0$, where

$$\begin{aligned} \mathcal{L}\{\dot{\mathbf{x}}\} &= s\tilde{\mathbf{X}}(\mathbf{s}) - \tilde{\mathbf{x}}(\mathbf{0}) = \mathbf{A}\tilde{\mathbf{X}}(\mathbf{s}), \\ \therefore \quad \tilde{\mathbf{X}}(\mathbf{s})(sI - \mathbf{A}) &= \tilde{\mathbf{x}}(\mathbf{0}) \end{aligned}$$

where $\tilde{\mathbf{x}}(\mathbf{0}) = \mathbf{x}(\mathbf{0}) - \mathbf{x}^*$. Solving for the function $\mathbf{X}(\mathbf{s})$, we find that

$$\begin{aligned} \mathbf{X}(\mathbf{s}) &= (sI - \mathbf{A})^{-1}\tilde{\mathbf{x}}(\mathbf{0}), \\ &= \frac{1}{|sI - \mathbf{A}|}(sI - \mathbf{A})^{\mathrm{T}}\tilde{\mathbf{x}}(\mathbf{0}). \end{aligned}$$

It is apparent that the determinant $|sI - \mathbf{A}|$ represents the poles of the state response. The eigenvalues of the system matrix $\mathbf{A}$ will, therefore, describe the stability of the system around the equilibrium point $\mathbf{x}^*$ with initial condition $\tilde{\mathbf{x}}(\mathbf{0})$, which is sufficiently close to $\mathbf{x}^*$. The following conclusions can be made of the stability around the operating point [2]:

(1) Asymptotic stability about $\mathbf{x}^*$ is guaranteed if all the eigenvalues are found in the left-hand complex plane (real-negative) [2].

(2) If any eigenvalue is found in the right-hand complex plane (real-positive) the system will have an unstable behaviour around the equilibrium point.

(3) No conclusion on the stability of the system can be made if all of the eigenvalues are found on the left hand plane with at least one eigenvalue found on the complex imaginary axis (real-zero). The higher-order terms that were

removed upon linearisation may have a significant role in the stability of the system about the operating point in this case.

These conclusions can also be applied for actuated systems upon the derivation of the system's linearised form. Such a system, located about an equilibrium point $\mathbf{x}^*$, is represented as

$$\dot{\mathbf{x}} = \mathbf{f}(\tilde{\mathbf{x}}) + \mathbf{g}(\tilde{\mathbf{x}})\mathbf{u}.$$

The Taylor expansion is used to introduce the linear form, whereby

$$\dot{\mathbf{x}} = \mathbf{f}(\tilde{\mathbf{x}})\Big|_{\substack{\mathbf{x}=\mathbf{x}^* \\ \mathbf{u}=\mathbf{0}}} + \left(\frac{\partial \mathbf{f}}{\partial \tilde{\mathbf{x}}}\right)\Bigg|_{\substack{\mathbf{x}=\mathbf{x}^* \\ \mathbf{u}=\mathbf{0}}} \tilde{\mathbf{x}} + \left(\frac{\partial \mathbf{g}}{\partial \mathbf{u}}\right)\Bigg|_{\substack{\mathbf{x}=\mathbf{x}^* \\ \mathbf{u}=\mathbf{0}}} \mathbf{u} + \mathcal{O}_{h.o.t}(\tilde{\mathbf{x}}).$$

Again, the dynamics at the equilibrium point are zero, and the higher-order terms are ignored to produce

$$\begin{aligned} \dot{\mathbf{x}} &\approx \left(\frac{\partial \mathbf{f}}{\partial \tilde{\mathbf{x}}}\right)\Bigg|_{\substack{\mathbf{x}=\mathbf{x}^* \\ \mathbf{u}=\mathbf{0}}} \tilde{\mathbf{x}} + \left(\frac{\partial \mathbf{g}}{\partial \mathbf{u}}\right)\Bigg|_{\substack{\mathbf{x}=\mathbf{x}^* \\ \mathbf{u}=\mathbf{0}}} \mathbf{u} \\ &= \mathbf{A}\tilde{\mathbf{x}} + \mathbf{B}\mathbf{u} \end{aligned} \tag{5.2}$$

which is in a first-order linearised format. The input is most commonly defined in terms of the states, producing an autonomous set of equations of motion. The input can, in this case, be described in terms of the states, where

$$\mathbf{u} = \left(\frac{\partial \mathbf{u}}{\partial \tilde{\mathbf{x}}}\right)\Bigg|_{\mathbf{x}=\mathbf{x}^*} \tilde{\mathbf{x}} = \mathbf{G}\tilde{\mathbf{x}}. \tag{5.3}$$

Therefore, substituting eq. (5.3) into eq. (5.2), we find that

$$\dot{\mathbf{x}} = (\mathbf{A} + \mathbf{B}\mathbf{G})\tilde{\mathbf{x}}. \tag{5.4}$$

The stability of the system around the equilibrium point can, once again, be found by following the procedure outlined above using the Laplace transform. The result of this procedure demonstrates that the eigenvalues of the matrix $(\mathbf{A} + \mathbf{B}\mathbf{G})$ must be determined to evaluate the stability of an actuated, autonomous, nonlinear system about a particular operating point [2]. This highlights an important, yet apparent, point about actuation and stability, which is exploited in the control of intrinsically unstable systems; **actuation can be used to influence the system's stability**.

Lyapunov's linearisation method provides important information about the stability of a system in small domains. It is difficult, however, to identify the size of this region of operation without testing every potential point using a trial-and-error approach. Additionally, it is an impossible task to implement this procedure over an infinite number of points to determine a system's global stability. The method discussed in the next section tackles these shortcomings.

5.2.2 Lyapunov's Direct Method (LDM)

A major problem with Lyapunov's linearisation method is not knowing the size of the linear range around an equilibrium point, i.e. how far away from the equilibrium point can an initial condition be set without nullifying the linear approximations derived in section 5.2.1? This issue may be circumnavigated by determining the behaviour of a system across a larger domain of operation. This possibility is presented by LDM.

The Lyapunov Function

Let us consider an autonomous unactuated mechanical system that is continuously losing energy due to some damping or friction. The mechanical energy of a system is a positive definite function, with its time-related differential being negative definite (this will be true for any system so long as the energy dissipated from the system is greater than the energy introduced into the system). The mechanical energy will, therefore, tend towards zero as time tends towards infinity. The system is guaranteed to settle at an equilibrium point when the system's total mechanical energy is zero, regardless of whether the system is linear or non-linear [2]. Additionally, if the friction is removed from the unactuated system, the change of energy in the system will be zero, resulting in the oscillation of the states within a bounded region of the equilibrium point associated with a zero-mechanical energy state. This is an important observation; a locally Lyapunov stable system, whose properties were described earlier in this chapter, will always be associated with an arbitrary scalar function, known as the Lyapunov function $(V(\mathbf{x}))$, that is positive definite, always has a negative semi-definite slope, and has continuous partial derivatives [2]. In mathematical terms,

$$\forall \dot{\mathbf{x}} = \mathbf{f}(\tilde{\mathbf{x}}),\ \exists \mathbf{R} > \mathbf{0}, \exists\, \mathbf{0} < \mathbf{r} \leq \mathbf{R}\ , \mathbf{x}(\mathbf{0}) \in \mathbf{B_r},\ \mathbf{x}(\mathbf{t}) \in \mathbf{B_R} => \begin{cases} \mathbf{x} \neq \mathbf{x}^*,\ \exists V(\mathbf{x}) > 0 \\ \forall\, \mathbf{t} \geq \mathbf{0},\ \dot{V}(\mathbf{x}) \leq \mathbf{0}. \end{cases}$$

It is apparent upon observation of this definition and the aforementioned stability concepts that if the derivative of the Lyapunov function for a autonomous nonlinear system $\dot{V}(\mathbf{x})$ is found to be strictly negative definite (i.e. $\dot{V}(\mathbf{x}) < 0$ for $\mathbf{x} \in \mathbf{B_R}$ and $\mathbf{x} \neq \mathbf{x}^*$), and the Lyapunov function is zero at the equilibrium point ($V(\mathbf{x}^*) = 0$) with $\mathbf{x}(\mathbf{0}) \in \mathbf{B_r}$, then the system is defined as being locally asymptotically stable [2]. The global stability variant of this condition occurs when the balls $\mathbf{B_R}$ and $\mathbf{B_r}$ are defined to be radially unbounded [2]. The asymptotically stable Lyapunov function $V(\mathbf{x})$ in figure 5.1 described by $\mathbf{x} \in \mathbb{R}^2$ would graphically correspond to the surface of an upright cup, with the equilibrium point forming the lowest point in the cup.

Invariant Set Theorem

It is less trivial to determine whether a system is asymptotically stable around an equilibrium point if the associated Lyapunov function has a negative semi-definite derivative. Tackling this problem involves the definition of what is known as

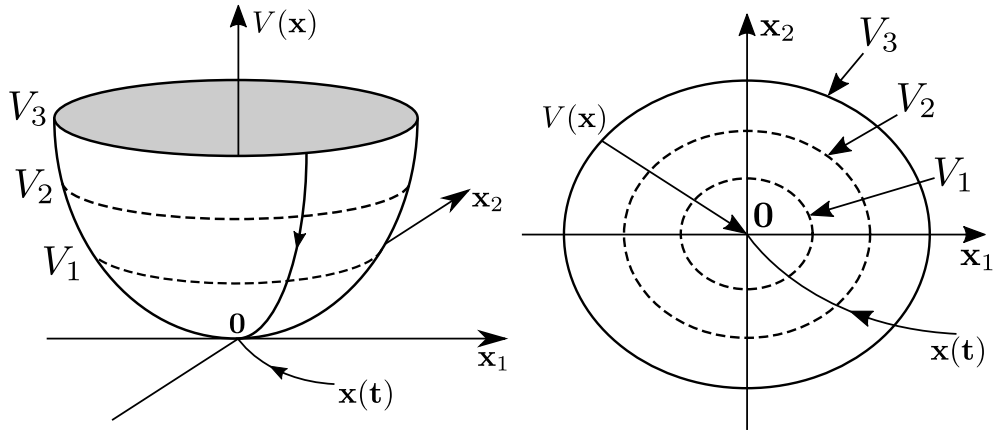

FIGURE 5.1: Typical upright cup shape of the Lyapunov function of an asymptotically stable equilibrium point $\mathbf{0}$ (left) with corresponding contour curves (right). Adapted from [2].

an *invariant set*, first defined by La Salle in his formulation of the *Invariant Set Theorems* [2]:

Definition 5.1. A set **G** is an <u>invariant set</u> if, for a system with dynamical equations, each system trajectory that begins in or enters **G** will remain in **G** for all future time.

The definition of an invariant set is subjective. For instance, an equilibrium point may form part of an invariant set as the system states will not move off this point once the equilibrium point has been reached. Alternatively, the entire state space of a system may also be defined as an invariant set as the system is never expected to leave this state space regardless of how it behaves. The definition of the invariant set determines how useful it is in determining system asymptotic stability.

The principle of invariant sets is well suited to Lyapunov stability theory as the Lyapunov function is expected to converge to zero once the system has reached the desired equilibrium point, which is invariant. This is clarified through the definition of the local invariant theorem [2]:

Theorem 5.1. ***(Local Invariant Set Theorem)*** *For a time-invariant system of the form* $\dot{\mathbf{x}} = \mathbf{f}(\tilde{\mathbf{x}})$*, where* $\mathbf{f}(\tilde{\mathbf{x}})$ *is continuous, there exists a continuously differentiable scalar function* $V(\mathbf{x}) < l$ *which defines a bounded neighbourhood* $\mathbf{\Omega_l}$ *where* $l > 0$*. Let the set* $\mathbf{R}$ *represent all states in* $\mathbf{\Omega_l}$ *where* $\dot{V}(\mathbf{x}) = 0$*, and the set* $\mathbf{M}$ *represents the union of all invariant sets in* $\mathbf{R}$*. If the time-differential of this function* $\dot{V}(\mathbf{x})$ *is negative semi-definite for all* $\mathbf{x}$ *in the region* $\mathbf{\Omega_l}$*, then every trajectory* $\mathbf{x}(\mathbf{t})$ *originating in the space* $\mathbf{\Omega_l}$ *will tend toward the space* $\mathbf{M}$ *as* $t \to \infty$*.*

More specifically, the invariant set $\mathbf{M}$ in figure 5.2 represents the collection of states that are associated with $\dot{V}(\mathbf{x}) = 0$ and will remain there as $\mathbf{t} \to \infty$. The set $\mathbf{R}$ will be completely composed of $\mathbf{M}$ if there are no states where $\dot{V}(\mathbf{x}) = 0$ for only a

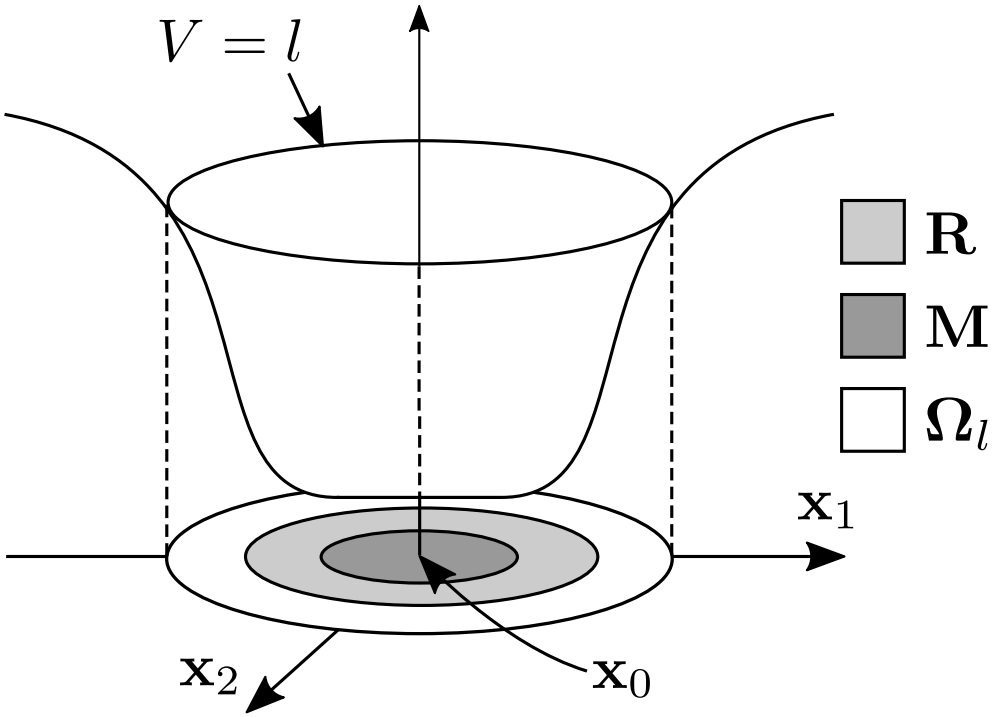

FIGURE 5.2: Lyapunov function converging to invariant set **M**. Adapted from [2].

finite amount of time.

An equilibrium point of a system that is associated with a negative semi-definite $\dot{V}(\mathbf{x})$ across the entire state space can be proven to be globally asymptotically stable by extending the radius of the neighbourhood $\mathbf{\Omega_l}$ toward an unbounded state (i.e. where $l \to \infty$), resulting in the *global invariant set theorem*.

Identification of Lyapunov Functions

It is trivial to construct a Lyapunov function for a LTI system, having the quadratic form

$$V(\mathbf{x}) = \tilde{\mathbf{x}}^{\mathrm{T}}\mathbf{P}\tilde{\mathbf{x}} \tag{5.5}$$

[2]. Differentiating the Lyapunov function, we find that

$$\dot{V}(\mathbf{x}) = \dot{\mathbf{x}}^{\mathrm{T}}\mathbf{P}\tilde{\mathbf{x}} + \tilde{\mathbf{x}}^{\mathrm{T}}\mathbf{P}\dot{\mathbf{x}} \tag{5.6}$$

[2]. Remembering that that structure of an unactuated LTI system with equilibrium point $\mathbf{x}^*$ is well-defined as $\dot{\mathbf{x}} = \mathbf{A}\tilde{\mathbf{x}}$, eq. (5.6) can be simplified as

$$\dot{V}(\mathbf{x}) = -\tilde{\mathbf{x}}^{\mathrm{T}}\mathbf{Q}\tilde{\mathbf{x}} \tag{5.7}$$

where

$$-\mathbf{Q} = \mathbf{A}^{\mathrm{T}}\mathbf{P} + \mathbf{P}\mathbf{A} \tag{5.8}$$

[2]. As stated in the definition of a Lyapunov function, the differential $\dot{V}(\mathbf{x})$ must be strictly negative semi-definite, therefore requiring that $\mathbf{Q}$ be strictly positive definite (where $\tilde{\mathbf{x}}^{\mathrm{T}}\mathbf{Q}\tilde{\mathbf{x}} > \mathbf{0}$ when $\tilde{\mathbf{x}} \neq \mathbf{0}$) [2]. Similarly, the Lyapunov function $V(\mathbf{x})$ must be positive definite, leading to the conclusion that the candidate matrix $\mathbf{P}$ must be defined as a positive definite matrix as a necessary condition for asymptotic stability around an equilibrium point. The procedure of determining the candidate matrix $\mathbf{P}$ is described as follows [2]:

(1) Define a positive definite matrix $\mathbf{Q}$.

(2) Solve for the candidate matrix $\mathbf{P}$ using eq. (5.8).

(3) Identify whether $\mathbf{P}$ is positive definite. If so, the LTI system in question is asymptotically stable around the equilibrium point $\tilde{\mathbf{x}} = \mathbb{O}$.

The most trivial example of a positive definite matrix is the identity matrix (I), which can be chosen for matrix $\mathbf{Q}$. This choice not only introduces mathematical simplicity, but also is the optimal choice for determining the exponential convergence rate of the asymptotically stable trajectory of a LTI system [2, pp. 91-93].

There are many available methodologies of estimating the Lyapunov function for non-linear systems, one of which is known as Krakovskii's method. This method allows for the definition of a Lyapunov function in the form

$$V(\mathbf{x}) = \mathbf{f}(\tilde{\mathbf{x}})\mathbf{P}\mathbf{f}(\tilde{\mathbf{x}}). \tag{5.9}$$

This method is based on the Krakovskii theorem, which is discussed in detail in [2, p. 85].

Another formal approach of determining Lyapunov functions of a nonlinear system is known as the Variable Gradient method [2]. This method involves the calculation of a Lyapunov function through the integral of a set of known gradient functions, where

$$V(\mathbf{x}) = \sum_{\mathbf{i=1}}^{\mathbf{N}} \int_{\mathbf{0}}^{\mathbf{x_i}} \nabla V_i(\mathbf{x}) \mathrm{d}x_i \tag{5.10}$$

and where $\nabla V(\mathbf{x}) = \left[\frac{\partial V(\mathbf{x})}{\partial x_1}, \ldots, \frac{\partial V(\mathbf{x})}{\partial x_N}\right]$. The variable gradient method can only be used to find the Lyapunov function $V(\mathbf{x})$ if and only if the matrix $\nabla^2 V(\mathbf{x})$ is

symmetric, where

$$\nabla^2 V(\mathbf{x}) = \begin{bmatrix} \frac{\partial^2 V(\mathbf{x})}{\partial x_1^2} & \frac{\partial^2 V(\mathbf{x})}{\partial x_1 \partial x_2} & \cdots & \frac{\partial^2 V(\mathbf{x})}{\partial x_1 \partial x_N} \\ \vdots & \vdots & \ddots & \vdots \\ \frac{\partial^2 V(\mathbf{x})}{\partial x_n \partial x_1} & \frac{\partial^2 V(\mathbf{x})}{\partial x_n \partial x_2} & \cdots & \frac{\partial^2 V(\mathbf{x})}{\partial x_N^2} \end{bmatrix} \tag{5.11}$$

[100]. It is evident that the following condition must be satisfied if this matrix is to be symmetric, where

$$\frac{\partial \nabla V(\mathbf{x})_i}{\partial x_j} = \frac{\partial \nabla V(\mathbf{x})_j}{\partial x_i} \qquad (i, j = 1, 2 \ldots, N) \tag{5.12}$$

[100]. This prerequisite is known as the *curl condition*. It can be assumed that the gradient functions have a specific form described by

$$\nabla V_i(\mathbf{x}) = \sum_{j=1}^{N} a_{ij} x_j \tag{5.13}$$

once the curl condition is satisfied [2]. The terms a_{ij} represent a set of unknown coefficients that are to be determined. The general procedure for determining a Lyapunov function for a nonlinear system using the Variable Gradient method is, therefore, described as follows:

(1) Express the elements of matrix $\nabla V(\mathbf{x})$ as $\nabla V_i(\mathbf{x}) = \sum_{j=1}^{N} a_{ij} x_j$.

(2) Determine the values of the coefficients a_{ij}, keeping in mind that the curl condition needs to be satisfied.

(3) Ensure that $\dot{V}(\mathbf{x}) = \nabla V(\mathbf{x}) \dot{\mathbf{x}}$ is negative definite in a neighbourhood Ω around the equilibrium point. Restrict the coefficients a_{ij} if necessary.

(4) Calculate the Lyapunov function $V(\mathbf{x})$ from $\nabla V(\mathbf{x})$ using integration.

(5) Identify whether $V(\mathbf{x})$ is positive definite.

There are not many other general methods of determining the Lyapunov function of a nonlinear system, an evidently major constraint to this technique of stability analysis. The autonomous nature of the Lyapunov function, however, allows for the expression of the time differential $\dot{V}(\mathbf{x})$ in terms of the system's dynamical equations, such as

$$\frac{\mathrm{d}V(\mathbf{x})}{\mathrm{dt}} = \frac{\partial V(\mathbf{x})}{\partial \mathbf{x}} \frac{\mathrm{d}\mathbf{x}}{\mathrm{dt}} = \frac{\partial V(\mathbf{x})}{\partial \mathbf{x}} \mathbf{f}(\mathbf{x}). \tag{5.14}$$

This expression does not provide an explicit means of determining the Lyapunov function, but can be used to check the validity of the choice of Lyapunov function.

In many cases, the implementation of the aforementioned methods does not produce an appropriate Lyapunov function. It is important to note, however, that the system cannot be identified as being unstable if the choice of Lyapunov function does not provide sufficient evidence to prove stability. The process must be iterated until a more accurate Lyapunov function.

General Procedure for Lyapunov Analysis

A summary of the procedure of Lyapunov's stability analysis is provided below:

(1) Identify the system's equations of motion and identify the relevant equilibrium point.

(2) Identify a candidate Lyapunov function $V(\mathbf{x})$ for the system. A quadratic Lyapunov function candidate will be sufficient for a linear system, whereas a positive definite function for a nonlinear system will require more intuition, and possibly the implementation of methods such as the Krakovskii or Variable Gradient methods.

(3) Determine if the candidate Lyapunov function remains positive definite within a satisfactory domain of operation $\mathbf{\Omega}$. Repeat the previous step if otherwise.

(4) Identify the behaviour of the candidate Lyapunov function by deriving $\dot{V}(\mathbf{x})$. If $\dot{V}(\mathbf{x})$ is negative definite throughout $\mathbf{\Omega}$, then the equilibrium point is asymptotically stable within $\mathbf{\Omega}$. The equilibrium point is Lyapunov stable within $\mathbf{\Omega}$ if $\dot{V}(\mathbf{x})$ is negative semi-definite within $\mathbf{\Omega}$. Invariant set theorem will be required to determine asymptotic stability in this case. If the candidate functions fails, it does not immediately suggest that the system is unstable around the equilibrium point. If there is a suspicion of stability, more candidate functions must be identified.

Example of the implementation of this method are shown in appendix B, including an example of the implementation of the aforementioned procedure using the system's mechanical energy as the Lyapunov function (Example B.1), and where the Lyapunov function of a system is found using Krakovskii's method (Example B.2). The steps in these examples are enumerated as seen in the generalised procedure presented in this section.

5.3 Feedback Linearisation

The work of Spong in [6, 76] highlights another popular technique used in the swing-up control of UMSs, namely the PFL technique. This chapter is dedicated to highlighting the important concepts that form the foundation of this technique.

5.3.1 Feedback Linearisation using the Controllability Canonical Form

Feedback linearisation involves the transformation of non-linear systems into equivalent linear representations to allow for the application of linear control methods [2]. This form of linearisation differs from that of the Lyapunov linearisation method highlighted in section 5.2.1 in that the linearised system dynamics of order n maintain their linear characteristics across a large region (if not all) of the domain $\mathbb{R}^n$ instead of only representing an approximation about an equilibrium point $\mathbf{x}^* \in \mathbb{R}^n$ [2]. This is achieved through state transformation as shown in figure 5.3, enforced by the actuators of the system through feedback [2].

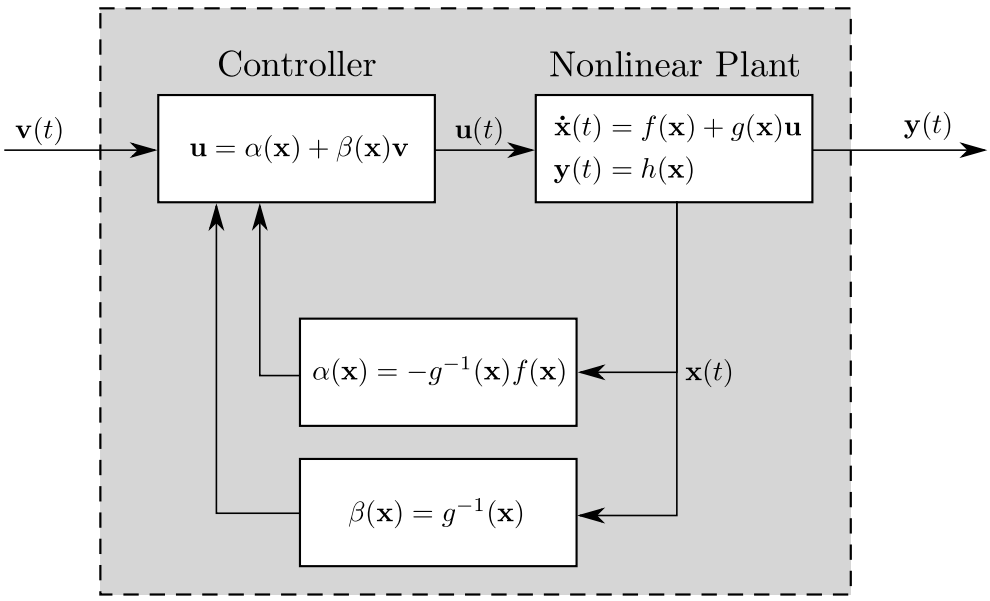

FIGURE 5.3: State transformation introduced through actuated feedback. Adapted from [4].

Therefore, for a MIMO nonlinear system with m inputs and outputs, whose dynamics are described by the companion form (or m^{th} order *controllability canonical form*)

$$\dot{\mathbf{x}} = \begin{bmatrix} x_2 \\ x_3 \\ \vdots \\ x_i \\ f_1(\mathbf{x}) + g_1(\mathbf{x})\mathbf{u}_1 \\ x_{i+2} \\ \vdots \\ x_{n-1} \\ x_n \\ f_m(\mathbf{x}) + g_m(\mathbf{x})\mathbf{u}_m \end{bmatrix}$$

where $\dot{\mathbf{x}} \in \mathbb{R}^n$, choosing the static feedback control law

$$\begin{aligned}\mathbf{u}(t) &= \alpha(\mathbf{x}) + \beta(\mathbf{x})\mathbf{v}(t) \\ &= -g^{-1}(\mathbf{x})f(\mathbf{x}) + g^{-1}(\mathbf{x})\mathbf{v}(t) \in \mathbb{R}^m\end{aligned}$$

with

$$g(\mathbf{x}) = \begin{bmatrix} g_1(\mathbf{x}) & 0 & 0 & \dots & 0 \\ 0 & g_2(\mathbf{x}) & 0 & \dots & 0 \\ \vdots & \ddots & \ddots & \ddots & \vdots \\ 0 & & \ddots & g_{m-1}(\mathbf{x}) & 0 \\ 0 & 0 & \dots & 0 & g_m(\mathbf{x}) \end{bmatrix} \in \mathbb{R}^{m \times m}$$

and

$$\begin{aligned} f(\mathbf{x}) &= \begin{bmatrix} f_1(\mathbf{x}) & f_2(\mathbf{x}) & \dots & f_m(\mathbf{x}) \end{bmatrix}^{\mathbf{T}} \in \mathbb{R}^m, \\ \mathbf{v} &= \begin{bmatrix} v_1 & v_2 & \dots & v_m \end{bmatrix}^{\mathbf{T}} \in \mathbb{R}^m \end{aligned}$$

results in the fully-linearised system dynamics described by

$$\dot{\mathbf{x}} = \begin{bmatrix} \overbrace{x_2 \quad x_3 \quad \dots \quad x_{i-1} \quad v_1}^{p_1 = i} & x_{i+1} & \dots & x_{n-1} & x_n & v_m \end{bmatrix}^{\mathbf{T}} \tag{5.15}$$

[2, 4]. A tracking controller may now be designed for each new input in $\mathbf{v}$, with each input v_j being associated with r_j states, as shown in eq. (5.15) (whereby v_1 is associated with $p_1 = i$ states, being $x_1, x_2, \dots, x_i$). Summing all of the associated coefficients would intuitively represent all n states (i.e. $\sum_{i=1}^{m} p_i = n$). The tracking controllers are represented as

$$\mathbf{v}(t) = \begin{bmatrix} v_1 \\ v_2 \\ \vdots \\ v_m \end{bmatrix} = \begin{bmatrix} \dot{x}^d_{\Sigma_1} - k_{0_1}e_1 - k_{1_1}\dot{e}_1 - \dots - k_{(p_1-1)_1}{e_1}^{(p_1-1)} \\ \dot{x}^d_{\Sigma_2} - k_{0_2}e_2 - k_{1_2}\dot{e}_2 - \dots - k_{(p_2-1)_2}{e_2}^{(p_2-1)} \\ \vdots \\ \dot{x}^d_{\Sigma_m} - k_{0_m}e_m - k_{1_m}\dot{e}_m - \dots - k_{(p_m-1)_m}{e_m}^{(p_m-1)} \end{bmatrix} \tag{5.16}$$

where

$$\Sigma_j = \sum_{i=1}^{j} p_i$$

and where the tracking error for the ith DOF measured in reference to the desired trajectory values is represented as ${e_i}^{(j)} = {x_{\alpha_i}}^{(j+1)} - {x^d_{\alpha_i}}^{(j+1)}$ with

$$\alpha_i = \sum_{q=2}^{i} p_{q-1} + 1 \qquad \text{for } 1 \leq i \leq m$$

and $0 \leq j \leq p_i - 1$ [2]. It is evident that $e_i^{(p_i)} = \dot{x}_{\Sigma_i} - \dot{x}^d_{\Sigma_i} = v_i - \dot{x}^d_{\Sigma_i}$. Substituting this expression into the entries of eq. (5.16) for $1 \leq i \leq m$ produces

$$\begin{aligned}
&e_1^{p_1} + k_{p_1-1} e_1^{(p_1-1)} + \cdots + k_{1_1}\dot{e}_1 + k_{0_1} e_1 = 0, \\
&e_2^{p_2} + k_{p_2-1} e_2^{(p_2-1)} + \cdots + k_{1_2}\dot{e}_2 + k_{0_2} e_2 = 0, \\
&\vdots \\
&e_m^{p_m} + k_{p_m-1} e_m^{(p_m-1)} + \cdots + k_{1_m}\dot{e}_m + k_{0_m} e_m = 0.
\end{aligned}$$

It is apparent that the poles of each of these differential equations are found on the left-half of the complex pole-zero plane, thus representing a set of stable signals that will tend towards the desired trajectory. Additionally, if the outputs are explicitly defined as

$$\begin{aligned}
\mathbf{y}(t) &= h(\mathbf{x}) \\
&= \begin{bmatrix} x_1 & x_{\Sigma_1} & x_{\Sigma_2} & \ldots & x_{\Sigma_{m-1}} \end{bmatrix}^{\mathbf{T}} \in \mathbb{R}^m
\end{aligned}$$

then p_i can be referred to as the *relative degree* of the system [2].

The procedure shown above demonstrates the basic principle behind feedback linearisation, but it can only be applied to a system that subscribes to the *controllability canonical form* [2]. More complex systems will require the implementation of a formalised feedback linearisation technique [2]. Two of these techniques are discussed in this section, namely the Exact Linearisation via Feedback Linearisation (ELFBL) and the Input-Output Feedback Linearisation (IOFBL) techniques. There is no introductory sections that are introduced in this chapter to discuss the mathematical tools that are used to derive each of these techniques (including the Lie derivative, coordinate transformations, the normal form, and relative degree). The reader is encouraged to refer to [2] if introductory material on these tools is required.

5.3.2 Exact Linearisation via Feedback Linearisation (ELFBL)

The objective of this technique (illustrated in figure 5.4) is to present a state-space of the form

$$\dot{\mathbf{z}}(t) = A\mathbf{z}(t) + B\mathbf{v}(t) \tag{5.17}$$

by means of a coordinate transformation of the $\mathbf{x}$ state-space (represented as the companion form of square control affine nonlinear system) and system feedback

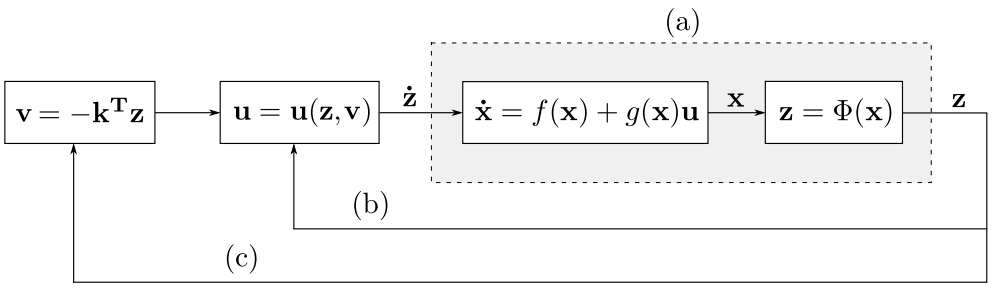

FIGURE 5.4: ELFBL, described by the (a) coordinate transformation (b) the linearisation loop and (c) the outer control loop. Figure adapted from [2].

using the static feedback control input

$$\mathbf{u}(t) = \alpha(\mathbf{x}) + \beta(\mathbf{x})\mathbf{v}(t)$$

where $\alpha(\mathbf{x}) \in \mathbb{R}^m$ and $\beta(\mathbf{x}) \in \mathbb{R}^{m\times m}$ [101]. A pole-placement linear state feedback control law is subsequently designed for the new input vector $\mathbf{v}$ to stabilise the dynamics of the closed-loop [2]. A diffeomorphism may simplify the dynamics of a complex nonlinear system if an appropriate transformation is selected [2]. It is quite evident, however, that the transformed state-space seen in eq. (5.17) is not guaranteed if there are internal dynamics in the system (i.e. if there are $n - r$ equations $\phi_{r+1},\ \phi_{r+2},\ \ldots\ ,\ \phi_n$ that fall out of the Lie derivative iteration) [2]. These equations may be intrinsically nonlinear and cannot be linearised by feedback since the dynamics are unobservable from a feedback perspective [101]. Therefore, it is possible to demonstrate the exact linearisation of a square control affine nonlinear system with relative degree $r = n$ about an operating point x_0 with the procedure found below.

Consider the transformed dynamics of a square control affine nonlinear system described by

$$\dot{\xi}^i = \begin{bmatrix} \dot{\xi}^i_1 \\ \dot{\xi}^i_2 \\ \vdots \\ \dot{\xi}^i_{r_i-1} \\ \dot{\xi}^i_{r_i} \end{bmatrix} = \begin{bmatrix} \xi^i_2 \\ \xi^i_3 \\ \vdots \\ \xi^i_{r_i} \\ b_i(\xi) + \sum\limits_{j=1}^{m} a_{ij}(\xi)u_j \end{bmatrix}$$

which is in normal form for $1 \leq i \leq m$ and $1 \leq j \leq m$, and where η is excluded since $r = n$ [101]. This state-space has m possible nonlinear components represented by $b_i(\xi) + \sum\limits_{j=1}^{m} a_{ij}(\xi)u_j$ [101]. These components will be linearised about the operating

point x_0 using the m control feedback inputs, choosing a new desired input v_i for each nonlinear component, where $1 \leq i \leq m$ [101]. Therefore, asserting the equality $\dot{\xi}^i_{r_i} = \mathbf{v} \in \mathbb{R}^m$ allows for the definition of

$$v_i = b_i(\xi) + \sum_{j=1}^{m} a_{ij}(\xi) u_j,$$
$$\therefore \ \mathbf{v}(t) = b(\xi) + C(\xi)\mathbf{u}(t)$$

where

$$b(\xi) = \begin{bmatrix} b_1(\xi) & b_2(\xi) & \dots & b_m(\xi) \end{bmatrix}$$

and $C(\xi)$ is the characteristic equation described in terms of ξ [2]. The control input can thus be defined as

$$\mathbf{u}(t) = C^{-1}(\xi)\big(v - b(\xi)\big) \tag{5.18}$$

[101]. Substituting this feedback control into the transformed state-space produces

$$\dot{\xi}^i = \begin{bmatrix} \dot{\xi}^i_1 \\ \dot{\xi}^i_2 \\ \vdots \\ \dot{\xi}^i_{r_i-1} \\ \dot{\xi}^i_{r_i} \end{bmatrix} = \begin{bmatrix} \xi^i_2 \\ \xi^i_3 \\ \vdots \\ \xi^i_{r_i} \\ v_i \end{bmatrix}.$$

Making

$$\begin{aligned} \mathbf{z} &= \xi(\mathbf{x}) \\ &= \begin{bmatrix} \xi^1_1 & \dots & \xi^1_{r_1} & \dots & \xi^m_1 & \dots & \xi^m_{r_m} \end{bmatrix}^{\mathbf{T}} \end{aligned}$$

we find that

$$\dot{\mathbf{z}}(t) = A\mathbf{z}(t) + B\mathbf{v}(t)$$

where

$$A = \begin{bmatrix} 0_{r_1-1,1} & I_{r_1-1} & 0_{r_1-1,n-\Sigma_1} \\ & 0_{1,n} & \\ 0_{r_2-1,\Sigma_1+1} & I_{r_2-1} & 0_{r_2-1,n-\Sigma_2} \\ & 0_{1,n} & \\ \vdots & \vdots & \vdots \\ 0_{r_m-1,\Sigma_{m-1}+1} & I_{r_m-1} & 0_0 \\ & 0_{1,n} & \end{bmatrix}, \quad B = \begin{bmatrix} & 0_{r_1-1,m} & \\ 0_0 & 1 & 0_{1,m-1} \\ & 0_{r_2-1,m} & \\ 0_{1,1} & 1 & 0_{1,m-2} \\ \vdots & \vdots & \vdots \\ & 0_{r_m-1,m} & \\ 0_{1,m-1} & 1 & 0_0 \end{bmatrix}$$

with $A \in R^{n \times n}$, $B \in \mathbb{R}^{n \times m}$, 0_0 representing an empty matrix, and

$$\Sigma_i = \sum_{j=1}^{i} r_j.$$

A pole-placement linear state feedback control law can now be designed for the new input $\mathbf{v}(t)$, which is defined as

$$\mathbf{v}(t) = -\mathbf{k}^{\mathbf{T}}\mathbf{z}$$

where $\mathbf{k}$ represents the gain matrix

$$\mathbf{k} = \begin{bmatrix} k_1 & k_2 & \dots & k_n \end{bmatrix}^{\mathbf{T}}.$$

This technique may produce elegant results, but it is limited in applications that are fully-actuated with respect to the chosen outputs $\mathbf{y}(t) = h(\mathbf{x})$ [2]. The technique discussed in the next subsection is more flexible to varying states of system actuation. An example of the application of the ELFBL technique is provided in appendix B (Example B.3).

5.3.3 Input-Output Feedback Linearisation (IOFBL)

Instead of focussing on the transformation of the entire system state-space, one could design a controller input $\mathbf{u}(t)$ such that the relationship between the newly introduced input $\mathbf{v}(t)$ and the output $\mathbf{y}(t)$ is linear (hence the term *input-output linearisation*) [4]. The result of this procedure produces a controllable output that places no requirement on the state of system actuation, provided that the internal dynamics of the system are stable [4]. There are a number of propositions and definitions that lead up to the final theorem behind the choice of IOFBL input $\mathbf{u}(t)$ for a MIMO system, but these are omitted for the sake of brevity (these definitions and propositions are explained in detail in [4, 102]).

Theorem 5.2. *(**Generalised Input-Output Feedback Linearisation**) If a system described by the companion form*

$$\begin{aligned} \dot{\mathbf{x}}(t) &= f(\mathbf{x}) + g(\mathbf{x})\mathbf{u}(t), \\ \mathbf{y}(t) &= h(\mathbf{x}) \end{aligned} \tag{5.19}$$

with $\mathbf{y}(t) \in \mathbb{R}^m$ and $\mathbf{u}(t) \in \mathbb{R}^m$ and described by relative degrees $r = \{r_1, r_2, \dots, r_m\}$ has a static feedback controller described by the general form

$$\mathbf{u}(t) = \alpha(\mathbf{x}) + \beta(\mathbf{x})\mathbf{v}(t)$$

which can be represented as

$$\mathbf{u}(t) = \Big(\Lambda_m C(\mathbf{x})\Big)^{-1}\left[\mathbf{v}(t) - \sum_{i=1}^{m}\sum_{k=0}^{r_i}\lambda_{i_k} L_f^k h_i(\mathbf{x})\right] \tag{5.20}$$

where

$$\Lambda_m = \begin{bmatrix}\lambda_{1_{r_1}} & \dots & \lambda_{m_{r_m}}\end{bmatrix} \in \mathbb{R}^{m\times m}$$

with each associated linear operator entry $\lambda_{i_k} = \left[\lambda_{i_k}^1, \lambda_{i_k}^2, \dots, \lambda_{i_k}^m\right]^{\boldsymbol{T}} \in \mathbb{R}^m$ *and with* $C(\mathbf{x})$ *defined as the characteristic equation, then the relationship between the new input* $\mathbf{v}(t) \in \mathbb{R}^m$ *and the output* $\mathbf{y}(t) \in \mathbb{R}^m$ *is described as*

$$\sum_{i=1}^{m}\sum_{k=0}^{r_i}\lambda_{i_k}\frac{d^k y_i}{dt^k} = \mathbf{v}(t) \tag{5.21}$$

provided that the relative degrees in r *are well defined and that* λ_{i_k} *satisfies*

$$\det\left(\left[\left(\sum_{k=0}^{r_1}\lambda_{1_k}s^k\right) \quad \left(\sum_{k=0}^{r_2}\lambda_{2_k}s^k\right) \quad \dots \quad \left(\sum_{k=0}^{r_m}\lambda_{1_r}s^k\right)\right]\right) = B(s) = \neq 0, \tag{5.22a}$$

$$\det\left(\begin{bmatrix}\lambda_{1_{r_1}} & \lambda_{2_{r_2}} & \dots \lambda_{m_{r_m}}\end{bmatrix}\right) = \Lambda_m \neq 0. \tag{5.22b}$$

The relationship between the desired input $\mathbf{v}(t)$ *and the output* $\mathbf{y}(t)$ *may be represented in the Laplace domain, whereby*

$$\mathbf{y}(s) = G(s)\mathbf{v}(s) = \Big[B(s)\Big]^{-1}\mathbf{v}(s).$$

An easy way of satisfying the conditions highlighted in eq. (5.22a) and (5.22b) is to define the linear operator λ_{i_k} as

$$\lambda_{i_k} = 0_{m\times 1} \quad \text{for} \quad \begin{cases} 1 \le i \le m; \\ 0 \le k < r_i. \end{cases},$$

$$\lambda_{i_{r_i}}^p = 0 \quad \text{for} \quad \begin{cases} 1 \le i \le m; \\ 1 \le p < i; \\ i < p \le m. \end{cases},$$

$$\lambda_{i_{r_i}}^p = 1 \quad \text{for} \quad \begin{cases} 1 \le i \le m; \\ p = i. \end{cases}.$$

This results in

$$\Lambda_m = I_m, \qquad\qquad B(s) = I_n \mathbf{s_k}$$

where

$$\mathbf{s_k} = \begin{bmatrix} s^{r_1} & s^{r_2} & \dots & s^{r_m} \end{bmatrix}^{\mathbf{T}} \in \mathbb{R}^m.$$

It is clear that eq. (5.22a) and eq. (5.22b) are satisfied in this instance. The control law in eq. (5.20) simplifies to

$$\begin{aligned} \mathbf{u}(t) &= C^{-1}(\mathbf{x}) \left[v - \sum_{i=1}^{m} \lambda_{i_{r_i}} L_f^{r_i} h_i(\mathbf{x}) \right], \\ &= C^{-1}(\mathbf{x})(\mathbf{v}(t) - b(\mathbf{x})) \end{aligned} \tag{5.23}$$

with the relationship seen in eq. (5.21) simplifying to

$$y_i^{(r_i)} = v_i \qquad \text{for } 1 \leq i \leq m. \tag{5.24}$$

An appropriate linear state feedback control law may now be designed to define the behaviour of each output y_i. The result depicted in eq. (5.24) is one that is typically seen in discussions on IOFBL (including [2]), and is a direct consequence of defining the relationship between $\mathbf{y}(t)$ and $\mathbf{v}(t)$ through the direct differentiation of $y_i(t)$ for $1 \leq i \leq m$ (the output is repeatedly differentiated until some input $u_k(t)$ appears in the associated expression). The number of differentiations for $y_i(t)$ strictly defines the relative degree r_i.

Continuing with this variant of IOFBL, and using the diffeomorphism principle discussed in [2], we can define the outputs $\mathbf{y}(t)$ in terms of the transformation $\Phi(\mathbf{x})$, whereby

$$\mathbf{y}(t) = \begin{bmatrix} h_1(\mathbf{x}) \\ h_2(\mathbf{x}) \\ \vdots \\ h_m(\mathbf{x}) \end{bmatrix} = \begin{bmatrix} \phi_1^1(\mathbf{x}) \\ \phi_1^2(\mathbf{x}) \\ \vdots \\ \phi_1^m(\mathbf{x}) \end{bmatrix}$$

with the derivatives of the ith output with respect to time (where $1 \leq i \leq m$) represented as

$$\begin{bmatrix} y_i \\ y_i^{(1)} \\ \vdots \\ y_i^{(r_i)} \end{bmatrix} = \begin{bmatrix} \phi_1^i \\ \phi_2^i \\ \vdots \\ \phi_{r_i}^i \end{bmatrix} = \begin{bmatrix} \xi_1^i \\ \xi_2^i \\ \vdots \\ \xi_{r_i}^i \end{bmatrix}.$$

If $r < n$, the internal dynamics of the system may be represented as

$$\eta(\mathbf{x}) = \begin{bmatrix} \phi_{r+1}(\mathbf{x}) \\ \phi_{r+2}(\mathbf{x}) \\ \vdots \\ \phi_n(\mathbf{x}) \end{bmatrix} = \begin{bmatrix} \eta_1(\mathbf{x}) \\ \eta_2(\mathbf{x}) \\ \vdots \\ \eta_n(\mathbf{x}) \end{bmatrix}$$

where $r = \sum_{i=1}^{m} r_i$. The total transformed state-space is therefore represented as

$$\begin{aligned} \dot{\xi}(\mathbf{x}) &= \begin{bmatrix} \dot{\xi}^1 & \dot{\xi}^2 & \dots & \dot{\xi}^m \end{bmatrix}^{\mathbf{T}} \in \mathbb{R}^r, \\ \dot{\eta} &= q(\xi, \eta) \in \mathbb{R}^{(n-r)}, \\ \mathbf{y}(t) &= \begin{bmatrix} \xi_1^1 & \xi_1^2 & \dots & \xi_1^m \end{bmatrix} \in \mathbb{R}^m \end{aligned}$$

where, according to the result in 5.24,

$$\dot{\xi}^i = \begin{bmatrix} \dot{\xi}_1^i \\ \dot{\xi}_2^i \\ \vdots \\ \dot{\xi}_{r_i-1}^i \\ \dot{\xi}_{r_i}^i \end{bmatrix} = \begin{bmatrix} \xi_2^i \\ \xi_3^i \\ \vdots \\ \xi_{r_i}^i \\ v_i \end{bmatrix}.$$

It is evident from the state-space model derived above that performing IOFBL on a system with $r = n$ will produce the same result as the ELFBL procedure. If the system is underactuated ($r < n$), however, exact linearisation cannot be performed, resulting in the population of the internal dynamics vector $\eta(t)$ [2]. It may, in some instances, be beneficial to linearise the observable dynamics to reduce the complexity of the system, regardless of the system's intrinsic underactuated nature [15]. This procedure, typically performed using IOFBL, is known as PFL, a popular technique in the field of swing-up control of underactuated mechanics, as highlighted in Spong's work (see [6, 9, 34, 76]). The PFL technique, its variants, and its application on UMSs will be discussed in greater detail in chapter 9. An example of the implementation of the IOFBL technique on a fully-actuated system is included in appendix B (Example B.4).

5.4 Conclusion

The objective of this chapter was to highlight key concepts pertaining to control methods that are relevant to this investigation, including Lyapunov's theories of stability and the feedback linearisation technique. Lyapunov's linearisation method is used to transform the nonlinear dynamics of a system into a linear state-space that is valid when found approximately near an operating point. This is useful when the stability of a nonlinear system across a large domain is difficult to determine, or if the system stability only needs to be determined for an approximate region

about an operating point. It is challenging, however, to intuit the size of the domain of attraction around the operating point when this method is used, whereby the appropriate region of operation about the equilibrium point can only be determined using trial-and-error. The identification of invariant sets in the state-space using a valid Lyapunov function provides a more accurate picture of nonlinear system stability on a larger domain (which may, in certain instances, be valid across the global state-space). Additionally, appropriate invariant sets may be created through actuated state-feedback, as outlined in the LDM technique. This method has been successfully used to perform swing-up control on a number of UMSs, as outlined in Xin and Liu's work. Identifying a valid Lyapunov function for any particular nonlinear system is typically challenging since there is no formalised identification technique currently available in existing literature, with the exception of Krakovskii's method and the variable gradient method (which are particularly situational). The feedback linearisation technique, in basic terms, involves the negation of the nonlinear dynamics of a system with the use of state feedback through system actuation. Two popular techniques discussed in this chapter include the ELFBL and IOFBL techniques. ELFBL involves both coordinate transformation and state-feedback, with the equivalence of the relative degree of the system (r) and the system order (n) being a prerequisite of this technique. IOFBL is more robust to differences in relative degree and system order, focussing on the linearisation of the system output dynamics rather than on the state-space; IOFBL may therefore be used to partially linearise an underactuated system. Despite this advantage, the partial linearisation of an underactuated system (with $r < n$) using feedback results in the formation of unobserved system dynamics (termed internal dynamics), which must be evaluated to ensure system stability. Performing IOFBL on a fully-actuated system produces the same results as the ELFBL technique, as demonstrated in the examples of this chapter.

As mentioned before, the techniques discussed in this chapter are all pertinent to this research investigation, and are implemented in the finalising chapters of this dissertation. The next two chapters, however, must first be introduced to discuss the important models that are derived for this investigation, beginning first with the friction model.

"This is what happens when an unstoppable force meets an immovable object."

— The Joker

Chapter 6

Viscous Damping Model

6.1 Chapter Overview

This chapter is dedicated to discussing the concept of viscous damping friction, a physical phenomenon that will be integrated into the conventional model chosen for this research, as discussed in the literature review. We generalise the behaviour of an unactuated compound pendulum system that has been integrated with this viscous damping friction model using LDM to demonstrate the effects of viscous damping friction on nonlinear systems. This generalisation is simulated on a viscously damped DIP. A high-level description of viscous damping using the linear mass-spring-damper system is provided in appendix C for supplementation, whereby the movement of the mass is described in the undamped, underdamped and damped cases.

6.2 Mathematical Representation of Viscous Damping Friction for Multi-body Pendulum Systems

As seen in the mass-spring-damper model in figure C.2 of appendix C, the damping torque produced as a result of the viscous damping friction model is directly proportional to some damping coefficient (b) and the velocity of the associated mass [82]. There is significant literature that suggests that viscous damping may be represented in a similar manner in the angular coordinate systems, whereby the viscous damping torque seen at a joint is directly proportional to the angular velocity of the rotational object [81, 103, 104]. The damping torque for a single joint is represented as

$$\tau_{d_i} = b_i \dot{q}_i. \tag{6.1}$$

These damping torques must be encompassed by the lossy matrix $\mathbf{R}(\mathbf{q}, \dot{\mathbf{q}})$ of the system's prototypical form as discussed in section 3.3.3. The viscous damping torques of the multi-link pendulum system are, therefore, represented in the prototypical

form, where

$$\mathbf{R}(\mathbf{q},\dot{\mathbf{q}}) = \begin{bmatrix} b_1\dot{q}_1 & 0 & 0 & \dots & 0 \\ 0 & b_2\dot{q}_2 & 0 & \ddots & \vdots \\ 0 & 0 & b_3\dot{q}_3 & \ddots & 0 \\ \vdots & \ddots & \ddots & \ddots & 0 \\ 0 & \dots & 0 & 0 & b_n\dot{q}_n \end{bmatrix} \tag{6.2}$$

and where the system energy is expected to change with respect to time as described by

$$\frac{\mathrm{d}}{\mathrm{dt}}E = -\dot{\mathbf{q}}^{\mathbf{T}}\mathbf{R}(\mathbf{q},\dot{\mathbf{q}}) + \dot{\mathbf{q}}^{\mathbf{T}}\mathbf{G}(\mathbf{q})\mathbf{u}. \tag{6.3}$$

This is similar to eq. (3.25), but the conservative torque matrix $\mathbf{J}(\mathbf{q},\dot{\mathbf{q}})$ is removed since $\dot{\mathbf{q}}^{\mathbf{T}}\mathbf{J}(\mathbf{q},\dot{\mathbf{q}})\dot{\mathbf{q}} = 0$.

6.3 Effect on the Dynamics of Pendulum Systems

It is evident that if a damped system is unactuated, the system energy will continue to dissipate until the system reaches a stable equilibrium point, as shown in eq. (6.3). It is, however, more difficult to mathematically prove that viscously damped nonlinear systems, such as the DIP, will exhibit this type of behaviour. The time-explicit behaviour of a damped pendulum system found approximately near a stable equilibrium point has been shown in [81, 103], but a global description of the behaviour of a damped system is not, to the knowledge of the author, included in existing literature. LDM may not provide a time-explicit equation describing the behaviour of each pendulum, but it can be used in this instance to determine the general tendency of the system dynamics. The behaviour of this system is described in the following section using LDM.

6.3.1 The Damped Pendulum and Lyapunov's Direct Method

If $\mathbb{S}$ is a set of all possible states of the pendulum system, let us define an invariant set $\mathbf{W}$ as a subset of this set $\mathbb{S}$, which is described by the state conditions

$$\mathbf{W} = \left\{ (\mathbf{q}^*, 0) \;\middle|\; V(\mathbf{q},\dot{\mathbf{q}}) = V^*;\ \dot{V}(\mathbf{q},\dot{\mathbf{q}}) = 0 \right\}; \qquad \mathbf{W} \subset \mathbb{S}; \qquad \mathbb{S} \in \mathbb{R}^{n\times 2}$$

where $V(\mathbf{q},\dot{\mathbf{q}})$ represents a Lyapunov candidate function, which must be formulated. To do this, consider the dynamical equations of an underactuated multi-body pendulum system demonstrated in chapter 7 (eq. (7.23)). The Lyapunov candidate function

$$V(\mathbf{q},\dot{\mathbf{q}}) = \frac{1}{2}(E - E_r)^2 \tag{6.4}$$

is arbitrarily constructed for this system where

$$E_r = -\sum_{i=1}^{n} m_i \left[l_i + \sum_{j=1}^{i-1} L_j \right]. \tag{6.5}$$

This function is evidently positive semi-definite for all time, with the function's minimum occurring when the pendulum system reaches the FPEP, which is the expected goal of a damped system. The time-differential of the Lyapunov function is described as

$$\begin{aligned} \dot{V}(\mathbf{q},\dot{\mathbf{q}}) &= (E - E_r)\dot{E} \\ &= -(E - E_r)\dot{\mathbf{q}}^{\mathrm{T}}\mathbf{R}(\mathbf{q},\dot{\mathbf{q}}). \end{aligned} \tag{6.6}$$

The $\mathbf{R}(\mathbf{q},\dot{\mathbf{q}})$ matrix is positive semi-definite, therefore $\dot{V}(\mathbf{q},\dot{\mathbf{q}})$ is guaranteed to be negative semi-definite. The following lemma is formally stated as a result of this scenario:

Lemma 6.1. The trajectory of a damped unactuated compound pendulum system will always tend toward the invariant set $\mathbf{W}$ as $t \to \infty$.

It is evident that the invariant set is made up of a collection of states that are associated with the equilibrium points of the system, whereby

$$\mathbf{q}^* = \begin{bmatrix} q_1^* \\ q_2^* \\ q_3^* \\ \vdots \\ q_n^* \end{bmatrix} = \begin{bmatrix} k_1\pi \\ k_2\pi \\ k_3\pi \\ \vdots \\ k_n\pi \end{bmatrix}, \quad \text{where } k_i \in \mathbb{Z}, \quad i = 1, 2, \ldots, n.$$

These equilibrium points will be found at varying potential energy levels, with the highest potential energy level ($E = |E_r|$) occurring at the UEP, whereby

$$\mathbf{q}_u^* = \begin{bmatrix} q_{u_1}^* \\ q_{u_2}^* \\ q_{u_3}^* \\ \vdots \\ q_{u_n}^* \end{bmatrix} = \begin{bmatrix} 2k_1\pi \\ 2k_2\pi \\ 2k_3\pi \\ \vdots \\ 2k_n\pi \end{bmatrix}. \tag{6.7}$$

These states are found in a newly defined invariant set $\mathbf{W}_u$, which is characterised by

$$\mathbf{W}_u = \left\{ (\mathbf{q}_u^*, 0) \;\middle|\; V(\mathbf{q},\dot{\mathbf{q}}) = 2{E_r}^2;\ \dot{V}(\mathbf{q},\dot{\mathbf{q}}) = 0 \right\}. \tag{6.8}$$

Additionally, the invariant set may be associated with many possible states (according to the values of k_i), but these states all result in the same physical configuration (i.e. with all pendulums found in the pendant position, represented by item (d) in

figure 4.1). This will be referred to, from now on, as the *equilibrium configuration*.

The lowest potential energy ($E = Er$) will occur at the FPEP, found within the newly defined invariant set $\mathbf{W}_p$ described by the states

$$\mathbf{q}_p^* = \begin{bmatrix} q_{p_1}^* \\ q_{p_2}^* \\ q_{p_3}^* \\ \vdots \\ q_{p_n}^* \end{bmatrix} = \begin{bmatrix} \pi + 2k_1\pi \\ 2k_2\pi \\ 2k_3\pi \\ \vdots \\ 2k_n\pi \end{bmatrix}. \tag{6.9}$$

$\mathbf{W}_p$ is defined by

$$\mathbf{W}_p = \left\{ (\mathbf{q}_p^*, 0) \;\middle|\; V(\mathbf{q},\dot{\mathbf{q}}) = 0;\ \dot{V}(\mathbf{q},\dot{\mathbf{q}}) = 0 \right\}. \tag{6.10}$$

The invariant sets $\mathbf{W}_u$ and $\mathbf{W}_p$ in figure 6.1 are, evidently, subsets of $\mathbf{W}$, along with the other equilibrium points (found in the invariant set Ω). Therefore

$$\mathbf{W} = \mathbf{W}_u \cup \mathbf{W}_p \cup \Omega, \qquad \mathbf{W}_u \cap \mathbf{W}_p = \varnothing, \qquad \mathbf{W}_u \cap \Omega = \varnothing, \qquad \mathbf{W}_p \cap \Omega = \varnothing.$$

It is important to note that the sets $\mathbf{W}_u$ and $\mathbf{W}_p$ are associated with one unique equilibrium configuration each (the fully-inverted and fully-pendant configuration respectively), whereas the set Ω is associated with multiple unique configurations. With the explicit statement of lemma 6.1, it is evident that the trajectory of the damped unactuated multi-body pendulum system must find a final equilibrium

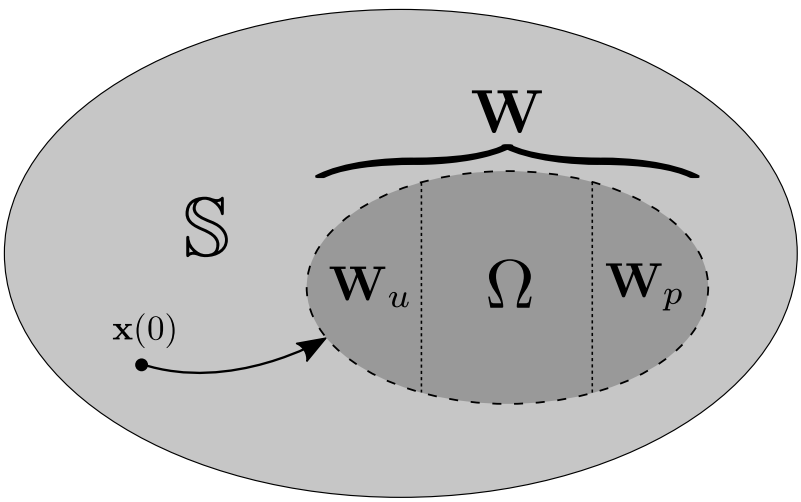

FIGURE 6.1: The invariant sets of the possible equilibrium coefficients found as a subset of $\mathbb{S}$. The system trajectory tends towards the invariant set $\mathbf{W}$ with initial conditions $\mathbf{x}(0)$ according to lemma 6.1.

point within the many subsets of $\mathbf{W}$, each associated with a particular equilibrium configuration. This begs the question: *which invariant set will be the eventual outcome of the system's trajectory?* There is certainly no true answer to this question that can be derived from invariant set theory. There are, however, a couple of considerations that provide substantial context to this problem.

The first consideration involves the relationship between the pendulum system's configuration at each possible equilibrium, the system energy seen at each configuration, and the associated Lyapunov function magnitudes. The argument of this observation is structured according to the following considerations:

(i) The mechanical energy of the pendulum system at any equilibrium point will be solely dependent on the system's potential energy, since $\dot{\mathbf{q}} = 0$ at equilibrium.

(ii) The Lyapunov function is directly proportional to the pendulum system's mechanical energy (as seen in eq. (6.4)).

(iii) The Lyapunov function has a negative semi-definite rate (as seen in eq. (6.6)).

(iv) Therefore, if the pendulum system is initialised with a mechanical energy that is less than that of the potential energy associated with an invariant set $\Phi_a \subset \mathbf{W}$, then the invariant set Φ_a is guaranteed to be excluded as an outcome of the system trajectory. This is because the system is initialised with a smaller Lyapunov function magnitude (step (ii)), and thus the outcome Φ_a cannot be achieved due to step (iii) of this argument.

This observation basically states that it is impossible to have a particular equilibrium configuration as an outcome of the damped system trajectory if the initialised mechanical energy of the system is smaller than that of the potential energy associated with the equilibrium configuration. Therefore, a number of invariant sets demonstrated in figure 6.2 can be excluded as possible outcomes according to the system's initialised mechanical energy. This concept is termed *configurational exclusion*, whereby the DIP contains four equilibrium points, namely the UEP, the Partially-Inverted Equilibrium Point (PIEP), the Partially-Pendant Equilibrium Point (PPEP) and the FPEP.

Another observation is made concerning the stability of each possible equilibrium configuration found in the invariant set $\mathbf{W}$. It is evident that the FPEP is stable, because the Lyapunov function associated with the invariant set $\mathbf{W}_p$ is zero. This represents the absolute minimum of the Lyapunov function. Any small disturbances about this equilibrium point will simply cause the system to drive back towards the FPEP once again, thus demonstrating asymptotic stability about this equilibrium point. This is not, however, true for the other equilibrium configurations. The positive semi-definite nature of the Lyapunov function for all other invariant sets has the potential to decay because the associated Lyapunov functions are all non-zero. Any disturbances about these equilibrium points will cause the system to tend towards

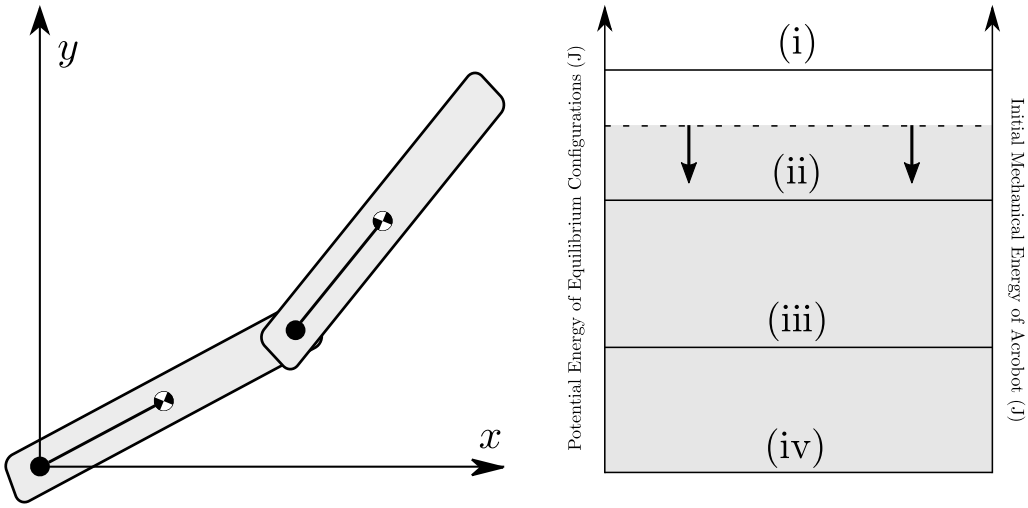

FIGURE 6.2: The principle of configurational exclusion. The Acrobot (left) is initialised with a mechanical energy (dashed line) that is lower than the potential energy found at the UEP (i), but is larger than the potential energies of the PIEP (ii), PPEP (iii) and the FPEP (iv). The invariant set associated with the UEP is thus excluded.

the pendant equilibrium point, where the associated Lyapunov function is zero.

Both of these observations lead to the expansion of lemma 6.1, which is stated as lemma 6.2

Lemma 6.2. The trajectory of a damped unactuated pendulum system is guaranteed to have a final outcome that is found within the invariant set $\mathbf{W}$, with the most probable outcome being the invariant set $\mathbf{W}_p$. Achieving an outcome in the sets $\mathbf{W}_u$ or Ω is improbable since the equilibrium points associated with these sets are locally unstable. Additionally, the equilibrium points found within the invariant set $\mathbf{W}_u$ and sets in Ω can potentially be excluded as an outcome candidate if the pendulum system is initialised with a smaller mechanical energy as compared to the potential energy associated with these equilibrium points.

6.3.2 Results

The effects of lemma 6.2 are simulated on an unactuated DIP for demonstration purposes (where the dynamical equations of the DIP are shown in section 7.4). Viscous damping friction is included in both the proximal and distal joints, with damping coefficients $b_1 = 5$ and $b_2 = 5$. The dynamics of the DIP are described by

$$\ddot{\mathbf{q}} = \mathbf{M}^{-1}(\mathbf{q})\left(-\mathbf{D}(\mathbf{q}, \dot{\mathbf{q}}) - \mathbf{K}(\mathbf{q})\right)$$

where the coefficient matrices are described in section 7.4. The $\mathbf{D}(\mathbf{q}, \dot{\mathbf{q}}$ matrix is populated with the viscous damping torques found in the $\mathbf{R}(\dot{\mathbf{q}})$ matrix. The masses, moments of inertia, and the lengths of the pendulums in the system accommodate the undamped oscillatory behaviour of the pendulum system, which is not expected to tend toward any invariant set. The integration of a non-zero damping coefficient b_2 causes the system to tend towards the FPEP, as proved by the analytical derivation in the previous section. Energy is thus dissipated from the system in this manner. The mechanical energy of the system is selected to represent the Lyapunov function. This function is related to the dynamical behaviour of the system, which is described by the aforementioned physical properties, but the function is a tool that can be used to predict the behaviour of the system. In this instance, we predicted that the system will tend towards an invariant set (represented by the FPEP) if the pendulum system is undamped. The function cannot predict the degree of damping in the behaviour of the system (i.e. whether the system is underdamped or critically damped for instance), but the function can be used to determine the final destination of the system trajectory.

The parameters of the DIP in this experiment are described by

$$\begin{aligned} m_1 &= 1 \text{ kg}, & L_1 &= 1 \text{ m}, \\ m_2 &= 1 \text{ kg}, & L_2 &= 2 \text{ m}, \\ l_1 &= 0.5 \text{ m}, & I_1 &= 0.083 \text{ kg.m}^2, \\ l_2 &= 1 \text{ m}, & I_2 &= 0.33 \text{ kg.m}^2. \end{aligned}$$

The DIP is initialised in the fully-horizontal configuration, described by the initial conditions

$$\begin{aligned} q_1(0) &= \theta(0) = \frac{\pi}{2}, & q_2(0) &= \alpha(0) = 0, \\ \dot{q}_1(0) &= \dot{\theta}(0) = 0, & \dot{q}_2(0) &= \dot{\alpha}(0) = 0. \end{aligned}$$

With these initial conditions in mind, it is apparent that the invariant sets associated with the partially-inverted and fully-inverted configurations are excluded from the potential choices of final trajectory outcomes as specified in lemma 6.2. The results of this simulation are demonstrated in figures 6.3-6.5. The behaviour of the proximal pendulum demonstrated in figure 6.3 oscillated for approximately 14 seconds before it settled at the FPEP ($-\pi$ rad for q_1). Similarly, the distal pendulum oscillates for the same amount of time before settling at the FPEP (0 rad for q_2). The pendulums tend towards the FPEP due to the presence of viscous damping friction, which dissipates energy from the system. The viscous damping friction introduces an explicitly time-dependent component into the Hamiltonian, which produces an asymmetrically time-translational system which, in turn, prevents energy conservation in the system (see section 3.2.2). The Lyapunov function that is represented in figure 6.5 tends towards the invariant set $\mathbf{W}_p$ as derived.

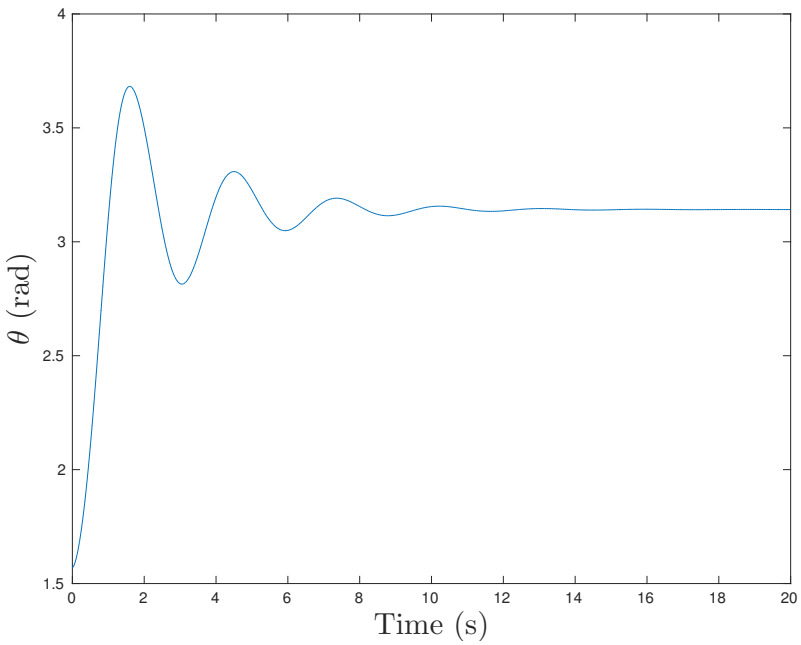

FIGURE 6.3: Angular displacement of the proximal pendulum of a damped DIP.

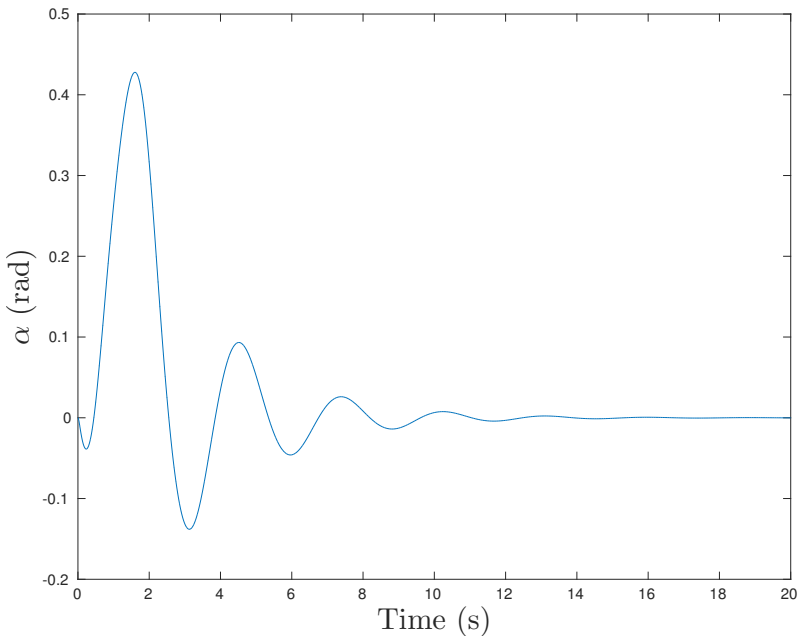

FIGURE 6.4: Angular displacement of the distal pendulum of a damped DIP.

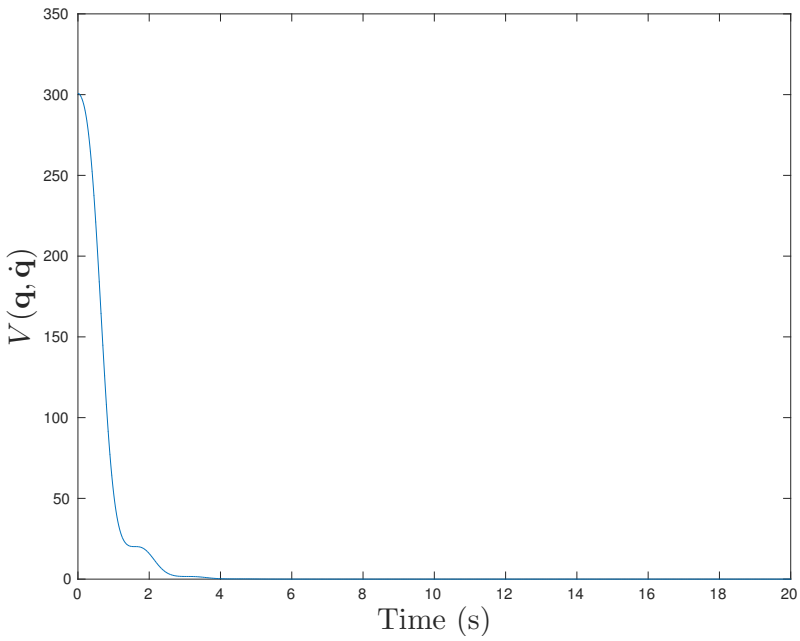

FIGURE 6.5: The behaviour of the Lyapunov function for a DIP shown in eq. (6.4).

6.4 Conclusion

The mathematical representation of the viscous damping friction model for multi-body pendulum systems was explicitly described in this chapter using supporting evidence from existing literature. The model may now be integrated into the conventional compound pendulum system as part of the model alteration discussed in the research methodology. Additionally, we analytically proved that the damped unactuated system will always tend toward some stable equilibrium point using LDM, regardless of whether the system is linear or nonlinear. This was done in an effort to describe the effects of viscous damping and provide the reader with an intuitive understanding of the behaviour of unactuated damped systems. Simulated results of this concept are provided for the unactuated and viscously damped DIP.

"Have you ever wondered if there was more to life, other than being really, really, ridiculously good looking?"

— Derek Zoolander

Chapter 7

Modelling

7.1 Chapter Overview

The objective of this chapter is to demonstrate the derivation the generalised mathematical model of the PA_{n-1} robot. This generalised classification encompasses a group of systems which include the Acrobot and the PAA robot, whose derivations are included this chapter as they will be used for swing-up control simulation in the chapters that follow. Preliminary assumptions and constraints are first stated to set the groundwork of the modelling procedure. The PA_{n-1} robot is subsequently modelled with the energy modelling methodology described in section 3.3 and using Virtual Composite Links (VCLs). The PA_{n-1} modelling procedures are followed by a discussion of the constraints of the PA_{n-1} robot, specifically referencing the work of Oriolo and Nakamura in [38]. These discussions lead to the derivation of the mathematical models of both the Acrobot and the PAA robot, which will be used to produce simulated results in later chapters. VCL coordinate transformations are also discussed since PA_{n-1} derivatives with system order $n > 2$ cannot be modelled conventionally if the execution of LDM-related swing-up control is desired.

7.2 Preliminaries

The PA_{n-1} robot is characterised by the following properties:

(1) The mass of each pendulum is represented as a point mass located at the centre of mass (COM) of the pendulum.

(2) The pendulums are modelled as rigid 1-dimensional rods (described only by a length) and are not deformable.

(3) The moment of inertia of each pendulum (I_i) subscribes to the inequality

$$I_i \leq m_i L_i l_i - m_i {l_i}^2. \tag{7.1}$$

These parameters are described in section 7.3. The moment of inertia of a rigid 1-dimensional rod is, however, typically described by

$$I_i = \frac{m_i L_i}{12} \tag{7.2}$$

as seen in [82, 105].

(4) The parameters of the system are constructed to ensure that the conditions

$$\beta_n \neq \beta_{n-1}, \qquad \beta_i > \sum_{j=i+1}^{n} \beta_j, \qquad \text{for } 2 \leq i < n-2$$

are satisfied. This set of conditions is derived and discussed in section 7.3.2.

(5) The system is square, having the same number of inputs as outputs.

(6) The system is affine in control.

(7) The term *proximal* is used to describe a pendulum that is closer to the joint found at the origin of the plane (i.e. the position of the first joint) when the system is fully-extended, whereas the term *distal* is used to describe a pendulum that is found further away from the origin of the plane when the system is fully extended. A system that is fully extended is described by $q_i = 0$ where $2 < i \leq n$.

The pendulum system operates under the following constraints:

(1) The system is constrained to a 2-dimensional plane.

(2) The pendulum systems introduced in this research operate under both holonomic and 2nd order nonholonomic constraints. This is thoroughly discussed in section 7.3.3.

Additionally, the following models are derived using the RCS, as discussed in section 2.3.

7.3 The PA$_{n-1}$ Robot

7.3.1 Modelling System Dynamics using the Energy Modelling Method

The n-link pendulum system has been modelled extensively using the traditional Lagrangian modelling method, as seen in [5, 6, 34]. It would be appropriate in this instance to add to this broad body of knowledge by deriving the mathematical model of the n-link pendulum using an alternative procedure, namely the energy modelling method outlined in section 3.3. The following formulation of the n-link pendulum model using the energy modelling method is thus conducted according to the stepwise structure as seen in section 3.3.4. This formulation does not consider

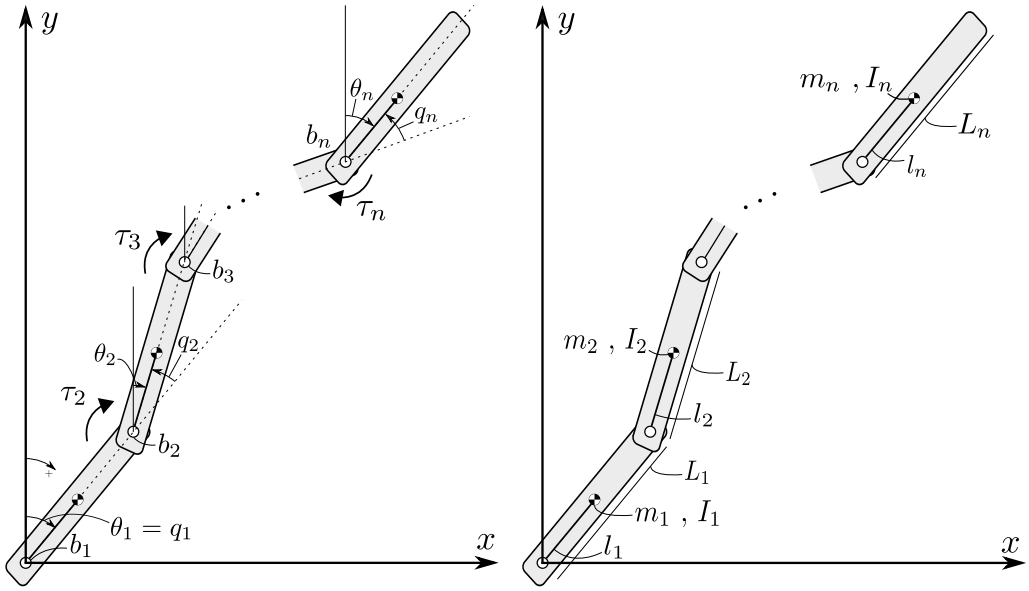

FIGURE 7.1: Generalised n-Link pendulum model. Adapted from [5].

all cases of the n-link pendulum system, but rather includes the explicit modelling of only the PA_{n-1} version of the n-link pendulum system, as discussed in the literature review. The modelling of the PA$_{n-1}$ robot is thus demonstrated below:

(1) Consider the generalised planar n-link pendulum system in figure 7.1. Each pendulum of the system (described generally as the ith pendulum) is characterised by the following properties:

   (i) mass (m_i),

   (ii) moment of inertia (I_i),

   (iii) length (L_i), and

   (iv) COM length (l_i)

   where $i = 1, 2, \ldots, n$. Additionally, the joints in the system may be actuated (τ_i) and viscously damped (with viscous damping friction coefficient b_i). The position of the pendulums in space can be measured using an angular coordinate system as opposed to conventional Cartesian coordinates; this is made possible by the system's intrinsic holonomic constraints [5]. This is discussed in more detail in section 7.3.3. Angular displacement of each pendulum is measured with reference to the y-axis (θ_i) and with reference to the preceding pendulum (q_i) [5]. These coordinates, known as the absolute and relative generalised coordinates, are represented in vector form, whereby

$$\theta = \begin{bmatrix}\theta_1 & \theta_2 & \ldots & \theta_n\end{bmatrix}^{\mathbf{T}}, \quad \mathbf{q} = \begin{bmatrix}q_1 & q_2 & \ldots & q_n\end{bmatrix}^{\mathbf{T}} \tag{7.3}$$

and where θ_i may be calculated as a summation of the preceding relative generalised coordinates described by

$$\theta_i = \sum_{k=1}^{i} q_k. \tag{7.4}$$

This is expressed in matrix format as

$$\theta = A\mathbf{q}, \quad \mathbf{q} = A^{-1}\theta \tag{7.5}$$

where

$$A = \begin{bmatrix} 1 & 0 & \dots & 0 \\ 1 & \ddots & \ddots & \vdots \\ \vdots & \ddots & 1 & 0 \\ 1 & \dots & 1 & 1 \end{bmatrix}, \quad A^{-1} = \begin{bmatrix} 1 & 0 & \dots & 0 & 0 \\ -1 & 1 & \ddots & \vdots & \vdots \\ 0 & -1 & \ddots & 0 & 0 \\ \vdots & \ddots & \ddots & 1 & 0 \\ 0 & \dots & 0 & -1 & 1 \end{bmatrix} \tag{7.6}$$

[5]. The principle of virtual work relates the torque applied to the system measured with reference to the y-axis ($\mathbf{u}_{\theta_i}$) and the torque applied to the system measured with reference to the preceding pendulum ($\mathbf{u}_i$), whereby

$$\mathbf{G}(\mathbf{q})\mathbf{u} = A^{\mathbf{T}}\mathbf{G}_\theta\mathbf{u}_\theta, \quad \mathbf{G}_\theta\mathbf{u}_\theta = \left(A^{\mathbf{T}}\right)^{-1}\mathbf{G}(\mathbf{q})\mathbf{u}. \tag{7.7}$$

(2) The mechanical energy of the n-link pendulum system, E_s, is calculated using

$$E_s = \sum_{i=1}^{n} \Big[T_i + P_i\Big]. \tag{7.8}$$

Following the technique demonstrated in [5], and using the information derived in the previous step, we find that

$$\begin{aligned} \mathbf{P} &= \sum_{i=1}^{n} P_i = \sum_{i=1}^{n} m_i g \sum_{j=1}^{n} l_{ij} \cos\theta_j \\ &= \sum_{j=1}^{n} \left[\sum_{i=1}^{n} m_i g l_{ij}\right] \cos\theta_j \\ &= \sum_{j=1}^{n} \beta_j \cos\theta_j \end{aligned} \tag{7.9}$$

where

$$\beta_j = \sum_{i=1}^{n} m_i g l_{ij} = m_j g l_j + g L_j \sum_{i=j+1}^{n} m_i.$$

Therefore

$$\mathbf{K}(\mathbf{q}) = A^{\mathbf{T}} \mathbf{K}_\theta(A\mathbf{q}) \tag{7.10}$$

where

$$\begin{aligned} \mathbf{K}_\theta &= \frac{\partial \mathbf{P}}{\partial \theta} \\ &= \begin{bmatrix} \frac{\partial \mathbf{P}}{\partial \theta_1} & \frac{\partial \mathbf{P}}{\partial \theta_2} & \dots & \frac{\partial \mathbf{P}}{\partial \theta_n} \end{bmatrix}^{\mathbf{T}}. \end{aligned} \tag{7.11}$$

Additionally, we find that

$$\mathbf{M}(\mathbf{q}) = A^{\mathbf{T}} \mathbf{M}_\theta(A\mathbf{q}) A \tag{7.12}$$

where

$$\Big[\mathbf{M}_\theta\Big]_{jk} = \alpha_{jk} \cos(\theta_j - \theta_k) \tag{7.13}$$

and

$$\alpha_{jk} = \begin{cases} I_j + m_j l_j^2 + {L_i}^2 \sum_{i=j+1}^{n} m_i & \text{if } j = k; \\ m_j l_j L_k + L_j L_k \sum_{i=j+1}^{n} m_i & \text{if } j \neq k. \end{cases}. \tag{7.14}$$

(3) The change in the mechanical energy with respect to time $\left(\frac{\mathrm{d}}{\mathrm{dt}} E_s\right)$ is represented as

$$\frac{\mathrm{d}}{\mathrm{dt}} E_s = \dot{\mathbf{q}}^{\mathrm{T}} \mathbf{M}(\mathbf{q}) \ddot{\mathbf{q}} + \frac{1}{2} \dot{\mathbf{q}}^{\mathrm{T}} \dot{\mathbf{M}}(\mathbf{q}) \dot{\mathbf{q}} + \dot{\mathbf{q}}^{\mathrm{T}} \mathbf{K}(\mathbf{q}) \tag{7.15}$$

which was originally derived in [93].

(4) The factors that have the potential to add/dissipate energy through actuation, and dissipate energy purely through damping in the system are grouped up in the $\mathbf{q}^{\mathbf{T}} \mathbf{G}(\mathbf{q}) \mathbf{u}$ and $\mathbf{q}^{\mathbf{T}} \mathbf{R}(\dot{\mathbf{q}})$ matrices respectively. In the PA_{n-1} robot version of the n-link pendulum, there are actuators found at each link except for the most proximal joint to the origin [5]. The actuation in the system can, thus, be represented as

$$\begin{aligned} \mathbf{G}(\mathbf{q})\mathbf{u} &= \begin{bmatrix} 0 & \tau_2 & \tau_3 & \dots & \tau_n \end{bmatrix}^{\mathbf{T}} \\ &= \tau, \\ \therefore \quad \dot{\mathbf{q}}^{\mathbf{T}} \mathbf{G}(\mathbf{q})\mathbf{u} &= \dot{\mathbf{q}}^{\mathbf{T}} \tau \\ &= \dot{q}_2 \tau_2 + \dot{q}_3 \tau_3 + \dots + \dot{q}_{n-1} \tau_{n-1} + \dot{q}_n \tau_n \\ &= \sum_{i=2}^{n} \dot{q}_i \tau_i \end{aligned}$$

where I_n represents a $n \times n$ identity matrix. The only lossy torques that exist intrinsically in the system, as predefined for this research, are the viscous damping torques that may occur at each joint. The mathematical model of the viscous damping phenomenon was described explicitly in section 6.2 by

$$\mathbf{R}(\dot{\mathbf{q}}) = \begin{bmatrix} b_1\dot{q}_1 & b_2\dot{q}_2 & \dots & b_{n-1}\dot{q}_{n-1} & b_n\dot{q}_n \end{bmatrix}^{\mathbf{T}} \tag{7.16}$$

where b_i represents the specific damping coefficient for the associated joint of the ith pendulum that is most proximal to the origin. Therefore

$$\begin{aligned} \dot{\mathbf{q}}^{\mathbf{T}}\mathbf{R}(\dot{\mathbf{q}}) &= b_1\dot{q}_1^2 + b_2\dot{q}_2^2 + \cdots + b_{n-1}\dot{q}_{n-1}^2 + b_n\dot{q}_n^2 \\ &= \sum_{i=1}^{n} b_i\dot{q}_i^2. \end{aligned}$$

The total change of energy in the system with respect to time is represented as

$$\begin{aligned} \frac{\mathrm{d}}{\mathrm{dt}}E_s &= \dot{\mathbf{q}}^{\mathbf{T}}\mathbf{G}(\mathbf{q})\mathbf{u} - \dot{\mathbf{q}}^{\mathbf{T}}\mathbf{R}(\dot{\mathbf{q}}) \\ &= -b_1\dot{q}_1^2 + \sum_{i=2}^{n} \dot{q}_i(\tau_i - b_i\dot{q}_i). \end{aligned}$$

This is, evidently, equivalent to the expression seen in eq. (7.15), whereby

$$\begin{aligned} \frac{\mathrm{d}}{\mathrm{dt}}E_s &= \dot{\mathbf{q}}^{\mathrm{T}}\mathbf{M}(\mathbf{q})\ddot{\mathbf{q}} + \frac{1}{2}\dot{\mathbf{q}}^{\mathrm{T}}\dot{\mathbf{M}}(\mathbf{q})\dot{\mathbf{q}} + \dot{\mathbf{q}}^{\mathrm{T}}\mathbf{K}(\mathbf{q}) = \dot{\mathbf{q}}^{\mathbf{T}}\mathbf{G}(\mathbf{q})\mathbf{u} - \dot{\mathbf{q}}^{\mathbf{T}}\mathbf{R}(\dot{\mathbf{q}}) \\ &= -b_1\dot{q}_1^2 + \sum_{i=2}^{n} \dot{q}_i(\tau_i - b_i\dot{q}_i). \end{aligned}$$

(5) The energy-shuffling vector $\mathbf{J}(\mathbf{q}, \dot{\mathbf{q}})\dot{\mathbf{q}}$ is calculated using

$$\mathbf{J}(\mathbf{q}, \dot{\mathbf{q}})\dot{\mathbf{q}} = \frac{1}{2}\dot{\mathbf{M}}(\mathbf{q}, \dot{\mathbf{q}})\dot{\mathbf{q}} - \left[\frac{\partial}{\partial \mathbf{q}}\left(\frac{1}{2}\dot{\mathbf{q}}^{\mathbf{T}}\mathbf{M}(\mathbf{q})\dot{\mathbf{q}}\right)\right]^{\mathbf{T}} \tag{7.17}$$

which was derived in section 3.3.3. This is not solved for in the case of the n-link pendulum, but instead may be implemented once n is defined. The entries of the square skew-symmetric matrix $\mathbf{J}(\mathbf{q}, \dot{\mathbf{q}})$ may be solved for deductively once the energy-shuffling matrix is calculated. It is important to note that the skew-symmetric properties of the $\mathbf{J}(\mathbf{q}, \dot{\mathbf{q}})$ matrix produces the quadratic result

$$\dot{\mathbf{q}}^{\mathbf{T}}\mathbf{J}(\mathbf{q}, \dot{\mathbf{q}})\dot{\mathbf{q}} = 0. \tag{7.18}$$

It is evident from this result that no power contribution is observed in the system as a result of the torques involved in energy shuffling. The quadratic form seen in eq. (7.18) can, therefore, be included in the system power equation

inconsequentially, whereby

$$\dot{\mathbf{q}}^{\mathrm{T}}\mathbf{M}(\mathbf{q})\ddot{\mathbf{q}} + \frac{1}{2}\dot{\mathbf{q}}^{\mathrm{T}}\dot{\mathbf{M}}(\mathbf{q},\dot{\mathbf{q}})\dot{\mathbf{q}} + \dot{\mathbf{q}}^{\mathrm{T}}\mathbf{K}(\mathbf{q}) = \dot{\mathbf{q}}^{\mathbf{T}}\mathbf{G}(\mathbf{q})\mathbf{u} - \dot{\mathbf{q}}^{\mathbf{T}}\mathbf{R}(\dot{\mathbf{q}}) - \dot{\mathbf{q}}^{\mathbf{T}}\mathbf{J}(\mathbf{q},\dot{\mathbf{q}})\dot{\mathbf{q}}. \tag{7.19}$$

(6) The system power equation seen in eq. (7.19) may be manipulated to produce the prototypical form through the implementation of the procedure that follows.

The system power equation is transformed into the system torque equation through the elimination of the common velocity vector $\dot{\mathbf{q}}^{\mathbf{T}}$. Therefore

$$\mathbf{M}(\mathbf{q})\ddot{\mathbf{q}} + \frac{1}{2}\dot{\mathbf{M}}(\mathbf{q},\dot{\mathbf{q}})\dot{\mathbf{q}} + \mathbf{K}(\mathbf{q}) = \mathbf{G}(\mathbf{q})\mathbf{u} - \mathbf{R}(\dot{\mathbf{q}}) - \mathbf{J}(\mathbf{q},\dot{\mathbf{q}})\dot{\mathbf{q}}. \tag{7.20}$$

The $\mathbf{R}(\dot{\mathbf{q}})$ and $\mathbf{J}(\mathbf{q},\dot{\mathbf{q}})\dot{\mathbf{q}}$ matrices are moved to the left-hand side of the equation and are collectively represented, along with the conservative torques that are associated with the change of the system's configuration $\left(\frac{1}{2}\dot{\mathbf{M}}(\mathbf{q})\dot{\mathbf{q}}\right)$, as the $\mathbf{D}(\mathbf{q},\dot{\mathbf{q}})$ matrix. Therefore

$$\mathbf{M}(\mathbf{q})\ddot{\mathbf{q}} + \underbrace{\frac{1}{2}\dot{\mathbf{M}}(\mathbf{q},\dot{\mathbf{q}})\dot{\mathbf{q}} + \mathbf{R}(\dot{\mathbf{q}}) + \mathbf{J}(\mathbf{q},\dot{\mathbf{q}})\dot{\mathbf{q}}}_{\mathbf{D}(\mathbf{q},\dot{\mathbf{q}})} + \mathbf{K}(\mathbf{q}) = \mathbf{G}(\mathbf{q})\mathbf{u}. \tag{7.21}$$

The final prototypical form is described as

$$\mathbf{M}(\mathbf{q})\ddot{\mathbf{q}} + \mathbf{D}(\mathbf{q},\dot{\mathbf{q}}) + \mathbf{K}(\mathbf{q}) = \mathbf{G}(\mathbf{q})\mathbf{u}. \tag{7.22}$$

The angular acceleration of each DOF may be calculated by inverting the mass matrix $\mathbf{M}(\mathbf{q})$, resulting in

$$\ddot{\mathbf{q}} = \mathbf{M}^{-\mathbf{1}}(\mathbf{q})\Big[\mathbf{G}(\mathbf{q})\mathbf{u} - \mathbf{D}(\mathbf{q},\dot{\mathbf{q}}) - \mathbf{K}(\mathbf{q})\Big] \in \mathbb{R}^n. \tag{7.23}$$

The $\mathbf{D}(\mathbf{q},\dot{\mathbf{q}})$ matrix would, in a general case, be constructed identically to what is seen in eq. (3.29) if the system was subject to nonconservative torques associated with a change in mass or moment of inertia in the system. This phenomenon is not, however, considered in this investigation.

(7) The system is now converted into the state-space representation through the selection of the transformations

$$\begin{aligned} \mathbf{x}_1 &= q_1, & \mathbf{x}_{n+1} &= \dot{q}_1, \\ \mathbf{x}_2 &= q_2, & \mathbf{x}_{n+2} &= \dot{q}_2, \\ &\vdots & &\vdots \end{aligned}$$

$$\mathbf{x}_n = q_n, \qquad \mathbf{x}_{2n} = \dot{q}_n.$$

Therefore

$$\begin{bmatrix} \dot{\mathbf{x}}_1 \\ \dot{\mathbf{x}}_2 \\ \vdots \\ \dot{\mathbf{x}}_n \\ \dot{\mathbf{x}}_{n+1} \\ \dot{\mathbf{x}}_{n+2} \\ \vdots \\ \dot{\mathbf{x}}_{2n} \end{bmatrix} = \begin{bmatrix} \mathbf{x}_{n+1} \\ \mathbf{x}_{n+2} \\ \vdots \\ \mathbf{x}_{2n} \\ f_1(\mathbf{x}) + g_1(\mathbf{x})\mathbf{u}_1 \\ f_2(\mathbf{x}) + g_2(\mathbf{x})\mathbf{u}_2 \\ \vdots \\ f_n(\mathbf{x}) + g_n(\mathbf{x})\mathbf{u}_n \end{bmatrix}$$

where

$$f_i(\mathbf{x}) = \Big[-\mathbf{M}^{-1}(\mathbf{q})\Big(\mathbf{D}(\mathbf{q}, \dot{\mathbf{q}}) + \mathbf{K}(\mathbf{q})\Big)\Big]_i, \qquad g_i(\mathbf{x}) = \Big[\mathbf{M}^{-1}(\mathbf{q})\mathbf{G}(\mathbf{q})\Big]_i.$$

The output $\mathbf{y}(\mathbf{x})$ is chosen according to the control technique, but must have the same number of entries as $\mathbf{u}(t)$ since the system is square (i.e. $\mathbf{y}(\mathbf{x}) \in \mathbb{R}^m$).

7.3.2 The VCL Modelling Protocol

The integration of VCLs into the modelling procedure of a n-link pendulum system was first introduced by Xin and Liu in [5] as a coordinate transformation used to address the breakdown in the formulation of LDM related swing-up control using the conventionally defined Lyapunov candidate function with $n > 2$ (a more detailed discussion of this deficiency is provided in [5, pp. 190-191]). A n-link pendulum system may be represented with $n-1$ VCLs, as shown in figure 7.2, with each VCL intrinsically incorporating the lengths, moments of inertia and masses of the pendulums found distal to an assigned joint [5]. More specifically, VCL$_i$ will account for the lengths, moments of inertia and the masses of the pendulums distal to pendulum $i-1$ (with the COM collectively represented as M_{VCL_i}). Each COM is associated with a newly defined angular displacement $\overline{q}_i$ and a length $\bar{l}_i$ (representing the distance between the COM and its associated joint). It is evident that the new coordinates may be represented by the transformation

$$\overline{q}_i = q_i + \xi_{i+1} \quad \text{for } 2 \leq i < n$$

where $\overline{q}_n = q_n$ [5]. Coordinate vectors are, therefore, defined to represent the coordinate transformation for the entire n-link pendulum, whereby

$$\begin{aligned} \mathbf{q}_a &= \begin{bmatrix} q_2 & q_3 & \dots & q_{n-1} & q_n \end{bmatrix}^{\mathbf{T}} && \text{for } \mathbf{q}_a \in \mathbb{R}^{n-1}, \\ \overline{\mathbf{q}}_a &= \begin{bmatrix} \overline{q}_2 & \overline{q}_3 & \dots & \overline{q}_{n-1} & \overline{q}_n \end{bmatrix}^{\mathbf{T}} && \text{for } \overline{\mathbf{q}}_a \in \mathbb{R}^{n-1}, \text{ and} \\ \xi_a &= \begin{bmatrix} \xi_3 & \xi_4 & \dots & \xi_n & 0 \end{bmatrix}^{\mathbf{T}} && \text{for } \xi_a \in \mathbb{R}^{n-1} \end{aligned}$$

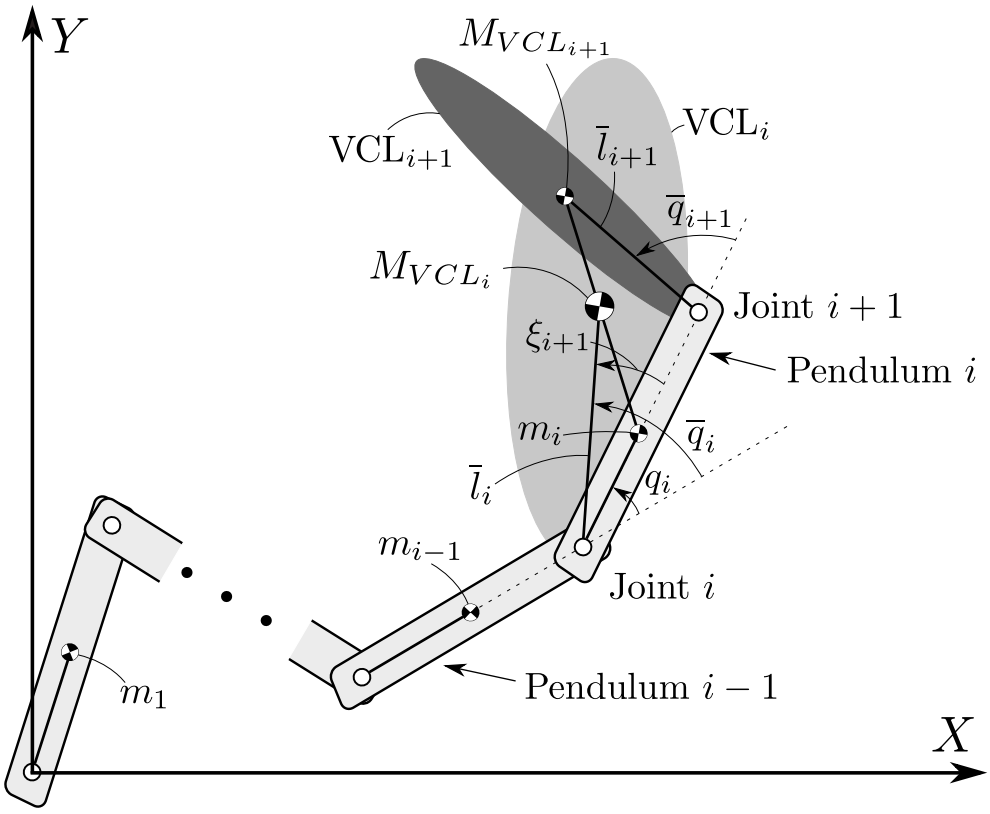

FIGURE 7.2: The implementation of the VCL modelling protocol on the PA_{n-1} robot. Adapted from [5].

with

$$\overline{\mathbf{q}}_a = \mathbf{q}_a + \xi_a.$$

This relationship is not trivial since ξ_a is not well defined in this case. It would be more beneficial to represent the coordinate transformation specifically in terms of $\mathbf{q}_a$, where

$$\overline{\mathbf{q}}_a = \mathbf{T}(\mathbf{q}_a)$$

[5]. It is evident that if the system were to be fully extended, that the two coordinates would directly map to zero, with

$$\overline{\mathbf{q}}_a = 0_{n-1} \longleftrightarrow \mathbf{q}_a = 0_{n-1} \tag{7.24}$$

[5]. The relationship between the VCL transformed coordinates $\overline{\mathbf{q}}_a$ and the generalised coordinates $\mathbf{q}_a$ was derived by Xin in Liu in [5], which results in the coordinate definition

$$\dot{\bar{q}}_i = \dot{q}_i + w_{i+1}\dot{\bar{q}}_{i+1} + v_{i+1}\dot{\overline{\beta}}_{i+1} \quad \text{for } 2 \leq i < n \tag{7.25}$$

and

$$\dot{\overline{\beta}}_i = f_{i+1}\dot{\overline{\beta}}_{i+1} + p_{i+1}\dot{\overline{q}}_{i+1} \tag{7.26}$$

where

$$w_{i+1} = \frac{\overline{\beta}_{i+1}(\beta_i \cos \overline{q}_{i+1} + \overline{\beta}_{i+1})}{\overline{\beta}_i^{\,2}}, \qquad v_{i+1} = \frac{\beta_i \sin \overline{q}_{i+1}}{\overline{\beta}_i^{\,2}},$$

$$f_{i+1} = \frac{\overline{\beta}_{i+1} + \beta_i \cos \overline{q}_{i+1}}{\overline{\beta}_i}, \qquad p_{i+1} = \frac{\overline{\beta}_{i+1}\beta_i \sin \overline{q}_{i+1}}{\overline{\beta}_i}.$$

Additionally, for the nth VCL, we find that

$$\overline{q}_n = q_n, \qquad \dot{\overline{q}}_n = \dot{q}_n, \tag{7.27}$$

$$\overline{\beta}_n = \beta_n, \qquad \dot{\overline{\beta}}_n = 0. \tag{7.28}$$

and

$$\beta_{n-1} \neq \beta_n \qquad \text{for } i = n-1, \text{ and}$$

$$\beta_i > \sum_{j=i+1}^{n} \beta_j \qquad \text{for } 2 \leq i \leq n-2.$$

A high-level description of the down-cascade iteration process is demonstrated below:

Down-cascade iteration procedure

FOR $k = 1 : n-2$

(i) $i = n - k$.

(ii) Solve for $\dot{\overline{q}}_i$ by substituting $\dot{\overline{\beta}}_{i+1}$ and $\dot{\overline{q}}_{i+1}$ into eq. (7.25).

(iii) Solve for $\dot{\overline{\beta}}_i$ by substituting $\dot{\overline{\beta}}_{i+1}$ and $\dot{\overline{q}}_{i+1}$ into eq. (7.26).

END

This procedure is demonstrated for $k = 1 : 3$ as an example in appendix B (Example B.5).

7.3.3 Constraints

The holonomic constraints of the n-link pendulum is demonstrated in figure 7.3. The n-link pendulum system is found, as stated in the preliminaries of this chapter, on a 2-D plane, whereby the position of the COM of each pendulum may be intuitively

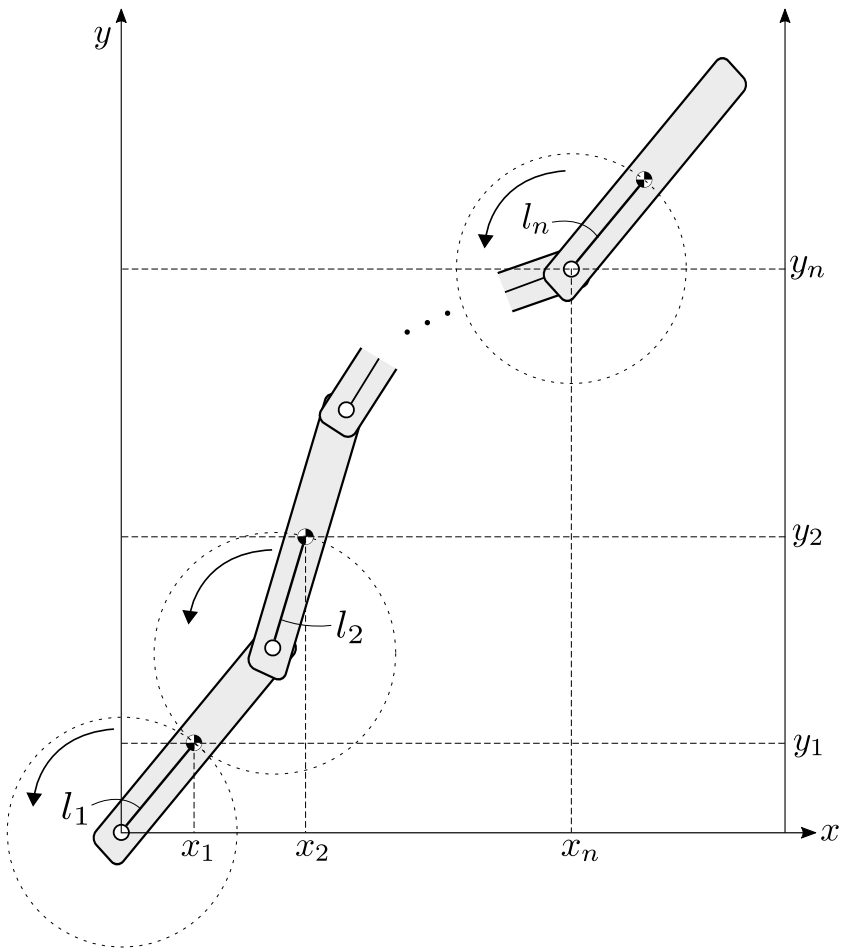

FIGURE 7.3: The holonomic constraints of the n-link pendulum.

described by the Cartesian coordinate (x_i, y_i). It is evident, however, that each pendulum mass cannot be found at any arbitrary coordinate. Instead, each COM is intrinsically constrained to move in a circular trajectory around its corresponding joint. These constraints allow for the transformation of the Cartesian coordinates of each pendulum COM into corresponding *angular coordinates* (θ_i and q_i). These constraints are mathematically described for the n-link pendulum system as

$$
\begin{aligned}
\mathbf{f}_1(\mathbf{x}, \mathbf{y}, t) &= x_1^2 + y_1^2 - l_1^2 = 0, \\
\mathbf{f}_2(\mathbf{x}, \mathbf{y}, t) &= \Big(x_2 - 2x_1\Big)^2 + \Big(y_2 - 2y_1\Big)^2 - l_2^2 = 0, \\
&\vdots \\
\mathbf{f}_n(\mathbf{x}, \mathbf{y}, t) &= \Big(x_n - 2\textstyle\sum_{j=1}^{n-1} x_j\Big)^2 + \Big(y_n - 2\textstyle\sum_{j=1}^{n-1} y_j\Big)^2 - l_i^2 = 0
\end{aligned}
$$

[106]. Therefore

$$\mathbf{f}_i(\mathbf{x}, \mathbf{y}, t) = \left(x_i - 2\sum_{j=1}^{i-1} x_j \right)^2 + \left(y_i - 2\sum_{j=1}^{i-1} y_j \right)^2 - l_i^2 = 0 \tag{7.29}$$

where $1 \leq i \leq \mathrm{n}$, $i \in \mathbb{Z}$. These constraints are strictly autonomous and are at least second-order differentiable, whereby constraints for the velocity and acceleration vectors of each pendulum can be directly derived from the original positional constraint. These constraints are therefore classified as *holonomic* [106]. Each pendulum, having a holonomic constraint $\mathbf{f}_i(\mathbf{x}, \mathbf{y}, t)$, can now be described by one DOF represented by the generalised angular coordinate q_i or θ_i (see section 7.3.1).

The aforementioned holonomic constraints of a pendulum system are evidently independent of the effect of actuation as they are constructed to accommodate the transformation between Cartesian and angular coordinates, a process that occurs before the definition of the prototypical form containing the control input vector. In the case of a fully-actuated undamped n-link pendulum system, each dynamical equation is associated with a control input, whereby

$$\begin{aligned}
&\mathbf{M}_1(\mathbf{q})\ddot{\mathbf{q}} + \mathbf{C}_1(\mathbf{q},\dot{\mathbf{q}}) + \mathbf{K}_1(\mathbf{q}) = \tau_1, \\
&\mathbf{M}_2(\mathbf{q})\ddot{\mathbf{q}} + \mathbf{C}_2(\mathbf{q},\dot{\mathbf{q}}) + \mathbf{K}_2(\mathbf{q}) = \tau_2, \\
&\quad\vdots \\
&\mathbf{M}_n(\mathbf{q})\ddot{\mathbf{q}} + \mathbf{C}_n(\mathbf{q},\dot{\mathbf{q}}) + \mathbf{K}_n(\mathbf{q}) = \tau_n
\end{aligned}$$

and where

$$\mathbf{M}_i(\mathbf{q}) = \begin{bmatrix} M_{i1}(\mathbf{q}) & M_{i2}(\mathbf{q}) & \dots & M_{in}(\mathbf{q}) \end{bmatrix} \in \mathbb{R}^n$$

with $1 \leq i \leq n$. In this case, the dynamics of each pendulum may be completely linearised by the control input, transforming the nonlinear dynamics of the pendulum system into a linear plant (this procedure is known as full-state feedback linearisation, and is discussed in section 5.3). Any constraints imposed by the natural dynamics of the system can, therefore, be negated effectively with the use of this control technique [2]. This is not the case with undamped underactuated systems, whose prototypical form may be generally described by m actuated dynamical equations and $n - m$ unactuated dynamical equations, described by

$$\begin{aligned}
&\mathbf{M}_1(\mathbf{q})\ddot{\mathbf{q}} + \mathbf{C}_1(\mathbf{q},\dot{\mathbf{q}}) + \mathbf{K}_1(\mathbf{q}) = \tau_1, \\
&\quad\vdots \\
&\mathbf{M}_m(\mathbf{q})\ddot{\mathbf{q}} + \mathbf{C}_m(\mathbf{q},\dot{\mathbf{q}}) + \mathbf{K}_m(\mathbf{q}) = \tau_m, \\
&\mathbf{M}_{m+1}(\mathbf{q})\ddot{\mathbf{q}} + \mathbf{C}_{m+1}(\mathbf{q},\dot{\mathbf{q}}) + \mathbf{K}_{m+1}(\mathbf{q}) = 0, \\
&\quad\vdots
\end{aligned}$$

$$\mathbf{M}_n(\mathbf{q})\ddot{\mathbf{q}} + \mathbf{C}_n(\mathbf{q},\dot{\mathbf{q}}) + \mathbf{K}_n(\mathbf{q}) = 0$$

[106]. These equations can be represented in matrix form as

$$\begin{bmatrix}\mathbf{M}_a(\mathbf{q})\\ \mathbf{M}_u(\mathbf{q})\end{bmatrix}\begin{bmatrix}\ddot{\mathbf{q}}_a\\ \ddot{\mathbf{q}}_u\end{bmatrix} + \begin{bmatrix}\mathbf{C}_a(\mathbf{q},\dot{\mathbf{q}})\\ \mathbf{C}_u(\mathbf{q},\dot{\mathbf{q}})\end{bmatrix} + \begin{bmatrix}\mathbf{K}_a(\mathbf{q})\\ \mathbf{K}_u(\mathbf{q})\end{bmatrix} = \begin{bmatrix}\tau\\ 0\end{bmatrix} \tag{7.30}$$

[38]. It is evident that full-feedback linearisation cannot be applied in this instant due to the distinct lack of actuators. The unactuated entries of the prototypical form may, therefore, be seen as a constraint that is defined as

$$\mathbf{M}_j(\mathbf{q})\ddot{\mathbf{q}} + \mathbf{C}_j(\mathbf{q},\dot{\mathbf{q}}) + \mathbf{K}_j(\mathbf{q}) = \mathbf{h}_j(\ddot{\mathbf{q}}, \dot{\mathbf{q}}, \mathbf{q}, \mathrm{t}) = 0 \tag{7.31}$$

where $m < j \leq n$ for the generalised form [38]. According to the proof provided in [38], the constraints seen in eq. (7.31) are classified as second-order nonholonomic constraints if:

(1) The mass matrix $\mathbf{M}_j$ is not dependent on the unactuated generalised coordinates $\mathbf{q_u}$.

(2) The gravitational torque $\mathbf{K}_j$ is not dependent on any generalised coordinate $\mathbf{q}$.

In the case of the n-link pendulum, it can be shown that the first condition is satisfied only if the joint related to the first generalised coordinate q_1 is the only unactuated joint in the system. This is true because the mass matrix $\mathbf{M}_j$ is never dependent on q_1. A proof of this independence is included in appendix A (Proof A.2). Despite the apparent possibility of satisfying the first condition for partial integrability, the vertical pendulum system is subject to gravitational torques that are dependent on the generalised coordinate system $\mathbf{q}$. The vertical underactuated n-link pendulum system, therefore, contains a combination of holonomic constraints (eq. 7.29) and second-order nonholonomic constraints, represented by the underactuated dynamical equations seen in eq. (7.31).

With the model for the PA_{n-1} robot clearly defined, we will now model the simplest derivatives of the PA_{n-1} robot, namely the Acrobot and the PAA robot. These models will be used to demonstrate simulated results in the chapters that follow.

7.4 The Acrobot

The Acrobot is a variation of the underactuated double-pendulum system and is the least complex derivative of the PA_{n-1} robot, and is demonstrated in figure 7.1). The Acrobot is characterised by an unactuated proximal joint (a) and an actuated distal joint (b) (this is conversely true for the other variation of underactuated double-pendulum system, the Pendubot) [15]. Each pendulum is associated with a mass (m_1 and m_2), a moment of inertia (I_1 and I_2), a length (L_1 and L_2) and a COM length (l_1 and l_2). Additionally, the joints may be subjected to viscous damping, and are

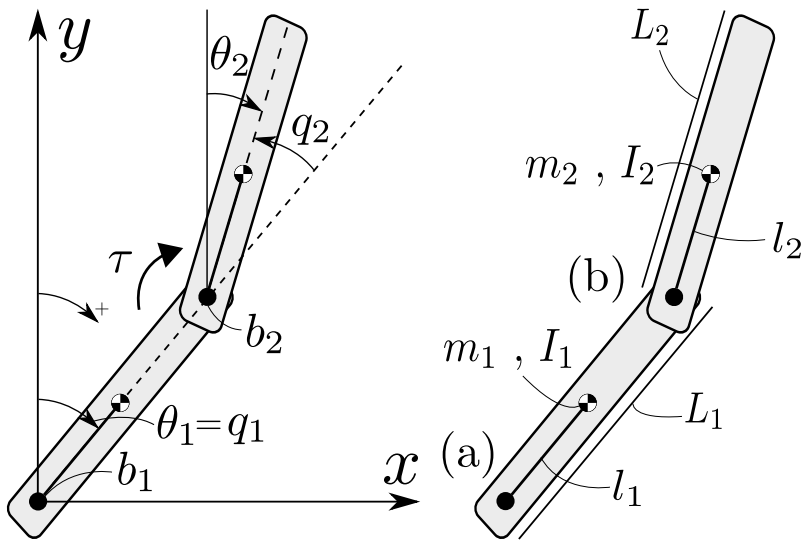

FIGURE 7.4: The Acrobot model. Adapted from [6].

thus each associated with a corresponding damping coefficient (b_1 for the proximal joint and b_2 for the distal joint).

The equations of motion for the Acrobot will be derived using the procedure highlighted in section 3.3.4 as seen with the case of the n-link pendulum (see section 7.3.1).

(1) The position of the proximal and distal pendulums can thus be described by generalised coordinates θ_1 and θ_2 (measured with respect to the y-axis) or generalised coordinates q_1 and q_2 respectively (measured with respect to the preceding pendulum. See figure 7.4). These generalised coordinates are represented in vector form as

$$\theta = \begin{bmatrix}\theta_1 & \theta_2\end{bmatrix}^{\mathbf{T}}, \qquad \mathbf{q} = \begin{bmatrix}q_1 & q_2\end{bmatrix}^{\mathbf{T}}$$

where the entries of the θ matrix are related to the entries of the generalised coordinate matrix $\mathbf{q}$ by

$$\theta_1 = q_1, \qquad \theta_2 = q_1 + q_2, \qquad q_2 = \theta_2 - \theta_1. \tag{7.32}$$

Therefore

$$\theta = A\mathbf{q}, \qquad \mathbf{q} = A^{-1}\theta$$

where

$$A = \begin{bmatrix}1 & 0\\ 1 & 1\end{bmatrix}, \qquad A^{-1} = \begin{bmatrix}1 & 0\\ -1 & 1\end{bmatrix}.$$

(2) Using [5], we find that

$$\mathbf{K}(\mathbf{q}) = \begin{bmatrix} -\beta_1 \sin q_1 - \beta_2 \sin(q_1 + q_2) \\ -\beta_2 \sin(q_1 + q_2) \end{bmatrix}$$

and

$$\mathbf{M}(\mathbf{q}) = \begin{bmatrix} \alpha_1 + \alpha_2 + 2\alpha_3 \cos q_2 & \alpha_2 + \alpha_3 \cos q_2 \\ \alpha_2 + \alpha_3 \cos q_2 & \alpha_2 \end{bmatrix}$$

where

$$\begin{aligned} \alpha_{11} &= \alpha_1 = I_1 + m_1 {l_1}^2 + m_2 {L_1}^2, \\ \alpha_{22} &= I_2 + m_2 {l_2}^2, \\ \alpha_{12} &= \alpha_{21} = \alpha_3 = m_2 L_1 l_2 \end{aligned}$$

and

$$\beta_1 = g(m_1 l_1 + m_2 L_1), \qquad \beta_2 = g m_2 l_2.$$

(3) The change in energy (power equation) of any system is trivially solved as

$$\frac{\mathrm{d}}{\mathrm{dt}} E_s = \dot{\mathbf{q}}^{\mathrm{T}} \mathbf{M}(\mathbf{q}) \ddot{\mathbf{q}} + \frac{1}{2} \dot{\mathbf{q}}^{\mathrm{T}} \dot{\mathbf{M}}(\mathbf{q}) \dot{\mathbf{q}} + \dot{\mathbf{q}}^{\mathrm{T}} \mathbf{K}(\mathbf{q}). \tag{7.33}$$

(4) The Acrobot is characterised by a single actuator found in its distal link. The actuation in the Acrobot is, thus, represented as

$$\begin{aligned} \mathbf{G}(\mathbf{q})\mathbf{u} &= \begin{bmatrix} 0 & \tau_2 \end{bmatrix}^{\mathbf{T}} \\ &= \tau. \end{aligned}$$

The power associated with the system actuator is represented by

$$\begin{aligned} \dot{\mathbf{q}}^{\mathbf{T}} \mathbf{G}(\mathbf{q})\mathbf{u} &= \dot{\mathbf{q}}^{\mathbf{T}} \tau \\ &= \tau_2 \dot{q}_2. \end{aligned}$$

The viscous damping torques are encapsulated within the lossy torque matrix $\mathbf{R}(\dot{\mathbf{q}})$ and, for the case of the Acrobot, is represented by

$$\mathbf{R}(\dot{\mathbf{q}}) = \begin{bmatrix} b_1 \dot{q}_1 & b_2 \dot{q}_2 \end{bmatrix}^{\mathbf{T}} \tag{7.34}$$

where b_1 and b_2 represent the damping coefficients of the viscous damping friction present at the proximal and distal pendulums respectively. The power

loss associated with the viscous damping is mathematically represented as

$$\dot{\mathbf{q}}^{\mathbf{T}}\mathbf{R}(\dot{\mathbf{q}}) = -b_1\dot{q}_1^2 - b_2\dot{q}_2^2. \tag{7.35}$$

The total power of the system is a combination of both of these factors, as shown with

$$\begin{aligned}\frac{\mathrm{d}}{\mathrm{dt}}E_s &= \dot{\mathbf{q}}^{\mathbf{T}}\mathbf{G}(\mathbf{q})\mathbf{u} - \dot{\mathbf{q}}^{\mathbf{T}}\mathbf{R}(\dot{\mathbf{q}}) \\ &= \tau\dot{q}_2 - b_1\dot{q}_1 - b_2\dot{q}_2.\end{aligned}$$

This is equivalent to the system power equation shown in step ((3)) of this procedure. Therefore

$$\begin{aligned}\frac{\mathrm{d}}{\mathrm{dt}}E_s &= \dot{\mathbf{q}}^{\mathbf{T}}\mathbf{M}(\mathbf{q})\ddot{\mathbf{q}} + \frac{1}{2}\dot{\mathbf{q}}^{\mathrm{T}}\dot{\mathbf{M}}(\mathbf{q})\dot{\mathbf{q}} + \dot{\mathbf{q}}^{\mathbf{T}}\mathbf{K}(\mathbf{q}) = \dot{\mathbf{q}}^{\mathbf{T}}\mathbf{G}(\mathbf{q})\mathbf{u} - \dot{\mathbf{q}}^{\mathbf{T}}\mathbf{R}(\dot{\mathbf{q}}) \\ &= \tau\dot{q}_2 - b_1\dot{q}_1 - b_2\dot{q}_2.\end{aligned}$$

(5) Following the structure of a skew-symmetric matrix given by eq. (3.32), the $\mathbf{J}(\mathbf{q},\dot{\mathbf{q}})\dot{\mathbf{q}}$ vector for the Acrobot is structured as

$$\mathbf{J}(\mathbf{q},\dot{\mathbf{q}})\dot{\mathbf{q}} = \begin{bmatrix} 0 & -J_1(\mathbf{q},\dot{\mathbf{q}}) \\ J_1(\mathbf{q},\dot{\mathbf{q}}) & 0 \end{bmatrix}\begin{bmatrix}\dot{q}_1 \\ \dot{q}_2\end{bmatrix} = \begin{bmatrix} -J_1(\mathbf{q},\dot{\mathbf{q}})\dot{q}_2 \\ J_1(\mathbf{q},\dot{\mathbf{q}})\dot{q}_1 \end{bmatrix}. \tag{7.36}$$

Note that the matrix has only one unique entry. This skew-symmetry prevents the observability of the energy and the power related to these torques, i.e.

$$\dot{\mathbf{q}}^{\mathbf{T}}\mathbf{J}(\mathbf{q},\dot{\mathbf{q}})\dot{\mathbf{q}} = 0 \qquad \text{and} \qquad \int \dot{\mathbf{q}}^{\mathbf{T}}\mathbf{J}(\mathbf{q},\dot{\mathbf{q}})\dot{\mathbf{q}}\,\mathrm{dt} = 0.$$

The entries of the matrix may now be found by implementing

$$\mathbf{J}(\mathbf{q},\dot{\mathbf{q}})\dot{\mathbf{q}} = \frac{1}{2}\dot{\mathbf{M}}(\mathbf{q},\dot{\mathbf{q}})\dot{\mathbf{q}} - \left[\frac{\partial}{\partial\mathbf{q}}\left(\frac{1}{2}\dot{\mathbf{q}}^{\mathrm{T}}\mathbf{M}(\mathbf{q})\dot{\mathbf{q}}\right)\right]^{\mathrm{T}} \tag{7.37}$$

where

$$\begin{aligned}\dot{\mathbf{M}}(\mathbf{q},\dot{\mathbf{q}}) &= \begin{bmatrix} -2\alpha_3\dot{q}_2\sin q_2 & -\alpha_3\dot{q}_2\sin q_2 \\ -\alpha_3\dot{q}_2\sin q_2 & 0 \end{bmatrix}, \\ \therefore \frac{1}{2}\dot{\mathbf{M}}(\mathbf{q})\dot{\mathbf{q}} &= \begin{bmatrix} -\alpha_3\left(\dot{q}_1\dot{q}_2 + \frac{1}{2}\dot{q}_2{}^2\right)\sin q_2 \\ -\frac{1}{2}\alpha_3\dot{q}_1\dot{q}_2\sin\alpha \end{bmatrix}\end{aligned}$$

and

$$\frac{1}{2}\dot{\mathbf{q}}^{\mathrm{T}}\mathbf{M}(\mathbf{q})\dot{\mathbf{q}} = \frac{1}{2}(\alpha_1 + \alpha_2 + 2\alpha_3\sin q_2)\dot{q}_1{}^2 + (\alpha_2 + \alpha_3\sin q_2)\dot{q}_1\dot{q}_2$$

$$+\frac{1}{2}\alpha_3 \dot{q}_2{}^2.$$

Therefore

$$\left[\frac{\partial}{\partial \mathbf{q}}\left(\frac{1}{2}\dot{\mathbf{q}}^{\mathrm{T}}\mathbf{M}(\mathbf{q})\dot{\mathbf{q}}\right)\right]^{\mathrm{T}} = \begin{bmatrix} 0 \\ -\alpha_3(\dot{q}_1^2 + \dot{q}_1\dot{q}_2)\sin q_2 \end{bmatrix}.$$

The expression for $\mathbf{J}(\mathbf{q},\dot{\mathbf{q}})\dot{\mathbf{q}}$ may now be solved for, resulting in

$$\begin{aligned}
\mathbf{J}(\mathbf{q},\dot{\mathbf{q}})\dot{\mathbf{q}} &= \frac{1}{2}\dot{\mathbf{M}}(\mathbf{q},\dot{\mathbf{q}})\dot{\mathbf{q}} - \left[\frac{\partial}{\partial \mathbf{q}}\left(\frac{1}{2}\dot{\mathbf{q}}^{\mathrm{T}}\mathbf{M}(\mathbf{q})\dot{\mathbf{q}}\right)\right]^{\mathrm{T}} \\
&= \begin{bmatrix} -\alpha_3\left(\dot{q}_1\dot{q}_2 + \frac{1}{2}\dot{q}_2{}^2\right)\sin q_2 \\ -\frac{1}{2}\alpha_3\dot{q}_1\dot{q}_2\sin q_2 \end{bmatrix} - \begin{bmatrix} 0 \\ -\alpha_3(\dot{q}_1^2 + \dot{q}_1\dot{q}_2)\sin q_2 \end{bmatrix} \\
&= \begin{bmatrix} -\alpha_3\sin q_2\left(\dot{q}_1\dot{q}_2 + \frac{1}{2}\dot{q}_2{}^2\right) \\ \alpha_3\sin q_2\left(\dot{q}_1{}^2 + \frac{1}{2}\dot{q}_1\dot{q}_2\right) \end{bmatrix} \\
&= \begin{bmatrix} -J_1(\mathbf{q},\dot{\mathbf{q}})\dot{q}_2 \\ J_1(\mathbf{q},\dot{\mathbf{q}})\dot{q}_1 \end{bmatrix}.
\end{aligned}$$

The solution to the entry $J_1(\mathbf{q},\dot{\mathbf{q}})$ may now be trivially calculated from the result above, which produces

$$J_1(\mathbf{q},\dot{\mathbf{q}}) = \alpha_3\sin q_2\left(\dot{q}_1 + \frac{1}{2}\dot{q}_2\right). \tag{7.38}$$

The internal energy shuffling matrix $\mathbf{J}(\mathbf{q},\dot{\mathbf{q}})$ is, therefore, represented as

$$\mathbf{J}(\mathbf{q},\dot{\mathbf{q}}) = \begin{bmatrix} 0 & -\alpha_3\sin q_2\left(\dot{q}_1 + \frac{1}{2}\dot{q}_2\right) \\ \alpha_3\sin q_2\left(\dot{q}_1 + \frac{1}{2}\dot{q}_2\right) & 0 \end{bmatrix}. \tag{7.39}$$

Calculating the quadratic equation $\dot{\mathbf{q}}^{\mathrm{T}}\mathbf{J}(\mathbf{q},\dot{\mathbf{q}})\dot{\mathbf{q}}$ produces the expected result of zero, confirming that the matrix is indeed skew-symmetric.

(6) The equations of motion of the system are now derived by constructing the prototypical form, which may now be solved for by equating the results found in steps (3) and (4), producing

$$\dot{\mathbf{q}}^{\mathrm{T}}\mathbf{M}(\mathbf{q})\ddot{\mathbf{q}} + \frac{1}{2}\dot{\mathbf{q}}^{\mathrm{T}}\dot{\mathbf{M}}(\mathbf{q},\dot{\mathbf{q}})\dot{\mathbf{q}} + \dot{\mathbf{q}}^{\mathrm{T}}\mathbf{K}(\mathbf{q}) = -\dot{\mathbf{q}}^{\mathrm{T}}\mathbf{R}(\mathbf{q},\dot{\mathbf{q}}) - \dot{\mathbf{q}}^{\mathrm{T}}\mathbf{J}(\mathbf{q},\dot{\mathbf{q}})\dot{\mathbf{q}} + \dot{\mathbf{q}}^{\mathrm{T}}\mathbf{G}(\mathbf{q})\mathbf{u}$$

[93]. The energy shuffling torque matrix is added to the power equation in its

quadratic form as it plays no role in changing the magnitude of the mechanical energy in the system. The prototypical form of the system is represented by

$$\mathbf{M}(\mathbf{q})\ddot{\mathbf{q}} + \mathbf{D}(\mathbf{q}, \dot{\mathbf{q}}) + \mathbf{K}(\mathbf{q}) = \mathbf{G}(\mathbf{q})\mathbf{u} \tag{7.40}$$

where

$$\mathbf{M}(\mathbf{q}) = \begin{bmatrix} \alpha_1 + \alpha_2 + \alpha_3 \cos q_2 & \alpha_2 + \alpha_3 \cos q_2 \\ \alpha_2 + \alpha_3 \cos q_2 & \alpha_2 \end{bmatrix},$$

$$\mathbf{K}(\mathbf{q}) = \begin{bmatrix} -\beta_1 \sin q_1 - \beta_2 \sin(q_1 + q_2) \\ -\beta_2 \sin(q_1 + q_2) \end{bmatrix},$$

$$\mathbf{G}(\mathbf{q})\mathbf{u} = \begin{bmatrix} 0 \\ \tau_2 \end{bmatrix}, \text{ and}$$

$$\begin{aligned} \mathbf{D}(\mathbf{q}, \dot{\mathbf{q}}) &= \mathbf{R}(\mathbf{q}, \dot{\mathbf{q}}) + \frac{1}{2}\dot{\mathbf{M}}(\mathbf{q}, \dot{\mathbf{q}})\dot{\mathbf{q}} + \mathbf{J}(\mathbf{q}, \dot{\mathbf{q}})\dot{\mathbf{q}} \\ &= \begin{bmatrix} b_1\dot{q}_1 - \alpha_3 \left(2\dot{q}_1\dot{q}_2 + \dot{q}_2^2\right) \sin q_2 \\ b_1\dot{q}_2 + \alpha_3\dot{q}_1^2 \sin q_2 \end{bmatrix} \end{aligned}$$

since

$$\mathbf{R}(\mathbf{q}, \dot{\mathbf{q}}) = \begin{bmatrix} b_1\dot{q}_1 \\ b_2\dot{q}_2 \end{bmatrix},$$

$$\dot{\mathbf{M}}(\mathbf{q}, \dot{\mathbf{q}}) = \begin{bmatrix} -2\dot{q}_2\alpha_3 \sin q_2 & -\dot{q}_2\alpha_3 \sin q_2 \\ -\dot{q}_2\alpha_3 \sin q_2 & 0 \end{bmatrix}, \text{ and}$$

$$\mathbf{J}(\mathbf{q}, \dot{\mathbf{q}}) = \begin{bmatrix} 0 & \alpha_3 \left(\dot{q}_1 + \frac{1}{2}\dot{q}_2\right) \sin q_2 \\ -\alpha_3 \left(\dot{q}_1 + \frac{1}{2}\dot{q}_2\right) \sin q_2 & 0 \end{bmatrix}.$$

The power equation also holds true when $\dot{q} = \mathbb{O}$ [93].

The equations of motion can be found by taking the inverse of the mass matrix, whereby

$$\ddot{\mathbf{q}} = \mathbf{M}^{-1}(\mathbf{q}) \left(-\mathbf{D}(\mathbf{q}, \dot{\mathbf{q}}) - \mathbf{K}(\mathbf{q}) + \mathbf{G}(\mathbf{q})\mathbf{u}\right). \tag{7.41}$$

The mass matrix is always invertible as it is always uniformly symmetric and positive definite [15]. This result is in agreement with the results produced through the classical modelling method, as confirmed by [6, 34, 64] (these

results do not include viscous damping friction).

(7) The system is represented in state-space form using the transformations

$$q_1 = \mathbf{x}_1, \qquad q_2 = \mathbf{x}_2,$$
$$\dot{q}_1 = \mathbf{x}_3, \qquad \dot{q}_2 = \mathbf{x}_4.$$

The system dynamics are thus represented in the companion form

$$\dot{\mathbf{x}} = \mathbf{f}(\mathbf{x}) + \mathbf{g}(\mathbf{x})\mathbf{u}$$

where

$$\mathbf{f}(\mathbf{x}) = \begin{bmatrix} \mathbf{x}_3 \\ \mathbf{x}_4 \\ f_1(\mathbf{x}) \\ f_2(\mathbf{x}) \end{bmatrix}$$

and

$$\begin{bmatrix} f_1(\mathbf{x}) \\ f_2(\mathbf{x}) \end{bmatrix} = \mathbf{M}^{-1}(\mathbf{x})\left(-\mathbf{D}(\mathbf{x}) - \mathbf{K}(\mathbf{x})\right).$$

Additionally, we find that

$$\mathbf{g}(\mathbf{x}) = \begin{bmatrix} g_1(\mathbf{x}) \\ g_2(\mathbf{x}) \end{bmatrix} = \mathbf{M}^{-1}(\mathbf{x})\mathbf{G}(\mathbf{x}).$$

7.5 The Passive-Active-Active (PAA) Robot

7.5.1 Conventional Modelling using the Energy-Modelling Method

The PAA robot is included as a slightly more complex supplementary model along with the Acrobot, and is specifically introduced to test the robustness of the analytical results of this research when the derived control is applied to higher-order systems. The PAA robot is a variation of the underactuated triple-pendulum system and is demonstrated in figure 7.5. The name of this model describes the actuation state of the joints in a progressive order, starting from the most proximal joint to the most distal joint. The most proximal joint (joint (a)) is, therefore, **P**assive and is followed by two **A**ctive joints (joints (b) and (c)). Excluding these differences, the PAA robot is identical to the Acrobot in terms of physical properties, whereby each pendulum is associated with a mass (m_1, m_2 and m_3), a moment of inertia (I_1, I_2 and I_3), a length (L_1, L_2 and L_3) and a COM length (l_1, l_2 and l_3). Additionally, each joint is also subject to the effects of viscous damping, with each joint being associated with a damping coefficient (b_1, b_2 and b_3).

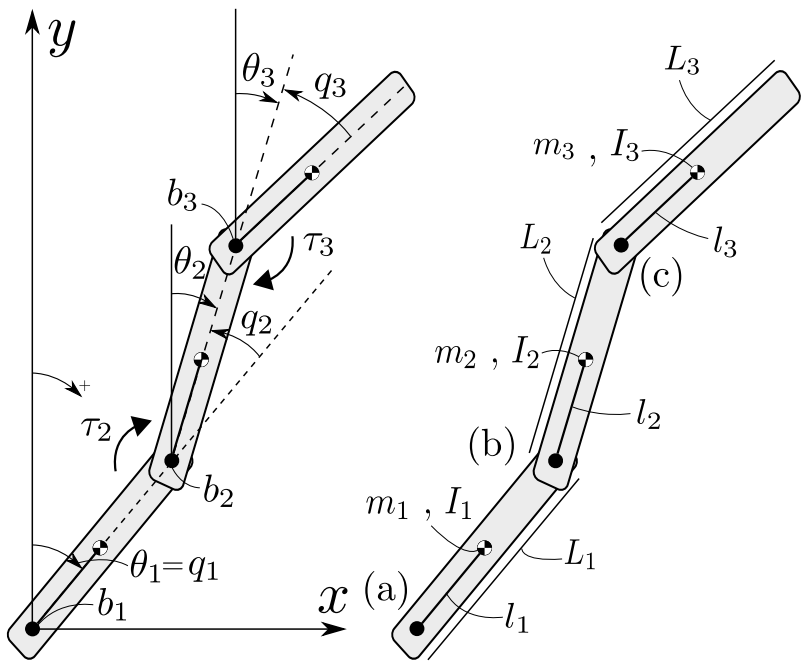

FIGURE 7.5: The PAA Robot.

The equations of motion for the PAA robot will be derived using the energy modelling methodology in section 3.3.4 as seen with the case of the n-link pendulum (section 7.3.1) and the Acrobot (section 7.4).

Important note: The model that emerges from this section will only be applicable to the PFL control method highlighted in chapter 9. The order of the system is too large to be implemented in such a conventional manner when applying LDM, thus requiring a model which incorporates the VCL modelling methodology. This is discussed in the next section (section 7.3.2).

(1) As with previous examples, there is one DOF that is associated with each pendulum once the Cartesian coordinates have been transformed into the generalised coordinates θ (absolute) and $\mathbf{q}$ (relative), where each of the coordinates are described in vector form, where

$$\theta = \begin{bmatrix}\theta_1 & \theta_2 & \theta_3\end{bmatrix}^{\mathbf{T}}, \qquad \mathbf{q} = \begin{bmatrix}q_1 & q_2 & q_3\end{bmatrix}^{\mathbf{T}}.$$

These generalised coordinates are related to one another by the transformations

$$\theta_1 = q_1, \qquad \theta_2 = q_1 + q_2, \qquad \theta_3 = q_1 + q_2 + q_3, \tag{7.42a}$$

$$q_2 = \theta_2 - \theta_1, \qquad q_3 = \theta_3 - \theta_2. \tag{7.42b}$$

Therefore

$$\theta = A\mathbf{q}, \qquad \mathbf{q} = A^{-1}\theta$$

where

$$A = \begin{bmatrix} 1 & 0 & 0 \\ 1 & 1 & 0 \\ 1 & 1 & 1 \end{bmatrix}, \qquad A^{-1} = \begin{bmatrix} 1 & 0 & 0 \\ -1 & 1 & 0 \\ 0 & -1 & 1 \end{bmatrix}.$$

(2) Applying the technique seen in [5] on the PAA robot, we find that

$$\mathbf{M}(\mathbf{q}) = A^{\mathbf{T}}\mathbf{M}_\theta(A\mathbf{q})A \tag{7.43}$$

where

$$\Big[\mathbf{M}(\mathbf{q})\Big]_{11} = \alpha_{11} + \alpha_{22} + \alpha_{33} + 2\alpha_{12}\cos q_2 + 2\alpha_{13}\cos(q_2+q_3) + 2\alpha_{23}\cos q_3, \tag{7.44}$$

$$\Big[\mathbf{M}(\mathbf{q})\Big]_{12} = \Big[\mathbf{M}(\mathbf{q})\Big]_{21} = \alpha_{22} + \alpha_{33} + \alpha_{12}\cos q_2 + \alpha_{13}\cos(q_2+q_3) + 2\alpha_{23}\cos q_3, \tag{7.45}$$

$$\Big[\mathbf{M}(\mathbf{q})\Big]_{13} = \Big[\mathbf{M}(\mathbf{q})\Big]_{31} = \alpha_{33} + \alpha_{13}\cos(q_2+q_3) + \alpha_{23}\cos q_3, \tag{7.46}$$

$$\Big[\mathbf{M}(\mathbf{q})\Big]_{22} = \alpha_{22} + \alpha_{33} + 2\alpha_{23}\cos q_3, \tag{7.47}$$

$$\Big[\mathbf{M}(\mathbf{q})\Big]_{23} = \Big[\mathbf{M}(\mathbf{q})\Big]_{32} = \alpha_{33} + \alpha_{23}\cos q_3, \tag{7.48}$$

$$\Big[\mathbf{M}(\mathbf{q})\Big]_{33} = \alpha_{33} \tag{7.49}$$

and where

$$\mathbf{K}(\mathbf{q}) = \begin{bmatrix} -\beta_1\sin q_1 - \beta_2\sin(q_1+q_2) - \beta_3\sin(q_1+q_2+q_3) \\ -\beta_2\sin(q_1+q_2) - \beta_3\sin(q_1+q_2+q_3) \\ -\beta_3\sin(q_1+q_2+q_3) \end{bmatrix} \tag{7.50}$$

with

$$\begin{aligned} \alpha_{11} &= I_1 + m_1{l_1}^2 + (m_2+m_3){L_1}^2, & \alpha_{12} &= \alpha_{21} = (m_2+m_3)L_1 l_2, \\ \alpha_{13} &= \alpha_{31} = m_3 L_1 l_3, & \alpha_{22} &= I_2 + m_2{l_2}^2 + m_3{L_2}^2, \\ \alpha_{23} &= \alpha_{32} = m_3 L_2 l_3, & \alpha_{33} &= I_3 + m_3{l_3}^2 \end{aligned}$$

and

$$\beta_1 = g\left(m_1 l_1 + (m_2+m_3)L_1\right), \quad \beta_2 = g\left(m_2 l_2 + m_3 L_2\right), \quad \beta_3 = g m_3 l_3.$$

(3) As explicitly stated in the sections that precede the modelling of the PAA robot, the power equation of any system is demonstrated as

$$\frac{\mathrm{d}}{\mathrm{dt}}E_s = \dot{\mathbf{q}}^{\mathrm{T}}\mathbf{M}(\mathbf{q})\ddot{\mathbf{q}} + \frac{1}{2}\dot{\mathbf{q}}^{\mathrm{T}}\dot{\mathbf{M}}(\mathbf{q},\dot{\mathbf{q}})\dot{\mathbf{q}} + \dot{\mathbf{q}}^{\mathrm{T}}\mathbf{K}(\mathbf{q}) \tag{7.51}$$

[93].

(4) The PAA robot is characterised by three joints, with an actuator fixed on each of the two most distal joints. The actuation in the PAA robot is, thus, represented as

$$\begin{aligned}\mathbf{G}(\mathbf{q})\mathbf{u} &= \begin{bmatrix}0 & \tau_2 & \tau_3\end{bmatrix}^{\mathbf{T}} \\ &= \tau.\end{aligned} \tag{7.52}$$

The power associated with these actuators is represented as

$$\begin{aligned}\dot{\mathbf{q}}^{\mathbf{T}}\mathbf{G}(\mathbf{q})\mathbf{u} &= \dot{\mathbf{q}}^{\mathbf{T}}\tau \\ &= \dot{q}_2\tau_2 + \dot{q}_3\tau_3.\end{aligned}$$

There are, once again, viscous damping torques that are associated with this robotic configuration. These associated torques are enclosed within the lossy torque matrix $\mathbf{R}(\dot{\mathbf{q}})$ and is represented for the PAA robot as

$$\mathbf{R}(\dot{\mathbf{q}}) = \begin{bmatrix}b_1\dot{q}_1 & b_2\dot{q}_2 & b_3\dot{q}_3\end{bmatrix}^{\mathbf{T}} \tag{7.53}$$

where b_1, b_2, and b_3 represent the damping coefficients of the viscous damping friction present at the pendulums. The power loss associated with the viscous damping friction is represented as

$$\dot{\mathbf{q}}^{\mathbf{T}}\mathbf{R}(\dot{\mathbf{q}}) = -b_1\dot{q}_1^2 - b_2\dot{q}_2^2 - b_3\dot{q}_3^2. \tag{7.54}$$

The total power of the system is a combination of both of viscous damping and actuation, where

$$\begin{aligned}\frac{\mathrm{d}}{\mathrm{dt}}E_s &= \dot{\mathbf{q}}^{\mathbf{T}}\mathbf{G}(\mathbf{q})\mathbf{u} - \dot{\mathbf{q}}^{\mathbf{T}}\mathbf{R}(\dot{\mathbf{q}}) \\ &= -b_1\dot{q}_1 + (\tau - b_2)\dot{q}_2 + (\tau_3 - b_3)\dot{q}_3.\end{aligned}$$

It is intuitive that this expression is equivalent to the system power equation shown in step (3) of this procedure, where

$$\begin{aligned}\frac{\mathrm{d}}{\mathrm{dt}}E_s &= \dot{\mathbf{q}}^{\mathrm{T}}\mathbf{M}(\mathbf{q})\ddot{\mathbf{q}} + \frac{1}{2}\dot{\mathbf{q}}^{\mathrm{T}}\dot{\mathbf{M}}(\mathbf{q},\dot{\mathbf{q}})\dot{\mathbf{q}} + \dot{\mathbf{q}}^{\mathrm{T}}\mathbf{K}(\mathbf{q}) = \dot{\mathbf{q}}^{\mathbf{T}}\mathbf{G}(\mathbf{q})\mathbf{u} - \dot{\mathbf{q}}^{\mathbf{T}}\mathbf{R}(\dot{\mathbf{q}}) \\ &= -b_1\dot{q}_1 + (\tau - b_2)\dot{q}_2 + (\tau_3 - b_3)\dot{q}_3.\end{aligned}$$

(5) Following the structure of a skew-symmetric matrix given by eq. (3.32), the $\mathbf{J}(\mathbf{q}, \dot{\mathbf{q}})$ matrix for the PAA robot is structured as

$$\begin{aligned}\mathbf{J}(\mathbf{q}, \dot{\mathbf{q}})\dot{\mathbf{q}} &= \begin{bmatrix} 0 & -J_1(\mathbf{q}, \dot{\mathbf{q}}) & -J_2(\mathbf{q}, \dot{\mathbf{q}}) \\ J_1(\mathbf{q}, \dot{\mathbf{q}}) & 0 & -J_3(\mathbf{q}, \dot{\mathbf{q}}) \\ J_2(\mathbf{q}, \dot{\mathbf{q}}) & J_3(\mathbf{q}, \dot{\mathbf{q}}) & 0 \end{bmatrix} \begin{bmatrix} \dot{q}_1 \\ \dot{q}_2 \\ \dot{q}_3 \end{bmatrix} \\ &= \begin{bmatrix} -J_1(\mathbf{q}, \dot{\mathbf{q}})\dot{q}_2 - J_2(\mathbf{q}, \dot{\mathbf{q}})\dot{q}_3 \\ J_1(\mathbf{q}, \dot{\mathbf{q}})\dot{q}_1 - J_3(\mathbf{q}, \dot{\mathbf{q}})\dot{q}_3 \\ J_2(\mathbf{q}, \dot{\mathbf{q}})\dot{q}_1 + J_3(\mathbf{q}, \dot{\mathbf{q}})\dot{q}_2 \end{bmatrix}.\end{aligned}$$

It is evident that the energy shuffling coefficient matrix $\mathbf{J}(\mathbf{q}, \dot{\mathbf{q}})$ has three unique entries. It is not necessary to calculate each of the elemental coefficients as the knowledge of the torque expressions alone are sufficient to describe the behaviour of the system. The coefficients are thus not calculated in this example.

Once again, the entries of the energy-shifting torque matrix may now be found with the implementation of

$$\mathbf{J}(\mathbf{q}, \dot{\mathbf{q}})\dot{\mathbf{q}} = \frac{1}{2}\dot{\mathbf{M}}(\mathbf{q}, \dot{\mathbf{q}})\dot{\mathbf{q}} - \left[\frac{\partial}{\partial \mathbf{q}}\left(\frac{1}{2}\dot{\mathbf{q}}^{\mathrm{T}}\mathbf{M}(\mathbf{q})\dot{\mathbf{q}}\right)\right]^{\mathrm{T}} \tag{7.55}$$

where the entries of the $\dot{\mathbf{M}}(\mathbf{q}, \dot{\mathbf{q}})$ are

$$\left[\dot{\mathbf{M}}(\mathbf{q}, \dot{\mathbf{q}})\right]_{11} = -2\left(\alpha_{12}\dot{q}_2 \sin q_2 + \alpha_{13}\left[\dot{q}_2 + \dot{q}_3\right]\sin(q_2 + q_3) + \alpha_{23}\dot{q}_3 \sin q_3\right), \tag{7.56}$$

$$\left[\dot{\mathbf{M}}(\mathbf{q}, \dot{\mathbf{q}})\right]_{12} = \left[\dot{\mathbf{M}}(\mathbf{q}, \dot{\mathbf{q}})\right]_{21} = -\alpha_{12}\dot{q}_2 \sin q_2 + \alpha_{13}\left[\dot{q}_2 + \dot{q}_3\right]\sin(q_2 + q_3) - 2\alpha_{23}\dot{q}_3 \sin q_3, \tag{7.57}$$

$$\left[\dot{\mathbf{M}}(\mathbf{q}, \dot{\mathbf{q}})\right]_{13} = \left[\dot{\mathbf{M}}(\mathbf{q}, \dot{\mathbf{q}})\right]_{31} = -\alpha_{13}\left[\dot{q}_2 + \dot{q}_3\right]\sin(q_2 + q_3) - \alpha_{23}\dot{q}_3 \sin q_3, \tag{7.58}$$

$$\left[\dot{\mathbf{M}}(\mathbf{q}, \dot{\mathbf{q}})\right]_{22} = -2\alpha_{23}\dot{q}_3 \sin q_3, \tag{7.59}$$

$$\left[\dot{\mathbf{M}}(\mathbf{q}, \dot{\mathbf{q}})\right]_{23} = \left[\dot{\mathbf{M}}(\mathbf{q}, \dot{\mathbf{q}})\right]_{32} = -\alpha_{23}\dot{q}_3 \sin q_3, \tag{7.60}$$

$$\left[\dot{\mathbf{M}}(\mathbf{q}, \dot{\mathbf{q}})\right]_{33} = 0 \tag{7.61}$$

and

$$\begin{aligned}\frac{1}{2}\dot{\mathbf{q}}^{\mathrm{T}}\mathbf{M}(\mathbf{q})\dot{\mathbf{q}} = \frac{1}{2}\Big[\Big(&\alpha_{11} + \alpha_{22} + \alpha_{33} + 2\alpha_{13}\cos(q_2 + q_3) + 2\alpha_{12}\cos q_2 + \\ &2\alpha_{23}\cos q_3\Big)\dot{q}_1{}^2 + \Big(\alpha_{22} + \alpha_{33} + 2\alpha_{23}\cos(q_2 + q_3)\Big)q_2{}^2 + \alpha_{33}\dot{q}_3^2\Big] +\end{aligned}$$

$$\Big(\alpha_{22} + \alpha_{33} + \alpha_{13}\cos(q_2+q_3) + \alpha_{12}\cos(q_2) + 2\alpha_{23}\cos q_3\Big)\dot{q}_1\dot{q}_2 + \Big(\alpha_{33} + \alpha_{13}\cos(q_2+q_3) + \alpha_{23}\cos q_3\Big)\dot{q}_1\dot{q}_3 + \Big(\alpha_{33} + \alpha_{23}\cos q_3\Big)\dot{q}_2\dot{q}_3.$$

Therefore

$$\left[\frac{\partial}{\partial \mathbf{q}}\left(\frac{1}{2}\dot{\mathbf{q}}^{\mathrm{T}}\mathbf{M}(\mathbf{q})\dot{\mathbf{q}}\right)\right]_{11} = 0,$$

$$\left[\frac{\partial}{\partial \mathbf{q}}\left(\frac{1}{2}\dot{\mathbf{q}}^{\mathrm{T}}\mathbf{M}(\mathbf{q})\dot{\mathbf{q}}\right)\right]_{12} = -\Big[\Big(\alpha_{13}\sin(q_2+q_3) + \alpha_{12}\sin q_2\Big)\dot{q}_1^2 + \Big(\alpha_{13}\sin(q_2+q_3) + \alpha_{12}\sin q_2\Big)\dot{q}_1\dot{q}_2 + \Big(\alpha_{13}\sin(q_2+q_3)\Big)\dot{q}_1\dot{q}_3\Big],$$

$$\left[\frac{\partial}{\partial \mathbf{q}}\left(\frac{1}{2}\dot{\mathbf{q}}^{\mathrm{T}}\mathbf{M}(\mathbf{q})\dot{\mathbf{q}}\right)\right]_{13} = -\Big[\Big(\alpha_{13}\sin(q_2+q_3) + \alpha_{23}\sin(q_3)\Big)\dot{q}_1^2 + \alpha_{23}\dot{q}_2^2\sin q_3 + \Big(\alpha_{13}\sin(q_2+q_3) + 2\alpha_{23}\sin q_3\Big)\dot{q}_1\dot{q}_2 + \Big(\alpha_{13}\sin(q_2+q_3) + \alpha_{23}\sin q_3\Big)\dot{q}_1\dot{q}_3 + \Big(\alpha_{23}\sin q_3\Big)\dot{q}_2\dot{q}_3\Big].$$

These results may be substituted in eq. (7.55), with the entries of the energy-shuffling torque matrix represented as

$$\Big[\mathbf{J}(\dot{\mathbf{q}},\mathbf{q})\dot{\mathbf{q}}\Big]_{11} = \frac{\alpha_{12}}{2}\Big[2\dot{q}_1 + \dot{q}_2\Big]\dot{q}_2\sin q_2 - \alpha_{13}\Big[2\dot{q}_1 + \dot{q}_2 + \dot{q}_3)(\dot{q}_2 + \dot{q}_3)\Big]\sin(q_2+q_3) - \frac{\alpha_{23}}{2}\Big[2\dot{q}_q + 2\dot{q}_2 + \dot{q}_3\Big]\dot{q}_3\sin q_3, \tag{7.62}$$

$$\Big[\mathbf{J}(\dot{\mathbf{q}},\mathbf{q})\dot{\mathbf{q}}\Big]_{21} = \frac{\alpha_{12}}{2}\Big[2\dot{q}_1 + \dot{q}_2\Big]\dot{q}_1\sin q_2 + \frac{\alpha_{13}}{2}\Big[2\dot{q}_1 + \dot{q}_2 + \dot{q}_3\Big]\dot{q}_1\sin(q_2 + q_3) - \frac{\alpha_{23}}{2}\Big[\dot{q}_1 + 2\dot{q}_2 + \dot{q}_3\Big]\dot{q}_3\sin q_3, \tag{7.63}$$

$$\Big[\mathbf{J}(\dot{\mathbf{q}},\mathbf{q})\dot{\mathbf{q}}\Big]_{31} = \frac{\alpha_{13}}{2}\Big[2\dot{q}_1 + \dot{q}_2 + \dot{q}_3\Big]\dot{q}_1\sin(q_2+q_3) + \frac{\alpha_{23}}{2}\Big[(\dot{q}_1 + \dot{q}_2)(2\dot{q}_1 + \dot{q}_2 + \dot{q}_3)\Big]\sin q_3. \tag{7.64}$$

Again, calculating the quadratic form $\dot{\mathbf{q}}^{\mathbf{T}}\mathbf{J}(\mathbf{q},\dot{\mathbf{q}})\dot{\mathbf{q}}$ produces the expected result of zero, confirming that the constituent coefficient matrix $\mathbf{J}(\mathbf{q},\dot{\mathbf{q}})$ is indeed skew-symmetric.

(6) The prototypical form is constructed through the equating of the two generalised expressions of the power equation, resulting in

$$\dot{\mathbf{q}}^{\mathrm{T}}\mathbf{M}(\mathbf{q})\ddot{\mathbf{q}}+\frac{1}{2}\dot{\mathbf{q}}^{\mathrm{T}}\dot{\mathbf{M}}(\mathbf{q},\dot{\mathbf{q}})\dot{\mathbf{q}}+\dot{\mathbf{q}}^{\mathrm{T}}\mathbf{K}(\mathbf{q})=-\dot{\mathbf{q}}^{\mathrm{T}}\mathbf{R}(\mathbf{q},\dot{\mathbf{q}})-\dot{\mathbf{q}}^{\mathbf{T}}\mathbf{J}(\mathbf{q},\dot{\mathbf{q}})\dot{\mathbf{q}}+\dot{\mathbf{q}}^{\mathrm{T}}\mathbf{G}(\mathbf{q})\mathbf{u}$$

[93]. The quadratic form of the energy-shuffling torque matrix $\left(\dot{\mathbf{q}}^{\mathbf{T}}\mathbf{J}(\mathbf{q},\dot{\mathbf{q}})\dot{\mathbf{q}}\right)$ is added to the power equation as it has no influence on the change of the magnitude of the system's mechanical energy. The prototypical form is represented as

$$\mathbf{M}(\mathbf{q})\ddot{\mathbf{q}}+\mathbf{D}(\mathbf{q},\dot{\mathbf{q}})+\mathbf{K}(\mathbf{q})=\mathbf{G}(\mathbf{q})\mathbf{u} \tag{7.65}$$

where the entries of the mass matrix $\mathbf{M}(\mathbf{q})$, the gravitational torque matrix $\mathbf{K}(\mathbf{q})$, and the actuator matrix $\mathbf{G}(\mathbf{q})\mathbf{u}$ are demonstrated in eqs. (7.44)-(7.49), eq. (7.50), and eq. (7.52) respectively. The $\mathbf{D}(\mathbf{q},\dot{\mathbf{q}})$ matrix, as stated in the preceding examples, is defined as

$$\mathbf{D}(\mathbf{q},\dot{\mathbf{q}})=\mathbf{R}(\mathbf{q},\dot{\mathbf{q}})+\frac{1}{2}\dot{\mathbf{M}}(\mathbf{q},\dot{\mathbf{q}})\dot{\mathbf{q}}+\mathbf{J}(\mathbf{q},\dot{\mathbf{q}})\dot{\mathbf{q}} \tag{7.66}$$

where the entries for the lossy torque matrix $\mathbf{R}(\mathbf{q},\dot{\mathbf{q}})$, the matrix relating to conservative configurational changes $\dot{\mathbf{M}}(\mathbf{q},\dot{\mathbf{q}})$, and the energy-shuffling torque matrix $\mathbf{J}(\mathbf{q},\dot{\mathbf{q}})$ are shown in eq. (7.53), eqs. (7.56)-(7.61), and eqs. (7.62)-(7.64) respectively. The final representation of the entries of the $\mathbf{D}(\mathbf{q},\dot{\mathbf{q}})$ matrix are calculated by substituting the relevant matrices into eq. (7.66). Therefore

$$\begin{aligned}\left[\mathbf{D}(\mathbf{q},\dot{\mathbf{q}})\right]_{11} &= b_1\dot{q}_1-\alpha_{12}\left[2\dot{q}_1+\dot{q}_2\right]\dot{q}_2\sin q_2-\alpha_{13}\Big[(\dot{q}_2+\dot{q}_3)(2\dot{q}_1+\dot{q}_2+ \\ &\quad \dot{q}_3)\Big]\sin(q_2+q_3)-\alpha_{23}\left[2\dot{q}_1+2\dot{q}_2+\dot{q}_3\right]\dot{q}_3\sin q_3,\end{aligned} \tag{7.67}$$

$$\begin{aligned}\left[\mathbf{D}(\mathbf{q},\dot{\mathbf{q}})\right]_{21} &= b_2\dot{q}_2+\alpha_{12}\dot{q}_1^2\sin q_2+\alpha_{13}\dot{q}_1^2\sin(q_2+q_3)-\alpha_{23}\dot{q}_3\Big[2\dot{q}_1 \\ &\quad +2\dot{q}_2+\dot{q}_3\Big]\sin q_3,\end{aligned} \tag{7.68}$$

$$\left[\mathbf{D}(\mathbf{q},\dot{\mathbf{q}})\right]_{31} = b_3\dot{q}_3+\alpha_{13}\dot{q}_1^2\sin(q_2+q_3)+\alpha_{23}\left[\dot{q}_1+\dot{q}_2\right]^2\sin q_3. \tag{7.69}$$

These entries are identical to the entries seen in the $\mathbf{D}(\mathbf{q},\dot{\mathbf{q}})$ matrix in [5] (when one ignores the effect of viscous damping friction) which was derived using Lagrangian mechanics.

The equations of motion for the PAA robot may now be determined by manipulating the prototypical form, specifically by retrieving the inverse of the mass matrix and shifting all of the relevant matrices to the right-hand side of the formula. Therefore

$$\ddot{\mathbf{q}}=\mathbf{M}^{-1}(\mathbf{q})\left(-\mathbf{D}(\mathbf{q},\dot{\mathbf{q}})-\mathbf{K}(\mathbf{q})+\mathbf{G}(\mathbf{q})\mathbf{u}\right).$$

(7) The PAA robot is represented in state-space format using the transformations

$$\begin{aligned} q_1 &= \mathbf{x}_1, & q_2 &= \mathbf{x}_2, & q_3 &= \mathbf{x}_3, \\ \dot{q}_1 &= \mathbf{x}_4, & \dot{q}_2 &= \mathbf{x}_5, & \dot{q}_3 &= \mathbf{x}_6. \end{aligned}$$

The system dynamics are thus represented in the companion form

$$\dot{\mathbf{x}} = \mathbf{f}(\mathbf{x}) + \mathbf{g}(\mathbf{x})\mathbf{u}$$

where

$$\mathbf{f}(\mathbf{x}) = \begin{bmatrix} \mathbf{x}_4 & \mathbf{x}_5 & \mathbf{x}_6 & f_1(\mathbf{x}) & f_2(\mathbf{x}) & f_3(\mathbf{x}) \end{bmatrix}^{\mathbf{T}}$$

and

$$\begin{bmatrix} f_1(\mathbf{x}) & f_2(\mathbf{x}) & f_3(\mathbf{x}) \end{bmatrix}^{\mathbf{T}} = \mathbf{M}^{-1}(\mathbf{x})\left(-\mathbf{D}(\mathbf{x}) - \mathbf{K}(\mathbf{x})\right).$$

Additionally,

$$\mathbf{g}(\mathbf{x}) = \begin{bmatrix} g_1(\mathbf{x}) & g_2(\mathbf{x}) & g_3(\mathbf{x}) \end{bmatrix}^{\mathbf{T}} = \mathbf{M}^{-1}(\mathbf{x})\mathbf{G}(\mathbf{x}).$$

7.5.2 VCL Modelling of the PAA Robot

The swing-up of the PAA robot through the implementation of LDM requires the modelling of the PAA robot using the VCL transformation protocol to ensure that the invariant set problem is solvable [5]. This is only applicable to n-link pendulum systems that have a system order $n > 2$, thus resulting in the exclusion of the VCL modelling of the Acrobot [5]. The reader may refer to [5] if supplementary discussions on the derivation of the VCL coordinate transformation for the n-link pendulum system is required. Additionally, the PAA robot is explicitly modelled using the VCL modelling method outlined in [5]. Only the necessary results of this derivation are included in this section.

The 2nd and 3rd pendulums of the PAA robot shown in figure 7.6 will be incorporated into a VCL. The set of coordinates $\mathbf{q}_a$ is transformed into the VCL coordinate set

$$\overline{\mathbf{q}}_a = \begin{bmatrix} \overline{q}_2 \\ q_3 \end{bmatrix}$$

[5]. Using the method VCL modelling method demonstrated in [5], we find that the total VCL coordinate transformation can be represented as

$$\overline{\mathbf{q}}_a = 0 \leftrightarrow \mathbf{q}_a = 0 \tag{7.70}$$

and

$$\dot{\overline{\mathbf{q}}}_a = \Psi(\mathbf{q}_a)\dot{\mathbf{q}}_a$$

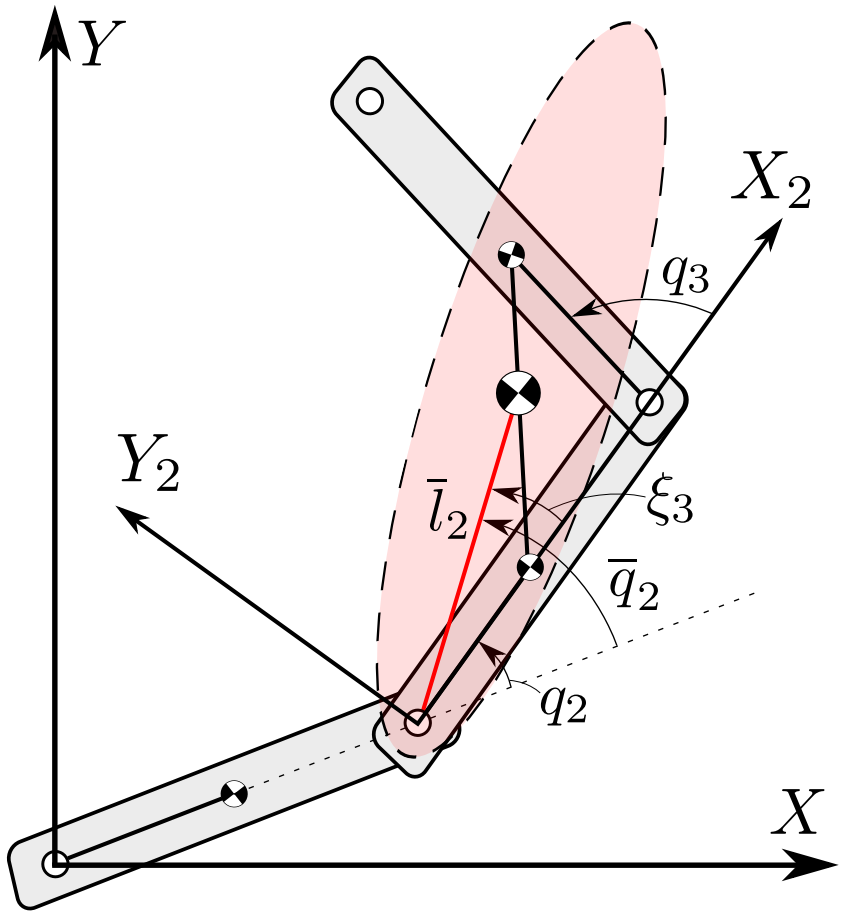

FIGURE 7.6: The VCL coordinate transformation of the PAA robot. Adapted from [5].

where

$$\Psi(\mathbf{q}_a) = \begin{bmatrix} 1 & \psi_{23} \\ 0 & 1 \end{bmatrix} \tag{7.71}$$

with

$$\psi_{23} = \beta_3 \Big[\beta_2 \cos q_3 \Big]$$

[5]. This is guaranteed so long as $\bar{l}_2 \neq 0$, which is ensured when

$$\beta_2 \neq \beta_3.$$

[5].

7.6 Conclusion

This chapter serves to present the derivation of the mathematical models for the PA_{n-1} robot and its derivatives, namely the Acrobot and the PAA robot. The models were derived using the *energy modelling method* as opposed to the conventional Lagrangian technique. The VCL coordinate transformation was implemented on the PA_{n-1} robot with system order $n > 2$ to accommodate LDM-related swing-up control. The Acrobot and the PAA robot are presented for swing-up control simulation, which will be covered in the following chapters.

"Man cannot discover new oceans unless he has the courage to lose sight of the shore."

— André Gide

Chapter 8

Identifying the Breaking Point:

The Swing-up Control of the Damped PA$_{n-1}$ Robot using Lyapunov's Direct Method

8.1 Chapter Overview

The preceding chapters of this dissertation were specifically included to introduce the reader to relevant concepts found within or surrounding the field of underactuated robotics, highlighting significant literature that can be used to formulate an appropriate research question. This literature review resulted in the identification of an appropriate **physical model** (the PA$_{n-1}$ robot), **control objective** (swing-up control), **control technique** (LDM) and an appropriate and relevant **system alteration** (integration of viscous damping). The work in this chapter seeks to fulfil the next requirements in the research methodology, namely, to prove or disprove the hypothesis of this research (highlighted in section 1.2). To do this, we shall first **replicate results** found in existing literature. Subsequent to this, we shall **alter** the system until the control objective can no longer be achieved (if possible).

This chapter is structured as follows. The analytical Lyapunov swing-up control formulation for the undamped PA$_{n-1}$ robot is first replicated, using the work of Xin and Liu as a reference point. This replication includes the proofs and lemmas involved in establishing the gain conditions. Subsequently, the analytical derivation of a swing-up control law for the actively damped and passively damped PA$_{n-1}$ robot is included, which is integrated as a system alteration. This results in the definition of the main finding of this chapter's investigation, the *matched damping condition*. This generalised derivation is followed by analytical and experimental results for the simplest derivatives of the PA$_{n-1}$ robot, namely the Acrobot and the PAA robot.

8.2 Preliminaries: The Undamped PA$_{n-1}$ Robot

In this section, we will first introduce the LDM related swing-up control design derived by Xin and Liu in [5] for the undamped PA$_{n-1}$ robot and its derivatives: the Acrobot, and the PAA Robot solely to **experimentally replicate** the work presented by Xin and Liu in [5]. These results are thus included as a preliminary discussion, which will lead up to the derivation of the swing-up control of the PA$_{n-1}$ robot that has been integrated with (i) active viscous damping (referred to as the tenable alteration) and (ii) passive viscous damping (referred to as the untenable alteration).

8.2.1 The Necessary Swing-up Control Torque for the Undamped PA$_{n-1}$ Robot

Following the control torque derivation highlighted in [5] for the conventionally modelled PA$_{n-1}$ robot, we find that the control torque

$$\tau_a = \Lambda^{-1}(\mathbf{q})\Big[k_D\mathbf{G}^{\mathbf{T}}(\mathbf{q})\mathbf{M}^{-1}(\mathbf{q})\Big[\mathbf{D}(\mathbf{q},\dot{\mathbf{q}}) + \mathbf{K}(\mathbf{q})\Big] - k_v\dot{\mathbf{q}}_a - k_P\psi^{\mathbf{T}}(\mathbf{q}_a)\overline{\mathbf{q}}_a\Big] \tag{8.1}$$

where

$$\Lambda(\mathbf{q},\dot{\mathbf{q}}) = (E - E_r)I_{n-1} + k_D\mathbf{G}^{\mathbf{T}}(\mathbf{q})\mathbf{M}^{-1}(\mathbf{q})\mathbf{G}(\mathbf{q}) \tag{8.2}$$

and

$$|\Lambda(\mathbf{q},\dot{\mathbf{q}})| \neq 0 \quad \forall\, \mathbf{q},\dot{\mathbf{q}} \tag{8.3}$$

are required to perform satisfactory swing-up control on the undamped PA$_{n-1}$ robot. We can thus replicate experimental results from [5] as required.

There are two outstanding objectives from this point in the derivation that are addressed in great detail in [5]. Firstly, the condition in eq. (8.3) must be proven to be true across the entire state-space to ensure that $\Lambda(\mathbf{q},\dot{\mathbf{q}})$ is invertible. Subsequent to this, the equilibrium points in the system, and their stability, must be evaluated to guarantee the swing-up behaviour of the system trajectory towards the UEP. These derivations result in a set of gain selection conditions for k_D and k_P which ensure that the system trajectory tends towards the UEP as $t \to \infty$. These proofs are outlined in great detail in [5], which indicates that for satisfactory swing-up control the gains k_P and k_D must be selected so that

$$\begin{aligned} k_D > k_{DM} &= \max_{\mathbf{q}_a}\{k_D(\mathbf{q}_a)\} \\ &= \max_{\mathbf{q}_a}\Big\{(E_r + \mathbf{\Phi}(\mathbf{q}_a))\lambda_{\max}\Big(\big(\mathbf{G}^{\mathbf{T}}(\mathbf{q})\mathbf{M}^{-1}(\mathbf{q})\mathbf{G}(\mathbf{q})\big)^{-1}\Big)\Big\} \end{aligned} \tag{8.4}$$

and

$$k_P > \max_{2\leq i\leq n}\{k_{mi}\} \tag{8.5}$$

where

$$k_{mi} = 2E_r\beta_{i-1}\frac{\sum_{j=1}^{n}\beta_j}{\sum_{j=i-1}^{n}\beta_j}.$$

In this chapter, we will highlight the traditional swing-up method of higher-order systems ($n > 2$) covered in [5], but we will also introduce an alternative method of approaching the swing-up control of the higher-order systems by approximately modelling the PA$_{n-1}$ robot as an Acrobot. The result of this approximation is referred to as the *Reduced-Order PA$_{n-1}$ robot* (ROPA$_{n-1}$ robot), and is realised, in this particular case, through the implementation of the Modified Collocated Partial Feedback Linearisation (MCPFL) technique. This technique, along with other pertinent variations of the PFL technique, are discussed in section 9.3. The modified version was chosen in this case to accommodate the independent derivation of the necessary swing-up torque for τ_2. Details of this derivation can be seen in section 9.3.1. The ROPA$_{n-1}$ robot is officially defined below.

Definition 8.1. The Reduced-Order PA$_{n-1}$ (ROPA$_{n-1}$) robot is a planar compound pendulum model that results from the PFL of the PA$_{n-1}$ robot. There are three variations of the ROPA$_{n-1}$ robot that correspond with the application of either the Traditional Collocated PFL (TCPFL), MCPFL, or the Noncollocated PFL (NCPFL) techniques. The general result of these techniques (and the application of non-oscillatory regulatory control) is the representation of the linearised PA$_{n-1}$ robot as an Acrobot. This is contingent on the selection of a sufficiently high response frequency for the controllers involved in regulation and the initialisation of the angular states of the regulated pendulums to zero.

Notable examples of the ROPA$_{n-1}$ robot are the ROPA$_1$ robot (the Acrobot) and the ROPA$_2$ robot (reduced order representation of the PAA robot). The reason for the inclusion of this model is not yet clear at this point of the derivation, but this will be carefully revealed once we encounter the *invertibility problem* (see section 8.4.1).

8.2.2 Modelling the Undamped PA$_{n-1}$ Robot as the MC-ROPA$_{n-1}$ Robot

The Modified Collocated ROPA$_{n-1}$ (MC-ROPA$_{n-1}$) robot is defined as follows:

Definition 8.2. The MC-ROPA$_{n-1}$ robot is a reduced-order representation of the PA$_{n-1}$ robot that results from the linearisation of the $n-2$ most distal pendulums of the system. The $n-1$ most distal pendulums thus collectively represent a single pendulum described by nonlinear dynamics. This system closely approximates the behaviour of an Acrobot, provided that the selected response frequency of the actuators involved in non-oscillatory regulation is sufficiently large and that $q_i(0) = 0$ for $2 < i < n$.

To define this model mathematically, we begin by first defining the torque required for each of the $n-2$ distal actuators that will be used to linearise the

dynamics of their respective joints, as derived in section 9.3.1. Each torque τ_i where $3 \leq i \leq n$ must satisfy

$$\tau_i = \hat{M}_{i3}(\mathbf{q})v_3 + \hat{M}_{i4}(\mathbf{q})v_4 + \cdots + \hat{M}_{in}(\mathbf{q})v_n + \hat{C}_i(\mathbf{q}, \dot{\mathbf{q}}) + \hat{K}_i(\mathbf{q}) + \hat{\tau}_i \tag{8.6}$$

where, for $3 \leq j \leq n$ and $2 \leq k \leq n$,

$$\hat{M}_{ij}(\mathbf{q}) = M_{ij}(\mathbf{q}) - \frac{\tilde{M}_{1j}(\mathbf{q})M_{i1}(\mathbf{q})}{M_{11}(\mathbf{q})} - \frac{\tilde{M}_{2j}(\mathbf{q})M_{i2}(\mathbf{q})}{\tilde{M}_{22}(\mathbf{q})},$$

$$\hat{C}_i(\mathbf{q}, \dot{\mathbf{q}}) = C_i(\mathbf{q}, \dot{\mathbf{q}}) - \frac{M_{i1}(\mathbf{q})}{M_{11}(\mathbf{q})}\tilde{C}_1(\mathbf{q}) - \frac{M_{i2}(\mathbf{q})}{\tilde{M}_{22}(\mathbf{q})}\tilde{C}_2(\mathbf{q}),$$

$$\hat{K}_i(\mathbf{q},) = K_i(\mathbf{q}) - \frac{M_{i1}(\mathbf{q})}{M_{11}(\mathbf{q})}\tilde{K}_1(\mathbf{q}) - \frac{M_{i2}(\mathbf{q})}{\tilde{M}_{22}(\mathbf{q})}\tilde{K}_2(\mathbf{q}),$$

$$\hat{\tau}_i = \frac{M_{i2}(\mathbf{q})}{\tilde{M}_{22}(\mathbf{q})}\tau_2 - \frac{M_{i1}(\mathbf{q})}{M_{11}(\mathbf{q})}\tilde{\tau}_2,$$

$$\tilde{\tau}_2 = \frac{M_{12}(\mathbf{q})}{\tilde{M}_{22}}\tau_2$$

and

$$\tilde{M}_{2k}(\mathbf{q}) = M_{2k}(\mathbf{q}) - \frac{M_{1k}(\mathbf{q})M_{21}(\mathbf{q})}{M_{11}(\mathbf{q})}, \qquad \tilde{M}_{1j}(\mathbf{q}) = M_{1j}(\mathbf{q}) - \frac{M_{12}(\mathbf{q})\tilde{M}_{2i}(\mathbf{q})}{\tilde{M}_{22}(\mathbf{q})},$$

$$\tilde{C}_2(\mathbf{q}, \dot{\mathbf{q}}) = C_2(\mathbf{q}, \dot{\mathbf{q}}) - \frac{M_{21}(\mathbf{q})}{M_{11}(\mathbf{q})}C_1(\mathbf{q}, \dot{\mathbf{q}}), \quad \tilde{C}_1(\mathbf{q}, \dot{\mathbf{q}}) = C_1(\mathbf{q}, \dot{\mathbf{q}}) - \frac{M_{12}(\mathbf{q})}{\tilde{M}_{22}(\mathbf{q})}\tilde{C}_2(\mathbf{q}, \dot{\mathbf{q}}),$$

$$\tilde{K}_2(\mathbf{q}) = K_2(\mathbf{q}) - \frac{M_{21}(\mathbf{q})}{M_{11}(\mathbf{q})}K_1(\mathbf{q}), \qquad \tilde{K}_1(\mathbf{q}) = K_1(\mathbf{q}) - \frac{M_{12}(\mathbf{q})}{\tilde{M}_{22}(\mathbf{q})}\tilde{K}_2(\mathbf{q}).$$

Implementing a linear controller law as seen in [2], where

$$v_i = -k_{D_i}\dot{q}_i - k_{P_i}q_i$$

we can ensure that the $n-2$ distal pendulums will collectively act as one pendulum provided that a sufficiently fast and damped response is chosen for k_{D_i} and k_{P_i}. The non-oscillatory behaviour of the $n-2$ distal pendulums can be guaranteed by choosing

$$k_{D_i} = 2\omega_{n_i}, \qquad k_{P_i} = {\omega_{n_i}}^2 \tag{8.7}$$

where ω_{n_i} represents the natural response frequency of the ith actuator.

Since we are guaranteed that

$$\begin{aligned} q_3 &\approx 0, \\ q_4 &\approx 0, \\ &\vdots \\ q_n &\approx 0 \end{aligned}$$

we can now model the PA$_{n-1}$ robot as a MC-ROPA$_{n-1}$ robot. The generalised result of modelling the PA$_{n-1}$ robot using MCPFL is shown in figure 8.1. The $n-1$ most distal pendulums of the generalised PA$_{n-1}$ robot on the left of figure 8.1 are linearised using the control gains in eq. (8.7), which will guarantee that the PA$_{n-1}$ robot will behave as an approximation of the Acrobot. The dynamics of this system can thus be described as

$$\overline{\mathbf{M}}(q_2)\ddot{\mathbf{q}} + \overline{\mathbf{D}}(q_2, \dot{\mathbf{q}}) + \overline{\mathbf{K}}(\mathbf{q}) = \mathbf{G}(\mathbf{q})\mathbf{u} \tag{8.8}$$

where

$$\overline{\mathbf{M}}(q_2) = \begin{bmatrix} \overline{M}_{11}(q_2) & \overline{M}_{12}(q_2) \\ \overline{M}_{21}(q_2) & \overline{M}_{22}(q_2) \end{bmatrix}$$

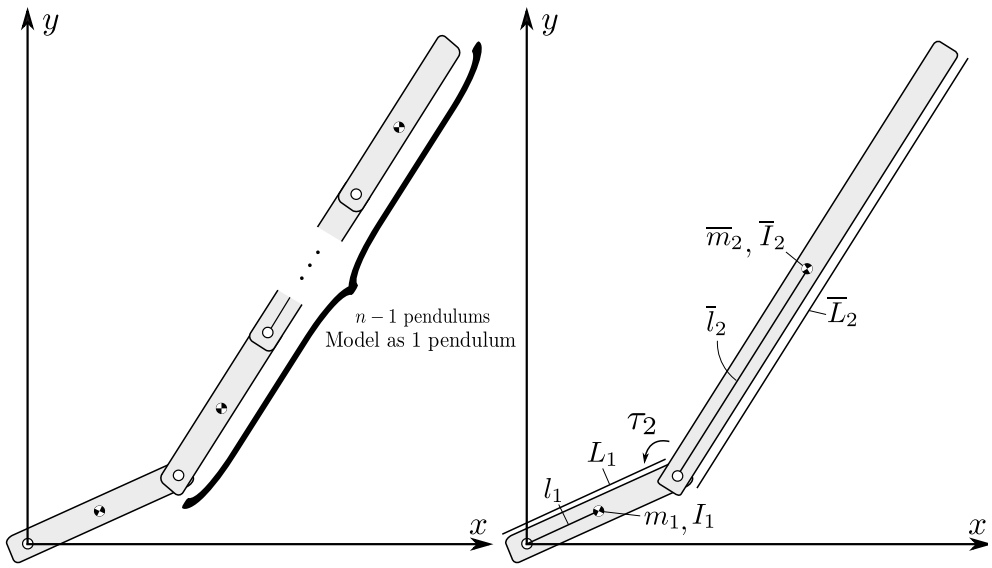

FIGURE 8.1: The PA$_{n-1}$ robot, linearised using MCPFL, represented as a MC-ROPA$_{n-1}$ robot.

$$\overline{\mathbf{D}}(q_2, \dot{\mathbf{q}}) = \overline{\mathbf{C}}(q_2, \dot{\mathbf{q}}) = \begin{bmatrix} \overline{\mathbf{C}}_1(q_2, \dot{\mathbf{q}}) \\ \overline{\mathbf{C}}_2(q_2, \dot{\mathbf{q}}) \end{bmatrix},$$

$$\overline{\mathbf{K}}(\mathbf{q}) = \begin{bmatrix} \overline{\mathbf{K}}_1(\mathbf{q}) \\ \overline{\mathbf{K}}_2(\mathbf{q}) \end{bmatrix}$$

with

$$\begin{aligned}
&\overline{M}_{11}(q_2) = \overline{\alpha}_1 + \overline{\alpha}_2 + 2\overline{\alpha}_3 \cos q_2, \\
&\overline{M}_{12}(q_2) = \overline{M}_{21}(q_2) = \overline{\alpha}_2 + \overline{\alpha}_3 \cos q_2, \\
&\overline{M}_{22}(q_2) = \overline{\alpha}_2, \\
&\overline{\mathbf{C}}_1(q_2, \dot{\mathbf{q}}) = -\overline{\alpha}_3(2\dot{q}_1\dot{q}_2 + \dot{q}_2^2) \sin q_2, \\
&\overline{\mathbf{C}}_2(q_2, \dot{\mathbf{q}}) = \overline{\alpha}_3\dot{q}_1^2 \sin q_2, \\
&\overline{\mathbf{K}}_1(\mathbf{q}) = -\overline{\beta}_1 \sin q_1 - \overline{\beta}_2 \sin(q_1 + q_2), \\
&\overline{\mathbf{K}}_2(\mathbf{q}) = -\overline{\beta}_2 \sin(q_1 + q_2)
\end{aligned}$$

and

$$\begin{aligned}
&\overline{\alpha}_1 = I_1 + m_1 {l_1}^2 + \overline{m}_2 {L_1}^2, && \overline{\alpha}_2 = \overline{I}_2 + \overline{m_2 {l_2}^2}, \\
&\overline{\alpha}_3 = \overline{m_2 l_2} L_1 && \overline{\beta}_1 = (m_1 l_1 + \overline{m}_2 L_1)\, g, \\
&\overline{\beta}_2 = \overline{m_2 l_2} g, && \\
&\overline{m}_2 = \sum_{i=2}^{n} m_i, && \overline{I}_2 = \sum_{i=2}^{n} I_i, \\
&\overline{m_2 l_2} = \sum_{i=2}^{n} m_i \left[l_i + \sum_{j=2}^{i-1} L_j \right], && \overline{m_2 {l_2}^2} = \sum_{i=2}^{n} m_i \left[l_i + \sum_{j=2}^{i-1} L_j \right]^2.
\end{aligned}$$

Therefore, the dynamical equations of motion of the newly defined MC-ROPA$_{n-1}$ robot may be defined as

$$\begin{aligned}
&\overline{M}_{11}(q_2)\ddot{q}_1 + \overline{M}_{12}(q_2)\ddot{q}_2 - \overline{\alpha}_3(2\dot{q}_1\dot{q}_2 + \dot{q}_2^2) \sin q_2 - \overline{\beta}_1 \sin q_1 \\
&- \overline{\beta}_2 \sin(q_1 + q_2) = 0, && \text{(8.9a)} \\
&\overline{M}_{21}(q_2)\ddot{q}_1 + \overline{M}_{22}(q_2)\ddot{q}_2 + \overline{\alpha}_3\dot{q}_1^2 \sin q_2 - \overline{\beta}_2 \sin(q_1 + q_2) = \tau_2. && \text{(8.9b)}
\end{aligned}$$

8.2.3 Necessary and Sufficient Gain Conditions for the Undamped MC-ROPA$_{n-1}$ Model

In this section, we will discuss the necessary and sufficient gain conditions that are required to swing-up the MC-ROPA$_{n-1}$ robot using LDM. These conditions are meticulously derived according to the procedural structure in [5], but only the most pertinent results of this derivation are included in this section. The more

mathematically rigorous sections of this derivation are included in appendix A. The derivation is treated with a significant amount of rigour since the success of the swing-up control is contingent on the satisfaction of these conditions. Altering the MC-ROPA$_{n-1}$ system (through the integration of viscous damping, for instance) may significantly impact these conditions. This impact will be best identified and understood if the derivation of the necessary conditions for swing-up of the undamped MC-ROPA$_{n-1}$ robot are meticulously described. Again, the importance of the MC-ROPA$_{n-1}$ robot will be made clear upon the definition of the *invertibility problem*, which is discussed in section 8.4.

It is apparent from eq. (8.1) that the necessary swing-up torque for the newly defined model above is defined as

$$\tau_2 = \frac{k_D \mathbf{G}^{\mathbf{T}}(\mathbf{q})\overline{\mathbf{M}}^{-1}(q_2)\Big[\overline{\mathbf{D}}(\mathbf{q},\dot{\mathbf{q}}) + \overline{\mathbf{K}}(\mathbf{q})\Big] - k_v\dot{q}_2 - k_P q_2}{\overline{\Lambda}(\mathbf{q},\dot{\mathbf{q}})} \tag{8.10}$$

where

$$\overline{\Lambda}(\mathbf{q},\dot{\mathbf{q}}) = (E - E_r) + k_D \mathbf{G}^{\mathbf{T}}(\mathbf{q})\overline{\mathbf{M}}^{-1}(q_2)\mathbf{G}(\mathbf{q})$$

whose dynamics is dictated by the Lyapunov candidate function

$$V = \frac{1}{2}(E - E_d)^2 + \frac{1}{2}k_D\dot{q}_2^2 + \frac{1}{2}k_P {q_2}^2 \tag{8.11}$$

and

$$\dot{V} = -k_V\dot{q}_2^2. \tag{8.12}$$

With this in mind, we can now demonstrate the feasibility of the swing-up control on this model by proving that

(i) The $\overline{\Lambda}(\mathbf{q},\dot{\mathbf{q}})$ matrix is invertible [5].

(ii) The system trajectory tends towards the UEP as $t \to \infty$ [5].

We will begin first with proving the invertible nature of $\overline{\Lambda}(\mathbf{q},\dot{\mathbf{q}})$.

It is shown in [5, pg. 204] that the $\Lambda(\mathbf{q},\dot{\mathbf{q}})$ matrix (and therefore the $\overline{\Lambda}(\mathbf{q},\dot{\mathbf{q}})$ matrix) is invertible as long as the necessary and sufficient condition

$$k_D > k_{DM} = \max_{\mathbf{q}}\Big\{\eta(\mathbf{q})\Big\} \tag{8.13}$$

is satisfied where

$$\eta(\mathbf{q}) = \Big[E_r + \mathbf{\Phi}(\mathbf{q}_a)\Big]\lambda_{\max}\Big[(\mathbf{G}^{\mathbf{T}}\mathbf{M}^{-1}\mathbf{G})^{-1}\Big].$$

This is proven in [5] for the PA$_{n-1}$ robot, but an adapted version of the proof is provided in appendix A (Proof A.3) to cater for the MC-ROPA$_{n-1}$ robot.

With this necessary condition proven, we must now show that the system trajectory of the MC-ROPA$_{n-1}$ robot will tend towards the UEP as $t \to \infty$ using invariant set theory. The result of this derivation is the gain condition

$$k_P > 2\overline{\beta}_1\overline{\beta}_2. \tag{8.14}$$

The satisfaction of this condition will ensure that there is only one other equilibrium point in the system (the FPEP). The FPEP will be unstable in this case, thus causing the system trajectory to follow a homoclinic orbit that tends toward the UEP [5]. The rigorous derivation of this condition is included in appendix A (Proof A.4) for the undamped MC-ROPA$_{n-1}$ robot, and follows the structure of the DDA proof shown in [5].

We have thus shown that the swing-up control of the MC-ROPA$_{n-1}$ robot is realisable. The modelling of the PA$_{n-1}$ robot as the MC-ROPA$_{n-1}$ robot will be useful in overcoming the *invertibility problem*, which will introduced at a later stage in this chapter.

The analytical results that have been derived for both the PA$_{n-1}$ robot and the MC-ROPA$_{n-1}$ must be supported by experimental results to demonstrate practical relevance. We must, therefore, construct defined variations of these robots, whose swing-up control can be practically demonstrated using simulation packages. We will begin by deriving the LDM-related swing-up control torque that is required to swing-up the least complex derivative of the PA$_{n-1}$ robot (and MC-ROPA$_{n-1}$ robot), namely the Acrobot (or MC-ROPA$_1$ robot). We will subsequently **replicate the simulated results** demonstrated in [5] for the undamped Acrobot. The modelling aspects of the Acrobot is covered in section 7.4.

8.2.4 The Undamped Acrobot

Derivation of the Necessary Swing-up Control Torque

The Lyapunov candidate function

$$V = \frac{1}{2}(E - E_r)^2 + \frac{1}{2}k_D\dot{q}_2^2 + \frac{1}{2}k_P{q_2}^2 \tag{8.15}$$

was chosen for the purpose of performing swing-up control on the Acrobot where

$$\dot{V} = (E - E_r)\dot{E} + k_D\ddot{q}_2\dot{q}_2 + k_P\dot{q}_2q_2 \tag{8.16}$$

represents the time-derivative of this Lyapunov function. The change in energy in the system, in this case, is only dependent on the actuation provided by torque τ_2.

Therefore

$$\dot{E} = \dot{q}_2 \tau_2. \tag{8.17}$$

This results in

$$\dot{V} = (E - E_r)\tau_2 \dot{q}_2 + k_D \ddot{q}_2 \dot{q}_2 + k_P q_2 \dot{q}_2 \tag{8.18}$$

through substitution. Furthermore, the dynamics $\ddot{q}_2$ is determined from the prototypical form, whereby

$$\ddot{q}_2 = \mathbf{G}^{\mathbf{T}}(\mathbf{q})\mathbf{M}^{-1}(\mathbf{q}) \left[\mathbf{G}(\mathbf{q})\tau_2 - \mathbf{C}(\mathbf{q}, \dot{\mathbf{q}}) - \mathbf{K}(\mathbf{q})\right].$$

Substituting this expression into eq. (8.18) produces

$$\begin{aligned}\dot{V} = \dot{q}_2 \big[\big[(E - E_r) + k_D \mathbf{G}^{\mathbf{T}}(\mathbf{q})\mathbf{M}^{-1}(\mathbf{q})\mathbf{G}(\mathbf{q})\big] \tau_2 - k_D \mathbf{G}^{\mathbf{T}}(\mathbf{q})\mathbf{M}^{-1}(\mathbf{q}) \left[\mathbf{C}(\mathbf{q}, \dot{\mathbf{q}})\right. \\ \left. + \mathbf{K}(\mathbf{q})\right] + k_p q_2 \big].\end{aligned}$$

As mentioned before, the Lyapunov function must have a negative semi-definite rate if the system trajectory is to tend towards the invariant set $\mathbf{W}_r$. The following Lyapunov function rate

$$\dot{V}_d = -k_v \dot{q}_2^2 \leq 0 \tag{8.19}$$

was selected for this application. Therefore, having $\dot{V} = \dot{V}_d$, we can solve for the necessary swing-up torque

$$\tau_2 = \frac{k_D \mathbf{G}^{\mathbf{T}}(\mathbf{q})\mathbf{M}^{-1}(\mathbf{q}) \left[\mathbf{C}(\mathbf{q}, \dot{\mathbf{q}}) + \mathbf{K}(\mathbf{q})\right] - k_V \dot{q}_2 - k_P q_2}{\Lambda(\mathbf{q}, \dot{\mathbf{q}})}$$

where

$$\Lambda(\mathbf{q}, \dot{\mathbf{q}}) = (E - E_r) + k_D \mathbf{G}^{\mathbf{T}}(\mathbf{q})\mathbf{M}^{-1}(\mathbf{q})\mathbf{G}(\mathbf{q}).$$

The gain conditions are demonstrated in eqs. (8.4) and (8.5) for $n = 2$ (which is identical to the results generated for the MC-ROPA$_{n-1}$ robot where $n = 2$, shown in eqs. (8.13) and (8.14)).

Simulation Results

Simulation results of the swing-up control formulate above is provided for the model demonstrated in section 7.4, we define the properties

$$\begin{aligned} m_1 &= 1 \text{ kg}, & m_2 &= 1 \text{ kg}, \\ l_1 &= 0.5 \text{ m}, & l_2 &= 1 \text{ m}, \\ L_1 &= 1 \text{ m}, & L_2 &= 2 \text{ m}, \\ I_1 &= 0.083 \text{ kg.m}^2, & I_2 &= 0.33 \text{ kg.m}^2, \\ g &= 9.81 \text{ m.s}^2 \end{aligned}$$

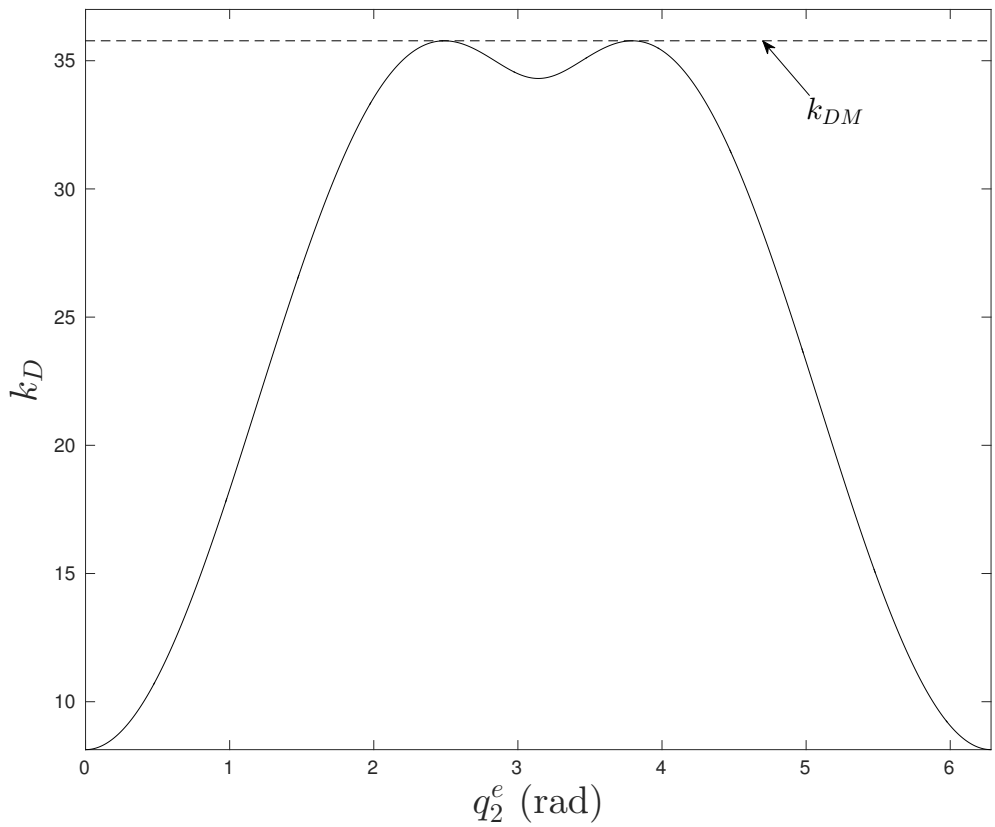

FIGURE 8.2: The behaviour of $k_D(\mathbf{q}_a)$ across $q_2^e \in [0, 2\pi]$, with k_{DM} shown as the suprenum.

for experimentation, as shown in [5]. The function $k_D(\mathbf{q}_a)$ (seen in eq. (8.4)) for this particular experiment is demonstrated in figure 8.2. The gain criterion k_{DM} represents the suprenum of this curve. We find that

$$k_{DM} = 35.777$$

through inspection of the data points of figure 8.2. The second gain condition (highlighted by eq. (8.14)) is selected to ensure that the straight-line function

$$f(q_2^e) = \frac{k_P}{\overline{\beta}_1 \overline{\beta}_2} q_2^e \tag{8.20}$$

will only intercept the function $\zeta(q_2^e)$ at the origin. We plotted the relationship between $\zeta(q_2^e)$ and two straight-line functions in figure 8.3, where the red dotted line represents the straight-line function whose behaviour is dictated by a gain k_P that satisfies eq. (8.14), and the blue dotted line represents a straight-line function that does not satisfy this gain condition. It is evident from the figure that selecting a

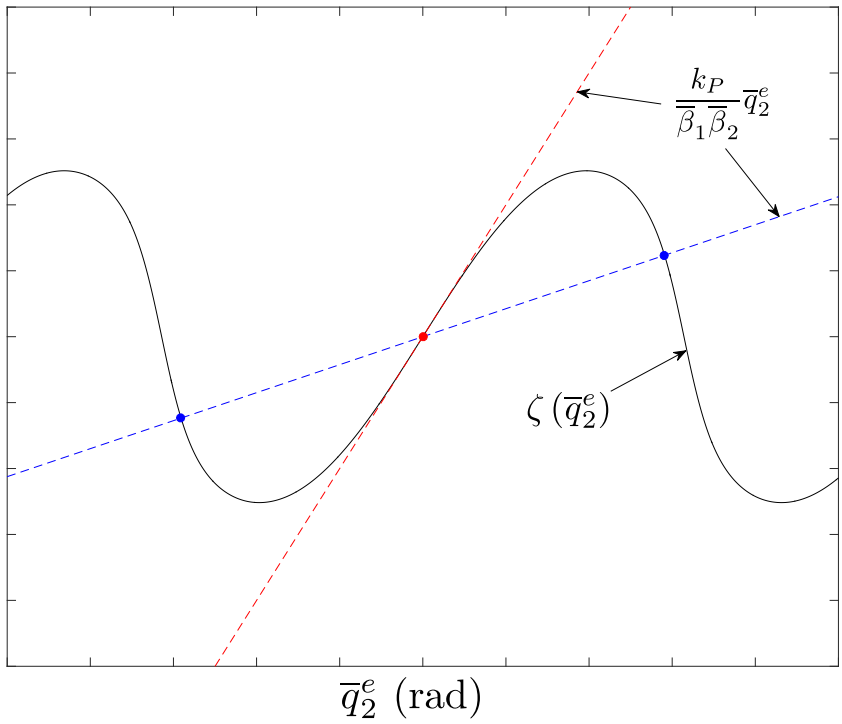

FIGURE 8.3: The intercepts of $\zeta\left(q_2^e\right)$ between (i) a straight line function that has a k_P that satisfies the condition in eq. (8.14) (red line) and (ii) a straight line function that has a k_P that only satisfies the condition in eq. (A.64).

gain k_P that satisfies the gain condition, whereby

$$k_P > 288.7083.$$

in this case, will ensure that the straight-line function only intercepts $\zeta\left(q_2^e\right)$ at the origin. Therefore, choosing

$$k_D = 35.8, \qquad k_P = 288.8$$

ensures that the $\Lambda(\mathbf{q}, \dot{\mathbf{q}})$ matrix is invertible $\forall t$ and that the FPEP is the only equilibrium point in Ω_-, with $\Omega_+ = \Omega_0 = \emptyset$. Additionally, we chose $k_V = 66.3$ to produce a rapid swing-up, as seen in [5] (since $k_V > 0$ is the only condition that must be satisfied). Therefore, a swing-up control simulation was performed using the selected gains and the initial conditions

$$q_1(0) = -\frac{\pi}{2} - 1.4, \qquad q_2(0) = 0,$$
$$\dot{q}_1(0), = 0 \qquad \dot{q}_2(0) = 0$$

as seen in [5]. The results of this swing-up control can be seen in figures 8.4 - 8.9.

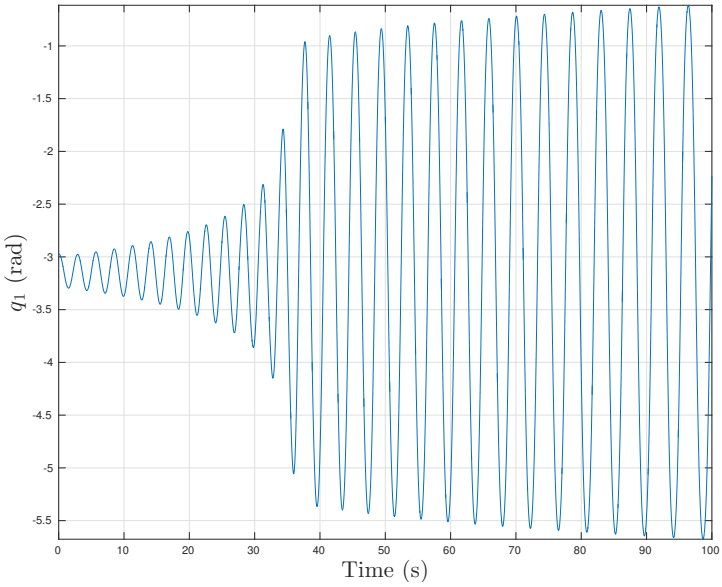

FIGURE 8.4: The angular displacement q_1 of the proximal pendulum for the undamped Acrobot with $k_P = 288.8$ during LDM-related swing-up control.

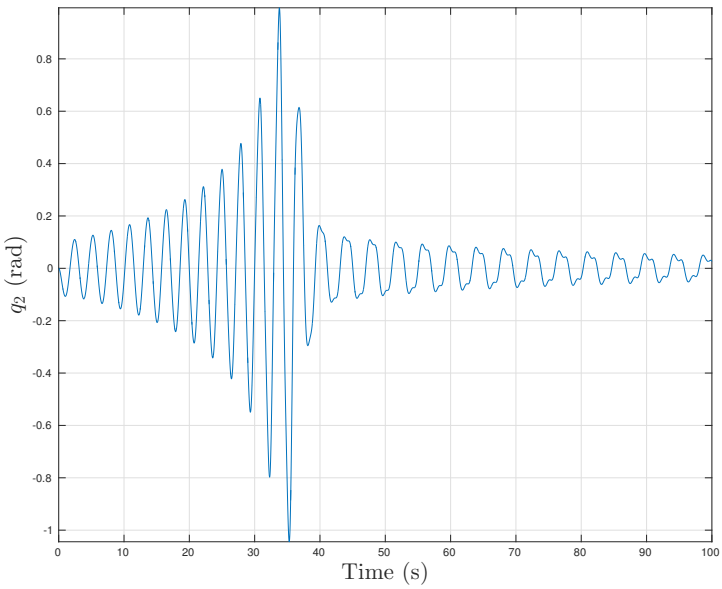

FIGURE 8.5: The angular displacement q_2 of the distal pendulum for the undamped Acrobot with $k_P = 288.8$ during LDM-related swing-up control.

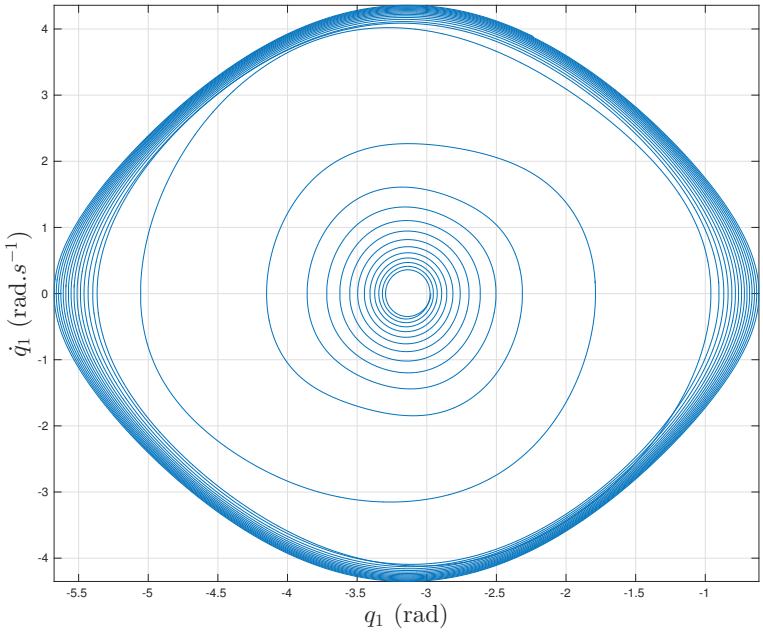

FIGURE 8.6: The phase portrait of the proximal pendulum of the undamped Acrobot with $k_P = 288.8$ during LDM-related swing-up control.

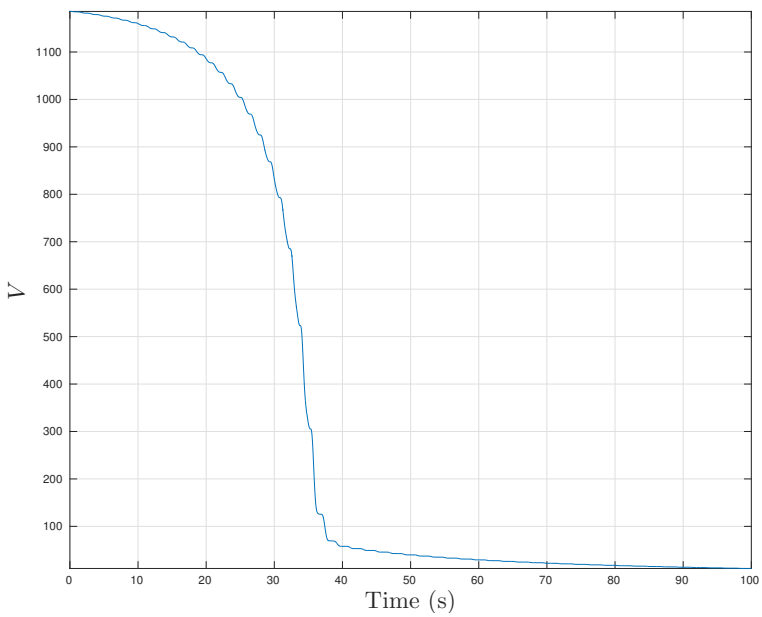

FIGURE 8.7: The Lyapunov candidate function of the undamped Acrobot with $k_P = 288.8$.

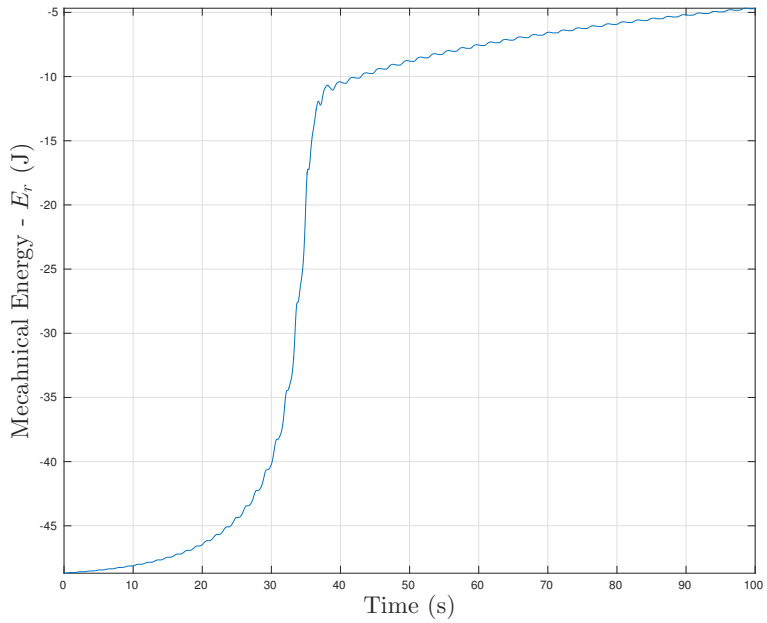

FIGURE 8.8: The difference between the mechanical energy of the undamped Acrobot and the energy state of E_r with $k_P = 288.8$ during LDM-related swing-up control.

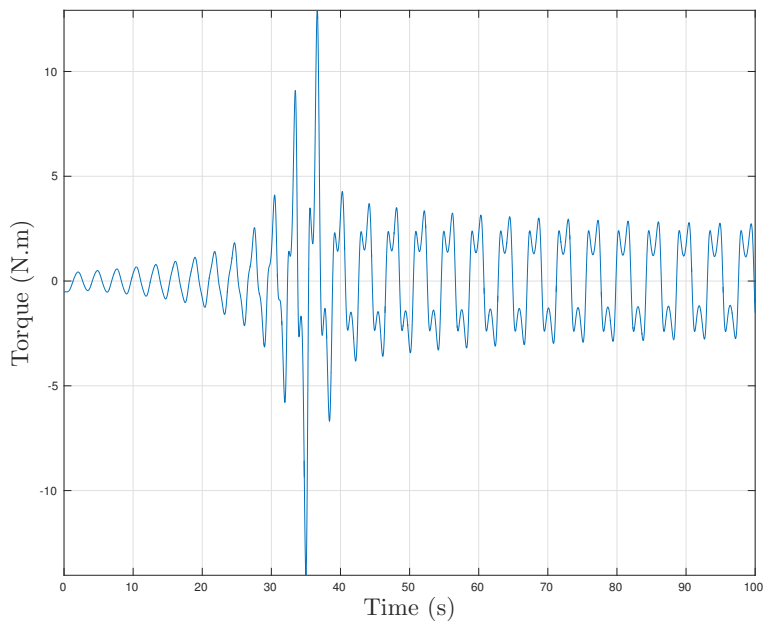

FIGURE 8.9: The LDM-related torque used to swing-up the undamped Acrobot with $k_P = 288.8$.

The Lyapunov function demonstrated in figure 8.7 predictably tends towards zero, demonstrating that the system tends towards the invariant set $\mathbf{W}_r$ as $t \to \infty$. This is confirmed by the behaviour of the angular trajectories q_1 and q_2 demonstrated in figures 8.4 and 8.5, whereby q_1 tends towards the UEP ($q_1^d = 0$), and q_2 tends towards $q_2^d = 0$. Additionally, figure 8.8 demonstrates that the system energy continued to tend towards the objective energy state E_r. The proximal pendulum entered into a limit cycle that approached the desired trajectory $q_1^d = 0$, and $\dot{q}_1^d = 0$ found on the far-right of the phase portrait in figure 8.6. The torque produced by the actuator found at the joint between the proximal and distal pendulum is demonstrated in figure 8.9. The peak of the torque corresponds to the point in the simulation when the proximal pendulum entered the outer boundaries of the limit cycle. The torque profile stabilises after this event, maintaining the limit cycle behaviour of the proximal pendulum whilst causing the distal pendulum to tend towards the desired trajectory. This behaviour is expected, but the Acrobot can, however, be swung-up at a faster rate by using the unstable nature of extra equilibrium points in the invariant set Ω_-, as shown in [5]. Therefore, we selected the gain

$$k_P = 61.3$$

that just satisfies the condition in eq. (A.64). This gain caused the three intercepts seen with the blue straight-line curve in figure 8.3. There are, therefore, three equilibrium points in Ω_-, which are all unstable. Furthermore, choosing

$$k_D = 35.8, \qquad k_V = 66.3$$

with the same initial conditions as the last swing-up control simulation, we find that the Acrobot is swung-up approximately near the UEP at a rate that is faster than the Acrobot that was swung-up with a k_P that allowed only one equilibrium point within Ω_-. The results of this swing-up control are shown in figure 8.10-8.15.

The results demonstrated in figures 8.10-8.15 are replications of the results demonstrated in [5] for the undamped DDA, which is expected. The response of the angular trajectories shown in figures 8.10 and 8.11 is faster than the response of the angular displacements shown in figures 8.4 and 8.5 since the control technique uses the unstable equilibrium point represented by the additional intercept in figure 8.3 to repel the trajectory towards the UEP. The slight plateau in the Lyapunov function shown in figure 8.13 and in the mechanical energy curve in figure 8.14 demonstrates the relative interception of this additional unstable equilibrium point in the invariant space $\mathbf{W}$. The response of this equilibrium point causes the proximal pendulum to exit the boundaries of the limit cycle demonstrated in figure 8.12. This behaviour is temporary, however, since the dynamics of the system obeys the constraints applied by the Lyapunov function, which dictates that the behaviour of the dynamics must tend towards the invariant set $\mathbf{W}_r$. The torque shown in figure 8.15 stabilises after the transience introduced by the interception of the unstable equilibrium point.

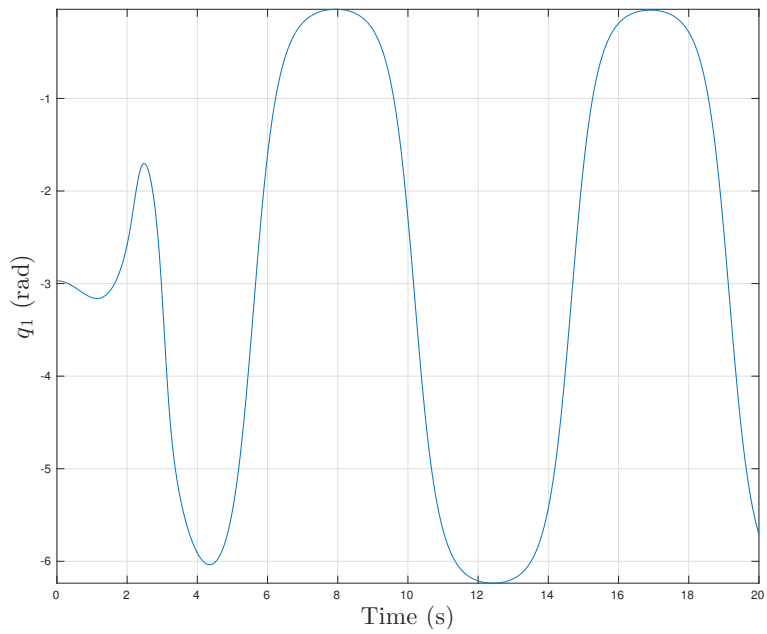

FIGURE 8.10: The angular displacement q_1 of the proximal pendulum of the undamped Acrobot with $k_P = 61.3$ during LDM-related swing-up control.

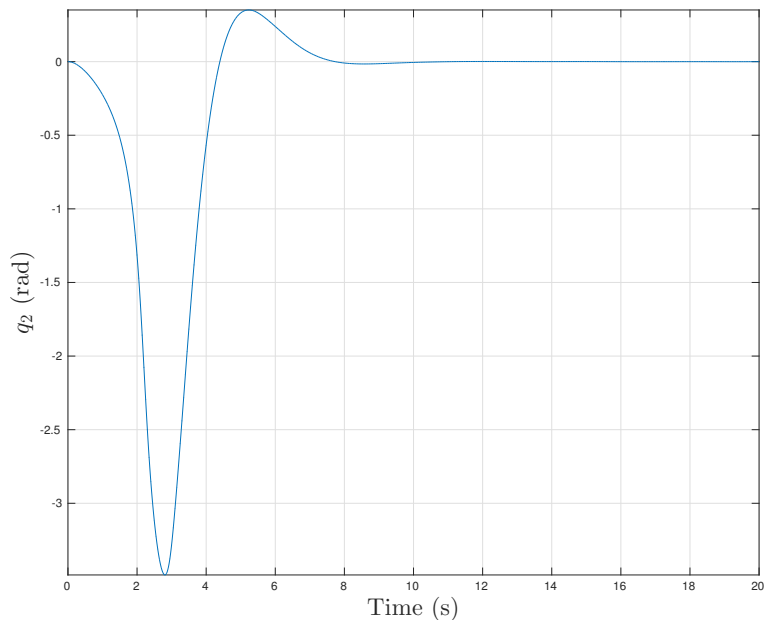

FIGURE 8.11: The angular displacement q_2 of the distal pendulum of the undamped Acrobot with $k_P = 61.3$ during LDM-related swing-up control.

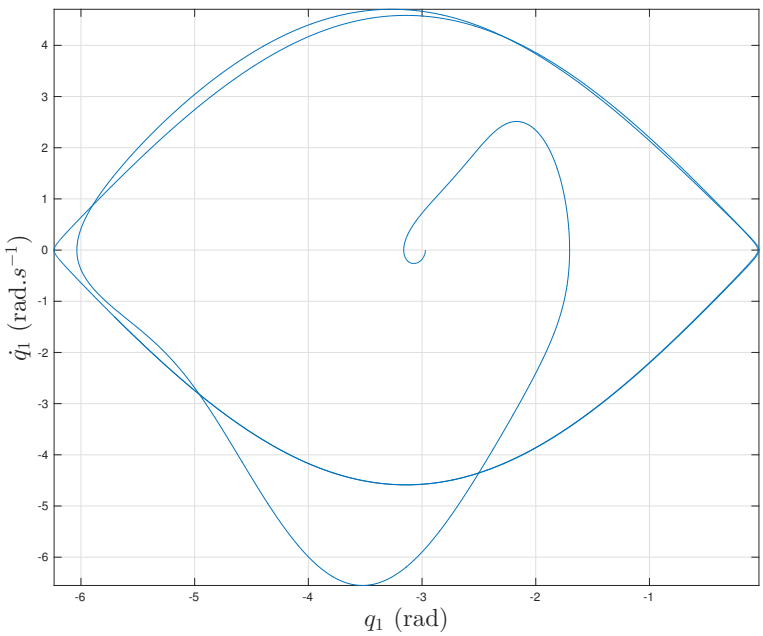

FIGURE 8.12: The phase portrait of the proximal pendulum of the undamped Acrobot with $k_P = 61.3$ during LDM-related swing-up control.

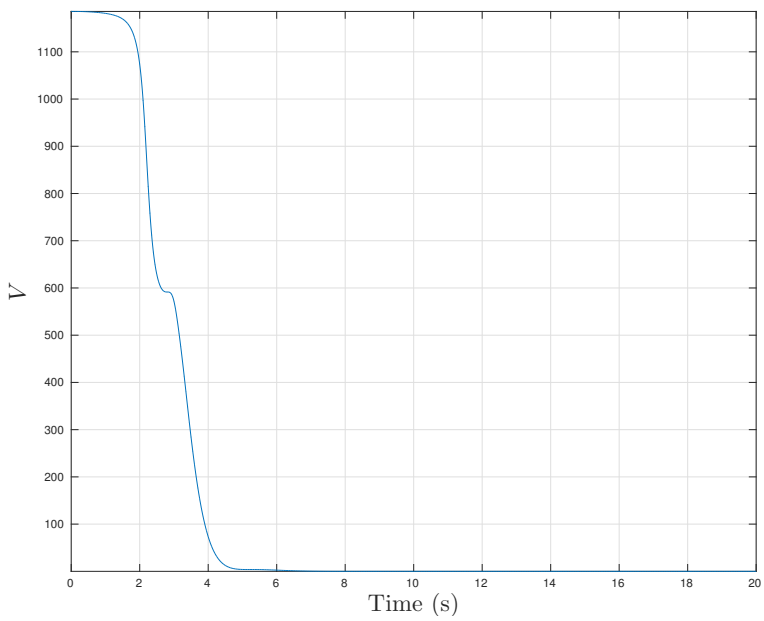

FIGURE 8.13: The Lyapunov candidate function of the undamped Acrobot with $k_P = 61.3$.

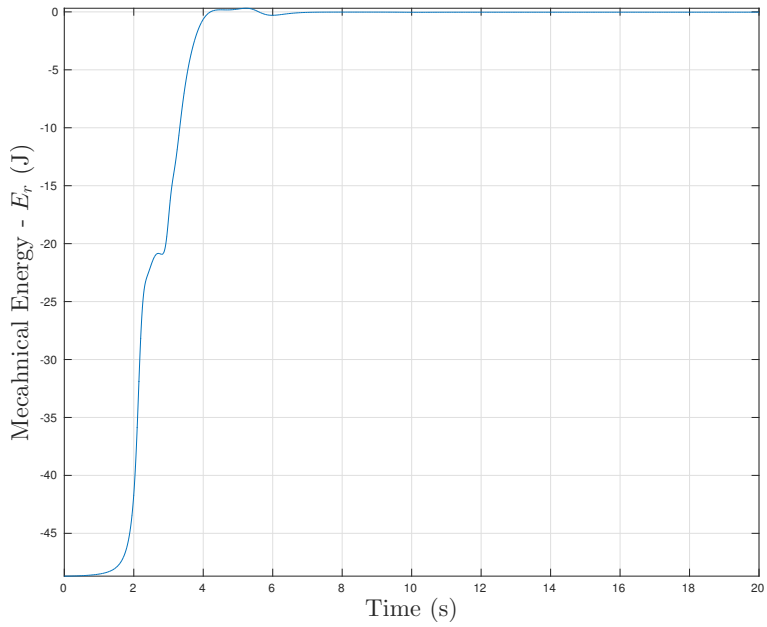

FIGURE 8.14: The difference between the mechanical energy of the undamped Acrobot and the energy state of E_r with $k_P = 61.3$ during LDM-related swing-up control.

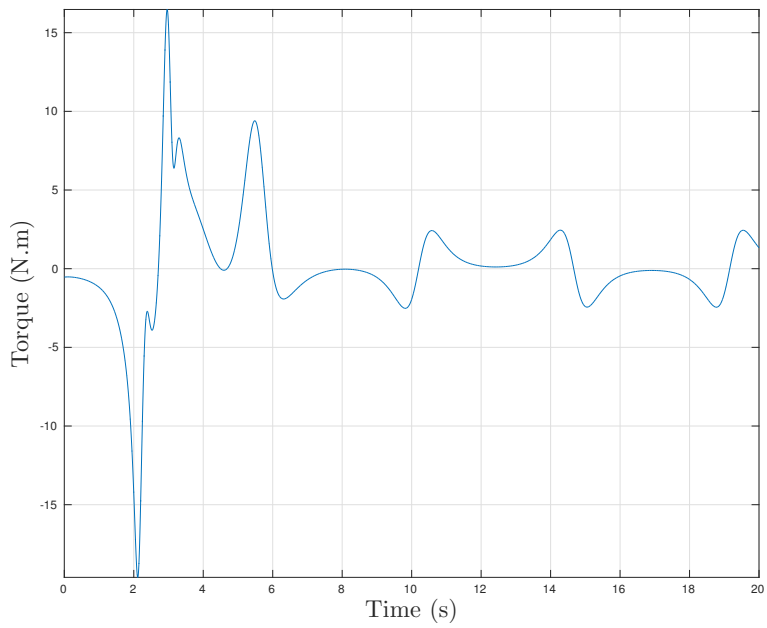

FIGURE 8.15: The LDM-related torque used to swing-up the undamped Acrobot with $k_P = 61.3$.

We will now demonstrate that relevant swing-up control results can be produced for undamped higher-order systems. A classic higher-order PA_{n-1} robot is the PAA robot. The PAA robot can be approximately modelled as the MC-ROPA_2 robot (whose control is discussed in the following section).

8.2.5 The Undamped PAA Robot

Derivation of the Necessary Swing-up Control Torque for the Traditional PAA Robot

The PAA robot is a triple inverted pendulum system that is actuated only at the most distal joints (being the 1st and 2nd joints in this configuration). The mathematical model of the PAA robot is discussed in great detail in section 7.5. We begin with the definition of the candidate Lyapunov function for the undamped PAA robot originally defined in [5], whereby

$$V = \frac{1}{2}(E - E_r)^2 + \frac{1}{2}k_D\dot{\mathbf{q}}_a^{\mathbf{T}}\dot{\mathbf{q}}_a + \frac{1}{2}k_P\overline{\mathbf{q}}_a{}^{\mathbf{T}}\overline{\mathbf{q}}_a$$

and where

$$\overline{q}_a = \begin{bmatrix}\overline{q}_2 & q_3\end{bmatrix}^{\mathbf{T}}$$

as stated in section 7.5. Taking the derivative of this Lyapunov function, we find that

$$\dot{V} = (E - E_r)\dot{E} + k_D\dot{\mathbf{q}}_a^{\mathbf{T}}\ddot{\mathbf{q}}_a + k_P\dot{\mathbf{q}}_a^{\mathbf{T}}\psi^{\mathbf{T}}\left(\overline{\mathbf{q}}_a\right)\overline{\mathbf{q}}_a. \tag{8.21}$$

The change of energy in the undamped PAA robot can only be caused by the two actuators. Therefore

$$\dot{E} = \dot{\mathbf{q}}_a^{\mathbf{T}}\tau_a$$

where

$$\tau_a = \begin{bmatrix}\tau_2 & \tau_3\end{bmatrix}^{\mathbf{T}}.$$

Substituting this expression into eq. (8.21) we find that

$$\dot{V} = \dot{\mathbf{q}}_a^{\mathbf{T}}\left[(E - E_r)\tau_a + k_D\ddot{\mathbf{q}}_a + k_P\psi^{\mathbf{T}}\left(\overline{\mathbf{q}}_a\right)\overline{\mathbf{q}}_a\right].$$

The equations of motion for the two most distal pendulums, represented by $\ddot{\mathbf{q}}_a$, may be solved for through the manipulation of the prototypical form for the PAA robot. The results in

$$\ddot{\mathbf{q}}_a = \mathbf{G}^{\mathbf{T}}(\mathbf{q})\mathbf{M}^{-1}(\mathbf{q})\left[\mathbf{G}(\mathbf{q})\tau_a - \mathbf{C}(\mathbf{q}, \dot{\mathbf{q}}) - \mathbf{K}(\mathbf{q})\right].$$

The substitution of this expression into eq. (8.21) produces

$$\begin{aligned}\dot{V} &= \dot{\mathbf{q}}_a^{\mathbf{T}} \left[\left[(E - E_r) I_2 + k_D \mathbf{G}^{\mathbf{T}}(\mathbf{q}) \mathbf{M}^{-1}(\mathbf{q}) \mathbf{G}(\mathbf{q}) \right] \tau_a - k_D \mathbf{G}^{\mathbf{T}}(\mathbf{q}) \mathbf{M}^{-1}(\mathbf{q}) \left[\mathbf{C}(\mathbf{q}, \dot{\mathbf{q}}) + \mathbf{K}(\mathbf{q}) \right] \right. \\ &\quad \left. + k_P \psi^{\mathbf{T}} \left(\overline{\mathbf{q}}_a \right) \overline{\mathbf{q}}_a \right] \\ &= \dot{\mathbf{q}}_a^{\mathbf{T}} \left[\Lambda(\mathbf{q}, \dot{\mathbf{q}}) \tau_a - k_D \mathbf{G}^{\mathbf{T}}(\mathbf{q}) \mathbf{M}^{-1}(\mathbf{q}) \left[\mathbf{C}(\mathbf{q}, \dot{\mathbf{q}}) + \mathbf{K}(\mathbf{q}) \right] + k_P \psi^{\mathbf{T}} \left(\overline{\mathbf{q}}_a \right) \overline{\mathbf{q}}_a \right]\end{aligned}$$

where

$$\Lambda(\mathbf{q}, \dot{\mathbf{q}}) = (E - E_r) I_2 + k_D \mathbf{G}^{\mathbf{T}}(\mathbf{q}) \mathbf{M}^{-1}(\mathbf{q}) \mathbf{G}(\mathbf{q}).$$

If the desired Lyapunov candidate function is chosen to be

$$\dot{V}_d = -k_V \dot{\mathbf{q}}_{\mathbf{a}}^{\mathbf{T}} \dot{\mathbf{q}}_a$$

then, allowing $\dot{V} = \dot{V}_d$ we can solve for the torque τ_a, since $\dot{\mathbf{q}}_a^{\mathbf{T}}$ is a common vector. Therefore

$$\tau_a = \Lambda^{-1}(\mathbf{q}, \dot{\mathbf{q}}) \left[k_D \mathbf{G}^{\mathbf{T}}(\mathbf{q}) \mathbf{M}^{-1}(\mathbf{q}) \left[\mathbf{C}(\mathbf{q}, \dot{\mathbf{q}}) + \mathbf{K}(\mathbf{q}) \right] - k_V \dot{\mathbf{q}}_a - k_P \psi^{\mathbf{T}} \left(\overline{\mathbf{q}}_a \right) \overline{\mathbf{q}}_a \right].$$

The necessary gain conditions for the undamped PAA robot are shown in eqs. (8.4) and (8.5).

Simulation Results: Traditional PAA Robot

To simulate the swing-up control of the PAA robot with the torque derived in the previous section, we choose the properties

$m_1 = 5.4$ kg,	$m_2 = 29.5$ kg,	$m_3 = 18.5$ kg,
$L_1 = 0.58$ m,	$L_2 = 0.5$ m,	$L_3 = 0.79$ m,
$l_1 = 0.31$ m,	$l_2 = 0.2$ m,	$l_3 = 0.33$ m,
$I_1 = 0.15$ kg.m^2,	$I_2 = 1.93$ kg.m^2,	$I_3 = 1.03$ kg.m^2

for the PAA robot, as seen in [5]. The gains are chosen by evaluating the gain selection conditions highlighted in eqs. (8.4) and (8.5), whereby

$$k_D > k_{DM} = \max_{\mathbf{q}_a} \left\{ (E_r + \mathbf{\Phi}(\mathbf{q}_a)) \lambda_{\max} \left(\left(\mathbf{G}^{\mathbf{T}}(\mathbf{q}) \mathbf{M}^{-1}(\mathbf{q}) \mathbf{G}(\mathbf{q}) \right)^{-1} \right) \right\} \tag{8.22}$$

and

$$k_P > k_{m_2} = 2\overline{\beta}_1 \left(\beta_2 + \beta_3 \right), \qquad k_P > k_{m_3} = \frac{2E_r \beta_2 \beta_3}{\beta_2 + \beta_3}. \tag{8.23}$$

For the condition on k_D, k_{DM} must be determined through an experimental method since eq. (8.22) offers no analytical solution, as seen with the Acrobot. We thus swept through a range of $[0, 2\pi]$ for both q_2 and q_3, and we plotted the function k_{DM} against these angular displacements, as shown in figures 8.16 and 8.17.

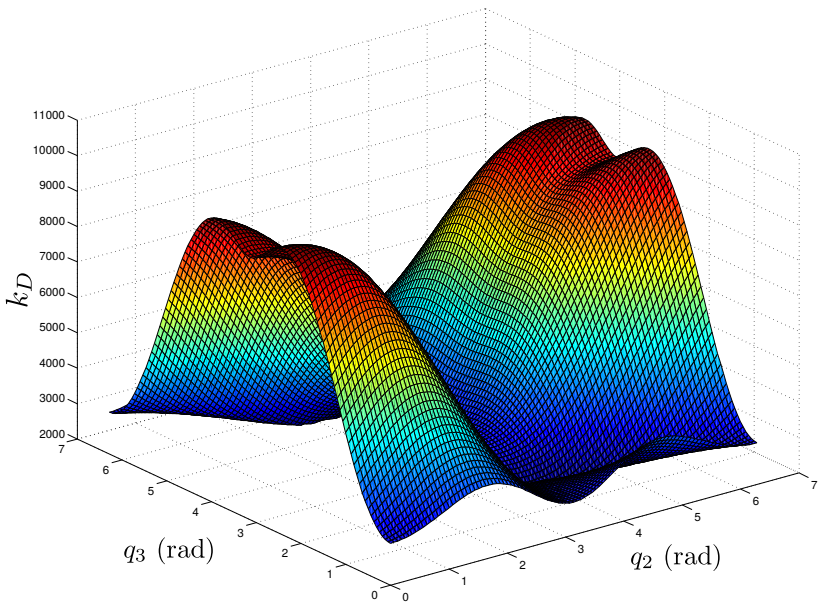

FIGURE 8.16: Contour plot (3D) of k_D for the PAA robot.

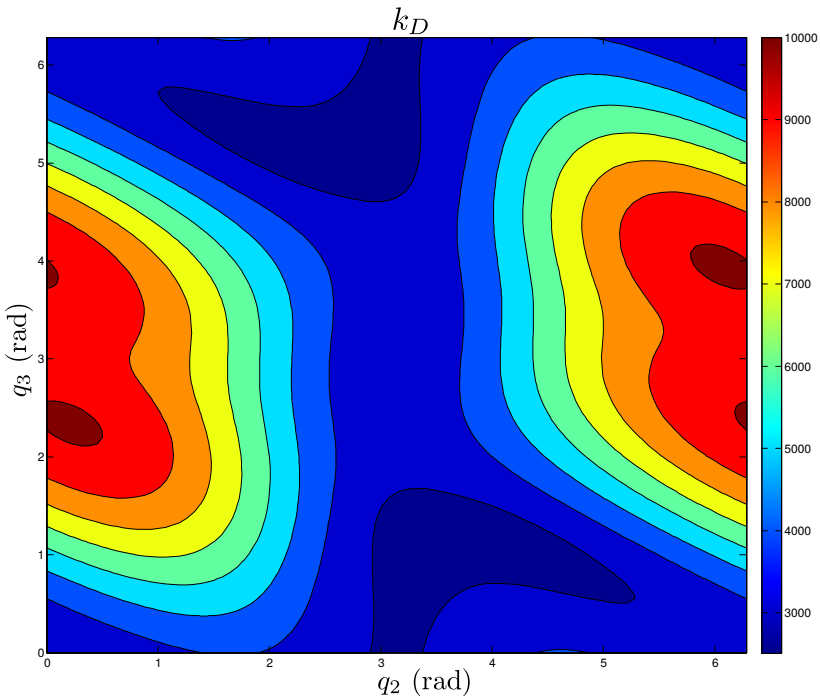

FIGURE 8.17: Contour plot (2D) of k_D for the PAA robot.

The maximum of the peaks of this curve is found to be $\max_{\mathbf{q}_a}\{k_D\} = k_{DM} = 10101$, which is approximate to the value determined in [5] for the PAA robot. The conditions on k_P (seen in eq. (8.23)) are solved for trivially, with

$$k_{m_2} = 120500, \qquad k_{m_3} = 42434.$$

Therefore, since $k_{m_2} > k_{m_3}$, $k_p > k_{m_2}$ is required to satisfy the gain selection criterion in eq. (8.23). Therefore

$$k_P > 120500.$$

To replicate the results seen in [5], the gains

$$k_D = 11500, \qquad k_P = 121700, \qquad k_V = 4550$$

were considered, according to their respective selection conditions. Additionally, we selected the initial conditions

$$q_1(0) = -1.4 - \frac{\pi}{2}, \qquad q_2(0) = q_3(0) = 0,$$
$$\dot{q}_1(0) = \dot{q}_2(0) = \dot{q}_3(0) = 0.$$

Figures 8.18-8.25 demonstrate the results of the simulation.

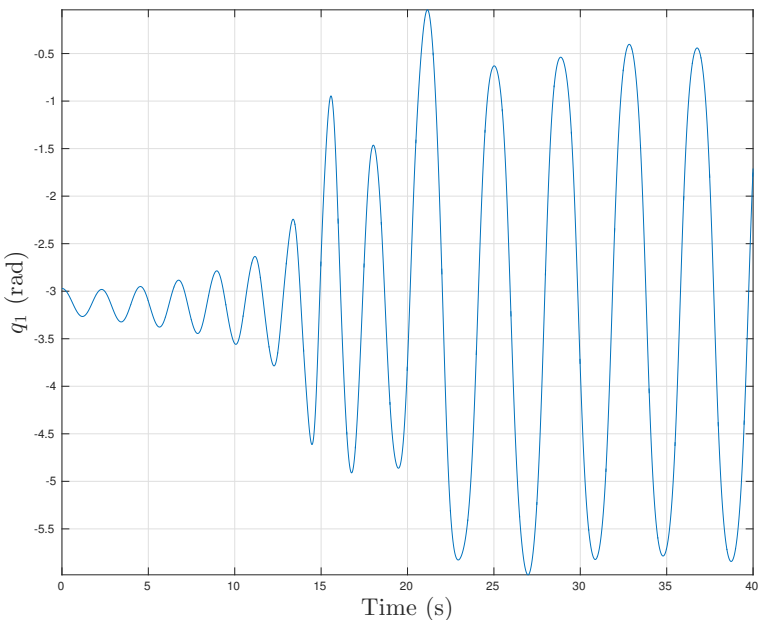

FIGURE 8.18: The angular displacement q_1 of the most proximal pendulum of the undamped PAA robot during LDM-related swing-up control.

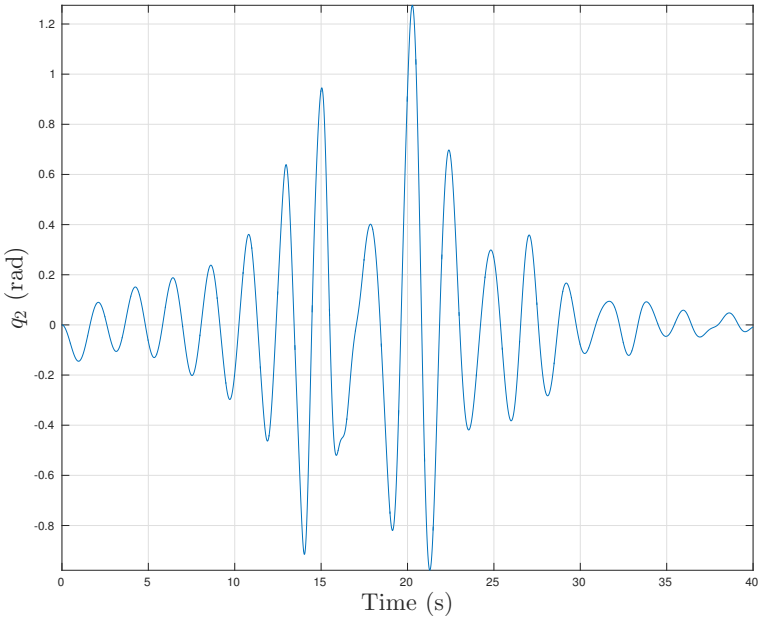

FIGURE 8.19: The angular displacement q_2 of the second pendulum of the undamped PAA robot during LDM-related swing-up control.

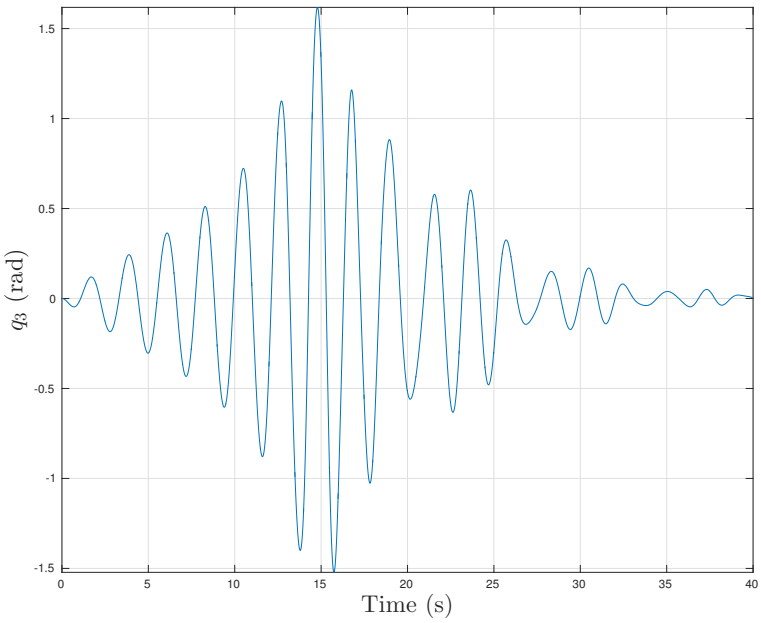

FIGURE 8.20: The angular displacement q_3 of the most distal pendulum of the undamped PAA robot during LDM-related swing-up control.

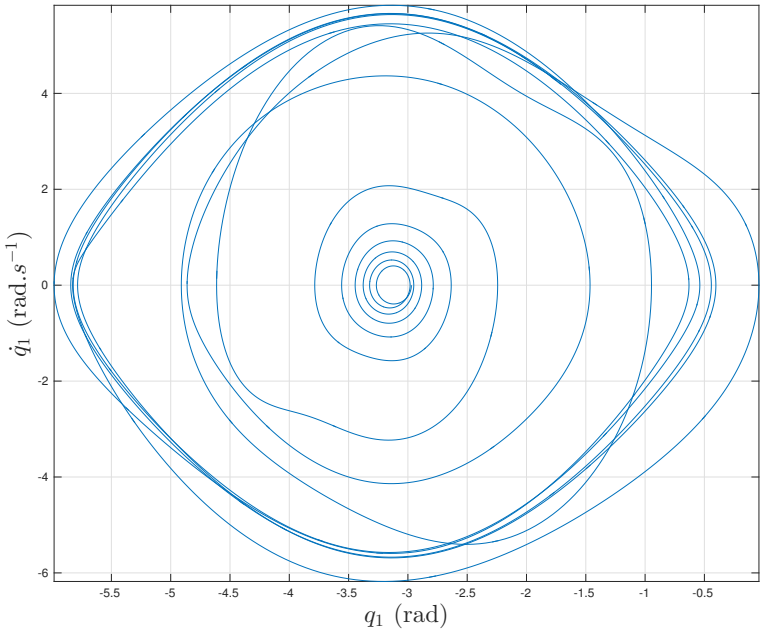

FIGURE 8.21: The phase portrait of the proximal pendulum of the undamped PAA robot during LDM-related swing-up control.

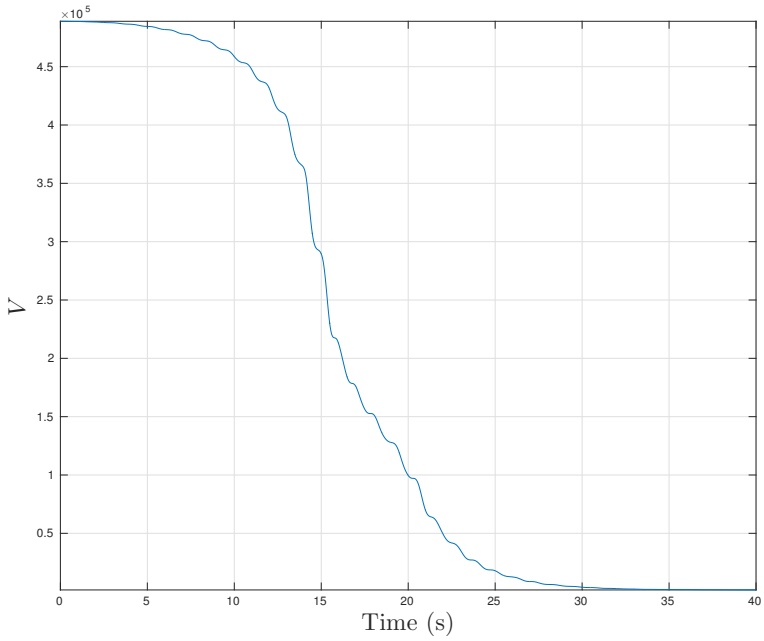

FIGURE 8.22: The Lyapunov candidate function of the undamped PAA robot.

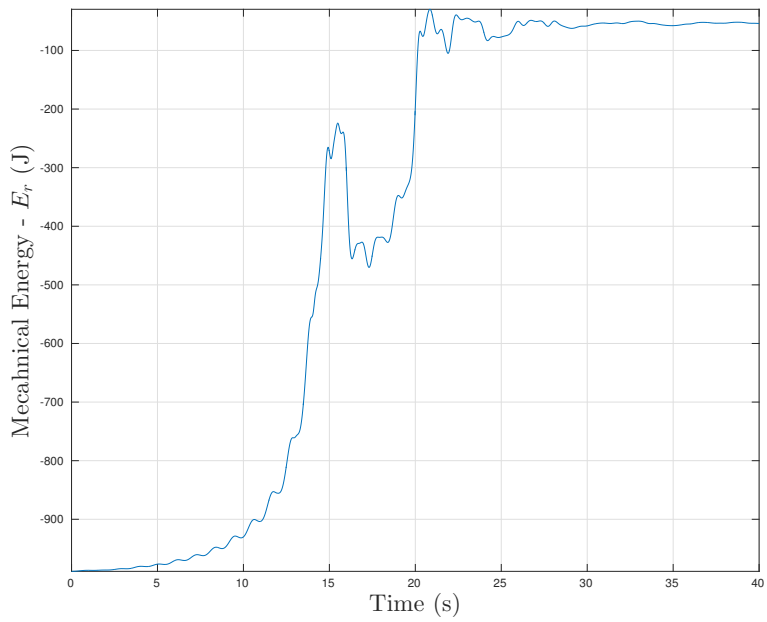

FIGURE 8.23: The difference between the mechanical energy of the undamped PAA robot and the energy state of E_r during LDM-related swing-up control.

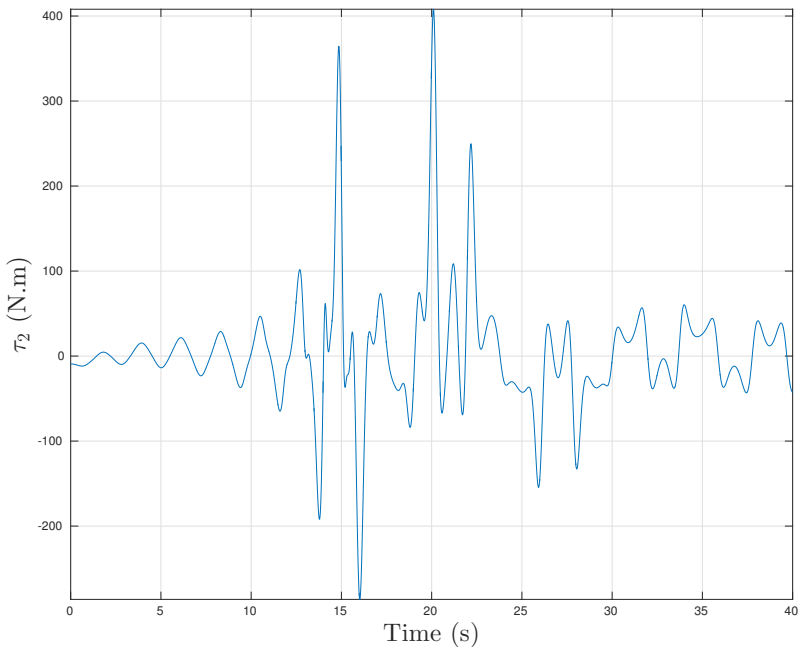

FIGURE 8.24: The LDM-related torque τ_2 used to swing-up the undamped PAA robot.

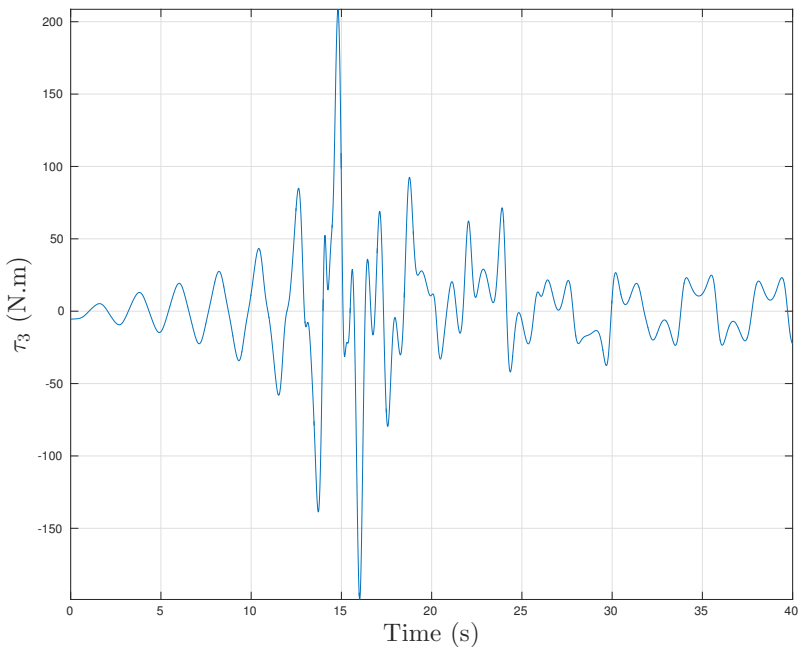

FIGURE 8.25: The LDM-related torque τ_3 used to swing-up the undamped PAA robot.

It is clear from figure 8.22 that the Lyapunov function tended towards zero, therefore reflecting the fact that the system dynamics approached the invariant set $\mathbf{W}_r$ throughout the simulation. This is confirmed by the behaviour of the angular trajectories shown in figures 8.18-8.20, whereby the proximal pendulum tended towards $q_1^d = 0$, the second pendulum approached $q_2^d = 0$, and the most distal pendulum approached $q_3^d = 0$ as $t \to \infty$. The trajectories q_2 and q_3 peaked at their greatest end-state deviations at approximately 15 seconds into the simulation. The transience attenuates after this point, allowing the proximal pendulum to enter into a limit cycle, as demonstrated by the phase portrait in figure 8.21. The trajectory exited the boundaries of this limit cycle during the transient phase of the simulation. The mechanical energy of the system is demonstrated in figure 8.23. It is evident that the mechanical energy of the PAA robot approximated the desired energy state E_r by the end of the simulation. The peak at 15 seconds occurred towards the end of the transience, which was the result of the high kinetic energies of the pendulums. The torques produced by the actuators in the system are demonstrated in figures 8.24 and 8.25. The profiles of these torques are similar, whereby the maximum torques are produced towards the end of the transient phase, forcing the system to approach the limit cycle in figure 8.21. The limit cycle is maintained by the steady-state torque profiles produced after the transience. These results are expected since they corroborate with the results produced in [5].

With the PAA robot having an order $n > 2$, we can model the PAA robot as a

MC-ROPA$_2$ robot, which approximates the behaviour of an Acrobot so long as the response frequency of the regulating controllers are sufficiently large. The modelling of the MC-ROPA$_2$ robot is, therefore, discussed in the next section.

Modelling the Undamped PAA Robot as the MC-ROPA$_2$ Robot

To model the PAA robot as an approximation of the Acrobot, the FBL torque

$$\tau_3 = \hat{M}_{33}(\mathbf{q})v_3 + \hat{C}_3(\mathbf{q}, \dot{\mathbf{q}}) + \hat{K}_3(\mathbf{q}) + \hat{\tau}_3$$

is required for τ_3, which is derived from eq. (8.6) where

$$\hat{M}_{33}(\mathbf{q}) = M_{33}(\mathbf{q}) - \frac{\tilde{M}_{13}(\mathbf{q})M_{31}(\mathbf{q})}{M_{11}(\mathbf{q})} - \frac{\tilde{M}_{23}(\mathbf{q})M_{32}(\mathbf{q})}{\tilde{M}_{22}(\mathbf{q})},$$

$$\hat{C}_3(\mathbf{q}, \dot{\mathbf{q}}) = C_3(\mathbf{q}, \dot{\mathbf{q}}) - \frac{M_{31}(\mathbf{q})}{M_{11}(\mathbf{q})}\tilde{C}_1(\mathbf{q}, \dot{\mathbf{q}}) - \frac{M_{32}(\mathbf{q})}{\tilde{M}_{22}(\mathbf{q})}\tilde{C}_2(\mathbf{q}, \dot{\mathbf{q}}),$$

$$\hat{K}_3(\mathbf{q}) = K_3(\mathbf{q}) - \frac{M_{31}(\mathbf{q})}{M_{11}(\mathbf{q})}\tilde{K}_1(\mathbf{q}) - \frac{M_{32}(\mathbf{q})}{\tilde{M}_{22}(\mathbf{q})}\tilde{K}_2(\mathbf{q}),$$

$$\hat{\tau}_3 = \frac{M_{32}(\mathbf{q})}{\tilde{M}_{22}(\mathbf{q})}\tau_2 - \frac{M_{31}(\mathbf{q})}{M_{11}(\mathbf{q})}\tilde{\tau}_2,$$

$$\tilde{\tau}_2 = \frac{M_{12}(\mathbf{q})}{\tilde{M}_{22}}\tau_2$$

and, for $2 \leq k \leq 3$,

$$\tilde{M}_{2k}(\mathbf{q}) = M_{2k}(\mathbf{q}) - \frac{M_{1k}(\mathbf{q})M_{21}(\mathbf{q})}{M_{11}(\mathbf{q})}, \qquad \tilde{M}_{13}(\mathbf{q}) = M_{13}(\mathbf{q}) - \frac{M_{12}(\mathbf{q})\tilde{M}_{23}(\mathbf{q})}{\tilde{M}_{22}(\mathbf{q})},$$

$$\tilde{C}_2(\mathbf{q}, \dot{\mathbf{q}}) = C_2(\mathbf{q}, \dot{\mathbf{q}}) - \frac{M_{21}(\mathbf{q})}{M_{11}(\mathbf{q})}C_1(\mathbf{q}, \dot{\mathbf{q}}), \quad \tilde{C}_1(\mathbf{q}, \dot{\mathbf{q}}) = C_1(\mathbf{q}, \dot{\mathbf{q}}) - \frac{M_{12}(\mathbf{q})}{\tilde{M}_{22}(\mathbf{q})}\tilde{C}_2(\mathbf{q}, \dot{\mathbf{q}}),$$

$$\tilde{K}_2(\mathbf{q}) = K_2(\mathbf{q}) - \frac{M_{21}(\mathbf{q})}{M_{11}(\mathbf{q})}K_1(\mathbf{q}), \qquad \tilde{K}_1(\mathbf{q}) = K_1(\mathbf{q}) - \frac{M_{12}(\mathbf{q})}{\tilde{M}_{22}(\mathbf{q})}\tilde{K}_2(\mathbf{q}).$$

Implementing this torque causes $\ddot{q}_3 = v_3$, which was selected to be

$$v_3 = -k_{D_3}\dot{q}_3 - k_{P_3}q_3.$$

With the application of the FBL torque, the PAA robot can be approximately modelled as an Acrobot described by the dynamical equations

$$\overline{M}_{11}(q_2)\ddot{q}_1 + \overline{M}_{12}(q_2)\ddot{q}_2 - \overline{\alpha}_3\left(2\dot{q}_1\dot{q}_2 + \dot{q}_2^2\right)\sin q_2 - \overline{\beta}_1 \sin q_1 - \overline{\beta}_2 \sin(q_1+q_2) = 0, \tag{8.24a}$$

$$\overline{M}_{21}(q_2)\ddot{q}_1 + \overline{M}_{22}(q_2)\ddot{q}_2 + \overline{\alpha}_3\dot{q}_1^2 \sin q_2 - \overline{\beta}_2 \sin(q_1+q_2) = \tau_2 \tag{8.24b}$$

where

$$\begin{aligned}
\overline{M}_{11}(q_2) &= \overline{\alpha}_1 + \overline{\alpha}_2 + 2\overline{\alpha}_3 \cos q_2,\\
\overline{M}_{12}(q_2) &= \overline{M}_{21}(q_2) = \overline{\alpha}_2 + \overline{\alpha}_3 \cos q_2,\\
\overline{M}_{22}(q_2) &= \overline{\alpha}_2,\\
\overline{\mathbf{C}}_1(q_2, \dot{\mathbf{q}}) &= -\overline{\alpha}_3(2\dot{q}_1\dot{q}_2 + \dot{q}_2^2)\sin q_2,\\
\overline{\mathbf{C}}_2(q_2, \dot{\mathbf{q}}) &= \overline{\alpha}_3\dot{q}_1^2 \sin q_2,\\
\overline{\mathbf{K}}_1(\mathbf{q}) &= -\overline{\beta}_1 \sin q_1 - \overline{\beta}_2 \sin(q_1+q_2),\\
\overline{\mathbf{K}}_2(\mathbf{q}) &= -\overline{\beta}_2 \sin(q_1+q_2)
\end{aligned}$$

and

$$\begin{aligned}
\overline{\alpha}_1 &= I_1 + m_1 {l_1}^2 + \overline{m}_2 {L_1}^2, & \overline{\alpha}_2 &= \overline{I}_2 + \overline{m_2 {l_2}^2},\\
\overline{\alpha}_3 &= \overline{m_2 l_2} L_1, & \overline{\beta}_1 &= (m_1 l_1 + \overline{m}_2 L_1)\, g,\\
\overline{\beta}_2 &= \overline{m_2 l_2} g, & &\\
\overline{m}_2 &= m_2 + m_3, & \overline{I}_2 &= I_2 + I_3,\\
\overline{m_2 l_2} &= m_2 l_2 + m_3\left[l_3 + L_2\right], & \overline{m_2 {l_2}^2} &= m_2 {l_2}^2 + m_3\left[l_3 + L_2\right]^2.
\end{aligned}$$

Derivation of the Necessary Swing-up Control Torque for the Undamped MC-ROPA$_2$ Robot

Choosing the Lyapunov function

$$V = \frac{1}{2}(E - E_r)^2 + \frac{1}{2}k_D\dot{q}_2^2 + \frac{1}{2}k_P {q_2}^2$$

results, according to eq. (8.10) in the necessary swing-up torque

$$\tau_2 = \frac{k_D \mathbf{G}^{\mathbf{T}}(\mathbf{q})\overline{\mathbf{M}}^{-1}(q_2)\left[\overline{\mathbf{D}}(\mathbf{q}, \dot{\mathbf{q}}) + \overline{\mathbf{K}}(\mathbf{q})\right] - k_v\dot{q}_2 - k_P q_2}{\overline{\Lambda}(\mathbf{q}, \dot{\mathbf{q}})} \tag{8.25}$$

where

$$\overline{\Lambda}(\mathbf{q}, \dot{\mathbf{q}}) = (E - E_r) + k_D \mathbf{G}^{\mathbf{T}}(\mathbf{q})\overline{\mathbf{M}}^{-1}(q_2)\mathbf{G}(\mathbf{q}).$$

The gain selection conditions

$$k_D > \max_{q_2} \left\{ \frac{\left(\overline{\mathbf{\Phi}}(q_2) + E_r\right) \left|\overline{\mathbf{M}}(q_2)\right|}{\overline{M}_{11}(q_2)} \right\}$$

must be satisfied to ensure that $\overline{\Lambda}(\mathbf{q}, \dot{\mathbf{q}})$ is invertible and that the system trajectory will tend towards the invariant set $\mathbf{W}_r$ as $t \to \infty$ with the invariant spaces $\Omega_+ = \Omega_0 = \emptyset$, where

$$\overline{\mathbf{\Phi}}(q_2) = \sqrt{\overline{\beta}_1{}^2 + \overline{\beta}_2{}^2 + 2\overline{\beta}_1\overline{\beta}_2 \cos q_2}$$

and

$$k_P > \frac{2}{\pi} \min \left\{ \overline{\beta}_1{}^2, \overline{\beta}_2{}^2 \right\}$$

as described by eqs (8.13) and (8.14).

Simulation Results: MC-ROPA$_2$ Robot

To find k_{DM}, we use an experimental analysis as performed with the Acrobot. In this instance, with the system parameters

$$\begin{array}{lll} m_1 = 1 \text{ kg}, & m_2 = 0.5 \text{ kg}, & m_3 = 0.5 \text{ kg}, \\ L_1 = 1 \text{ m}, & L_2 = 1 \text{ m}, & L_3 = 1 \text{ m}, \\ l_1 = 0.5 \text{ m}, & l_2 = 0.5 \text{ m}, & l_3 = 0.5 \text{ m}, \\ I_1 = 0.083 \text{ kg.m}^2, & I_2 = 0.165 \text{ kg.m}^2, & I_3 = 0.165 \text{ kg.m}^2 \end{array}$$

which produces

$$\begin{array}{ll} \overline{m}_2 = 1 \text{ kg}, & \overline{I}_2 = 0.33 \text{ kg.m}^2, \\ \overline{m_2 l_2} = 1 \text{ kg.m}, & \overline{m_2 l_2{}^2} = 1.25 \text{ kg.m}^2. \end{array}$$

Using these parameters, we plotted the behaviour of $k_D\left(q_2\right)$ for the MC-ROPA$_2$ robot. The behaviour of $k_D\left(q_2\right)$ for this particular MC-ROPA$_2$ robot was found to be identical to that of the Acrobot shown in figure 8.2. As explained before, the suprenum of this curve is $k_{DM} = 37.5134$. The gain selection criterion

$$k_P > 61.2658$$

was trivially solved. Therefore, we selected the gains

$$k_D = 38, \qquad k_P = 61.3, \qquad k_V = 66.3.$$

Additionally, we chose the gains

$$k_{D_3} = 40, \qquad k_{P_3} = 400$$

taken from eq. (8.7), with $\omega_{n_3} = 20$ rad.s^{-1} along with the initial conditions

$$q_1(0) = -1.4 - \frac{\pi}{2}, \qquad q_2(0) = q_3(0) = 0,$$
$$\dot{q}_1(0) = \dot{q}_2(0) = \dot{q}_3(0) = 0.$$

The results of the swing-up control of this MC-ROPA$_2$ robot are demonstrated in figures 8.26-8.33. It is expected that these results should be approximately the same as the results produced for the Acrobot earlier in this chapter. The angular displacement of the most proximal pendulum of the MC-ROPA$_2$ robot is demonstrated in figure 8.26. The most proximal pendulum enters a limit cycle after experiencing a 2π radian negative phase shift during the transient phase of the swing-up control. This is not evident in the Acrobot simulation result shown in figure 8.10, and is attributed to the approximations of the system dynamics that were made in the formulation of the MC-ROPA$_2$ robot. The angular displacement of the second pendulum of the MC-ROPA$_2$ robot is demonstrated in figure 8.27. The behaviour of this function closely approximates the response of the most distal pendulum of the Acrobot shown in figure 8.11, but there are more significant oscillations in the steady-state present for q_2 of the MC-ROPA$_2$ robot. This can be attributed to the approximations which are intrinsic to this model. The result of the simulated angular displacement of the most distal pendulum is demonstrated in figure 8.28. It is evident that this pendulum is tightly regulated about the $q_3 = 0$ axis since it has a maximum deviation of approximately 8×10^{-13} radians.

The phase portrait of the most proximal pendulum of the MC-ROPA$_2$ robot during swing-up control is demonstrated in figure 8.29. The 2π radian negative phase shift is evident in this figure, which occurs during transience. The MC-ROPA$_2$ robot subsequently enters a limit cycle that closely approximates the behaviour of the limit cycle of the Acrobot shown in figure 8.12. The Lyapunov function demonstrated in figure 8.30 tends towards zero, with an almost identical behaviour to the Lyapunov function of the Acrobot seen in figure 8.13. The mechanical energy demonstrated in figure 8.31 tends towards the desired energy state E_r, which is expected. More importantly, the behaviour of the mechanical energy is also almost identical to the behaviour of the mechanical energy of the Acrobot demonstrated in figure 8.14. The torques produced by the proximal and distal actuators are demonstrated in figures 8.32 and 8.33. The behaviour of the torque produced by the actuator found between the most proximal pendulum and the second pendulum is almost identical to that of the result produced in figure 8.15 for the Acrobot. The torque produced by the actuator found between the second pendulum and the most distal pendulum is used to linearise the dynamics of the most distal pendulum, and thus reacts similarly to τ_2 since the dynamics induced by this actuator must be negated.

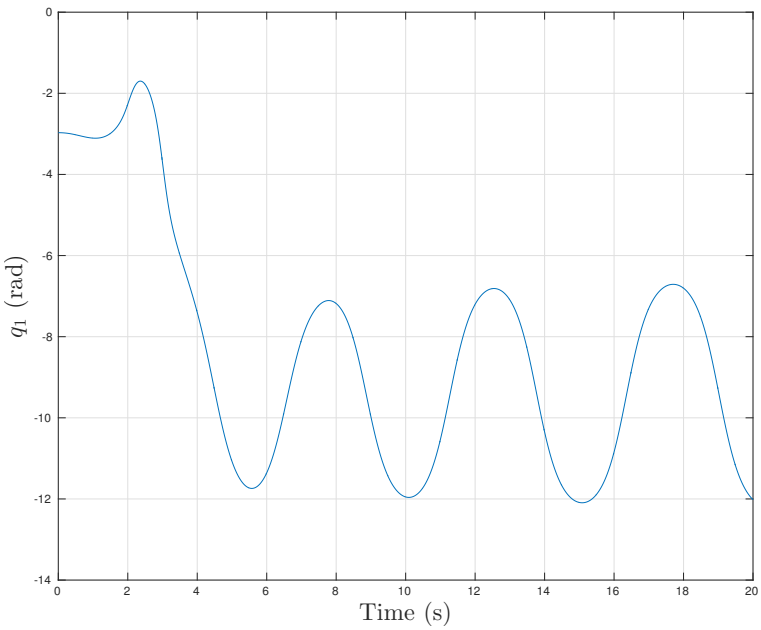

FIGURE 8.26: The angular displacement q_1 of the most proximal pendulum of the undamped MC-ROPA$_2$ robot during LDM-related swing-up control.

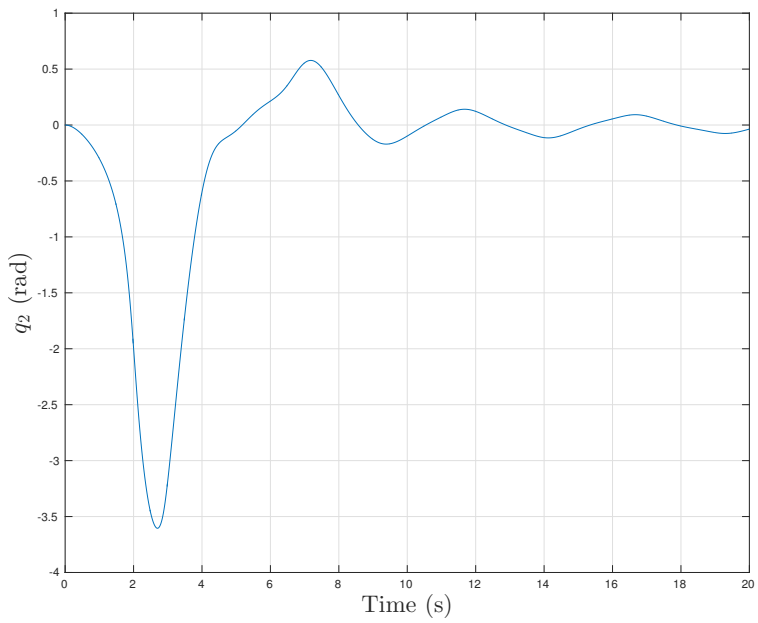

FIGURE 8.27: The angular displacement q_2 of the second pendulum of the undamped MC-ROPA$_2$ robot during LDM-related swing-up control.

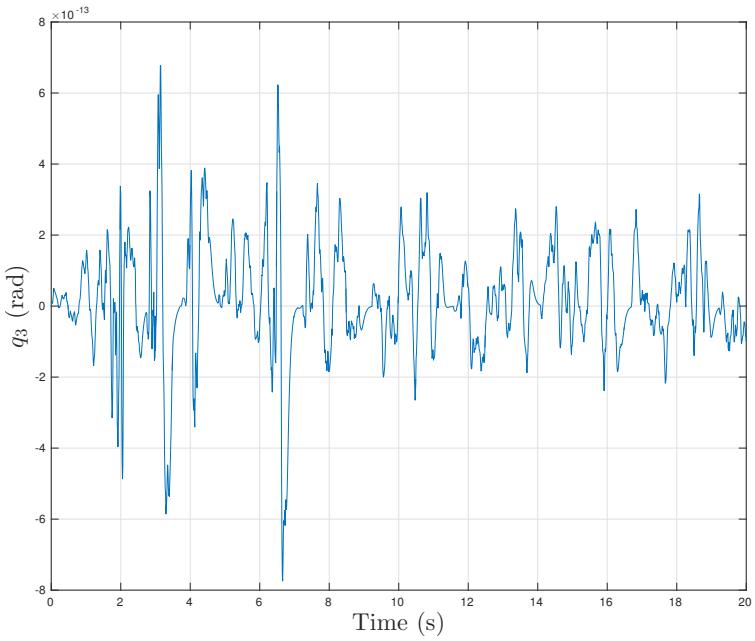

FIGURE 8.28: The angular displacement q_3 of the most distal pendulum of the undamped MC-ROPA$_2$ robot during LDM-related swing-up control.

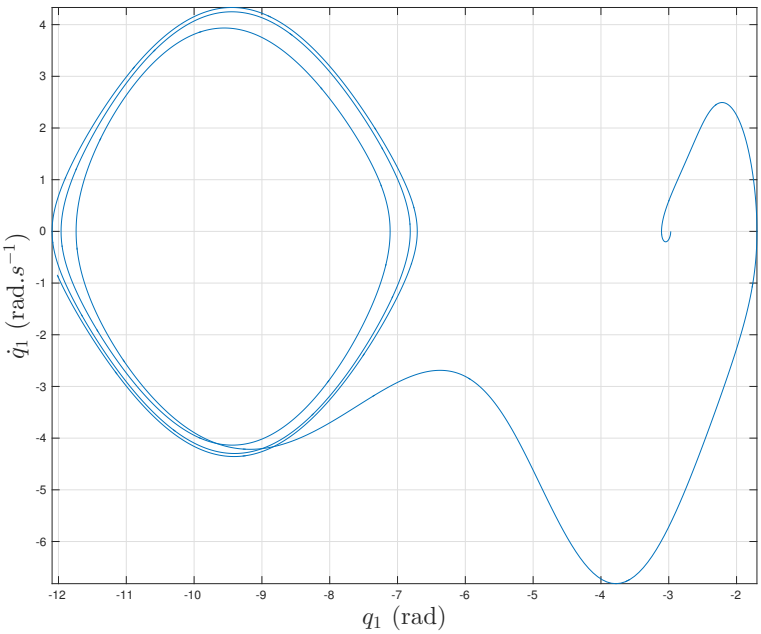

FIGURE 8.29: The phase portrait of the proximal pendulum of the undamped MC-ROPA$_2$ robot during LDM-related swing-up control.

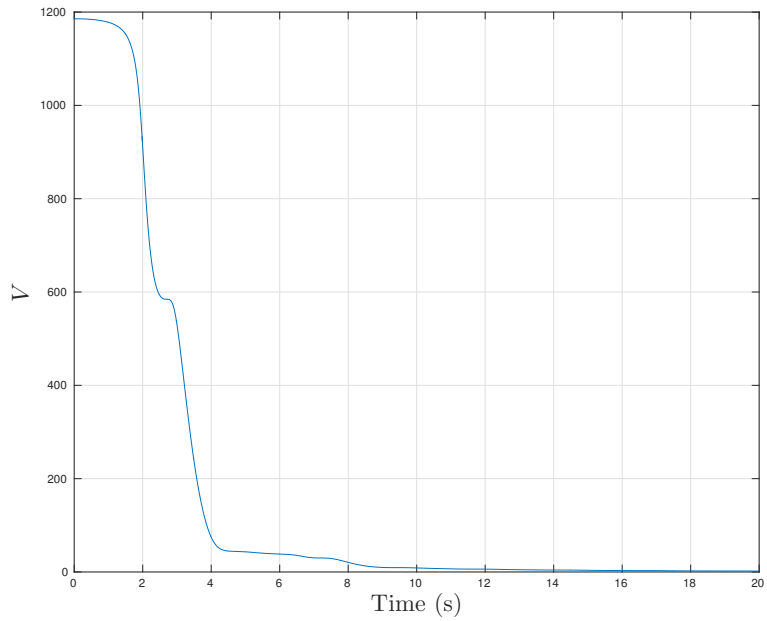

FIGURE 8.30: The Lyapunov candidate function of the undamped MC-ROPA$_2$ robot.

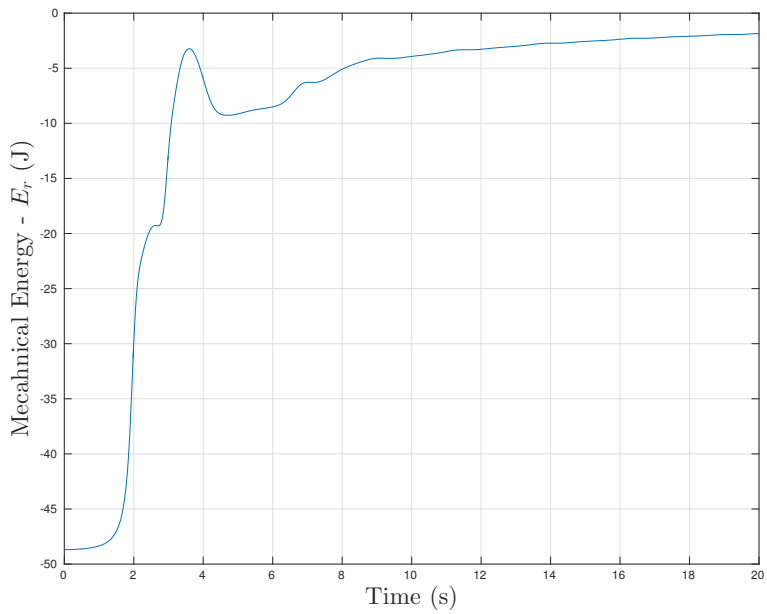

FIGURE 8.31: The difference between the mechanical energy of the undamped MC-ROPA$_2$ robot and the energy state of E_r during LDM-related swing-up control.

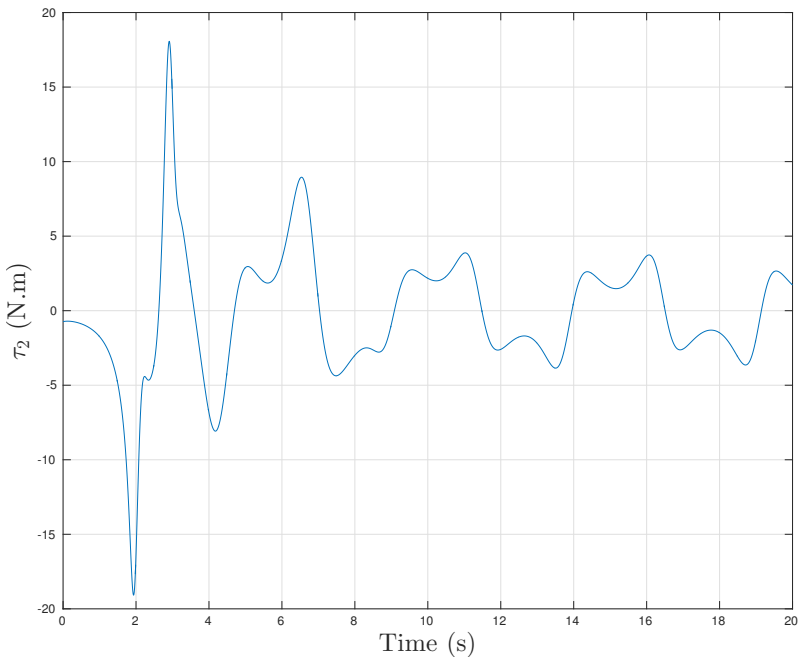

FIGURE 8.32: The LDM-related torque τ_2 used to swing-up the undamped MC-ROPA$_2$ robot.

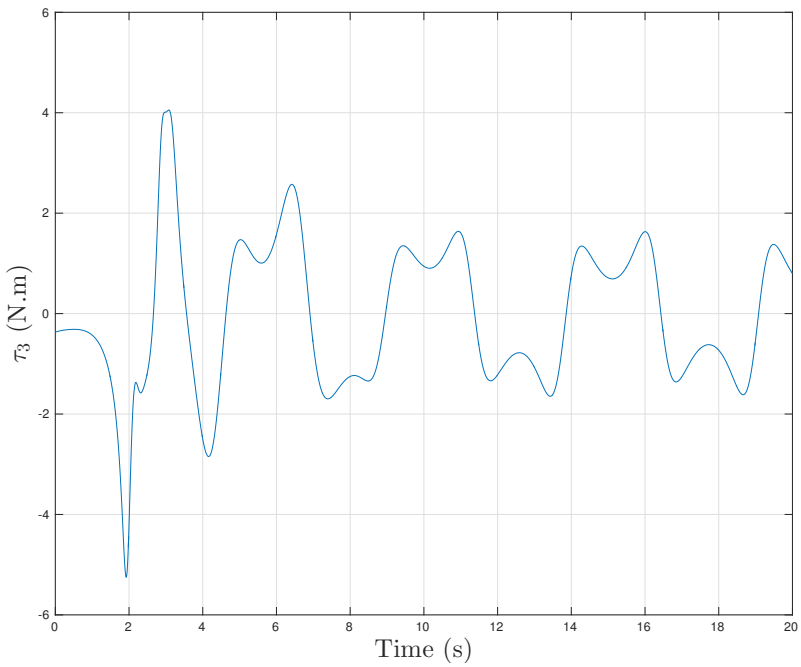

FIGURE 8.33: The LDM-related torque τ_3 used to swing-up the undamped MC-ROPA$_2$ robot.

The results of the swing-up control of the MC-ROPA$_2$ robot closely approximated the swing-up control results produced for the Acrobot as predicted. There were, however, slight deviations in the behaviour of the pendulum displacements, whereby the most proximal pendulum did not enter the limit cycle within the predicted phase range, and the second pendulum experienced more oscillations in the steady-state as compared to the most distal pendulum of the Acrobot during swing-up control. Despite this, we can conclude that the implementation of a swing-up torque τ_2 which was designed on the MC-ROPA$_2$ system accommodates the satisfactory swing-up control of the PAA robot. This is attributed to the FBL torques that respond sufficiently well to changes in the velocity and angular displacement of the most distal pendulum, regulating the pendulum within ranges of 8×10^{-13} radians about $q_3 = 0$.

We have now demonstrated the swing-up control of the undamped PA$_{n-1}$, the MC-ROPA$_{n-1}$ and two of their derivatives: the Acrobot (which is identical to the MC-ROPA$_1$ robot), the PAA robot, and the MC-ROPA$_2$ robot. We were able to successfully replicate the simulated results for the Acrobot and the PAA robot demonstrated in [5]. We have thus built the foundation on which to test our hypothesis highlighted in section 1.2, which involves the integration of the viscous damping model into the PA$_{n-1}$ robot model. We will begin the execution of the next step of the research methodology by first integrating the viscous damping model into the actuated joints, referred to as active damping.

8.3 The Tenable Alteration: The Actively Damped PA$_{n-1}$ Robot

8.3.1 Derivation of the Necessary Swing-up Torque

For the case of the actively damped PA$_{n-1}$ robot, we will follow the same procedure outlined in the last section and in [5] with the addition of an appropriately defined lossy torque matrix $\mathbf{R}(\dot{\mathbf{q}})$ (original definition in eq. (7.16)). With this definition, we define $\mathbf{R}(\dot{\mathbf{q}})$ as

$$\mathbf{R}(\dot{\mathbf{q}}) = \mathbf{b}^{\mathbf{T}}\dot{\mathbf{q}} = \begin{bmatrix} 0 & b_2\dot{q}_2 & \dots & b_{n-1}\dot{q}_{n-1} & b_n\dot{q}_n \end{bmatrix}^{\mathbf{T}}$$

where the viscous damping coefficients are represented collectively as

$$\mathbf{b} = \begin{bmatrix} b_1 & b_2 & \dots & b_{n-1} & b_n \end{bmatrix}^{\mathbf{T}}$$

with, in the case of active damping, $b_1 = 0$ since there is no damping on the passive joint. Therefore, we can represent the non-zero components of the system damping as

$$\mathbf{R}_a(\dot{\mathbf{q}}_a) = \mathbf{G}^{\mathbf{T}}(\mathbf{q})\mathbf{R}(\dot{\mathbf{q}})$$

where

$$\mathbf{G}(\mathbf{q}) = \begin{bmatrix} \mathbf{0}_{1\times n-1} \\ I_{n-1} \end{bmatrix}.$$

We once again chose

$$V = \frac{1}{2}\left(E - E_r\right)^2 + \frac{1}{2}k_D\dot{\mathbf{q}}_a^{\mathbf{T}}\dot{\mathbf{q}}_a + \frac{1}{2}k_P\overline{\mathbf{q}}_a{}^{\mathbf{T}}\overline{\mathbf{q}}_a$$

as the Lyapunov candidate function seen in [5] where

$$\overline{\mathbf{q}}_a = \overline{0} \leftrightarrow \mathbf{q}_a = \overline{0}, \qquad \dot{\overline{\mathbf{q}}}_a = \psi\left(\mathbf{q}_a\right)\dot{\mathbf{q}}_a \tag{8.26}$$

with $\psi(\mathbf{q}_a)$ described in [5]. The desired rate of this Lyapunov candidate function was, once again, chosen to be

$$\dot{V}_d = -k_V\dot{\mathbf{q}}_a^{\mathbf{T}}\dot{\mathbf{q}}_a \leq 0 \tag{8.27}$$

where $k_V > 0$. The actual time derivative of the Lyapunov function is

$$\dot{V} = (E - E_r)\dot{E} + k_D\dot{\mathbf{q}}_a^{\mathbf{T}}\ddot{\mathbf{q}}_a + k_P\dot{\mathbf{q}}_a^{\mathbf{T}}\psi^{\mathbf{T}}(\mathbf{q}_a)\overline{\mathbf{q}}_a. \tag{8.28}$$

The equations of motion for the most distal pendulums of the actively damped PA_{n-1} robot, $\ddot{\mathbf{q}}_a$, are derived from eq. (7.23) are represented by

$$\ddot{\mathbf{q}}_a = \mathbf{G}^{\mathbf{T}}(\mathbf{q})\mathbf{M}^{-1}(\mathbf{q})\left[\mathbf{G}(\mathbf{q})\tau_a - \mathbf{D}(\mathbf{q},\dot{\mathbf{q}}) - \mathbf{K}(\mathbf{q})\right] \tag{8.29}$$

$$= \mathbf{G}^{\mathbf{T}}(\mathbf{q})\mathbf{M}^{-1}(\mathbf{q})\left[\mathbf{G}(\mathbf{q})\tau_a - \mathbf{C}(\mathbf{q},\dot{\mathbf{q}}) - \mathbf{R}(\dot{\mathbf{q}}) - \mathbf{K}(\mathbf{q})\right] \tag{8.30}$$

where

$$\mathbf{D}(\mathbf{q},\dot{\mathbf{q}}) = \mathbf{C}(\mathbf{q},\dot{\mathbf{q}}) + \mathbf{R}(\dot{\mathbf{q}}).$$

Additionally, the change of energy in the system is attributed to both actuation and damping in this case as represented by

$$\dot{E} = \dot{\mathbf{q}}_a^{\mathbf{T}}\left[\tau_a - \mathbf{R}_a(\dot{\mathbf{q}}_a)\right]. \tag{8.31}$$

Substituting eqs. (8.30) and (8.31) into eq. (8.28) produces

$$\dot{V}(\mathbf{q},\dot{\mathbf{q}}) = \dot{\mathbf{q}}_a^{\mathbf{T}}\left[(E - E_d)\left[\tau_a - \mathbf{R}_a(\dot{\mathbf{q}}_a)\right] + k_D\mathbf{G}^{\mathbf{T}}(\mathbf{q})\mathbf{M}^{-1}(\mathbf{q})\left(\mathbf{G}(\mathbf{q})\tau_a - \mathbf{C}(\mathbf{q},\dot{\mathbf{q}}) - \right.\right.$$
$$\left.\left.\mathbf{R}(\dot{\mathbf{q}}) - \mathbf{K}(\mathbf{q})\right)\right] + k_P\dot{\overline{\mathbf{q}}}_a^{\mathbf{T}}\overline{\mathbf{q}}_a.$$

From eq. (8.26) the above expression simplifies to

$$\dot{V}(\mathbf{q},\dot{\mathbf{q}}) = \dot{\mathbf{q}}_a^{\mathbf{T}}\left[(E - E_d)\left[\tau_a - \mathbf{R}_a(\dot{\mathbf{q}}_a)\right] + k_D\mathbf{G}^{\mathbf{T}}(\mathbf{q})\mathbf{M}^{-1}(\mathbf{q})\left(\mathbf{G}(\mathbf{q})\tau_a - \mathbf{C}(\mathbf{q},\dot{\mathbf{q}}) - \right.\right.$$
$$\left.\left.\mathbf{R}(\dot{\mathbf{q}}) - \mathbf{K}(\mathbf{q})\right) + k_P\psi^{\mathbf{T}}(\mathbf{q}_a)\overline{\mathbf{q}}_a\right].$$

We will solve for the expression τ_a that is required to realise the desired Lyapunov dynamics shown in eq. (8.27). We begin this derivation by equating the real and desired Lyapunov dynamics, which produces

$$\begin{aligned}-k_V\dot{\mathbf{q}}_a^{\mathbf{T}}\dot{\mathbf{q}}_a = \dot{\mathbf{q}}_a^{\mathbf{T}}\big[&(E-E_d)\left[\tau_a - \mathbf{R}_a(\dot{\mathbf{q}}_a)\right] + k_D\mathbf{G}^{\mathbf{T}}(\mathbf{q})\mathbf{M}^{-1}(\mathbf{q})\left(\mathbf{G}(\mathbf{q})\tau_a - \mathbf{C}(\mathbf{q},\dot{\mathbf{q}})\right.\\ &\left.-\mathbf{G}^{\mathbf{T}}(\mathbf{q})\mathbf{R}_a(\dot{\mathbf{q}}) - \mathbf{K}(\mathbf{q})\right) + k_P\psi^{\mathbf{T}}(\mathbf{q}_a)\overline{\mathbf{q}}_a\big].\end{aligned}$$

It is evident that the vector $\dot{\mathbf{q}}_a^{\mathbf{T}}$ is a common factor among both sides of the equation, and can thus fall away, resulting in

$$\begin{aligned}-k_V\dot{\mathbf{q}}_a = &(E-E_d)\left[\tau_a - \mathbf{R}_a(\dot{\mathbf{q}}_a)\right] + k_D\mathbf{G}^{\mathbf{T}}(\mathbf{q})\mathbf{M}^{-1}(\mathbf{q})\left(\mathbf{G}(\mathbf{q})\tau_a - \mathbf{C}(\mathbf{q},\dot{\mathbf{q}})\right.\\ &\left.-\mathbf{G}^{\mathbf{T}}(\mathbf{q})\mathbf{R}_a(\dot{\mathbf{q}}) - \mathbf{K}(\mathbf{q})\right) + k_P\psi^{\mathbf{T}}(\mathbf{q}_a)\overline{\mathbf{q}}_a.\end{aligned} \tag{8.32}$$

Solving for τ_a requires that

$$|\Lambda(\mathbf{q},\dot{\mathbf{q}})| \neq 0 \quad \forall \mathbf{q},\dot{\mathbf{q}}.$$

If this is true, then $\Lambda(\mathbf{q},\dot{\mathbf{q}})$ is invertible. Solving for τ_a, therefore, produces

$$\begin{aligned}\tau_a = &\Lambda^{-1}(\mathbf{q},\dot{\mathbf{q}})\left[-k_V\dot{\mathbf{q}}_a + k_D\mathbf{G}^{\mathbf{T}}(\mathbf{q})\mathbf{M}^{-1}(\mathbf{q})\left[\mathbf{C}(\mathbf{q},\dot{\mathbf{q}}) + \mathbf{K}(\mathbf{q})\right] - k_P\psi^{\mathbf{T}}\overline{\mathbf{q}}_a\right]\\ &+ \mathbf{R}_a(\dot{\mathbf{q}})\end{aligned} \tag{8.33}$$

where

$$\Lambda(\mathbf{q},\dot{\mathbf{q}}) = (E-E_d)\,I_{n-1} + k_D\mathbf{G}^{\mathbf{T}}(\mathbf{q})\mathbf{M}^{-1}(\mathbf{q})\mathbf{G}(\mathbf{q}).$$

It is evident from eq. (8.33) that, in the case of the actively damped PA_{n-1} robot, each actuator is responsible for negating the damping torques present at the respective joint. Therefore, so long as the $|\mathbf{\Lambda}(\mathbf{q},\dot{\mathbf{q}})|$ is invertible and we can prove that there exists an invariant set $\mathbf{W}_r$ that contains the UEP and is dictated by a homoclinic orbit that is approached from the set $\mathbb{S} \in \mathbb{R}^n$, as seen in the undamped case, the behaviour of the actively damped PA_{n-1} robot that is being swung-up by a set of controllers, whose torques are dictated by τ_a in eq. (8.33), will behave identically to the swing-up controlled undamped PA_{n-1} robot. The only difference that can be seen between the undamped and actively damped cases is the presence of a superimposed damping-negation torque found in the final swing-up torque. Additionally, the gain condition proofs performed in [5] are satisfactory for a viscously damped PA_{n-1} robot since the viscous damping is dependent on $\dot{\mathbf{q}}_a$, which does not interfere with the proof since the majority of the analysis occurs at the equilibrium points. The gain selection conditions derived in [5] to ensure that $|\Lambda(\mathbf{q},\dot{\mathbf{q}})|$ is invertible and that $\mathbf{W}_r$ is approached as $t \to \infty$ is shown in eqs. (8.4) and (8.5).

It is apparent, therefore, that the integration of active damping into the PA_{n-1} robot is a **tenable alteration**, since this alteration does not lead to the derivation of a control torque that does not achieve the control objective. A discussion on

the actively damped MC-ROPA$_{n-1}$ robot is not included in this section since the swing-up control of the actively damped PA$_{n-1}$ has been proven to be satisfactory.

We shall now explicitly demonstrate the swing-up behaviour of the actively damped Acrobot and PAA robot using simulated results, beginning with the Acrobot.

8.3.2 The Actively Damped Acrobot

Derivation of the Necessary Swing-up Control Torque

For the case of the actively damped Acrobot, we chose

$$\mathbf{R}(\dot{\mathbf{q}}) = \begin{bmatrix} 0 & b_2\dot{q}_2 \end{bmatrix}^{\mathbf{T}}$$

as the viscous damping profile. The Lyapunov candidate function was chosen as

$$V = \frac{1}{2}(E - E_r)^2 + \frac{1}{2}k_D\dot{q}_2^2 + \frac{1}{2}k_P{q_2}^2$$

which is identical to that of the undamped case where the time-derivative of this candidate function is described by

$$\dot{V} = (E - E_r)\dot{E} + k_D\ddot{q}_2\dot{q}_2 + k_P\dot{q}_2q_2.$$

The change of energy in the system is dependent on both the viscous damping and the system actuation. Therefore

$$\dot{E} = \dot{q}_2\left[\tau_2 - b_2\dot{q}_2\right]$$

which leads to

$$\dot{V} = \dot{q}_2\left[(E - E_r)\left[\tau_2 - b_2\dot{q}_2\right] + k_D\ddot{q}_2 + k_Pq_2\right].$$

To complete the definition of the Lyapunov time-derivative, we solve for $\ddot{q}_2$ from the prototypical form of the actively damped Acrobot, with

$$\ddot{q}_2 = \mathbf{G}^{\mathbf{T}}(\mathbf{q})\mathbf{M}^{-1}(\mathbf{q})\left[\mathbf{G}(\mathbf{q})\tau_2 - \mathbf{C}(\mathbf{q},\dot{\mathbf{q}}) - \mathbf{R}(\dot{\mathbf{q}}) - \mathbf{K}(\mathbf{q})\right].$$

Substituting this expression into the time-derivative of the Lyapunov function produces

$$\begin{aligned}\dot{V} &= \dot{q}_2\left[\left[(E - E_r) + k_D\mathbf{G}^{\mathbf{T}}(\mathbf{q})\mathbf{M}^{-1}(\mathbf{q})\mathbf{G}(\mathbf{q})\right]\tau_2 - (E - E_r)b_2\dot{q}_2 + k_pq_2\right.\\ &\quad\left.-k_D\mathbf{G}^{\mathbf{T}}(\mathbf{q})\mathbf{M}^{-1}(\mathbf{q})\left[\mathbf{C}(\mathbf{q},\dot{\mathbf{q}}) + \mathbf{R}(\dot{\mathbf{q}}) + \mathbf{K}(\mathbf{q})\right]\right]\\ &= \dot{q}_2\left[\left[(E - E_r) + k_D\mathbf{G}^{\mathbf{T}}(\mathbf{q})\mathbf{M}^{-1}(\mathbf{q})\mathbf{G}(\mathbf{q})\right]\left[\tau_2 - b_2\dot{q}_2\right] + k_pq_2\right.\\ &\quad\left.-k_D\mathbf{G}^{\mathbf{T}}(\mathbf{q})\mathbf{M}^{-1}(\mathbf{q})\left[\mathbf{C}(\mathbf{q},\dot{\mathbf{q}}) + \mathbf{K}(\mathbf{q})\right]\right].\end{aligned}$$

Therefore, choosing the negative semi-definite Lyapunov rate

$$\dot{V}_d = -k_V \dot{q}_2^2$$

and choosing $\dot{V} = \dot{V}_d$, we can now solve for the necessary swing-up torque

$$\tau_2 = \frac{k_D \mathbf{G}^{\mathbf{T}}(\mathbf{q})\mathbf{M}^{-1}(\mathbf{q})\left[\mathbf{C}(\mathbf{q},\dot{\mathbf{q}}) + \mathbf{K}(\mathbf{q})\right] - k_V \dot{q}_2 - k_P q_2}{\Lambda(\mathbf{q},\dot{\mathbf{q}})} + b_2 \dot{q}_2 \tag{8.34}$$

where

$$\Lambda(\mathbf{q},\dot{\mathbf{q}}) = (E - E_r) + k_D \mathbf{G}^{\mathbf{T}}(\mathbf{q})\mathbf{M}^{-1}(\mathbf{q})\mathbf{G}(\mathbf{q}).$$

The gain conditions for the Acrobot are demonstrated in eqs. (8.4) and (8.5) where $n = 2$.

Simulation Results

The actuator torque τ_2, shown in eq. (8.34), evidently negates the damping torque present at the actuated joint. Therefore, the results demonstrated in figures 8.4-8.8 also represents the behaviour of the actively damped Acrobot system, regardless of the value of the damping coefficient b_2 (so long as $b_2 \nrightarrow \infty$). It is important to note, however, that the torque required to swing-up an actively damped Acrobot will have a different magnitude. We demonstrate this by simulating the swing-up control of an actively damped Acrobot. The resultant torques of the actuators involved in the swing-up control of the actively damped Acrobot (with $b_2 = 10$) are demonstrated in figures 8.34 and 8.35, with the red curves representing the superposition of both the swing-up torque and the damping-negation torque, and the blue curves representing the torques required to swing-up an undamped Acrobot. The same physical parameters, initial conditions, and gains were selected for this example according to what is seen in section 8.2.4.

The comparison between the torques required to swing up the undamped and actively damped Acrobot when using $k_P = 288.8$ is demonstrated in figure 8.34. The same comparison using $k_P = 61.3$ is demonstrated in figure 8.34. In both cases, the magnitude of the torques during transience are at least twice the magnitude of the torque required to swing-up the undamped Acrobot. The torques closely approximate one another once the transient phase has ended. The change in the scaling factor is due to the strict regulation of the most distal pendulum about $q_2 = 0$, which only occurs after the transient phase. This behaviour was expected.

We shall now demonstrate that this damping negation phenomenon is also evident in higher-order systems, using the actively damped PAA robot as a representative.

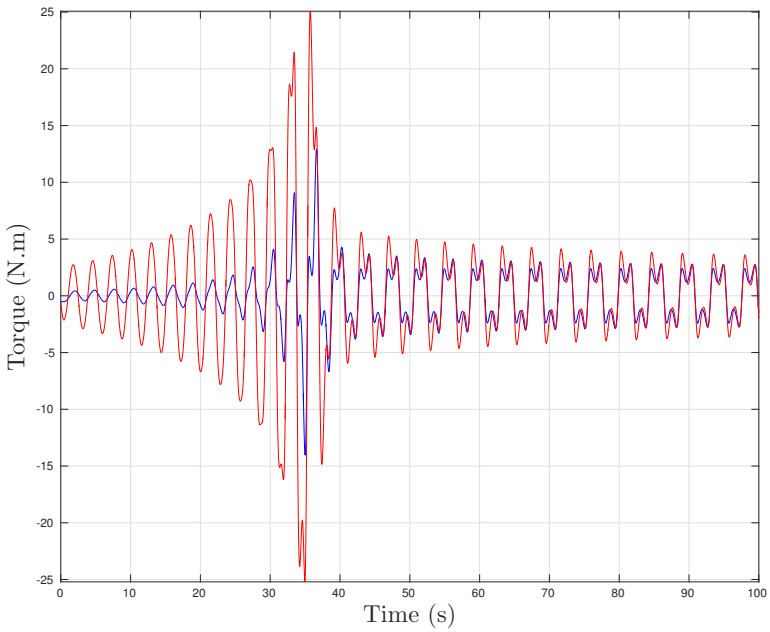

FIGURE 8.34: A comparison of the necessary swing-up control torques for the undamped Acrobot (blue) and the actively damped Acrobot (red) with $b_2 = 10$ and $k_P = 288.8$.

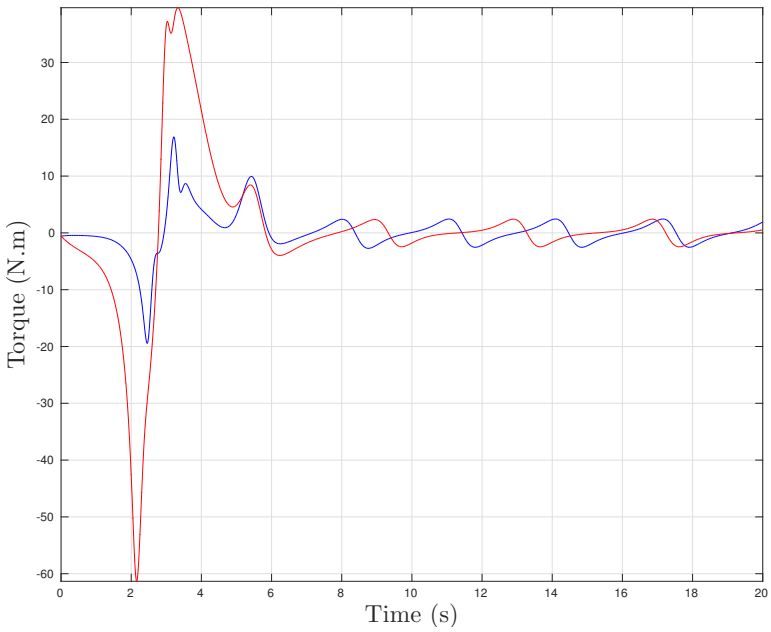

FIGURE 8.35: A comparison of the necessary swing-up control torques for the undamped Acrobot (blue) and the actively damped Acrobot (red) with $b_2 = 10$ and $k_P = 61.3$.

8.3.3 The Actively Damped PAA Robot

Derivation of the Necessary Swing-up Control Torque

In the case where active viscous damping is integrated into the PAA model, we describe the damping torques in the system collectively as

$$\mathbf{R}(\dot{\mathbf{q}}) = \begin{bmatrix} 0 & b_2\dot{q}_2 & b_3\dot{q}_3 \end{bmatrix}^{\mathbf{T}}$$

whereby

$$\mathbf{R}_a(\dot{\mathbf{q}}) = \mathbf{G}(\mathbf{q})\mathbf{R}(\dot{\mathbf{q}}).$$

We defined the candidate Lyapunov function

$$V = \frac{1}{2}(E - E_r)^2 + \frac{1}{2}k_D\dot{\mathbf{q}}_a^{\mathbf{T}}\dot{\mathbf{q}}_a + \frac{1}{2}k_P\overline{\mathbf{q}}_a{}^{\mathbf{T}}\overline{\mathbf{q}}_a$$

for this instance where

$$\overline{q}_a = \begin{bmatrix} \overline{q}_2 & q_3 \end{bmatrix}^{\mathbf{T}}.$$

The derivative of this candidate Lyapunov function was selected as

$$\dot{V} = (E - E_r)\dot{E} + k_D\dot{\mathbf{q}}_a^{\mathbf{T}}\ddot{\mathbf{q}}_a + k_P\dot{\mathbf{q}}_a^{\mathbf{T}}\psi^{\mathbf{T}}\left(\overline{\mathbf{q}}_a\right)\overline{\mathbf{q}}_a. \tag{8.35}$$

Both the actuation and the viscous damping in this case is responsible for the change of energy in the viscously damped PAA robot. Therefore

$$\dot{E} = \dot{\mathbf{q}}_a^{\mathbf{T}}\left[\tau_a - \mathbf{R}_a(\dot{\mathbf{q}})\right]$$

where

$$\tau_a = \begin{bmatrix} \tau_2 & \tau_3 \end{bmatrix}^{\mathbf{T}}.$$

The substitution of this torque expression into eq. (8.35) produces

$$\dot{V} = \dot{\mathbf{q}}_a^{\mathbf{T}}\left[(E - E_r)\left[\tau_a - \mathbf{R}_a(\dot{\mathbf{q}})\right] + k_D\ddot{\mathbf{q}}_a + k_P\psi^{\mathbf{T}}\left(\overline{\mathbf{q}}_a\right)\overline{\mathbf{q}}_a\right]. \tag{8.36}$$

The dynamics of the two most distal pendulums may be solved for through the manipulation of the prototypical form of the PAA robot, resulting in

$$\ddot{\mathbf{q}}_a = \mathbf{G}^{\mathbf{T}}(\mathbf{q})\mathbf{M}^{-1}(\mathbf{q})\left[\mathbf{G}(\mathbf{q})\left[\tau_a - \mathbf{R}_a(\dot{\mathbf{q}})\right] - \mathbf{C}(\mathbf{q},\dot{\mathbf{q}}) - \mathbf{K}(\mathbf{q})\right].$$

Substituting this expression into eq. (8.36) produces

$$\begin{aligned}\dot{V} &= \dot{\mathbf{q}}_a^{\mathbf{T}}\Big[\left[(E - E_r)I_2 + k_D\mathbf{G}^{\mathbf{T}}(\mathbf{q})\mathbf{M}^{-1}(\mathbf{q})\mathbf{G}(\mathbf{q})\right]\left[\tau_a - \mathbf{R}_a(\dot{\mathbf{q}})\right] \\ &\quad -k_D\mathbf{G}^{\mathbf{T}}(\mathbf{q})\mathbf{M}^{-1}(\mathbf{q})\left[\mathbf{C}(\mathbf{q},\dot{\mathbf{q}}) + \mathbf{K}(\mathbf{q})\right] + k_P\psi^{\mathbf{T}}\left(\overline{\mathbf{q}}_a\right)\overline{\mathbf{q}}_a\Big] \\ &= \dot{\mathbf{q}}_a^{\mathbf{T}}\left[\Lambda(\mathbf{q},\dot{\mathbf{q}})\left[\tau_a - \mathbf{R}_a(\dot{\mathbf{q}})\right] - k_D\mathbf{G}^{\mathbf{T}}(\mathbf{q})\mathbf{M}^{-1}(\mathbf{q})\left[\mathbf{C}(\mathbf{q},\dot{\mathbf{q}}) + \mathbf{K}(\mathbf{q})\right] + k_P\psi^{\mathbf{T}}\left(\overline{\mathbf{q}}_a\right)\overline{\mathbf{q}}_a\right]\end{aligned}$$

where

$$\Lambda(\mathbf{q}, \dot{\mathbf{q}}) = (E - E_r)I_2 + k_D \mathbf{G}^{\mathbf{T}}(\mathbf{q})\mathbf{M}^{-1}(\mathbf{q})\mathbf{G}(\mathbf{q}).$$

The desired behaviour of the Lyapunov time-derivative must be negative semi-definite. Therefore, we selected

$$\dot{V}_d = -k_V \dot{\mathbf{q}}_a^{\mathbf{T}} \dot{\mathbf{q}}_a.$$

Then with $\dot{V} = \dot{V}_d$, the necessary swing-up control torque for the actively damped PAA robot may be solved for, resulting in

$$\begin{aligned}\tau_a = \Lambda^{-1}(\mathbf{q}, \dot{\mathbf{q}}) \left[k_D \mathbf{G}^{\mathbf{T}}(\mathbf{q})\mathbf{M}^{-1}(\mathbf{q}) \left[\mathbf{C}(\mathbf{q}, \dot{\mathbf{q}}) + \mathbf{K}(\mathbf{q})\right] - k_V \dot{\mathbf{q}}_a - k_P \psi^{\mathbf{T}}\left(\overline{\mathbf{q}}_a\right) \overline{\mathbf{q}}_a\right] \\ + \mathbf{R}_a(\dot{\mathbf{q}}).\end{aligned}$$

It is evident that, as seen with the Acrobot example, each swing-up torque negates the viscous damping found on the corresponding joint, thus resulting in an identical swing-up control performance, albeit with a resultant torque that represents the superposition of the swing-up torque and damping-negation torque.

Simulation Results

We will now demonstrate the torque results of the simulated swing-up control on the actively damped PAA robot using the physical parameters values

$$\begin{aligned} &m_1 = 5.4 \text{ kg}, && m_2 = 29.5 \text{ kg}, && m_3 = 18.5 \text{ kg}, \\ &L_1 = 0.58 \text{ m}, && L_2 = 0.5 \text{ m}, && L_3 = 0.79 \text{ m}, \\ &l_1 = 0.31 \text{ m}, && l_2 = 0.2 \text{ m}, && l_3 = 0.33 \text{ m}, \\ &I_1 = 0.15 \text{ kg.m}^2, && I_2 = 1.93 \text{ kg.m}^2, && I_3 = 1.03 \text{ kg.m}^2. \end{aligned}$$

The gains were chosen to satisfy the gain conditions highlighted in eqs. (8.4) and (8.5), since the active damping has been proven to not interfere with the gain selection condition proofs highlighted in [5]. We chose the gains

$$k_D = 11500, \qquad k_P = 121700, \qquad k_V = 4550$$

alongside the initial conditions

$$\begin{aligned} &q_1(0) = -1.4 - \frac{\pi}{2}, && q_2(0) = q_3(0) = 0, \\ &\dot{q}_1(0) = \dot{q}_2(0) = \dot{q}_3(0) = 0. \end{aligned}$$

The execution of this simulation for the PAA robot produced results that are identical to the trajectories demonstrated in figures 8.18-8.23. There is, however, a discrepancy between the resultant torques used for swing-up control in the undamped and damped cases. The results of the torques τ_2 and τ_3 that are required to swing-up

an actively damped PAA robot (where $b_2 = 100$ and $b_3 = 100$) are shown as the red curves in figures 8.36 and 8.37 respectively. The corresponding torques required to swing-up the undamped PAA robot are shown in blue on the same figures.

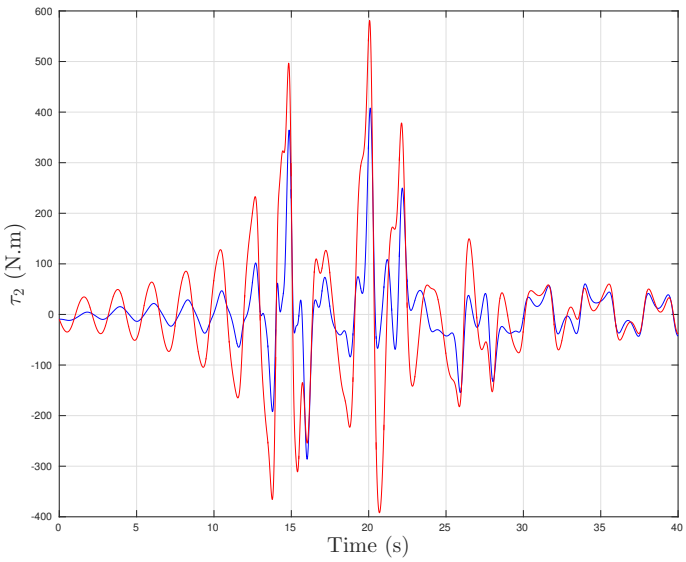

FIGURE 8.36: Comparison of the torque τ_2 that is required to swing-up the undamped PAA robot (blue) and the actively damped PAA robot with $b_2 = 100$ (red) using LDM-related swing-up control.

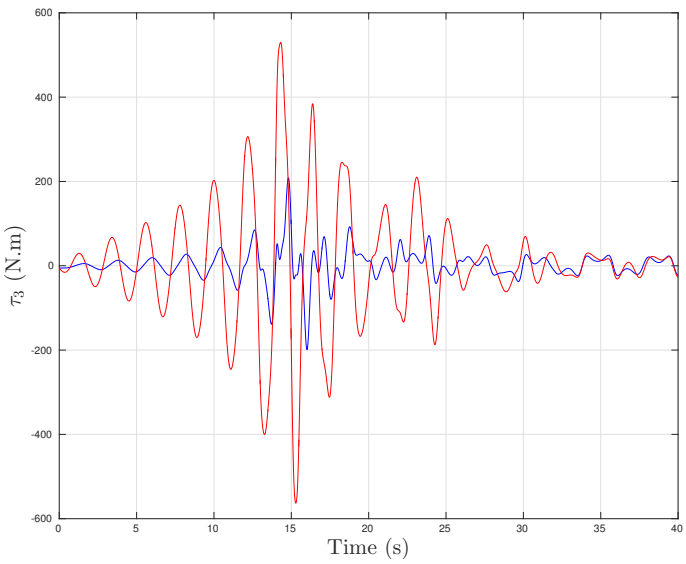

FIGURE 8.37: Comparison of the torque τ_3 that is required to swing-up the undamped PAA robot (blue) and the actively damped PAA robot with $b_3 = 100$ (red) using LDM-related swing-up control.

It is evident that the magnitude of the torques required to swing up the actively damped PAA robot are larger in magnitude during the transient phase, but the magnitude difference is relatively small during the steady-state. This difference is caused by the dynamic second pendulum which deviates well off the objective $q_2 = 0$ during the transient phase. The controllers constrain the second pendulum to fall within an approximate region of $q_2 = 0$ once the transient phase ends, thus reducing the contribution of the damping torques at the second joint. The damping torque contribution of the most distal pendulum is insignificant because the most distal pendulum is regulated quite tightly about $q_3 = 0$ throughout the entire simulation.

We have thus shown that the integration of active damping into the PA_{n-1} robot has no effect on the LDM control technique's ability to satisfy the swing-up control objective. The hypothesis described in section 1.2 has thus failed in this instance since the alteration is **tenable** when considering the possibility of achieving the swing-up control objective using the LDM technique. We shall now test the hypothesis in the instance where viscous damping is integrated into the unactuated joint of the PA_{n-1} robot. This alteration is known as passive damping, and is discussed in the next section.

8.4 The Untenable Alteration: The Passively Damped PA_{n-1} Robot

8.4.1 Derivation of the Necessary Swing-up Control Torque: The Invertibility Problem

For the case of the passively damped PA_{n-1} robot, we will follow the same procedure demonstrated for both the undamped and actively damped PA_{n-1} robots whilst attempting to accommodate the lossy torque which has been integrated into the unactuated joint (the first joint). In this case, the damping matrix $\mathbf{R}(\dot{\mathbf{q}})$ is defined as

$$\mathbf{R}(\dot{\mathbf{q}}) = \mathbf{b}^{\mathbf{T}}\dot{\mathbf{q}} = \begin{bmatrix} b_1\dot{q}_1 & 0 & \dots & 0 \end{bmatrix}^{\mathbf{T}}$$

where the viscous damping coefficients are represented as

$$\mathbf{b} = \begin{bmatrix} b_1 & b_2 & \dots & b_{n-1} & b_n \end{bmatrix}^{\mathbf{T}}$$

with $b_2, b_3, \dots, b_n$ equalling zero in the case of passive damping.

We select the Lyapunov candidate function

$$V = \frac{1}{2}(E - E_r)^2 + \frac{1}{2}k_D\dot{\mathbf{q}}_a^{\mathbf{T}}\dot{\mathbf{q}}_a + \frac{1}{2}\overline{\mathbf{q}}_a{}^{\mathbf{T}}\overline{\mathbf{q}}_a$$

where

$$\overline{\mathbf{q}}_a = \overline{0} \leftrightarrow \mathbf{q}_a = \overline{\mathbf{q}}_a = \overline{0}, \qquad \dot{\overline{\mathbf{q}}}_a = \psi(\mathbf{q}_a)\dot{\mathbf{q}}_a$$

and where $\psi(\mathbf{q}_a)$ is described in [5]. The time-derivative of the Lyapunov candidate function is chosen to be

$$\dot{V}_d = -k_V \dot{\mathbf{q}}_a^{\mathbf{T}} \dot{\mathbf{q}}_a \leq 0 \tag{8.37}$$

where $k_V > 0$. Taking the derivative of the Lyapunov candidate function with respect to time produces

$$\dot{V} = (E - E_r)\dot{E} + k_D \dot{\mathbf{q}}_a^{\mathbf{T}} \ddot{\mathbf{q}}_a + k_P \dot{\mathbf{q}}_a^{\mathbf{T}} \psi^{\mathbf{T}}(\mathbf{q}_a)\, \overline{\mathbf{q}}_a. \tag{8.38}$$

The equations of motion for the most distal pendulums in the system are required to solve the necessary swing-up torque. This is expressed as

$$\ddot{\mathbf{q}}_a = \mathbf{G}^{\mathbf{T}}(\mathbf{q})\mathbf{M}^{-1}(\mathbf{q})\left[\mathbf{G}(\mathbf{q})\tau_a - \mathbf{C}(\mathbf{q}, \dot{\mathbf{q}}) - \mathbf{R}(\dot{\mathbf{q}}) - \mathbf{K}(\mathbf{q})\right] \tag{8.39}$$

where

$$\mathbf{D}(\mathbf{q}, \dot{\mathbf{q}}) = \mathbf{C}(\mathbf{q}, \dot{\mathbf{q}}) + \mathbf{R}(\dot{\mathbf{q}}).$$

The change of mechanical energy in the system is attributed to both the torque produced by the actuators and the passive damping located on the most proximal joint, which is represented by

$$\dot{E} = \dot{\mathbf{q}}_a^{\mathbf{T}} \tau_a - b_1 \dot{q}_1^2. \tag{8.40}$$

Substituting eqs. (8.39) and (8.40) into eq. (8.38) produces

$$\begin{aligned}\dot{V}(\mathbf{q}, \dot{\mathbf{q}}) = (E - E_d)\left[\dot{\mathbf{q}}_a^{\mathbf{T}} \tau_a - b_1 \dot{q}_1^2\right] + \dot{\mathbf{q}}_a^{\mathbf{T}} \Big[k_D \mathbf{G}^{\mathbf{T}}(\mathbf{q})\mathbf{M}^{-1}(\mathbf{q})\left(\mathbf{G}(\mathbf{q})\tau_a\right. \\ \left. -\mathbf{C}(\mathbf{q}, \dot{\mathbf{q}}) - \mathbf{R}(\dot{\mathbf{q}}) - \mathbf{K}(\mathbf{q})\right) + k_P \psi^{\mathbf{T}}(\mathbf{q}_a)\overline{\mathbf{q}}_a\Big].\end{aligned} \tag{8.41}$$

Equating eqs. (8.37) and (8.41), we find

$$\begin{aligned}-k_V \dot{\mathbf{q}}_a^{\mathbf{T}} \dot{\mathbf{q}}_a = (E - E_d)\left[\dot{\mathbf{q}}_a^{\mathbf{T}} \tau_a - b_1 \dot{q}_1^2\right] + \dot{\mathbf{q}}_a^{\mathbf{T}} \Big[k_D \mathbf{G}^{\mathbf{T}}(\mathbf{q})\mathbf{M}^{-1}(\mathbf{q})\left(\mathbf{G}(\mathbf{q})\tau_a - \mathbf{C}(\mathbf{q}, \dot{\mathbf{q}})\right. \\ \left. -\mathbf{R}(\dot{\mathbf{q}}) - \mathbf{K}(\mathbf{q})\right) + k_P \psi^{\mathbf{T}}(\mathbf{q}_a)\overline{\mathbf{q}}_a\Big].\end{aligned}$$

It is here where we encounter a fundamental problem with this formulation. In the undamped and actively damped case, we could simply factor out the vector $\dot{\mathbf{q}}_a^{\mathbf{T}}$ since it was a common factor on both sides of the equation. In this case, however, the viscous damping is dependent on $\dot{q}_1^2$, preventing the negation of the $\dot{\mathbf{q}}_a^{\mathbf{T}}$ vector. This is problematic since the vector is not traditionally invertible, and the implementation of a pseudo-inverse (such as the Moore-Penrose pseudo-inverse) is typically performed on systems that are over-actuated (see [107]). This is termed the *invertibility problem*. The swing-up control problem for the passively damped PA_{n-1}

robot cannot, therefore, be solved in this form. The integration of passive damping into the PA$_{n-1}$ robot is thus referred to as the **untenable alteration**.

To overcome this problem, we must reduce the order of the system, so that the vector will be simplified to an element ($\dot{q}_2$) which can be easily divided through. This is where the MC-ROPA$_{n-1}$ robot becomes relevant, since the MC-ROPA$_{n-1}$ is used to approximately model a system of order $n > 2$ as an Acrobot. Additionally, the swing-up control of the MC-ROPA$_{n-1}$ robot is possible, as proven in section 8.2.3. We shall, therefore, attempt to circumnavigate the *invertibility problem* by modelling the passively damped PA$_{n-1}$ robot as a MC-ROPA$_{n-1}$ robot.

8.4.2 Modelling the Passively Damped PA$_{n-1}$ robot as the MC-ROPA$_{n-1}$ robot

From section 9.3.1, we define the torques

$$\tau_i = \hat{M}_{i3}(\mathbf{q})v_3 + \hat{M}_{i4}(\mathbf{q})v_4 + \cdots + \hat{M}_{in}(\mathbf{q})v_n + \hat{D}_i(\mathbf{q}, \dot{\mathbf{q}}) + \hat{K}_i(\mathbf{q}, \dot{\mathbf{q}}) + \hat{\tau}_i$$

which are required to linearise the dynamics of the $n-2$ most distal pendulums of the PA$_{n-1}$ robot, where, for $3 \leq j \leq n$ and $2 \leq k \leq n$,

$$\hat{M}_{ij}(\mathbf{q}) = M_{ij}(\mathbf{q}) - \frac{\tilde{M}_{1j}(\mathbf{q})M_{i1}(\mathbf{q})}{M_{11}(\mathbf{q})} - \frac{\tilde{M}_{2j}(\mathbf{q})M_{i2}(\mathbf{q})}{\tilde{M}_{22}(\mathbf{q})},$$

$$\hat{D}_i(\mathbf{q}, \dot{\mathbf{q}}) = D_i(\mathbf{q}, \dot{\mathbf{q}}) - \frac{M_{i1}(\mathbf{q})}{M_{11}(\mathbf{q})}\tilde{D}_1(\mathbf{q}) - \frac{M_{i2}(\mathbf{q})}{\tilde{M}_{22}(\mathbf{q})}\tilde{D}_2(\mathbf{q}),$$

$$\hat{K}_i(\mathbf{q}) = K_i(\mathbf{q}) - \frac{M_{i1}(\mathbf{q})}{M_{11}(\mathbf{q})}\tilde{K}_1(\mathbf{q}) - \frac{M_{i2}(\mathbf{q})}{\tilde{M}_{22}(\mathbf{q})}\tilde{K}_2(\mathbf{q}),$$

$$\hat{\tau}_i = \frac{M_{i2}(\mathbf{q})}{\tilde{M}_{22}(\mathbf{q})}\tau_2 - \frac{M_{i1}(\mathbf{q})}{M_{11}(\mathbf{q})}\tilde{\tau}_2$$

and

$$\tilde{M}_{2k}(\mathbf{q}) = M_{2k}(\mathbf{q}) - \frac{M_{1k}(\mathbf{q})M_{21}(\mathbf{q})}{M_{11}(\mathbf{q})}, \qquad \tilde{M}_{1j}(\mathbf{q}) = M_{1j}(\mathbf{q}) - \frac{M_{12}(\mathbf{q})\tilde{M}_{2i}(\mathbf{q})}{\tilde{M}_{22}(\mathbf{q})},$$

$$\tilde{D}_2(\mathbf{q}, \dot{\mathbf{q}}) = D_2(\mathbf{q}, \dot{\mathbf{q}}) - \frac{M_{21}(\mathbf{q})}{M_{11}(\mathbf{q})}D_1(\mathbf{q}, \dot{\mathbf{q}}), \quad \tilde{D}_1(\mathbf{q}, \dot{\mathbf{q}}) = D_1(\mathbf{q}, \dot{\mathbf{q}}) - \frac{M_{12}(\mathbf{q})}{\tilde{M}_{22}(\mathbf{q})}\tilde{D}_2(\mathbf{q}, \dot{\mathbf{q}}),$$

$$\tilde{K}_2(\mathbf{q}) = K_2(\mathbf{q}) - \frac{M_{21}(\mathbf{q})}{M_{11}(\mathbf{q})}K_1(\mathbf{q}), \qquad \tilde{K}_1(\mathbf{q}) = K_1(\mathbf{q}) - \frac{M_{12}(\mathbf{q})}{\tilde{M}_{22}(\mathbf{q})}\tilde{K}_2(\mathbf{q}).$$

Noting that for $2 \leq m \leq n$, $D_m(\mathbf{q}, \dot{\mathbf{q}}) = C_m(\mathbf{q}, \dot{\mathbf{q}})$, $D_1(\mathbf{q}, \dot{\mathbf{q}}) = C_1(\mathbf{q}, \dot{\mathbf{q}}) + R_1(\dot{\mathbf{q}})$, and $R_1(\dot{q}) = b_1\dot{q}_1$ in the passively damped case.

The prototypical form of the passively damped MC-ROPA$_{n-1}$ robot is thus shown in eq. (8.8) as a result of this linearisation, with the expanded form shown as

$$\begin{aligned}
&\overline{M}_{11}(q_2)\ddot{q}_1 + \overline{M}_{12}(q_2)\ddot{q}_2 - \overline{\alpha}_3(2\dot{q}_1\dot{q}_2 + \dot{q}_2^2)\sin q_2 - \overline{\beta}_1 \sin q_1, && \text{(8.42a)}\\
&- \overline{\beta}_2 \sin(q_1 + q_2) = -b_1\dot{q}_1 &&\\
&\overline{M}_{21}(q_2)\ddot{q}_1 + \overline{M}_{22}(q_2)\ddot{q}_2 + \overline{\alpha}_3\dot{q}_1^2 \sin q_2 - \overline{\beta}_2 \sin(q_1 + q_2) = \tau_2 && \text{(8.42b)}
\end{aligned}$$

where

$$\overline{M}_{11}(q_2) = \overline{\alpha}_1 + \overline{\alpha}_2 + 2\overline{\alpha}_3 \cos q_2, \tag{8.43}$$

$$\overline{M}_{12}(q_2) = \overline{M}_{21}(q_2) = \overline{\alpha}_2 + \overline{\alpha}_3 \cos q_2, \tag{8.44}$$

$$\overline{M}_{22}(q_2) = \overline{\alpha}_2 \tag{8.45}$$

and

$$\begin{aligned}
&\overline{\alpha}_1 = I_1 + m_1 {l_1}^2 + \overline{m}_2 {L_1}^2, && \overline{\alpha}_2 = \overline{I}_2 + \overline{m_2 {l_2}^2},\\
&\overline{\alpha}_3 = \overline{m_2 l_2} L_1, && \overline{\beta}_1 = (m_1 l_1 + \overline{m}_2 L_1)\, g,\\
&\overline{\beta}_2 = \overline{m_2 l_2} g, &&\\
&\overline{m}_2 = \sum_{i=2}^{n} m_i, && \overline{I}_2 = \sum_{i=2}^{n} I_i,\\
&\overline{m_2 l_2} = \sum_{i=2}^{n} m_i \left[l_i + \sum_{j=2}^{i-1} L_j \right], && \overline{m_2 {l_2}^2} = \sum_{i=2}^{n} m_i \left[l_i + \sum_{j=2}^{i-1} L_j \right]^2.
\end{aligned}$$

With the model of the passively damped MC-ROPA$_{n-1}$ defined, we shall now construct the LDM-related swing-up control problem in an attempt to circumnavigate the invertibility problem.

8.4.3 Derivation of the Necessary Swing-up Control Torque for the Passively Damped MC-ROPA$_{n-1}$ Robot: The Singularity Problem

To begin, we construct the candidate Lyapunov function

$$V = \frac{1}{2}(E - E_r)^2 + \frac{1}{2}k_D\dot{q}_2^2 + \frac{1}{2}k_P {q_2}^2$$

with the time-derivative of this function being

$$\dot{V} = (E - E_r)\dot{E} + k_D\ddot{q}_2\dot{q}_2 + k_P\dot{q}_2 q_2 \tag{8.46}$$

where

$$\dot{E} = \tau_2 \dot{q}_2 - b_1 \dot{q}_1^2. \tag{8.47}$$

The vector $\ddot{q}_2$ can be derived by solving separately for $\ddot{q}_1$ in eq. (8.42a) and substituting it into eq. (8.42b). This will result in

$$\ddot{q}_2 = \mathbf{G}^{\mathbf{T}}(\mathbf{q})\overline{\mathbf{M}}^{-1}(q_2)\left[\mathbf{G}(\mathbf{q})\tau_2 - \overline{\mathbf{C}}(q_2, \dot{\mathbf{q}}) - \overline{\mathbf{R}}(\dot{\mathbf{q}}) - \overline{\mathbf{K}}(\mathbf{q})\right] \tag{8.48}$$

where $\mathbf{G}(\mathbf{q}) = \begin{bmatrix} 0 & 1 \end{bmatrix}^{\mathbf{T}}$ and

$$\overline{\mathbf{M}}(q_2) = \begin{bmatrix} \overline{M}_{11}(q_2) & \overline{M}_{12}(q_2) \\ \overline{M}_{21}(q_2) & \overline{M}_{22}(q_2) \end{bmatrix},$$

$$\overline{\mathbf{C}}(q_2, \dot{\mathbf{q}}) = \begin{bmatrix} \overline{\mathbf{C}}_1(q_2, \dot{\mathbf{q}}) \\ \overline{\mathbf{C}}_2(q_2, \dot{\mathbf{q}}) \end{bmatrix},$$

$$\overline{\mathbf{R}}\left(\dot{\mathbf{q}}\right) = \begin{bmatrix} \overline{\mathbf{R}}_1\left(\dot{\mathbf{q}}\right) \\ \overline{\mathbf{R}}_2\left(\dot{\mathbf{q}}\right) \end{bmatrix},$$

$$\overline{\mathbf{K}}(\mathbf{q}) = \begin{bmatrix} \overline{\mathbf{K}}_1(\mathbf{q}) \\ \overline{\mathbf{K}}_2(\mathbf{q}) \end{bmatrix}$$

with

$$\begin{aligned}
&\overline{\mathbf{C}}_1(q_2, \dot{\mathbf{q}}) = -\overline{\alpha}_3(2\dot{q}_1\dot{q}_2 + \dot{q}_2^2)\sin q_2, \\
&\overline{\mathbf{C}}_1(q_2, \dot{\mathbf{q}}) = -\overline{\alpha}_3(2\dot{q}_1\dot{q}_2 + \dot{q}_2^2)\sin q_2, \\
&\overline{\mathbf{C}}_2(q_2, \dot{\mathbf{q}}) = \overline{\alpha}_3\dot{q}_1^2 \sin q_2, \\
&\overline{\mathbf{R}}_1\left(\dot{\mathbf{q}}\right) = b_1\dot{q}_1, \\
&\overline{\mathbf{R}}_2\left(\dot{\mathbf{q}}\right) = 0, \\
&\overline{\mathbf{K}}_1(\mathbf{q}) = -\overline{\beta}_1 \sin q_1 - \overline{\beta}_2 \sin(q_1 + q_2), \\
&\overline{\mathbf{K}}_2(\mathbf{q}) = -\overline{\beta}_2 \sin(q_1 + q_2).
\end{aligned}$$

Therefore, substituting eqs. (8.47) and (8.48) into eq. (8.46) produces

$$\begin{aligned}
\dot{V} = (E - E_r)\left[\tau_2\dot{q}_2 - b_1\dot{q}_1^2\right] + k_D\dot{q}_2\mathbf{G}^{\mathbf{T}}(\mathbf{q})\overline{\mathbf{M}}^{-1}(q_2)\left[\mathbf{G}(\mathbf{q})\tau_2 - \overline{\mathbf{C}}(q_2, \dot{\mathbf{q}})\right. \\
\left. -\overline{\mathbf{R}}(\dot{\mathbf{q}}) - \overline{\mathbf{K}}(\mathbf{q})\right] + k_P\dot{q}_2 q_2.
\end{aligned}$$

The desired Lyapunov time-derivative is chosen as

$$\dot{V}_d = -k_V\dot{q}_2^2.$$

Therefore, choosing $\dot{V} = \dot{V}_d$ we find that

$$-k_V \dot{q}_2^2 = (E - E_r)\left[\tau_2 \dot{q}_2 - b_1 \dot{q}_1^2\right] + k_D \dot{q}_2 \mathbf{G}^{\mathbf{T}}(\mathbf{q}) \overline{\mathbf{M}}^{-1}(q_2)\left[\mathbf{G}(\mathbf{q})\tau_2 - \overline{\mathbf{C}}(q_2, \dot{\mathbf{q}}) - \overline{\mathbf{R}}(\dot{\mathbf{q}}) - \overline{\mathbf{K}}(\mathbf{q})\right] + k_P \dot{q}_2 q_2.$$

We can, therefore, solve for the required torque

$$\tau_2 = \frac{k_D \mathbf{G}^{\mathbf{T}}(\mathbf{q}) \overline{\mathbf{M}}^{-1}(q_2)\left[\overline{\mathbf{C}}(q_2, \dot{\mathbf{q}}) + \overline{\mathbf{R}}(\dot{\mathbf{q}}) + \overline{\mathbf{K}}(\mathbf{q})\right] - k_V \dot{q}_2 - k_P q_2}{\overline{\Lambda}(\mathbf{q}, \dot{\mathbf{q}})} + \frac{(E - E_r) b_1 \dot{q}_1^2}{\dot{q}_2 \overline{\Lambda}(\mathbf{q}, \dot{\mathbf{q}})}.$$

The torque is now, evidently, solvable, but it seems as if, in certain cases, it will not be practically realisable. This is due to the conditional singularity in the second term of the expression, which is guaranteed to occur when $\dot{q}_2 \to 0$ and $\dot{q}_1 \neq 0$, which is guaranteed to occur if the system is to follow the expected homoclinic orbit that describes $\mathbf{W_r}$ (see eq. (A.21)). This is termed the *singularity problem*. Therefore, since this conditional singularity is guaranteed to occur in the swing-up control, then we conclude that the swing-up control of the passively damped PA$_{n-1}$ robot cannot be achieved using the Lyapunov candidate function described for the generalised PA$_{n-1}$ robot, even if the order of the system is reduced to that of an Acrobot using the MC-ROPA$_{n-1}$ modelling protocol.

8.4.4 The Matched Damping Condition

The *invertibility problem* and the *singularity problem* thus leads to the definition of a necessary and sufficient condition known as the *matched damping condition*.

Criterion 8.1. ***Matched Damping Condition:*** The LDM-related swing-up control of the PA$_{n-1}$ robot is realisable if and only if the PA$_{n-1}$ robot is undamped or actively damped. The presence of passive damping is a prerequisite of the *invertibility problem* (for $n > 2$) or the *singularity problem* (for $n = 2$), which results in unsatisfactory Lyapunov-related swing-up control.

The hypothesis mentioned in section 1.2 is thus confirmed through the integration of passive damping into the PA$_{n-1}$ robot. This is referred to as the **untenable alteration**.

The analytical results obtained that lead to the definition of the *matched damping condition* will now be experimentally demonstrated on the passively damped Acrobot, PAA robot, and MC-ROPA$_2$ robot to demonstrate the unsatisfactory performance of the swing-up controllers.

8.4.5 The Passively Damped Acrobot

Derivation of the Necessary Swing-up Control Torque: The Singularity Problem

For the case of the passively damped Acrobot, we choose the viscous damping profile

$$\mathbf{R}(\dot{\mathbf{q}}) = \begin{bmatrix} b_1\dot{q}_1 & 0 \end{bmatrix}^{\mathbf{T}}.$$

As with the previous cases, the Lyapunov candidate function

$$V = \frac{1}{2}(E - E_r)^2 + \frac{1}{2}k_D\dot{q}_2^2 + \frac{1}{2}k_P{q_2}^2$$

was selected. The behaviour of the Lyapunov function is determined by taking its differential with respect to time. Therefore

$$\dot{V} = (E - E_r)\dot{E} + k_D\ddot{q}_2\dot{q}_2 + k_P\dot{q}_2q_2.$$

The change of energy in the system is, once again, dependent on the both the actuation and viscous damping present in the system, whereby the system is passively damped in this example. The change of the system's mechanical energy is represented as

$$\dot{E} = \dot{q}_2\tau_2 - b_1\dot{q}_1^2.$$

Therefore

$$\dot{V} = \dot{q}_2\left[(E - E_r)\tau_2 + k_D\ddot{q}_2 + k_Pq_2\right] - (E - E_r)b_1\dot{q}_1.$$

This expression is completed, once again, through the substitution of the distal pendulum's equation of motion, described by

$$\ddot{q}_2 = \mathbf{G}^{\mathbf{T}}(\mathbf{q})\mathbf{M}^{-1}(\mathbf{q})\left[\mathbf{G}(\mathbf{q})\tau_2 - \mathbf{C}(\mathbf{q},\dot{\mathbf{q}}) - \mathbf{R}(\dot{\mathbf{q}}) - \mathbf{K}(\mathbf{q})\right].$$

Therefore

$$\begin{aligned}\dot{V} = \dot{q}_2\Big[&\left[(E - E_r) + k_D\mathbf{G}^{\mathbf{T}}(\mathbf{q})\mathbf{M}^{-1}(\mathbf{q})\mathbf{G}(\mathbf{q})\right]\tau_2 + k_pq_2 \\ &-k_D\mathbf{G}^{\mathbf{T}}(\mathbf{q})\mathbf{M}^{-1}(\mathbf{q})\left[\mathbf{C}(\mathbf{q},\dot{\mathbf{q}}) + \mathbf{R}(\dot{\mathbf{q}}) + \mathbf{K}(\mathbf{q})\right]\Big] - (E - E_r)b_1\dot{q}_1^2.\end{aligned}$$

Knowing that the desired dynamics of the Lyapunov candidate function is described as

$$\dot{V}_d = -k_V\dot{q}_2^2$$

and letting $\dot{V} = \dot{V}_d$, we can thus solve for the necessary swing-up torque described by

$$\tau_2 = \frac{k_D \mathbf{G}^{\mathbf{T}}(\mathbf{q})\mathbf{M}^{-1}(\mathbf{q})\left[\mathbf{C}(\mathbf{q},\dot{\mathbf{q}}) + \mathbf{R}(\dot{\mathbf{q}}) + \mathbf{K}(\mathbf{q})\right] - k_V \dot{q}_2 - k_P q_2}{\Lambda(\mathbf{q},\dot{\mathbf{q}})} + \frac{(E - E_r) b_1 \dot{q}_1^2}{\dot{q}_2 \Lambda(\mathbf{q},\dot{\mathbf{q}})}.$$

The *singularity problem* is clearly present in this torque expression, since $n = 2$ for the Acrobot.

Simulation Results

We selected the gains

$$k_P = 61.3, \qquad k_D = 35.8, \qquad k_V = 66.3$$

which are identical to the gains chosen in the undamped and actively damped cases, to demonstrate the effects of the *singularity problem*. We also selected the initial conditions

$$q_1(0) = -\frac{\pi}{2} - 1.4, \qquad q_2(0) = 0,$$
$$\dot{q}_1(0) = 0, \qquad \dot{q}_2(0) = 0.1$$

which are also identical to the initial conditions used in the undamped case. We integrated passive damping into the proximal joint using the damping coefficient

$$b_1 = 1.$$

The simulated results of the swing-up control of the passively damped Acrobot are demonstrated in figures 8.38-8.42.

The angular displacement of the proximal pendulum q_1 is demonstrated in figure 8.38. The controller is responsible for tracking the objective $q_1^d = 0$, but the pendulum follows a trajectory that does not fulfil this objective unlike what is seen in the undamped and actively damped cases. The angular displacement of the distal pendulum is demonstrated in figure 8.39. Again, the controller is expected to direct the distal pendulum toward the objective $q_2^d = 0$, but the control torque is clearly unsatisfactory since the angular position of the distal pendulum oscillates erratically across a 9 radian range. The phase portrait of the proximal pendulum is demonstrated in figure 8.40. Whilst it seems, upon inspection of this figure, that the controller attempts to initiate a limit cycle, there is no conclusive evidence that suggests that this is intentional. It is safer to assume that the results shown in this figure have no determinable pattern, and that it is solely the result of an unsatisfactory control law.

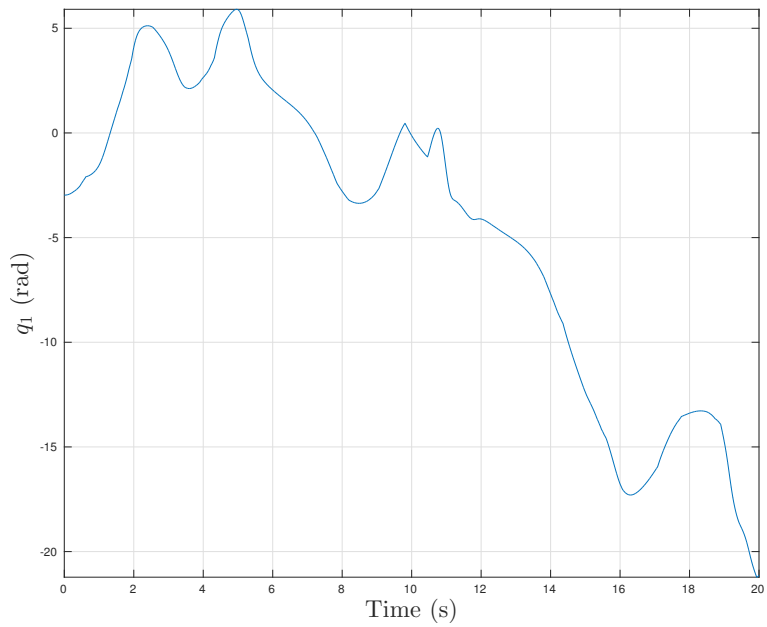

FIGURE 8.38: The angular displacement q_1 of the proximal pendulum for the passively damped Acrobot with $k_P = 61.3$ and $b_1 = 1$ during LDM-related swing-up control.

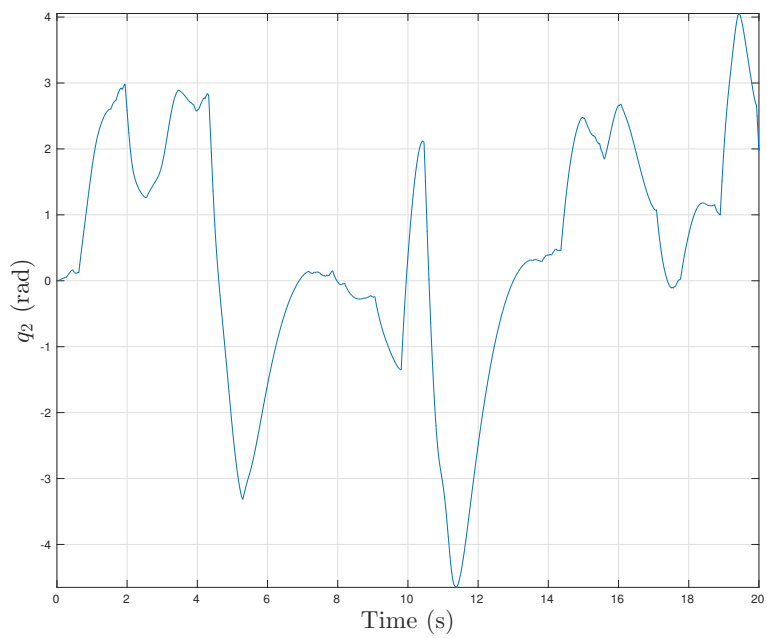

FIGURE 8.39: The angular displacement q_2 of the distal pendulum for the passively damped Acrobot with $k_P = 61.3$ and $b_1 = 1$ during LDM-related swing-up control.

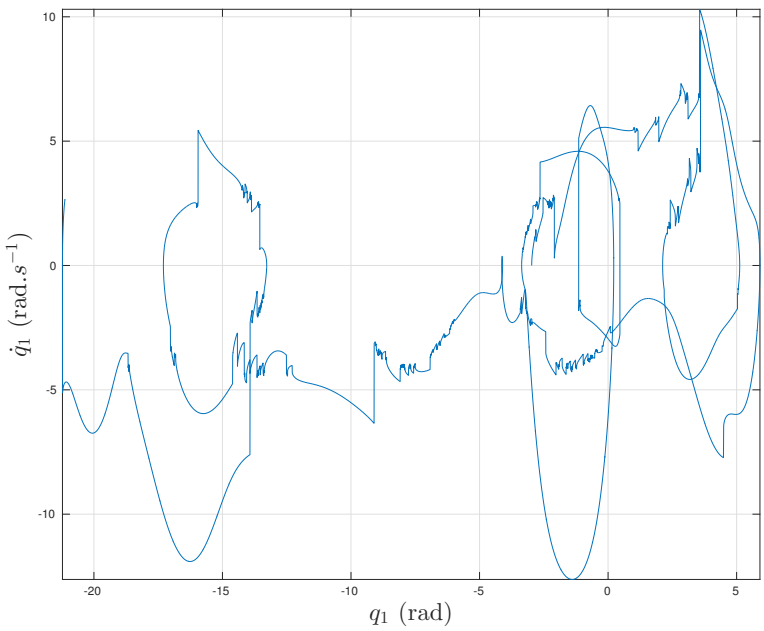

FIGURE 8.40: The phase portrait of the proximal pendulum of the passively damped Acrobot with $k_P = 61.3$ and $b_1 = 1$ during LDM-related swing-up control.

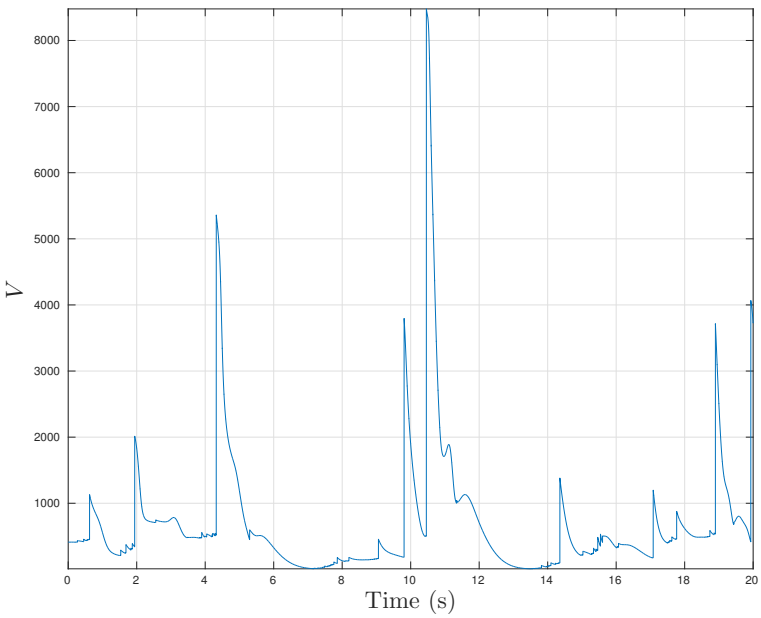

FIGURE 8.41: The Lyapunov candidate function of the passively damped Acrobot with $k_P = 61.3$ and $b_1 = 1$.

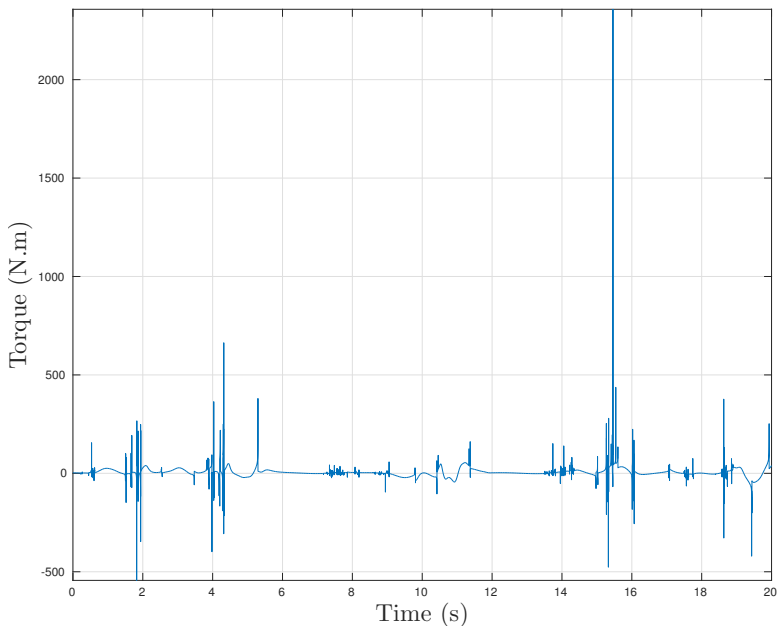

FIGURE 8.42: The LDM-related torque used to swing-up the passively damped Acrobot with $k_P = 61.3$ and $b_1 = 1$.

The behaviour of the selected Lyapunov function is demonstrated in figure 8.9. It is clear that the system dynamics does not adhere to an invariant set with semi-negative gradient since the function does not exponentially tend toward zero throughout the simulation. Instead, the function follows a steep positive gradient in certain instances, reaching magnitudes that surpass 8000. The function, therefore, does not follow a negatively sloping stable manifold as required for satisfactory LDM-related swing-up control. The torque produced by the actuator during swing-up control is demonstrated in figure 8.42. The torque profile does not contain a transient phase followed by a steady-state as seen in the undamped and actively damped cases. Instead, the actuator is constantly required to produce sharp torques in an attempt to satisfy the applied control law. The large spikes coincide with the plateaus seen in the angular displacement of q_2 (figure 8.39). This is expected since the plateaus represent $\dot{q}_2 \approx 0$, which will introduce a singularity in the control torque.

The results clearly demonstrate that, despite the fact that we have implemented the same gains and initial conditions, we cannot achieve satisfactory swing-up control performance that is seen in both the undamped and actively damped cases when the *matched damping condition* is not satisfied. We shall now demonstrate the effects on the control of a higher-order system, namely the PAA robot, when the *matched damping condition* is violated.

8.4.6 The Passively Damped PAA Robot

Derivation of the Necessary Swing-up Control Torque: The Invertibility Problem

The passively damped PAA robot is associated with the following viscous damping profile

$$\mathbf{R}(\dot{\mathbf{q}}) = \begin{bmatrix} b_1\dot{q}_1 & 0 & 0 \end{bmatrix}.$$

The Lyapunov function

$$V = \frac{1}{2}(E - E_r)^2 + \frac{1}{2}k_D\dot{\mathbf{q}}_a^{\mathbf{T}}\dot{\mathbf{q}}_a + \frac{1}{2}k_P\overline{\mathbf{q}}_a{}^{\mathbf{T}}\overline{\mathbf{q}}_a$$

was chosen for the PAA robot, as seen in the undamped and actively damped cases along with the time-related differential of this Lyapunov function described by

$$\dot{V} = (E - E_r)\dot{E} + k_D\dot{\mathbf{q}}_a^{\mathbf{T}}\ddot{\mathbf{q}}_a + k_P\psi^{\mathbf{T}}(\overline{\mathbf{q}}_a)\dot{\mathbf{q}}_a^{\mathbf{T}}\overline{\mathbf{q}}_a. \tag{8.49}$$

The change of energy of the system is dictated by the actuation of the system and the passive damping, resulting in

$$\dot{E} = \dot{\mathbf{q}}_a^{\mathbf{T}}\tau_a - b_1\dot{q}_1^2.$$

Substituting this expression into eq. (8.49) produces

$$(E - E_r)\left[\dot{\mathbf{q}}_a^{\mathbf{T}}\tau_a - b_1\dot{q}_1^2\right] + k_D\dot{\mathbf{q}}_a^{\mathbf{T}}\ddot{\mathbf{q}}_a + k_P\psi^{\mathbf{T}}(\overline{\mathbf{q}}_a)\dot{\mathbf{q}}_a^{\mathbf{T}}\overline{\mathbf{q}}_a.$$

The dynamics of the two most distal pendulums in the PAA robot are represented as

$$\ddot{\mathbf{q}}_a = \mathbf{G}^{\mathbf{T}}(\mathbf{q})\mathbf{M}^{-1}(\mathbf{q})\left[\mathbf{G}(\mathbf{q})\tau_a - \mathbf{C}(\mathbf{q},\dot{\mathbf{q}}) - \mathbf{R}(\dot{\mathbf{q}}) - \mathbf{K}(\mathbf{q})\right].$$

Therefore

$$\begin{aligned}\dot{V} = \dot{\mathbf{q}}_a^{\mathbf{T}}\Big[\big[(E - E_r)I_2 + k_D\mathbf{G}^{\mathbf{T}}(\mathbf{q})\mathbf{M}^{-1}(\mathbf{q})\mathbf{G}(\mathbf{q})\big]\tau_a + k_pq_2 \\ -k_D\mathbf{G}^{\mathbf{T}}(\mathbf{q})\mathbf{M}^{-1}(\mathbf{q})\left[\mathbf{C}(\mathbf{q},\dot{\mathbf{q}}) + \mathbf{R}(\dot{\mathbf{q}}) + \mathbf{K}(\mathbf{q})\right]\Big] - (E - E_r)b_1\dot{q}_1^2.\end{aligned} \tag{8.50}$$

Knowing that $\dot{V}_d = -k_V\dot{\mathbf{q}}_a^{\mathbf{T}}\dot{\mathbf{q}}_a$, and $\dot{V} = \dot{V}_d$, we conclude that

$$\begin{aligned}-k_V\dot{\mathbf{q}}_a^{\mathbf{T}}\dot{\mathbf{q}}_a &= \dot{\mathbf{q}}_a^{\mathbf{T}}\Big[\big[(E - E_r)I_2 + k_D\mathbf{G}^{\mathbf{T}}(\mathbf{q})\mathbf{M}^{-1}(\mathbf{q})\mathbf{G}(\mathbf{q})\big]\tau_a + k_pq_2 \\ &\quad -k_D\mathbf{G}^{\mathbf{T}}(\mathbf{q})\mathbf{M}^{-1}(\mathbf{q})\left[\mathbf{C}(\mathbf{q},\dot{\mathbf{q}}) + \mathbf{R}(\dot{\mathbf{q}}) + \mathbf{K}(\mathbf{q})\right]\Big] - (E - E_r)b_1\dot{q}_1^2, \\ &= \dot{\mathbf{q}}_a^{\mathbf{T}}\left[\Lambda(\mathbf{q},\dot{\mathbf{q}})\tau_a + k_pq_2 - k_D\mathbf{G}^{\mathbf{T}}(\mathbf{q})\mathbf{M}^{-1}(\mathbf{q})\left[\mathbf{C}(\mathbf{q},\dot{\mathbf{q}}) + \mathbf{R}(\dot{\mathbf{q}}) + \mathbf{K}(\mathbf{q})\right]\right] \\ &\quad - (E - E_r)b_1\dot{q}_1^2\end{aligned}$$

where

$$\Lambda(\mathbf{q},\dot{\mathbf{q}}) = \left[(E - E_r)I_2 + k_D\mathbf{G}^{\mathbf{T}}(\mathbf{q})\mathbf{M}^{-1}(\mathbf{q})\mathbf{G}(\mathbf{q})\right].$$

It is apparent that the isolation of τ_a is contingent on the factoring out of the $\dot{\mathbf{q}}_a^{\mathbf{T}}$ vector, which is not practically possible since the vector is not invertible, and the implementation of a pseudo-inverse is typically used in instances where the system is over-actuated, as stated in section 8.4. The swing-up torque cannot, therefore, be solved for the passively damped PAA robot as a consequence of the *invertibility problem* (since for the PAA robot, $n > 2$). This issue can be circumnavigated through the reduction of the order of the system using the MC-ROPA$_2$ modelling protocol. This evidently results in the presence of the *singularity problem* (as stated by the matched damping condition). We shall demonstrate the effect of the singularity problem on the MC-ROPA$_2$ robot subsequent to the highlighting of the MC-ROPA$_2$ modelling protocol.

Modelling the Passively Damped PAA Robot as the MC-ROPA$_2$ Robot

The MC-ROPA$_2$ robot is first constructed through the implementation of the FBL torque

$$\tau_3 = \hat{M}_{33}(\mathbf{q})v_3 + \hat{D}_3(\mathbf{q}, \dot{\mathbf{q}}) + \hat{K}_3(\mathbf{q}) + \hat{\tau}_3$$

where

$$\hat{M}_{33}(\mathbf{q}) = M_{33}(\mathbf{q}) - \frac{\tilde{M}_{13}(\mathbf{q})M_{31}(\mathbf{q})}{M_{11}(\mathbf{q})} - \frac{\tilde{M}_{23}(\mathbf{q})M_{32}(\mathbf{q})}{\tilde{M}_{22}(\mathbf{q})},$$

$$\hat{D}_3(\mathbf{q}, \dot{\mathbf{q}}) = D_3(\mathbf{q}, \dot{\mathbf{q}}) - \frac{M_{31}(\mathbf{q})}{M_{11}(\mathbf{q})}\tilde{D}_1(\mathbf{q}) - \frac{M_{32}(\mathbf{q})}{\tilde{M}_{22}(\mathbf{q})}\tilde{D}_2(\mathbf{q}),$$

$$\hat{K}_3(\mathbf{q}) = K_3(\mathbf{q}) - \frac{M_{31}(\mathbf{q})}{M_{11}(\mathbf{q})}\tilde{K}_1(\mathbf{q}) - \frac{M_{32}(\mathbf{q})}{\tilde{M}_{22}(\mathbf{q})}\tilde{K}_2(\mathbf{q}),$$

$$\hat{\tau}_3 = \frac{M_{32}(\mathbf{q})}{\tilde{M}_{22}(\mathbf{q})}\tau_2 - \frac{M_{31}(\mathbf{q})}{M_{11}(\mathbf{q})}\tilde{\tau}_2,$$

$$\tilde{\tau}_2 = \frac{M_{12}(\mathbf{q})}{\tilde{M}_{22}}\tau_2$$

and, for $2 \leq k \leq 3$,

$$\tilde{M}_{2k}(\mathbf{q}) = M_{2k}(\mathbf{q}) - \frac{M_{1k}(\mathbf{q})M_{21}(\mathbf{q})}{M_{11}(\mathbf{q})}, \qquad \tilde{M}_{13}(\mathbf{q}) = M_{13}(\mathbf{q}) - \frac{M_{12}(\mathbf{q})\tilde{M}_{23}(\mathbf{q})}{\tilde{M}_{22}(\mathbf{q})},$$

$$\tilde{D}_2(\mathbf{q}, \dot{\mathbf{q}}) = D_2(\mathbf{q}, \dot{\mathbf{q}}) - \frac{M_{21}(\mathbf{q})}{M_{11}(\mathbf{q})}D_1(\mathbf{q}, \dot{\mathbf{q}}), \quad \tilde{D}_1(\mathbf{q}, \dot{\mathbf{q}}) = D_1(\mathbf{q}, \dot{\mathbf{q}}) - \frac{M_{12}(\mathbf{q})}{\tilde{M}_{22}(\mathbf{q})}\tilde{D}_2(\mathbf{q}, \dot{\mathbf{q}}),$$

$$\tilde{K}_2(\mathbf{q}) = K_2(\mathbf{q}) - \frac{M_{21}(\mathbf{q})}{M_{11}(\mathbf{q})} K_1(\mathbf{q}), \qquad \tilde{K}_1(\mathbf{q}) = K_1(\mathbf{q}) - \frac{M_{12}(\mathbf{q})}{\tilde{M}_{22}(\mathbf{q})} \tilde{K}_2(\mathbf{q})$$

with the $\mathbf{D}(\mathbf{q}, \dot{\mathbf{q}})$ matrix entries defined as

$$D_1(\mathbf{q}, \dot{\mathbf{q}}) = C_1(\mathbf{q}, \dot{\mathbf{q}}) + R_1(\dot{\mathbf{q}}), \quad D_2(\mathbf{q}, \dot{\mathbf{q}}) = C_2(\mathbf{q}, \dot{\mathbf{q}}), \quad D_3(\mathbf{q}, \dot{\mathbf{q}}) = C_3(\mathbf{q}, \dot{\mathbf{q}})$$

for the passively damped case. The implementation of this torque results in $\ddot{q}_3 = v_3$, thus causing the most distal two pendulums to behave approximately as a single pendulum. The equations of motion of the passively damped MC-ROPA$_2$ robot and its physical parameters can now be defined as

$$\begin{aligned} &\overline{M}_{11}(q_2)\ddot{q}_1 + \overline{M}_{12}(q_2)\ddot{q}_2 - \overline{\alpha}_3(2\dot{q}_1\dot{q}_2 + \dot{q}_2^2)\sin q_2 - \overline{\beta}_1 \sin q_1 \\ &- \overline{\beta}_2 \sin(q_1 + q_2) = -b_1\dot{q}_1, \end{aligned} \tag{8.51a}$$

$$\overline{M}_{21}(q_2)\ddot{q}_1 + \overline{M}_{22}(q_2)\ddot{q}_2 + \overline{\alpha}_3\dot{q}_1^2 \sin q_2 - \overline{\beta}_2 \sin(q_1 + q_2) = \tau_2. \tag{8.51b}$$

The individual entries are defined as seen in section 8.2.5.

Derivation of the Necessary Swing-up Control Torque for the Passively Damped MC-ROPA$_2$ Robot: The Singularity Problem

Now that the PAA robot is modelled as a MC-ROPA$_2$ robot, we can use the Lyapunov function

$$V = \frac{1}{2}(E - E_r)^2 + \frac{1}{2}k_D\dot{q}_2^2 + \frac{1}{2}k_P {q_2}^2$$

to derive the swing-up control, with the time-related differential of the candidate function represented as

$$\dot{V} = (E - E_r)\dot{E} + k_D\ddot{q}_2\dot{q}_2 + k_P\dot{q}_2 q_2.$$

The change of energy can be modelled according to the damping experienced on the most proximal joint and the actuation that occurs at the second joint. This results in

$$\dot{E} = \tau_2\dot{q}_2 - b_1\dot{q}_1^2$$

with

$$\dot{V} = (E - E_r)\left[\tau_2\dot{q}_2 - b_1\dot{q}_1^2\right] + k_D\ddot{q}_2\dot{q}_2 + k_P\dot{q}_2 q_2. \tag{8.52}$$

The dynamics of the collective distal pendulum $\ddot{q}_2$ is represented as

$$\ddot{q}_2 = \mathbf{G}^{\mathbf{T}}(\mathbf{q})\overline{\mathbf{M}}^{-1}(q_2)\left[\mathbf{G}(\mathbf{q})\tau_2 - \overline{\mathbf{C}}(q_2, \dot{\mathbf{q}}) - \overline{\mathbf{R}}(\dot{\mathbf{q}}) - \overline{\mathbf{K}}(\mathbf{q})\right] \tag{8.53}$$

where $\mathbf{G}(\mathbf{q}) = \begin{bmatrix} 0 & 1 \end{bmatrix}^{\mathbf{T}}$ and

$$\overline{\mathbf{M}}(q_2) = \begin{bmatrix} \overline{M}_{11}(q_2) & \overline{M}_{12}(q_2) \\ \overline{M}_{21}(q_2) & \overline{M}_{22}(q_2) \end{bmatrix},$$

$$\overline{\mathbf{C}}(q_2, \dot{\mathbf{q}}) = \begin{bmatrix} \overline{\mathbf{C}}_1(q_2, \dot{\mathbf{q}}) \\ \overline{\mathbf{C}}_2(q_2, \dot{\mathbf{q}}) \end{bmatrix},$$

$$\overline{\mathbf{R}}\left(\dot{\mathbf{q}}\right) = \begin{bmatrix} \overline{\mathbf{R}}_1\left(\dot{\mathbf{q}}\right) \\ \overline{\mathbf{R}}_2\left(\dot{\mathbf{q}}\right) \end{bmatrix},$$

$$\overline{\mathbf{K}}(\mathbf{q}) = \begin{bmatrix} \overline{\mathbf{K}}_1(\mathbf{q}) \\ \overline{\mathbf{K}}_2(\mathbf{q}) \end{bmatrix}$$

with

$$\begin{aligned}
&\overline{\mathbf{C}}_1(q_2, \dot{\mathbf{q}}) = -\overline{\alpha}_3(2\dot{q}_1\dot{q}_2 + \dot{q}_2^2)\sin q_2, \\
&\overline{\mathbf{C}}_1(q_2, \dot{\mathbf{q}}) = -\overline{\alpha}_3(2\dot{q}_1\dot{q}_2 + \dot{q}_2^2)\sin q_2, \\
&\overline{\mathbf{C}}_2(q_2, \dot{\mathbf{q}}) = \overline{\alpha}_3\dot{q}_1^2\sin q_2, \\
&\overline{\mathbf{R}}_1\left(\dot{\mathbf{q}}\right) = b_1\dot{q}_1, \\
&\overline{\mathbf{R}}_2\left(\dot{\mathbf{q}}\right) = 0, \\
&\overline{\mathbf{K}}_1(\mathbf{q}) = -\overline{\beta}_1\sin q_1 - \overline{\beta}_2\sin(q_1 + q_2), \\
&\overline{\mathbf{K}}_2(\mathbf{q}) = -\overline{\beta}_2\sin(q_1 + q_2).
\end{aligned}$$

The expression found in eq. (8.52) can thus be represented as

$$\begin{aligned}
\dot{V} = (E - E_r)\left[\tau_2\dot{q}_2 - b_1\dot{q}_1^2\right] + k_D\dot{q}_2\mathbf{G}^{\mathbf{T}}(\mathbf{q})\overline{\mathbf{M}}^{-1}(q_2)\left[\mathbf{G}(\mathbf{q})\tau_2 - \overline{\mathbf{C}}(q_2, \dot{\mathbf{q}})\right. \\
\left. -\overline{\mathbf{R}}(\dot{\mathbf{q}}) - \overline{\mathbf{K}}(\mathbf{q})\right] + k_P\dot{q}_2q_2.
\end{aligned}$$

The desired Lyapunov time-derivative is chosen as

$$\dot{V}_d = -k_V\dot{q}_2^2.$$

Therefore, choosing $\dot{V} = \dot{V}_d$ results in the definition of the torque expression

$$\begin{aligned}
\tau_2 = &\frac{k_D\mathbf{G}^{\mathbf{T}}(\mathbf{q})\overline{\mathbf{M}}^{-1}(q_2)\left[\overline{\mathbf{C}}(q_2, \dot{\mathbf{q}}) + \overline{\mathbf{R}}(\dot{\mathbf{q}}) + \overline{\mathbf{K}}(\mathbf{q})\right] - k_V\dot{q}_2 - k_Pq_2}{\overline{\Lambda}\left(\mathbf{q}, \dot{\mathbf{q}}\right)} \\
&+ \frac{(E - E_r)b_1\dot{q}_1^2}{\dot{q}_2\overline{\Lambda}\left(\mathbf{q}, \dot{\mathbf{q}}\right)}
\end{aligned} \tag{8.54}$$

as seen in the case of the passively damped Acrobot. The *singularity problem* is clearly visible in this torque expression, thus confirming the prediction made by the *matched damping condition*. The torque τ_2 in this case is thus guaranteed to tend towards infinity as $\dot{q}_2 \to 0$ and $\dot{q}_1 \neq 0$.

Simulation Results

The consequences of this problem are demonstrated on the passively damped MC-ROPA$_2$ robot, using the system parameters

$$\begin{aligned} &m_1 = 1 \text{ kg}, && m_2 = 0.5 \text{ kg}, && m_3 = 0.5 \text{ kg}, \\ &L_1 = 1 \text{ m}, && L_2 = 1 \text{ m}, && L_3 = 1 \text{ m}, \\ &l_1 = 0.5 \text{ m}, && l_2 = 0.5 \text{ m}, && l_3 = 0.5 \text{ m}, \\ &I_1 = 0.083 \text{ kg.m}^2, && I_2 = 0.165 \text{ kg.m}^2, && I_3 = 0.165 \text{ kg.m}^2 \end{aligned}$$

which produces

$$\begin{aligned} &\overline{m}_2 = 1 \text{ kg}, && \overline{I}_2 = 0.33 \text{ kg.m}^2, \\ &\overline{m_2 l_2} = 1 \text{ kg.m}, && \overline{m_2 {l_2}^2} = 1.25 \text{ kg.m}^2. \end{aligned}$$

Additionally, we implement the gains

$$\begin{aligned} &k_D = 38, && k_P = 61.3, && k_V = 66.3, \\ &k_{D_3} = 40, && k_{P_3} = 400 \end{aligned}$$

and the initial conditions

$$\begin{aligned} &q_1(0) = -1.4 - \frac{\pi}{2}, && q_2(0) = q_3(0) = 0, \\ &\dot{q}_1(0) = \dot{q}_3(0) = 0, && \dot{q}_2(0) = 0.1. \end{aligned}$$

The results of the simulation of the passively damped MC-ROPA$_2$ robot are demonstrated in figures 8.43-8.47.

The angular displacement of the most proximal pendulum of the MC-ROPA$_2$ robot is demonstrated in figure 8.43. The proximal pendulum demonstrated no behaviour that suggests that it converged with the desired trajectory towards the UEP, unlike what is seen with the undamped MC-ROPA$_2$ robot. The angular displacement of the second pendulum of the MC-ROPA$_2$ robot is demonstrated in figure 8.44. The second pendulum also did not follow an exponentially stable path toward the UEP, demonstrating that the control law did not establish a smooth stable manifold on which the system trajectory could be established towards the desired objective.

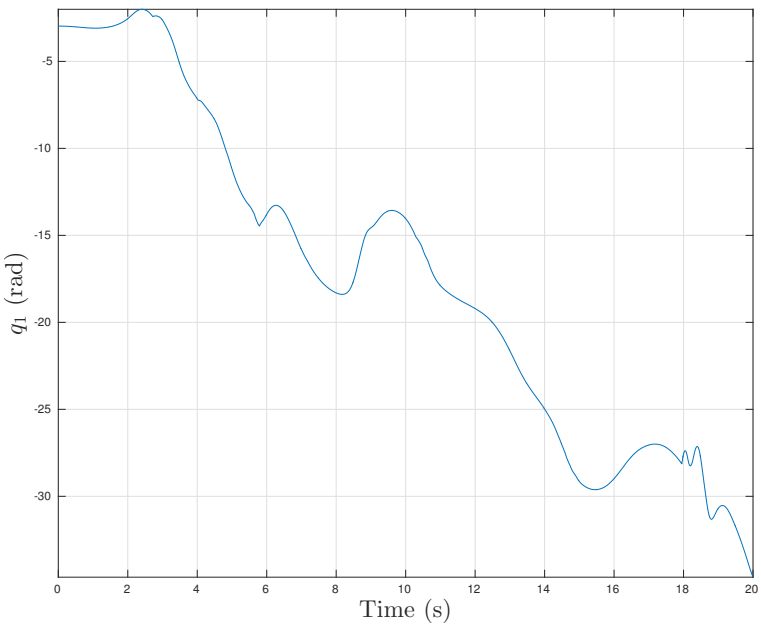

FIGURE 8.43: The angular displacement q_1 of the most proximal pendulum of the passively damped MC-ROPA$_2$ robot during LDM-related swing-up control.

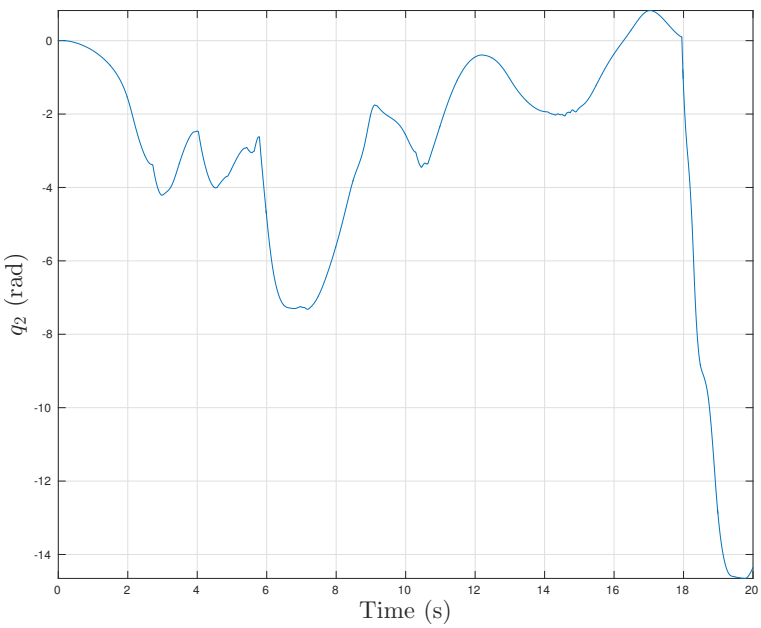

FIGURE 8.44: The angular displacement q_2 of the second pendulum of the passively damped MC-ROPA$_2$ robot during LDM-related swing-up control.

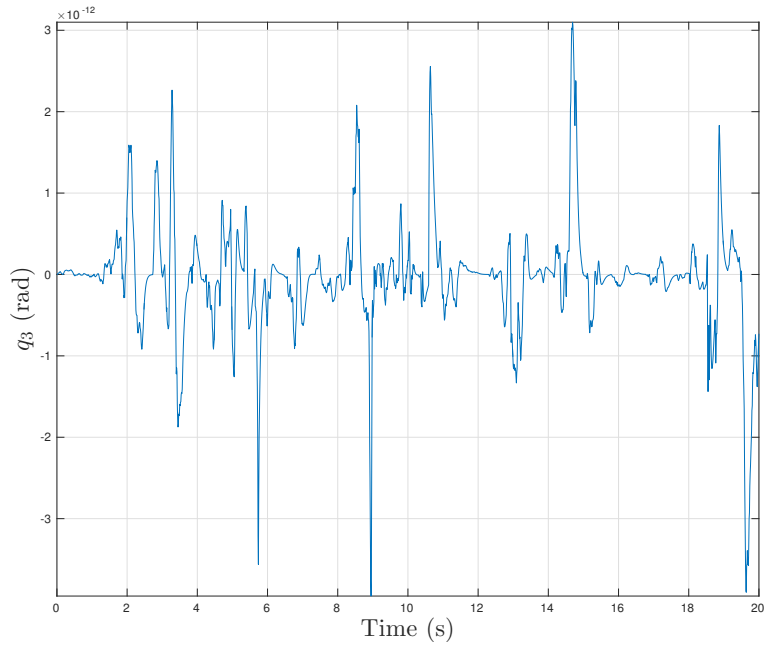

FIGURE 8.45: The angular displacement q_3 of the most distal pendulum of the passively damped MC-ROPA$_2$ robot during LDM-related swing-up control.

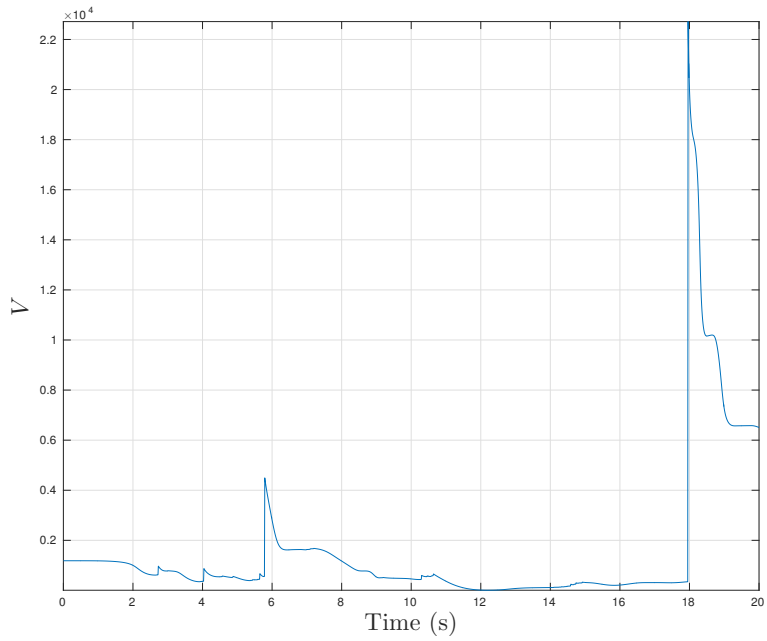

FIGURE 8.46: The Lyapunov candidate function of the passively damped MC-ROPA$_2$ robot.

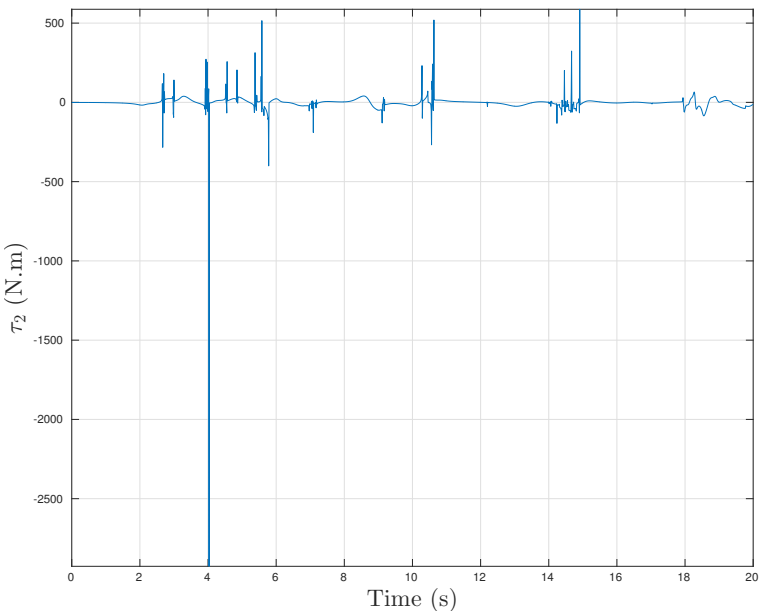

FIGURE 8.47: The torque τ_2 used to swing-up the passively damped MC-ROPA$_2$ robot during LDM-related swing-up control.

The angular displacement of the most distal pendulum is demonstrated in figure 8.45. The pendulum is tightly regulated about $q_3^d = 0$, deviating off the objective by a maximum 4×10^{-12} radians. This control ensured that the second and most distal pendulum acted collectively as a single pendulum, as is expected when applying MCPFL.

The behaviour of the Lyapunov function of the passively damped MC-ROPA$_2$ robot is demonstrated in figure 8.46. The control law was not sustained in this simulation since the Lyapunov function did not conform to an exponentially stable semi-negative invariant set. There are many instances throughout the simulation where the Lyapunov function demonstrated positive growth, which violates the premise of LDM-related control. The UEP is thus not a realisable control objective in this case. The torque produced by the actuator found between the most proximal and second pendulum is demonstrated in figure 8.47. The actuator attempted to sustain LDM-related control through the production of large spike torques as seen in the swing-up control of the passively damped Acrobot. These spikes coincide with the plateaus seen in figure 8.44, which corresponds to instances where $\dot{q}_2 \approx 0$ as seen with the passively damped Acrobot. Despite these large torque spikes, it is evident that the control law could not be adhered to. Therefore, **implementing MCPFL in an attempt to circumvent the *invertibility problem* is not a satisfactory work-around since the Acrobot and MC-ROPA$_2$ robot are susceptible to the singularity problem.**

8.5 Conclusion

In this chapter, we managed to confirm that the successful LDM-related swing-up control of the PA_{n-1} robot model is contingent on the satisfaction of a criterion termed the *matched damping condition*, which is the key result of this chapter. This condition highlights the following phenomena:

The integration of viscous damping on the actuated joints (known as active damping) has no effect on the derivation of the control law or the determination of the specific necessary gain conditions for the PA_{n-1} robot and its derivatives. The behaviour of the actively damped system remains identical to the undamped PA_{n-1} robot, with the resultant swing-up torque for the actively damped case having a superimposed damping-negating torque. Conversely, integrating viscous damping into the unactuated joint of the PA_{n-1} robot (known as passive damping) results in the derivation of an unsuitable swing-up torque expression. Specifically, for passively damped PA_{n-1} robot derivatives that are of order ($n > 2$), the necessary torque expression cannot be solved due to the non-invertible properties of a the $\dot{\mathbf{q}}_a^{\mathbf{T}}$ vector. This is referred to as the *invertibility problem*. This problem can be circumnavigated through the implementation of a modelling technique that accommodates the transformation of PA_{n-1} robot derivatives of higher-order ($n > 2$) into a system that approximates the Acrobot using MCPFL (termed the MC-ROPA_{n-1} robot). Despite these efforts, it became evident that the torque expression that is necessary to swing-up the passively damped MC-ROPA_{n-1} robot or Acrobot model is also unsuitable since it is subject to a conditional singularity. This is referred to as the *singularity problem*. It is, therefore, evident that the Lyapunov related swing-up control is limited to applications on undamped or actively damped derivatives of the PA_{n-1} robot.

The author believes that this limitation is significant since the presence of passive damping in a true physical underactuated robotic system is not improbable. The application of underactuated robotic systems is becoming increasingly popular, as mentioned in the introduction of this dissertation. We thus believe that addressing this issue will increase the probability of swing-up control becoming prevalent in real-world applications. The objective of this research is to, thus, develop a work-around for this limitation.

"Where there is a will there is a way."
— Samuel Smiles

Chapter 9

Work-Around:

The Swing-up Control of the Damped PA_{n-1} Robot using Partial Feedback Linearisation

9.1 Chapter Overview

The work presented in this chapter is dedicated to the development of a work-around for the limitation highlighted by the **matched damping condition**, which was introduced in the last chapter. This limitation pertains to the application of Lyapunov-related swing-up control on the passively damped PA_{n-1} robot. There are two contributions that are highlighted in this chapter, namely the **gain selection criterion** and the **convergence algorithm**. These contributions are provided for the undamped, actively damped, and passively damped PA_{n-1} robot.

The rest of this chapter is structured as follows. A brief discussion on the control strategy that is implemented to address the *matched damping condition* is introduced to justify the use of swing-up control using PFL as a possible work-around, and is summarised as a **research question**. This is followed by a formalisation of the PFL technique applied on the PA_{n-1} robot, which includes the Traditional Collocated (TCPFL), Modified Collocated (MCPFL) and Noncollocated (NCPFL) forms. The MCPFL technique is not explicitly implemented in this chapter, but it is formally defined here to prevent unnecessary discontinuity. The *matched damping condition* is first addressed in this chapter through the application of TCPFL on the undamped, actively damped and passively damped PA_{n-1} robot, which results in the analytical contribution referred to as the *gain selection criterion*. This is achieved as follows: the PA_{n-1} robot is first modelled as a ROPA_{n-1} robot using TCPFL (TC-ROPA_{n-1} robot). The TC-ROPA_{n-1} model is subsequently integrated with an ATAN swing-up controller and the equilibrium points of this resultant system are thus determined. Lastly, the stability of the FPEP of the TC-ROPA_{n-1} robot is determined through the implementation of the Routh-Hurwitz criterion. The results of this set of analytical conditions are demonstrated on the undamped, actively damped and passively damped Acrobot and PAA robot, which are the simplest derivatives of the PA_{n-1} robot. The *matched damping condition* is also addressed through the implementation

of NCPFL on the undamped, actively damped and passively damped ROPA$_{n-1}$ robot modelled using NCPFL (referred to as the Noncollocated ROPA$_{n-1}$ robot, or NC-ROPA$_{n-1}$ robot), which results in the experimental solution known as the *convergence algorithm*. The structure of this algorithm is highlighted in the latter sections of this chapter, along with the results of this algorithm when applied on the undamped, actively damped, and passively damped Acrobot (NC-ROPA$_1$ robot).

9.2 Control Strategy and Research Question

In the last chapter, we highlighted a key limitation in the Lyapunov-related swing-up control of the passively damped PA$_{n-1}$ robot, which is summarised as an application prerequisite known as the *matched damping condition*. The objective of this research project is the development of a work-around that will address this condition, resulting in an increased robustness in the field of swing-up control. There are three ways in which this condition can be addressed:

(i) Identify an appropriate Lyapunov candidate function that is not subject to the invertibility and singularity problems.

(ii) Identify multiple Lyapunov functions that are valid within a certain region of operation, and implement a controller switching algorithm that will switch between these controllers when appropriate (based on Artstein's theorem, which states that the existence of a smooth control related Lyapunov function will entail smooth stabilisability [108]).

(iii) Implement a different control technique that will achieve the same desired objective without being subject to the *invertibility* and *singularity* problems.

Whilst it would be beneficial to develop either a single or multiple valid Lyapunov candidate functions for this application (since the control is designed specifically to actively track the UEP), it cannot be guaranteed that these functions will (or even can) be found within a defined time-frame. This is due to the absence of a rigorous and formalised candidate function identification method (existing conditional techniques are discussed in section 5.2.2). It is for this reason that we have opted with option (iii) for this project, but we encourage other interested researchers to explore options (i) and (ii).

Logically, the next question one would ask at this stage would be: **Which control technique will be most appropriate in this application?** Whilst there are a number of relevant nonlinear control techniques found in existing literature highlighted in section 2.4.2 (which include, and is not limited to, fuzzy control, NN adaptive control, and feedforward control), the PFL technique, first implemented by Mark Spong in [6], was deemed to be most appropriate for the following reasons:

(1) There is a significant body of existing literature that discusses the application of this technique on varying orders of robotic systems, which includes, and

is not limited to, [6, 34, 75, 76]. This provides us with a significantly broad foundation on which we may base our investigation.

(2) The technique evidently does not actively track the control objective. This is evident in the fact that:

(i) The Collocated form of PFL swing-up control relies on the definition of an 'energy-pump' ATAN controller, which is designed specifically to introduce energy into the system indiscriminately through a number of swing-up cycles, thus allowing the system to 'swing-up' from a lower energy-state to a higher-energy state [6]. The controller does not, therefore, have a final energy state in mind, but is simply responsible for causing the system to behave in an unstable manner. The swing-up controller's performance is monitored through the system's internal and zero dynamics.

(ii) The Noncollocated form of PFL swing-up control relies on a set of perfectly tuned initial conditions, since the most proximal limb is immediately swung-up to the inverted position without requiring multiple swing-up cycles [6]. A correctly paired set of angular initial conditions must, therefore, be chosen for the distal pendulum to guarantee that the entire system approaches and settles near (or exactly at) the UEP. The controller, therefore, does not track the UEP as the final objective.

These variations of PFL are discussed in section 9.3. Whilst the inability of the PFL controller to track the UEP may be perceived as an inconvenient property, it is a direct consequence of the flexibility of the control technique, allowing it to be more robust to changes in the system's physical properties. This will become evident once the final work-around is derived. With these justifications in mind, we decided to continue onto the next step of the research, which involved answering the following research question:

RQ: Using PFL as a work-around for the key limitation in LDM highlighted by the *matched damping condition*, what are the specific conditions (if any) that need to be satisfied to accommodate the satisfactory swing-up control of a passively damped PA$_{n-1}$ robot?

The answer to this question will be highlighted in the upcoming sections for both the collocated and noncollocated forms of PFL, which are first defined prior to the derivation of the conditions necessary to facilitate the swing-up of the passively damped PA$_{n-1}$ robot.

9.3 Partial Feedback Linearisation

Partial feedback linearisation (PFL) describes the implementation of the IOFBL technique to linearise a portion of the dynamics of an underactuated system [6]. The

application of the PFL technique was implemented in chapter 8 to accommodate the derivation of the MC-ROPA$_{n-1}$ robot, but information about this technique was discussed at a superficial level. This section is dedicated to discussing each of the PFL techniques whilst referring to their rigorous derivations included in appendix D. There are currently two traditional forms of PFL that were originally defined in [6], namely the *collocated* and *noncollocated* forms. These variants are discussed in the subsections that follows, and are subsequently applied to the PA$_{n-1}$ robot.

9.3.1 Collocated Partial Feedback Linearisation

Collocated PFL (CPFL) is defined in [6] for the Acrobot as a procedure that involves the linearisation of the dynamics of the actuated joint (i.e. the distal joint). This accommodates the design of a linear state feedback controller for the distal pendulum, whose behaviour can be precisely controlled. The dynamics of the proximal pendulum, however, can only be influenced indirectly by the dynamics of the distal pendulum since it is unactuated. These dynamics are, thus, internal and unobservable to the control input [2]. Despite this formal definition of CPFL for the Acrobot, it does not consider higher-order systems, such as the PA$_{n-1}$ robot. This formal definition of CPFL will be expanded in this section to include applications on systems that have a higher order than that of the Acrobot. We identify two variations of the CPFL technique, namely the *Traditional* and the *Modified*.

Traditional Collocated Partial Feedback Linearisation

The method of Collocated PFL performed on a PA$_{n-1}$ robot is shown in figure 9.1. It is evident that the most distal $n-1$ pendulums of the PA$_{n-1}$ robot found on the left of this figure are configured in such a way that they can be collectively represented as a single pendulum (as seen on the right of figure 8.1). It is not possible, however, to keep the $n-1$ most distal pendulums in this configuration unless the actuators of the $n-2$ most distal pendulums are used for the purpose of regulation. The dynamics of the 2nd pendulum are also linearised, but the linear state feedback controller that is designed for this joint will be responsible for producing the swing-up control rather than just regulating the pendulum. This control technique is formally defined as Traditional Collocated Partial Feedback Linearisation.

Definition 9.1. Traditional Collocated Partial Feedback Linearisation (TCPFL) involves the linearisation of the dynamics of the $n-1$ most distal pendulums in the PA$_{n-1}$ robot. The linear state feedback controllers for the $n-2$ most distal pendulums (v_i where $3 \leq i \leq n$) are responsible for regulating the pendulum about $q_i = 0$ whilst the linear state feedback controller of the 2nd pendulum is designed specifically to achieve the intended control objective.

The torques required to perform this control technique are defined as

$$\tau_i = \hat{M}_{i2}(\mathbf{q})v_2 + \hat{M}_{i3}(\mathbf{q})v_3 + \cdots + \hat{M}_{in}(\mathbf{q})v_n + \hat{D}_i(\mathbf{q}, \dot{\mathbf{q}}) + \hat{K}_i(\mathbf{q}) \tag{9.1}$$

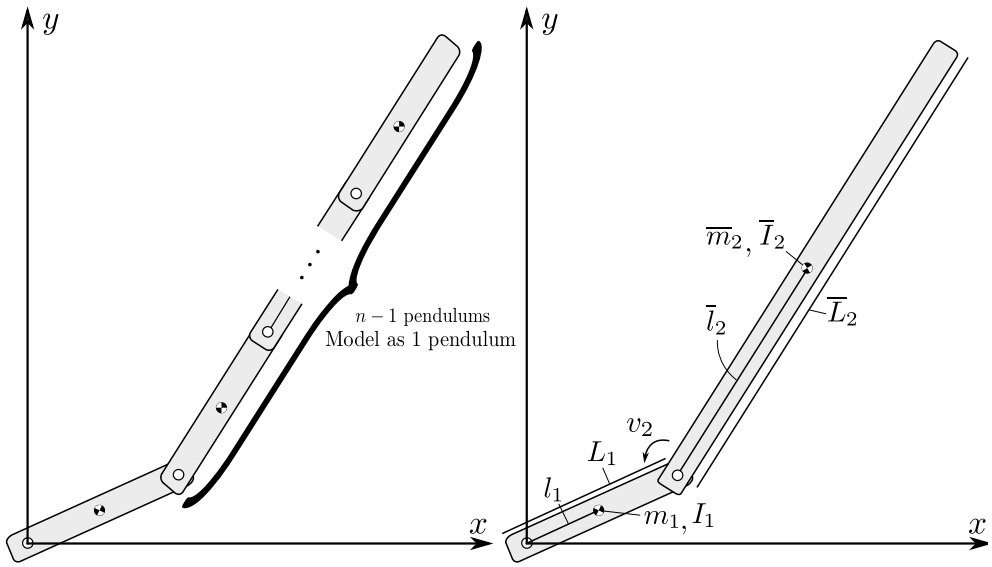

FIGURE 9.1: The PA_{n-1} robot, linearised using TCPFL, represented as a TC-$ROPA_{n-1}$ robot.

where, for $2 \leq j \leq n$,

$$\hat{M}_{ij}(\mathbf{q}) = M_{ij}(\mathbf{q}) - \frac{M_{i1}(\mathbf{q})M_{1j}(\mathbf{q})}{M_{11}(\mathbf{q})},$$
$$\hat{D}_i(\mathbf{q}, \dot{\mathbf{q}}) = D_i(\mathbf{q}, \dot{\mathbf{q}}) - \frac{M_{i1}(\mathbf{q})}{M_{11}(\mathbf{q})} D_1(\mathbf{q}, \dot{\mathbf{q}}),$$
$$\hat{K}_i(\mathbf{q}) = K_i(\mathbf{q}) - \frac{M_{i1}(\mathbf{q})}{M_{11}(\mathbf{q})} K_1(\mathbf{q}).$$

This results in a set of dynamical equations described by

$$\ddot{q}_1 = \frac{-M_{12}(\mathbf{q})v_2 - M_{13}(\mathbf{q})v_3 - \cdots - M_{1n}(\mathbf{q})v_n - D_1(\mathbf{q}, \dot{\mathbf{q}}) - K_1(\mathbf{q})}{M_{11}(\mathbf{q})}, \tag{9.2a}$$
$$\ddot{q}_2 = -k_{D_2}\dot{q}_2 - k_{P_2}q_2, \tag{9.2b}$$
$$\ddot{q}_3 = -k_{D_3}\dot{q}_3 - k_{P_3}q_3, \tag{9.2c}$$
$$\vdots$$
$$\ddot{q}_n = -k_{D_n}\dot{q}_n - k_{P_n}q_n \tag{9.2d}$$

where

$$M_{11}(\mathbf{q}) \neq 0 \; \forall \mathbf{q} \tag{9.3}$$

must be ensured. The full derivation of the TCPFL control technique is included in section D.1 of appendix D.

Modified Collocated Partial Feedback Linearisation

The MCPFL method has a similar objective to the TCPFL technique, whereby, upon application of this technique, the behaviour of the most distal $n-1$ pendulums of the PA$_{n-1}$ robot may be collectively represented as a single pendulum. The key difference between these two techniques is the state of linearisation concerning the second pendulum. In the traditional case, the dynamics of the second pendulum is linearised and replaced with the linear state feedback controller

$$\ddot{q}_2 = v_2.$$

There are instances, however, where this would not be convenient. This is evident in the instance where LDM-related swing-up control is applied to the ROPA$_{n-1}$ robot that has been linearised using TCPFL (TC-ROPA$_{n-1}$ robot). The existing literature, including the derivation of the gain selection criterion, have all been derived for the nonlinear PA$_{n-1}$ robot and its derivatives. It would be counterproductive in this case to derive a new set of conditions and swing-up control torques for partially linearised systems. Instead, it is more practical to linearise the dynamics of the $n-2$ most distal pendulums and to leave τ_2 unchanged in this formulation. The $n-1$ pendulums can still be collectively represented as one pendulum, but it accommodates the substitution of an already existing control torque τ_2 without the need for reformulation. The MCPFL technique is introduced here specifically to supplement its application in chapter 8, and is not implemented to address the *matched damping condition*. With this in mind, we can now formally define the technique.

Definition 9.2. As with the TCPFL method, the application of this technique accommodates the collective representation of the $n-1$ most proximal pendulums as a single pendulum. In this case, however, the dynamics of the $n-2$ most distal pendulums of the PA$_{n-1}$ robot are linearised. The control objective torque τ_2 is reserved specifically for the substitution of an existing torque solution derived for the traditional Acrobot. Linear state feedback controllers are defined for the $n-2$ most distal pendulums (v_i where $3 \leq i \leq n$), and are responsible for regulating the corresponding pendulum about $q_i = 0$.

The torque expression required to perform MCPFL on a multi-link system is described by

$$\tau_i = \hat{M}_{i3}(\mathbf{q})v_3 + \hat{M}_{i4}(\mathbf{q})v_4 + \cdots + \hat{M}_{in}(\mathbf{q})v_n + \hat{D}_i(\mathbf{q}, \dot{\mathbf{q}}) + \hat{K}_i(\mathbf{q}) + \hat{\tau}_i \tag{9.4}$$

where, for $3 \leq i \leq n$, $3 \leq j \leq n$ and $2 \leq k \leq n$,

$$\hat{M}_{ij}(\mathbf{q}) = M_{ij}(\mathbf{q}) - \frac{\tilde{M}_{1j}(\mathbf{q})M_{i1}(\mathbf{q})}{M_{11}(\mathbf{q})} - \frac{\tilde{M}_{2j}(\mathbf{q})M_{i2}(\mathbf{q})}{\tilde{M}_{22}(\mathbf{q})},$$

$$\hat{D}_i(\mathbf{q}, \dot{\mathbf{q}}) = D_i(\mathbf{q}, \dot{\mathbf{q}}) - \frac{M_{i1}(\mathbf{q})}{M_{11}(\mathbf{q})}\tilde{D}_1(\mathbf{q}, \dot{\mathbf{q}}) - \frac{M_{i2}(\mathbf{q})}{\tilde{M}_{22}(\mathbf{q})}\tilde{D}_2(\mathbf{q}, \dot{\mathbf{q}}),$$

$$\hat{K}_i(\mathbf{q}) = K_i(\mathbf{q}) - \frac{M_{i1}(\mathbf{q})}{M_{11}(\mathbf{q})}\tilde{K}_1(\mathbf{q}) - \frac{M_{i2}(\mathbf{q})}{\tilde{M}_{22}(\mathbf{q})}\tilde{K}_2(\mathbf{q}),$$

$$\hat{\tau}_i = \frac{M_{i2}(\mathbf{q})}{\tilde{M}_{22}(\mathbf{q})}\tau_2 - \frac{M_{i1}(\mathbf{q})}{M_{11}(\mathbf{q})}\tilde{\tau}_2,$$

$$\tilde{\tau}_2 = \frac{M_{12}(\mathbf{q})}{\tilde{M}_{22}(\mathbf{q})}\tau_2$$

and

$$\tilde{M}_{2k}(\mathbf{q}) = M_{2k}(\mathbf{q}) - \frac{M_{1k}(\mathbf{q})M_{21}(\mathbf{q})}{M_{11}(\mathbf{q})}, \qquad \tilde{M}_{1j}(\mathbf{q}) = M_{1j}(\mathbf{q}) - \frac{M_{12}(\mathbf{q})\tilde{M}_{2i}(\mathbf{q})}{\tilde{M}_{22}(\mathbf{q})},$$

$$\tilde{D}_2(\mathbf{q},\dot{\mathbf{q}}) = D_2(\mathbf{q},\dot{\mathbf{q}}) - \frac{M_{21}(\mathbf{q})}{M_{11}(\mathbf{q})}D_1(\mathbf{q},\dot{\mathbf{q}}), \quad \tilde{D}_1(\mathbf{q},\dot{\mathbf{q}}) = D_1(\mathbf{q},\dot{\mathbf{q}}) - \frac{M_{12}(\mathbf{q})}{\tilde{M}_{22}(\mathbf{q})}\tilde{D}_2(\mathbf{q},\dot{\mathbf{q}}),$$

$$\tilde{K}_2(\mathbf{q}) = K_2(\mathbf{q}) - \frac{M_{21}(\mathbf{q})}{M_{11}(\mathbf{q})}K_1(\mathbf{q}), \qquad \tilde{K}_1(\mathbf{q}) = K_1(\mathbf{q}) - \frac{M_{12}(\mathbf{q})}{\tilde{M}_{22}(\mathbf{q})}\tilde{K}_2(\mathbf{q}).$$

This form of linearisation results in a set of equations of motion for the MC-ROPA$_{n-1}$ robot described by

$$\ddot{q}_1 = \frac{-\tilde{M}_{13}(\mathbf{q})v_3 - \tilde{M}_{14}(\mathbf{q})v_4 - \cdots - \tilde{M}_{1n}(\mathbf{q})v_n - \tilde{D}_1(\mathbf{q},\dot{\mathbf{q}}) - \tilde{K}_1(\mathbf{q})}{M_{11}(\mathbf{q})},$$
$$\ddot{q}_2 = \frac{\tau_2 - \tilde{M}_{23}(\mathbf{q})v_3 - \tilde{M}_{24}(\mathbf{q})v_4 - \cdots - \tilde{M}_{2n}(\mathbf{q})v_n - \tilde{D}_2(\mathbf{q},\dot{\mathbf{q}}) - \tilde{K}_2(\mathbf{q})}{M_{11}(\mathbf{q})}.$$

Additionally, a set of physical parameters must be selected to ensure that

$$M_{11}(\mathbf{q}) \neq 0 \; \forall \mathbf{q}. \tag{9.5}$$

The detailed derivation of the necessary torque expression is included in section D.2 of appendix D.

9.3.2 Noncollocated Partial Feedback Linearisation

With CPFL and its variants defined, we will now consider the noncollocated case. Suppose we present the PA$_{n-1}$ robot in a configuration as seen on the left portion of figure 9.2. It is apparent that if the system remains in this configuration throughout the entire operation, the most proximal $n-1$ pendulums may collectively be represented as a single pendulum (as seen on the right of figure 9.2). It is not possible,

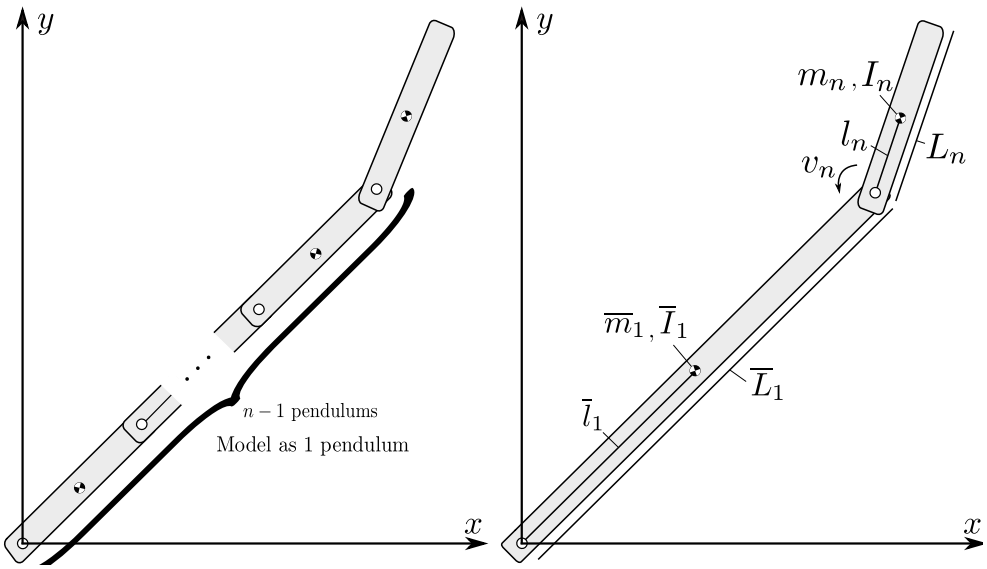

FIGURE 9.2: The PA$_{n-1}$ robot represented as a NC-ROPA$_{n-1}$.

however, to maintain this configuration throughout the entire operation unless the actuators of the $n-2$ pendulums found precisely distal to the first pendulum are used to enforce this configuration. The dynamics of the most proximal pendulum are also linearised, but the linear state feedback controller that is designed for this joint will be responsible for producing the swing-up control rather than just regulating the pendulum about a particular axis. This control technique is formally defined as the Noncollocated Partial Feedback Linearisation technique.

Definition 9.3. Noncollocated Partial Feedback Linearisation (NCPFL) involves the linearisation of the dynamics of the $n-1$ most proximal pendulums of the PA$_{n-1}$ robot. The linear state feedback controllers assigned to the $n-2$ pendulums precisely distal to the most proximal pendulum (v_i where $2 \leq i \leq n-1$) are responsible for regulating the pendulum about $q_i = 0$ whilst the linear state feedback controller of the most proximal pendulum is designed specifically to achieve the intended control objective.

The necessary torque expression required to perform NCPFL on the PA$_{n-1}$ robot is described by

$$\tau_i = \hat{M}_{i1}(\mathbf{q})v_1 + \hat{M}_{i2}(\mathbf{q})v_2 + \cdots + \hat{M}_{in-1}(\mathbf{q})v_{n-1} + \hat{D}_i(\mathbf{q}, \dot{\mathbf{q}}) + \hat{K}_i(\mathbf{q})$$

where

$$\hat{M}_{ij}(\mathbf{q}) = M_{ij}(\mathbf{q}) - \frac{M_{in}(\mathbf{q})M_{1j}(\mathbf{q})}{M_{1n}(\mathbf{q})},$$
$$\hat{D}_i(\mathbf{q}, \dot{\mathbf{q}}) = D_i(\mathbf{q}, \dot{\mathbf{q}}) - \frac{M_{in}(\mathbf{q})}{M_{1n}(\mathbf{q})}D_1(\mathbf{q}, \dot{\mathbf{q}}),$$

$$\hat{K}_i(\mathbf{q}) = K_i(\mathbf{q}) - \frac{M_{in}(\mathbf{q})}{M_{1n}(\mathbf{q})} K_1(\mathbf{q}).$$

for $1 \leq j \leq n-1$. This results in a set of dynamical equations which are described by

$$\ddot{q}_1 = -k_{D_1}\dot{q}_1 - k_{P_1}q_1, \tag{9.6a}$$
$$\ddot{q}_2 = -k_{D_2}\dot{q}_2 - k_{P_2}q_2, \tag{9.6b}$$
$$\vdots$$
$$\ddot{q}_{n-1} = -k_{D_{n-1}}\dot{q}_{n-1} - k_{P_{n-1}}q_{n-1}, \tag{9.6c}$$
$$\ddot{q}_n = \frac{-M_{11}(\mathbf{q})v_1 - M_{12}(\mathbf{q})v_2 - \cdots - M_{1n-1}(\mathbf{q})v_{n-1} - D_1(\mathbf{q}, \dot{\mathbf{q}}) - K_1(\mathbf{q})}{M_{1n}(\mathbf{q})} \tag{9.6d}$$

where

$$M_{1n}(\mathbf{q}) \neq 0 \; \forall \mathbf{q}. \tag{9.7}$$

The details of the derivation of the NCPFL control technique is described in section D.3 of appendix D.

9.4 Gain Selection Criterion

With the PFL technique now defined, we will derive the first work-around for the *matched damping condition* using TCPFL, known as the *gain selection criterion*.

As mentioned before, the TCPFL technique accommodates the reduced-order representation of the PA$_{n-1}$ robot as a TC-ROPA$_{n-1}$ robot. The dynamics of the collective single pendulum must, therefore, be swung in a calculated fashion to facilitate the introduction of energy into the system and to indirectly influence the behaviour of the most proximal pendulum. This must be done to allow the system to move away from a lower energy state (near the FPEP, as an example) and towards the UEP. Spong addresses this issue by introducing the 'energy-pump' ATAN controller, which was designed to mimic the technique a gymnast would use when attempting to reach an upright position on the high bar [6, 109]. The gymnast uses its hips and lower body to introduce energy into its manoeuvre by performing multiple sinusoidal swing-cycles [109]. The system's response is, thus, **unstable** but **predictable**. The ATAN controller is described as

$$v_2 = -k_D\dot{q}_2 + k_P\left(q_2^d - q_2\right)$$

where

$$q_2^d = \left(\frac{2\alpha}{\pi}\right)\arctan\dot{q}_1$$

[6]. The design of this controller is justified by Spong in the following statement:

> *The basic idea behind our swingup strategy is to swing the second link between fixed values $\pm\alpha$ in order to pump energy into the system and then to schedule the transition of the second link between these two values $\pm\alpha$ 'in phase' with the motion of the first link in such a way that the amplitude of the swing of the first link increases with each swing. [6]*

Spong demonstrates that the swing-up control of an undamped Acrobot using the ATAN controller is possible [6,34], but his work is limited for the following reasons:

(1) The simulations for his investigation were initialised with one set of initial conditions, which aren't reflective of the behaviour of the system throughout a larger domain of operation.

(2) There is no prescription on what magnitude of gains must be chosen for k_D and k_P to ensure satisfactory swing-up control. Instead, Spong observes the system's internal and zero dynamics to determine whether the behaviour of the controller is satisfactory. This observation can only be made once a simulation is performed, and does not provide a prescriptive and analytical means of ensuring swing-up.

This leads to the following questions:

1. **Can an ATAN controller perform satisfactory swing-up control when initialised across the domain $\mathbf{q_1}, \mathbf{q_2} \in (-\pi, \pi]$ with the assumption that $\dot{\mathbf{q}}_\mathbf{1}(\mathbf{0}), \dot{\mathbf{q}}_\mathbf{2}(\mathbf{0}) = \mathbf{0}$?**

2. **What magnitudes for the gains k_D and k_P must I choose to ensure that the swing-up is satisfactory?**

It is difficult to provide a definitive answer to these questions since the ATAN control demonstrated by Spong does not actively track some objective. In other words, we are not able to guarantee satisfactory swing-up performances in all cases, but it is possible, however, to highlight certain conditions that will guarantee unsatisfactory controller performance. For instance, if the system trajectory is found sufficiently close to a stable equilibrium point that is not the UEP (e.g. the FPEP), it is evident that the system trajectory will tend towards this equilibrium point, resulting in unsatisfactory swing-up control performance. The stability of this equilibrium point may depend on the magnitudes of k_P and k_D. The values of k_P and k_D must be designed carefully to prevent the stability of these equilibrium points, resulting in a possible contribution in the form of a *gain selection criterion*. If this contribution is analytical in nature, it would alleviate the need to monitor the system's internal and zero dynamics, as seen in Spong's work. The feasibility of this venture must be explored through the determination of the equilibrium points in the TC-ROPA$_{n-1}$ robot (expanding on the possibility of developing solutions for higher-order systems not covered in [6]). Additionally, we will first attempt to demonstrate the feasibility of the *gain selection criterion* by evaluating the undamped

PA$_{n-1}$ robot. The modelling of the undamped TC-ROPA$_{n-1}$ robot using TCPFL is thus discussed in the next section, followed by an evaluation of the TC-ROPA$_{n-1}$ robot's equilibrium points when it is integrated with the ATAN controller seen in [6]. These processes are subsequently performed on the actively damped and passively damped TC-ROPA$_{n-1}$ robot.

9.4.1 Preliminaries: The Undamped PA$_{n-1}$ Robot

Modelling the Undamped PA$_{n-1}$ Robot as the TC-ROPA$_{n-1}$ Robot

Similar to what is done in chapter 8, we will first proceed to derive the mathematical model of the undamped TC-ROPA$_{n-1}$ robot. The generalised TC-ROPA$_{n-1}$ robot is formally defined below:

Definition 9.4. The TC-ROPA$_{n-1}$ robot is a reduced-order representation of the PA$_{n-1}$ robot that results from the linearisation of the $n-1$ most distal pendulums of the system, with the dynamics of the $n-2$ most distal pendulums being regulated about $q_i = 0$, where $2 < i < n$. The $n-1$ most distal pendulums thus collectively represent a single pendulum described by linear dynamics. The system closely approximates the behaviour of an Acrobot that has been linearised using TCPFL, provided that the selected response frequency of the actuators involved in non-oscillatory regulation is sufficiently large and that $q_i(0) = 0$.

The TCPFL technique is used in this case since the swing-up control torque τ_2 does not need to be reserved for the substitution of a known control law. This will become more apparent when we derive the *gain selection criterion* for the PFL-related swing-up control of the TC-ROPA$_{n-1}$ robot.

The application of the TCPFL technique on the PA$_{n-1}$ robot results in the dynamical equations shown in eqs. (9.2a)-(9.2d), where

$$D_i(\mathbf{q}, \dot{\mathbf{q}}) = C_i(\mathbf{q}, \dot{\mathbf{q}}) \qquad \text{for } 1 \leq i \leq n$$

in the undamped case. Choosing the initial conditions

$$\begin{aligned} q_3(0) &= 0, & \dot{q}_3(0) &= 0, \\ q_4(0) &= 0, & \dot{q}_4(0) &= 0, \\ &\vdots & &\vdots \\ q_n(0) &= 0, & \dot{q}_n(0) &= 0 \end{aligned}$$

then it is guaranteed that

$$q_3 \approx 0, \qquad q_4 \approx 0, \qquad \ldots \qquad q_n \approx 0$$

$\forall t$. So long as the natural response frequency of each of the linearising actuators is sufficiently large (this ensures satisfactory angular regulation). This will accommodate the modelling of the PA$_{n-1}$ robot to the TC-ROPA$_{n-1}$ robot, and will be described by the dynamical equations

$$\overline{M}_{11}(\mathbf{q})\ddot{q}_1 + \overline{M}_{12}(\mathbf{q})v_2 + \overline{D}_1(\mathbf{q}, \dot{\mathbf{q}}) + \overline{K}_1(\mathbf{q}) = 0, \tag{9.8a}$$

$$\ddot{q}_2 = v_2 \tag{9.8b}$$

where

$$\begin{aligned}
&\overline{M}_{11}(q_2) = \overline{\alpha}_1 + \overline{\alpha}_2 + 2\overline{\alpha}_3 \cos q_2, \\
&\overline{M}_{12}(q_2) = \overline{\alpha}_2 + \overline{\alpha}_3 \cos q_2, \\
&\overline{D}_1(q_2, \dot{\mathbf{q}}) = \overline{C}_1(q_2, \dot{\mathbf{q}}) = -\overline{\alpha}_3 \left(2\dot{q}_1\dot{q}_2 + \dot{q}_2^2\right) \sin q_2, \\
&\overline{K}_1(\mathbf{q}) = -\overline{\beta}_1 \sin q_1 - \overline{\beta}_2 \sin(q_1 + q_2)
\end{aligned}$$

and

$$\begin{aligned}
&\overline{\alpha}_1 = I_1 + m_1 {l_1}^2 + \overline{m}_2 {L_1}^2, && \overline{\alpha}_2 = \overline{I}_2 + \overline{m_2 {l_2}^2}, \\
&\overline{\alpha}_3 = \overline{m_2 l_2} L_1, && \overline{\beta}_1 = (m_1 l_1 + \overline{m}_2 L_1)\, g, \\
&\overline{\beta}_2 = \overline{m_2 l_2} g, && \\
&\overline{m}_2 = \sum_{i=2}^{n} m_i, && \overline{I}_2 = \sum_{i=2}^{n} I_i, \\
&\overline{m_2 l_2} = \sum_{i=2}^{n} m_i \left[l_i + \sum_{j=2}^{i-1} L_j \right], && \overline{m_2 {l_2}^2} = \sum_{i=2}^{n} m_i \left[l_i + \sum_{j=2}^{i-1} L_j \right]^2
\end{aligned}$$

whereby the physical parameters of the system are constrained, as seen in eq. (9.3).

Equilibrium Point Analysis of the TC-ROPA$_{n-1}$ Robot Integrated with an ATAN Controller and the Gain Selection Criterion

We shall integrate the ATAN controller into the TC-ROPA$_{n-1}$ robot model by choosing the linear state feedback controller

$$v_2 = k_P \left(q_2^d - q_2\right) - k_D \dot{q}_2$$

as shown in [34], where

$$q_2^d = \left(\frac{2\alpha}{\pi}\right) \arctan \dot{q}_1$$

represents the ATAN control with $\alpha \in \mathbb{R}^+$. Substituting this expression into the equations that describe the TC-ROPA$_{n-1}$ robot's motion in eqs. (9.8a) and (9.8b) produces the following finalised TCPFL swing-up dynamics for the TC-ROPA$_{n-1}$

robot, whereby

$$\overline{M}_{11}(\mathbf{q})\ddot{q}_1 + \overline{M}_{12}(\mathbf{q})\left(k_P\left[\left(\frac{2\alpha}{\pi}\right)\arctan\dot{q}_1 - q_2\right] - k_D\dot{q}_2\right) - \overline{\alpha}_3\left(2\dot{q}_1\dot{q}_2 + \dot{q}_2^2\right)\sin q_2 - \overline{\beta}_1\sin q_1 - \overline{\beta}_2\sin\left(q_1+q_2\right) = 0, \tag{9.9a}$$

$$\ddot{q}_2 = k_P\left[\left(\frac{2\alpha}{\pi}\right)\arctan\dot{q}_1 - q_2\right] - k_D\dot{q}_2 \tag{9.9b}$$

which can be represented as

$$\ddot{q}_1 = \left[-\overline{M}_{12}(\mathbf{q})\left(k_P\left[\left(\frac{2\alpha}{\pi}\right)\arctan\dot{q}_1 - q_2\right] - k_D\dot{q}_2\right) + \overline{\alpha}_3\left(2\dot{q}_1\dot{q}_2 + \dot{q}_2^2\right)\sin q_2 + \overline{\beta}_1\sin q_1 + \overline{\beta}_2\sin\left(q_1+q_2\right)\right] \Big/ \left[\overline{M}_{11}(\mathbf{q})\right], \tag{9.10a}$$

$$\ddot{q}_2 = k_P\left[\left(\frac{2\alpha}{\pi}\right)\arctan\dot{q}_1 - q_2\right] - k_D\dot{q}_2. \tag{9.10b}$$

The equilibrium point states of the TC-ROPA$_{n-1}$ robot are thus represented by

$$\begin{aligned} q_1^e &= q_1^*, & q_2^e &= q_2^*, \\ \dot{q}_1^e &= 0, & \dot{q}_2^e &= 0, \\ \ddot{q}_1^e &= 0, & \ddot{q}_2^e &= 0. \end{aligned}$$

Additionally, we select

$$q_2^d = 0$$

since the UEP is the desired trajectory. Therefore, if the TC-ROPA$_{n-1}$ robot is found at an equilibrium point, its dynamical equations demonstrated in eqs. (9.9a) and (9.9b) simplify into

$$-\overline{M}_{12}k_P q_2^e - \overline{\beta}_1\sin q_1^e - \overline{\beta}_2\sin\left(q_1^e + q_2^e\right) = 0, \tag{9.11}$$

$$k_P q_2^e = 0. \tag{9.12}$$

With $k_P > 0$, we see that

$$q_2^e = 0$$

from eq. (9.12). Therefore, substituting $q_2^e = 0$ into eq. (9.11) we find that

$$\left[\overline{\beta}_1 + \overline{\beta}_2\right]\sin q_1^e = 0. \tag{9.13}$$

Since $\overline{\beta}_1 > 0$, and $\overline{\beta}_2 > 0$ it is evident that the condition

$$q_1^e = \pm\pi k, \qquad k \in \mathbb{Z}$$

must hold for eq. (9.13) to be satisfied. Therefore, there are two classifications of equilibrium points which exist in this configuration, the UEP and the FPEP, whereby

$$(\mathbf{q^e}, \dot{\mathbf{q}}^\mathbf{e})_{\text{UEP}} = (0, 0, 0, 0),$$
$$(\mathbf{q^e}, \dot{\mathbf{q}}^\mathbf{e})_{\text{FPEP}} = (\pm\pi k, 0, 0, 0)$$

and where $k \in \mathbb{Z}$. These points can be defined within the region $q_1^e, q_2^e \in (-\pi, \pi]$. Therefore

$$(\mathbf{q^e}, \dot{\mathbf{q}}^\mathbf{e})_{\text{UEP}} = (0, 0, 0, 0),$$
$$(\mathbf{q^e}, \dot{\mathbf{q}}^\mathbf{e})_{\text{FPEP}} = (\pi, 0, 0, 0).$$

There are no equilibrium points (other than the UEP) that the trajectory can tend towards if the system is initialised approximately near the FPEP (provided that the FPEP is an unstable equilibrium point). We can thus conclude the following, assuming that the local stability of the FPEP is dependent on the gains k_P and k_D:

Proposition 9.1. ***Gain selection criterion***: Choosing appropriate values for the gains k_P and k_D will ensure that the FPEP is **unstable**. This is a necessary condition for satisfactory swing-up control of a UMS that is initialised near the FPEP. This will eliminate a large domain of possible value combinations for k_P and k_D that cannot be used if satisfactory swing-up control is desired.

The stability of the FPEP can be determined through the derivation of the characteristic equation of the system linearised about the FPEP. We, therefore, highlight the following set of directives that must be completed for the derivation of the *gain selection criterion* for the undamped TC-ROPA$_{n-1}$ robot:

(i) Use Lyapunov's linearisation technique to linearise the undamped TC-ROPA$_{n-1}$ robot about the FPEP. Use the linearised model to determine a characteristic equation, describing local stability about the FPEP.

(ii) Implement the Routh-Hurwitz stability criterion (using the Routh array) to determine conditions that ensure that the FPEP is locally unstable.

The detailed derivation of this gain selection criterion is included in section A.5 of appendix A. The result of this proof is summarised as follows:

Criterion 9.1. ***Gain selection criterion (undamped TC-ROPA$_{n-1}$):*** The FPEP of the undamped TC-ROPA$_{n-1}$ robot is guaranteed to be locally unstable so long as the following selection conditions for the gains k_P and k_D are satisfied:

(1) For $\dfrac{\overline{\beta}_2}{\overline{\alpha}_2 + \overline{\alpha}_3} < k_P < \dfrac{\overline{\beta}_1 + \overline{\beta}_2}{\overline{\alpha}_1 + \overline{\alpha}_2 + 2\overline{\alpha}_3}$:

$$0 \leq k_D < \frac{2\alpha k_P}{\pi} \left[\frac{[\overline{\alpha}_2 + \overline{\alpha}_3]\, k_P - \overline{\beta}_2}{\overline{\beta}_1 + \overline{\beta}_2 - k_P\, [\overline{\alpha}_1 + \overline{\alpha}_2 + \overline{\alpha}_3]} \right];$$

(2) For $k_P \geq \dfrac{\overline{\beta}_1 + \overline{\beta}_2}{\overline{\alpha}_1 + \overline{\alpha}_2 + 2\overline{\alpha}_3}$; $\quad k_D \geq 0$:

We shall demonstrate the application of the *gain selection criterion* for practical versions of the TC-ROPA$_{n-1}$ robot. The parameters that have been selected in the experiments that follow are taken from [5] and [6] since the results produced in this chapter can easily be verified and compared to results in existing literature. It is important to note, however, that any set of parameters can be selected since the *gain selection criterion* is analytical in nature.

The Undamped Acrobot

The swing-up control of the undamped Acrobot (which is an identical manifestation of the TC-ROPA$_1$ robot) using TCPFL is demonstrated to provide a practical application of the *gain selection criterion*. The application of the FBL torque

$$\tau_2 = \hat{M}_{22}(\mathbf{q})v_2 + \hat{D}_2(\mathbf{q}, \dot{\mathbf{q}}) + \hat{K}_2(\mathbf{q})$$

derived from eq. (9.1) with $i = 2$ where

$$\begin{aligned}
\hat{M}_{22}(\mathbf{q}) &= M_{22}(\mathbf{q}) - \frac{M_{21}(\mathbf{q})M_{12}(\mathbf{q})}{M_{11}(\mathbf{q})}, \\
\hat{D}_2(\mathbf{q}, \dot{\mathbf{q}}) &= D_2(\mathbf{q}, \dot{\mathbf{q}}) - \frac{M_{21}(\mathbf{q})}{M_{11}(\mathbf{q})} D_1(\mathbf{q}, \dot{\mathbf{q}}), \\
\hat{K}_2(\mathbf{q}) &= K_2(\mathbf{q}) - \frac{M_{21}(\mathbf{q})}{M_{11}(\mathbf{q})} K_1(\mathbf{q})
\end{aligned}$$

and where

$$D_1(\mathbf{q}, \dot{\mathbf{q}}) = C_1(\mathbf{q}, \dot{\mathbf{q}}), \qquad D_2(\mathbf{q}, \dot{\mathbf{q}}) = C_2(\mathbf{q}, \dot{\mathbf{q}})$$

results in the linearised dynamics

$$\begin{aligned}
\ddot{q}_1 &= \frac{-M_{12}(\mathbf{q})v_2 - D_1(\mathbf{q}, \dot{\mathbf{q}}) - K_1(\mathbf{q})}{M_{11}(\mathbf{q})}, \\
\ddot{q}_2 &= v_2
\end{aligned}$$

for the undamped Acrobot where

$$v_2 = k_P \left(q_2^d - q_2 \right) - k_D \dot{q}_2$$

with $q_2^d = \left(\dfrac{2\alpha}{\pi} \right) \arctan \dot{q}_1$. The permissible region of gains that you can select for the aforementioned control law (referred to as the *Region of Appropriate Gains*, or RAG) is demonstrated in figure 9.3 for an Acrobot described by the parameters

$$m_1 = 1 \text{ kg}, \qquad m_2 = 1 \text{ kg},$$

$$l_1 = 0.5 \text{ m}, \qquad l_2 = 1 \text{ m},$$
$$L_1 = 1 \text{ m}, \qquad L_2 = 2 \text{ m},$$
$$I_1 = 0.0833 \text{ kg.m}^2, \qquad I_2 = 0.3333 \text{ kg.m}^2,$$
$$g = 9.81 \text{ m.s}^2$$

which adhere to the constraint in eq. (9.3). This corresponds to the relationship between appropriate gains and the negative magnitude of the critical Routh coefficient $\overline{c}_1$, as seen in figure 9.4.

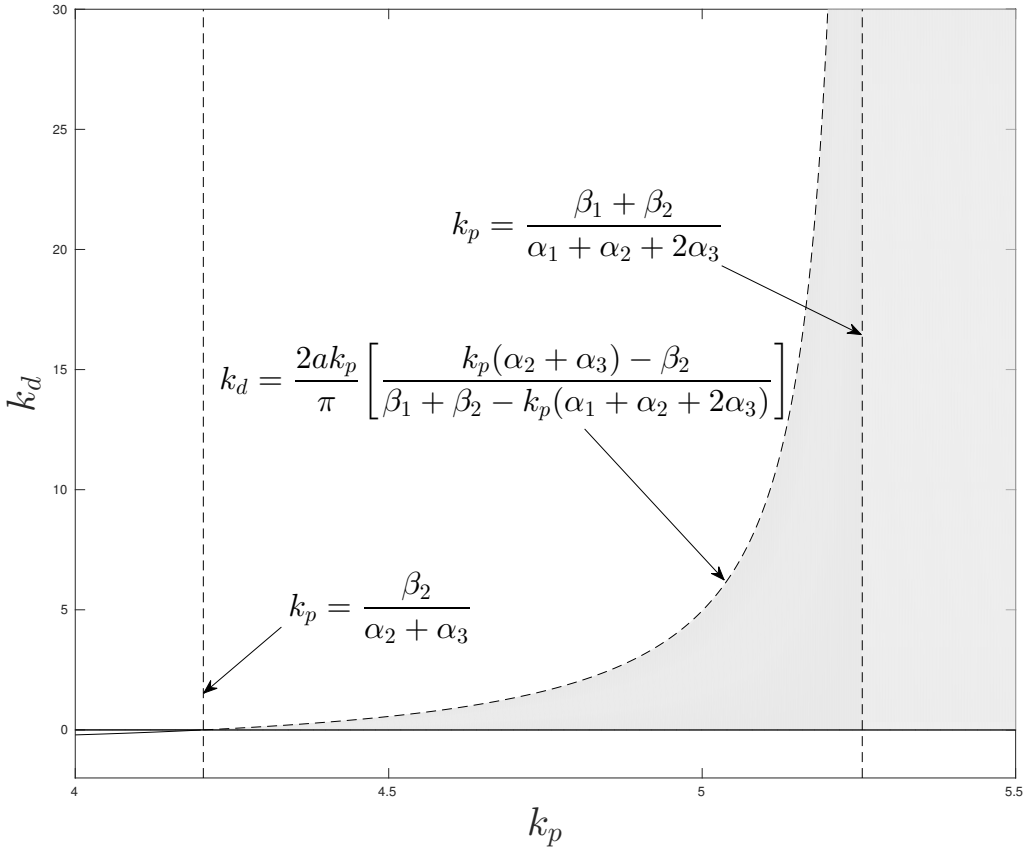

FIGURE 9.3: The *gain selection criterion* of the undamped Acrobot, which forms borders around the *region of appropriate gains* (shaded in grey).

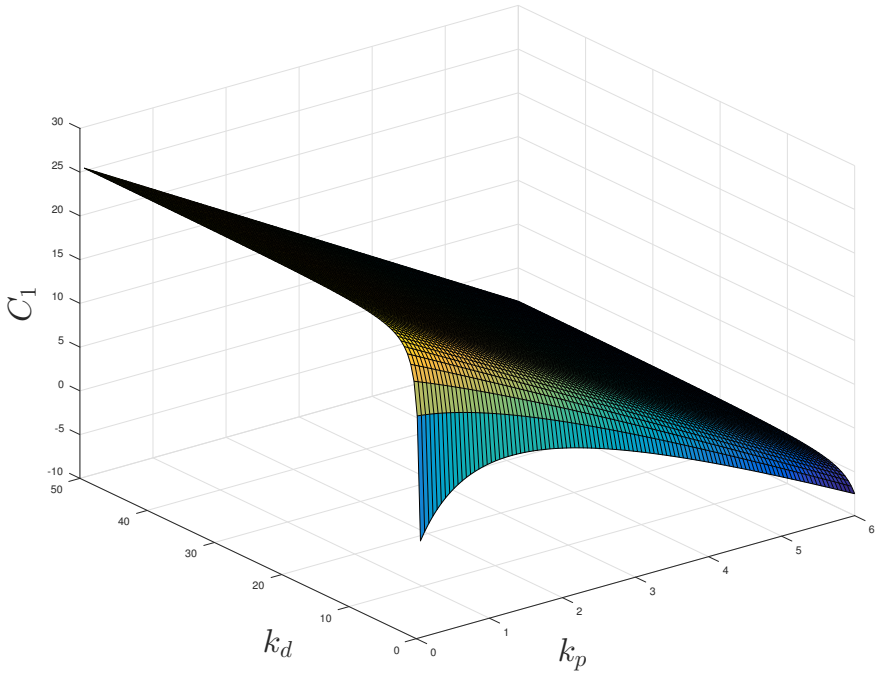

FIGURE 9.4: The critical Routh coefficient $\bar{c}_1$ plotted against a range of possible values for k_D and k_P.

Selecting a set of gains that fall within the RAG will ensure that the FPEP of the Acrobot is locally unstable, thus sufficing as a prerequisite to swing-up control if the Acrobot is initialised approximately near to the FPEP. The simulated change of energy of the Acrobot described earlier in this section with the selection of magnitudes for gains k_P and k_D that either fall into or outside of the RAG are demonstrated in figures 9.5-9.10. An increasing level of mechanical energy of the Acrobot with a gain selection of $k_P = 4.21$ and $k_D = 0.001$, which falls within the RAG, is demonstrated in figure 9.5. A decreasing level of mechanical energy of the Acrobot with a gain selection of $k_P = 4.19$ and $k_D = 0.001$, which falls outside of the RAG, is demonstrated in figure 9.6. An increasing level of mechanical energy of the Acrobot with a gain selection of $k_P = 4.7$ and $k_D = 1$, which falls within the RAG, is demonstrated in figure 9.7. A decreasing level of mechanical energy of the Acrobot with a gain selection of $k_P = 4.7$ and $k_D = 2$, which falls outside of the RAG, is demonstrated in figure 9.8. An increasing level of mechanical energy of the Acrobot with a gain selection of $k_P = 5.25$ and $k_D = 0.001$, which falls within the RAG, is demonstrated in figure 9.9. An increasing level of mechanical energy of the Acrobot with a gain selection of $k_P = 5.355$ and $k_D = 10$, which falls within the RAG, is demonstrated in figure 9.10. All these results demonstrate that a gain selection found outside of the RAG will cause the loss of mechanical energy from the system, and that a gain selection in the RAG will cause the mechanical energy of the system to increase. These results are expected since they comply with the *gain selection criterion*.

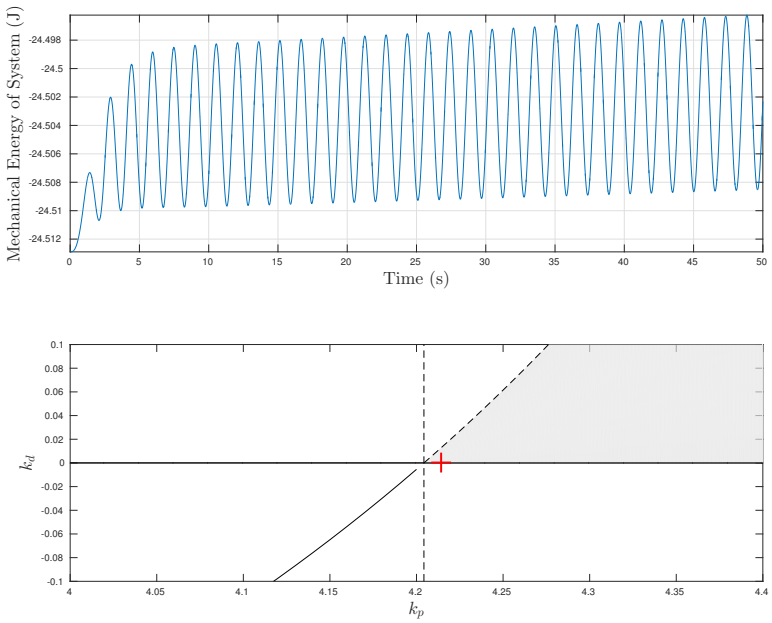

FIGURE 9.5: The unstable response of an undamped Acrobot initialised near the FPEP with a gain selection within the left-bottom boundary of the RAG.

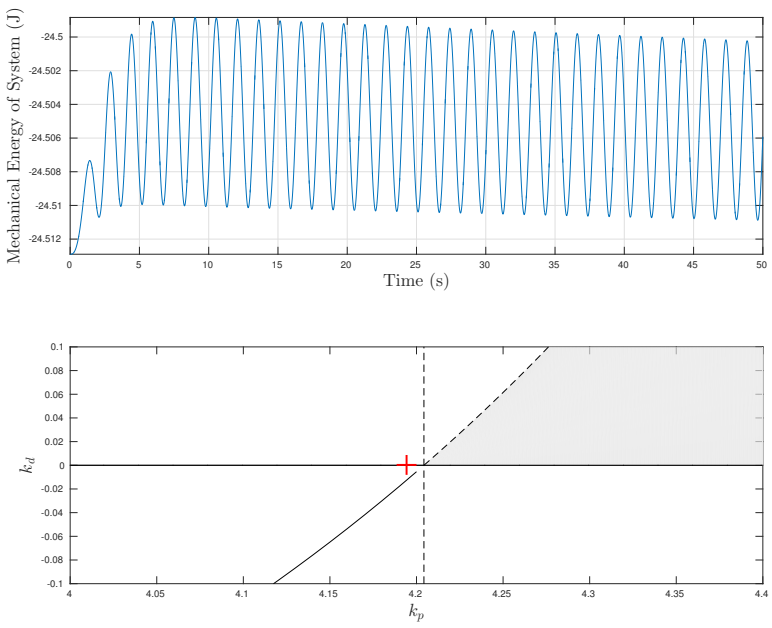

FIGURE 9.6: The stable response of an undamped Acrobot initialised near the FPEP with a gain selection outside of the left-bottom boundary of the RAG.

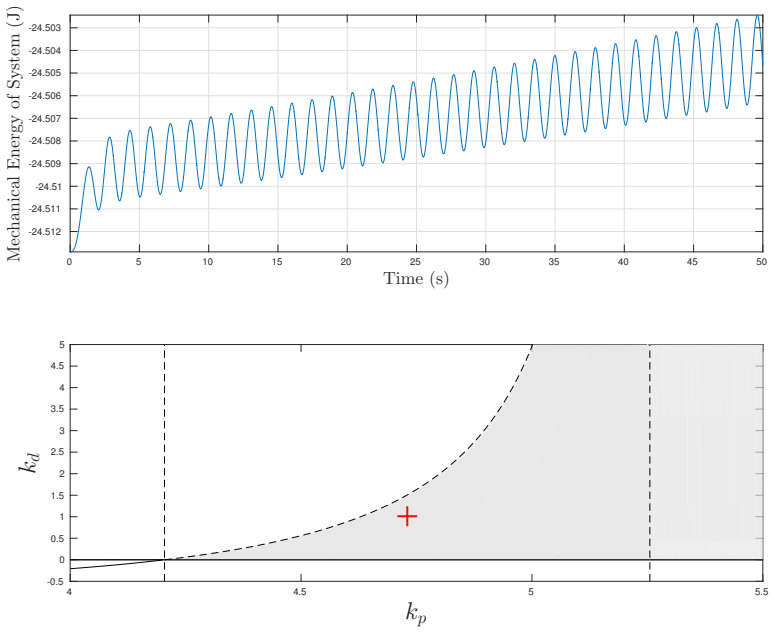

FIGURE 9.7: The unstable response of an undamped Acrobot initialised near the FPEP with a gain selection within the middle-top boundary of the RAG.

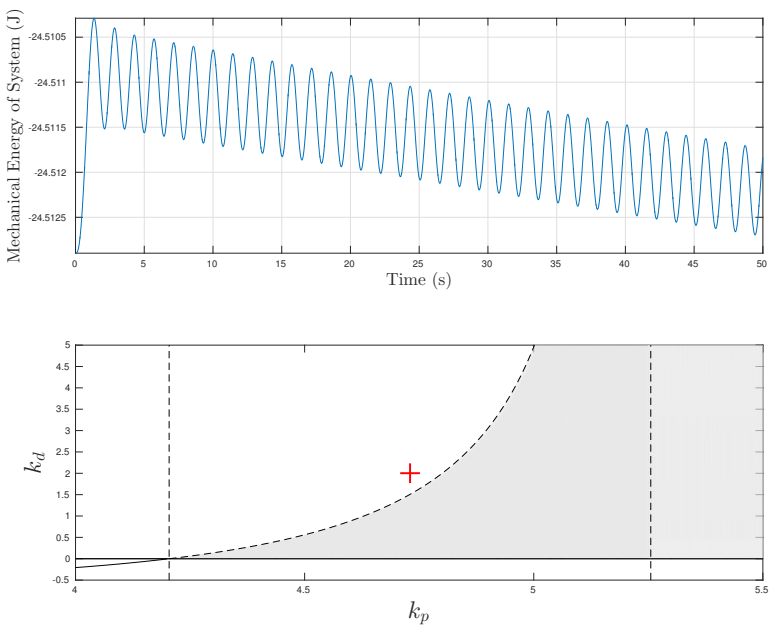

FIGURE 9.8: The stable response of an undamped Acrobot initialised near the FPEP with a gain selection outside of the middle-top boundary of the RAG.

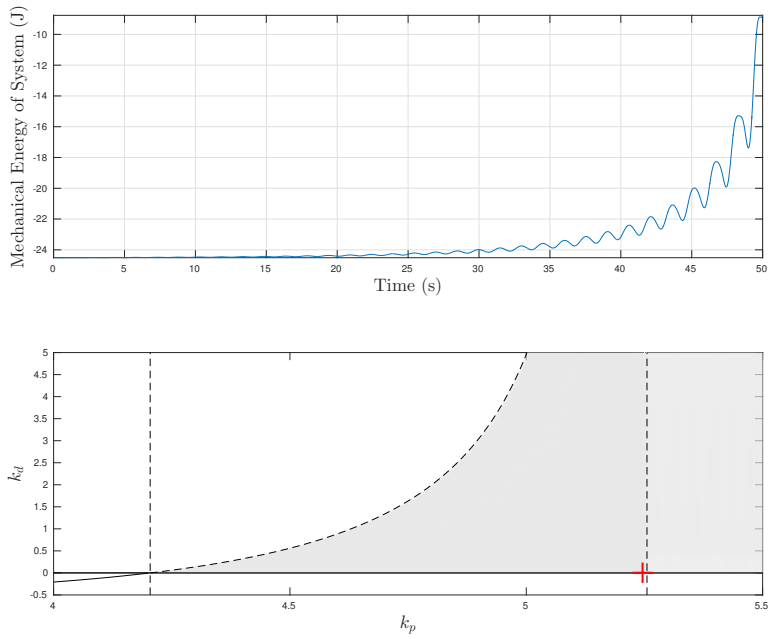

FIGURE 9.9: The unstable response of an undamped Acrobot initialised near the FPEP with a gain selection within the bottom boundary of the RAG.

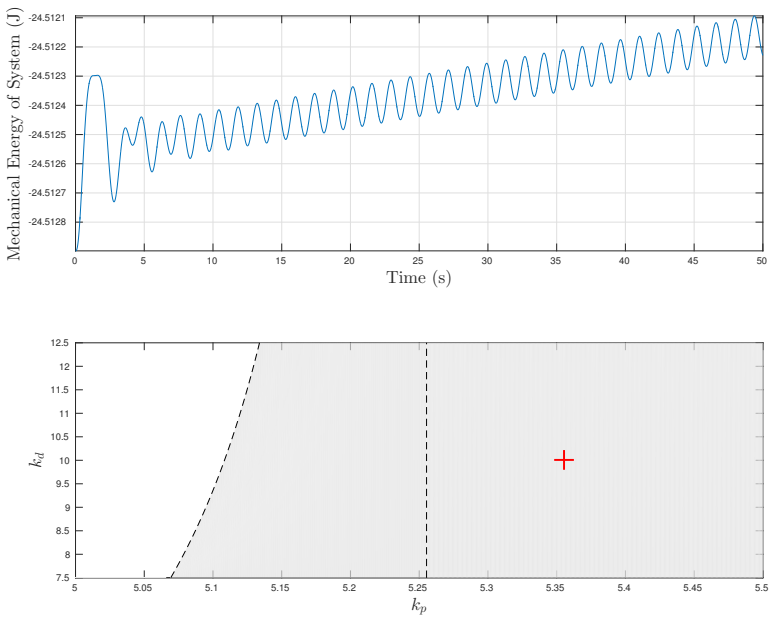

FIGURE 9.10: The unstable response of an undamped Acrobot initialised near the FPEP with a gain selection within the boundaries of the RAG.

We can thus demonstrate the swing-up control of the Acrobot using gains found within the RAG. In the case of an aggressive swing-up (as shown in [6]), we chose $\alpha = \pi/2$ for the ATAN controller, and the gains

$$k_D = 7.55482, \qquad k_P = 100.$$

An LQR controller was used to balance the Acrobot using the gains

$$k_1 = -246.216, \qquad k_2 = -98.5841, \tag{9.14a}$$

$$k_3 = -106.3313, \qquad k_4 = -50.0957. \tag{9.14b}$$

The implementation of a LQR controller simply demonstrates the possibility of regulating the system about the UEP once it has been swung-up. The results of the swing-up of this Acrobot are demonstrated in figures 9.11-9.14 using the initial conditions

$$q_1(0) = -\frac{101}{100}\pi, \qquad q_2(0) = 0, \qquad \dot{q}_1(0) = 0, \qquad \dot{q}_2(0) = 0$$

found approximately near the FPEP. The simulations were performed using the Dormand-Prince fixed time-interval integrator package using a 0.01 seconds resolution. The swing-up controller is switched to the LQR controller after 37 seconds. The angular displacement of the proximal pendulum during PFL-related swing-up control is demonstrated in figure 9.11. The displacement from the initial condition increases exponentially throughout the experiment, with the pendulum continually oscillating about $q_1^d = 0$ until the LQR controller is introduced at 37 seconds. The proximal pendulum is regulated about the UEP after the LQR controller is introduced, demonstrating successful swing-up control. The angular displacement of the distal pendulum during the PFL-related swing-up control is demonstrated in figure 9.12. The displacement of the distal pendulum demonstrates an increasing exponential behaviour as seen with the proximal pendulum. This continues until the LQR controller is introduced at 37 seconds, whereby the pendulum is stabilised at the UEP (with $q_2^d = 0$). The increasing displacement is determined by the gain factor α, which was set at $\pi/2$ for this experiment. The swing-up and LQR torque produced by the actuator is demonstrated in figure 9.13. The controller introduces an exponentially growing torque throughout the experiment since its magnitude was dependent on the displacements of the pendulums (which increased as more energy was introduced into the system). This produces the swing-cycles seen in the angular displacements. The actuator reduces the torque magnitude between 33-35 seconds since $q_2 \approx 0$ and $q_1 \approx 0$. A small negative torque is applied after 37 seconds to regulate pendulum about the UEP. The mechanical energy of the undamped Acrobot is demonstrated in figure 9.14. The energy of the system increases with every swing-cycle, with the peaks occurring when $\dot{q}_2 = 0$ and $q_1 = -\pi$ (as the pendulums are swinging past the FPEP with maximum kinetic energy). The energy dips slightly with each cycle since the actuator introduces a braking torque at the point when the system reaches the highest possible potential energy. It is believed that this was done

to ensure that the system achieved the appropriate states before the initiation of a new swing-cycle. The energy stabilises at E_r after the LQR controller is introduced at 37 seconds. This confirms that the swing-up control was successful in this case.

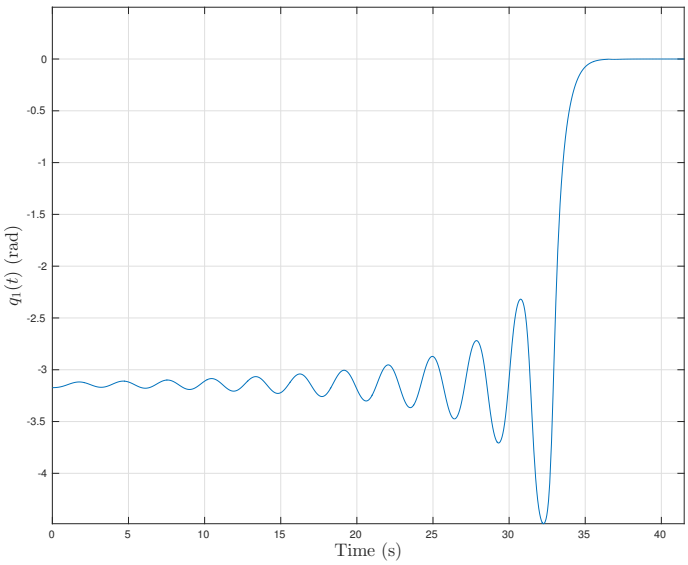

FIGURE 9.11: The angular position of the most proximal pendulum (q_1) of the undamped Acrobot during swing-up control using TCPFL and the ATAN controller.

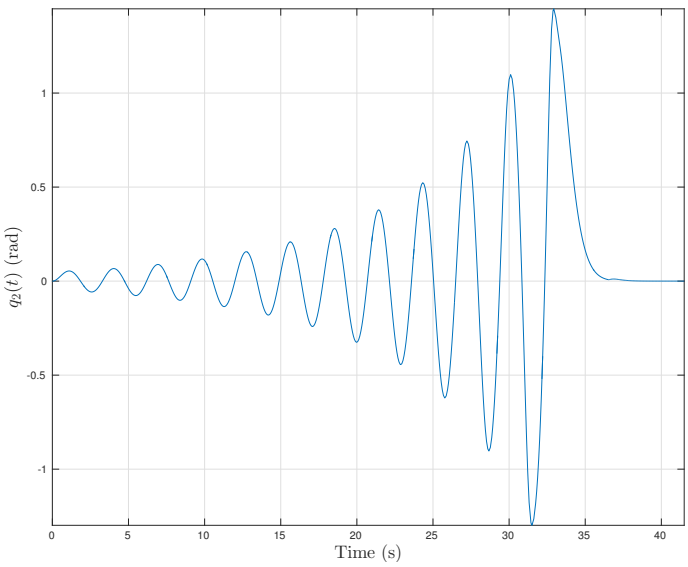

FIGURE 9.12: The angular position of the most distal pendulum (q_2) of the undamped Acrobot during swing-up control using TCPFL and the ATAN controller.

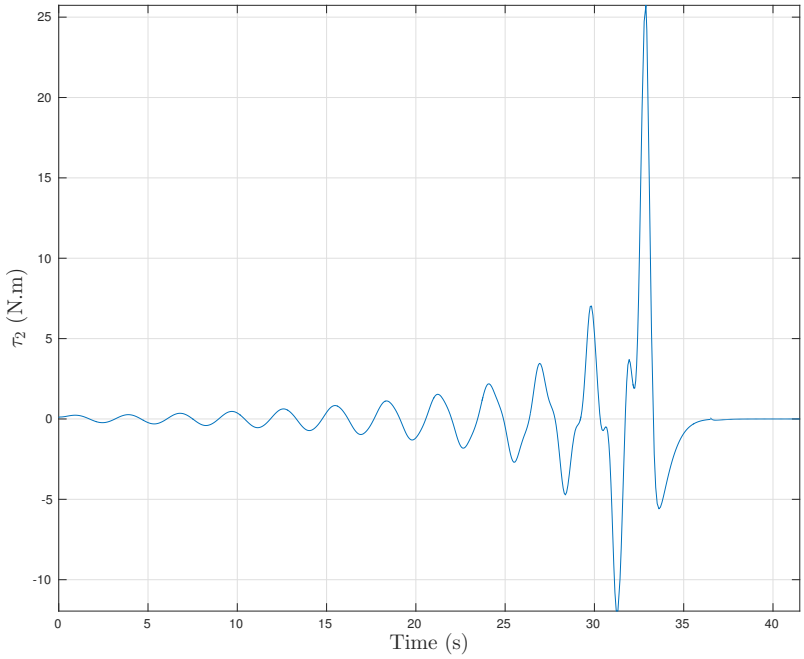

FIGURE 9.13: The torque required to perform swing-up control on an undamped Acrobot using TCPFL and the ATAN controller.

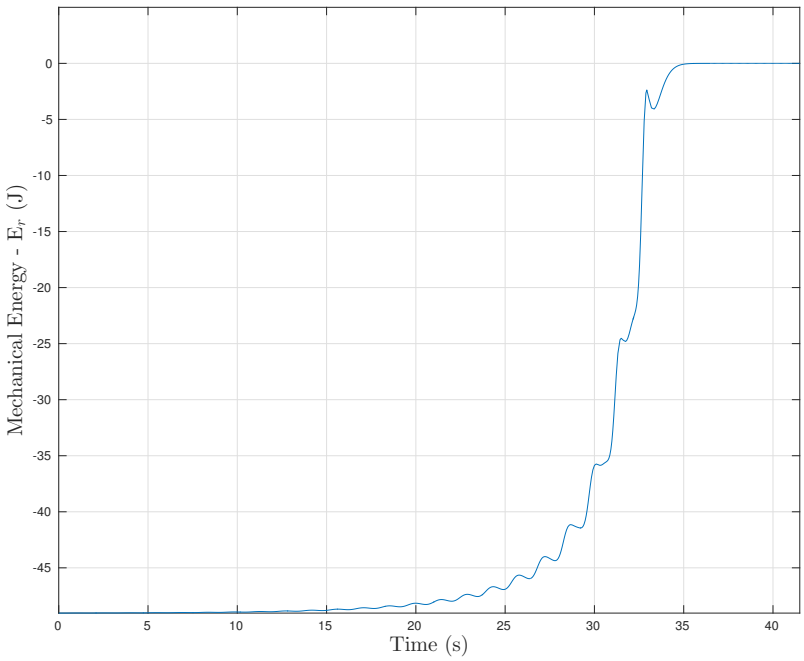

FIGURE 9.14: The difference between the mechanical energy of the undamped Acrobot and E_r during TCPFL-related swing-up control.

The *gain selection criterion* for the undamped Acrobot has been included in a paper that has been accepted into the IEEE AFRICON17 conference proceedings [110]. The full paper has been included in appendix F. There may be instances where a more gentle swing-up approach may be more appropriate. A more gentle swing-up is demonstrated using the gains

$$k_D = 1.1280225, \qquad k_P = 5.2554 = \frac{\beta_1 + \beta_2}{\alpha_1 + \alpha_2 + 2\alpha_3}, \qquad \alpha = \frac{\pi}{2}.$$

These gains are chosen specifically because they satisfy the *gain selection criterion* despite having low magnitudes as compared to the more aggressive swing-up control that was demonstrated in the previous set of results. We chose the initial conditions

$$q_1(0) = -\frac{101}{100}\pi, \qquad q_2(0) = 0,$$
$$\dot{q}_1(0) = 0, \qquad \dot{q}_2(0) = 0$$

as with the previous simulations. The simulations were performed using the Dormand-Prince fixed time-interval integrator package using a resolution of 0.01 seconds. The swing-up controller, in this case, is switched for the LQR controller (which is described by the gains shown in eqs. (9.14a)-(9.14b)) at 172 seconds. The gentle swing-up control of the undamped Acrobot is demonstrated in figures 9.15-9.18.

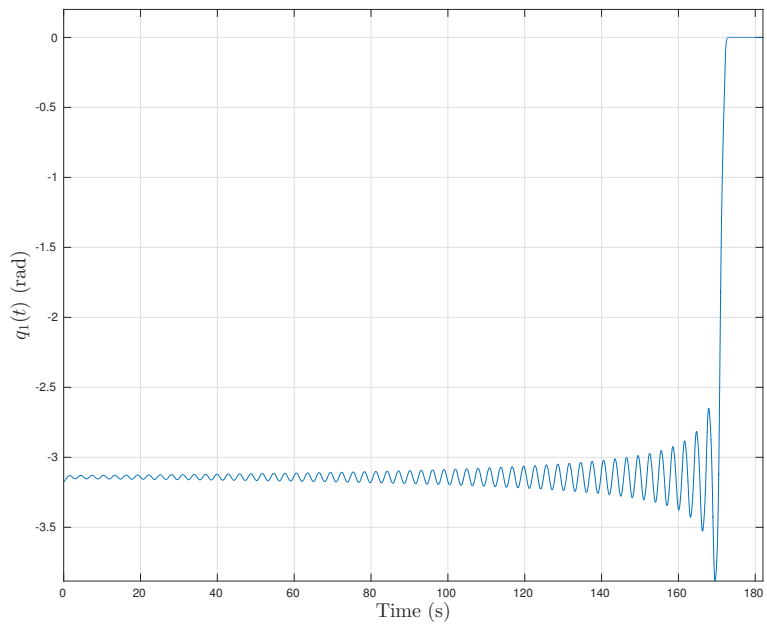

FIGURE 9.15: The angular position of the most proximal pendulum (q_1) of the undamped Acrobot during gentle swing-up control using TCPFL and the ATAN controller.

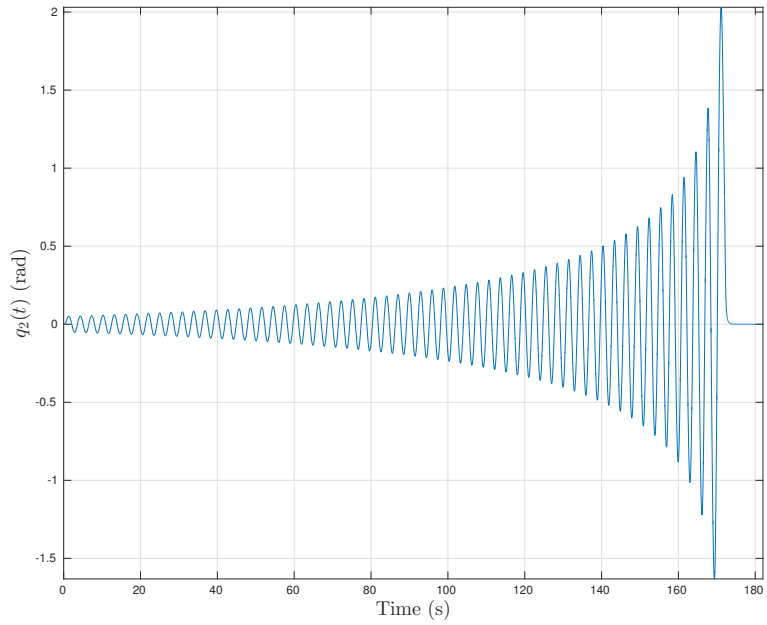

FIGURE 9.16: The angular position of the most distal pendulum (q_2) of the undamped Acrobot during gentle swing-up control using TCPFL and the ATAN controller.

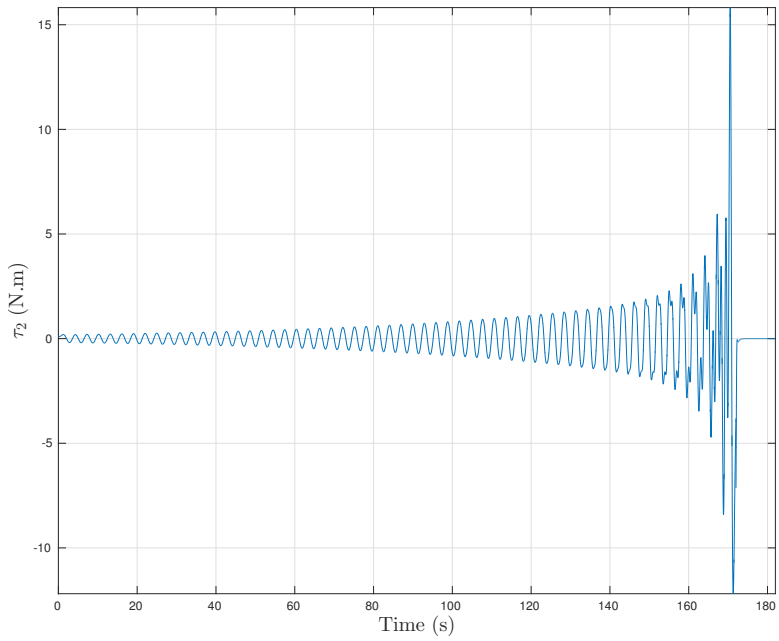

FIGURE 9.17: The torque required to perform gentle swing-up control on an undamped Acrobot using TCPFL and the ATAN controller.

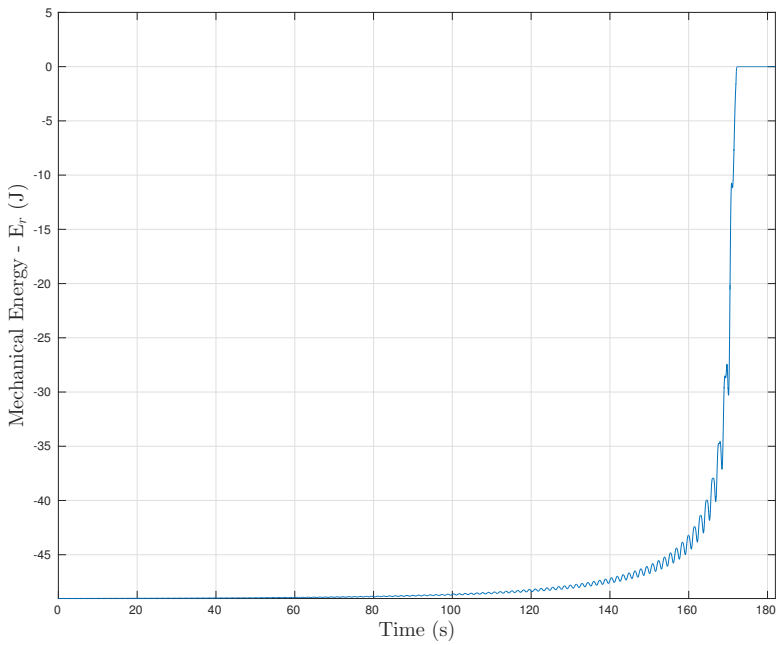

FIGURE 9.18: The difference between the mechanical energy of the undamped Acrobot and E$_r$ during gentle TCPFL-related swing-up control.

The angular displacement of the proximal pendulum of the undamped Acrobot during a more gentle instance of swing-up control is demonstrated in figure 9.15. The displacement of the proximal pendulum increases exponentially throughout the experiment but at a slower rate as compared to the result demonstrated in figure 9.11. This is expected since a smaller magnitude for the gain k_P was selected in this instance, but the exponential increase in the displacement is attributed to the satisfaction of the *gain selection criterion*, since the selected gains still fell within the RAG. The pendulum was regulated at $q_1 = 0$ after the LQR controller was introduced (at 172 seconds). The angular displacement of the distal pendulum during a more gentle instance of swing-up control is demonstrated in figure 9.16. The displacement of the distal pendulum also increases exponentially throughout the experiment and at a slower rate as compared to the result in figure 9.12. The distal pendulum was regulated at $q_2 = 0$ after the LQR controller was introduced at 172 seconds as expected. The torque produced by the actuator during the gentle swing-up control is demonstrated in figure 9.17. The torque increases exponentially throughout the experiment, but at a slower rate as compared to the torque results shown in figure 9.13. The torque levels off at approximately 0 N.m after 172 seconds since the controller was no longer producing a swing-up torque but was instead regulating the system about the UEP. The mechanical energy of the undamped Acrobot during this experiment is demonstrated in figure 9.18. As with the previous experiment, the swing-up torque increased the mechanical energy of the system exponentially until the UEP was reached. The mechanical energy remained unchanged at the value E_r

after the LQR controller was initiated.

As expected, the swing-up controller required significantly more time to execute the swing-up control when a lower magnitude for the gain k_P was selected, but the objective was evidently attained since the *gain selection criterion* was satisfied. It is thus apparent that the *gain selection criterion* acts as a prerequisite to swing-up control provided that the TC-ROPA$_{n-1}$ robot is to be swung from approximately near the FPEP. If this criterion is not satisfied, the robot's trajectory will tend toward the FPEP, guaranteeing unsatisfactory swing-up control.

We shall now demonstrate that the *gain selection criterion* is valid for higher-order systems by performing TCPFL-related swing-up control on the undamped PAA robot.

The Undamped PAA Robot

The undamped PAA robot is modelled as the TC-ROPA$_2$ robot using TCPFL through the application of the FBL torques

$$\begin{aligned}\tau_2 &= \hat{M}_{22}(\mathbf{q})v_2 + \hat{M}_{23}(\mathbf{q})v_3 + \hat{D}_2(\mathbf{q},\dot{\mathbf{q}}) + \hat{K}_2(\mathbf{q}),\\ \tau_3 &= \hat{M}_{32}(\mathbf{q})v_2 + \hat{M}_{33}(\mathbf{q})v_3 + \hat{D}_3(\mathbf{q},\dot{\mathbf{q}}) + \hat{K}_3(\mathbf{q})\end{aligned}$$

where

$$\begin{aligned}
\hat{M}_{22}(\mathbf{q}) &= M_{22}(\mathbf{q}) - \frac{M_{21}(\mathbf{q})M_{12}(\mathbf{q})}{M_{11}(\mathbf{q})}, & \hat{M}_{23}(\mathbf{q}) &= M_{23}(\mathbf{q}) - \frac{M_{21}(\mathbf{q})M_{13}(\mathbf{q})}{M_{11}(\mathbf{q})},\\
\hat{M}_{32}(\mathbf{q}) &= M_{32}(\mathbf{q}) - \frac{M_{31}(\mathbf{q})M_{12}(\mathbf{q})}{M_{11}(\mathbf{q})}, & \hat{M}_{33}(\mathbf{q}) &= M_{33}(\mathbf{q}) - \frac{M_{31}(\mathbf{q})M_{13}(\mathbf{q})}{M_{11}(\mathbf{q})},\\
\hat{D}_2(\mathbf{q},\dot{\mathbf{q}}) &= D_2(\mathbf{q},\dot{\mathbf{q}}) - \frac{M_{21}(\mathbf{q})}{M_{11}(\mathbf{q})}D_1(\mathbf{q},\dot{\mathbf{q}}), & \hat{D}_3(\mathbf{q},\dot{\mathbf{q}}) &= D_3(\mathbf{q},\dot{\mathbf{q}}) - \frac{M_{31}(\mathbf{q})}{M_{11}(\mathbf{q})}D_1(\mathbf{q},\dot{\mathbf{q}}),\\
\hat{K}_2(\mathbf{q}) &= K_2(\mathbf{q}) - \frac{M_{21}(\mathbf{q})}{M_{11}(\mathbf{q})}K_1(\mathbf{q}), & \hat{K}_3(\mathbf{q}) &= K_3(\mathbf{q}) - \frac{M_{31}(\mathbf{q})}{M_{11}(\mathbf{q})}K_1(\mathbf{q})
\end{aligned}$$

and where $D_1(\mathbf{q},\dot{\mathbf{q}}) = C_1(\mathbf{q},\dot{\mathbf{q}})$, $D_2(\mathbf{q},\dot{\mathbf{q}}) = C_2(\mathbf{q},\dot{\mathbf{q}})$, and $D_3(\mathbf{q},\dot{\mathbf{q}}) = C_3(\mathbf{q},\dot{\mathbf{q}})$. This results in a set of dynamical equations described by

$$\begin{aligned}\ddot{q}_1 &= \frac{-M_{12}(\mathbf{q})v_2 - M_{13}(\mathbf{q})v_3 - D_1(\mathbf{q},\dot{\mathbf{q}}) - K_1(\mathbf{q})}{M_{11}(\mathbf{q})},\\ \ddot{q}_2 &= v_2,\\ \ddot{q}_3 &= -k_{D_3}\dot{q}_3 - k_{P_3}q_3\end{aligned}$$

where

$$\begin{aligned}
\overline{\alpha}_1 &= I_1 + m_1{l_1}^2 + \overline{m}_2{L_1}^2, & \overline{\alpha}_2 &= \overline{I}_2 + \overline{m_2{l_2}^2},\\
\overline{\alpha}_3 &= \overline{m_2 l_2}L_1, & \overline{\beta}_1 &= (m_1 l_1 + \overline{m}_2 L_1)\,g,
\end{aligned}$$

$$\overline{\beta}_2 = \overline{m_2 l_2} g,$$
$$\overline{m}_2 = m_2 + m_3, \qquad \overline{I}_2 = I_2 + I_3,$$
$$\overline{m_2 l_2} = m_2 l_2 + m_3 \left[l_3 + L_2\right], \qquad \overline{m_2 {l_2}^2} = m_2 {l_2}^2 + m_3 \left[l_3 + L_2\right]^2.$$

Additionally, we define

$$k_{D_3} = 2\omega_{n_3}, \qquad k_{P_3} = {\omega_{n_3}}^2$$

and

$$v_2 = k_P \left(q_2^d - q_2\right) - k_D \dot{q}_2$$

with

$$q_2^d = \left(\frac{2\alpha}{\pi}\right) \arctan \dot{q}_1.$$

We modelled the behaviour of the TC-ROPA$_2$ robot through the selection of the parameters

$$m_1 = 1 \text{ kg}, \quad m_2 = 0.5 \text{ kg}, \quad m_3 = 0.5 \text{ kg},$$
$$l_1 = 0.5 \text{ m}, \quad l_2 = 0.5 \text{ m}, \quad l_3 = 0.5 \text{ m},$$
$$L_1 = 1 \text{ m}, \quad L_2 = 1 \text{ m}, \quad L_3 = 1 \text{ m},$$
$$I_1 = 0.083 \text{ kg.m}^2, \quad I_2 = 0.165 \text{ kg.m}^2, \quad I_3 = 0.165 \text{ kg.m}^2,$$
$$g = 9.81 \text{ m.s}^2$$

which adheres to the constraint highlighted in eq. (9.3) and which we used to outline the gain selection criterion shown in Definition 9.1. These produced a similar set of boundaries as seen in the Acrobot example shown in section 9.4.1. We thus selected the gains

$$k_{D_2} = 9.640222, \quad k_{P_2} = 100, \quad \alpha = \frac{\pi}{2},$$
$$k_{D_3} = 40, \quad k_{P_3} = 400$$

which fall well within the RAG. Additionally, we selected

$$q_1(0) = -\frac{99}{100}\pi, \quad q_2(0) = 0, \quad q_3(0) = 0,$$
$$\dot{q}_1(0) = 0, \quad \dot{q}_2(0) = 0, \quad \dot{q}_3(0) = 0$$

as the initial conditions of this experiment. The results of the TCPFL-related swing-up control of the undamped PAA robot are shown in figures 9.19-9.23, which were simulated using the Dormand-Prince fixed time-interval integrator package using a 0.01 seconds resolution.

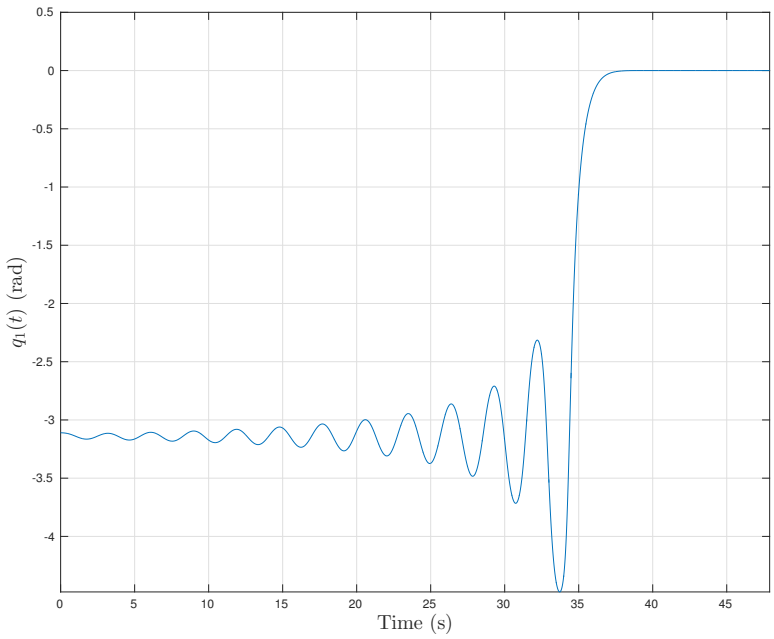

FIGURE 9.19: The angular displacement of the most proximal pendulum of the undamped TC-ROPA$_2$ robot during TCPFL-related swing-up control.

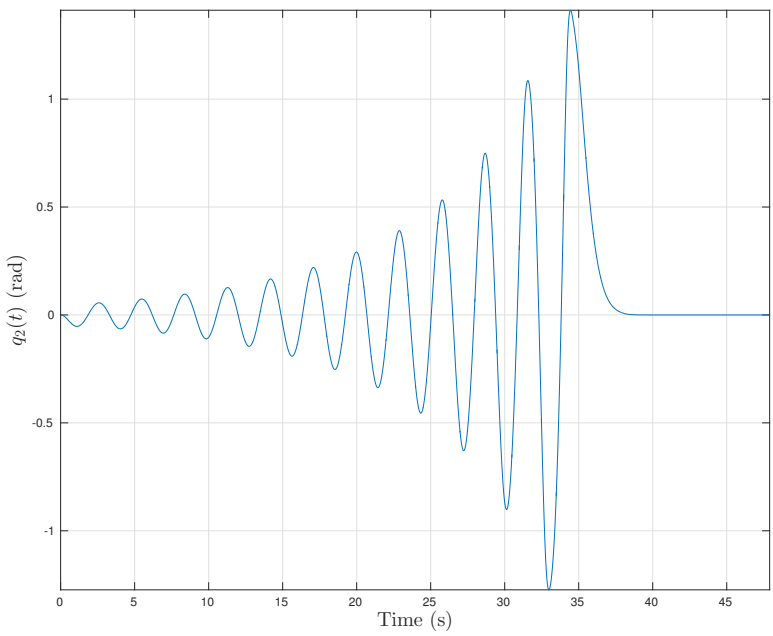

FIGURE 9.20: The angular displacement of the second pendulum of the undamped TC-ROPA$_2$ robot during TCPFL-related swing-up control.

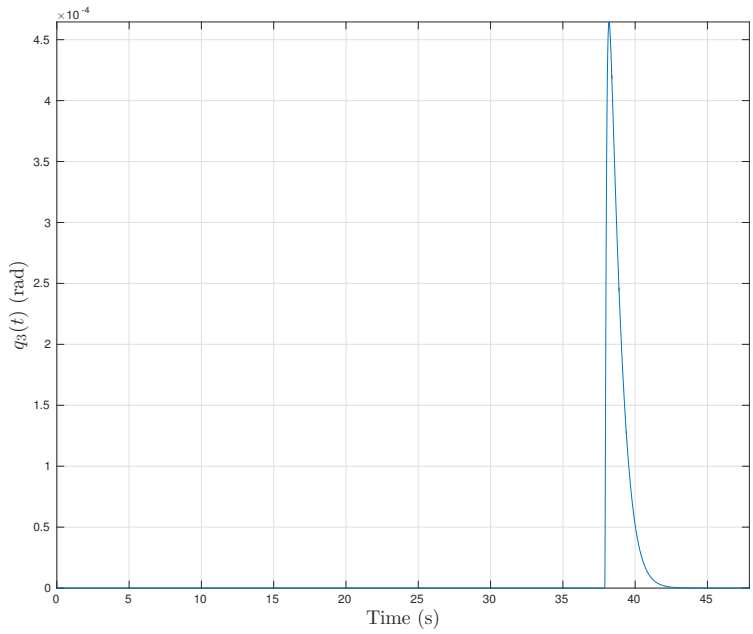

FIGURE 9.21: The angular displacement of the most distal pendulum of the undamped TC-ROPA$_2$ robot during TCPFL-related swing-up control.

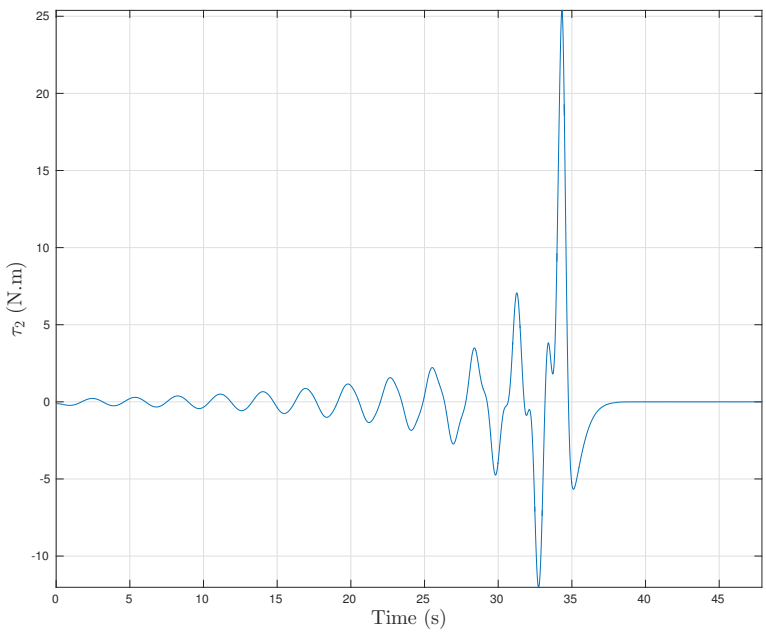

FIGURE 9.22: The torque τ_2 that is required to perform TCPFL-related swing-up control on the undamped TC-ROPA$_2$ robot.

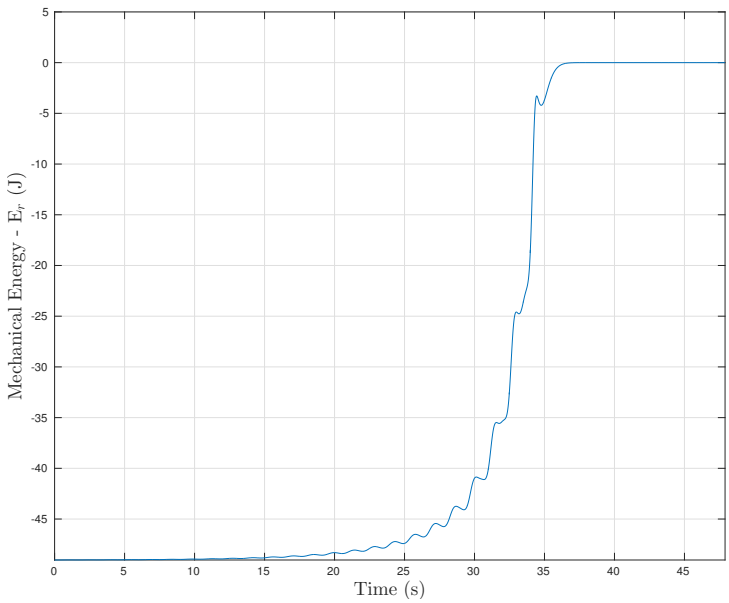

FIGURE 9.23: The difference between the mechanical energy and the objective energy E_r during the TCPFL-related swing-up control of the TC-ROPA$_2$ robot.

The swing-up controller was switched to an LQR controller at 37.9 seconds. The LQR controller is described by the gains

$$k_{11} = -239.7244, \quad k_{12} = -95.3162, \quad k_{13} = -25.2219, \tag{9.15a}$$
$$k_{14} = -103.4730, \quad k_{15} = -48.5752, \quad k_{16} = -13.6428, \tag{9.15b}$$
$$k_{21} = -77.3684, \quad k_{22} = -32.5982, \quad k_{23} = -4.7272, \tag{9.15c}$$
$$k_{24} = -33.3699, \quad k_{25} = -16.0123, \quad k_{26} = -3.3075. \tag{9.15d}$$

The angular displacement of the most proximal pendulum of the TC-ROPA$_2$ robot during PFL-related swing-up control is demonstrated in figure 9.19. The displacement of the most proximal pendulum off $q_1 = -\pi$ increased exponentially in magnitude throughout the experiment, as seen with the swing-up control of the undamped Acrobot. The pendulum plateaued at $q_1 = 0$ after the substitution of the swing-up controller with the LQR controller 37.9 seconds into the simulation. The angular displacement of the second pendulum of the undamped TC-ROPA$_2$ robot during PFL-related swing-up control is demonstrated in figure 9.20. The pendulum oscillated about $q_2 = 0$, with the displacement increasing exponentially with each swing-cycle. The pendulum was regulated about $q_2 = 0$ after the LQR controller was initiated 37.9 seconds into the experiment. The angular displacement of the most distal pendulum of the undamped TC-ROPA$_2$ robot that occurred during PFL-related swing-up control is demonstrated in figure 9.21. The TCPFL control technique ensured that the most distal pendulum was strictly regulated about the neighbourhood of $q_3 = 0$ throughout the swing-up control phase of the simulation.

The spike in the figure occurred at the point when the swing-up controller was switched with the LQR controller, and was a result of the LQR control law. The deviation is, however, relatively small as compared to the displacements seen with the more proximal pendulums, reaching a maximum deflection of 4.6×10^{-4} radians.

The torque produced by the PFL-related swing-up controller located between the most proximal pendulum and the second pendulum is demonstrated in figure 9.22. The torque increases exponentially in magnitude in response to the behaviour of the displacements q_1 and q_2 (and their respective angular velocities). The pattern continued until the TC-ROPA$_2$ fell within the approximate neighbourhood of the UEP (the swing-cycle before the LQR is introduced). The system was regulated using an LQR-related torque after the swing-up phase (which ended 37. seconds into the simulation). The mechanical energy of the TC-ROPA$_2$ robot recorded during the swing-up control of the undamped TC-ROPA$_2$ robot is demonstrated in figure 9.23. The mechanical energy exponentially increased throughout the experiment, with each swing-cycle demonstrating a peak and a trough in the mechanical energy. The peak in mechanical energy during any particular swing-cycle corresponds to the point when the TC-ROPA$_2$ robot contained the largest kinetic energy (as it swung past the FPEP). The trough corresponds to the point when the TC-ROPA$_2$ robot had the highest potential energy in the swing-cycle (when the robot reached the largest possible deflection off the FPEP). The author believes that this dip in the energy occurred due to the introduction of a braking torque by the actuator responsible for swing-up control to ensure that the system reached the appropriate states before initiating a new swing-cycle instance.

The results depicted in figures 9.19-9.23 demonstrate the successful swing-up of the TC-ROPA$_2$ robot. The behaviour of the controller was particularly aggressive, reaching the UEP after 37.9 seconds. We will now demonstrate that successful swing-up control can be achieved when the specific gain selection is found closer to the boundaries of, but still within, the RAG. Using the same physical parameters that were selected in the aggressive swing-up experiment, we selected the gains

$$k_{D_2} = 1.1279685675, \qquad k_{P_2} = 5.2554 = \frac{\overline{\beta}_1 + \overline{\beta}_2}{\overline{\alpha}_1 + \overline{\alpha}_2 + 2\overline{\alpha}_3}, \qquad \alpha = \frac{\pi}{2},$$
$$k_{D_3} = 40, \qquad k_{P_3} = 400$$

and the initial conditions

$$q_1(0) = -\frac{101}{100}\pi, \qquad q_2(0) = 0, \qquad q_3(0) = 0,$$
$$\dot{q}_1(0) = 0, \qquad \dot{q}_2(0) = 0, \qquad \dot{q}_3(0) = 0$$

which initialised the system near the FPEP. The simulation of the gentle swing-up of the undamped PAA robot using PFL was performed using the Dormand-Prince fixed time-interval integrator package with a 0.01 seconds resolution. The results of

this simulation are demonstrated in figures 9.24-9.28. The swing-up controller was switched to an LQR controller at 171.79 seconds. The LQR controller is described by the gains shown in eqs. (9.15a)-(9.15d).

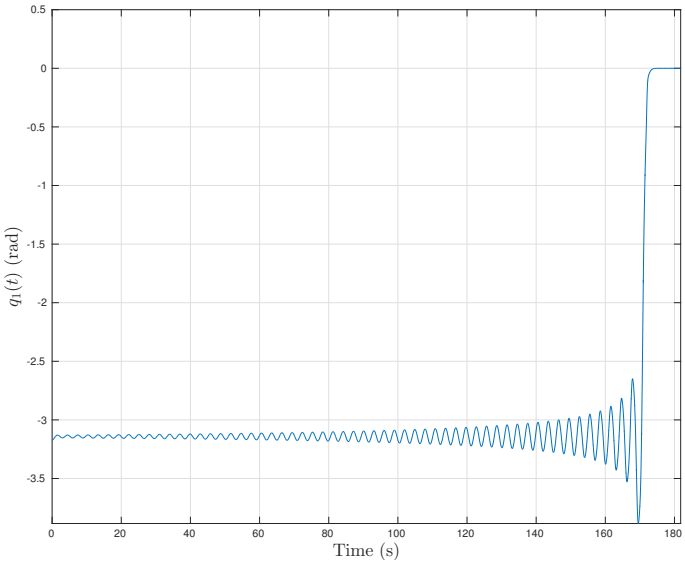

FIGURE 9.24: The angular displacement of the most proximal pendulum of the undamped TC-ROPA$_2$ robot during gentle TCPFL-related swing-up control.

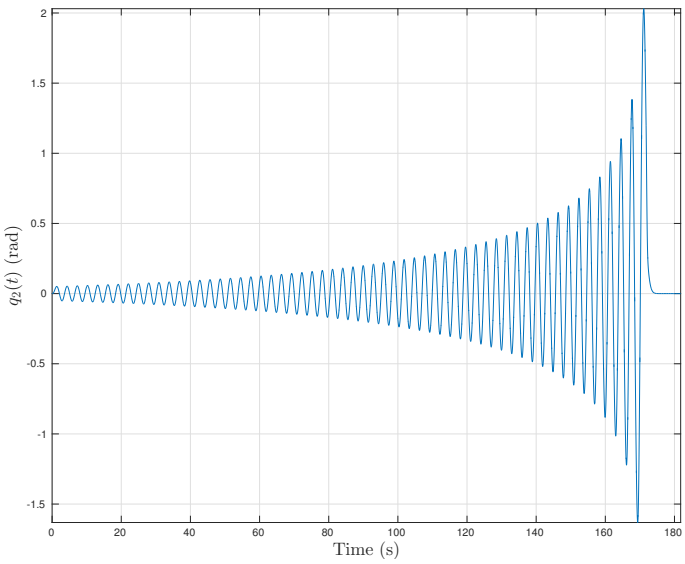

FIGURE 9.25: The angular displacement of the second pendulum of the undamped TC-ROPA$_2$ robot during gentle TCPFL-related swing-up control.

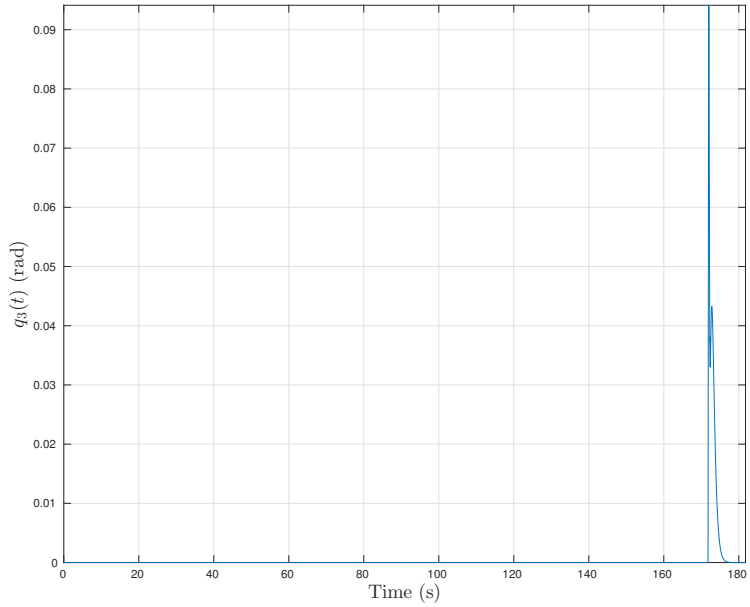

FIGURE 9.26: The angular displacement of the most distal pendulum of the undamped TC-ROPA$_2$ robot during gentle TCPFL-related swing-up control.

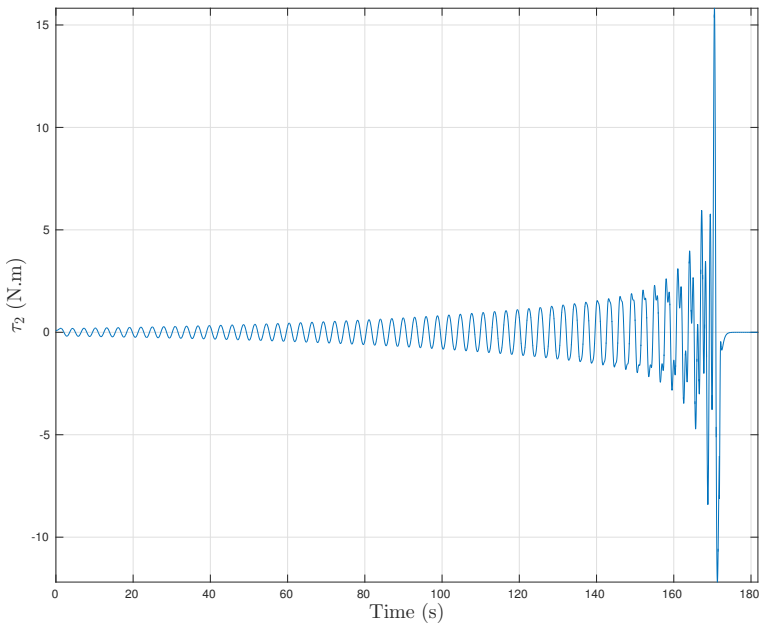

FIGURE 9.27: The torque τ_2 that is required to perform gentle TCPFL-related swing-up control on the undamped TC-ROPA$_2$ robot.

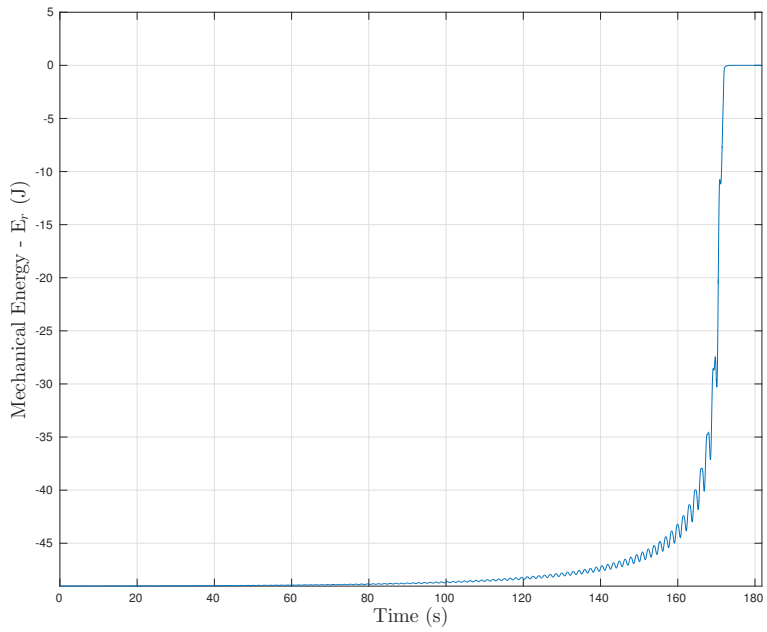

FIGURE 9.28: The difference between the mechanical energy and the objective energy E_r during the gentle TCPFL-related swing-up control of the TC-ROPA$_2$ robot.

The angular displacement of the most proximal pendulum of the TC-ROPA$_2$ robot during gentle swing-up control is demonstrated in figure 9.24. The pendulum oscillated about $q_1 = -\pi$, but increased exponentially in magnitude throughout the experiment, with < 1 radian range deflections occurring with almost every swing-cycle (with the last swing-cycle being the exception). The states of the TC-ROPA$_2$ fell approximately within the neighbourhood of the UEP after approximately 170 seconds, taking nearly 5 times longer than the previous experiment. The proximal pendulum was regulated using an LQR controller 171.9 seconds into the simulation. The angular displacement of the second pendulum of the TC-ROPA$_2$ robot during gentle TCPFL-related swing-up control is demonstrated in figure 9.25. The displacement of the second pendulum increased exponentially throughout the experiment until the LQR controller was initiated 171.9 seconds into the experiment, whereby the pendulum remained within an approximate neighbourhood of $q_2 = 0$. The angular displacement of the most distal pendulum of the TC-ROPA$_2$ robot that was recorded during gentle TCPFL-related swing-up control is demonstrated in figure 9.26. The actuator found between the second and most distal pendulums exerted a torque that ensured the strict regulation of the most distal pendulum about $q_3 = 0$ throughout the swing-up cycle of the TC-ROPA$_2$ robot. The spike that is evident in the figure was the result of the response of the actuator when it was assigned with a new LQR-related control law (occurred 171.9 seconds into the simulation). The swing-up and LQR-related control torque that was exerted by the actuator found between the second and most proximal pendulums of the TC-ROPA$_2$ robot

during gentle TCPFL-related swing-up control is demonstrated in figure 9.27. The magnitude of the torque increased exponentially throughout the swing-up phase as the behaviour of the torque was dependent on the magnitudes of q_1 and q_2 as well as their respective velocities. A regulating torque was applied after 171.9 seconds into the simulation as described by the LQR control law. The mechanical energy of the TC-ROPA$_2$ robot that was recorded during the gentle TCPFL-related swing-up control is demonstrated in figure 9.28. The mechanical energy of the system increased exponentially as energy was introduced by the unstable control torque applied by the actuator responsible for swing-up control. Each swing-cycle is clearly associated with a peak and trough of mechanical energy. The peak of the cycle occurred when the system reached its maximum possible kinetic energy (when the system crossed the FPEP). The troughs occurred at the point in the cycle where the maximum potential energy was achieved (when the proximal pendulum achieved the largest deviation away from $q_1 = -\pi$ for the swing-cycle). The troughs are believed to be a result of the application of a braking torque that was required to ensure that the pendulums are synchronised before the initiation of the new swing-up cycle.

The swing-up control of the TC-ROPA$_2$ robot was evidently successful despite the selection of a lower magnitude for k_P. The system required many more swing-cycles to achieve the objective, but this simulation demonstrates that **it is possible to swing-up an undamped and underactuated multi-body pendulum system using TCPFL so long as the *gain selection criterion* is satisfied**. Therefore, a constraint in the gain magnitudes may increase the amount of time required to perform satisfactory swing-up control on an undamped underactuated robotic system, but the objective can, nonetheless, be achieved so long as the *gain selection criterion* is satisfied. Additionally, this experiment demonstrates that the reduction in the magnitude of k_P produces a more gentle swing-up control. It is not known whether this is specific to this example, but further investigations into this phenomenon is recommended for future research, especially since the RAG can be dissected into areas of varying system response rates.

The *gain selection criterion* has been proven to be an effective tool in determining the relevant gains that are required to swing-up an undamped TC-ROPA$_{n-1}$ system from the FPEP; This is an important milestone in this research. We shall now evaluate the potential of using this principle to develop conditions with which a damped TC-ROPA$_{n-1}$ robot can be swung-up from the FPEP, beginning first with the actively damped case.

9.4.2 Actively Damped PA$_{n-1}$ Robot

TC-ROPA$_{n-1}$ Robot Modelling, Equilibrium Point Analysis and Gain Selection Criterion

The implementation of the TCPFL technique on the actively damped PA$_{n-1}$ robot results in the dynamical equations shown in eqs. (9.2a) and (9.2d) which describes

the behaviour of the TC-ROPA$_{n-1}$ robot, where

$$\begin{aligned} D_i(\mathbf{q}, \dot{\mathbf{q}}) &= C_i(\mathbf{q}, \dot{\mathbf{q}}) + R_i(\dot{\mathbf{q}}) && \text{for } 2 \leq i \leq n, \\ D_1(\mathbf{q}, \dot{\mathbf{q}}) &= C_i(\mathbf{q}, \dot{\mathbf{q}}) \end{aligned}$$

in the case of an actively damped system, and $R_i(\dot{\mathbf{q}}) = b_i \dot{q}_i$. The formulation of the model follows the derivation seen in section 9.4.1, resulting in the TC-ROPA$_{n-1}$ model described by eqs. (9.8a) and (9.8b). The active damping has thus been linearly negated from the system dynamics, with the effects of this damping only evident once the magnitude of the FBL torques τ_i are evaluated. The active damping therefore has no implications on the derivation of the TC-ROPA$_{n-1}$ robot's equilibrium points and its respective swing-up *gain selection criterion*. The results of sections 9.4.1 thus adequately describes the derivation of the *gain selection criterion* for the actively damped PA$_{n-1}$ robot. We shall practically demonstrate this on the simplest derivatives of the PA$_{n-1}$ robot, beginning with the actively damped Acrobot.

Actively Damped Acrobot

The actively damped Acrobot requires the FBL torque

$$\tau_2 = \hat{M}_{22} v_2 + \hat{D}_2(\mathbf{q}, \dot{\mathbf{q}}) + \hat{K}(\mathbf{q})$$

to linearise the dynamics of the most distal pendulum, which is damped in this case, where

$$\begin{aligned} \hat{M}_{22}(\mathbf{q}) &= M_{22}(\mathbf{q}) - \frac{M_{21}(\mathbf{q}) M_{12}(\mathbf{q})}{M_{11}(\mathbf{q})}, \\ \hat{D}_2(\mathbf{q}, \dot{\mathbf{q}}) &= D_2(\mathbf{q}, \dot{\mathbf{q}}) - \frac{M_{21}(\mathbf{q})}{M_{11}(\mathbf{q})} D_1(\mathbf{q}, \dot{\mathbf{q}}), \\ \hat{K}_2(\mathbf{q}) &= K_2(\mathbf{q}) - \frac{M_{21}(\mathbf{q})}{M_{11}(\mathbf{q})} K_1(\mathbf{q}) \end{aligned}$$

and where

$$\begin{aligned} D_1(\mathbf{q}, \dot{\mathbf{q}}) &= C_1(\mathbf{q}, \dot{\mathbf{q}}), && D_2(\mathbf{q}, \dot{\mathbf{q}}) = C_2(\mathbf{q}, \dot{\mathbf{q}}) + R_2(\dot{\mathbf{q}}), \\ R_2(\dot{\mathbf{q}}) &= b_2 \dot{q}_2. \end{aligned}$$

This torque produces a set of equations of motion described by

$$\ddot{q}_1 = \frac{-M_{12} v_2 - D_1(\mathbf{q}, \dot{\mathbf{q}}) - K_1(\mathbf{q})}{M_{11}(\mathbf{q})}$$

with

$$v_2 = k_P \left(q_2^d - q_2 \right) - k_D \dot{q}_2$$

and $q_2^d = \left(\frac{2\alpha}{\pi}\right) \arctan \dot{q}_1$. To compare the effects of active damping on the torque of the swing-up controller, we select the system properties

$$\begin{aligned} m_1 &= 1 \text{ kg}, & m_2 &= 1 \text{ kg}, \\ l_1 &= 0.5 \text{ m}, & l_2 &= 1 \text{ m}, \\ L_1 &= 1 \text{ m}, & L_2 &= 2 \text{ m}, \\ I_1 &= 0.083 \text{ kg.m}^2, & I_2 &= 0.33 \text{ kg.m}^2, \\ g &= 9.81 \text{ m.s}^2 \end{aligned}$$

as seen in section 9.4.1. This set of parameters, with the gain selection criterion highlighted in Definition 9.1, produces identical results for the actively damped Acrobot as what is seen in figures 9.3-9.10. The only difference that is seen in the simulation results is in the torque, whereby, in the actively damped case, the resultant torque represents a superposition of the swing-up torque and the damping-negation torque. We demonstrate this by performing swing-up control on the actively damped Acrobot using

$$k_D = 1.01, \qquad k_P = 5.2554 = \frac{\overline{\beta}_1 + \overline{\beta}_2}{\overline{\alpha}_1 + \overline{\alpha}_2 + 2\overline{\alpha_3}},$$

the ATAN controller constant

$$\alpha = \frac{\pi}{40},$$

the damping coefficient

$$b_2 = 10,$$

and the initial conditions

$$\begin{aligned} q_1(0) &= -\frac{101}{100}\pi, & q_2(0) &= 0, \\ \dot{q}_1(0) &= 0, & \dot{q}_2(0) &= 0. \end{aligned}$$

The gains were chosen using the *gain selection criterion* highlighted in criterion 9.1. A swing-up control simulation was performed on the actively damped and undamped Acrobot. The dynamics of the actively damped Acrobot were unaffected by the active damping torques since these torques were negated by the controller torque. The behaviour of the actively damped Acrobot described by the aforementioned properties is thus identically represented in the swing-up control results of the undamped Acrobot demonstrated in figures 9.11,9.12, and 9.14. The only discernible difference between these cases would be the magnitudes in torque produced by the swing-up controllers. The comparison of the torques required to swing-up an undamped Acrobot and an actively damped Acrobot using TCPFL is demonstrated in figure 9.29.

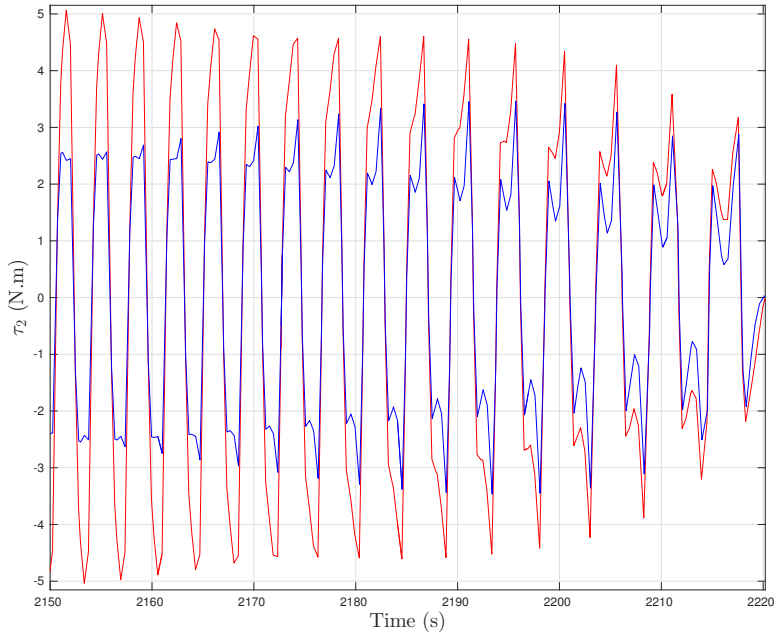

FIGURE 9.29: Torque required to perform TCPFL-related swing-up control on the undamped Acrobot (blue) and the actively damped Acrobot (red) where $b_2 = 10$.

The torque required to swing-up an undamped Acrobot using TCPFL is shown by the blue curve, whereas the red curve represents the torque required to swing-up an identically configured Acrobot that has been integrated with viscous damping on the active joint (with a damping coefficient of $b_2 = 10$). The two curves are in phase with one another, with the difference between the magnitudes of the red and blue curves representing the torque that is required to negate the damping friction present at the active joint. The magnitude of this curve will evidently increase if the damping coefficient of the damping friction torque found at the active joint is increased. It is, therefore, evident that the *gain selection criterion* can be applied to actively damped Acrobots.

We shall now demonstrate that higher-order actively damped underactuated systems may also be swung-up using the *gain selection criterion*.

Actively Damped PAA Robot

The actively damped PAA robot is linearised, as with the undamped case, with the FBL torques

$$\tau_2 = \hat{M}_{22}(\mathbf{q})v_2 + \hat{M}_{23}(\mathbf{q})v_3 + \hat{D}_2(\mathbf{q}, \dot{\mathbf{q}}) + \hat{K}_2(\mathbf{q}),$$
$$\tau_3 = \hat{M}_{32}(\mathbf{q})v_2 + \hat{M}_{33}(\mathbf{q})v_3 + \hat{D}_3(\mathbf{q}, \dot{\mathbf{q}}) + \hat{K}_3(\mathbf{q})$$

where the parameters are identical to that of the undamped case with the exception of

$$D_2(\mathbf{q}, \dot{\mathbf{q}}) = C_2(\mathbf{q}, \dot{\mathbf{q}}) + R_2(\dot{\mathbf{q}}),$$
$$D_3(\mathbf{q}, \dot{\mathbf{q}}) = C_3(\mathbf{q}, \dot{\mathbf{q}}) + R_3(\dot{\mathbf{q}})$$

where $R_2(\dot{\mathbf{q}}) = b_2\dot{q}_2$, and $R_3(\dot{\mathbf{q}}) = b_3\dot{q}_3$. This results in a set of dynamical equations described by

$$\begin{aligned}
\ddot{q}_1 &= \frac{-M_{12}(\mathbf{q})v_2 - M_{13}(\mathbf{q})v_3 - D_1(\mathbf{q}, \dot{\mathbf{q}}) - K_1(\mathbf{q})}{M_{11}(\mathbf{q})}, \\
\ddot{q}_2 &= v_2, \\
\ddot{q}_3 &= -k_{D_3}\dot{q}_3 - k_{P_3}q_3
\end{aligned}$$

with the elements above defined as seen in the undamped PAA robot case. The gains

$$k_{D_3} = 2\omega_{n_3}, \qquad k_{P_3} = {\omega_{n_3}}^2$$

were identified to produce a non-oscillating regulation of the most distal pendulum along with

$$v_2 = k_P\left(q_2^d - q_2\right) - k_D\dot{q}_2$$

and

$$q_2^d = \left(\frac{2\alpha}{\pi}\right)\arctan\dot{q}_1.$$

It is evident that the linearising torques have negated the active damping torques. The gain selection criterion for the actively damped PAA robot is identical to that of the undamped PAA robot. Choosing the parameters

$$\begin{aligned}
&m_1 = 1 \text{ kg}, && m_2 = 0.5 \text{ kg}, && m_3 = 0.5 \text{ kg}, \\
&l_1 = 0.5 \text{ m}, && l_2 = 0.5 \text{ m}, && l_3 = 0.5 \text{ m}, \\
&L_1 = 1 \text{ m}, && L_2 = 1 \text{ m}, && L_3 = 1 \text{ m}, \\
&I_1 = 0.083 \text{ kg.m}^2, && I_2 = 0.165 \text{ kg.m}^2, && I_3 = 0.165 \text{ kg.m}^2, \\
&g = 9.81 \text{ m.s}^2, && b_2 = 10, && b_3 = 10
\end{aligned}$$

and the control properties

$$\begin{aligned}
&k_D = 1.05, && k_P = 5.3027 = \frac{\overline{\beta}_1 + \overline{\beta}_2}{\overline{\alpha}_1 + \overline{\alpha}_2 + 2\overline{\alpha}_3}, \\
&k_{D_3} = 40, && k_{P_3} = 400,
\end{aligned}$$

$$\alpha = \frac{\pi}{2}$$

with the gains k_D and k_P chosen using the *gain selection criterion* highlighted in criterion 9.1. Simulating the swing-up control of the actively damped TC-ROPA$_2$ using the initial conditions

$$\begin{aligned} q_1(0) &= -\frac{101}{100}\pi, & q_2(0) &= 0, & q_3(0) &= 0, \\ \dot{q}_1(0) &= 0, & \dot{q}_2(0) &= 0, & \dot{q}_3(0) &= 0 \end{aligned}$$

we find that the performance of the actively damped TC-ROPA$_2$ robot is identical to that of the undamped TC-ROPA$_2$ robot demonstrated in figures 9.19-9.21, and figure 9.23. A comparison between the torques produced by the actuator found between the most proximal and second pendulums of the TC-ROPA$_2$ robot for the undamped and actively damped cases is demonstrated in figure 9.30, with the torque in the undamped system represented by the blue curve, and the torque in the actively damped system represented by the red curve. The controller compensates for the viscous damping by producing a damping-negation torque, which is superimposed on the swing-up torque. The linearising torque τ_3 is not affected tangibly by the presence of viscous damping on the most distal joint since the angular velocity of

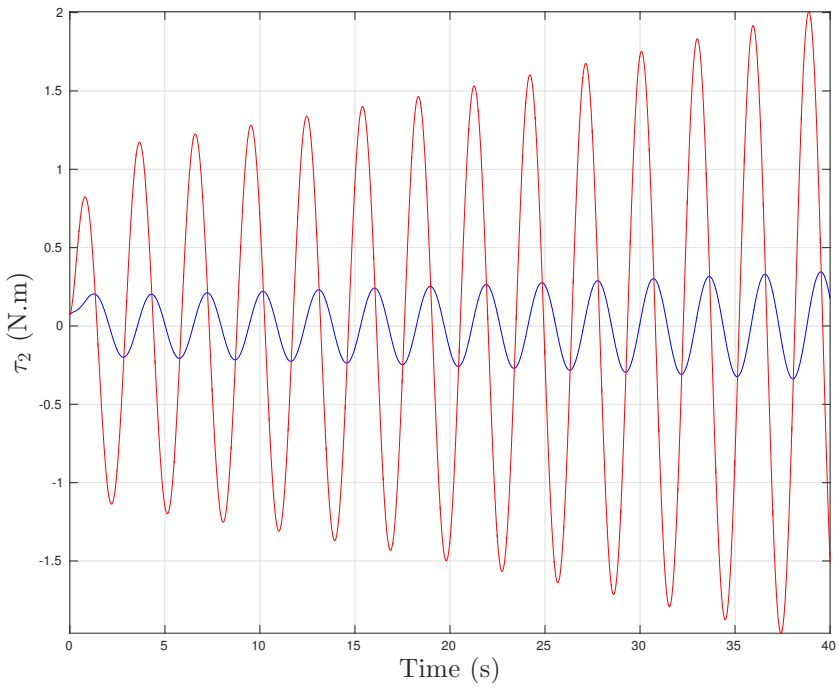

FIGURE 9.30: Torque required to perform TCPFL-related swing-up control on the undamped PAA robot (blue) and the actively damped PAA robot (red) where $b_2 = 10$.

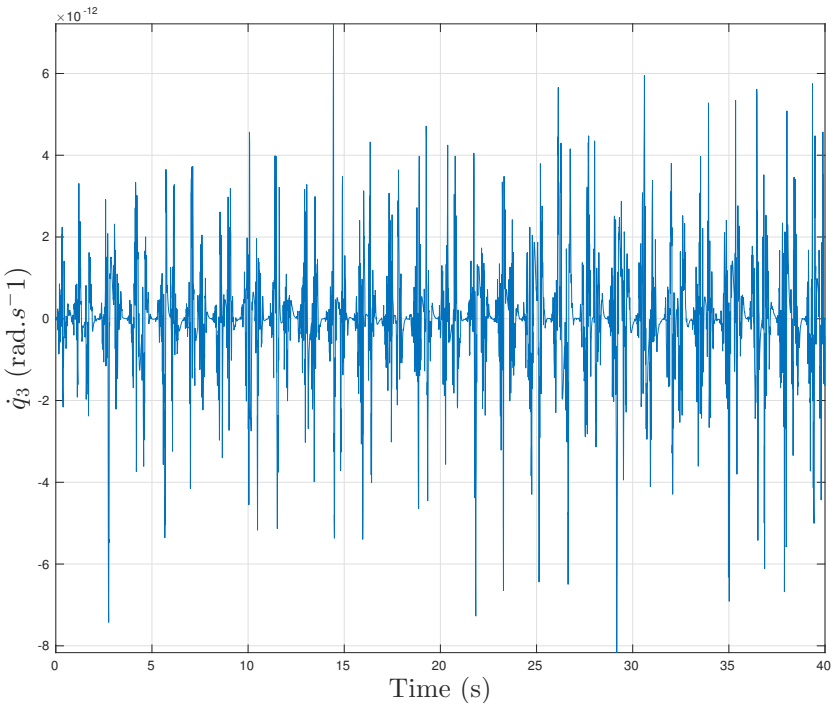

FIGURE 9.31: Angular velocity of the most distal pendulum of the actively damped PAA robot during TCPFL-related swing-up control.

the most distal pendulum is regulated sufficiently by the FBL torque τ_3, as shown in the figure 9.31.

We can now finally address the issue of developing a work-around for the limitation of the Lyapunov-related swing-up control highlighted in the *matched damping condition* by investigating the potential of applying TCPFL swing-up control using an ATAN controller on the passively damped PA$_{n-1}$ robot. If this technique can successfully swing-up a passively damped derivative of the PA$_{n-1}$ robot, the prerequisites of this control shall be outlined by a set of conditions collectively referred to as the *gain selection criterion*, which is similar in principle to the set of conditions derived for the undamped and actively damped PA$_{n-1}$ robot, but will be unique to the application on passively damped PA$_{n-1}$ robots.

9.4.3 Passively Damped PA$_{n-1}$ Robot

This derivation begins with the reduced-order modelling of the passively damped PA$_{n-1}$ robot, which results in the definition of the passively damped TC-ROPA$_{n-1}$ robot.

Modelling the Passively Damped PA$_{n-1}$ Robot as the TC-ROPA$_{n-1}$ Robot

As seen in section 9.4.1, the application of the TCPFL technique on the PA$_{n-1}$ robot produces the set of dynamical equations shown in eqs. (9.2a)-(9.2d), where

$$\begin{aligned} D_i(\mathbf{q}, \dot{\mathbf{q}}) &= C_1(\mathbf{q}, \dot{\mathbf{q}}) && \text{for } 2 \leq i \leq n, \\ D_1(\mathbf{q}, \dot{\mathbf{q}}) &= C_1(\mathbf{q}, \dot{\mathbf{q}}) + R_1(\dot{\mathbf{q}}) \end{aligned}$$

in the passively damped case with $R_1(\dot{\mathbf{q}}) = b_1 \dot{q}_1$. Selecting the initial conditions

$$\begin{aligned} q_3(0) &= 0, & \dot{q}_3(0) &= 0, \\ q_4(0) &= 0, & \dot{q}_4(0) &= 0, \\ &\vdots & &\vdots \\ q_n(0) &= 0, & \dot{q}_n(0) &= 0 \end{aligned}$$

we can guarantee that

$$q_3 \approx 0, \qquad q_4 \approx 0, \qquad \ldots \qquad q_n \approx 0.$$

This is contingent on the choice of a sufficiently large response frequency for each of the linearising actuators. The linearising torque accommodates the modelling of the PA$_{n-1}$ robot as a TC-ROPA$_{n-1}$ robot, with the dynamics of this TC-ROPA$_{n-1}$ robot described by

$$\begin{aligned} &\overline{M}_{11}(\mathbf{q})\ddot{q}_1 + \overline{M}_{12}(\mathbf{q})v_2 + \overline{D}_1(\mathbf{q}, \dot{\mathbf{q}}) + \overline{K}_1(\mathbf{q}) = 0, \\ &\ddot{q}_2 = v_2 \end{aligned}$$

where

$$\begin{aligned} &\overline{M}_{11}(q_2) = \overline{\alpha}_1 + \overline{\alpha}_2 + 2\overline{\alpha}_3 \cos q_2, \\ &\overline{M}_{12}(q_2) = \overline{\alpha}_2 + \overline{\alpha}_3 \cos q_2, \\ &\overline{D}_1(q_2, \dot{\mathbf{q}}) = \overline{C}_1(q_2, \dot{\mathbf{q}}) + R_1(\dot{\mathbf{q}}) = -\overline{\alpha}_3 \left(2\dot{q}_1\dot{q}_2 + \dot{q}_2^2\right) \sin q_2 + b_1\dot{q}_1, \\ &\overline{K}_1(\mathbf{q}) = -\overline{\beta}_1 \sin q_1 - \overline{\beta}_2 \sin(q_1 + q_2) \end{aligned}$$

and

$$\begin{aligned} \overline{\alpha}_1 &= I_1 + m_1 {l_1}^2 + \overline{m}_2 {L_1}^2, & \overline{\alpha}_2 &= \overline{I}_2 + \overline{m_2 {l_2}^2}, \\ \overline{\alpha}_3 &= \overline{m_2 l_2} L_1, & \overline{\beta}_1 &= (m_1 l_1 + \overline{m}_2 L_1)\, g, \\ \overline{\beta}_2 &= \overline{m_2 l_2} g, \\ \overline{m}_2 &= \sum_{i=2}^{n} m_i, & \overline{I}_2 &= \sum_{i=2}^{n} I_i, \end{aligned}$$

$$\overline{m_2 l_2} = \sum_{i=2}^{n} m_i \left[l_i + \sum_{j=2}^{i-1} L_j \right], \qquad \overline{m_2 {l_2}^2} = \sum_{i=2}^{n} m_i \left[l_i + \sum_{j=2}^{i-1} L_j \right]^2$$

which is constrained by the condition in eq. (9.3).

Equilibrium Point Analysis of the Passively Damped TC-ROPA$_{n-1}$ Robot Integrated with an ATAN Controller

The identification of the equilibrium points in the ATAN control integrated passively damped TC-ROPA$_{n-1}$ robot is necessary to understand whether there may be equilibrium points that will pull the system off of the swing-up trajectory towards the UEP. The TC-ROPA$_{n-1}$ model is thus integrated with a linear state feedback controller described by

$$v_2 = k_P \left(q_2^d - q_2 \right) - k_D \dot{q}_2$$

where the ATAN control is represented using the desired angular trajectory

$$q_2^d = \left(\frac{2\alpha}{\pi} \right) \arctan \dot{q}_1 \qquad \text{where } \alpha \in \mathbb{R}^+.$$

Substituting v_2 into eqs. (9.2a)-(9.2d) produces the expressions

$$\overline{M}_{11}(\mathbf{q})\ddot{q}_1 + \overline{M}_{12}(\mathbf{q}) \left(k_P \left[\left(\frac{2\alpha}{\pi} \right) \arctan \dot{q}_1 - q_2 \right] - k_D \dot{q}_2 \right) - \overline{\alpha}_3 \left(2\dot{q}_1 \dot{q}_2 + \dot{q}_2^2 \right) \sin q_2 + b_1 \dot{q}_1 - \overline{\beta}_1 \sin q_1 - \overline{\beta}_2 \sin(q_1 + q_2) = 0, \tag{9.16}$$

$$\ddot{q}_2 = k_P \left[\left(\frac{2\alpha}{\pi} \right) \arctan \dot{q}_1 - q_2 \right] - k_D \dot{q}_2 \tag{9.17}$$

which describe the dynamics of the TC-ROPA$_{n-1}$ model that has been integrated with an ATAN controller. These dynamical equation can also be represented as a set of equations of motion described by

$$\ddot{q}_1 = \left[-\overline{M}_{12}(\mathbf{q}) \left(k_P \left[\left(\frac{2\alpha}{\pi} \right) \arctan \dot{q}_1 - q_2 \right] - k_D \dot{q}_2 \right) + \overline{\alpha}_3 \left(2\dot{q}_1 \dot{q}_2 + \dot{q}_2^2 \right) \sin q_2 - b_1 \dot{q}_1 + \overline{\beta}_1 \sin q_1 + \overline{\beta}_2 \sin(q_1 + q_2) \right] \Big/ \left[\overline{M}_{11}(\mathbf{q}) \right], \tag{9.18}$$

$$\ddot{q}_2 = k_P \left[\left(\frac{2\alpha}{\pi} \right) \arctan \dot{q}_1 - q_2 \right] - k_D \dot{q}_2. \tag{9.19}$$

The states which exists at any equilibrium point $(q_1, q_2, \dot{q}_1, \dot{q}_2) = (q_1^e, q_2^e, \dot{q}_1^e, \dot{q}_2^e)$ are selected as

$$q_1^e = q_1^*, \qquad q_2^e = q_2^*,$$

$$\dot{q}_1^e = 0, \qquad \dot{q}_2^e = 0,$$
$$\ddot{q}_1^e = 0, \qquad \ddot{q}_2^e = 0$$

along with

$$q_2^d = 0.$$

Substituting these equilibrium points into the dynamical equations shown in eqs. (9.9a) and (9.9b) produces the expressions

$$-\overline{M}_{12} k_P q_2^e - \overline{\beta}_1 \sin q_1^e - \overline{\beta}_2 \sin(q_1^e + q_2^e) = 0,$$
$$k_P q_2^e = 0$$

that describe the dynamics of the TC-ROPA$_{n-1}$ robot. These expressions are identical to those seen in eqs. (9.11) and (9.12). It is evident, therefore, that the passive damping has no effect on the location and number of equilibrium points in the state-space of the TC-ROPA$_{n-1}$ robot. We can thus conclude that there are two classifications of equilibrium points found in this system, namely the UEP and the FPEP. These equilibrium points are described as

$$(\mathbf{q^e}, \dot{\mathbf{q}}^\mathbf{e})_{\text{UEP}} = (0, 0, 0, 0),$$
$$(\mathbf{q^e}, \dot{\mathbf{q}}^\mathbf{e})_{\text{FPEP}} = (\pm\pi k, 0, 0, 0)$$

respectively where $k \in \mathbb{Z}$. These points are defined within the region $q_1^e, q_2^e \in (-\pi, \pi]$ where

$$(\mathbf{q^e}, \dot{\mathbf{q}}^\mathbf{e})_{\text{UEP}} = (0, 0, 0, 0),$$
$$(\mathbf{q^e}, \dot{\mathbf{q}}^\mathbf{e})_{\text{FPEP}} = (\pi, 0, 0, 0).$$

Therefore, assuming that the stability of the FPEP is dependent upon the gains k_P and k_D (as done in the undamped case), then the statement in Preposition 9.1 remains relevant in the case of the passively damped TC-ROPA$_{n-1}$ robot. We shall thus state the following directives that are necessary to derive a set of conditions (termed the *gain selection criterion*) for the swing-up control of the passively damped TC-ROPA$_{n-1}$ robot:

(i) Linearise the passively damped TC-ROPA$_{n-1}$ robot about the FPEP using Lyapunov's linearisation technique. Determine the characteristic equation that describes the local stability of the FPEP using this linearised system.

(ii) Implement the Routh-Hurwitz stability criterion (using the Routh array) to determine conditions that ensure that the FPEP is locally unstable.

The execution of these directives results in the derivation of the *gain selection criterion* for passively damped underactuated TC-ROPA$_{n-1}$ robots.

Criterion 9.2. ***Gain selection criterion for the passively damped TC-ROPA$_{n-1}$ robot*** The FPEP of the passively damped TC-ROPA$_{n-1}$ robot when $b_1 > b_{1_{\text{lim}}}$ is guaranteed

to be locally unstable so long as the conditions

$$\frac{\overline{\beta}_2}{\overline{\alpha}_2 + \overline{\alpha}_3} < k_P < \frac{\overline{n}_2 b_1}{\overline{n}_1 b_1 - \overline{w}_2}, \quad k_D = 0$$

are satisfied. Additionally, the FPEP of the passively damped TC-ROPA$_{n-1}$ robot when $0 < b_1 < b_{1_{\text{lim}}}$ is guaranteed to be locally unstable so long as the conditions

$$k_P > \frac{\overline{\beta}_2}{\overline{\alpha}_2 + \overline{\alpha}_3}, \quad k_D = 0$$

are satisfied.

The derivation of this criterion is included in section A.6 in appendix A. We shall now demonstrate the application of the *gain selection criterion* on derivatives of the passively damped TC-ROPA$_{n-1}$ robot, beginning with the Acrobot.

The Passively Damped Acrobot

The passively damped Acrobot is partially linearised with the implementation of the FBL torque

$$\tau_2 = \hat{M}_{22}(\mathbf{q})v_2 + \hat{D}_2(\mathbf{q}, \dot{\mathbf{q}}) + \hat{K}_2(\mathbf{q})$$

where

$$\begin{aligned}
\hat{M}_{22}(\mathbf{q}) &= M_{22}(\mathbf{q}) - \frac{M_{12}(\mathbf{q})M_{21}(\mathbf{q})}{M_{11}(\mathbf{q})}, \\
\hat{D}_2(\mathbf{q}, \dot{\mathbf{q}}) &= D_2(\mathbf{q}, \dot{\mathbf{q}}) - \frac{M_{21}(\mathbf{q})}{M_{11}(\mathbf{q})} D_1(\mathbf{q}), \\
\hat{K}_2(\mathbf{q}) &= K_2(\mathbf{q}) - \frac{M_{21}(\mathbf{q})}{M_{11}(\mathbf{q})} K_1(\mathbf{q})
\end{aligned}$$

and where

$$D_1(\mathbf{q}, \dot{\mathbf{q}}) = C_1(\mathbf{q}, \dot{\mathbf{q}}) + R_1(\dot{\mathbf{q}}), \qquad D_2(\mathbf{q}, \dot{\mathbf{q}}) = C_2(\mathbf{q}, \dot{\mathbf{q}})$$

with $R_1(\dot{\mathbf{q}}) = b_1 \dot{q}_1$. This results in the dynamics

$$\begin{aligned}
\ddot{q}_1 &= \frac{-M_{12}(\mathbf{q})v_2 - D_1(\mathbf{q}, \dot{\mathbf{q}}) - K_1(\mathbf{q})}{M_{11}(\mathbf{q})}, \\
\ddot{q}_2 &= v_2
\end{aligned}$$

where

$$v_2 = k_P \left(q_2^d - q_2 \right) - k_D \dot{q}_2.$$

Following the suggestions as highlighted in [6], the ATAN control is selected for the desired angular displacement of the most distal pendulum, whereby

$$q_2^d = \left(\frac{2\alpha}{\pi}\right) \arctan \dot{q}_1.$$

With all the control parameters selected, we chose the physical parameters

$$\begin{aligned} m_1 &= 1 \text{ kg}, & m_2 &= 1 \text{ kg}, \\ l_1 &= 0.5 \text{ m}, & l_2 &= 1 \text{ m}, \\ L_1 &= 1 \text{ m}, & L_2 &= 2 \text{ m}, \\ I_1 &= 0.083 \text{ kg.m}^2, & I_2 &= 0.33 \text{ kg.m}^2, \\ g &= 9.81 \text{ m.s}^2 \end{aligned}$$

for the Acrobot (as chosen in the undamped case), which will be used to demonstrate the validity of the *gain selection criterion*. With these parameters, we demonstrate

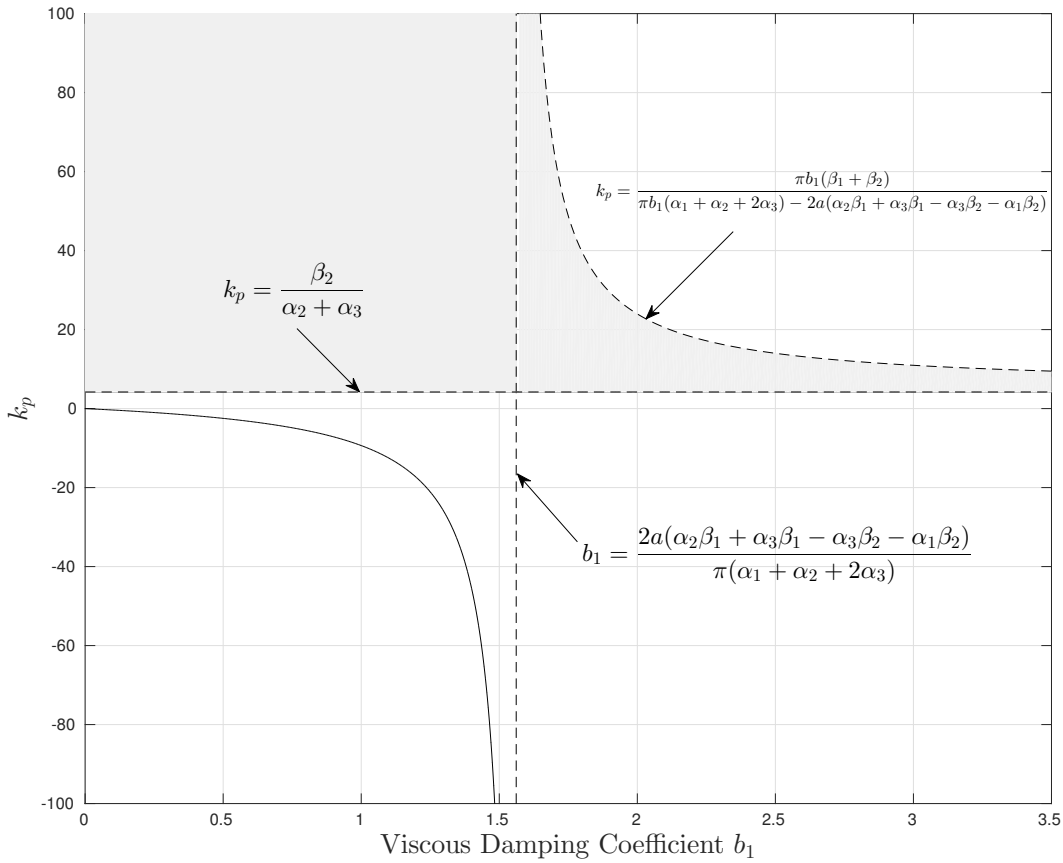

FIGURE 9.32: The RAG (grey shaded area) relating the gain k_P to the passive damping coefficient b_1.

the *gain selection criterion* for k_P that is associated with an unstable response about the FPEP for the Acrobot when compared to the value of passive damping found in the most proximal joint, indicated by the grey area in figure 9.32. This area is formally termed the *region of appropriate gains* (RAG). The boundaries of the RAG are demarcated by the minimum gain requirement described by

$$k_p = \frac{\beta_2}{\alpha_2 + \alpha_3} \tag{9.20}$$

and the damping coefficient dependent gain magnitude

$$k_p = \frac{\pi b_1 \left(\overline{\beta}_1 + \overline{\beta}_2\right)}{\pi b_1 \left(\overline{\alpha}_1 + \overline{\alpha}_2 + 2\overline{\alpha}_3\right) - 2\alpha \left(\overline{\beta}_1\overline{\alpha}_2 + \overline{\beta}_1\overline{\alpha}_3 - \overline{\beta}_2\overline{\alpha}_1 - \overline{\beta}_2\overline{\alpha}_3\right)}.$$

This gain magnitude converges with the k_P magnitude described in eq. (9.20) when $b_1 \to \infty$ and tends to $+\infty$ when

$$b_1 = b_{1_{\text{lim}}} = \frac{2\alpha \left(\overline{\beta}_1\overline{\alpha}_2 + \overline{\beta}_1\overline{\alpha}_3 - \overline{\beta}_2\overline{\alpha}_1 - \overline{\beta}_2\overline{\alpha}_3\right)}{\pi \left(\overline{\alpha}_1 + \overline{\alpha}_2 + 2\overline{\alpha}_3\right)}.$$

We shall now demonstrate the nature of the stability of the FPEP by initialising the Acrobot with the initial conditions

$$\begin{aligned} q_1(0) &= -\frac{101}{100}\pi, & q_2(0) &= 0, \\ \dot{q}_1(0) &= 0, & \dot{q}_2(0) &= 0 \end{aligned}$$

which places the Acrobot within an approximate neighbourhood of the FPEP, and by selecting a range of values for both k_P and b_1 that falls within and outside of the RAG. The results of these tests are shown in the figures 9.33-9.37. A decreasing level of mechanical energy of the Acrobot with a gain selection of $k_P = 3$ and damping coefficient selection $b_1 = 1.45$, which falls outside of the RAG, is demonstrated in figure 9.33. An increasing level of mechanical energy of the Acrobot with a gain selection of $k_P = 5$ and a damping coefficient selection of $b_1 = 1.45$, which falls within the RAG, is demonstrated in figure 9.34. A decreasing level of mechanical energy of the Acrobot with a gain selection of $k_P = 15$ and damping coefficient selection $b_1 = 2.6$, which falls outside of the RAG, is demonstrated in figure 9.35. An increasing level of mechanical energy of the Acrobot with a gain selection of $k_P = 12$ and a damping coefficient selection of $b_1 = 2.6$, which falls within the RAG, is demonstrated in figure 9.36. An increasing level of mechanical energy of the Acrobot with a gain selection of $k_P = 5$ and a damping coefficient selection of $b_1 = 11$, which falls within the RAG, is demonstrated in figure 9.37. These results are expected since they comply with the *gain selection criterion*.

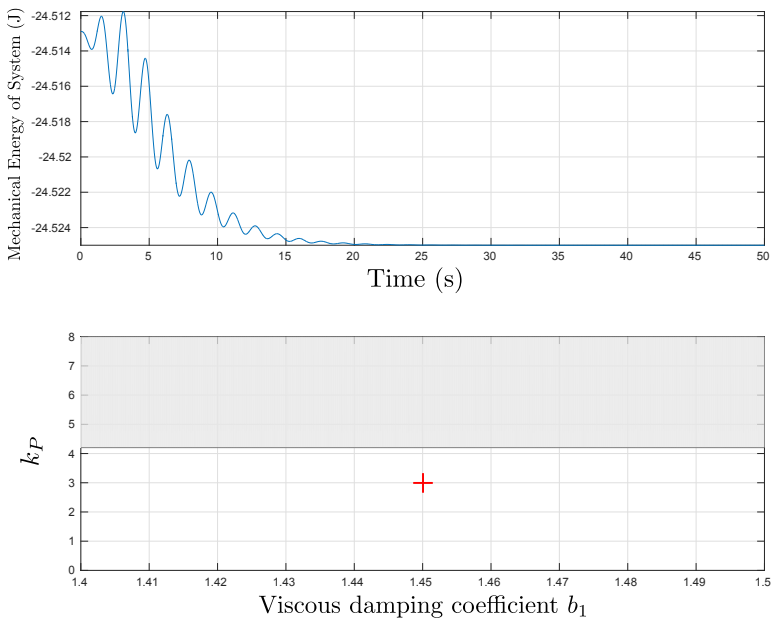

FIGURE 9.33: The stable response of a passively damped Acrobot initialised near the FPEP, with $k_P = 3$ ($0 < k_P < k_{P_2}$) and $b_1 = 1.45$ ($b_1 < b_{1_{\text{lim}}}$).

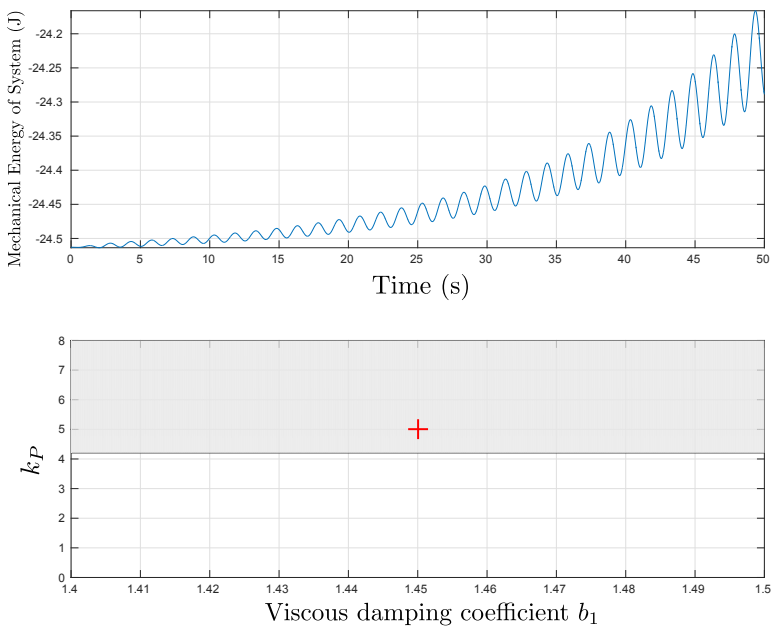

FIGURE 9.34: The unstable response of a passively damped Acrobot initialised near the FPEP, with $k_P = 5$ ($k_{P_2} < k_P < k_{P_3}$) and $b_1 = 1.45$ ($b_1 < b_{1_{\text{lim}}}$).

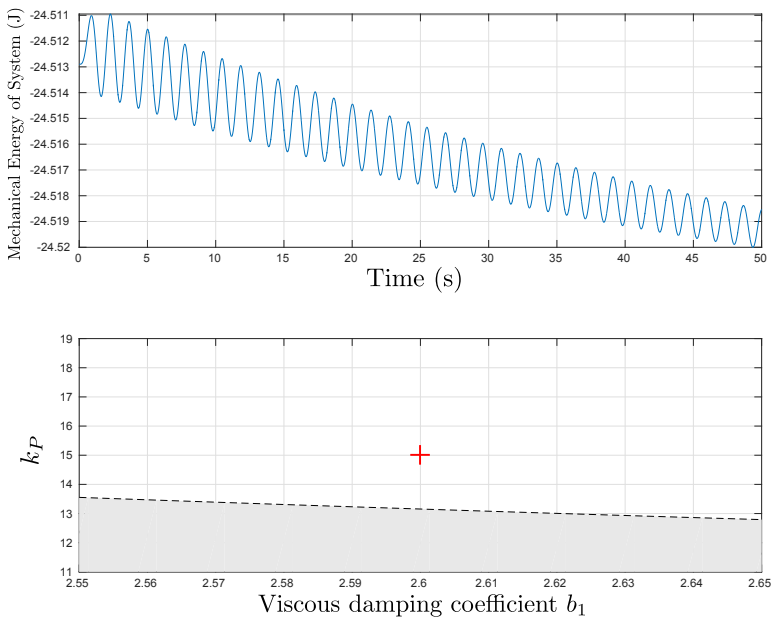

FIGURE 9.35: The stable response of a passively damped Acrobot initialised near the FPEP, with $k_P = 15$ ($k_P > k_{P_3}$) and $b_1 = 2.6$ ($b_1 > b_{1_{\text{lim}}}$).

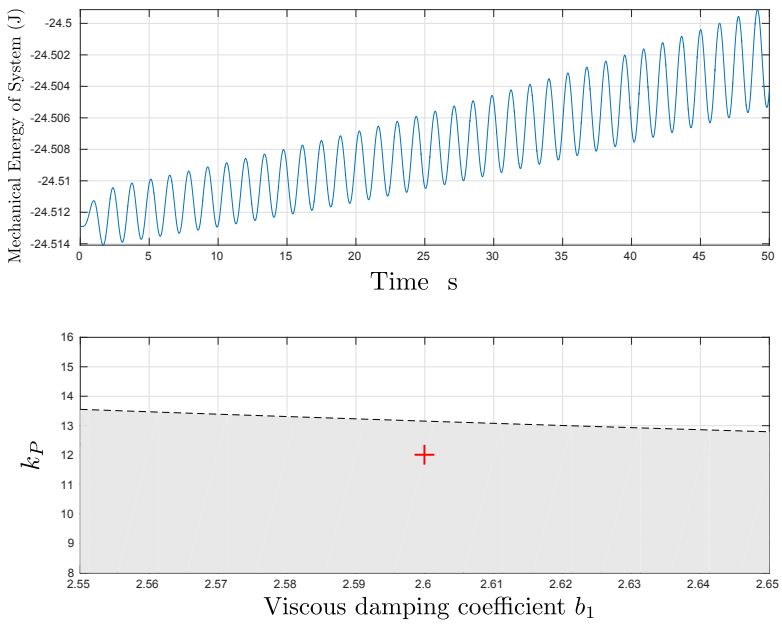

FIGURE 9.36: The unstable response of a passively damped Acrobot initialised near the FPEP, with $k_P = 12$ ($k_{P_2} < k_P < k_{P_3}$) and $b_1 = 2.6$ ($b_1 > b_{1_{\text{lim}}}$).

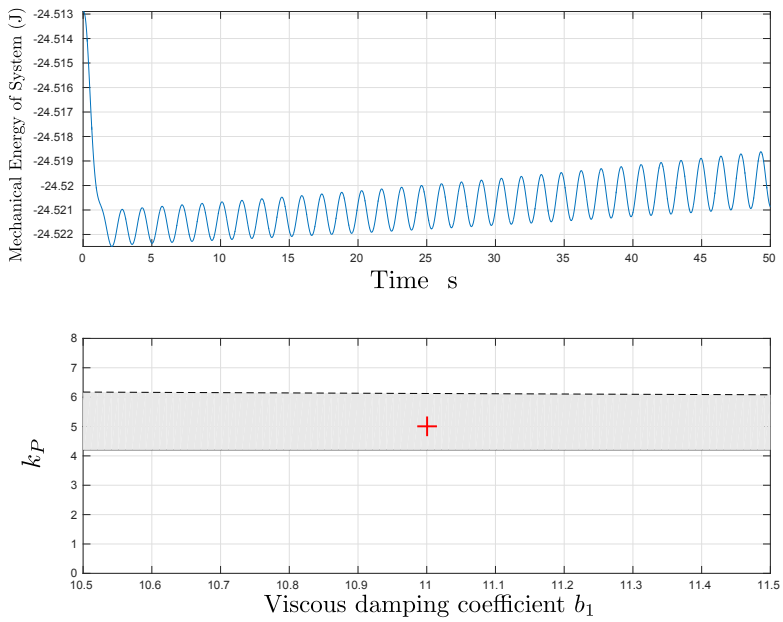

FIGURE 9.37: The unstable response of a passively damped Acrobot initialised near the FPEP, with $k_P = 5$ ($k_{P_2} < k_P < k_{P_3}$) and $b_1 = 11$ ($b_1 >> b_{1_{\text{lim}}}$).

We now demonstrate that the swing-up control of the passively damped Acrobot is possible through the choice of a passive damping coefficient b_1 and gain k_P that falls within the RAG. We selected the gains

$$k_D = 0, \qquad\qquad k_P = 19.58$$

desired swing angle

$$\alpha = \frac{\pi}{2}$$

and damping coefficient

$$b_1 = 2.4$$

with the initial conditions remaining the same as before. With these selections, we simulated the swing-up control of a passively damped Acrobot. The results of this simulation are demonstrated in the figures 9.38-9.41.

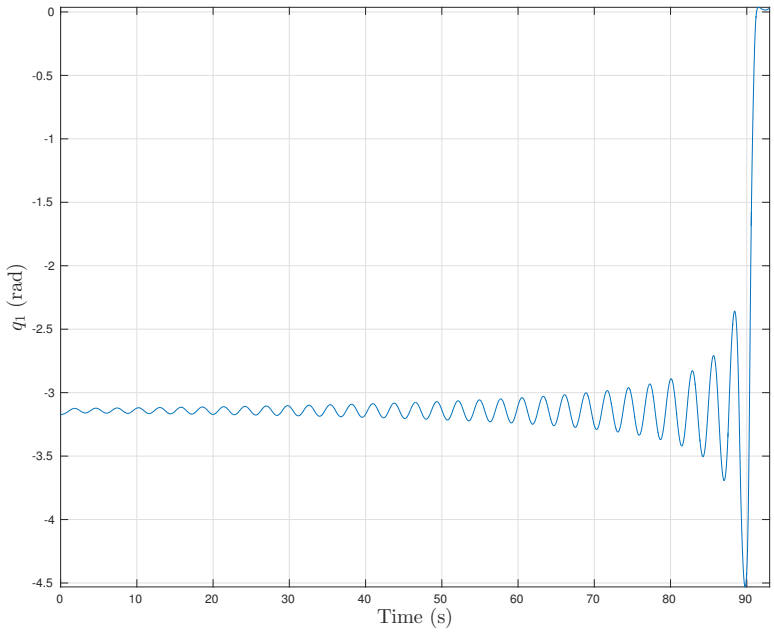

FIGURE 9.38: The angular displacement of the most proximal pendulum (q_1) of the passively damped Acrobot during ATAN swing-up control.

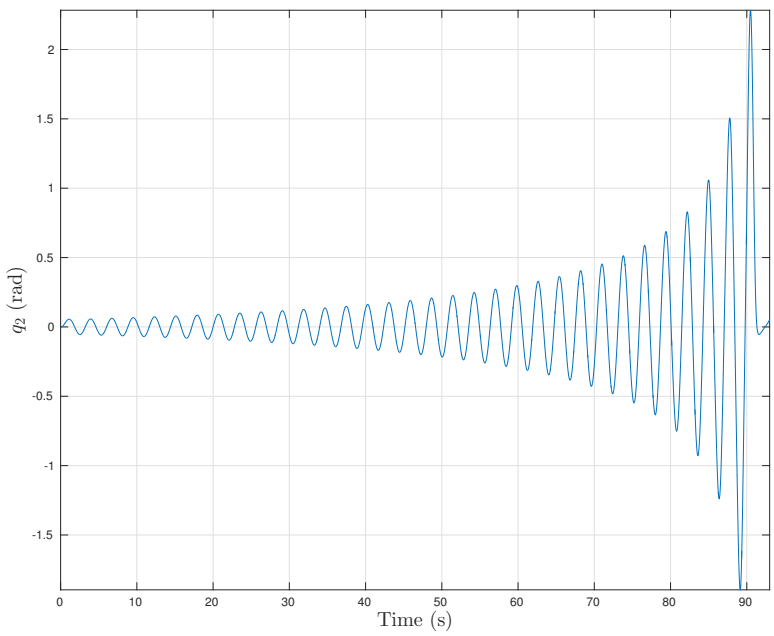

FIGURE 9.39: The angular displacement of the most distal pendulum (q_2) of the passively damped Acrobot during ATAN swing-up control.

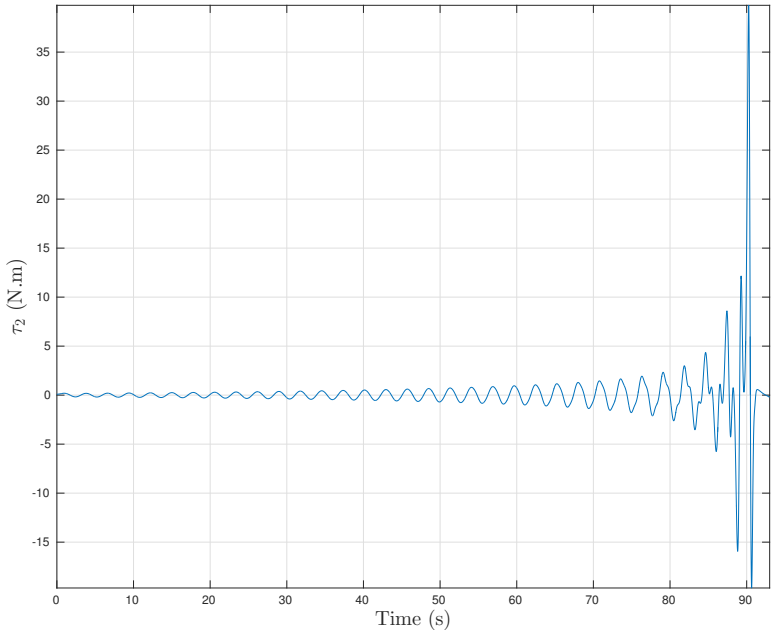

FIGURE 9.40: The torque used to produced swing-up control on the passively damped Acrobot using TCPFL and the ATAN controller.

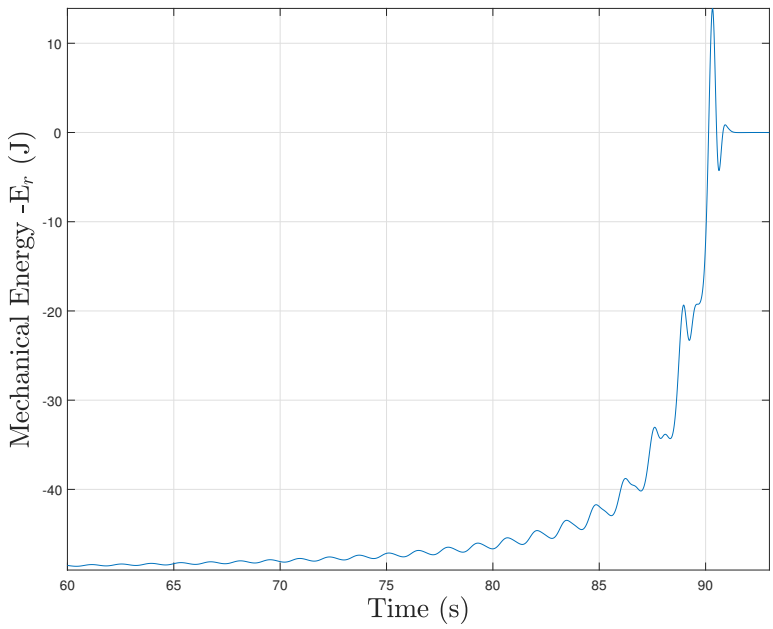

FIGURE 9.41: The difference between the mechanical energy of the passively damped Acrobot and E_r during swing-up control using TCPFL and the ATAN controller (beginning at 60 seconds).

The angular displacement of the proximal pendulum of the passively damped Acrobot that occurred during the swing-up control simulation is demonstrated in figure 9.38. The displacement of the proximal pendulum away from $q_1 = 0$ increased exponentially throughout the experiment, falling within the region of the UEP during the final swing-cycle which ended approximately 92 seconds into the simulation. The swing-up controller was not switched to an LQR controller during this simulation since the general LQR control law does not perform satisfactorily when passive damping is integrated into the system. A more robust regulator is required in this instance, but could not be applied to this system due to the stringent time constraints of the project. The angular displacement of the distal pendulum of the passively damped Acrobot that occurred during the swing-up control simulation is demonstrated in figure 9.39. The displacement of the distal pendulum away from $q_2 = 0$ increased exponentially throughout the simulation, falling within an approximate neighbourhood of the UEP after 92 seconds. The displacement did not plateau at $q_2 = 0$ after reaching this approximate neighbourhood since a regulator was not implemented. The torque that was exerted by the actuator on the passively damped Acrobot during the simulated swing-up control is demonstrated in figure 9.40. The magnitude of the torque increased exponentially throughout the experiment in response to the exponentially increasing angular displacements and angular velocities. The oscillating torque produced the unstable response seen in the angular displacements since the actuator introduced energy into the system with every swing-cycle. The mechanical energy of the passively damped Acrobot that was recorded during the swing-up control simulation is demonstrated in figure 9.41. The mechanical energy of the system increased exponentially throughout the experiment, with increments in the energy occurring with every swing cycle. The mechanical energy oscillated with every cycle, where the energy would initially reach a peak before rapidly dropping into a trough. The largest peak evidently occurred in the last swing-cycle before the energy fell within an approximate neighbourhood of E_r. The author believes that the spikes are a result of overexcitation by the actuator (which is rapidly corrected), but this assumption has not been confirmed.

We will now demonstrate that the *gain selection criterion* may be used to perform satisfactory swing-up control of higher-order passively damped TC-ROPA$_{n-1}$ robots, specifically the passively damped PAA robot in this case.

The Passively Damped PAA Robot

The PAA robot is modelled as the TC-ROPA$_2$ robot through the implementation of the FBL torques

$$\tau_2 = \hat{M}_{22}(\mathbf{q})v_2 + \hat{M}_{23}(\mathbf{q})v_3 + \hat{D}_2(\mathbf{q}, \dot{\mathbf{q}}) + \hat{K}_2(\mathbf{q}),$$
$$\tau_3 = \hat{M}_{32}(\mathbf{q})v_2 + \hat{M}_{33}(\mathbf{q})v_3 + \hat{D}_3(\mathbf{q}, \dot{\mathbf{q}}) + \hat{K}_3(\mathbf{q})$$

where

$$\hat{M}_{22}(\mathbf{q}) = M_{22}(\mathbf{q}) - \frac{M_{12}(\mathbf{q})M_{21}(\mathbf{q})}{M_{11}(\mathbf{q})}, \qquad \hat{M}_{23}(\mathbf{q}) = M_{23}(\mathbf{q}) - \frac{M_{13}(\mathbf{q})M_{21}(\mathbf{q})}{M_{11}(\mathbf{q})},$$
$$\hat{M}_{32}(\mathbf{q}) = M_{32}(\mathbf{q}) - \frac{M_{12}(\mathbf{q})M_{31}(\mathbf{q})}{M_{11}(\mathbf{q})}, \qquad \hat{M}_{33}(\mathbf{q}) = M_{33}(\mathbf{q}) - \frac{M_{13}(\mathbf{q})M_{31}(\mathbf{q})}{M_{11}(\mathbf{q})},$$
$$\hat{D}_2(\mathbf{q},\dot{\mathbf{q}}) = D_2(\mathbf{q},\dot{\mathbf{q}}) - \frac{M_{21}(\mathbf{q})}{M_{11}(\mathbf{q})}D_1(\mathbf{q},\dot{\mathbf{q}}), \quad \hat{D}_3(\mathbf{q},\dot{\mathbf{q}}) = D_3(\mathbf{q},\dot{\mathbf{q}}) - \frac{M_{31}(\mathbf{q})}{M_{11}(\mathbf{q})}D_1(\mathbf{q},\dot{\mathbf{q}}),$$
$$\hat{K}_2(\mathbf{q}) = K_2(\mathbf{q}) - \frac{M_{21}(\mathbf{q})}{M_{11}(\mathbf{q})}K_1(\mathbf{q}), \qquad \hat{K}_3(\mathbf{q}) = K_3(\mathbf{q}) - \frac{M_{31}(\mathbf{q})}{M_{11}(\mathbf{q})}K_1(\mathbf{q})$$

with

$$D_1(\mathbf{q},\dot{\mathbf{q}}) = C_1(\mathbf{q},\dot{\mathbf{q}}) + R_1(\dot{\mathbf{q}}), \qquad D_2(\mathbf{q},\dot{\mathbf{q}}) = C_2(\mathbf{q},\dot{\mathbf{q}}) \qquad D_3(\mathbf{q},\dot{\mathbf{q}}), = C_3(\mathbf{q},\dot{\mathbf{q}})$$

and $R_1(\dot{\mathbf{q}}) = b_1\dot{q}_1$. The application of these torques results in

$$\begin{aligned}
\ddot{q}_1 &= \frac{-M_{12}(\mathbf{q})v_2 - M_{13}(\mathbf{q})v_3 - D_1(\mathbf{q},\dot{\mathbf{q}}) - K_1(\mathbf{q})}{M_{11}(\mathbf{q})},\\
\ddot{q}_2 &= v_2,\\
\ddot{q}_3 &= -k_{D_3}\dot{q}_3 - k_{P_3}q_3
\end{aligned}$$

where

$$k_{D_3} = 2\omega_{n_3}, \qquad k_{P_3} = {\omega_{n_3}}^2$$

and

$$v_2 = k_P\left(q_2^d - q_2\right) - k_D\dot{q}_2.$$

Additionally, we selected

$$q_2^d = \left(\frac{2\alpha}{\pi}\right)\arctan\dot{q}_1.$$

The swing-up control of the TC-ROPA$_2$ robot is performed using the parameters

$$k_D = 0, \qquad k_P = 24.6, \qquad \alpha = \frac{\pi}{2}, \qquad b_1 = 2.4$$

as suggested by the *gain selection criterion*. The initial conditions

$$\begin{aligned}
&q_1(0) = -\frac{101}{100}\pi, && q_2(0) = 0, && q_3(0) = 0,\\
&\dot{q}_1(0) = 0, && \dot{q}_2(0) = 0, && \dot{q}_3(0) = 0
\end{aligned}$$

were selected for this experiment along with the system parameters

$$\begin{array}{lll} m_1 = 1 \text{ kg}, & m_2 = 1 \text{ kg}, & m_3 = 0.5 \text{ kg}, \\ l_1 = 0.5 \text{ m}, & l_2 = 0.5 \text{ m}, & l_3 = 0.5 \text{ m}, \\ L_1 = 1 \text{ m}, & L_2 = 1 \text{ m}, & L_3 = 1 \text{ m}, \\ I_1 = 0.083 \text{ kg.m}^2, & I_2 = 0.165 \text{ kg.m}^2, & I_3 = 0.165 \text{ kg.m}^2, \\ g = 9.81 \text{ m.s}^2 & & \end{array}$$

which adhere to the constraint shown in eq. (9.3). The results of the simulated swing-up control of the passively damped PAA robot are demonstrated in figures 9.42-9.47. The angular displacement of the most proximal pendulum of the passively damped TC-ROPA$_2$ robot that occurred during the swing-up control simulation is demonstrated in figure 9.42. The angular displacement of the proximal pendulum about $q_1 = 0$ increased exponentially throughout the simulation until it entered into a limit cycle approximately 56 seconds into the simulation (oscillating in the approximate range $-4.75 < q_1 < 0$). Ordinarily, the pendulum would eventually overshoot the objective since the control torque would continue to inject energy into the system. In this case, the energy that was introduced into the system by the swing-up controller was dissipated by the viscous damping friction present at the most proximal joint when the highest possible angular velocity was achieved, thus allowing the proximal pendulum to enter into a limit cycle. The angular displacement of the second pendulum of the passively damped TC-ROPA$_2$ robot that occurred during the swing-up control simulation is demonstrated in figure 9.43. The angular displacement of the second pendulum about $q_2 = 0$ increased exponentially until it entered into a limit cycle (approximately 56 seconds into the simulation), similar to what is seen with the proximal pendulum. This cycling behaviour is not seen in the second pendulum when LDM-related swing-up control is applied to the system, since the controller ensures that $q_2 \to 0$ during the steady-state phase of the swing-up control. A sufficiently robust regulator would need to be applied to ensure that the system achieves the desired inverted configuration. The angular displacement of the most distal pendulum of the passively damped TC-ROPA$_2$ robot that occurred during the swing-up control simulation is demonstrated in figure 9.44. The pendulum was strictly regulated about $q_3 = 0$ as required by the TCPFL controller, deviating off the objective by a maximum 4.1×10^{-12} radians, which is sufficiently small.

The phase portrait of the most proximal pendulum of the passively damped TC-ROPA$_2$ robot that occurred during the simulated swing-up control is demonstrated in figure 9.45. The boundaries of the limit cycle are not as symmetrical and uniform as what is seen in the undamped PAA robot during LDM-related swing-up control (figure 8.29), but the behaviour of the trajectory of the proximal pendulum was consistent throughout the experiment, with a slight deviation in the trajectory occurring with the very first swing-up in the limit cycle. The non-uniformity in the shape of the limit cycle is believed to be caused by the behaviour of the second

pendulum, which enters its own limit cycle. The torque produced by the actuator found between the second and most proximal joint during the swing-up control simulation is demonstrated in figure 9.46. The torque produced by the swing-up controller increased exponentially throughout the experiment in response to the exponentially increasing displacements and velocities of the most proximal and second pendulums. The torque then switched rapidly between the approximate range $-40 \leq \tau_2$ (N.m) < 50 as the system entered the limit cycle. This control torque profile would not be recommended in practical application since the rapid switching would place tremendous stress on the actuator. This can be solved through the introduction of a robust regulator as the system enters the limit cycle. The mechanical energy of the passively damped TC-ROPA$_2$ robot that occurred during the swing-up control simulation is demonstrated in figure 9.47. The mechanical energy increased exponentially throughout the experiment until the system reached the limit cycle. The mechanical energy would spike and dip over a large range (described approximately by $-25 < E$ (J) < 11) with each swing-cycle in the limit cycle. The system settled at the approximate magnitude E_r between each of these peaks and troughs. These spikes and dips are believed to be associated with the energy that is added to and dissipated from the system by the actuator (which produces large impulse torques during the transitions between peak and trough energy states).

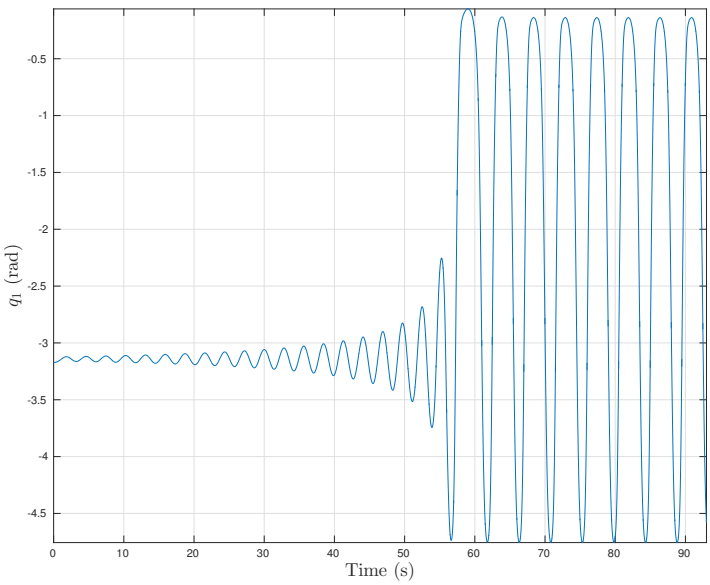

FIGURE 9.42: The angular displacement of the most proximal pendulum (q_1) of the passively damped PAA robot during TCPFL-related swing-up control.

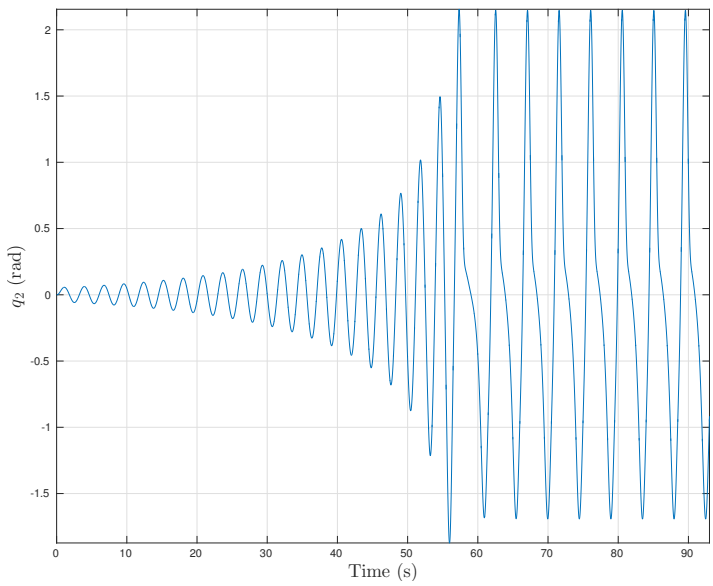

FIGURE 9.43: The angular displacement of the second pendulum (q_2) of the passively damped PAA robot during TCPFL-related swing-up control.

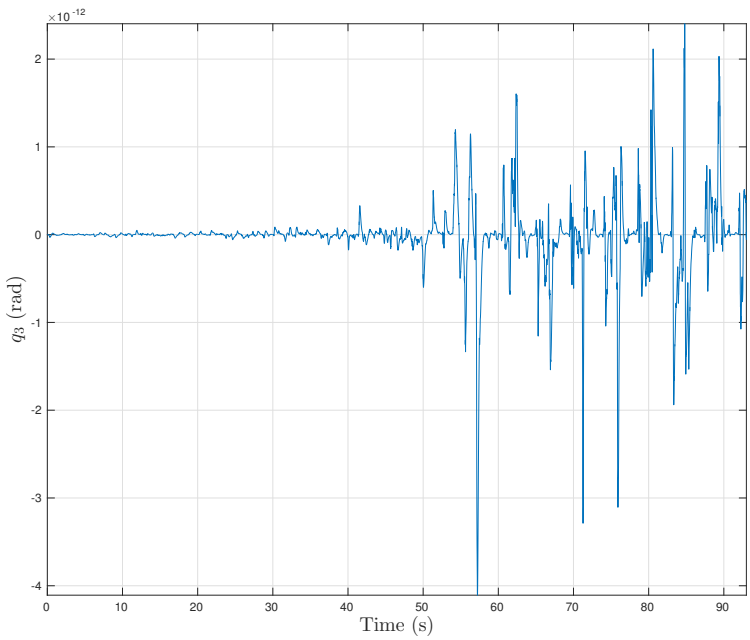

FIGURE 9.44: The angular displacement of the most distal pendulum (q_3) of the passively damped PAA robot during TCPFL-related swing-up control.

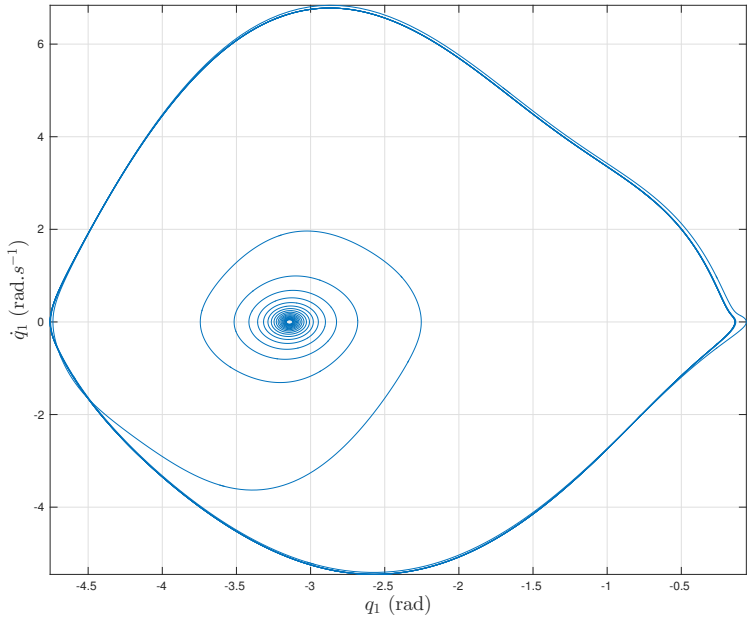

FIGURE 9.45: Phase plot of the most proximal pendulum of the passively damped PAA robot during TCPFL-related swing-up control.

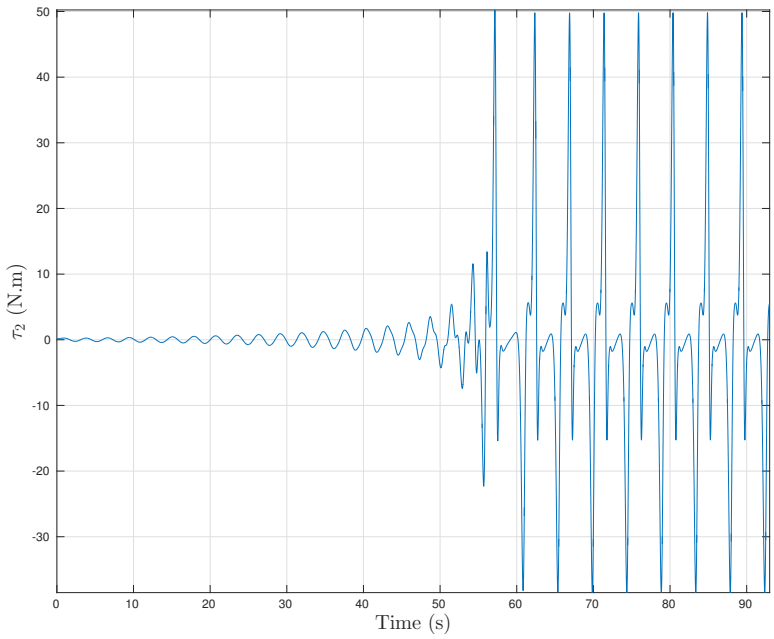

FIGURE 9.46: The torque used to produced swing-up control on the passively damped PAA robot using TCPFL and the ATAN controller.

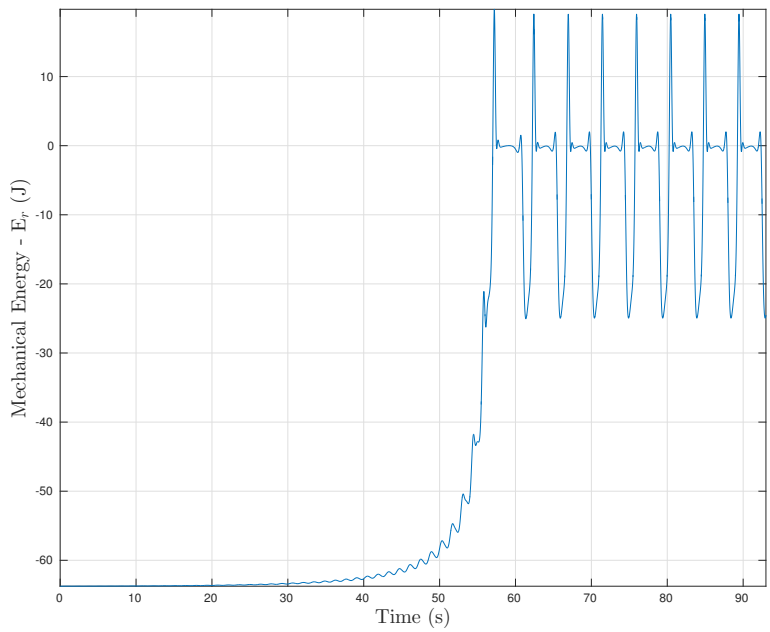

FIGURE 9.47: The mechanical energy of the passively damped PAA robot during swing-up control using TCPFL and the ATAN controller.

9.4.4 Discussion

We have demonstrated that the *gain selection criterion* is an important and relevant set of prerequisite conditions that will prevent undesirable stable responses by the underactuated robotic system when initiated approximately near to the FPEP. This set of conditions is not restricted to application on the Acrobot alone, since the implementation of the TCPFL technique allows for the reduced-order modelling of higher-order system (resulting in the TC-ROPA$_{n-1}$ robot). Despite the fact that we have been able to provide examples of how the implementation of ATAN swing-up control can overcome the limitation of Lyapunov-related control highlighted by the *matched damping condition*, there are a number of limitations that must be considered:

(i) This set of conditions is only applicable to the case of the viscously damped PA$_{n-1}$ robot. The effects of other forms of damping (including Coulomb and the Stribeck effect) are not considered, and will affect the performance of the system significantly if these friction models are integrated.

(ii) The control does not track the UEP. Instead, the feedback gains need to be perfectly tuned so that the system approaches an approximate neighbourhood of the UEP, where it can then be regulated about the UEP.

(iii) Traditional LQR controllers have a significantly smaller domain of operation when viscous damping is integrated into the PA$_{n-1}$ robot. More robust regulators are required to regulate the system about the UEP in the event that the gains cannot be perfectly tuned.

(iv) The fulfilment of the *gain selection criterion* will not guarantee satisfactory swing-up control. It only guarantees that the system will move away from the FPEP when the system is found sufficiently close to it. The trajectory may move towards the UEP subsequent to this, but it may also tend towards an orbit that results from the merging of two unstable manifold, one originating from the FPEP and the other from the UEP.

(v) It is apparent that the mass and length related proportions of the pendulums found in the system may affect the performance of the swing-up control, since the most proximal pendulum remains unactuated and relies on the transfer of energy from the distal set of pendulums. In the examples provided in this dissertation, the lengths and masses of each pendulum are relatively similar to one another. There are instances where, however, the proportions of the pendulum mass and lengths won't be so well aligned. For instance, if the most proximal pendulum is much longer and heavier than the combined lengths and masses of the distal set of pendulums, it will be difficult to perform full swing-up control, despite having a locally unstable FPEP, since a larger amount of energy will be required to deflect the most proximal pendulum as compared to the distal pendulums. Nothing can be done in this instance, but if the opposite were to occur (where the distal set of pendulums have a larger mass and length proportion as compared to the most proximal pendulum) this scenario can be remedied by relocating the swing-up control input further down the system (instead of allocating v_2 as the swing-up controller and v_i where $2 < i \leq n$ as the linearising controllers, one could instead choose v_2 as a linearising controller and v_j as the swing-up controller, where j represents the index of any pendulum found distal to the second pendulum). Such disproportionate systems may be rare to encounter, but this phenomenon must be considered. It is also important to note that the system parameters are also subject to the constraint highlighted in eq. (9.3). Failure to satisfy this constraint will result in the presence of a singularity in the system dynamics.

We shall now consider the circumnavigation of the limitation highlighted in the *matched damping condition* using NCPFL.

9.5 Convergence Algorithm

As with the TCPFL technique, the implementation of the NCPFL technique on the PA$_{n-1}$ results in the linearisation of a portion of the system's dynamics, resulting in the NC-ROPA$_{n-1}$ robot. This robot is formally defined below:

Definition 9.5. The NC-ROPA$_{n-1}$ robot is a reduced-order representation of the PA$_{n-1}$ robot that results from the linearisation of the $n-1$ most proximal pendulums of the system, where the dynamics of the ith pendulum (where $1 < i < n-1$) is regulated about $q_i = 0$. The $n-1$ most proximal pendulums thus collectively represent a single pendulum described by linear dynamics. The system closely approximates the behaviour of a Noncollocated Partial Feedback Linearised Acrobot, provided that the selected response frequency of the actuators involved in non-oscillatory regulation is sufficiently large and that $q_i(0) = 0$.

The nature of the setup obviates the need for multiple swing-up cycles since the most proximal pendulum is directly controllable, and thus can be actuated by a control law that tracks the upright configuration. Successful swing-up control, however, requires that all the system's pendulums be configured in the inverted position. This requirement exists despite the fact that the nth pendulum is unable to track the UEP. How can we, therefore, achieve swing-up control? We offer the following proposition, as first suggested by Spong in [6]:

Proposition 9.2. ***Noncollocated-related Swing-up control of the NC-ROPA$_{n-1}$ robot:*** Swing-up control of the NC-ROPA$_{n-1}$ robot can be successfully executed if the system's configuration is perfectly tuned.

In other words, if the $n-1$ most proximal pendulums are collectively swung-up using a non-oscillatory linear feedback controller described by the actuator's response frequency ω_n, then the system will naturally tend toward the UEP if a perfectly tuned set of initial conditions are chosen for both the proximal $n-1$ pendulums and the nth pendulum. This has been suggested in [6] but the application of this solution is not provided. With this possible solution in mind, there are a few concerns that must be considered:

(i) If the linear state feedback control law for the most proximal $n-1$ pendulums is swung-up with a response frequency ω_n and an initial angular condition $q_1(0)$, what angular position $q_n(0)$ must the nth pendulum be initialised with to allow the satisfactory swing-up control of the system?

(ii) What is the minimum response frequency ω_n that must be used to produce satisfactory swing-up control if the $n-1$ proximal pendulums are collectively initialised at any angular position $q_1(0)$ within the range $q_1 \in (-\pi, \pi]$.

(iii) Can this form of swing-up control be used as a work-around for the limitation of the Lyapunov-related swing-up control of passively damped PA$_{n-1}$ robots highlighted in the *matched damping condition*?

Swing-up control in this case will be deemed satisfactory if, once the most appropriate end-states are achieved, the system can be regulated successfully with the use of a conventional LQR controller. The LQR controller is designed using MATLAB, as seen in [34].

At this point, we believe that there is no analytical method that can be used to address these concerns. Instead, we have developed an algorithm (referred to as the *convergence algorithm*) that graphically generates a set of solutions to the highlighted concerns for a NC-ROPA$_{n-1}$ robot described by a known set of physical properties (i.e. known masses, lengths etc.). This algorithm is based on the idea of convergence demonstrated by the convergent series

$$\lim_{n\to\infty}\sum_{i=1}^{n}\left(\frac{1}{2}\right)^{i}=1.$$

This idea of convergence is useful since we will be applying an iterative process to determine what value of $q_n(0)$ will be most appropriate in the NCPFL-related swing-up control using a particular actuator response frequency ω_n. We can manipulate the above convergent series to produce

$$2\pi\lim_{n\to\infty}\sum_{i=1}^{n}\left(\frac{1}{2}\right)^{i}=2\pi \tag{9.21}$$

which illustrates this point. Therefore, using an infinite number of iterations will allow us, in one extreme, to circle around the entire range of $q_n(0)$, where $q_n(0)\in(-\pi,\pi]$, halving the difference each time so we approach a certain value of $q_n(0)$ according to whether it overshoots ($q_n(T)>0$) or undershoots ($q_n(T)<0$) the inverted position by the end of the simulation at time T. It is evidently impossible to iterate an infinite number of times to determine the exact value of $q_n(0)$, but it is expected that the system will converge around the appropriate value of $q_n(0)$ with a small associated error if a sufficient number of iterations are used. This is shown by the series

$$q_{n_d}(0)=\pi\left(\pm\frac{1}{2}\pm\frac{1}{4}\pm\cdots\pm\left(\frac{1}{2}\right)^{k_{\max}}\right)$$

which either subtracts or adds a difference depending on the performance of the swing-up, where $q_{n_d}(0)$ represents value of $q_n(0)$ that results in the best swing-up performance and $k_{\max}$ represents the maximum number of iterations that is chosen by the user, referred to from here as the *maximum convergence index*.

This chapter is less detailed as compared to previous chapters due to this solution's experimental nature. Nevertheless, details of the execution of this algorithm (including results) are provided below, beginning with the representation of the NCPFL linearised PA$_{n-1}$ robot as a NC-ROPA$_{n-1}$ robot.

9.5.1 Preliminaries

Modelling the PA$_{n-1}$ Robot as the NC-ROPA$_{n-1}$ Robot

The NCPFL technique (derived in section 9.3.2) involves the linearisation of the most proximal pendulums, allowing for the representation of the PA$_{n-1}$ robot as an NC-ROPA$_{n-1}$ robot, as seen in figure 9.2. The implementation of the NCPFL technique results in the dynamical equations that are shown in eqs. (9.6a)-(9.6d). If one selects the initial conditions

$$\begin{aligned} q_2(0) &= 0, & \dot{q}_2(0) &= 0, \\ q_3(0) &= 0, & \dot{q}_3(0) &= 0, \\ &\vdots & &\vdots \\ q_{n-1}(0) &= 0, & \dot{q}_{n-1}(0) &= 0 \end{aligned}$$

then we can ensure that

$$q_2 \approx 0, \qquad q_3 \approx 0, \qquad \dots \qquad q_{n-1}(0) \approx 0$$

$\forall t$. This will be true so long as the response frequency of the linearising actuators are sufficiently large. The PA$_{n-1}$ robot can now be represented as a NC-ROPA$_{n-1}$ robot, described by the dynamics

$$\ddot{q}_1 = v_1, \tag{9.22a}$$

$$\overline{M}_{11}(\mathbf{q})v_1 + \overline{M}_{12}(\mathbf{q})\ddot{q}_n + \overline{D}_1(\mathbf{q}, \dot{\mathbf{q}}) + \overline{K}_1(\mathbf{q}) = 0 \tag{9.22b}$$

where

$$\begin{aligned} \overline{M}_{11}(\mathbf{q}) &= \overline{\alpha}_1 + \alpha_2 + 2\overline{\alpha}_3 \cos q_n, \\ \overline{M}_{12} &= \alpha_2 + \overline{\alpha}_3 \cos q_n, \\ \overline{D}_1(q_2, \dot{\mathbf{q}}) &= b_1\dot{q}_1 - \overline{\alpha}_3 \left(2\dot{q}_1\dot{q}_n + \dot{q}_n^2\right) \sin q_n, \\ \overline{K}_1(\mathbf{q}) &= -\overline{\beta}_1 \sin q_1 - \beta_2 \sin(q_1 + q_n) \end{aligned}$$

and

$$\begin{aligned} \overline{\alpha}_1 &= \overline{I}_1 + \overline{m_1 l_1}^2 + m_n \overline{L}_1^{\,2}, & \alpha_2 &= I_n + m_n l_n^{\,2}, \\ \overline{\alpha}_3 &= m_n l_n \overline{L}_1, & \overline{\beta}_1 &= \left(\overline{m_1 l_1} + m_n \overline{L}_1\right) g, \\ \beta_2 &= m_n l_n g, \\ \overline{m}_1 &= \sum_{i=1}^{n-1} m_i, & \overline{I}_1 &= \sum_{i=1}^{n-1} I_i, \\ \overline{L}_1 &= \sum_{i=1}^{n-1} L_i, & \overline{m_1 l_1} &= \sum_{i=1}^{n-1} m_i \left[l_i + \sum_{j=1}^{i-1} L_j \right], \end{aligned}$$

$$\overline{m_1 l_1{}^2} = \sum_{i=1}^{n-1} m_i \left[l_i + \sum_{j=1}^{i-1} L_j \right]^2 .$$

These parameters are constrained by the condition highlighted in eq. (9.7).

Algorithm Structure

The *convergence algorithm* is separated into two parts, each having a unique purpose. The first part of the algorithm is responsible for determining, if possible, the necessary initial configuration of the NC-ROPA$_{n-1}$ robot that would result in the end-states most closely approximating the UEP. This is done for $q_1(0) \in (-\pi, \pi]$ within a user-designated range of actuator response frequencies ω_n. The second (and latter) part of the algorithm is responsible for determining whether the end-states that were derived in the previous stage of the algorithm are sufficiently close enough to the UEP to be regulated by a conventional LQR controller. These unique partitions of the algorithm, referred to as the *swing-up* and *balance test* segments, are demonstrated in the following high-level flow charts respectively, with the application of the algorithm originally designed for execution in MATLAB. These figures are followed by an in-depth description of each function in the flow-charts, which are labelled numerically. It is also important to note that the success of the algorithm is contingent on the design of two separate Simulink models, one where the torque τ_2 is dedicated to swing-up the system, and another model where the torque τ_2 is used to regulate the system about the UEP using a LQR controller. The Simulink models used in this particular investigation are demonstrated in Appendix E.

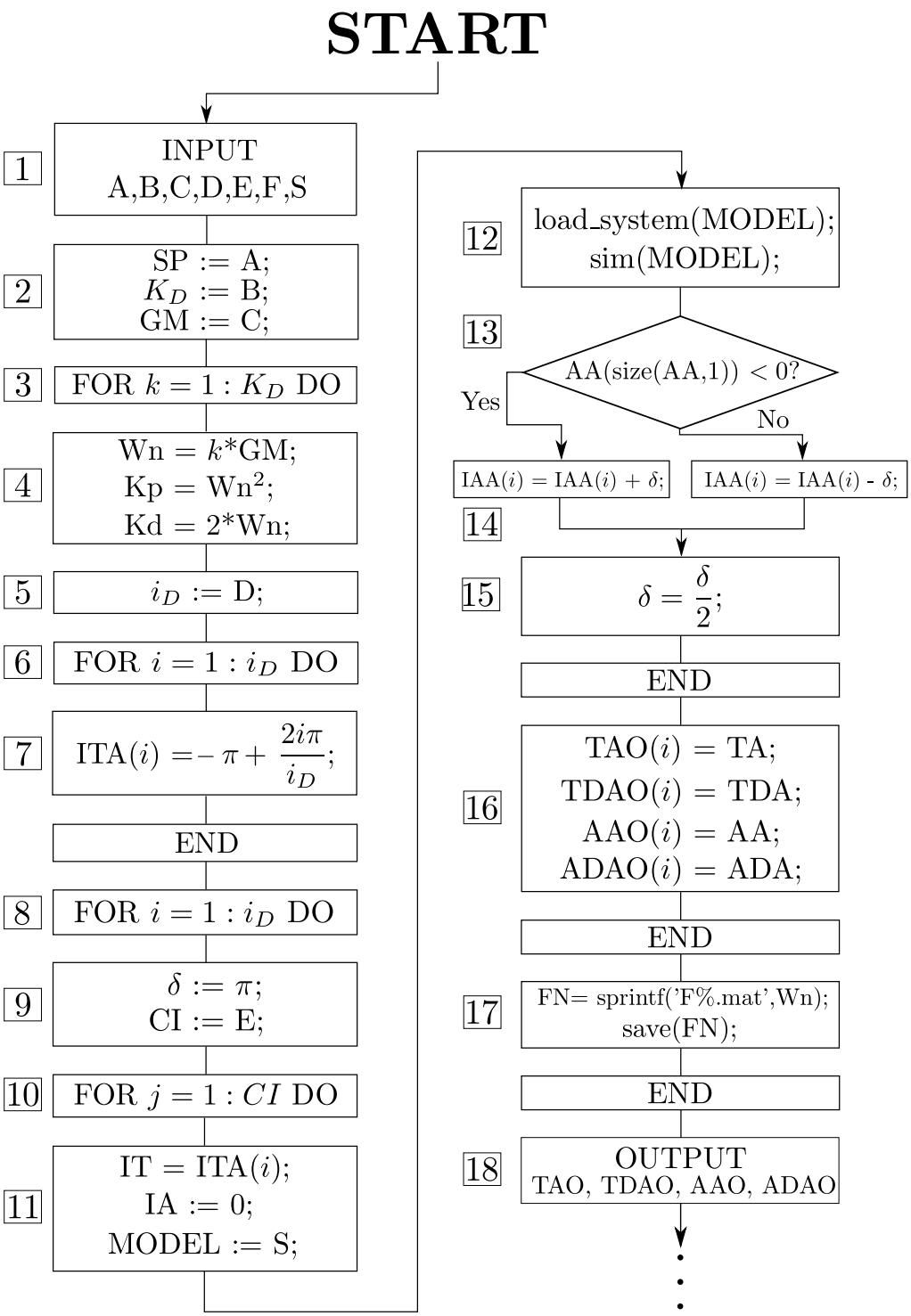

FIGURE 9.48: A high-level flow chart of the *swing-up* segment of the Convergence algorithm.

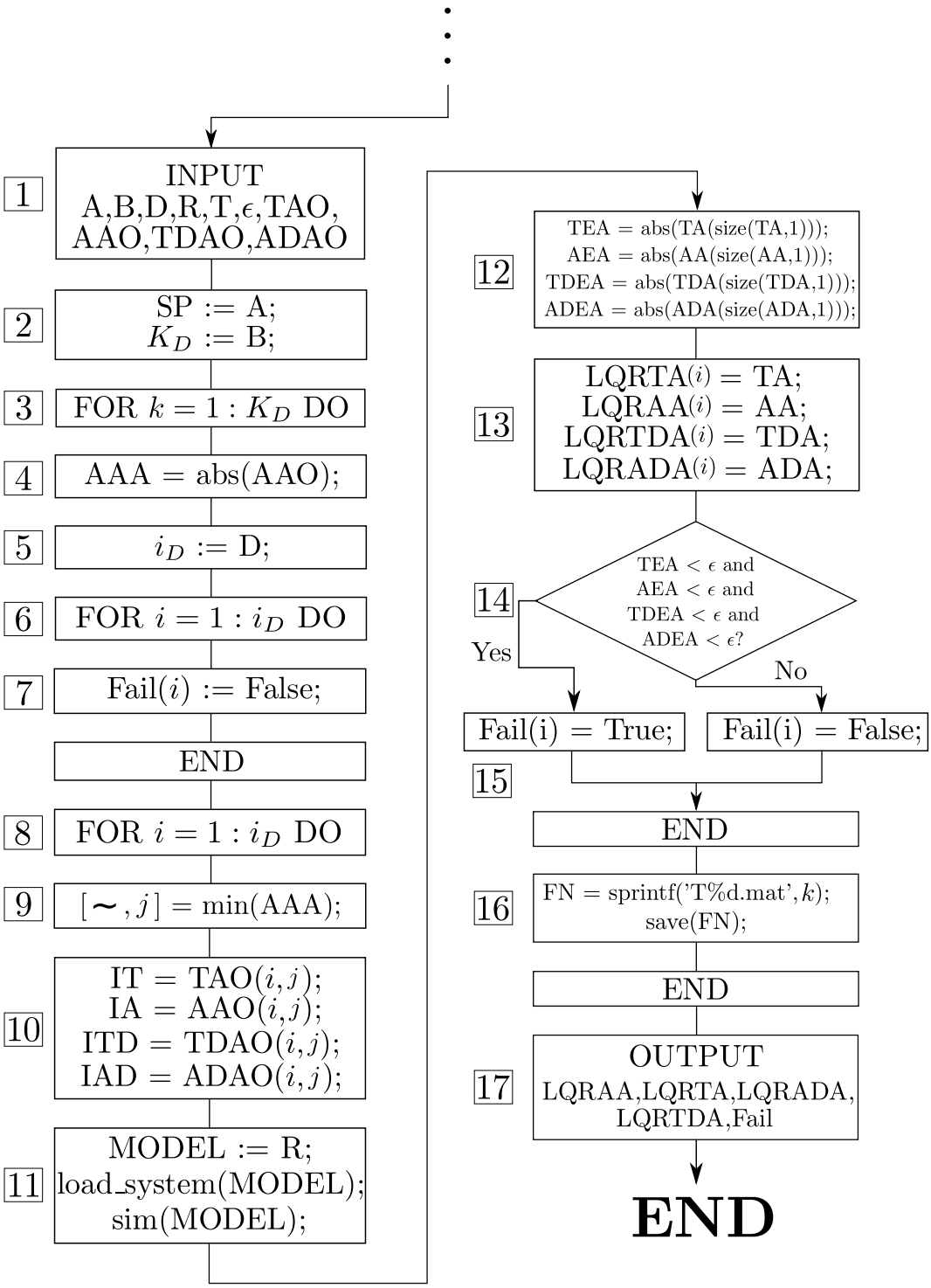

FIGURE 9.49: A high-level flow chart of the *balance test* segment of the Convergence algorithm.

Swing-up segment of convergence algorithm:

1 Declare the necessary input variables, which includes the system parameters described by the pendulum masses, lengths, damping coefficients etc. (A) , the actuator response frequency maximum index (B), the gain multiplication factor (C), the resolution of q_1 within the range $(-\pi, \pi]$ (D), the maximum convergence index (E), the filename prefix where the simulated data and algorithm segment output is stored (F), and the filename of the appropriate Simulink model that is simulated in this algorithm (S).

2 Initialise the systems parameters (SP), the actuator response frequency maximum index K_D, and the gain multiplication factor GM using the relevant input variables. It is important to note that varying sets of system parameters will be associated with varying sets of *convergence algorithm* results.

3 Iterate through each possible actuator response index from 1 to K_D. This will help to provide information on how the NCPFL-related swing-up control performs with respect to the implemented swing-up gains.

4 Set the actuator response frequency Wn which will be used to create a non-oscillatory tracking input using Kp and Kd.

5 Initialise the resolution of $q_1(0)$ within the range $(-\pi, \pi]$ (i_D) using the appropriate input variable D.

6 Iterate through each possible index between 1 and i_D so that each possible configuration of $q_1(0)$ may be populated in an array (with resolution i_D).

7 Populate the Initial Theta Array (ITA) with all possible values of $q_1(0) \in (-\pi, \pi]$ using the resolution i_D (Theta represents q_1 in this instance).

8 Iterate through each possible index between 1 and i_D so that each of the possible configurations of $q_1(0)$ within ITA may be tested with respect to the current actuator response frequency Wn.

9 Initialise the angular difference value δ to π. This variable will be used to converge the solution of $q_n(0)$ towards the most appropriate initial condition that will produce the best swing-up for the currently chosen Wn and $q_1(0)$. Additionally, initialise the maximum convergence index CI to the variable E. The value of CI represents the maximum number of iterations that the algorithm will perform until the system assumes convergence.

10 Iterate through each index between 1 and CI to generate a converged solution for $q_n(0)$.

11 Configure the current setup of the NC-ROPA$_{n-1}$ robot by initialising the Initial Theta (IT, which represents $q_1(0)$) to the ith entry of ITA and the Initial Alpha (represents $q_n(0)$) to zero (always begin with $q_n(0) = 0$ and use the difference variable δ to change $q_n(0)$ in the next simulation according to the performance

of the swing-up control). Initialise the MODEL variable to the appropriate filename of the Simulink model that will be simulated (S).

12 Load the Simulink model into MATLAB and simulate (using exception handling if required). This generates the results of the swing-up control using the currently chosen $q_1(0)$, $q_n(0)$, and Wn. These results are stored in the form of the following arrays: Theta Array (TA, which represents the stored values q_1 during this particular swing-up control), Alpha Array (AA, representing q_n), Theta Dot Array (TDA, representing the angular velocity of the most proximal pendulum $\dot{q}_1$), and Alpha Dot Array (ADA, representing $\dot{q}_n$).

13 Check the end-state value of AA (the last value in the array). Has the most distal pendulum overshot the target of an inverted configuration (is the end-state of AA > 0) or has it undershot (end-state of AA < 0)?

14 If the most distal pendulum has overshot, then decrease the initial condition of the most distal pendulum ($q_n(0)$) by the difference variable δ and store it in the IAA array. Conversely, if the most distal pendulum has undershot, then increase $q_n(0)$ by δ.

15 Half the difference variable δ for the next cycle so that a solution may be converged upon, as highlighted by the convergence series in eq. (9.21).

16 Populate the output arrays TAO (Theta Array Output), TDAO (Theta Dot Array Output), Alpha Array Output (AAO), and Alpha Dot Array Output (ADAO) with the resultant outputs of the simulation, namely TA, TDA, AA, and ADA respectively.

17 Create a file with the chosen filename prefix F and merge it with the suffix Wn to give the file a unique identification. Save the file.

18 The outputs TAO, TDAO, AAO, and ADAO are fed into the next segment of the algorithm, the *balance test* segment.

Balance test segment of convergence algorithm:

1 Declare the following new input variables: the file name of the appropriate Simulink model that will be used in this segment of the algorithm (R), the file name of the file which will ultimately store the results of the LQR results (T), and the acceptable range away from UEP (ϵ). Re-declare variables A,B, and D from the previous segment and retrieve the output variables TAO, AAO, TDAO, and ADAO.

2 Initialise the system parameters (SP) and the actuator response frequency maximum index K_D to the relevant input variables A and B respectively.

3 Iterate through each possible actuator response index from 1 to K_D. We shall, therefore, test the efficacy of the swing-up control for each possible actuator frequency up to the maximum actuator frequency, which is related to K_D.

4 Declare a new array name Absolute Alpha Array (AAA) which is the magnitude of AAO. This will be used to determine the angle that is closest to zero and its corresponding index in the array AA.

5 Initialise the resolution of $q_1(0)$ within the range $(-\pi, \pi]$ (i_D) using the appropriate input variable D.

6 Iterate through each of the possible indices from 1 to i_D for purposes of populating the Fail array, one of the main outputs of this segment.

7 Initialise the ith element of the Fail array with the Boolean value 'False'. This array will store the results of the LQR regulatory control (false if the regulation is successful, and true if it fails).

8 Iterate, once again, through the indices 1 to i_D to test the best swing-up solution of each instance of $q_1(0)$ within the kth gain selection to determine whether it will pass the LQR regulation test.

9 Find the angle within the array AAA that is closest to 0. This represents the point of the simulation where the second pendulum is closest to the inverted configuration. Initialise the index of this minimum value to the variable j.

10 Initialise the Initial Theta (IT), Initial Alpha (IA), Initial Theta Dot (ITD), and the Initial Alpha Dot (IAD) variables to the elements found in the ith row and the jth column. These variables are used to initialise the conditions for the model which is simulated in the next step.

11 Initialise the variable MODEL with the file name of the appropriate LQR model (R). Load the model onto MATLAB and simulate it (using exception handling if required). The results of this simulation are stored in the arrays Theta Array (TA), Alpha Array (AA), Theta Dot Array (TDA), and Alpha Dot Array (ADA).

12 Find the magnitudes of the end states of each of the resultant arrays of the simulation (TA, AA, TDA, ADA) and store them in the variables Theta End Array (TEA), Alpha End Array (AEA), Theta Dot End Array (TDEA), and Alpha Dot End Array (ADEA) respectively.

13 Choose the output matrix variables of this algorithm segment LQR Theta Array (LQRTA), LQR Alpha Array (LQRAA), LQR Theta Dot Array (LQRTDA), and LQR Alpha Dot Array to store the results of the simulation (TA, AA, TDA, and ADA respectively) in their i^{th} rows.

14 Check to see if the end-states fall within a small range of the UEP set by the variable ϵ after LQR control simulation.

15 If any of the end-states fall out of this region, then it is apparent that the LQR control has failed, and thus shows that the actuator response frequency Wn related to the index k is not large enough to swing-up the system to within

an acceptable domain of operation for the conventional LQR regulator. If the end-states do fall within this range, then LQR regulation was successful in this case. Store the results as a Boolean as the ith entry of the array Fail.

16 Create a file with the chosen filename prefix T and merge it with the suffix k to give the file a unique identification. Save the file.

17 The outputs LQRAA, LQRTA, LQRADA, LQRTDA, and Fail are regarded as outputs of this algorithm, which will be used in conjunction with the outputs of the previous segment to draw up a number of graphical figures.

The results of this convergence algorithm are demonstrated for the Acrobot (NCROPA$_1$ robot) in the section that follows. These results, along with the aforementioned break-down of the *convergence algorithm* have been included in a paper that has been accepted into the Control Conference Africa 2017 proceedings [111]. The full paper has been included in appendix F.

9.5.2 The Acrobot

Undamped Acrobot

The NCPFL-related swing-up control of the undamped Acrobot is achieved through the application of the FBL torque

$$\tau_2 = \hat{M}_{21}(\mathbf{q})v_1 + \hat{D}_2(\mathbf{q}, \dot{\mathbf{q}}) + \hat{K}_2(\mathbf{q})$$

derived in section 9.3.2, where

$$\begin{aligned}
\hat{M}_{21}(\mathbf{q}) &= M_{21}(\mathbf{q}) - \frac{M_{22}(\mathbf{q})M_{11}(\mathbf{q})}{M_{1n}(\mathbf{q})}, \\
\hat{D}_2(\mathbf{q}, \dot{\mathbf{q}}) &= D_2(\mathbf{q}, \dot{\mathbf{q}}) - \frac{M_{2n}(\mathbf{q})}{M_{1n}(\mathbf{q})} D_1(\mathbf{q}, \dot{\mathbf{q}}), \\
\hat{K}_2(\mathbf{q}) &= K_2(\mathbf{q}) - \frac{M_{2n}(\mathbf{q})}{M_{1n}(\mathbf{q})} K_1(\mathbf{q})
\end{aligned}$$

and

$$D_1(\mathbf{q}, \dot{\mathbf{q}}) = C_1(\mathbf{q}, \dot{\mathbf{q}}), \qquad D_2(\mathbf{q}, \dot{\mathbf{q}}) = C_2(\mathbf{q}, \dot{\mathbf{q}}).$$

This results in the dynamical equations

$$\begin{aligned}
\ddot{q}_1 &= v_1 = -k_D \dot{q}_1 - k_P q_1, \\
\ddot{q}_2 &= \frac{-M_{11}(\mathbf{q})v_1 - D_1(\mathbf{q}, \dot{\mathbf{q}}) - K_1(\mathbf{q})}{M_{12}(\mathbf{q})}.
\end{aligned}$$

As seen with the application of regulating FBL torques, we chose the non-oscillatory gains

$$k_D = 2\omega_n, \qquad k_P = {\omega_n}^2.$$

The *convergence algorithm* is executed with the system parameters

$$\begin{aligned} m_1 &= 1 \text{ kg}, & m_2 &= 1 \text{ kg}, \\ l_1 &= 0.5 \text{ m}, & l_2 &= 1 \text{ m}, \\ L_1 &= 1 \text{ m}, & L_2 &= 2 \text{ m}, \\ I_1 &= 0.083 \text{ kg.m}^2, & I_2 &= 0.33 \text{ kg.m}^2, \\ g &= 9.81 \text{ m.s}^2. \end{aligned}$$

which satisfy the condition in eq. (9.7) and have been selected specifically since swing-up control has been successfully achieved with this model in existing literature. The algorithm was simulated using an angular resolution of $\pi/128$ (for $q_1(0)$), a maximum convergence index of 25, a maximum actuator response index of 40 and a gain multiplication factor of 1. The simulations were performed using the Dortmund-Price fixed-time integrator package with a time-step of 0.01 seconds. Additionally, the gains

$$k_1 = -245.9821, \qquad k_2 = -98.4906, \qquad k_3 = -106.2845, \qquad k_4 = -50.0736$$

were used for the LQR controller that was implemented in the *balance test* segment of the *convergence algorithm*. The results of the convergence algorithm applied to the undamped Acrobot are demonstrated in figures 9.50-9.51.

The maximum values of the angular position of the most proximal pendulum ($q_1(0)$) that can be swung-up using NCPFL-related swing-up control described by the actuator response frequency ω_n evaluated after the *balance test* phase of the *convergence algorithm* is presented in figure 9.50. It is evident that a larger actuator response frequency will be required if the most proximal pendulum is initialised further away from the inverted position. It is also apparent that if an actuator response frequency of $\omega_n \geq 18$ rad.s^{-1} is used with this particular Acrobot, the controller will be able to swing-up the Acrobot from the most extreme position (the pendant position).

The angular initial condition that is required for the most distal pendulum ($q_2(0)$) if successful swing-up control is to be achieved using NCPFL for any particular initial condition $q_1(0)$ is presented in figure 9.51. This is demonstrated for three selected gains, namely $\omega_n = 5$ rad.s^{-1}, $\omega_n = 10$ rad.s^{-1}, and $\omega_n = 40$ rad.s^{-1}. It is evident that using an actuator response frequency $\omega_n \geq 18$ rad.s^{-1} ensures that swing-up can be achieved with any initial condition $q_1(0)$. Gains that exceed this limit accommodate for the linear relationship between $q_1(0)$ and $q_2(0)$. The range of successful initial conditions, however, reduces as ω_n drops below this limit. In

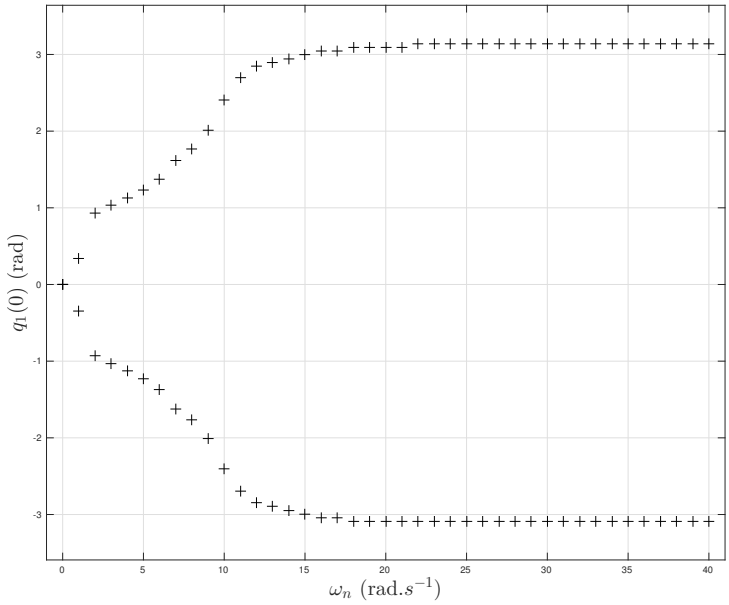

FIGURE 9.50: The minimum gain threshold required to swing-up an undamped Acrobot using NCPFL evaluated after the *balance test* phase of the *convergence algorithm*.

other words, the values of $q_1(0)$ that are found near the extremities (the pendant position) are not suitable for swing-up with a gain that is not sufficiently large since the Acrobot fails the *balance test*. This problem becomes more evident as ω_n drops well below the limit $\omega_{n_{\text{lim}}} = 18$. Additionally, the relationship between the initial conditions becomes non-linear, with the tails of the curves shown in figure 9.51 demonstrating a sharper gradient as compared to what is seen in the centre of the figure. We can thus conclude that it is possible to experimentally generate a set of necessary conditions with which to perform NCPFL-related swing-up control on the undamped Acrobot, but this has only been proven in one particular case.

We now demonstrate the NCPFL-related swing-up control on the undamped Acrobot using the information derived with the *convergence algorithm*. The initial conditions

$$q_1(0) = -2.3071, \qquad q_2(0) = 5.8562,$$
$$\dot{q}_1(0) = 0, \qquad \dot{q}_2(0) = 0$$

and actuator response frequency

$$\omega_n = 10 \text{ rad.s}^{-1}$$

were therefore selected. The results of this NCPFL-related swing-up control of the undamped Acrobot are shown in figures 9.52-9.54.

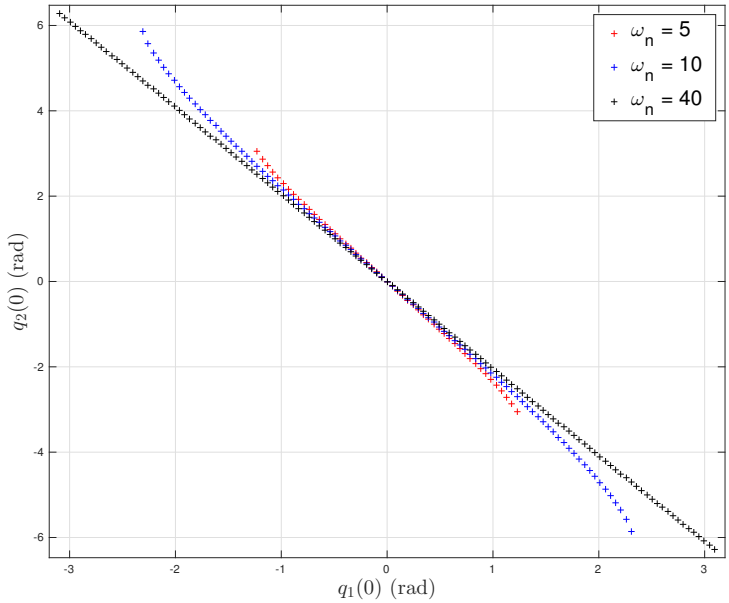

FIGURE 9.51: The relationship between the angular initial conditions that result in successful swing-up of the undamped Acrobot using the actuator response frequency $\omega_n = 5$ rad.s^{-1} (red), $\omega_n = 10$ rad.s^{-1} (blue), and $\omega_n = 40$ rad.s^{-1} (black).

The angular displacement of the proximal pendulum of the undamped Acrobot during the NCPFL-related swing-up control simulation is demonstrated in figure 9.52. The proximal pendulum tended exponentially towards $q_1^d = 0$ without the need for multiple swing-cycles as seen in the TCPFL case. The angular displacement of the distal pendulum of the undamped Acrobot during the NCPFL-related swing-up control simulation is demonstrated in figure 9.53. This pendulum was not controlled during the simulation, but was initialised at the specific initial condition indicated by the *convergence algorithm*. The natural dynamics of the system caused this pendulum to tend exponentially towards $q_2^d = 0$. The torque produced by the actuator on the undamped Acrobot during NCPFL-related swing-up control is demonstrated in figure 9.54. The torque transitioned once between negative and positive magnitudes to counteract the coupled dynamics introduced by the distal pendulum on the proximal pendulum during the swing-cycle. The torque subsequently tended towards zero as the pendulums approached their desired objectives. These results demonstrate that the *convergence algorithm* does indeed provide crucial information about system initialisation characteristics that are required to ensure the satisfactory NCPFL-related swing-up control of the Acrobot.

We shall now test the robustness of this algorithm by integrating the Acrobot with the viscous damping model, beginning first with the active viscous damping model.

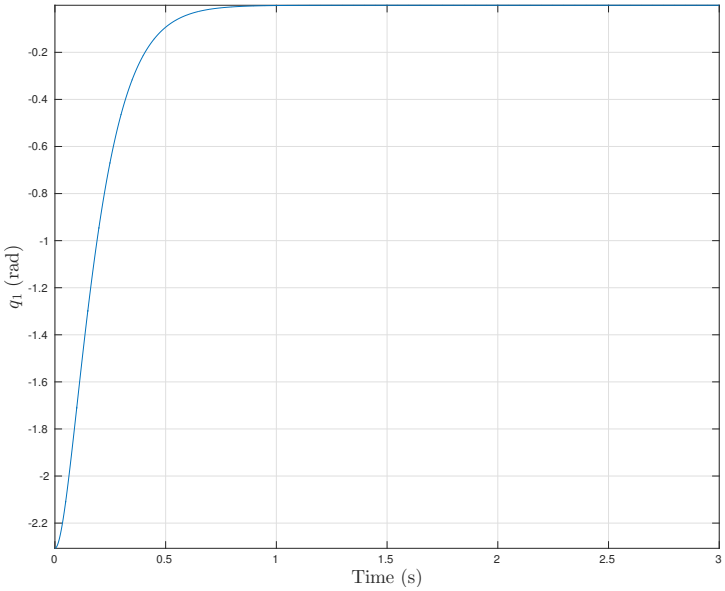

FIGURE 9.52: The angular position of the most proximal pendulum (q_1) of the undamped Acrobot during NCPFL-related swing-up control.

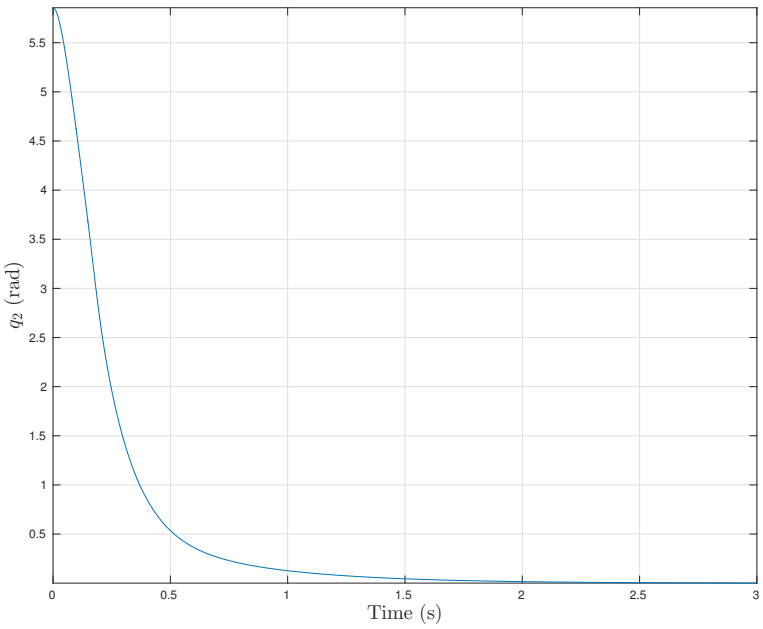

FIGURE 9.53: The angular position of the most distal pendulum (q_2) of the undamped Acrobot during NCPFL-related swing-up control.

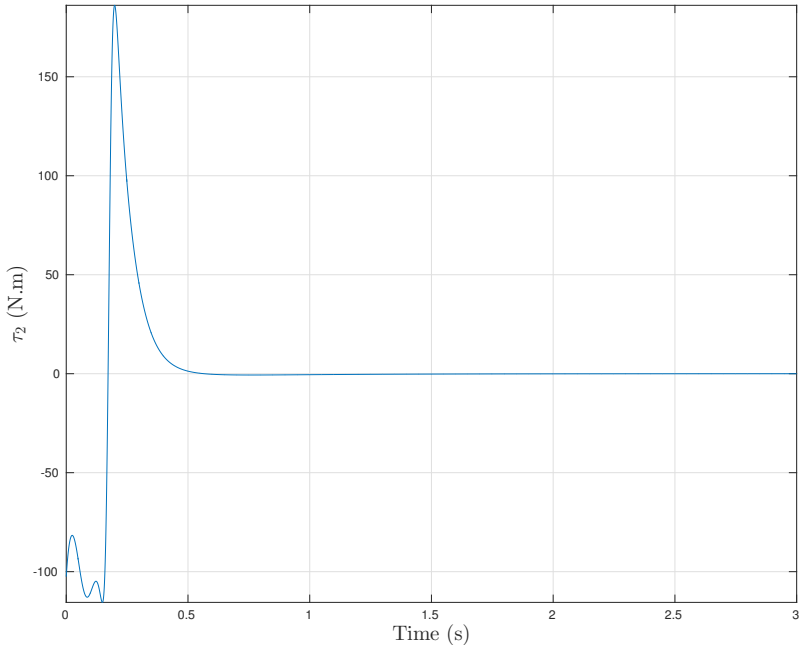

FIGURE 9.54: The torque required to perform swing-up control on an undamped Acrobot using NCPFL-related swing-up control.

Actively Damped Acrobot

As seen with the undamped case, the actively damped Acrobot is linearised with the NCPFL torque

$$\tau_2 = \hat{M}_{21} v_1 + \hat{D}_2(\mathbf{q}, \dot{\mathbf{q}}) + \hat{K}_2(\mathbf{q})$$

where

$$\begin{aligned}
\hat{M}_{21}(\mathbf{q}) &= M_{21}(\mathbf{q}) - \frac{M_{22}(\mathbf{q}) M_{11}(\mathbf{q})}{M_{1n}(\mathbf{q})}, \\
\hat{D}_2(\mathbf{q}, \dot{\mathbf{q}}) &= D_2(\mathbf{q}, \dot{\mathbf{q}}) - \frac{M_{2n}(\mathbf{q})}{M_{1n}(\mathbf{q})} D_1(\mathbf{q}, \dot{\mathbf{q}}), \\
\hat{K}_2(\mathbf{q}) &= K_2(\mathbf{q}) - \frac{M_{2n}(\mathbf{q})}{M_{1n}(\mathbf{q})} K_1(\mathbf{q})
\end{aligned}$$

and

$$D_1(\mathbf{q}, \dot{\mathbf{q}}) = C_1(\mathbf{q}, \dot{\mathbf{q}}).$$

The difference between the undamped and the actively damped case is seen in the definition of

$$D_2(\mathbf{q}, \dot{\mathbf{q}}) = C_2(\mathbf{q}, \dot{\mathbf{q}}) + R_2(\dot{\mathbf{q}})$$

where $R_2(\dot{\mathbf{q}}) = b_2\dot{q}_2$. Nevertheless, the application of this torque results in the dynamics

$$\ddot{q}_1 = v_1 = -k_D\dot{q}_1 - k_P q_1,$$
$$\ddot{q}_2 = \frac{-M_{11}(\mathbf{q})v_1 - D_1(\mathbf{q}, \dot{\mathbf{q}}) - K_1(\mathbf{q})}{M_{1n}(\mathbf{q})}$$

which is identical to that of the undamped case. We can thus conclude that the addition of active damping to the Acrobot has no effect on the results of the *convergence algorithm* (when evaluated after the *swing-up* segment of the *convergence algorithm*) since the active damping is effectively negated by the swing-up torque τ_2. This results in the superposition of the swing-up torque and the damping-negation torque, but ultimately the *swing-up* segment of the *convergence algorithm* will generate identical gain selection thresholds and angular initial condition relationships seen in the undamped case. The integration of viscous damping does, however, affect the results produced by the *balance test* segment of the algorithm. These effects will be discussed in the section that follows.

The NCPFL-related swing-up control torque that is required to swing-up an undamped Acrobot (blue curve) and the actively damped Acrobot (red curve) is demonstrated in figure 9.55 for comparative purposes. This simulation was performed with the same gain, physical parameters and initial conditions seen in the undamped case, with $b_2 = 10$.

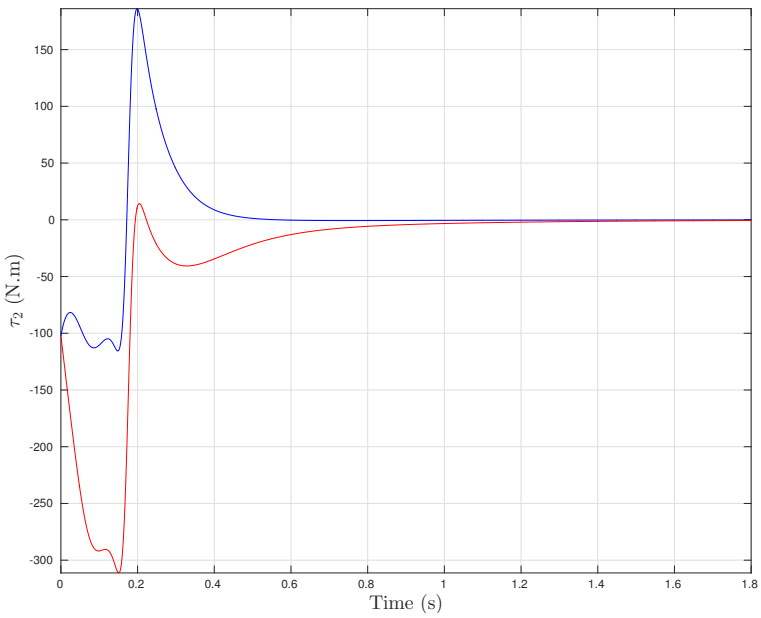

FIGURE 9.55: A comparison between the undamped swing-up torque (blue) and actively damped swing-up torque (red) required to perform NCPFL-related swing-up control on the Acrobot.

The discrepancy between the two curves represents the torque that was produced by the actuator to negate the viscous damping torques that were found at the active joint. Despite the presence of this discrepancy, the actively damped Acrobot behaved identically to the undamped Acrobot (figures 9.52 and 9.53) as predicted through the analytical analysis presented before these results. The convergence algorithm can thus be used to perform NCPFL-related swing-up control on the actively damped Acrobot.

We shall now investigate the performance of the *convergence algorithm* in the instance where NCPFL-related swing-up control is applied on a passively damped Acrobot. This experiment will demonstrate whether NCPFL-related swing-up control of a passively damped underactuated system is possible (and thus demonstrates the appropriateness of NCPFL-related swing-up control when applied as a work-around to the limitation highlighted by the *matched damping condition*).

Passively Damped Acrobot

The NCPFL torque,

$$\tau_2 = \hat{M}_{21} v_1 + \hat{D}_2(\mathbf{q}, \dot{\mathbf{q}}) + \hat{K}_2(\mathbf{q})$$

which has been used in the undamped and actively damped cases, is used to linearise the passively damped Acrobot, where

$$\begin{aligned}
\hat{M}_{21}(\mathbf{q}) &= M_{21}(\mathbf{q}) - \frac{M_{22}(\mathbf{q}) M_{11}(\mathbf{q})}{M_{1n}(\mathbf{q})}, \\
\hat{D}_2(\mathbf{q}, \dot{\mathbf{q}}) &= D_2(\mathbf{q}, \dot{\mathbf{q}}) - \frac{M_{2n}(\mathbf{q})}{M_{1n}(\mathbf{q})} D_1(\mathbf{q}, \dot{\mathbf{q}}), \\
\hat{K}_2(\mathbf{q}) &= K_2(\mathbf{q}) - \frac{M_{2n}(\mathbf{q})}{M_{1n}(\mathbf{q})} K_1(\mathbf{q})
\end{aligned}$$

and

$$D_2(\mathbf{q}, \dot{\mathbf{q}}) = C_2(\mathbf{q}, \dot{\mathbf{q}}).$$

The definition of $D_1(\mathbf{q}, \dot{\mathbf{q}})$ differs in this case, whereby

$$D_1(\mathbf{q}, \dot{\mathbf{q}}) = C_1(\mathbf{q}, \dot{\mathbf{q}}) + R_1(\dot{\mathbf{q}})$$

and where $R_1(\dot{\mathbf{q}}) = b_1 \dot{q}_1$. The application of this torque results in the dynamics

$$\begin{aligned}
\ddot{q}_1 &= v_1 = -k_D \dot{q}_1 - k_P q_1, \\
\ddot{q}_2 &= \frac{-M_{11}(\mathbf{q}) v_1 - D_1(\mathbf{q}, \dot{\mathbf{q}}) - K_1(\mathbf{q})}{M_{1n}(\mathbf{q})}.
\end{aligned}$$

The selection of the gains

$$k_D = 2\omega_n, \qquad k_P = {\omega_n}^2$$

results in the non-oscillatory tracking of the inverted position for q_1. We shall now demonstrate the results of the application of the *convergence algorithm* on the passively undamped Acrobot that is described by the physical parameters

$$\begin{aligned} m_1 &= 1 \text{ kg}, & m_2 &= 1 \text{ kg}, \\ l_1 &= 0.5 \text{ m}, & l_2 &= 1 \text{ m}, \\ L_1 &= 1 \text{ m}, & L_2 &= 2 \text{ m}, \\ I_1 &= 0.083 \text{ kg.m}^2, & I_2 &= 0.33 \text{ kg.m}^2, \\ g &= 9.81 \text{ m.s}^2, & b_1 &= 2.4 \end{aligned}$$

as seen in the undamped case (aside from the damping coefficient), and an angular resolution of $\pi/128$ (for $q_1(0)$), a maximum convergence index of 25, a maximum actuator response index of 40, and a gain multiplication factor of 10. The simulations were performed using the Dormand-Prince fixed-time integrator package with a time-step of 0.01 seconds. Additionally, the gains

$$k_1 = 80328, \qquad k_2 = 32131, \qquad k_3 = 31332, \qquad k_4 = 15668$$

were used for the LQR controller that was implemented in the *balance test* segment of the *convergence algorithm*. This results in the minimum gain threshold and relationships between the appropriate initial conditions demonstrated in figures 9.56 and 9.57.

The minimum gain threshold results that were produced upon evaluation of the *convergence algorithm* for the passively damped Acrobot after the *swing-up* segment (black) and after the *balance test* segment (red) is presented in figure 9.56. The end-states produced by the *swing-up* segment of the *convergence algorithm* are deemed, in this case, to be sufficiently close to the UEP if they fall within an absolute range $\epsilon = 1 \times 10^{-4}$ of the respective UEP state, where

$$|q_i(T) - q_{i_{\text{UEP}}}| < \epsilon, \tag{9.23a}$$

$$|\dot{q}_i(T) - \dot{q}_{i_{\text{UEP}}}| < \epsilon \tag{9.23b}$$

and where $1 \leq i \leq 2$. In this case, it seems that sufficient swing-up control can be performed for a maximum range $-2.3562 \leq q_1(0) \leq 2.3562$ when $\omega_n \geq 240$ rad.s^{-1}. If, however, we feed the end-states into the *balance test* segment, we find that the conventional LQR controller is significantly less capable of balancing the Acrobot as compared to the undamped case despite the fact that the Acrobot is found within a significantly small neighbourhood of the UEP (guaranteed by the conditions seen in eqs. (9.23a) and (9.23b)). It is evident, therefore, that the algorithm does in fact manage to determine the appropriate minimum gain threshold and initial condition

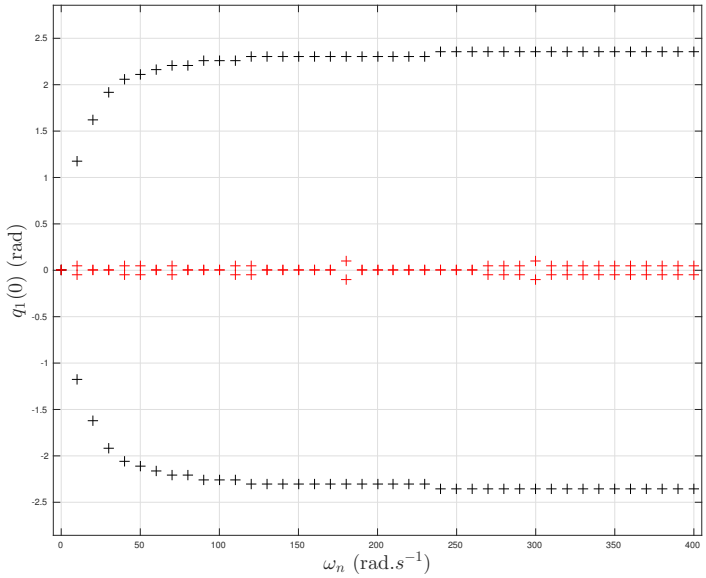

FIGURE 9.56: The minimum gain threshold required to swing-up a passively damped Acrobot using NCPFL evaluated after the *swing-up* phase (black) and after the *balance test* phase (red) of the *convergence algorithm*.

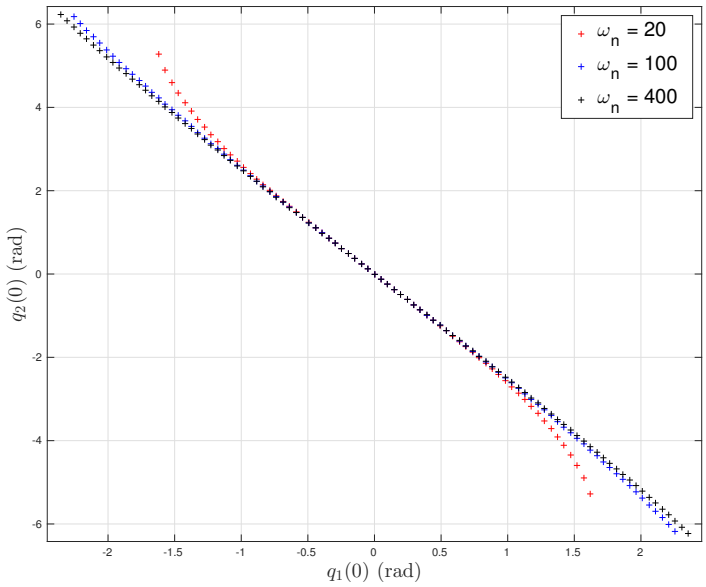

FIGURE 9.57: The relationship between the angular initial conditions that result in successful swing-up of the passively damped Acrobot using the actuator response frequency $\omega_n = 20$ rad.s^{-1} (red), $\omega_n = 100$ rad.s^{-1} (blue), and $\omega_n = 400$ rad.s^{-1} (black) evaluated after the *swing-up* phase of the *convergence algorithm*.

requirements to swing-up the Acrobot to within an approximate neighbourhood of the UEP, but a more robust regulating controller must be implemented when the Acrobot is viscously damped. This phenomenon is also evident in the actively damped case.

The angular initial condition that is required for the most distal pendulum ($q_2(0)$) if successful swing-up control is to be achieved using NCPFL for any particular initial condition $q_1(0)$ for the passively damped Acrobot is presented in figure 9.51. Drawing our attention to the results produced by the *swing-up* segment of the *convergence algorithm* demonstrated in figure 9.56, it is apparent that the possible range of angles for $q_1(0)$ shown in figure 9.57 plateaus at a value that is not representative of the fully-pendant configuration ($q_1(0) = \pi$), despite the fact that the maximum actuator response frequency selected in this instance is $10\times$ larger than the magnitude used in the undamped case. Therefore, regardless of the magnitude of actuator response frequency, this passively damped Acrobot cannot be swung-up successfully if $q_1(0)$ exceeds ± 2.3562 radians. The relationship between the appropriate initial conditions loses its linearity when the magnitude of the actuator response frequency ω_n falls below the limit of ≈ 240 rad.s^{-1}.

Despite the deficiency in regulating control, we are able to demonstrate the swing-up control of the passively damped Acrobot through the selection of an appropriate gain and angular initial condition pairing derived using the *convergence algorithm*, where

$$\begin{aligned} q_1(0) &= -2.3071, & q_2(0) &= 5.8562, \\ \dot{q}_1(0) &= 0, & \dot{q}_2(0) &= 0, \\ \omega_n &= 10 \text{ rad.s}^{-1}. \end{aligned}$$

The results of the NCPFL-related swing-up control of the passively damped Acrobot where $b_1 = 2.4$ is demonstrated in figures 9.58-9.60.

The angular displacement of the proximal pendulum of the passively damped Acrobot during the NCPFL-related swing-up control simulation is demonstrated in figure 9.58. The proximal pendulum tended exponentially towards q_1^d, which is expected. A robust regulator is required, however, to keep the pendulum within the neighbourhood of q_1^d. An LQR controller could not be implemented in this instance since it performed poorly (as demonstrated in figure 9.56). The angular displacement of the distal pendulum of the passively damped Acrobot during the NCPFL-related swing-up control simulation is demonstrated in figure 9.59. The pendulum was exponentially tending towards q_2^d, but the response of this pendulum was slower than that of the proximal pendulum since the damping torque could not be negated. The torque produced by the actuator on the passively damped Acrobot during NCPFL-related swing-up control is demonstrated in figure 9.60, which produced a similar response to what is seen in the undamped case.

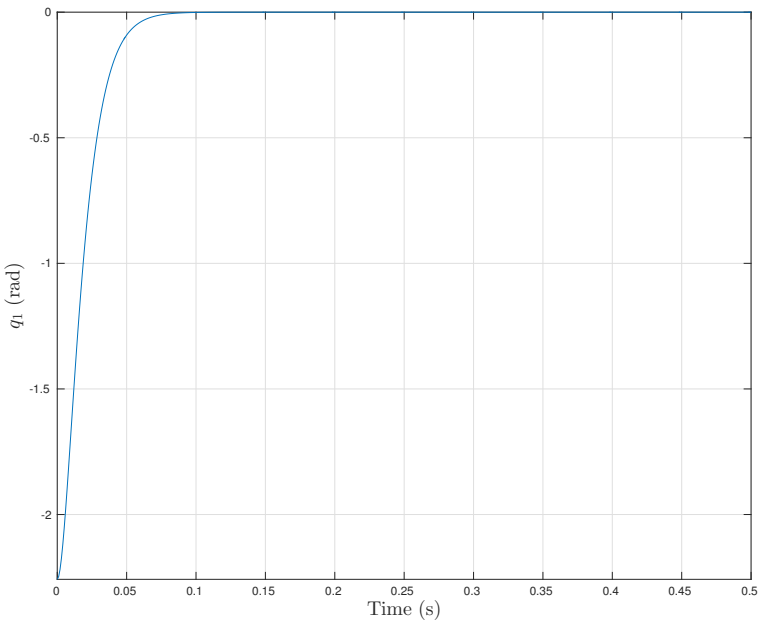

FIGURE 9.58: The angular position of the most proximal pendulum (q_1) of the passively damped Acrobot during NCPFL-related swing-up control.

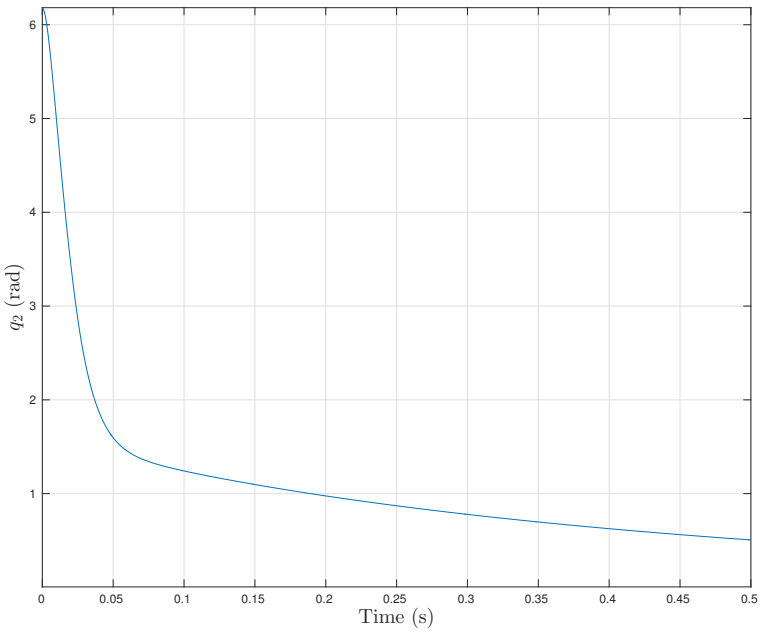

FIGURE 9.59: The angular position of the most distal pendulum (q_2) of the passively damped Acrobot during NCPFL-related swing-up control.

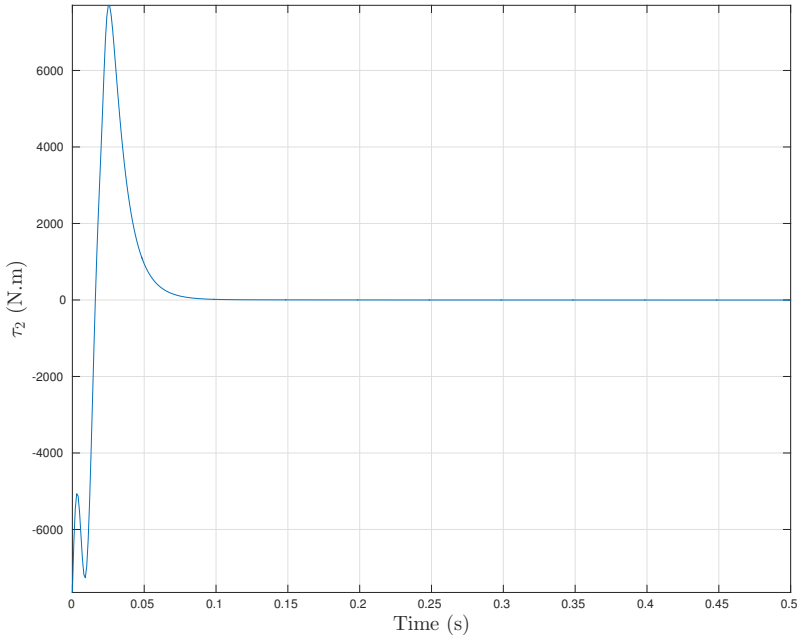

FIGURE 9.60: The torque required to perform swing-up control on a passively damped Acrobot using NCPFL-related swing-up control.

Whilst it is evident from these results that we can circumnavigate the *matched damping condition* using NCPFL-related swing-up control on the passively damped Acrobot, the performance of this controller can be improved with the use of a robust regulator. It is possible to implement the NCPFL-related swing-up control using the *convergence algorithm* on systems with an order $n > 2$ (such as the PAA robot), but we could not, unfortunately, produce these results due to the project's stringent time constraints. The higher-order system will, however, have to be modelled as the NC-ROPA$_{n-1}$ robot. We thus recommend that these simulations be produced in future work.

9.5.3 Discussion

Despite the fact that we could not generate an analytical solution for this application, we have demonstrated that the *convergence algorithm* can be used to facilitate the NCPFL-related swing-up control of an undamped, actively damped, and passively damped Acrobot, and thus provides an alternative work-around to the limitation of Lyapunov-related swing-up control highlighted in the *matched damping condition*. There are, however, a number of advantages and disadvantages that are associated with this form of PFL-related swing-up control:

(i) It is unknown whether the *convergence algorithm* will be able to demonstrate satisfactory swing-up control for a system that has been integrated with a different damping model.

(ii) Unlike the TCPFL-related swing-up control method, the NCPFL-related swing-up controller is able to bring the system to the completely inverted configuration without the need of swing-up cycles.

(iii) Whilst the controller does actively track the inverted position of the most proximal set of collective pendulums, the dynamics of the distal pendulum are unobservable. This control does not, therefore, track the UEP, a problem that is common among the PFL-related swing-up control techniques.

(iv) We have demonstrated that full-range swing-up control of all configurations of the passively-damped Acrobot (where $q_1(0) \in (-\pi, \pi]$) cannot be guaranteed.

(v) We have not experimentally demonstrated NCPFL-related swing-up control for systems described by $n > 2$.

(vi) The performance of the NCPFL-related swing-up control may also be affected by the disproportionate distribution of the masses and lengths of the pendulums within the pendulum system (a problem that may also affect the performance of the TCPFL-related swing-up control variant). If one imagines, for instance, that the distal pendulum is significantly smaller in length and mass as compared to the collectively represented set of proximal pendulums, it is apparent that a very large angular deflection of this distal pendulum would be needed for every incremental angular difference between the proximal collective set of pendulums and its inverted position to ensure satisfactory swing-up control. These disproportionate systems may not be commonly found in the field of underactuated robotics, but this issue must be considered in such an instance.

9.5.4 Conclusion

In this chapter, we addressed the *matched damping condition*, which highlights the inability to practically swing-up up a passively damped PA$_{n-1}$ robot using LDM-related swing-up control, through the implementation of PFL as a work-around. This resulted in the production of two contributions, namely the *gain selection criterion* (TCPFL) and the *convergence algorithm* (NCPFL). It is evident that, in both cases, the control torque used to produce the swing-up control on the passively damped PA$_{n-1}$ robot is not subject to the *invertibility* and *singularity* problems that were identified in the *matched damping condition*. Indeed, using both the *gain selection criterion* and the *convergence algorithm*, we were able to demonstrate the possibility of achieving swing-up control of passively damped systems using simulated results. There are, however, a number of advantages and disadvantages that are associated with each contribution.

Firstly, concerning the implementation of TCPFL, the associated contribution (the *gain selection criterion*) is analytical in nature, and is thus true for TC-ROPA$_{n-1}$ robots that are defined by any set of parameters. This control does, however, require

multiple swing-up cycles to achieve the objective since the dynamics of the most proximal pendulum are unobservable to the actuator. Additionally, the control does not track the UEP, and thus the gains need to be finely tuned if the system is to reach a sufficiently close neighbourhood of the UEP that will allow for appropriate regulation (using an LQR controller, for instance). The *gain selection criterion* guarantees that the system will have an unstable response if it is initialised within a sufficiently close neighbourhood of the FPEP.

Regarding NCPFL-related swing-up control, the swing-up control occurs without the need for multiple swing-up cycles since the most proximal pendulum is directly controllable. A non-oscillatory tracking control law can thus be designed for this pendulum, which results in the active tracking of its inverted state. The dynamics of the most distal pendulum remains unobserved, however, and thus the minimum gain and appropriate angular initial condition of the most distal pendulum are required to ensure satisfactory swing-up control. These parameters cannot be determined through analytical means, thus leading to the derivation of the *convergence algorithm*. As a result, the *convergence algorithm* must be executed for every NC-ROPA$_{n-1}$ robot that has a unique set of system parameters and damping properties. We were able to experimentally demonstrate simulated results of the *convergence algorithm* for the Acrobot, but we could not, unfortunately, demonstrate NCPFL-related swing-up control on higher-order systems due to time constraints. We suggest that these results should be demonstrated in future work. The simulated results demonstrated that the conventional LQR controller is not a satisfactory candidate regulator when attempting to balance the viscously damped system. The *balance test* segment of the *convergence algorithm* must thus implement a more robust regulator in future work. Additionally, we could not demonstrate an example in this research where a passively damped system could be swung-up using NCPFL from within an approximate neighbourhood of the FPEP. It is difficult to conclude whether such a range of swing-up control using NCPFL is possible due to the experimental nature of this contribution.

With these findings in mind, we can conclude that the implementation of PFL-related swing-up control can be used as a work-around to the limitation of LDM-related swing-up control highlighted in the *matched damping condition*, but this is contingent on the highlighted advantages and disadvantages of each variation of the PFL technique and their associated contributions.

"There is no real ending. It's just the place where you stop the story."
— Frank Herbert

Chapter 10

Conclusion and Recommendations

10.1 Conclusion

The objective of this research was to produce significant contributions to the field of mechatronics and underactuated robotics. To achieve this, we first constructed a control problem that is relevant to the field through the identification of an appropriate model (PA_{n-1} robot), control objective (swing-up control), and control technique (LDM) using existing literature. The results generated from the executed control problem were compared to the results found in existing literature. Upon the confirmation of the successful replication of these results, the robustness of the control technique was tested through the alteration of the model (integration of viscous damping). The contributions of this research are presented as work-arounds to the identified limitations in the control.

The implementation of swing-up control using LDM requires a substantial amount of mathematical rigour. Despite this, there is a substantial amount of literature that exists pertaining to the application of Lyapunov-related swing-up control, which justifies its selection for this project. This existing literature formed a solid foundation of reference for this research. Additionally, the control torque that results from this technique is designed specifically to track the UEP, thus requiring little intervention to achieve swing-up control. We were able to replicate the analytical and practical results seen in the work of Xin and Liu, which pertained to the LDM-related swing-up control of the undamped PA_{n-1} robot. We found that the integration of viscous damping into the actuated joints had no effect on the control since the actuator found on the same joint would simply negate the damping torques. The actively damped PA_{n-1} robot thus produced the same swing-up behaviour as the undamped PA_{n-1} robot. The addition of viscous damping on the passive joint, however, lead to the derivation of the control law that could not be solved due the *invertibility problem* (for systems that had $n > 2$). To address this issue, we attempted to reduce the order of the PA_{n-1} robot so that it may be approximately modelled as an Acrobot using the MCPFL technique (the resultant model is known as the MC-ROPA_{n-1} robot). However, it became evident that the swing-up control torque for the MC-ROPA_{n-1} robot (including the Acrobot, or MC-ROPA_2 robot) was subject to a conditional singularity (*singularity problem*). It became evident, therefore, that it is not possible

to derive a practical control law that will achieve the swing-up control objective when LDM-related swing-up control is applied to passively damped PA$_{n-1}$ robots, regardless of the order of the PA$_{n-1}$ robot. This is described as the *matched damping condition*.

There are a few ways to circumnavigate this problem. One such solution involves the derivation of another Lyapunov controller that is not subject to the invertibility and singularity problems. Another possible solution involves the application of Artstein's law, which suggests that the implementation of multiple LDM-related swing-up controllers which are activated when the control trajectory entered a particular operational domain, thus allowing for smooth stabilisability of the system trajectory. These solutions, while perfectly valid, are not practical since there is no truly formalised method of developing an appropriate Lyapunov function for any specific scenario. It is more practical, in this case, to implement another control technique that is fundamentally different to LDM in a theoretical nature. We thus chose to implement Partial Feedback Linearisation (PFL) related swing-up control that was originally demonstrated by Spong. The application of this technique is less mathematically rigorous, and the resultant control laws are derived not to track to the UEP, but to instead increase the system's mechanical energy until the system coincidently ends up sufficiently near the UEP (in the case of TCPFL) or to swing the proximal pendulum to the inverted position and assume that the most distal pendulums would follow suit (in the case of Noncollocated PFL, or NCPFL). We expected that the lack of rigidity in the control torque derivation would allow the system to be more robust to changes in system parameters, such as the introduction of passive damping, which was proven true since the derived torques for both variants of the PFL control law was not subject to the invertibility or singularity problems that are highlighted by the *matched damping condition*. We thus derived and presented two contributions that arose from the applications of the TCPFL and NCPFL techniques on the TC-ROPA$_{n-1}$ and NC-ROPA$_{n-1}$ robots respectively, namely the *gain selection criterion* and the *convergence algorithm*.

The *gain selection criterion* describes a set of analytically derived conditions that, when satisfied, guarantees the unstable behaviour of the TC-ROPA$_{n-1}$ robot when it is initialised within an approximate neighbourhood of the FPEP. The conditions refer to the selection of appropriate magnitudes for the swing-up gains k_P and k_D. This criterion acts as a necessary condition for swing-up control when the TC-ROPA$_{n-1}$ robot is initialised near the FPEP. Two separate cases of the *Gain Selection criterion* are derived for the undamped and passively damped TC-ROPA$_{n-1}$ robot. The *convergence algorithm* is an experimental solution that, once executed, determines the minimum actuator response frequency ω_n and the appropriate angular initial condition of the most distal pendulum ($q_2(0)$) that is required to perform NCPFL-related swing-up control on an undamped, actively damped, or passively damped NC-ROPA$_{n-1}$ robot that is initialised with a known set of system parameters, damping coefficients, and proximal pendulum initial angular condition ($q_1(0)$). Simulated

results of the ROPA$_2$ robot (Acrobot) and the TC-ROPA$_3$ robot (Traditional collocated Reduced-order PAA robot) demonstrate that it is indeed possible to swing-up a passively damped model using PFL-related swing-up control methods, but each of the variants (and the related contributions) are associated with a number of advantages and disadvantages. Firstly, the *gain selection criterion* (associated with the TCPFL technique) is an analytical solution, and thus the conditions described by this criterion holds true for TC-ROPA$_{n-1}$ robots with any unique set of system parameters and passive damping coefficient. Despite this, the nature of this form of control requires the steady introduction of energy into the system. This is done through multiple swing-up cycles, which may be disadvantageous if an instantaneous swing-up is desired. The result of these multiple swing-up cycles will produce a desirable swing-up if and only if the gains are finely-tuned. Finding these appropriate gains may be laborious, but the fine-tuning procedure is necessary to prevent undershooting or overshooting of the UEP. The application of the NCPFL-related swing-up control technique accommodates the instantaneous swing-up of the system since the dynamics of the proximal pendulum are linearised and directly controllable. The controller cannot, however, track the inverted position for the distal pendulum. Instead, the controller relies on the tuned positioning of the distal pendulum that will, once influenced by the dynamics of the proximal pendulum, follow a trajectory that will coincidently lead it to a neighbourhood that is sufficiently close to the UEP. The minimum gain and the initial angular condition of the distal pendulum ($q_n(0)$) cannot, to the knowledge of the author, be determined analytically, thus justifying the introduction of the *convergence algorithm*. The algorithm, since it is experimental in nature, needs to be executed for each uniquely configured NC-ROPA$_{n-1}$ robot. Simulation results of the *convergence algorithm* could only be provided for the Acrobot due to the project's stringent time constraints. These results demonstrated that it is indeed possible to determine minimum gain thresholds and appropriate initial conditions for a range of actuator response frequencies, but the integration of viscous damping into the system model results in the significant reduction of the region of operation of the conventional LQR controller, which ultimately compromises the performance of the *balance test* segment of the algorithm. Additionally, we could not show that NCPFL-related swing-up control could be performed for the full range $q_1(0) \in (-\pi, \pi]$.

In conclusion, the execution of the aforementioned research methodology accommodated the discovery of a key limitation in the implementation of LDM that prevents the swing-up control of passively damped underactuated robotic systems from becoming practically realisable. We have, however, demonstrated that this limitation can be overcome through the implementation of PFL-related swing-up control (as shown with the simulated results of the Acrobot and the PAA robot). The success of this swing-up control is, however, contingent on the satisfactory application of the *gain selection criterion* or the *convergence algorithm*. Additionally, each variant of swing-up control is associated with a number of advantages and disadvantages, which must be considered before a control technique is selected.

10.2 Recommendations

The results of the *gain selection criterion* demonstrates that the selection of a larger k_P value will increase the rate at which the system swings-up. It is believed, therefore, that the criterion can be optimised in terms of rate of swing-up, whereby the RAG can be dissected into areas which provide varying swing-up responses. The stringent time constraints of this project prevented the simulation of the NCPFL-related swing-up control of the NC-ROPA$_{n-1}$ robot with $n > 2$ using the *convergence algorithm*. These results should be provided in future work to supplement the results that have included in this dissertation. Additionally, a regulator that is better suited to the balancing of viscously damped systems should be integrated into the *balance test* segment of the *convergence algorithm* to improve its performance. Furthermore, the performance of the *convergence algorithm* could be improved through the integration of existing algorithms, such as the Newton method.

The contributions provided in this research project can be extended on through the integration of more complex friction models that will more closely approximate the frictional effects that are observed in real-world rotational mechanical systems, such as Coulomb damping, the Stribeck effect and the absolute damping observed in [104]. Additionally, focussing on the development of economical solutions, it may be beneficial to investigate the ability to replace certain regulating actuators in an underactuated system with torsional springs. The feasibility of this application can first be tested on a planar system that acts perpendicularly to the field of gravity. The effects of viscous damping and other frictional forces can be added in once this concept is proven. The project can then be expanded to consider the simulation of the swing-up control technique on 3D models, with the ultimate extension involving the replication of the presented simulated results upon practical models of the undamped, actively damped, and passively damped Acrobot and the PAA robot.

References

[1] J. G. Broida, *Calculus of Variations*. University of Colorado, Boulder, October 2009.

[2] J.-J. E. Slotine and W. Li, *Applied Nonlinear Control*. New Jersey: Prentice-Hall Inc., 1991.

[3] Massachusetts Institute of Technology. Understanding poles and zeros. Department of Mechanical Engineering. Boston. From Chapter 2.14 of Lecture Notes: Analysis and Design of Feedback Control Systems. [Online]. Available: http://web.mit.edu/2.14/www/Handouts/PoleZero.pdf

[4] F. Garces, V. M. Becerra, C. Kambhampati, and K. Warwick, *Strategies for Feedback Linearisation: A Dynamic Neural Network Approach*. Springer-Verlag London, 2003.

[5] X. Xin and Y. Liu, *Control Design and Analysis for Underactuated Robotic Systems*. Springer-Verlag London, 2014.

[6] M. W. Spong, "Partial feedback linearisation of underactuated mechanical systems," *Proceedings of the IEEE/RSJ/GI International conference on Intelligent Robots and Systems '94 'Advanced Robotics and the Real World'*, vol. 1, pp. 314–321, September 1994.

[7] S. Lichiardopol, *A Survey on Teleoperation*, Technische Universiteit Eindhoven, Department of Mechanical Engineering, Dynamics and Control Group, Eindhoven, December 2007.

[8] J. Vertut and P. Coiffet, *Teleoperation and Robotics: Evolutions and Development*. Konan Page, 1986.

[9] M. W. Spong and M. Fujita, "Selected application domains for control: Control in robotics," in *The Impact of Control Technology*. IEEE, 2011, ch. 1.

[10] S. B. Fisher and S. Schnittger, "Innovation and autonomous technologies in the mining industry," *Autonomous and Remote Operation Technologies in the Mining Industry: Benefits and Costs*, pp. 23–24, February 2012.

[11] P. Coiffet and M. Chirouze, *An Introduction to Robot Technology*, 1st ed. Springer Netherlands, 1983.

[12] C. R. Janakiraman and B. M. Das, *Application of Artificial Intelligence and Robotics to Mining*. Springer Berlin Heidelberg, 1988.

[13] Y. Liu and H. Yu, "A survey of underactuated mechanical systems," Published through the University of Aberdeen, United Kingdom, 5 May 2012.

[14] H. Herr, G. P. Whiteley, and D. Childress, *Biologically Inspired Intelligent Robots*. SPIE Press, 2003, chapter 5: Cyborg Technology - Biomimetic Orthotic and Prosthetic Technology.

[15] R. Tedrake, *Underactuated Robotics: Learning, Planning and Control for Efficient and Agile Machines*. Massachusetts Institute of Technology, 2009.

[16] R. Full and D. Koditschek, "Templates and anchors: Neuromechanical hypothesis of legged locomotion on land," *The Journal of Experimental Biology*, vol. 202, pp. 3325–3332, 16 November 1999.

[17] A. Shkolnik and R. Tedrake, "High-dimensional underactuated motion planning via task space control," in *IEEE/RSJ International Conference on Robotics and Intelligent Systems*. IEEE, 22-26 September 2008, pp. 3762–3768.

[18] R. M. Murray, Z. Li, and S. Sastry, *A Mathematical Introduction to Robotic Manipulation: Robot Dynamics and Control*. CRC Press, 1994, ch. 4, pp. 155–210.

[19] M. Raibert, K. Blankespoor, G. Nelson, and R. Playter, "Bigdog, the rough-terrain quaduped robot," Boston Dynamics, Waltham, MA, Tech. Rep., 2008.

[20] X. Hu, T. J. Scharshmidt, D. D. Ohnmeiss, and I. H. Lieberman, "Robotic assisted surgeries for the treatment of spine tumours," *International Journal of Spine Surgery*, February 2015.

[21] Honda Motors Co. Ltd., *ASIMO: The Honda Humanoid Robot*, September 2007. [Online]. Available: http://asimo.honda.com/downloads/pdf/asimo-technical-information.pdf

[22] B. J. Hernandez and S. Piatrovich, "Spacex dragon air circulation system," American Institute of Aeronautics and Astronautics, Hawthorn, CA, Tech. Rep., 2011, published on NASA's journal archive.

[23] S. Thrun, M. Montemerlo, H. Dahlkand *et al.*, "Stanley: The robot that won the darpa grand challenge," *Journal of Field Robotics*, vol. 23, no. 9, pp. 661–692, June 2006.

[24] H. A. Yanco, A. Norton, W. Ober *et al.*, "Analysis of human-robot interaction at the darpa robotics challenge trials," *Journal of Field Robotics*, 2015, special Issue on the DARPA Robotics Challenge.

[25] J. I. Neimark and N. A. Fufaev, *Dynamics of nonholonomic systems*, ser. Translations of Mathematical Monographs. American Mathematical Society, Reprinted edition (July 16, 2004), vol. 33.

[26] A. M. Bloch, M. Reyanoglu, and N. H. McClamroch, "Control and stabilisation of nonholonomic dynamic systems," *IEEE Transactions on Automatic Control*, vol. 37, no. 11, pp. 1746–1757, November 1992.

[27] A. M. Bloch, J. E. Marsden, and D. V. Zenkov, "Nonholonomic dynamics," *Notices of the AMS*, vol. 52, no. 3, pp. 320–329, 2005.

[28] I. E. Paromtchik and C. Laugier, "Autonomous parallel parking of a nonholonomic vehicle," in *Proceedings of the 1996 IEEE Intelligent Vehicles Symposium*. Tokyo, Japan: IEEE, 19-20 September 1996, pp. 13–18.

[29] M. A. Fairus, S. N. S. Salim, I. W. Jamaludin, and M. N. Kamarudin, "Development of an automatic parallel parking system for a nonholonomic mobile robot," in *International Conference on Electrical, Control and Computer Engineering (INECCE)*. Pahang: IEEE, 21-22 June 2011 2011, pp. 45–49.

[30] K. Jiang, "A sensor guided parallel parking system for nonholonomic vehicles," in *Proceedings of the 2000 IEEE Conference on Intelligent Transportation Systems*. Dearborn, MI: IEEE, 1-3 October 2000, pp. 270–275.

[31] M. Grossman and A. Gmiterko, "n-link inverted pendulum, lqr control, some observations," in *AT&P Journal PLUS1*. Riadenie Mechatronickych Systemov, 2008, pp. 62–65.

[32] A. Gmiterko and M. Grossman, *Recent Advances in Mechatronics 2008-2009*. Springer, 2009, ch. 27: n-link Inverted Pendulum Modeling, pp. 151–157.

[33] A. K. Stimac, "Standup and stabilization of the inverted pendulum," Master's thesis, Department of Mechanical Engineering at the Massachusetts Institute of Technology, Boston, USA, June 1999.

[34] M. W. Spong, "The swing-up control problem for the acrobot," in *Proceedings of the Conference of IEEE Control Systems*, vol. 15, no. 1. IEEE, February 1995, pp. 45–55.

[35] H. H. Niemann and J. K. Poulsen, "Analysis and design of controllers for a double inverted pendulum," in *Proceedings of the American Control Conference*, vol. 4. Denver, Colorado: IEEE, 4-6 June 2003, pp. 2803–2808.

[36] P. Larcombe, "On the control of a two dimensional multi-link inverted pendulum: Co-ordinate system suitability for dynamic formulation," in *Proceedings of the 30th Conference on Decision and Control*, vol. 1, IEEE. Brighton, England: IEEE, December 1991, pp. 136–141.

[37] H. P. Gavin, "Generalized coordinates, lagrange's equations, and constraints," Department of Civil and Environmental Engineering, Duke University, CEE 541 Structural Dynamics Notes, 2014, published through the University.

[38] G. Oriolo and Y. Nakamura, "Control of mechanical systems with second-order nonholonomic constraints: Underactuated manipulators," in *Proceedings of the 30th Conference on Decision and Control*. Brighton, England: IEEE, December 1991.

[39] N. Muskinja and B. Tovornik, "Swinging up and stabilisation of a real inverted pendulum," *IEEE Transactions on Industrial Electronics*, vol. 53, no. 2, pp. 631–639, April 2006.

[40] K. Furuta and M. Yamakita, "Swing-up control of inverted pendulum using pseudo-state feedback," *Proceedings of the Institute of Mechanical Engineers, Part I: Journal of Systems and Control Engineering*, vol. 206, no. 4, pp. 263–269, November 1992.

[41] K. Furuta, M. Yamakita, and S. Kobayashi, "Swing up control of inverted pendulum," in *Proceedings of the International Conference on Industrial Electronics, Control and Instrumentation (IECON '91)*, vol. 3. Kobe: IEEE, 28th Oct. - 1st Nov. 1991, pp. 2193–2198.

[42] P. Dang and F. L. Lewis, "Controller for swing-up and balance of single inverted pendulum using sdre-based solution," in *31st Annual Conference of IEEE Industrial Electronics Society (IECON)*, IEEE. IEEE, 6-10 November 2005, pp. 304–309.

[43] B. Widrow and F. W. Smith, "Pattern recognising control systems," in *Proceedings of the 1963 International Symposium of Computer and information Sciences (COINS)*. Washington, DC: Spartan, 1964, pp. 288–317.

[44] B. Widrow, "The original adaptive neural net broom-balancer," in *Proceedings of the IEEE International Symposium on Circuits and Systems*. Philadelphia, Pennsylvania: Stanford University, 4-7 May 1987, pp. 351–357.

[45] N. Singh and S. K. Yadav, "Comparison of lqr and pd controller for stabilising double inverted pendulum," *International Journal of Engineering Research and Development*, vol. 1, no. 12, pp. 69–74, July 2012.

[46] A. Bogdanov, "Optimal control of a double inverted pendulum on a cart," Department of Computer Science & Electrical Engineering, Oregan Health & Science University, Portland, OR, USA, Tech. Rep. CSE-04-006, December 2004.

[47] K. Srikanth and G. V. N. Kumar, "Stabilisation at upright equilibrium position of a double inverted pendulum with unconstrained bat optimisation," *International Journal on Computational Science and Applications (IJCSA)*, vol. 5, no. 5, p. 101, October 2015.

[48] X.-S. Yang, "Bat algorithm: Literature review and applications," *International Journal for Bio-Inspired Computation*, vol. 5, no. 3, pp. 141–149, 2013.

[49] T. Fujinaka, Y. Kishida, M. Yoshioka, and S. Omatu, "Stabilisation of double inverted pendulum with self-tuning neuro-pid," in *Proceedings of the IEEE-INNS-ENNS International Joint Conference on Neural Networks (IJCNN)*, vol. 4. Como: IEEE, 24-27 July 2000, pp. 345–348.

[50] H. M. Z. Farwig and H. Unbehauen, "Discrete computer control of a triple-inverted pendulum," *Optimal Control Applications & Methods*, vol. 11, pp. 151–171, 1990.

[51] V. A. Tsachouridis and G. A. Medrano-Cerda, "Discrete-time h-∞ control of a triple inverted pendulum with single control input," in *IEE Proceedings - Control Theory and Applications*, vol. 146, no. 6, IET. IET, November 1999, pp. 567–577.

[52] V. A. Tsachouridis, "Robust control of a triple inverted pendulum," in *Proceedings of the 1999 IEEE International Conference on Control Applications*. Hohala Coast-Island of Hawaii, USA: IEEE, 22-27 August 1999, pp. 1235–1240.

[53] G. A. Medrano-Cerda, "Robust stabilisation of a triple inverted pendulum-cart," *International Journal of Control*, vol. 68, no. 4, pp. 849–865, 1997.

[54] G. A. Medrano-Cerda, E. E. Eldukhri, and M. Cetin, "Balancing and attitude control of double and triple inverted pendulums," *Transactions of the Institute of Measurement and Control*, vol. 17, no. 3, pp. 143–154, August 1995.

[55] K. G. Eltohamy and C. Y. Kuo, "Real time stabilisation of a triple inverted pendulum using single control input," in *IEE Proceedings - Control Theory and Applications*, vol. 144, no. 5. IET, September 1997, pp. 498–504.

[56] S. Sengal and S. Tiwari, "Lqr control for stabilising triple link inverted pendulum system," in *2nd International Conference on Power, Control and Embedded Systems (ICPCES)*. Allahabad: IEEE, 17-19 December 2012, pp. 1–5.

[57] S. Lam and E. J. Davison, *Real Stability and Stabilizability Radii of the Multi-Link Inverted Pendulum*, Department of Electrical and Computer Engineering Systems and Control Research Report 0502, May 2005, supported by the National Sciences and Engineering Research Council of Canada (NSERC).

[58] H. O. Wang, K. Tanaka, and M. F. Griffin, "An approach to fuzzy control of nonlinear systems: stability and design issues," *IEEE Transactions on Fuzzy Systems*, vol. 4, no. 1, pp. 14–23, February 1996.

[59] C. W. Anderson, "Learning to control an inverted pendulum using neural networks," *IEEE Control Systems Magazine*, vol. 9, no. 3, pp. 31–37, April 1989.

[60] Q. Wei, W. P. Dayawansa, and W. S. Levine, "Nonlinear controller for an inverted pendulum having restricted travel," *Automatica*, vol. 31, no. 6, pp. 841–850, 1995.

[61] K. Yoshida, "Swing-up control of an inverted pendulum by energy-based methods," in *Proceedings of the American Control Conference*, vol. 6, San Diego, CA, June 1999, pp. 4045–4047.

[62] M. Bugeja, "Non-linear swing-up and stabilising control of an inverted pendulum," in *EUROCON 2003*, vol. 2. IEEE, 22-24 September 2003, pp. 437–441.

[63] K. J. Åström and K. Furuta, "Swinging up a pendulum by energy control," in *13th IFAC World Congress*. San Francisco, CA: IFAC, 1996, pp. 1–15.

[64] X. Xin and M. Kaneda, "The swing up control for the acrobot based on energy control approach," in *Proceedings of the 41st IEEE Conference on Decision and Control*, vol. 3. IEEE, December 2002, pp. 3261–3266.

[65] G. Boone, "Minimum-time control of the acrobot," in *Proceedings of the 1997 IEEE Conference of Robotics and Automation*, vol. 4, Albuquerque, New Mexico, April 1997, pp. 3281–3287.

[66] R. N. Ranavar and A. D. Mahindrakar, "Energy-based swing-up of the acrobot and time-optimal motion," *Proceedings of 2003 IEEE Conference on Control Applications CCA*, vol. 1, pp. 706–711, June 2003.

[67] A. D. Mahindrakar and R. N. Ranavar, "Sub time-optimal swing up of the acrobot," in *European Control Conference (ECC)*, Porto, Portugal, September 2001, pp. 588–593.

[68] S. C. Brown and K. M. Passino, "Intelligent control for an acrobot," *Journal of Intelligent and Robotic Systems*, vol. 18, pp. 209–248, November 1997.

[69] J. Yoshimoto, M. Nishimura, Y. Tokita, and S. Ishii, "Acrobot control by learning the switching of multiple controllers," *Artificial Life and Robotics*, vol. 9, pp. 67–71, May 2005.

[70] A. D. Mahindrakar and R. N. Ranavar, "A swing-up of the acrobot based on a simple pendulum strategy," *International Journal of Control*, vol. 78, no. 6, pp. 424–429, December 2005.

[71] G. DeJong, "A case study of explanation-based control," in *Proceedings of the 12th International Conference of Machine Learning*, A. Prieditis, Ed., Tahoe City, California, July 1995.

[72] R. Jafari, F. B. Mathis, and R. Mukherjee, "Swing-up control of the acrobot: An impulse-momentum approach," in *American Control Conference*, O'Farrell street, San Francisco, CA, USA, July 2011, pp. 262–267.

[73] T. Glück, A. Eder, and A. Kugi, "Swing-up control of a triple inverted pendulum on a cart with experimental validation," *Automatica*, vol. 49, no. 3, pp. 801–808, 2013.

[74] K. Graichen, M. Treuer, and M. Zeitz, "Fast side-stepping of the triple inverted pendulum via contrained nonlinear feedforward control design," in *Proceedings of the 44th IEEE Conference on Decision and Control, and the European Control Conference 2005*. Seville, Spain: IEEE, 12-15 December 2005, pp. 1096–1101.

[75] M. Spong, *Control Problem in Robotics and Automation*. Springer-Verlag London Ltd., 1998, vol. 230, ch. 9: Underactuated Mechanical Systems, pp. 135–150.

[76] M. W. Spong, "Energy based control of a class of underactuated mechanical systems," in *1996 IFAC World Congress*. Citeseer, 1996, pp. 431–435.

[77] X. Xin, J.-H. She, T. Yamasaki, and Y. Liu, "Swing-up control based on virtual composite links for n-link underactuated robot with passive first joint," *Automatica*, vol. 45, pp. 1986–1994, 18 June 2009.

[78] X. Xin, J.-H. She, and T. Yamasaki, "Swing-up control for the n-link planar robot with single passive joint using notion of virtual composite links," in *Proceedings of the 47th IEEE Conference on Decision and Control*. Cancun, Mexico: IEEE, December 9-11 2008, pp. 4339–4344.

[79] X. Xin, J.-H. She, and Y. Liu, "A unified solution to swing-up control for n-link planar robot with single passive joint based on virtual composite links and passivity," *Nonlinear Dynamics*, vol. 67, no. 2, pp. 909–923, 16 April 2011.

[80] C. C. de Wit, H. Olsson, K. J. Åström, and P. Lischinsky, "Dynamic friction models and control design," in *American Control Conference '93*. San Francisco, CA, USA: IEEE, 2-4 June 1993, pp. 1920–1926.

[81] L. F. C. Zonetti, A. S. S. Camargo, J. Sartori, D. F. de Sousa, and L. A. O. Nunes, "Demonstration of dry and viscous damping of an oscillating pendulum," *European Journal of Physics*, vol. 20, 1999.

[82] R. A. Serway, R. J. Beichner, and J. W. Jewett, *Physics for Scientists and Engineers with Modern Physics*, 6th ed. Cengage Learning, 2000.

[83] G. W. van der Linden and P. F. Lambrechts, "H-∞ control of an experimental inverted pendulum with dry friction," *IEEE Control Systems*, vol. 13, no. 4, pp. 44–50, August 1993.

[84] S. A. Campbell, S. Crawford, and K. Morris, "Friction and the inverted pendulum stabilisation problem," *Journal of Dynamic Systems, Measurement, and Control*, vol. 130, no. 5, 2008.

[85] D. Park, D. Chwa, and S. kyo Hong, "An estimation and compensation of the friction in an inverted pendulum," in *2006 SICE-ICASE International Joint Conference*. Busan: IEEE, 18-21 October 2006, pp. 779–783.

[86] T. Kubo, G. Anwar, and M. Tomizuka, "Application of nonlinear friction compensation to robot arm control," in *Proceedings of the 1986 IEEE International Conference on Robotics and Automation*, vol. 3. IEEE, April 1986, pp. 722–727.

[87] L. Fang, W. J. Chen, and S. U. Cheang, "Friction compensation for a double inverted pendulum," in *Proceedings of the 2001 IEEE International Conference on Control Applications (CCA '01)*. IEEE, 5-7 September 2001, pp. 908–913.

[88] A. Nejadfard and M. J. Yazdanpanah, "Friction compensation of double inverted pendulum on a cart using locally linear neuro-fuzzy model," *Neural Computing and Applications*, vol. 22, no. 2, pp. 337–347, 2013.

[89] W. Greiner, *Classical Mechanics: Systems of Particles and Hamiltonian Dynamics*. Springer Berlin Heidelberg, 1962.

[90] L. Komzsik, *Applied Calculus of Variations for Engineers*. CRC Press, 2009.

[91] P. J. Olver, *Introduction into the Calculus of Variations*, University of Minnesota, Minnesota, USA, 2016, lecture Notes.

[92] D. Baumann, *Concepts in Theoretical Physics*. Cambridge Univeristy, 2012, ch. 1: Principle of Least Action, pp. 3–12.

[93] J. Naude, "Control design using energy-shaping methods," Masters of Science in Engineering (MSc. Eng.), University of the Witwatersrand, Braamfontein, Johannesburg, South Africa, 2012.

[94] D. Morin, *Problems and Solutions in Introductory Mechanics*. Harvard University, 2014.

[95] K. J. Åström and R. M. Murray, *Analysis and Design of Feedback Systems*. Princeton University Press, 2004, ch. 6, pp. 139–166.

[96] Utah University. (2014, 16 March) Chapter 8: Laplace transform. Electronic Publication. Engineering Math 2250. Lecture Notes. [Online]. Available: http://www.math.utah.edu/~gustafso/s2015/2250/2250laplaceTheory2008.pdf

[97] The University of Vermont. (2015, November) Routh-hurwitz criteria. Chapter 4: Linear Differential Equations: Theory and Examples. [Online]. Available: http://www.cems.uvm.edu/~tlakoba/08_fall/EE_295/Routh_Hurwitz_Criterion.pdf

[98] Indiana University. (2007, 13 June) Routh's stability criterion. ECE 680 Modern Control Theory. Supplementary notes. [Online]. Available: http://www.engr.iupui.edu/~skoskie/ECE680/Routh.pdf

[99] F. R. Gantmacher, *The Theory of Matrices*. Chelsea Publishing Company, 1959.

[100] H. Márquez, *Nonlinear Control Systems: Analysis and Design*. Hoboken, New Jersey, USA: John Wiley & Sons, Inc., 2003.

[101] A. Isidori, *Nonlinear Control Systems: An Introduction*, 2nd ed. Springer-Verlag Berlin Heidelberg GmbH, 1989.

[102] C. Kravaris and M. Soroush, "Synthesis of multivariable nonlinear controllers by input-output linearisation," *American Institute of Chemical Engineers (AIChE)*, vol. 36, no. 2, pp. 249–264, 1990.

[103] M. I. Molina, "Exponential versus linear amplitude decay in damped oscillators," *The Physics Teacher: America Association of Physics Teachers*, vol. 42, no. 8, July 2004.

[104] M. E. Bacon and D. D. Nguyen, "Real-world damping of a physical pendulum," *European Journal of Physics*, no. 26, pp. 651–655, May 2005.

[105] A. A. Shabana, *Dynamics of Multibody Systems*, 3rd ed. Cambridge, UK: Cambridge University Press, 2005, ch. 3.5: Application to Rigid Body Dynamics, p. 135.

[106] C. Torre, "Some examples. constraints and lagrange multipliers," in *Physics 6010*. Utah State University, Fall 2010. [Online]. Available: http://www.physics.usu.edu/torre/6010_Fall_2010/Lectures/03.pdf

[107] S. Kolavennu, S. Palanki, and C. J. C, "Nonlinear control of nonsquare multivariable systems," *Chemical Engineering Science*, no. 56, pp. 2103–2110, 2001.

[108] E. D. Sontag, "A 'universal' construction of artstein's theorem on nonlinear stabilization," *Systems & Control Letters*, no. 13, pp. 117–123, 1989.

[109] S. Takashima, "Control of gymnast on a high bar," in *IEEE RSJ International Workshop on Intelligent Robots and Systems IROS '91*, Osaka, Japan, November 3-5 1991.

[110] R. De Almeida and O. Nyandoro, "Gain selection criteria for the swing-up control of the acrobot using collocated partial feedback linearisation," in *IEEE AFRICON17*, Cape Town, South Africa, 2017.

[111] ——, "Swing-up control of the acrobot using noncollocated partial feedback linearisation: an iterative approach," in *Control Conference Africa*, IFAC. Johannesburg, South Africa: Elsevier, 2017.

Appendix A

Proofs

A number of mathematical proofs that are used to generate the key analytical results that are described in the main body of the dissertation are discussed in this appendix. There are six sections included in this appendix which include proofs related to:

1. The conservation of energy and time-translational symmetry.
2. The independence of the mass matrix of a square affine system from $\mathbf{q_u}$.
3. The necessary and sufficient gain condition (k_D) for swing-up control of the MC-ROPA$_{n-1}$ robot.
4. The necessary and sufficient gain condition (k_P) for swing-up control of the MC-ROPA$_{n-1}$ robot.
5. The *gain selection criterion* for the undamped TC-ROPA$_{n-1}$ robot.
6. The *gain selection criterion* for the passively damped TC-ROPA$_{n-1}$ robot.

A.1 Conservation of Energy and Time-Translational Symmetry

The time differential of the Lagrangian function can be described as follows with the implementation of the chain rule, where

$$\frac{d\mathbf{L}(\mathbf{q},\dot{\mathbf{q}},t)}{dt} = \frac{\partial \mathbf{L}(\mathbf{q},\dot{\mathbf{q}},t)}{\partial \mathbf{q}}\dot{\mathbf{q}} + \frac{\partial \mathbf{L}(\mathbf{q},\dot{\mathbf{q}},t)}{\partial \dot{\mathbf{q}}}\ddot{\mathbf{q}} + \frac{\partial \mathbf{L}(\mathbf{q},\dot{\mathbf{q}},t)}{\partial t}. \tag{A.1}$$

This expression may seem complicated, but the Euler-Lagrange function can be manipulated to produce an expression that simplifies the problem. We can thus show that

$$\begin{aligned} \frac{d}{dt}\frac{\partial \mathbf{L}(\mathbf{q},\dot{\mathbf{q}},t)}{\partial \dot{\mathbf{q}}} - \frac{\partial \mathbf{L}(\mathbf{q},\dot{\mathbf{q}},t)}{\partial \mathbf{q}} &= 0, \\ \therefore \frac{d}{dt}\frac{\partial \mathbf{L}(\mathbf{q},\dot{\mathbf{q}},t)}{\partial \dot{\mathbf{q}}} &= \frac{\partial \mathbf{L}(\mathbf{q},\dot{\mathbf{q}},t)}{\partial \mathbf{q}}. \end{aligned} \tag{A.2}$$

Substituting eq. (A.2) into eq. (A.1), we find that

$$\frac{d\mathbf{L}(\mathbf{q},\dot{\mathbf{q}},t)}{dt} = \left[\frac{d}{dt}\frac{\partial \mathbf{L}(\mathbf{q},\dot{\mathbf{q}},t)}{\partial \dot{\mathbf{q}}}\dot{\mathbf{q}} + \frac{\partial \mathbf{L}(\mathbf{q},\dot{\mathbf{q}},t)}{\partial \dot{\mathbf{q}}}\ddot{\mathbf{q}}\right] + \frac{\partial \mathbf{L}(\mathbf{q},\dot{\mathbf{q}},t)}{\partial t}. \tag{A.3}$$

This substitution clearly demonstrates that the bracketed expressions are the result of a time-differentiation on a product, i.e. $\frac{d}{dt}(\mathbf{uv}) = \dot{\mathbf{u}}\mathbf{v} + \mathbf{u}\dot{\mathbf{v}}$. Eq. (A.3) can therefore be represented as

$$\frac{d\mathbf{L}(\mathbf{q},\dot{\mathbf{q}},t)}{dt} = \frac{d}{dt}\left(\frac{\partial \mathbf{L}(\mathbf{q},\dot{\mathbf{q}},t)}{\partial \dot{\mathbf{q}}}\dot{\mathbf{q}}\right) + \frac{\partial \mathbf{L}(\mathbf{q},\dot{\mathbf{q}},t)}{\partial t}. \tag{A.4}$$

We know that the angular momentum of the system $\mathbf{p}$ is represented by the expression $\frac{\partial \mathbf{L}(\mathbf{q},\dot{\mathbf{q}},t)}{\partial \dot{\mathbf{q}}}$. Therefore

$$\frac{d}{dt}\left(\frac{\partial \mathbf{L}(\mathbf{q},\dot{\mathbf{q}},t)}{\partial \dot{\mathbf{q}}}\right) = \frac{d\mathbf{p}}{dt} = \dot{\mathbf{p}}. \tag{A.5}$$

The time-derivative of the Lagrangian equation can, therefore, be represented as

$$\begin{aligned} \frac{d\mathbf{L}(\mathbf{q},\dot{\mathbf{q}},t)}{dt} &= \frac{d}{dt}\left(\mathbf{p}^{T}\dot{\mathbf{q}}\right) + \frac{\partial \mathbf{L}(\mathbf{q},\dot{\mathbf{q}},t)}{\partial t}, \\ &= \frac{d}{dt}\sum_{i=1}^{N}(p_i\dot{q}_i) + \frac{\partial \mathbf{L}(\mathbf{q},\dot{\mathbf{q}},t)}{\partial t}, \\ &= 2\frac{d\mathbf{T}}{dt} + \frac{\partial \mathbf{L}(\mathbf{q},\dot{\mathbf{q}},t)}{\partial t}. \end{aligned} \tag{A.6}$$

Integrating eq. (A.6) with respect to time produces

$$\mathbf{L}(\mathbf{q}, \dot{\mathbf{q}}, \mathrm{t}) = 2\mathbf{T} + \int \frac{\partial \mathbf{L}(\mathbf{q}, \dot{\mathbf{q}}, \mathrm{t})}{\partial \mathrm{t}} \mathrm{dt} - \mathcal{H}$$

where $\mathcal{H}$ represents the constant of this integration process (and is referred to as the Hamiltonian). We know that

$$\mathbf{L}(\mathbf{q}, \dot{\mathbf{q}}, \mathrm{t}) = \sum_{i=1}^{N} (T_n - P_n) = \mathbf{T} - \mathbf{P}.$$

Therefore,

$$\mathcal{H} = \mathbf{T} + \mathbf{P} + \int \frac{\partial \mathbf{L}(\mathbf{q}, \dot{\mathbf{q}}, \mathrm{t})}{\partial \mathrm{t}} \mathrm{dt}. \tag{A.7}$$

We can thus conclude from eq. (A.7) that the mechanical energy of the system, represented by $\mathbf{T} + \mathbf{P}$ will only be equal to the Hamiltonian (and thus constant) if and only if

$$\int \frac{\partial \mathbf{L}(\mathbf{q}, \dot{\mathbf{q}}, \mathrm{t})}{\partial \mathrm{t}} \mathrm{dt} = 0.$$

This can only be true if

$$\frac{\partial \mathbf{L}(\mathbf{q}, \dot{\mathbf{q}}, \mathrm{t})}{\partial \mathrm{t}} = 0. \tag{A.8}$$

The system thus contains time-translational symmetry if and only if the Lagrangian is not explicitly time dependent. This time dependency is introduced into the system by an external force or torque (such as damping or actuation). □

A.2 Independence of the Mass matrix of a Square Affine System from $\mathbf{q_u}$

It is shown in section 7.3 and in [5] that

$$\mathbf{M}_\theta(\theta)_{jk} = \alpha_{jk}\cos(\theta_j - \theta_k)$$

whereby

$$\theta_j = \sum_{m=1}^{j} q_m, \qquad \theta_k = \sum_{m=1}^{k} q_m.$$

Substituting these expressions for θ_j and θ_k produces

$$\theta_j - \theta_k = \sum_{m=1}^{j} q_m - \sum_{m=1}^{k} q_m,$$

$$\therefore \theta_j - \theta_k = \sum_{m=k+1}^{i} q_m \quad \text{for } j > k, \text{ and} \tag{A.9}$$

$$\theta_j - \theta_k = -\sum_{m=j+1}^{k} q_m \quad \text{for } k > j. \tag{A.10}$$

It is apparent that $j \neq 0$ and $k \neq 0$ for all time, the consequence of which excludes the generalised coordinate q_1 from the final summation of generalised coordinates seen in eqs. (A.9) and (A.10). We can conclude, therefore, that $\mathbf{M}_\theta(\theta)$ cannot depend on q_1. The true mass matrix $\mathbf{M}(\mathbf{q})$ is transformed from the $\mathbf{M}_\theta(\theta)$ where

$$\mathbf{M}(\mathbf{q}) = A^{\mathbf{T}}\mathbf{M}_\theta(\theta)A \tag{A.11}$$

and where the definition of A can be found in section 7.3.1. This transformation cannot introduce the coordinate q_1 into the expression, therefore $\mathbf{M}(\mathbf{q})$ is also independent of q_1. The mass matrix is independent of the unactuated generalised coordinates $\mathbf{q_u}$ in this case if $\mathbf{q_u} = q_1$. □

A.3 Necessary and Sufficient Gain Condition (k_D) for Swing-up Control of the MC-ROPA$_{n-1}$ Robot

Choosing $\mathbf{M}_a = \left(\mathbf{G}^{\mathbf{T}}\mathbf{M}^{-1}\mathbf{G}\right)^{-1}$, we define $\Lambda(\mathbf{q}, \dot{\mathbf{q}})$ as

$$\begin{aligned}\Lambda(\mathbf{q}, \dot{\mathbf{q}}) &= (E - E_r)I_{n-1} + k_D\mathbf{M}_a^{-1} \\ &= \mathbf{M}_a^{-1}\Big[(E - E_r)\mathbf{M}_a + k_D I_n\Big] \\ &= \mathbf{M}_a^{-1}\mathbf{v}^{-1}\Big[\lambda(E - E_r) + k_D I_{n-1}\Big]\mathbf{v}\end{aligned}$$

where $\mathbf{v} \in \mathbb{R}^{(n-1)\times(n-1)}$ matrix contains all the eigenvectors of $\mathbf{M}_a$ and $\lambda \in \mathbb{R}^{(n-1)\times(n-1)}$ is an identity matrix that is populated with the eigenvalues of the matrix $\mathbf{M}_a$ such that

$$\lambda = \begin{bmatrix} \lambda_1 & 0 & \dots & 0 \\ 0 & \lambda_2 & \ddots & \vdots \\ \vdots & \ddots & \ddots & 0 \\ 0 & \dots & 0 & \lambda_{n-1} \end{bmatrix}.$$

Therefore

$$\begin{aligned}|\Lambda(\mathbf{q}, \dot{\mathbf{q}})| &= \left|\mathbf{M}_a^{-1}\mathbf{v}^{-1}\Big[\lambda(E - E_r) + k_D I_{n-1}\Big]\mathbf{v}\right| \\ &= \underbrace{\left|\mathbf{M}_a^{-1}\right|}_{\neq 0}\underbrace{\left|\mathbf{v}^{-1}\right|}_{\neq 0}\left|\Big[\lambda(E - E_r) + k_D I_{n-1}\Big]\right|\underbrace{\left|\mathbf{v}\right|}_{\neq 0},\end{aligned}$$

$$\therefore \quad |\Lambda(\mathbf{q}, \dot{\mathbf{q}})| \neq 0 \leftrightarrow \left|\lambda(E - E_r) + k_D I_{n-1}\right| \neq 0. \tag{A.12}$$

This determinant can be represented as

$$\det \begin{bmatrix} \lambda_1(E - E_r) + k_D & 0 & \dots & 0 \\ 0 & \lambda_2(E - E_r) + k_D & \ddots & \vdots \\ \vdots & \ddots & \ddots & 0 \\ 0 & \dots & 0 & \lambda_{n-1}(E - E_r) + k_D \end{bmatrix}.$$

It is evident that this determinant is guaranteed to be non-zero if

$$k_D \neq (E_r - E)\lambda_i$$

where $1 \leq i < n$. This condition will be satisfied if

$$k_D > \left(E_r - \min_{\mathbf{q}}\{E\}\right)\lambda_{\max}$$

where $\lambda_{\max} = \max\{\lambda\}$. Additionally

$$\begin{aligned} E(\mathbf{q}, \dot{\mathbf{q}}) &= \underbrace{\frac{1}{2}\dot{\mathbf{q}}^{\mathbf{T}}\mathbf{M}(\mathbf{q})\dot{\mathbf{q}}}_{\geq 0} + \mathbf{P}(\mathbf{q}) \\ &\geq \mathbf{P}(\mathbf{q}) \end{aligned}$$

where $-E_r \leq \mathbf{P}(\mathbf{q}) \leq E_r$. We can therefore define $\min_q\{E\} \geq \min_q\{\mathbf{P}(\mathbf{q})\}$, which leads to

$$\begin{aligned} k_D &> (E_r - \min_{\mathbf{q}}\{\mathbf{P}(\mathbf{q})\})\lambda_{\max} \\ &= \max_{\mathbf{q}}\{(E_r - \mathbf{P}(\mathbf{q}))\lambda_{\max}\} \\ &= \max_{\mathbf{q}}\{\eta(\mathbf{q})\}. \end{aligned}$$

To show that this condition is indeed necessary, we will show that for $0 < k_D \leq \max_{\mathbf{q}}\{\eta(\mathbf{q})\}$ there is an initial condition $(\mathbf{q}(0), \dot{\mathbf{q}}(0))$ in which the condition in eq. (8.3) is not satisfied. We first define

$$k_D = \max_{\mathbf{q}}\{\eta(\mathbf{q}) - d_0\lambda_{\max}\} \tag{A.13}$$

where d_0 is a constant bounded by $0 \leq d_0 < E_r - \min_{\mathbf{q}} P(\mathbf{q})$. Additionally, we define a set of states $\zeta \in \mathbb{R}^n$ that represents the values of $\mathbf{q}$ that, at any point in time t, maximises $\eta(\mathbf{q})$ (i.e. minimises $\mathbf{P}(\mathbf{q})$). We also define the resulting velocity vector as

$$\zeta_d = \mathbf{M}(\zeta)^{-1/2}\mathbf{v}_\zeta$$

where $\zeta_d \in \mathbb{R}^n$ and

$$\mathbf{v}_\zeta = \begin{bmatrix}\sqrt{2d_0} & 0 & \dots & 0\end{bmatrix}^{\mathbf{T}}.$$

Therefore, choosing $(\mathbf{q}(0), \dot{\mathbf{q}}(\mathbf{0})) = (\zeta, \zeta_d)$, we find that the mechanical energy at $t = 0$ is described as

$$\begin{aligned} E(\zeta, \zeta_d) &= \frac{1}{2}{\zeta_d}^{\mathbf{T}}\mathbf{M}(\zeta)\zeta_d + \mathbf{P}(\zeta) \\ &= \frac{1}{2}{\mathbf{v}_\zeta}^{\mathbf{T}}\left(\mathbf{M}(\zeta)^{-1/2}\right)^{\mathbf{T}}\mathbf{M}(\zeta)\mathbf{M}(\zeta)^{-1/2}\mathbf{v}_\zeta. \end{aligned}$$

It is important to note that $\mathbf{M}(\zeta)$ is a positive definite matrix, thus resulting in

$$\left(\mathbf{M}(\zeta)^{-1/2}\right)^{\mathbf{T}}\mathbf{M}(\zeta)\mathbf{M}(\zeta)^{-1/2} = I_n.$$

Therefore

$$\begin{aligned} E(\zeta) &= \frac{1}{2}\mathbf{v}_\zeta{}^{\mathbf{T}}\mathbf{v}_\zeta + \mathbf{P}(\zeta) \\ &= d_0 + \mathbf{P}(\zeta). \end{aligned}$$

Therefore $\mathbf{P}(\zeta) \leq E(\zeta) < E_r$. Substitution of the aforementioned expression into eq. (A.12) produces

$$\begin{aligned} |\Lambda(\zeta, \zeta_d)| &= \Big|\lambda(E(\zeta, \zeta_d) - E_r) + k_D I_{n-1}\Big| \\ &= \Big|\underbrace{\lambda(d_0 + \mathbf{P}(\zeta) - E_r) + k_D I_{n-1}}_{\mathbf{W}_\zeta}\Big| \end{aligned}$$

where

$$\mathbf{W}(\zeta) = \begin{bmatrix} W_{1,1} & 0 & \dots & 0 \\ 0 & W_{2,2} & \ddots & \vdots \\ \vdots & \ddots & \ddots & 0 \\ 0 & \dots & 0 & W_{n-1,n-1} \end{bmatrix} \in \mathbb{R}^{(n-1)\times(n-1)}.$$

Each non-zero entry in the $\mathbf{W}(\zeta)$ matrix is thus represented as

$$W_{i,i}(\zeta) = \lambda_i(d_0 + \mathbf{P}(\zeta) - E_r) + k_D \tag{A.14}$$

where $1 \leq i \leq n-1$. The substitution of eq. (A.13) into eq. (A.14) produces

$$\begin{aligned} W_{i,i}(\zeta) &= \lambda_i(d_0 + \mathbf{P}(\zeta) - E_r) + \eta(\zeta) - d_0\lambda_{\max}(\mathbf{M}_a) \\ &= \lambda_i(d_0 + \mathbf{P}(\zeta) - E_r) + (E_r - \mathbf{P}(\zeta))\lambda_{\max}(\mathbf{M}_a) - d_0\lambda_{\max}(\mathbf{M}_a) \\ &= (E_r - \mathbf{P}(\zeta) - d_0)\Big[\lambda_{\max}(\mathbf{M}_a) - \lambda_i\Big]. \end{aligned}$$

We note that $0 \leq d_0 < E_r - \mathbf{P}(\zeta)$. Therefore

$$\min_{d_0}\Big\{W_{i,i}\Big\} = \epsilon\Big[\lambda_{\max}(\mathbf{M}_a) - \lambda_i\Big] \geq 0$$

where ϵ is an infinitesimally small positive number. It is guaranteed, therefore, one of the entries of the $\mathbf{W}(\zeta)$ matrix will be zero, resulting in

$$W_{i,i} = 0 \leftrightarrow \lambda_{\max}(\mathbf{M}_a) - \lambda_i = 0$$

where i in this case represents the index where $\lambda_i = \lambda_{\max}(\mathbf{M}_a)$. This condition is guaranteed since $\lambda_{\max}(\mathbf{M}_a)$ forms part of the λ matrix. Therefore

$$|\Lambda(\mathbf{q}, \dot{\mathbf{q}})| = 0 \leftrightarrow k_D \leq \max_{\mathbf{q}}\Big\{\eta(\mathbf{q})\Big\}.$$

If, however, k_D is changed so that it is guaranteed to be larger than $\max_{\mathbf{q}}\left\{\eta(\mathbf{q})\right\}$, by choosing

$$k_D = \eta(\zeta) + \epsilon$$

then the entries for matrix $\mathbf{W}(\zeta)$ are expressed as

$$\begin{aligned} W_{i,i}(\zeta) &= \lambda_i(d_0 + \mathbf{P}(\zeta) - E_r) + \eta(\zeta) + \epsilon \\ &= \lambda_i(d_0 + \mathbf{P}(\zeta) - E_r) + (E_r - \mathbf{P}(\zeta))\lambda_{\max}(\mathbf{M}_a) \\ &= \underbrace{(E_r - \mathbf{P}(\zeta))\Big[\lambda_{\max}(\mathbf{M}_a) - \lambda_i\Big] + \lambda_i d_0}_{\geq 0} + \underbrace{\epsilon}_{>0}. \end{aligned}$$

Therefore, $k_D > \max_{\mathbf{q}} \eta(\mathbf{q})$ is both a sufficient and a necessary condition for $|\Lambda(\mathbf{q}, \dot{\mathbf{q}})| \neq 0$.

The expression $\eta(\mathbf{q}) = (E_r - \mathbf{P}(\mathbf{q}))\lambda_{\max}$ can be simplified to be expressed solely in terms of the states $\mathbf{q}_a$ [5]. Choosing $q_1 = \zeta_1$ (a value that maximises $\eta(\mathbf{q})$ with respect to q_1), we find that

$$\left.\frac{\partial \eta(\mathbf{q})}{\partial q_1}\right|_{q_1=\zeta_1} = -\lambda_{\max}\left.\frac{\partial \mathbf{P}(\mathbf{q})}{\partial q_1}\right|_{q_1=\zeta_1} = -\lambda_{\max} K_1(\mathbf{q}) = 0$$

according to 3.15. It is evident that $\lambda_{\max} \neq 0$ since $\mathbf{M}_a$ is positive definite. Therefore

$$\left.K_1(\mathbf{q})\right|_{q_1=\zeta_1} = 0. \tag{A.15}$$

We can, thus, use this expression to describe $\left.\mathbf{P}(\mathbf{q})\right|_{q_1=\zeta_1}$ solely in terms of $\mathbf{q}_a$, where

$$\mathbf{P}^2(\zeta_1, \mathbf{q}_a) = \mathbf{P}^2(\zeta_1, \mathbf{q}_a) + {K_1}^2(\zeta_1, \mathbf{q}_a).$$

It is evident that

$$\begin{aligned} \mathbf{P}^2(\zeta_1, \mathbf{q}_a) &= \left(\sum_{i=1}^{n} {\beta_i}^2 \cos^2\left[\sum_{j=1}^{i} q_j\right] + 2\sum_{i=1}^{n-1} \beta_i \cos\left[\sum_{k=1}^{i} q_k\right] \sum_{j=i+1}^{n} \beta_j \cos\left[\sum_{l=1}^{j} q_l\right]\right), \\ {K_1}^2(\zeta_1, \mathbf{q}_a) &= \left(\sum_{i=1}^{n} {\beta_i}^2 \sin^2\left[\sum_{j=1}^{i} q_j\right] + 2\sum_{i=1}^{n-1} \beta_i \sin\left[\sum_{k=1}^{i} q_k\right] \sum_{j=i+1}^{n} \beta_j \sin\left[\sum_{l=1}^{j} q_l\right]\right) \end{aligned}$$

where $q_1 = \zeta_1$. Therefore

$$\mathbf{P}^2(\zeta_1, \mathbf{q}_a) + {K_1}^2(\zeta_1, \mathbf{q}_a) = \left(\sum_{i=1}^{n} {\beta_i}^2 + 2\sum_{i=1}^{n-1}\sum_{j=i+1}^{n} \beta_i\beta_j\left(\sin\left[\sum_{k=1}^{i} q_k\right] \sin\left[\sum_{l=1}^{j} q_l\right] + \right.\right.$$

$$
\begin{aligned}
&\cos\left[\sum_{k=1}^{i} q_k\right]\cos\left[\sum_{l=1}^{j} q_l\right]\Bigg)\Bigg)\Bigg|_{q_1=\zeta_1} \\
&= \sum_{i=1}^{n} {\beta_i}^2 + 2\sum_{i=1}^{n-1}\sum_{j=i+1}^{n} \beta_i\beta_j\left(\cos\left[\sum_{k=i+1}^{j} q_k\right]\right) \\
&= \mathbf{P}^2(\mathbf{q}_a).
\end{aligned}
$$

Furthermore

$$
\mathbf{P}(\mathbf{q}_a) = \pm\mathbf{\Phi}(\mathbf{q}_a) = \pm\left[\sum_{i=1}^{n} {\beta_i}^2 + 2\sum_{i=1}^{n-1}\sum_{j=i+1}^{n} \beta_i\beta_j\left(\cos\left[\sum_{k=i+1}^{j} q_k\right]\right)\right]^{1/2}.
$$

From this observation, we find that

$$
\max_{\mathbf{q}}\left\{\mathbf{P}(\mathbf{q})\right\} = \max_{\mathbf{q}_a}\left\{\mathbf{P}(\zeta_1,\mathbf{q}_a)\right\} = \max_{\mathbf{q}_a}\left\{\mathbf{P}(\mathbf{q}_a)\right\} \tag{A.16}
$$

$$
= \max_{\mathbf{q}_a}\left\{\pm\mathbf{\Phi}(\mathbf{q}_a)\right\} = \max_{\mathbf{q}_a}\left\{\mathbf{\Phi}(\mathbf{q}_a)\right\}. \tag{A.17}
$$

Therefore, the condition seen in eq. (8.13) is represented as

$$
k_D > k_{DM} = \max_{\mathbf{q}_a}\left\{\left[E_r + \mathbf{\Phi}(\mathbf{q}_a)\right]\lambda_{\max}\left[\left(\mathbf{G^T M^{-1} G}\right)^{-1}\right]\right\}. \tag{A.18}
$$

□

A.4 Necessary and Sufficient Gain Condition (k_P) for Swing-up Control of the MC-ROPA$_{n-1}$ Robot

It is evident that the time-dependent behaviour of the Lyapunov function shown in eq. (8.11) is guaranteed to be negative semi-definite so long as the torque expression for τ_2 is described as seen in eq. (8.10), with k_D satisfying the condition seen in eq. (8.3). Therefore, the system trajectories are described as

$$\lim_{t\to\infty} V = V^*, \qquad \lim_{t\to\infty} E = E^*,$$
$$\lim_{t\to\infty} \overline{\mathbf{q}}_2 = \overline{\mathbf{q}}_2^*$$

where the asterix superscript identifies the equilibrium value of the particular state trajectories [5]. Figure A.1 demonstrates a collection of subsets in the real state-space. We define the state-space $\mathbb{S} \in \mathbb{R}^n$ which encompasses the compact set Γ_c described by

$$\Gamma_c = \Big\{(\mathbf{q}, \dot{\mathbf{q}}) \in \mathbb{S} \mid V(\mathbf{q}, \dot{\mathbf{q}}) \leq c\Big\}$$

with $c \in \mathbb{R}^+$ [5]. It is evident that the compact set Γ_c is an invariant set since the torque expression in eq. (8.1) guarantees that $\dot{V} \leq 0$. Therefore, the set

$$\mathbf{S} = \Big\{(\mathbf{q}, \dot{\mathbf{q}}) \in \Gamma_c \mid V(\mathbf{q}, \dot{\mathbf{q}}) \leq c;\ \dot{V}(\mathbf{q}, \dot{\mathbf{q}}) = 0\Big\}$$

forms a subset of the compact set Γ_c. The entire set $\mathbf{S}$ is not itself invariant, since there is a possibility of achieving $\dot{V} < 0$ after $\dot{V} = 0$. We can, however, define the largest invariant set within this set, $\mathbf{W}$, where

$$\mathbf{W} = \Big\{(\mathbf{q}, \dot{\mathbf{q}}) \in \mathbf{S} \mid \dot{q}_1 \in \mathbb{R};\ q_2 = q_2^*\Big\}. \tag{A.19}$$

The definition of $\mathbf{W}$ shown in eq. (A.19) is not complete, however, since there is no definition of the behaviour of the state q_1. Knowing that

$$E = \frac{1}{2}\dot{\mathbf{q}}^{\mathbf{T}}\mathbf{M}(\mathbf{q})\dot{\mathbf{q}} + \mathbf{P}(\mathbf{q})$$

and that $\dot{q}_2 = 0$ when $E = E^*$, we find that

$$E^* = \frac{1}{2}M_{11}(\mathbf{q})\dot{q}_1^2 + \mathbf{P}(q_1, \mathbf{q}_a).$$

Therefore

$$\dot{q}_1^2 = \frac{2\Big[E^* - \mathbf{P}(q_1, \mathbf{q}_a^*)\Big]}{M_{11}(\mathbf{q}_a^*)}.$$

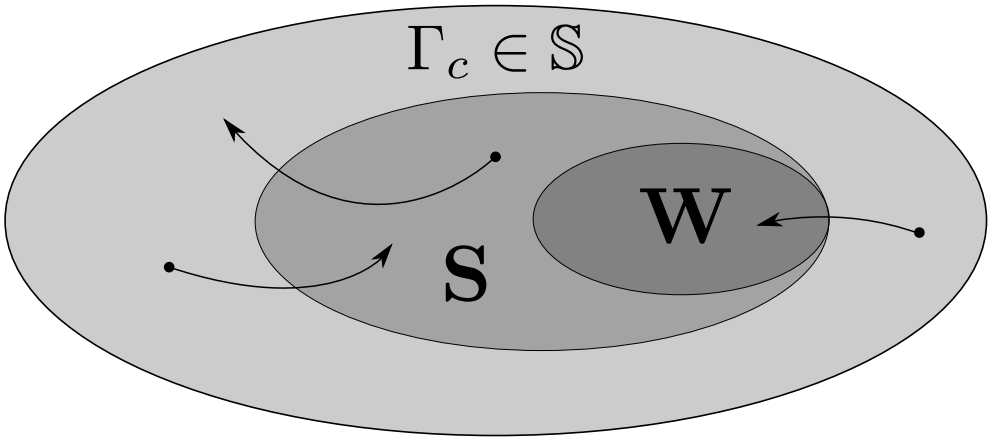

FIGURE A.1: The invariant sets in the state-space $\mathbb{S} \in \mathbb{R}^n$.

The complete definition of the invariant set $\mathbf{W}$ is thus defined as follows

$$\mathbf{W} = \left\{ (\mathbf{q}, \dot{\mathbf{q}}) \in \mathbf{S} \;\middle|\; \dot{q}_1^2 = \frac{2\Big[E^* - \mathbf{P}(q_1, \mathbf{q}_a^*)\Big]}{M_{11}(\mathbf{q}_a^*)};\; q_2 = q_2^* \right\}$$

[5]. The trajectories of the system will therefore, according to invariant set theory, tend toward the invariant set $\mathbf{W}$ as $t \to \infty$. The dynamics of the system described by $\ddot{\mathbf{q}}_a$ simplifies as a consequence of the states being found at an equilibrium point, where $E = E^*$ and $\ddot{q}_2 = \dot{q}_2 = 0$ [5]. Therefore

$$(E^* - E_r)\tau_2 + k_P q_2^* = 0. \tag{A.20}$$

There may be a number of possible equilibrium points that exist within the invariant set $\mathbf{W}$, of which includes both the UEP and the FPEP. We will thus classify the equilibrium points according to the mechanical energy of the system found at the equilibrium point E^*, whereby the equilibrium point of greatest concern is the UEP (where $E^* = E_r$). There are two specific groups of equilibrium points within $\mathbf{W}$ defined in [5], which are catered for in this proof.

Case 1: $E^* = E_r$.

In this case, it is clear that eq. (A.20) simplifies to the expression

$$k_P q_2^* = 0.$$

It is, therefore, evident that $q_2^* = 0$ since $k_P \neq 0$. This leads to the observation that $V^* = 0$ when $E^* = E_r$ (as seen in [5]) through the substitution of the relevant variables). Additionally, $q_2 = 0$. We can thus define an invariant set $\mathbf{W}_r$, which is a

subset of the invariant set $\mathbf{W}$ and is described by

$$\mathbf{W}_r = \left\{ (\mathbf{q}, \dot{\mathbf{q}}) \in \mathbf{W} \;\middle|\; \dot{q}_1^2 = \frac{2\Big[E_r - \mathbf{P}(q_1)\Big]}{M_{11}(0)};\; q_2^* = 0 \right\} \tag{A.21}$$

[5]. This definition can be refined through simplification involving eq. (7.9), where

$$\begin{aligned} \mathbf{P}(q_1, q_2^*)\Big|_{q_2^*=0} &= \overline{\beta}_1 \cos(q_1) + \overline{\beta}_2 \cos(q_1) \\ &= \left[\overline{\beta}_1 + \overline{\beta}_2\right] \cos(q_1) = E_r \cos(q_1). \end{aligned}$$

Therefore, taking the conditions of the set $\mathbf{W}_r$ in eq. (A.21), we find that

$$\begin{aligned} \dot{q}_1^2 &= \frac{2\Big[E_r - \mathbf{P}(q_1)\Big]}{M_{11}(0)} \\ &= \frac{2(E_r - E_r \cos q_1)}{M_{11}(0)} \\ &= \frac{2E_r(1 - \cos q_1)}{M_{11}(0)} \end{aligned}$$

[5]. This trajectory represents a homoclinic orbit with the equilibrium point

$$\mathbf{x}^* = (q_1, \dot{q}_1) = (2\pi k, 0), \quad k \in \mathbb{Z}$$

which is the UEP [5]. We therefore define the homoclinic orbit according to [5, pg. 27]:

Definition A.1. If an equilibrium point $\mathbf{x} = \mathbf{x}^*$ exists, then the trajectory $\phi(t)$ is a homoclinic orbit if

$$\phi(t) \to \mathbf{x}^* \quad \text{as } t \to \pm\infty.$$

The homoclinic orbit rests on the intersection between a stable and unstable manifold.

Therefore, the trajectory of the system will tend toward the equilibrium point $\mathbf{x}^*$ in $\mathbf{W}_r$ as $t \to \pm\infty$, thus resulting in successful swing-up of the robot to the UEP.

Case 2: $E^* \neq E_r$

The following derivation aims to demonstrate the possibility of the trajectory tending towards an equilibrium point outside of the invariant set $\mathbf{W}_r$, i.e.

$$(q_1, q_2, \dot{q}_1, \dot{q}_2) \to (q_1^*, q_2^*, 0, 0)$$

[5]. This is achieved by proving that the state q_1 tends towards some constant value q_1^* as $t \to \infty$, since it has already been proven that $\lim_{t\to\infty} q_2 = q_2^*$ in $\mathbf{W}$.

We now proceed with the proof through the execution of the following steps, as seen in [5].

Step (i): We will first assume that $q_1 \neq q_1^*$ in an attempt to proof $q_1 = q_1^*$ through contradiction. With this assumption in mind, we will prove that $\tau_2 = \tau_2^*$ and derive a set of conditions that must be adhered to if $q_1(t) \neq q_1^*$.

Step (ii): We will then prove, using a set of nonlinear equations derived in the previous step, that $\cos q_2^* = -1$ satisfies $q_1(t) \neq q_1^*$ along with the equality

$$(\overline{\alpha}_1 - \overline{\alpha}_3)\overline{\beta}_2 + (\overline{\alpha}_2 - \overline{\alpha}_3)\overline{\beta}_1 = 0.$$

Additionally, we will use this equality to prove that $\tau_2 = 0$ and that $q_2^* = 0$, which demonstrates a contradiction, proving that $q_1(t) = q_1^*$.

We shall now derive this proof for the undamped MC-ROPA$_{n-1}$ robot.

Proof A.4.1. ***Step (i):*** *In the case where $E^* \neq E_r$, the dynamical equation of the states represented in eq. (A.20) simplifies to*

$$k_p q_2^* + (E^* - E_r)\tau_2 = 0. \tag{A.22}$$

It is evident that since all of the components of eq. (A.22) are constant except for τ_2, it can be concluded that τ_2 itself must be a constant. Additionally, it has been established that the invariant set $\mathbf{W}$ is characterised by $q_2 = q_2^*$ and $q_1(t)$. Taking this into consideration, eqs. (8.9a) and (8.9b) are simplified to

$$\overline{M}_{11}\left(q_2^*\right)\ddot{q}_1 - \overline{\beta}_1 \sin q_1 - \overline{\beta}_2 \sin(q_1 + q_2^*) = 0, \tag{A.23a}$$

$$\overline{M}_{21}\left(q_2^*\right)\ddot{q}_1 + \overline{\alpha}_3 \dot{q}_1^2 \sin q_2^* - \overline{\beta}_2 \sin(q_1 + q_2^*) = \tau_2^*. \tag{A.23b}$$

Therefore, manipulating eq. (A.23a), we find that

$$\ddot{q}_1 = \frac{\overline{\beta}_1 \sin(q_1) + \overline{\beta}_2 \sin(q_1 + q_2^*)}{\overline{M}_{11}\left(q_2^*\right)}. \tag{A.24}$$

Substituting eq. (A.24) into eq. (A.23b) produces

$$\frac{\overline{M}_{21}\left(q_2^*\right)}{\overline{M}_{11}\left(q_2^*\right)}\left[\overline{\beta}_1 \sin(q_1) + \overline{\beta}_2 \sin(q_1 + q_2^*)\right] + \overline{\alpha}_3 \dot{q}_1^2 \sin q_2^* - \overline{\beta}_2 \sin(q_1 + q_2^*) = \tau_2^*. \tag{A.25}$$

Taking the time derivative of eq. (A.25) results

$$\dot{q}_1 \left[\frac{\overline{M}_{21}\left(q_2^*\right)}{\overline{M}_{11}\left(q_2^*\right)} \left(\overline{\beta}_1 \cos(q_1) + \overline{\beta}_2 \cos(q_1 + q_2^*)\right) + 2\overline{\alpha}_3 \ddot{q}_1 \sin q_2^* \right. \tag{A.26}$$
$$\left. - \overline{\beta}_2 \cos(q_1 + q_2^*) \right] = 0.$$

We, once again, substitute eq. (A.24) into eq. (A.26), which produces

$$\dot{q}_1 \left[\left(\frac{\overline{M}_{21}\left(q_2^*\right)}{\overline{M}_{11}\left(q_2^*\right)} \left[\overline{\beta}_1 + \overline{\beta}_2 \cos q_2^*\right] + \frac{2\overline{\alpha}_3 \overline{\beta}_2 \sin^2 q_2^*}{\overline{M}_{11}\left(q_2^*\right)} - \overline{\beta}_2 \cos q_2^* \right) \cos q_1 - \right.$$
$$\left. \left(\frac{\overline{M}_{21}\left(q_2^*\right)}{\overline{M}_{11}\left(q_2^*\right)} \overline{\beta}_2 \sin q_2^* - 2\overline{\alpha}_3 \left[\frac{\overline{\beta}_1 + \overline{\beta}_2 \cos q_2^*}{\overline{M}_{11}\left(q_2^*\right)} \right] \sin q_2^* - \overline{\beta}_2 \sin q_2^* \right) \sin q_1 \right] = 0.$$

This equation is represented as

$$\dot{q}_1 \Big[A_0\left(q_2^*\right) \cos q_1 - B_0\left(q_2^*\right) \sin q_1 \Big] = 0 \tag{A.27}$$

where

$$A_0\left(q_2^*\right) = \frac{\overline{M}_{21}\left(q_2^*\right)}{\overline{M}_{11}\left(q_2^*\right)} \left[\overline{\beta}_1 + \overline{\beta}_2 \cos q_2^*\right] + \frac{2\overline{\alpha}_3 \overline{\beta}_2 \sin^2 q_2^*}{\overline{M}_{11}\left(q_2^*\right)} - \overline{\beta}_2 \cos q_2^*, \tag{A.28}$$

$$B_0\left(q_2^*\right) = \frac{\overline{M}_{21}\left(q_2^*\right)}{\overline{M}_{11}\left(q_2^*\right)} \overline{\beta}_2 \sin q_2^* - 2\overline{\alpha}_3 \left[\frac{\overline{\beta}_1 + \overline{\beta}_2 \cos q_2^*}{\overline{M}_{11}\left(q_2^*\right)} \right] \sin q_2^* - \overline{\beta}_2 \sin q_2^*. \tag{A.29}$$

It is, therefore, apparent through the inspection of eq. (A.27) that if $q_1 \neq q_1^*$, then

$$A_0\left(q_2^*\right) \cos q_1 - B_0\left(q_2^*\right) \sin q_1 = 0.$$

This can only be true if $A_0\left(q_2^*\right) = 0$ and $B_0\left(q_2^*\right) = 0$, as shown in lemma A.1 (as seen in [5]).

Lemma A.1. If $q_1 \neq q_1^*$, we can represent eq. (A.27) as

$$\dot{q}_1 \Big[A_0\left(q_2^*\right) \cos q_1 - B_0\left(q_2^*\right) \sin q_1 \Big] = 0$$
$$= \dot{q}_1 \sqrt{{A_0}^2\left(q_2^*\right) + {B_0}^2\left(q_2^*\right)} \left[\frac{A_0\left(q_2^*\right) \cos q_1}{\sqrt{{A_0}^2\left(q_2^*\right) + {B_0}^2\left(q_2^*\right)}} - \frac{B_0\left(q_2^*\right) \sin q_1}{\sqrt{{A_0}^2\left(q_2^*\right) + {B_0}^2\left(q_2^*\right)}} \right].$$

Choosing

$$\cos \phi\left(q_2^*\right) = \frac{A_0\left(q_2^*\right)}{\sqrt{{A_0}^2\left(q_2^*\right) + {B_0}^2\left(q_2^*\right)}}, \tag{A.30a}$$

$$\sin\phi\left(q_2^*\right) = \frac{B_0\left(q_2^*\right)}{\sqrt{{A_0}^2\left(q_2^*\right) + {B_0}^2\left(q_2^*\right)}} \tag{A.30b}$$

we find that

$$\begin{aligned}
&\dot{q}_1\sqrt{{A_0}^2\left(q_2^*\right) + {B_0}^2\left(q_2^*\right)}\left[\cos\phi\left(q_2^*\right)\cos q_1 - \sin\phi\left(q_2^*\right)\sin q_1\right] \\
&= \dot{q}_1\sqrt{{A_0}^2\left(q_2^*\right) + {B_0}^2\left(q_2^*\right)}\cos\left(q_1 + \phi\left(q_2^*\right)\right) = 0.
\end{aligned} \tag{A.31}$$

Integrating eq. (A.31) with respect to time, we find that

$$\sqrt{{A_0}^2\left(q_2^*\right) + {B_0}^2\left(q_2^*\right)}\int \dot{q}_1(t)\cos\left(q_1(t) + \phi\left(q_2^*\right)\right)\mathrm{d}t = 0.$$

Using u-substitution, we choose

$$\begin{aligned}
u &= q_1(t), \\
\frac{\mathrm{d}u}{\mathrm{d}t} &= \dot{q}_1(t), \\
\therefore\ \mathrm{d}t &= \frac{\mathrm{d}u}{\dot{q}_1(t)}.
\end{aligned}$$

Performing the u-substitution produces

$$\begin{aligned}
&\sqrt{{A_0}^2\left(q_2^*\right) + {B_0}^2\left(q_2^*\right)}\int \cos\left(u + \phi\left(q_2^*\right)\right)\mathrm{d}u \\
&= \sqrt{{A_0}^2\left(q_2^*\right) + {B_0}^2\left(q_2^*\right)}\sin\left(q_1(t) + \phi\left(q_2^*\right)\right) + \underbrace{C}_{\text{Const. of Int.}} = 0, \\
&\therefore \sqrt{{A_0}^2\left(q_2^*\right) + {B_0}^2\left(q_2^*\right)}\sin\left(q_1(t) + \phi\left(q_2^*\right)\right) = -C = K.
\end{aligned} \tag{A.32}$$

This demonstrates a contradiction, since $q_1(t) = q_1^*(t)$ for the left-hand side of the equation in eq. (A.32) to equal the constant K. It has thus been proven through contradiction that for $q_1(t) = q_1^*$, $A_0\left(q_2^*\right) = 0$ and $B_0\left(q_2^*\right) = 0$. □

Step (ii): *Since $A_0\left(q_2^*\right) = 0$ and $B_0\left(q_2^*\right) = 0$, we can redefine the expressions seen in eqs. (A.28) and (A.29) as*

$$\begin{aligned}
A_0\left(q_2^*\right) &= \frac{\overline{M}_{21}\left(q_2^*\right)}{\overline{M}_{11}\left(q_2^*\right)}\left[\overline{\beta}_1 + \overline{\beta}_2\cos q_2^*\right] + \frac{2\overline{\alpha}_3\overline{\beta}_2\sin^2 q_2^*}{\overline{M}_{11}\left(q_2^*\right)} - \overline{\beta}_2\cos q_2^* \\
&= \frac{-1}{\overline{M}_{11}\left(q_2^*\right)}\left[-\overline{M}_{21}\left(q_2^*\right)\left[\overline{\beta}_1 + \overline{\beta}_2\cos q_2^*\right] - 2\overline{\alpha}_3\overline{\beta}_2\sin^2 q_2^* + \overline{M}_{11}\left(q_2^*\right)\overline{\beta_2}\cos q_2^*\right] \\
&= \frac{-1}{\overline{M}_{11}\left(q_2^*\right)}\left[\left[\overline{\alpha}_2 + \overline{\alpha}_3\cos q_2^*\right]\left[\overline{\beta}_1 + \overline{\beta}_2\cos q_2^*\right]\right] - 2\overline{\alpha}_3\overline{\beta}_2\sin^2 q_2^* + \left(\overline{\alpha}_1 + \overline{\alpha}_2 + \right. \\
&\qquad \left. 2\overline{\alpha}_3\cos q_2^*\right)\overline{\beta}_2\cos q_2^*\Big]
\end{aligned}$$

starting with $A_0\left(q_2^*\right) = 0$. *This simplifies to*

$$A_0\left(q_2^*\right) = \frac{-1}{\overline{M}_{11}\left(q_2^*\right)}\left[3\overline{\alpha}_3\overline{\beta}_2\cos^2 q_2^* - \left[\overline{\alpha}_3\overline{\beta}_1 - \overline{\alpha}_1\overline{\beta}_2\right]\cos q_2^* - \overline{\alpha}_2\overline{\beta}_1 - 2\overline{\alpha}_3\overline{\beta}_2\right] = 0,$$
$$\therefore\ A_0\left(q_2^*\right) = 3\overline{\alpha}_3\overline{\beta}_2\cos^2 q_2^* - \left[\overline{\alpha}_3\overline{\beta}_1 - \overline{\alpha}_1\overline{\beta}_2\right]\cos q_2^* - \overline{\alpha}_2\overline{\beta}_1 - 2\overline{\alpha}_3\overline{\beta}_2.$$

For $B_0\left(q_2^*\right)$, *we find that*

$$\begin{aligned}
B_0\left(q_2^*\right) &= \frac{\overline{M}_{21}\left(q_2^*\right)}{\overline{M}_{11}\left(q_2^*\right)}\overline{\beta}_2\sin q_2^* - 2\overline{\alpha}_3\left[\frac{\overline{\beta}_1 + \overline{\beta}_2\cos q_2^*}{\overline{M}_{11}\left(q_2^*\right)}\right]\sin q_2^* - \overline{\beta}_2\sin q_2^* \\
&= \frac{-1}{\overline{M}_{11}\left(q_2^*\right)}\left[-\overline{M}_{21}\left(q_2^*\right)\overline{\beta}_2\sin q_2^* + 2\overline{\alpha}_3\left[\overline{\beta}_1 + \overline{\beta}_2\cos q_2^*\right]\sin q_2^* + \right. \\
&\quad \left.\overline{M}_{11}\left(q_2^*\right)\overline{\beta}_2\sin q_2^*\right] \\
&= \frac{-1}{\overline{M}_{11}\left(q_2^*\right)}\left[-\left(\overline{\alpha}_2 + \overline{\alpha}_3\cos q_2^*\right)\overline{\beta}_2\sin q_2^* + 2\overline{\alpha}_3\left[\overline{\beta}_1 + \overline{\beta}_2\cos q_2^*\right]\sin q_2^* + \left(\overline{\alpha}_1 + \right.\right. \\
&\qquad \left.\left.\overline{\alpha}_2 + 2\overline{\alpha}_3\cos q_2^*\right)\overline{\beta}_2\sin q_2^*\right].
\end{aligned}$$

This simplifies to

$$B_0\left(q_2^*\right) = \frac{-1}{\overline{M}_{11}\left(q_2^*\right)}\left[\left(3\overline{\alpha}_3\overline{\beta}_2\cos q_2^* + 2\overline{\alpha}_3\overline{\beta}_1 + \overline{\alpha}_1\overline{\beta}_2\right)\sin q_2^*\right] = 0,$$
$$\therefore\ B_0\left(q_2^*\right) = \left(3\overline{\alpha}_3\overline{\beta}_2\cos q_2^* + 2\overline{\alpha}_3\overline{\beta}_1 + \overline{\alpha}_1\overline{\beta}_2\right)\sin q_2^*.$$

Manipulating $B_0\left(q_2^*\right)$ *further we can show that*

$$\begin{aligned}
B_0\left(q_2^*\right) &= 3\overline{\alpha}_3\overline{\beta}_2\left[\cos q_2^* + \frac{2\overline{\alpha}_3\overline{\beta}_1 + \overline{\alpha}_1\overline{\beta}_2}{3\overline{\alpha}_3\overline{\beta}_2}\right]\sin q_2^* \\
&= 3\overline{\alpha}_3\overline{\beta}_2\left[\cos q_2^* + \overline{\alpha}_0\right]\left[1 - \cos^2 q_2^*\right]^{1/2}
\end{aligned}$$

where

$$\overline{\alpha}_0 = \frac{2\overline{\alpha}_3\overline{\beta}_1 + \overline{\alpha}_1\overline{\beta}_2}{3\overline{\alpha}_3\overline{\beta}_2}. \tag{A.33}$$

It is evident, therefore, that if $B_0\left(q_2^*\right) = 0$, *then*

$$\begin{array}{lll}
\textit{(i)} & \cos q_2^* = -\overline{\alpha}_0, & \textit{or} \\
\textit{(ii)} & \cos q_2^* = 1, & \textit{or} \\
\textit{(iii)} & \cos q_2^* = -1. &
\end{array} \tag{A.34}$$

We shall first assume that $\cos q_2^* = -\overline{\alpha}_0$. *If this is the case, then*

$$A_0\left(q_2^*\right)\Big|_{\cos q_2^* = -\overline{\alpha}_0} = \overline{\alpha}_3\overline{\beta}_2\overline{\alpha}_0{}^2 + \left[\overline{\alpha}_3\overline{\beta}_1 - \overline{\alpha}_1\overline{\beta}_2\right]\overline{\alpha}_0 - \overline{\alpha}_2\overline{\beta}_1 - 2\overline{\alpha}_3\overline{\beta}_2$$

$$
\begin{aligned}
&= 6\overline{\alpha_3}^2\overline{\beta}_1{}^2 + 3\overline{\alpha}_1\overline{\alpha}_3\overline{\beta}_1\overline{\beta}_2 - 3\overline{\alpha}_2\overline{\alpha}_3\overline{\beta}_1\overline{\beta}_2 - 6\overline{\alpha}_3{}^2\overline{\beta}_2{}^2 \\
&= 2\overline{\alpha}_3\left[\overline{\beta}_1{}^2 - \overline{\beta}_2{}^2\right] + \overline{\beta}_1\overline{\beta}_2\left[\overline{\alpha}_1 - \overline{\alpha}_2\right] = 0. \qquad \text{(A.35)}
\end{aligned}
$$

Knowing that

$$
\overline{\alpha}_3 = \overline{m}_2\bar{l}_2L_1, \qquad \overline{\beta}_2 = \overline{m}_2\bar{l}_2g \qquad \text{(A.36)}
$$

we can simplify eq. (A.35) to

$$
\overline{\alpha}_2g\overline{\beta}_1 + 2L_1\beta_2{}^2 = \left[2L_1\overline{\beta}_1 + \overline{\alpha}_1g\right]\overline{\beta}_1. \qquad \text{(A.37)}
$$

We can further manipulate this inequality to make $\overline{\alpha}_1$ the subject of the equation, resulting in

$$
\overline{\alpha}_1 \leq \frac{L_1\left(3\overline{\beta}_2 - 2\overline{\beta}_1\right)}{g}. \qquad \text{(A.38)}
$$

Additionally, if $\cos q_2^* = -\overline{\alpha}_0$, then $-1 \leq \overline{\alpha}_0 \leq 1$. But, according to eq. (A.33),

$$
\overline{\alpha}_0 = \frac{2\overline{\alpha}_3\overline{\beta}_1 + \overline{\alpha}_1\overline{\beta}_2}{3\overline{\alpha}_3\overline{\beta}_2} \nleq 0.
$$

Therefore, $0 < \overline{\alpha}_0 \leq 1$. We can also show that

$$
2\overline{\alpha}_3\overline{\beta}_1 + \overline{\alpha}_1\overline{\beta}_2 \leq 3\overline{\alpha}_3\overline{\beta}_2
$$

through the manipulation of the expression in eq. (A.33). With the substitution of the expressions of eq. (A.36) into the above equation, we find that

$$
2L_1\overline{\beta}_1 + \overline{\alpha}_1g \leq 3L_1\overline{m}_2\bar{l}_2g.
$$

The inequality above can be further manipulated to bring the length of the COM of the VCL $\bar{l}_2$ into focus, whereby

$$
\bar{l}_2 \geq \frac{2L_1\overline{\beta}_1 + \overline{\alpha}_1g}{3L_1\overline{m}_2g}. \qquad \text{(A.39)}
$$

A new inequality is now derived through the substitution of the equality shown in eq. (A.38) into the expression in eq. (A.39), which results in

$$
\frac{\overline{\alpha}_2\overline{\beta}_1g + 2L_1\overline{\beta}_2{}^2 - 2L_1\overline{\beta}_1{}^2}{g\overline{\beta}_1} = \overline{\alpha}_1 \leq \frac{3L_1\overline{\beta}_2 - 2L_1\overline{\beta}_1}{g}.
$$

This simplifies to

$$
\frac{\overline{\alpha}_2g}{\overline{\beta}_2} \leq \frac{3L_1\overline{\beta}_1 - 2L_1\overline{\beta}_2}{\overline{\beta}_1}.
$$

Additionally, we find that

$$\begin{aligned}\frac{\overline{\alpha}_2 g}{\overline{\beta}_2} &= \frac{\overline{I}_2 + \overline{m}_2 \bar{l}_2{}^2}{\overline{m}_2 \bar{l}_2} \\ &= \frac{\overline{I}_2}{\overline{m}_2 \bar{l}_2} + \bar{l}_2 > \bar{l}_2.\end{aligned}$$

Therefore

$$\bar{l}_2 < \frac{\overline{\alpha}_2 g}{\overline{\beta}_2} \leq \frac{L_1\left(3\overline{\beta}_1 - 2\overline{\beta}_2\right)}{\overline{\beta}_1}.$$

This implies, therefore, that

$$\bar{l}_2 < \frac{L_1\left(3\overline{\beta}_1 - 2\overline{\beta}_2\right)}{\overline{\beta}_1}.$$

Substituting $\overline{\beta}_2$ from eq. (A.36) into the expression above produces

$$\bar{l}_2 < \frac{3L_1\overline{\beta}_1}{\overline{\beta}_1 + 2L_1\overline{m}_2 g}.$$

Therefore, $\bar{l}_2$ is bounded by

$$\frac{2L_1\overline{\beta}_1 + \overline{\alpha}_1 g}{3L_1\overline{m}_2 g} \leq \bar{l}_2 < \frac{3L_1\overline{\beta}_1}{\overline{\beta}_1 + 2L_1\overline{m}_2 g}. \tag{A.40}$$

Therefore

$$\frac{2L_1\overline{\beta}_1 + \overline{\alpha}_1 g}{3L_1\overline{m}_2 g} < \frac{3L_1\overline{\beta}_1}{\overline{\beta}_1 + 2L_1\overline{m}_2 g}$$

which simplifies to

$$5\overline{m}_2 L_1{}^2 > \frac{2L_1\overline{\beta}_1}{g} + \overline{\alpha}_1 + \frac{2\overline{\alpha}_1 L_1\overline{m}_2 g}{\overline{\beta}_1}. \tag{A.41}$$

We know that

$$\overline{\alpha}_1 = I_1 + m_1 l_1{}^2 + \overline{m}_2 L_1{}^2.$$

Therefore $\overline{\alpha}_1 > \overline{m}_2 L_1{}^2$. Additionally, using the inequality $a + b \geq 2\sqrt{ab}$ for $a > 0$ and $b > 0$ (shown in [5, pg. 55]), with

$$a = \frac{2L_1\overline{\beta}_1}{g}, \qquad b = \frac{2\overline{\alpha}_1 L_1\overline{m}_2 g}{\overline{\beta}_1}$$

we find that

$$\frac{2L_1\overline{\beta}_1}{g} + \frac{2\overline{\alpha}_1 L_1 \overline{m}_2 g}{\overline{\beta}_1} \geq 4L_1\sqrt{\overline{\alpha}_1\overline{m}_2}.$$

But, if $\overline{\alpha}_1 > \overline{m}_2 {L_1}^2$ *then*

$$4L_1\sqrt{\overline{\alpha}_1\overline{m}_2} > 4\overline{m}_2{L_1}^2.$$

Therefore

$$\overline{\alpha_1} + \frac{2\overline{m}_2\overline{\alpha}_1 g L_1}{\overline{\beta}_1} + \frac{2L_1\overline{\beta}_1}{g} > 5\overline{m}_2{L_1}^2.$$

This is contradictory to the inequality demonstrated in eq. (A.41). It is evident, therefore, that $\cos q_2^* \neq \overline{\alpha}_0$.

If $\cos q_2^* = 1$, *then*

$$\begin{aligned} A_0\left(q_2^*\right)\Big|_{\cos q_2^*=1} &= 3\overline{\alpha}_3\overline{\beta}_2 - \left[\overline{\alpha}_3\overline{\beta}_1 - \overline{\alpha}_1\overline{\beta}_2\right] - \left[\overline{\alpha}_2\overline{\beta}_1 + 2\overline{\alpha}_3\overline{\beta}_2\right] \\ &= \overline{\alpha}_3\overline{\beta}_2 - \overline{\alpha}_3\overline{\beta}_1 + \overline{\alpha}_1\overline{\beta}_2 - \overline{\alpha}_2\overline{\beta}_1. \end{aligned}$$

A modification on Lemma 2.1 in [5] shows that

$$\overline{\alpha}_2\overline{\beta}_1 + \overline{\alpha}_3\overline{\beta}_1 - \overline{\alpha}_1\overline{\beta}_2 - \overline{\alpha}_3\overline{\beta}_2 > 0. \tag{A.42}$$

This shows, therefore, that $A_0\left(q_2^*\right) < 0$, *but this does not satisfy the necessary condition shown in lemma A.1, which states that* $A_0\left(q_2^*\right)$ *must equal 0. This, therefore, proves that* $\cos q_2^* \neq 1$ *through contradiction.*

The only possible solution that satisfies lemma A.1 is $\cos q_2^* = -1$. *If this is the case, we find that*

$$\sin q_2^* = \sqrt{1 - \cos^2 q_2^*} = 0. \tag{A.43}$$

We also find that

$$A_0\left(q_2^*\right)\Big|_{\cos q_2^*=-1} = \left(\overline{\alpha}_1 - \overline{\alpha}_3\right)\overline{\beta}_2 + \left(\overline{\alpha}_2 - \overline{\alpha}_3\right)\overline{\beta}_1 = 0. \tag{A.44}$$

This must hold when $q_1(t) \neq q_1^*$. *The dynamical equation of the VCL shown in eq. (8.9b) simplifies with the consideration of eq. (A.43) and* $\cos q_2^*$ *into*

$$\begin{aligned} &\overline{M}_{21}\left(q_2^*\right)\ddot{q}_1 - \overline{\beta}_2 \sin\left(q_1 + q_2^*\right) \\ &= \overline{M}_{21}\left(q_2^*\right)\ddot{q}_1 + \overline{\beta}_2 \sin q_1 = \tau_2^*. \end{aligned}$$

Substituting eq. (A.24) into the expression above produces

$$\begin{aligned}
&\overline{M}_{21}\left(q_2^*\right)\left[\frac{\overline{\beta}_1 \sin q_1 + \overline{\beta}_2 \sin\left(q_1 + q_2^*\right)}{\overline{M}_{11}\left(q_2^*\right)}\right] + \overline{\beta}_2 \sin q_1 \\
&= \left[\frac{\left[\overline{\alpha}_2 - \overline{\alpha}_3\right]\left[\overline{\beta}_1 - \overline{\beta}_2\right]}{\overline{\alpha}_1 + \overline{\alpha}_2 - 2\overline{\alpha}_3} \sin q_1 + \overline{\beta}_2\right] \sin q_1 \\
&= \left[\frac{\left[\overline{\alpha}_2 - \overline{\alpha}_3\right]\overline{\beta}_1 + \left[\overline{\alpha}_1 - \overline{\alpha}_3\right]\overline{\beta}_2}{\overline{\alpha}_1 + \overline{\alpha}_2 - 2\overline{\alpha}_3}\right] \sin q_1 = \tau_2^*. \qquad \text{(A.45)}
\end{aligned}$$

It is evident, however, that eq. (A.45) is equal to zero because of eq. (A.44). Therefore, $\tau_2 = \tau_2^* = 0$. *If we substitute this expression for the torque into eq. (A.20) we find that*

$$k_P q_2^* = 0.$$

Therefore, the only solution to the equality would be if $q_2^* = 0$. *This, however, contradicts* $\cos q_2^* = -1$. *We thus have proven through contradiction that* $q_1(t) = q_1^*$. *This shows that when* $E^* \neq E_r$ *and* $k_D > k_{DM}$, $k_P > 0$, *and* $k_V > 0$ *then* $(q_1, q_2, \dot{q}_1, \dot{q}_2) = (q_1^*, q_2^*, 0, 0)$ *as* $t \to \infty$. □

So at this point in the evaluation of the MC-ROPA$_{n-1}$ system trajectory in the invariant set $\mathbf{W}$ when $E \neq E_r$, we know that

$$\begin{aligned}
q_1(t) = q_1^* = q_1^e, \qquad & \qquad \ddot{q}_1 = \dot{q}_1 = 0, \\
E^* &= P\left(q_2^e\right), \\
\tau_2 &= \tau_2^* = \tau_2^e, \\
\mathbf{q}_a &= q_2^* = q_2^e.
\end{aligned}$$

Substituting these expressions into eq. (8.9a) and (8.9b) produces

$$\overline{\beta}_1 \sin q_1^e + \overline{\beta}_2 \sin\left(q_1^e + q_2^e\right) = 0$$

and

$$\tau_2^e = -\overline{\beta}_2 \sin\left(q_1^e + q_2^e\right).$$

Evaluating eq. (A.20) considering the newly derived expressions above we find that

$$k_P q_2^e - \left[P\left(\mathbf{q}^e\right) - E_r\right]\overline{\beta}_2 \sin\left(q_1^e + q_2^e\right) = 0.$$

We now define a new invariant set

$$\Omega = \left\{ \left(\mathbf{q}^e, 0\right) \in \mathbf{W} \;\middle|\; \begin{array}{l} k_P q_2^e - \left[\mathbf{P}\left(q_2^e\right) - E_r\right]\overline{\beta}_2 \sin\left(q_1^e + q_2^e\right) = 0; \\ \overline{\beta}_1 \sin q_1^e + \overline{\beta}_2 \sin\left(q_1^e + q_2^e\right) = 0. \end{array} \;\middle|\; \mathbf{P}\left(\mathbf{q}^e\right) \neq E_r \right\} \qquad \text{(A.46)}$$

which is a subset of $\mathbf{W}$. From this definition, it is evident that Ω encloses all

equilibrium points in $\mathbf{W}$ except for the UEP. Therefore, if $k_D > k_{DM}$, $k_P > 0$, and $k_V > 0$, then the invariant set $\mathbf{W}$ satisfies

$$\mathbf{W} = \mathbf{W}_r \cup \Omega, \qquad \mathbf{W}_r \cap \Omega = \emptyset$$

where $\mathbf{W}_r$ corresponds to the UEP and contains a trajectory described by a homoclinic orbit. The invariant set Ω encapsulates the equilibrium points that correspond with the condition $E \neq E_r$.

We have now established two specific invariant sets that are of importance to the swing-up control through the application of LDM. Ideally, to achieve the goal of swing-up control, the UEP should be the only equilibrium point in the system that has a basin of attraction. If any other equilibrium points (i.e. the equilibrium points in Ω) can be characterised as stable, even within an approximate neighbourhood, then it is impossible to guarantee satisfactory swing-up control. We must, therefore, identify the existing equilibrium points and determine what conditions will render these equilibrium points unstable. We will begin this derivation by first proving that the subsets of Ω related to a positive or zero potential energy for the undamped MC-ROPA$_{n-1}$ robot are empty sets, as seen in [5]. This results in the gain condition

$$\Omega_+ = \Omega_0 = \emptyset \leftrightarrow k_P > \frac{2}{\pi} \min\left\{\overline{\beta}_1, \overline{\beta}_2\right\}$$

[5].

Proof A.4.2. *To begin the proof, we identify the following subsets of Ω according to their relationship with the potential energy of the encapsulated equilibrium points, $\mathbf{P}(\mathbf{q}^e)$, where*

$$\begin{aligned}
\Omega_0 &= \left\{(\mathbf{q}^e, 0) \in \Omega \;\middle|\; \mathbf{P}(\mathbf{q}^e) = 0\right\}, \\
\Omega_+ &= \left\{(\mathbf{q}^e, 0) \in \Omega \;\middle|\; \mathbf{P}(\mathbf{q}^e) > 0\right\}, \\
\Omega_- &= \left\{(\mathbf{q}^e, 0) \in \Omega \;\middle|\; \mathbf{P}(\mathbf{q}^e) < 0\right\}
\end{aligned}$$

and where

$$\Omega = \Omega_0 \cup \Omega_+ \cup \Omega_-.$$

The objective of this proof, ideally, is to ensure that all of these subsets are null sets through the careful selection of an appropriate gain for k_P. We shall begin by evaluating the invariant set Ω_0.

As discussed earlier in this section, we find that,

$$\mathbf{P}(\mathbf{q}^e)\Big|_{\Omega_0} = \mathbf{\Phi}(q_2^e)$$

$$= \sqrt{\overline{\beta}_1{}^2 + \overline{\beta}_2{}^2 + 2\overline{\beta}_1\overline{\beta}_2 \cos q_2^e} = 0$$

according to eq. (A.17). Therefore

$$\overline{\beta}_1{}^2 + \overline{\beta}_2{}^2 + 2\overline{\beta}_1\overline{\beta}_2 \cos q_2^e = 0 \quad \textit{where } \mathbf{q} \in \Omega_0.$$

This can only be true if $\overline{\beta}_1 = \overline{\beta}_2$ *and* $\cos q_2^e = -1$*. This results in* $\sin q_2^e = 0$*. If this is true, then the combined COM of the VCL and the most proximal pendulum will fall exactly on the origin, resulting in* $\mathbf{P}\left(\mathbf{q}^e\right) = 0$*.*

Substituting these newly defined expressions into eq. (8.9b) produces

$$\begin{aligned} \tau_2^e &= -\overline{\beta}_2 \sin\left(q_1^e + q_2^e\right) \\ &= \overline{\beta}_2 \sin q_1^e. \end{aligned} \tag{A.47}$$

Substituting eq. (A.47) into eq. (A.20) results in

$$k_P q_2^e + \left(\mathbf{P}\left(\mathbf{q}^e\right) - E_r\right)\overline{\beta}_2 \sin q_1^e = 0. \tag{A.48}$$

But in the case of the MC-ROPA$_{n-1}$ *model, considering the fact that* $\overline{\beta}_1 = \overline{\beta}_2$*, we find that*

$$E_r = \overline{\beta}_1 + \overline{\beta}_2 = 2\overline{\beta}_1. \tag{A.49}$$

Therefore, substituting eq. (A.49) into eq. (A.48) produces

$$\begin{aligned} k_P q_2^e - 2\overline{\beta}_1{}^2 \sin q_1^e &= 0, \\ \therefore\ k_P &= \frac{2\overline{\beta}_1{}^2 \sin q_1^e}{q_2^e}. \end{aligned}$$

If $\cos q_2^e = -1$*, then it is evident that* $q_2^e = \pi \pm 2k\pi$ *where* $k \in \mathbb{Z}$*. It is also evident, therefore, that*

$$\min\left\{q_2^e\right\} = \pi.$$

Therefore

$$\begin{aligned} \sup_{q_2^e}\left\{k_P\right\} &= \max_{q_1^e}\left\{\frac{2\overline{\beta}_1{}^2 \sin q_1^e}{\pi}\right\}, \\ \therefore\ \sup_{(q_1^e, q_2^e)}\left\{k_P\right\} &= \frac{2\overline{\beta}_1{}^2}{\pi} \end{aligned} \tag{A.50}$$

since $\max_{q_1^e}\{\sin q_1^e\} = 1$. *Therefore, the invariant set* $\Omega_0 = \emptyset$ *if the value for* k_P *chosen exceeds the suprenum of* k_P *(shown in eq. (A.50)). Therefore*

$$k_P > \frac{2\overline{\beta}_1{}^2}{\pi}, \quad \overline{\beta}_1 = \overline{\beta}_2 \tag{A.51}$$

results in $\Omega_0 = \emptyset$ *since*

$$|k_P q_2^e| \geq k_P \pi > 2\overline{\beta}_1{}^2 \geq 2\overline{\beta}_1{}^2 \left|\sin q_1^e\right|$$

[5]. We now move on to evaluate the invariant set Ω_+.

In Ω_+, *the potential energy* $\mathbf{P}\left(\mathbf{q}^e\right)$, *considering eq. (7.11), is described as*

$$\mathbf{P}\left(\mathbf{q}^e\right)\Big|_{\Omega_+} = +\mathbf{\Phi}(q_2^e) = \sqrt{\overline{\beta}_1{}^2 + \overline{\beta}_2{}^2 + 2\overline{\beta}_1\overline{\beta}_2 \cos q_2^e} \tag{A.52}$$

$$= \overline{\beta}_1 \cos q_1^e + \overline{\beta}_2 \cos\left(q_1^e + q_2^e\right) > 0, \quad \textit{where } \mathbf{q} \in \Omega_+. \tag{A.53}$$

We can deduce from eq. (A.52) that $q_2^e \neq 2\pi k$ *where* $k \in \mathbb{Z}$ *since that would imply that* $\mathbf{\Phi}\left(q_2^e\right) = E_r$, *which cannot be the case since the equilibrium point associated with* $E^* = E_r$ *is found within the* $\mathbf{W}_r$ *invariant set. Additionally, the torque* τ_2^e *is defined through the simplification of eq. (8.9b), where*

$$\tau_2^e = -\overline{\beta}_2\left(q_1^e + q_2^e\right). \tag{A.54}$$

The dynamics of the system at the equilibrium can thus be described by

$$k_P q_2^e - \left[\mathbf{\Phi}\left(q_2^e\right) - E_r\right]\overline{\beta}_2 \sin\left(q_1^e + q_2^e\right) = 0 \tag{A.55}$$

through the substitution of eqs. (A.52) and (A.54) into eq. (A.20). It is difficult, in this case, to establish sufficient conditions for k_P *since both* q_1^e *and* q_2^e *are unknown. To solve this, we will eliminate* q_1^e *from this expression through the execution of the procedure that follows.*

We know that for all equilibrium points, the potential torque exerted on the most proximal pendulum, $\overline{K}_1(\mathbf{q}) = 0$ *(as shown in eq. (A.15)). Therefore,*

$$\overline{K}_1(\mathbf{q}^*) = -\overline{\beta}_1 \sin q_1^e - \overline{\beta}_2 \sin\left(q_1^e + q_2^e\right) = 0 \tag{A.56}$$

according to eq. (7.11). Therefore

$$\overline{\beta}_1 \sin q_1^e + \overline{\beta}_2 \sin\left(q_1^e + q_2^e\right) = 0.$$

We can thus eliminate q_1^e *in eq. (A.20) through*

$$\begin{aligned}\mathbf{P}\left(\mathbf{q}^e\right)\sin\left(q_1^e + q_2^e\right) &= \mathbf{P}\left(\mathbf{q}^e\right)\sin\left(q_1^e + q_2^e\right) + \overline{K}_1(\mathbf{q})\cos\left(q_1^e + q_2^e\right) \\ &= \left[\overline{\beta}_1 \cos q_1^e + \overline{\beta}_2 \cos\left(q_1^e + q_2^e\right)\right]\sin\left(q_1^e + q_2^e\right) - \left[\overline{\beta}_1 \sin q_1^e + \right.\end{aligned}$$

$$\begin{aligned}
&\overline{\beta}_2 \sin\left(q_1^e + q_2^e\right)\Big] \cos\left(q_1^e + q_2^e\right) \\
&= \overline{\beta}_1 \left[\cos q_1^e \sin\left(q_1^e + q_2^e\right) - \sin q_1^e \cos\left(q_1 + q_2^e\right)\right] \\
&= \overline{\beta}_1 \sin q_2^e. \qquad \text{(A.57)}
\end{aligned}$$

Therefore

$$\begin{aligned}
\mathbf{P}\left(\mathbf{q}^e\right) \sin\left(q_1^e + q_2^e\right) &= \overline{\beta}_1 \sin q_2^e, \\
\therefore \ \sin\left(q_1^e + q_2^e\right) &= \frac{\overline{\beta}_1 \sin q_2^e}{\mathbf{P}\left(\mathbf{q}^e\right)} = \frac{\overline{\beta}_1 \sin q_2^e}{\mathbf{\Phi}\left(q_2^e\right)}. \qquad \text{(A.58)}
\end{aligned}$$

Substituting eq. (A.58) into eq. (A.55) produces

$$k_P q_2^e - \left[\mathbf{\Phi}\left(q_2^e\right) - E_r\right] \left[\frac{\overline{\beta}_1 \overline{\beta}_2 \sin q_2^e}{\mathbf{\Phi}\left(q_2^e\right)}\right] = 0.$$

Therefore

$$\frac{k_P q_2^e}{\overline{\beta}_1 \overline{\beta}_2} = \frac{\left[\mathbf{\Phi}\left(q_2^e\right) - E_r\right] \sin q_2^e}{\mathbf{\Phi}\left(q_2^e\right)} = \lambda\left(q_2^e\right) \qquad \text{(A.59)}$$

where $\mathbf{\Phi}\left(q_2^e\right) \neq E_r$. *The expression in eq. (A.59) can be simplified to*

$$q_2^e \left[\frac{k_P}{\overline{\beta}_1 \overline{\beta}_2} - \rho\left(q_2^e\right)\right] = 0 \qquad \text{(A.60)}$$

where $q_2^e \neq 2\pi k$ *with* $k \in \mathbb{Z}$ *and*

$$\rho\left(q_2^e\right) = \frac{\left[\mathbf{\Phi}\left(q_2^e\right) - E_r\right]}{\mathbf{\Phi}\left(q_2^e\right) q_2^e} \sin q_2^e.$$

Therefore, to ensure that eq. (A.60) is not realisable, and thus resulting in $\Omega_+ = \emptyset$, *the condition*

$$k_P > \overline{\beta}_1 \overline{\beta}_2 \sup_{q_2^e \neq 0} \left\{\rho\left(q_2^e\right)\right\} \qquad \text{(A.61)}$$

must be adhered to. An example of the function $\rho\left(q_2^e\right)$ *is plotted with its suprenum in figure A.2. Therefore, eq. (A.61) suggests that the value of* $k_P / \overline{\beta}_1 \overline{\beta}_2$ *must be greater than the suprenum of* $\rho\left(q_2^e\right)$ *for* $\Omega_+ = \emptyset$ *[5].*

Another way of approaching this problem is by comparing the straight line function on the left-hand side of eq. (A.59) with $\lambda\left(q_2^e\right)$. *An example of the relationship between* $\lambda\left(q_2^e\right)$ *and* $\lambda\left(q_2^e\right)$ *is plotted in figure A.3. It is evident that a sufficiently large gain must be chosen to prevent an intercept between the straight-line function and* $\lambda\left(q_2^e\right)$ *(as seen with the red dashed line in the figure). If the gain is insufficiently large, more intercepts between these two functions will occur (as shown by the blue dashed line), which demonstrates that* $\Omega_+ \neq \emptyset$. *The intercept at the origin is not of concern since* $q_2^e \neq 0$. *This must, however, be proven*

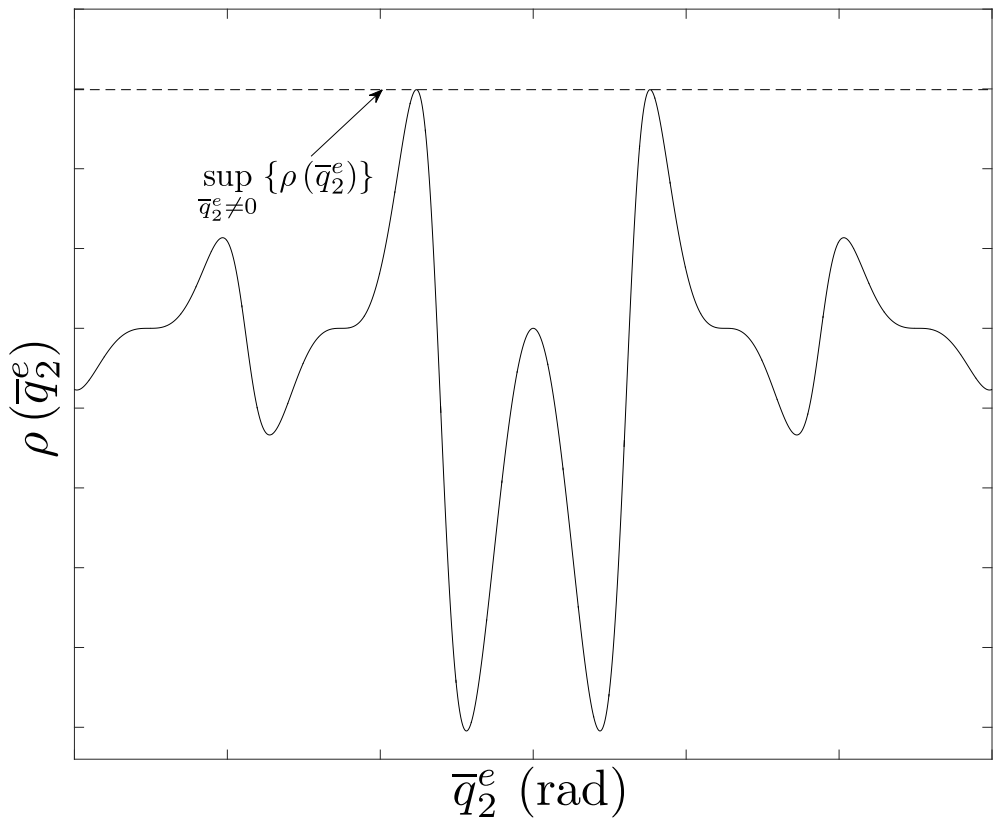

FIGURE A.2: An example of a function $\rho(q_2^e)$ with its suprenum value.

analytically, to guarantee that for all examples a sufficiently large gain can be chosen to ensure that $\Omega_+ = \emptyset$.

It is evident that the function $\rho(q_2^e)$ *is an even function, demonstrating symmetry across the vertical axis. Indeed, it is also evident that, since* $\mathbf{\Phi}(q_2^e) < E_r \; \forall q_2^e$ *and* $\sin q_2^e < 0$ *when* $(2k-1)\pi < q_2^e < 2\pi k$ *where* $k \in \mathbb{Z}$*, then*

$$\sup_{q_2^e \neq 0} \{\rho(q_2^e)\} = \sup_k \left\{ \sup_{q_2^e \in ((2k-1)\pi, 2\pi k)} \rho(q_2^e) \right\}$$

[5]. This is true since the suprenum cannot be located within boundaries that are guaranteed to have a negatively valued function. It is also apparent that the function $\rho(q_2^e)$ *will be attenuated as* $q_2^e \to \pm\infty$*. The true suprenum of* $\rho(q_2^e)$ *must, therefore, be located between the limits of the first possible positive peak (i.e. when* $k = 1$*). This leads to*

$$\sup_{q_2^e \neq 0} \{\rho(q_2^e)\} = \sup_k \left\{ \sup_{q_2^e \in ((2k-1)\pi, 2\pi k)} \rho(q_2^e) \right\} \Bigg|_{k=1} = \sup_{q_2^e \in (\pi, 2\pi)} \{\rho(q_2^e)\}$$

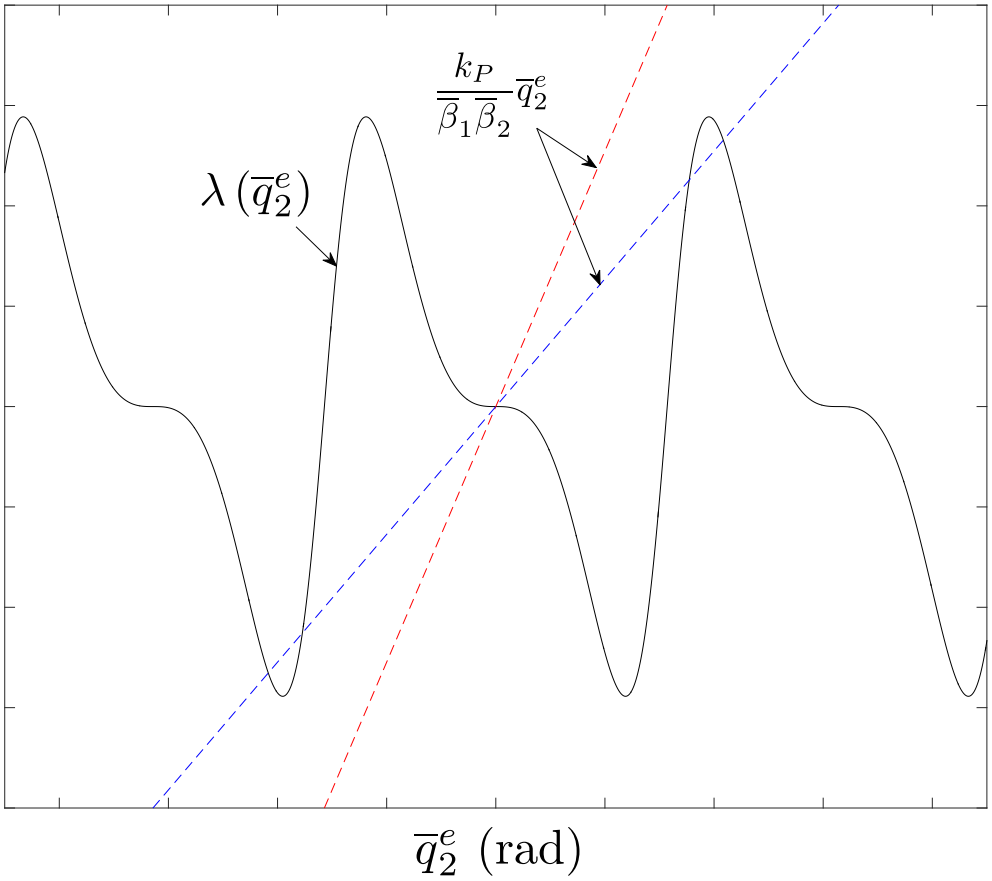

FIGURE A.3: An example of the intercepts between the straight-line functions governed by k_P (red line has a sufficiently large gradient, unlike the blue line) and the function $\lambda\left(q_2^e\right)$ with its suprenum value. Adapted from [5].

[5]. The expression above is manipulated and represented as

$$\sup_{q_2^e \in (\pi, 2\pi)} \left\{\rho\left(q_2^e\right)\right\} = \sup_{q_2^e \in (\pi, 2\pi)} \left\{\left[\frac{\mathbf{\Phi}\left(q_2^e\right) - E_r}{q_2^e}\right]\left(\frac{\sin q_2^e}{\mathbf{\Phi}\left(q_2^e\right)}\right)\right\} \tag{A.62}$$

[5]. We know, from [5, pg. 46], that

$$|\sin z| \leq \min\left\{\frac{1}{b}, \frac{1}{x}\right\} h(b, x, z).$$

So since $\mathbf{\Phi}\left(q_2^e\right) = h\left(\overline{\beta}_1, \overline{\beta}_2, q_2^e\right)$ *and* $\mathbf{\Phi}\left(q_2^e\right) = \left|\mathbf{\Phi}\left(q_2^e\right)\right|$ *since* $\mathbf{\Phi}\left(q_2^e\right) > 0$*, then*

$$\left|\frac{\sin q_2^e}{\mathbf{\Phi}\left(q_2^e\right)}\right| \leq \min\left\{\frac{1}{\overline{\beta}_1}, \frac{1}{\overline{\beta}_2}\right\}. \tag{A.63}$$

Additionally

$$\sin q_2^e|_{q_2^e \in (\pi, 2\pi)} = -\left|\sin q_2^e\right|.$$

Therefore, eq. (A.62) may be represented as

$$\begin{aligned}\sup_{q_2^e \in (\pi,2\pi)} \{\rho(q_2^e)\} &= \sup_{q_2^e \in (\pi,2\pi)} \left\{ \left[\frac{E_r - \mathbf{\Phi}(q_2^e)}{q_2^e} \right] \left| \frac{\sin q_2^e}{\mathbf{\Phi}(q_2^e)} \right| \right\} \\ &\leq \sup_{q_2^e \in (\pi,2\pi)} \left\{ \left[\frac{E_r - \mathbf{\Phi}(q_2^e)}{q_2^e} \right] \right\} \min\left\{ \frac{1}{\overline{\beta}_1}, \frac{1}{\overline{\beta}_2} \right\}\end{aligned}$$

[5]. From here, it is apparent that the suprenum will occur at $q_2^e = \pi$ since $\mathbf{\Phi}(q_2^e) = \left|\overline{\beta}_1 - \overline{\beta}_2\right| = \min_{q_2^e}\{\mathbf{\Phi}(q_2^e)\}$ (made evident by eq. (A.52)) where $\overline{\beta}_1 \neq \overline{\beta}_2$. Therefore

$$\begin{aligned}\sup_{q_2^e \in (\pi,2\pi)} \{\rho(q_2^e)\} &\leq \left[\frac{E_r - \left|\overline{\beta}_1 - \overline{\beta}_2\right|}{\pi} \right] \min\left\{ \frac{1}{\overline{\beta}_1}, \frac{1}{\overline{\beta}_2} \right\} \\ &\leq \left[\frac{\overline{\beta}_1 + \overline{\beta}_2 - \left|\overline{\beta}_1 - \overline{\beta}_2\right|}{\pi} \right] \min\left\{ \frac{1}{\overline{\beta}_1}, \frac{1}{\overline{\beta}_2} \right\}.\end{aligned}$$

Now, for the case where $\overline{\beta}_1 > \overline{\beta}_2$, we know that $\left|\overline{\beta}_1 - \overline{\beta}_2\right| = \overline{\beta}_1 - \overline{\beta}_2$. Additionally we find that

$$\min\left\{ \frac{1}{\overline{\beta}_1}, \frac{1}{\overline{\beta}_1} \right\} = \frac{1}{\overline{\beta}_1}.$$

Therefore

$$\sup_{q_2^e \in (\pi,2\pi)} \{\rho(q_2^e)\} \leq \frac{2}{\pi} \frac{\overline{\beta}_2}{\overline{\beta}_1}$$

where $\overline{\beta}_1 > \overline{\beta}_2$. For the case where $\overline{\beta}_2 > \overline{\beta}_1$, we know that $\left|\overline{\beta}_1 - \overline{\beta}_2\right| = \overline{\beta}_2 - \overline{\beta}_1$. We can also conclude that

$$\min\left\{ \frac{1}{\overline{\beta}_1}, \frac{1}{\overline{\beta}_2} \right\} = \frac{1}{\overline{\beta}_2}.$$

Therefore

$$\sup_{q_2^e \in (\pi,2\pi)} \{\rho(q_2^e)\} \leq \frac{2}{\pi} \frac{\overline{\beta}_1}{\overline{\beta}_2}$$

where $\overline{\beta}_2 > \overline{\beta}_1$. This result can be summarised as

$$\sup_{q_2^e \in (\pi,2\pi)} \{\rho(q_2^e)\} \leq \frac{2}{\pi} \min\left\{ \frac{\overline{\beta}_1}{\overline{\beta}_2}, \frac{\overline{\beta}_2}{\overline{\beta}_1} \right\}$$

which can also be represented as

$$\overline{\beta}_1\overline{\beta}_2 \sup_{q_2^e\in(\pi,2\pi)} \{\rho\left(q_2^e\right)\} \leq \frac{2}{\pi}\min\left\{\overline{\beta}_1{}^2, \overline{\beta}_2{}^2\right\}.$$

It is, therefore, apparent that for $\Omega_+ = \emptyset$, the condition

$$k_P > \frac{2}{\pi}\min\left\{\overline{\beta}_1{}^2, \overline{\beta}_2{}^2\right\} \tag{A.64}$$

must be satisfied, as seen from eq. (A.61) [5]. This is the same condition derived for the case of $\Omega_0 = \emptyset$, as seen in eq. (A.51). Therefore, it is evident that the gain condition $k_P > \frac{2}{\pi}\min\left\{\overline{\beta}_1{}^2, \overline{\beta}_2{}^2\right\}$ guarantees that $\Omega_0 = \emptyset$ and $\Omega_+ = \emptyset$.

We are now left with the Ω_- invariant set, which, if the *gain selection criterion* in eq. (A.64) is satisfied, can be represented as $\Omega_- = \Omega$. There are a number of objectives that remain outstanding in this regard, which will all be covered in the proof that follows. We, therefore, must prove that

(i) Ω_- has a finite number of equilibrium points.

(ii) All of the equilibrium points within the invariant set Ω_- are unstable.

(iii) The only equilibrium point within Ω_- is the FPEP.

(iv) The FPEP is unstable.

(v) The trajectory of the system will tend towards the invariant set $\mathbf{W}_r$ by following a homoclinic orbit.

Once again, all these items are demonstrated for the DDA in [5], but it is of use to the reader to include a proof specifically for the MC-ROPA$_{n-1}$ model, as justified in the beginning of this derivation.

Proof A.4.3. *(i) For Ω_-, we define the potential energy $\mathbf{P}\left(\mathbf{q}^e\right)$ as*

$$\mathbf{P}\left(\mathbf{q}^e\right) = \mathbf{P}\left(q_2^e\right) = -\mathbf{\Phi}\left(q_2^e\right).$$

Therefore

$$\sin\left(q_1^e + q_2^e\right) = -\frac{\overline{\beta}_1 \sin q_2^e}{\mathbf{\Phi}\left(q_2^e\right)}$$

according to eq. (A.57). This, along with the equilibrium point torque expression in eq. (A.54) is substituted into eq. (A.20) to produce

$$k_P q_2^e - \overline{\beta}_1\overline{\beta}_2\left[\frac{\mathbf{\Phi}\left(q_2^e\right) + E_r}{\mathbf{\Phi}\left(q_2^e\right)}\right]\sin q_1^e = 0.$$

Therefore

$$\frac{k_p}{\overline{\beta}_1\overline{\beta}_2}q_2^e = \frac{[\mathbf{\Phi}\left(q_2^e\right) + E_r]}{\mathbf{\Phi}\left(q_2^e\right)}\sin q_2^e = \zeta\left(q_2^e\right) \tag{A.65}$$

which can also be presented as

$$q_2^e\left[\frac{k_p}{\overline{\beta}_1\overline{\beta}_2} - \xi\left(q_2^e\right)\right] = 0 \tag{A.66}$$

where

$$\xi\left(q_2^e\right) = \frac{[\mathbf{\Phi}\left(q_2^e\right) + E_r]}{\mathbf{\Phi}\left(q_2^e\right)q_2^e}\sin q_2^e.$$

An example of the relationship between $\zeta\left(q_2^e\right)$ and the straight line functions which are dependent on the gain k_P is demonstrated in figure A.4. As seen with Ω_+, the function $\zeta\left(q_2^e\right)$ is bounded and odd, and is therefore guaranteed to have at least one intercept with the straight line function on the left-hand side of eq. (A.65). There is, however, a minimum gradient that will ensure that the only intercept between these two functions will occur at the origin.

It is possible to determine the value of q_2^e through graphical inspection, but there is, as of yet, no method of obtaining the value of q_1^e. This can be achieved through the implementation of the method that follows.

From A.57, we know that

$$\sin\left(q_1^e + q_2^e\right) = -\frac{\overline{\beta}_1\sin q_2^e}{\mathbf{\Phi}\left(q_2^e\right)}. \tag{A.67}$$

Additionally, from eq. (A.56), we find that

$$\sin\left(q_1^e + q_2^e\right) = -\frac{\overline{\beta}_1\sin q_1^e}{\overline{\beta}_2}. \tag{A.68}$$

Therefore, substituting eq. (A.67) into eq. (A.68) produces

$$\sin q_1^e = \frac{\overline{\beta}_2}{\mathbf{\Phi}\left(q_2^e\right)}. \tag{A.69}$$

Using the expression above, we define

$$\cos q_1^e = \pm\sqrt{1 - \frac{\overline{\beta}_2{}^2\sin^2 q_2^e}{\mathbf{\Phi}^2\left(q_2^e\right)}}$$

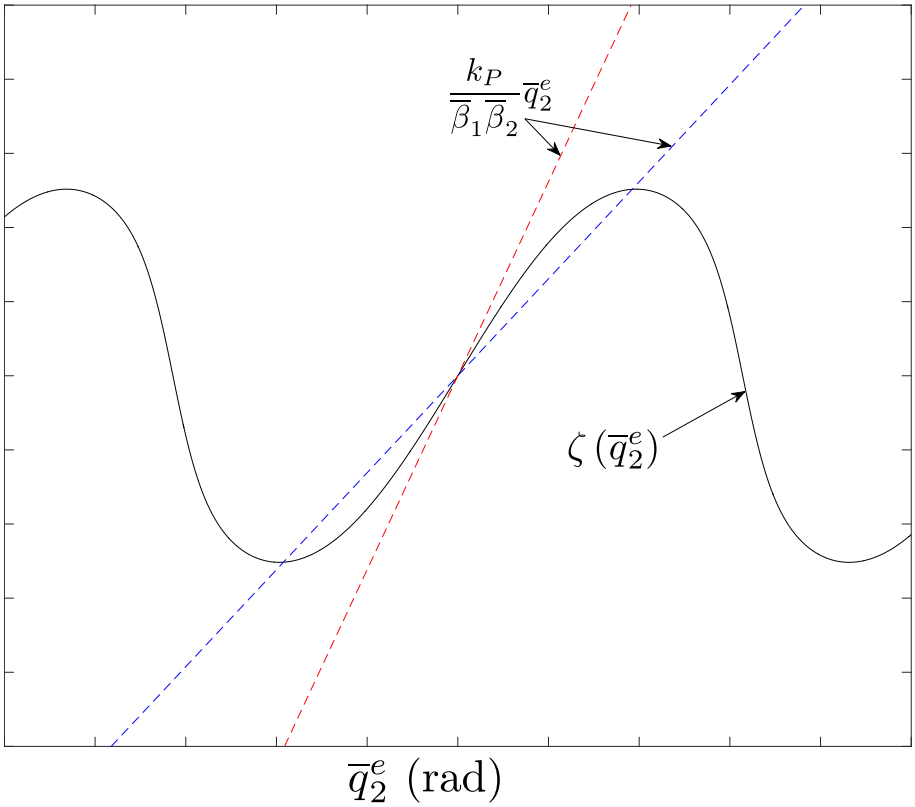

FIGURE A.4: The intercepts between the function $\zeta\left(\overline{q}_2^a\right)$ and the straight-line function with sufficiently large k_P (red line) and with an insufficient k_P (blue line).

$$
\begin{aligned}
&= \pm\sqrt{1 - \frac{\overline{\beta}_2{}^2\left[1-\cos^2 q_2^e\right]}{\mathbf{\Phi}^2\left(q_2^e\right)}} \\
&= \pm\frac{1}{\mathbf{\Phi}\left(q_2^e\right)}\sqrt{\mathbf{\Phi}^2\left(q_2^e\right) - \overline{\beta}_2{}^2 + \overline{\beta}_2{}^2\cos^2 q_2^e} \\
&= \pm\frac{1}{\mathbf{\Phi}\left(q_2^e\right)}\sqrt{\overline{\beta}_1{}^2 + 2\overline{\beta}_1\overline{\beta}_2\cos q_2^e + \overline{\beta}_2{}^2\cos^2 q_2^e} \\
&= \pm\frac{1}{\mathbf{\Phi}\left(q_2^e\right)}\left(\overline{\beta}_1 + \overline{\beta}_2\cos q_2^e\right).
\end{aligned}
$$

But

$$
\begin{aligned}
\mathbf{P}\left(q_2^e\right)\Big|_{\Omega_-} &= \overline{\beta}_1\cos q_1^e + \overline{\beta}_2\cos\left(q_1^e + q_2^e\right) = -\mathbf{\Phi}\left(q_2^e\right) \\
&= \overline{\beta}_1\cos\overline{q}_1^e + \overline{\beta}_2\left[\cos q_1^e\cos q_2^e - \sin q_1^e\sin q_2^e\right].
\end{aligned}
$$

Substituting eq. (A.69) into the expression above results in

$$\begin{aligned}\cos q_1^e \left[\overline{\beta}_1 + \overline{\beta}_2 \cos q_2^e\right] &= \frac{\overline{\beta}_2{}^2 \sin^2 q_2^e - \mathbf{\Phi}^2\left(q_2^e\right)}{\mathbf{\Phi}\left(q_2^e\right)} \\ &= \frac{\overline{\beta}_2{}^2 \left[1 - \cos^2 q_2^e\right] - \mathbf{\Phi}^2\left(q_2^e\right)}{\mathbf{\Phi}\left(q_2^e\right)} \\ &= \frac{-\left[\overline{\beta}_1 + \overline{\beta}_2 \cos q_2^e\right]^2}{\mathbf{\Phi}\left(q_2^e\right)}.\end{aligned}$$

Therefore

$$\cos q_1^e = -\left[\frac{\overline{\beta}_1 + \overline{\beta}_2 \cos q_2^e}{\mathbf{\Phi}\left(q_2^e\right)}\right]. \tag{A.70}$$

The value of q_1^e can be uniquely determined, thus demonstrating that there are a finite number of equilibrium points contained in the subset Ω_-.

(ii) The candidate Lyapunov function for the MC-ROPA$_{n-1}$ model is represented as

$$V = \frac{1}{2}\left(E - E_r\right)^2 + \frac{1}{2}k_D \dot{q}_2^2 + \frac{1}{2}k_P {q_2}^2$$

with reference to eq. (8.11). This Lyapunov candidate function will be represented as

$$V\left(q_1^e, q_2^e, 0, 0\right) = \frac{1}{2}\left[P\left(q_1^e, q_2^e\right) - E_r\right]^2 + \frac{1}{2}k_P q_2^{e2}$$

when found at an equilibrium point [5]. If the trajectory is moved off of the equilibrium point by an angle δ on the q_1^e coordinate, then

$$V\left(q_1^e + \delta, q_2^e, 0, 0\right) = \frac{1}{2}\left[P\left(q_1^e + \delta, q_2^e\right) - E_r\right]^2 + \frac{1}{2}k_P q_2^{e2}$$

where

$$\begin{aligned}P\left(q_1^e + \delta, q_2^e\right) &= \overline{\beta}_1 \cos\left(q_1^e + \delta\right) + \overline{\beta}_2 \cos\left(q_1^e + q_2^e + \delta\right) \\ &= \left[\overline{\beta}_1 \cos\left(q_1^e\right) + \overline{\beta}_2 \cos\left(q_1^e + q_2^e\right)\right] \cos\delta - \left[\overline{\beta}_1 \sin\left(q_1^e\right)\right. \\ &\quad \left. + \overline{\beta}_2 \sin\left(q_1^e + q_2^e\right)\right] \sin\delta \\ &= P(q_1^e, q_2^e)\cos\delta + \underbrace{\overline{K}_1(q_1^e, q_2^e)}_{=0} \sin\delta \\ &= P(q_1^e, q_2^e)\cos\delta\end{aligned}$$

with $P(q_1^e, q_2^e) < 0$ [5]. It is, therefore, evident that

$$P\left(q_1^e + \delta, q_2^e\right) > P\left(q_1^e, q_2^e\right), \qquad \left|P\left(q_1^e + \delta, q_2^e\right)\right| < \left|P\left(q_1^e, q_2^e\right)\right|$$

[5]. Therefore

$$[P(q_1^e+\delta, q_2^e) - E_r]^2 < [P(q_1^e, q_2^e) - E_r]^2$$

which results in

$$V(q_1^e+\delta, q_2^e, 0, 0) < V(q_1^e, q_2^e, 0, 0)$$

[5]. It is evident, therefore, that since $\dot{V}(\mathbf{q}, \dot{\mathbf{q}}) < 0$ if the torque τ_2 satisfies eq. (8.1) with $k_D > k_{DM}$, $k_V > 0$ and k_P satisfying eq. (A.64), then it is impossible for the trajectory to converge on the equilibrium points in Ω_- since the candidate Lyapunov function values found in the neighbourhood of the equilibrium points will always be less than the Lyapunov candidate function at the equilibrium point. This, therefore, proves that all equilibrium points in Ω_- are unstable.

(iii) It has been mentioned in the previous portion of this proof that the function $\zeta(q_2^e)$ is an odd and bounded function that does not decay as $q_2^e \to \pm\infty$. Therefore, it is evident from the relationship between $\zeta(q_2^e)$ and $\xi(q_2^e)$ represented by

$$\xi(q_2^e) = \frac{[\mathbf{\Phi}(q_2^e) + E_r]}{\mathbf{\Phi}(q_2^e)\, q_2^e} \sin q_2^e = \frac{\zeta(q_2^e)}{q_2^e}$$

that $\xi(q_2^e)$ is in fact an even function that will decay as $q_2^e \to \pm\infty$. An example of the $\xi(q_2^e)$ function is demonstrated in figure A.5. We can thus conclude that the suprenum of $\xi(q_2^e)$ will be found at $q_2^e = 0$ if $\xi(q_2^e) > 0$ at $q_2^e = 0$. Taking the limit as $q_2^e \to 0$ we find that

$$\lim_{q_2^e \to 0} \{\xi(q_2^e)\} = \lim_{q_2^e \to 0} \left\{ \frac{[\mathbf{\Phi}(q_2^e) + E_r]}{\mathbf{\Phi}(q_2^e)\, q_2^e} \sin q_2^e \right\} = \left. \frac{[\mathbf{\Phi}(q_2^e) + E_r]}{\mathbf{\Phi}(q_2^e)\, q_2^e} \sin q_2^e \right|_{q_2^e=0}$$

which, upon initial inspection, is not defined. We can, however, use L'Hôpital's rule to find a defined limit, whereby

$$\begin{aligned}
\lim_{q_2^e \to 0} \left\{ \frac{[\mathbf{\Phi}(q_2^e) + E_r]}{\mathbf{\Phi}(q_2^e)\, q_2^e} \sin q_2^e \right\} &= \lim_{q_2^e \to 0} \left\{ \frac{\dfrac{d}{dq_2^e}\left[[\mathbf{\Phi}(q_2^e) + E_r] \sin q_2^e\right]}{\dfrac{d}{dq_2^e}\left[\mathbf{\Phi}(q_2^e)\, q_2^e\right]} \right\} \\
&= \lim_{q_2^e \to 0} \left\{ \frac{\mathbf{\Phi}'(q_2^e) \sin q_2^e + [\mathbf{\Phi}(q_2^e) + E_r] \cos q_2^e}{\mathbf{\Phi}'(q_2^e)\, q_2^e + \mathbf{\Phi}(q_2^e)} \right\} \\
&= \frac{\mathbf{\Phi}(0) + E_r}{\mathbf{\Phi}(0)}.
\end{aligned}$$

It is apparent that $\mathbf{\Phi}(0) = \overline{\beta}_1 + \overline{\beta}_2$. Therefore

$$\sup_{q_2^e \neq 0} \{\xi(q_2^e)\} = \lim_{q_2^e \to 0} \left\{ \frac{[\mathbf{\Phi}(q_2^e) + E_r]}{\mathbf{\Phi}(q_2^e)\, q_2^e} \sin q_2^e \right\} = 2.$$

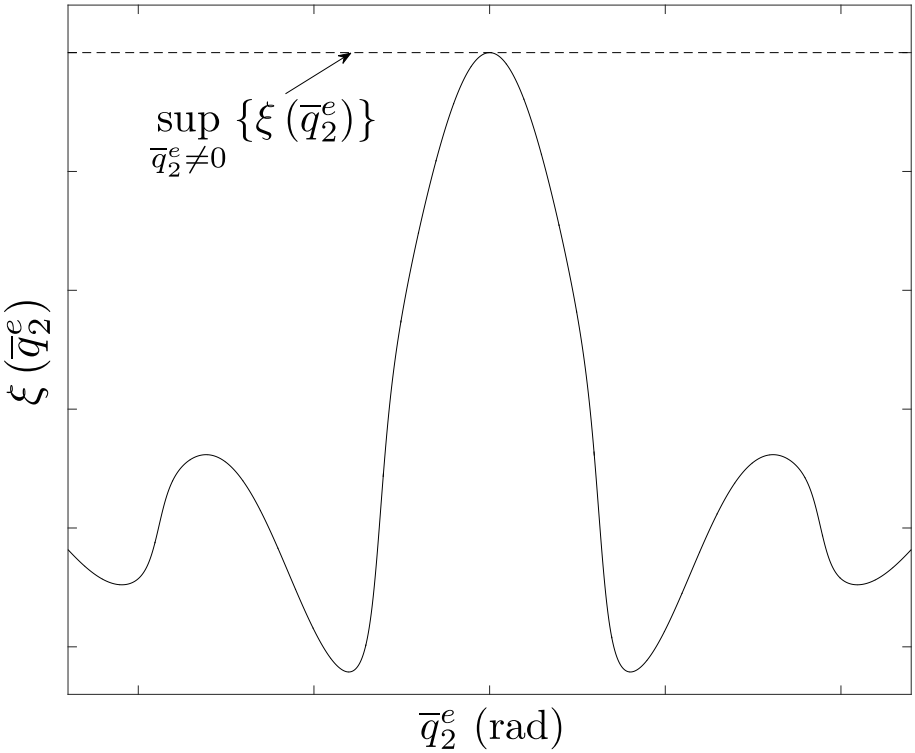

FIGURE A.5: The suprenum of $\xi(q_2^e)$.

Therefore, to ensure that eq. (A.66) only has the solution $q_2^e = 0$, the condition

$$k_P > 2\overline{\beta}_1\overline{\beta}_2 \tag{A.71}$$

must be satisfied [5]. This supersedes the gain conditions seen in eqs. (A.64) and (A.51) since

$$\begin{aligned} \overline{\beta}_1\overline{\beta}_2 &> \min\left\{\overline{\beta}_1{}^2, \overline{\beta}_2{}^2\right\}, && \textit{for } \overline{\beta}_1 \neq \overline{\beta}_2, \textit{ and} \\ \overline{\beta}_1\overline{\beta}_2 &= \min\left\{\overline{\beta}_1{}^2, \overline{\beta}_2{}^2\right\}, && \textit{for } \overline{\beta}_1 = \overline{\beta}_2. \end{aligned}$$

With the only solution for eq. (A.66) being $q_2^e = 0$, we will use the expressions found in eqs. (A.69) and (A.70) to determine q_1^e as a unique solution, whereby

$$\sin q_1^e|_{q_2^e=0} = 0, \qquad \cos q_1^e|_{q_2^e=0} = \frac{-\overline{\beta}_1 - \overline{\beta}_2}{\overline{\beta}_1 + \overline{\beta}_2} = -1.$$

From these results, it is evident that

$$q_1^e = \pi \pm 2k\pi$$

with $k \in \mathbb{Z}$. Therefore

$$\left(q_1^e, q_2^e, \dot{q}_1^e, \dot{\overline{q}}_2^e\right) = (\pi + 2k\pi, 0, 0, 0)\,.$$

Thus, we have proven that the only equilibrium point in Ω_- is the FPEP.

(iv) The behaviour of the system trajectory when found within an approximate neighbourhood of the FPEP can be determined through the development of a characteristic equation, which will contain information about the poles of the system when approximately linearised about the FPEP. The MC-ROPA$_{n-1}$ model is represented by the companion form when it is transformed into the state-space described by

$$\dot{\mathbf{x}} = f(\mathbf{x}). \tag{A.72}$$

The state-space was constructed by choosing the transformations

$$q_1 = \mathbf{x}_1, \qquad \dot{q}_1 = \mathbf{x}_2,$$
$$q_2 = \mathbf{x}_3, \qquad \dot{q}_2 = \mathbf{x}_4.$$

The approximately linearised system about the FPEP is derived using Lyapunov's Linearisation technique (see section 5.2.1 for more information), whereby

$$A = \left.\frac{\partial f(\mathbf{x})}{\partial \mathbf{x}}\right|_{(\mathbf{x}_1,\mathbf{x}_2,\mathbf{x}_3,\mathbf{x}_4)=(\pi,0,0,0)} \tag{A.73}$$

and where $A \in \mathbb{R}^{4\times 4}$ in this particular scenario. The characteristic equation can thus be generated as

$$\lambda(s) = \det\left(sI_4 - A\right) = 0$$

where $s = \sigma + j\omega \in \mathbb{C}$ (see section 4.4 for more information). This results in the characteristic equation

$$\lambda(s) = s^4 + \overline{a}_1 s^3 + \overline{a}_2 s^2 + \overline{a}_3 s + \overline{a}_4 \tag{A.74}$$

which pertains specifically to the undamped MC-ROPA$_{n-1}$ robot, where

$$\overline{a}_1 = \frac{k_V}{\overline{\gamma}}, \qquad \overline{a}_2 = \frac{k_P + \overline{\Psi}^2\left[k_D - 2\left(\overline{\alpha}_2\overline{\beta}_1 + \overline{\alpha}_1\overline{\beta}_2\right)\right]}{\overline{\gamma}},$$
$$\overline{a}_3 = \frac{k_V\overline{\Psi}^2}{\overline{\gamma}}, \qquad \overline{a}_4 = \frac{\overline{\Psi}^2\left(k_P - 2\overline{\beta}_1\overline{\beta}_2\right)}{\overline{\gamma}}$$

and

$$\overline{\Psi}^2 = \frac{E_r}{\overline{\alpha}_1 + \overline{\alpha}_2 + 2\overline{\alpha}_3}, \qquad \overline{\gamma} = k_D - 2\overline{\Psi}^2\left(\overline{\alpha}_1\overline{\alpha}_2 - \overline{\alpha}_3{}^2\right) \tag{A.75}$$

[5]. $\overline{\Psi}^2$ is evidently > 0. We shall now prove that $\gamma > 0$ [5].

It has been shown in Proof A.3 that $k_D > k_{DM}$ for $|\Lambda(\mathbf{q}, \dot{\mathbf{q}})| \neq 0$ (see eq. (8.13)). This expression can be simplified for the VCL transformed PA_{n-1} robot, which results in

$$\begin{aligned} k_{DM} &= \max_{q_2} \left\{ \left[\mathbf{\Phi}\left(q_2\right) + E_r \right] \lambda_{\max} \left[\left(G(\mathbf{q})^{\boldsymbol{T}} \, \overline{M}^{-1}\left(q_2\right) G\left(\mathbf{q}\right) \right)^{-1} \right] \right\} \\ &= \max_{q_2} \left\{ \left[\mathbf{\Phi}\left(q_2\right) + E_r \right] \frac{\left|\overline{M}\left(q_2\right)\right|}{\overline{M}_{11}\left(q_2\right)} \right\} \end{aligned}$$

where $G\left(\mathbf{q}\right) = \begin{bmatrix} 0 & 1 \end{bmatrix}^{\boldsymbol{T}}$ and where

$$\begin{aligned} \left|\overline{M}\left(q_2\right)\right| &= \overline{M}_{11}\left(q_2\right) \overline{M}_{22}\left(q_2\right) - \overline{M}_{12}\left(q_2\right) \overline{M}_{21}\left(q_2\right) \\ &= \overline{\alpha}_1 \overline{\alpha}_2 + \left[\overline{\alpha}_1 + 2\overline{\alpha}_3\right] \overline{\alpha}_3 \cos q_2. \end{aligned}$$

Therefore

$$k_{DM} = \max_{q_2} \left\{ \left[\mathbf{\Phi}\left(q_2 + E_r\right) \right] \left[\frac{\overline{\alpha}_1 \overline{\alpha}_2 + \left[\overline{\alpha}_1 + 2\overline{\alpha}_3\right] \overline{\alpha}_3 \cos q_2}{\overline{\alpha}_1 + \overline{\alpha}_2 + 2\overline{\alpha}_3 \cos q_2} \right] \right\}$$

We constructed

$$\begin{aligned} k_{D_1} &= \left[\mathbf{\Phi}\left(q_2 + E_r\right) \right] \left[\frac{\overline{\alpha}_1 \overline{\alpha}_2 + \left[\overline{\alpha}_1 + 2\overline{\alpha}_3\right] \overline{\alpha}_3 \cos q_2}{\overline{\alpha}_1 + \overline{\alpha}_2 + 2\overline{\alpha}_3 \cos q_2} \right] \Bigg|_{q_2 = 0} \\ &= 2E_r \left[\frac{\overline{\alpha}_1 \overline{\alpha}_2 + \left[\overline{\alpha}_1 + 2\overline{\alpha}_3\right] \overline{\alpha}_3}{\overline{\alpha}_1 + \overline{\alpha}_2 + 2\overline{\alpha}_3} \right] \end{aligned}$$

an example of such a gain, k_{D_1}. Substituting $k_D = k_{D_1}$ into the expression for $\overline{\gamma}$ seen in eq. (A.75) produces

$$\overline{\gamma}\big|_{k_D = k_{D_1}} = \frac{2E_r \overline{\alpha}_3}{\overline{\alpha}_1 + \overline{\alpha}_2 + 2\overline{\alpha}_3} \left[\overline{\alpha}_1 + 3\overline{\alpha}_3\right] > 0$$

with $k_{D_1} \leq k_{DM}$ and $k_{D_1} > 2\overline{\Psi}^2 \left(\overline{\alpha}_1 \overline{\alpha}_2 - \overline{\alpha}_3{}^2\right)$. Therefore

$$k_{DM} > 2\overline{\Psi}^2 \left(\overline{\alpha}_1 \overline{\alpha}_2 - \overline{\alpha}_3{}^2\right)$$

which will lead to

$$k_D > 2\overline{\Psi}^2 \left(\overline{\alpha}_1 \overline{\alpha}_2 - \overline{\alpha}_3{}^2\right)$$

if the condition in eq. (8.3) is satisfied. Therefore, $\overline{\gamma} > 0$. Additionally, $k_V > 0$, therefore $\overline{a}_1 > 0$ and $\overline{\alpha}_3 > 0$.

Information about the positions of the eigenvalues in the characteristic equation

shown in eq. (A.74) can be revealed with the use of the Routh-Hurwitz criterion (see section 4.4 for more information). We thus construct the Routh array and populate it using the coefficients of the characteristic equation, as seen with

s^4	1	$\overline{a}_2$	$\overline{a}_4$
s^3	$\overline{a}_1$	$\overline{a}_3$	0
s^2	$\overline{b}_1$	$\overline{b}_2$	0
s^1	$\overline{c}_1$	0	0
s^0	$\overline{d}_1$	0	0

where

$$\overline{b}_1 = \frac{\overline{a}_1\overline{a}_2 - \overline{a}_3}{\overline{a}_1} = \frac{\overline{D}_2}{\overline{a}_1}, \qquad \overline{b}_2 = \overline{a}_4$$

and

$$\begin{aligned}\overline{c}_1 &= \frac{\overline{b}_1\overline{a}_3 - \overline{a}_1\overline{b}_2}{\overline{b}_1} \\ &= \frac{\left[\overline{a}_1\overline{a}_2 - \overline{a}_3\right]\overline{a}_3 - \overline{a}_1{}^2\overline{a}_4}{\overline{a}_1\overline{a}_2 - \overline{a}_3} \\ &= \frac{\overline{D}_3}{\overline{D}_2}\end{aligned}$$

and where, for clarity, $\overline{D}_2 = \overline{a}_1\overline{a}_2 - \overline{a}_3$ *and* $\overline{D}_3 = \left[\overline{a}_1\overline{a}_2 - \overline{a}_3\right]\overline{a}_3 - \overline{a}_1{}^2\overline{a}_4$*. Solving for* $\overline{D}_3$ *produces*

$$\overline{D}_3 = -\frac{2\left[\overline{\alpha}_2\overline{\beta}_1 + \overline{\alpha}_3\overline{\beta}_1 - \overline{\alpha}_1\overline{\beta}_2 - \overline{\alpha}_3\overline{\beta}_2\right]^2\overline{\Psi}^2 k_V{}^2}{\left(\overline{\alpha}_1 + \overline{\alpha}_2 + 2\overline{\alpha}_3\right)^2\overline{\gamma}^2} < 0.$$

Therefore, $\overline{D}_3 < 0$ *regardless of the gains chosen for* k_P *and* k_V*. This is sufficient to prove that the FPEP is unstable since this condition will always guarantee a sign change in the left-hand column of the Routh array [5]. If, for instance* $\overline{D}_2 > 0$*, then* $\overline{b}_1 > 0$ *and* $\overline{c}_1 < 0$*, guaranteeing at least two eigenvalues in the right-hand side of the complex plane. If* $\overline{D}_2 < 0$*, then* $\overline{b}_1 < 0$ *and* $\overline{c}_1 > 0$*, once again guaranteeing at least two eigenvalues in the right-hand side of the complex plane.*

To extend this proof, we will derive, in detail, the eigenvalues positional states with respect to the gain k_P*, as originally derived in [5]. This will be useful for the upcoming derivations in the next chapter. There are three specific cases in this proof, where*

(i) $0 < k_P < 2\overline{\beta}_1\overline{\beta}_2$*,*

(ii) $k_P = 2\overline{\beta}_1\overline{\beta}_2$*, and*

(iii) $k_P > 2\overline{\beta}_1\overline{\beta}_2$*.*

If $0 < k_P < 2\overline{\beta}_1\overline{\beta}_2$*, the following conditions arise:*

(1) $\overline{a}_4 < 0$,

(2) $\overline{D}_3 = [\overline{a}_1\overline{a}_2 - \overline{a}_3]\,\overline{a}_3 - \overline{a}_1{}^2\overline{a}_4 < 0$,
$\therefore \quad \underbrace{[\overline{a}_1\overline{a}_2 - \overline{a}_3]}_{\overline{D}_2}\,\overline{a}_3 < \overline{a}_1{}^2\overline{a}_4 < 0$, *and*

(3) $\overline{D}_2 < 0$ *from condition (2) if* $\overline{\alpha}_3 > 0$.

These conditions result in $\dfrac{\overline{D}_3}{\overline{D}_2} > 0$, *which produces the coefficient signs* $\{+,+,-,+,-\}$ *on the left-hand column of the Routh array. Therefore, if* $0 < k_P < 2\overline{\beta}_1\overline{\beta}_2$, *the characteristic equation will have three poles in the right-hand side of the complex plane and one eigenvalue in the left-hand side of the complex plane [5].*

For the second case, if $k_P = 2\overline{\beta}_1\overline{\beta}_2$, *then the following conditions arise:*

(1) $\overline{a}_4 = 0$,

(2) $\overline{D}_3 = [\overline{a}_1\overline{a}_2 - \overline{a}_3]\,\overline{a}_3 < 0$, *and*

(3) $\overline{D}_2 < 0$ *from condition (2) if* $\overline{\alpha}_3 > 0$.

Additionally, if $\overline{a}_4 = 0$ *then*

$$\begin{aligned}\lambda(s) &= s^4 + \overline{a}_1 s^3 + \overline{a}_2 s^2 + \overline{a}_3 s \\ &= s\left[s^3 + \overline{a}_1 s^2 + \overline{a}_2 s + \overline{a}_3\right].\end{aligned}$$

From this, we can construct a new Routh array, knowing that one of the poles is found at the origin ($s = 0$). *Therefore*

s^3	1	$\overline{a}_2$	0
s^2	$\overline{a}_1$	$\overline{a}_3$	0
s^1	$\overline{b}_1$	0	0
s^0	$\overline{c}_1$	0	0

where

$$\overline{b}_1 = \frac{\overline{D}_2}{\overline{a}_1} < 0, \qquad\qquad \overline{c}_1 = \overline{a}_3 > 0.$$

This results in the left-hand column coefficient signs: $\{+,+,-,+\}$. *Therefore, one eigenvalue is found at the origin, and two eigenvalues are found on both the right-hand side and left-hand side of the complex plane [5].*

If $k_P > 2\overline{\beta}_1\overline{\beta}_2$, *then the following conditions arise:*

(1) $\overline{a}_4 > 0$,

(2) $\overline{D}_3 = [\overline{a}_1\overline{a}_2 - \overline{a}_3]\,\overline{a}_3 - \overline{a}_1{}^2\overline{a}_4 < 0,$
$\therefore \underbrace{[\overline{a}_1\overline{a}_2 - \overline{a}_3]}_{\overline{D}_2}\,\overline{a}_3 < \overline{a}_1{}^2\overline{a}_4,$

which means that $[\overline{a}_1\overline{a}_2 - \overline{a}_3]\,\overline{a}_3 \begin{cases} > 0 \\ = 0 \\ < 0 \end{cases}$ *, and*

(3) $\overline{D}_2 = \overline{a}_1\overline{a}_2 - \overline{a}_3 \begin{cases} > 0 \\ = 0 \\ < 0 \end{cases}$ *from condition (2) if* $\overline{\alpha}_3 > 0$.

In the case where $\overline{D}_2 > 0$*, then* $\dfrac{\overline{D}_3}{\overline{D}_2} < 0$*, which results in the left-hand column coefficients* $\{+,+,+,-,+\}$*. If* $\overline{D}_2 < 0$*, then* $\dfrac{\overline{D}_3}{\overline{D}_2} > 0$*, which results in the left-hand column coefficients* $\{+,+,-,+,+\}$*. So for both cases where* $\overline{D}_2 < 0$ *and* $\overline{D}_2 > 0$*, both the left-hand and right-hand sides of the complex plane will each contain two eigenvalues [5].*

If, however, $\overline{D}_2 = 0$*, we won't be able to solve for the positions of the eigenvalues directly. Instead, we can assume that* $\overline{D}_2$ *is an infinitely small number with either a negative or positive sign to determine the behaviour of the system with* $\overline{D}_2 \approx 0$ *[5]. We, therefore, choose*

$$\overline{D}_2 = \epsilon$$

[5]. Therefore

$$\frac{\overline{D}_2}{\overline{a}_1} = \frac{\epsilon}{\overline{a}_1} = \epsilon = \overline{b}_1.$$

If $\epsilon > 0$*, then the coefficients of the left-hand column of the Routh array will be* $\{+,+,+,-,+\}$*. Similarly, if* $\epsilon < 0$*, then the coefficients of the left-hand column of the Routh array will be* $\{+,+,-,+,+\}$*. Therefore, if* $k_P > 2\overline{\beta}_1\overline{\beta}_2$*, then the characteristic equation of the undamped MC-ROPA*$_{n-1}$ *robot about the FPEP will have two eigenvalues in each of the left-hand and right-hand sides of the complex plane [5].*

Each solution shows that the FPEP is unstable, since there are at least two eigenvalues in the right-hand half of the complex plane. Therefore, choosing $k_P > 2\overline{\beta}_1\overline{\beta}_2$ *not only guarantees that the FPEP is the only equilibrium point in* Ω_-*, it also guarantees that FPEP is unstable and hyperbolic (has no eigenvalues on the imaginary axis), and is therefore a saddle point (as explained in Definition 2.7 of [5, pg. 25]).*

(v) It has already been proven that, in the case where $E^* = E_r$*, there is an invariant set* $\mathbf{W}_r$ *(shown in eq. (A.21)) that contains the UEP, which is associated with a trajectory that is described by a homoclinic orbit. Therefore, since the FPEP is unstable and*

is a saddle point, it is apparent that, if $k_D > k_{DM}$, $k_V > 0$ and $k_P > 2\overline{\beta}_1\overline{\beta}_2$, that every closed loop solution will approach the invariant set $\mathbf{W}_r$ (the UEP) as $t \to \infty$. This does not mean that the UEP is a stable equilibrium point, however, since the homoclinic orbit rests between a stable and unstable manifold. The unstable nature of the UEP is proven below, as seen in [5].

Considering the companion form representation of the MC-ROPA$_{n-1}$ robot seen in eq. (A.72), the approximately linear system representation about the UEP is represented as

$$A = \left.\frac{\partial f(\mathbf{x})}{\partial \mathbf{x}}\right|_{(\mathbf{x}_1,\mathbf{x}_2,\mathbf{x}_3,\mathbf{x}_4)=(0,0,0,0)}.$$

The characteristic equation is derived as per the last example, and is presented as

$$\lambda(s) = s^4 + \overline{a}_1 s^3 + \overline{a}_2 s^2 + \overline{a}_3 s + \overline{a}_4$$

whereby

$$\overline{a}_1 = \frac{k_V}{k_D}, \qquad \overline{a}_2 = \frac{k_P}{k_D} - \overline{\Psi}^2,$$
$$\overline{a}_3 = -\frac{k_V}{k_D}\overline{\Psi}^2, \qquad \overline{a}_4 = -\frac{k_P}{k_D}\overline{\Psi}^2.$$

To our convenience, the characteristic equation can thus be neatly represented as

$$\left(s^2 - \overline{\Psi}^2\right)\left[s^2 + \frac{k_V}{k_D}s + \frac{k_P}{k_D}\right] = 0,$$
$$\therefore \ \left(s - \overline{\Psi}\right)\left(s + \overline{\Psi}\right)\left[s^2 + \frac{k_V}{k_D}s + \frac{k_P}{k_D}\right] = 0.$$

It is apparent, upon inspection of the expression above, that the UEP has three eigenvalues in the left-hand half of the complex plane and one eigenvalue in the right-hand half of the complex plane. Thus, according to Definition 2.7 of [5, 25], the UEP is also a saddle point.

□

It is apparent that, despite the fact that all closed-loop solutions in $\mathbb{S}$ will tend toward the invariant set $\mathbf{W}_r$, it will never reach this equilibrium point within a defined length of time. It is, therefore, imperative that a balancing controller, such as an LQR controller, be employed once the pendulum system finds itself approximately near the UEP. This is important for practical applications, but an extensive discussion on this topic is not included in this dissertation since the realisation of the homoclinic orbit is deemed sufficient for this application as stated in chapter 1.

There is, however, a sufficient discussion on the topic included in [5], and the reader is encouraged to read this section if necessary. □

A.5 The Gain Selection Criterion for the Undamped TC-ROPA$_{n-1}$ Robot

The equations of motion of the undamped TC-ROPA$_{n-1}$ robot is transformed into the state-space by choosing the equalities

$$q_1 = \mathbf{x}_1, \qquad q_2 = \mathbf{x}_2,$$
$$\dot{q}_1 = \mathbf{x}_3, \qquad \dot{q}_2 = \mathbf{x}_4$$

which results in the expression

$$\mathbf{f}(\mathbf{x}) = \begin{bmatrix} \mathbf{x}_3 \\ \mathbf{x}_4 \\ f_1(\mathbf{x}) \\ f_2(\mathbf{x}) \end{bmatrix} \tag{A.76}$$

where, from eqs. (9.10a) and (9.10b),

$$f_1(\mathbf{x}) = \left[-\overline{M}_{12}(\mathbf{x}) \left(k_P \left[\left(\frac{2\alpha}{\pi} \right) \arctan \mathbf{x}_3 - \mathbf{x}_2 \right] - k_D \mathbf{x}_4 \right) + \overline{\alpha}_3 \left(2\mathbf{x}_3\mathbf{x}_4 + {\mathbf{x}_4}^2 \right) \sin \mathbf{x}_2 \right.$$
$$\left. + \overline{\beta}_1 \sin \mathbf{x}_1 + \overline{\beta}_2 \sin \left(\mathbf{x}_1 + \mathbf{x}_2 \right) \right] \Big/ \left[\overline{M}_{11}(\mathbf{x}) \right],$$
$$f_2(\mathbf{x}) = k_P \left[\left(\frac{2\alpha}{\pi} \right) \arctan \mathbf{x}_3 - \mathbf{x}_2 \right] - k_D \mathbf{x}_4.$$

The linearised system about the FPEP is represented as

$$\mathbf{f}(\tilde{\mathbf{x}}) \approx \mathbf{A}\tilde{\mathbf{x}}$$

as seen in section 5.2.1, where

$$\mathbf{A} = \left(\frac{\partial \mathbf{f}(\mathbf{x})}{\partial \tilde{\mathbf{x}}} \right) \Bigg|_{\mathbf{x}=\mathbf{x}^*}$$

with $\mathbf{x}^* = (\pi, 0, 0, 0)$. Therefore, with $\mathbf{f}(\mathbf{x})$ defined in eq. (A.76) we can calculate the matrix $\mathbf{A}$, resulting in

$$\mathbf{A} = \begin{bmatrix} 0 & 0 & 1 & 0 \\ 0 & 0 & 0 & 1 \\ a_{31} & a_{32} & a_{33} & a_{34} \\ a_{41} & a_{42} & a_{43} & a_{44} \end{bmatrix} \tag{A.77}$$

where

$$a_{31} = \frac{-\overline{\beta}_1 - \overline{\beta}_2}{\overline{\alpha}_1 + \overline{\alpha}_2 + 2\overline{\alpha}_3}, \qquad a_{41} = 0,$$

$$a_{32} = \frac{k_P\left(\overline{\alpha}_2 + \overline{\alpha}_3\right) - \overline{\beta}_2}{\overline{\alpha}_1 + \overline{\alpha}_2 + 2\overline{\alpha}_3}, \qquad a_{42} = -k_P,$$
$$a_{33} = -2k_P\alpha\left[\frac{\overline{\alpha}_2 + \overline{\alpha}_3}{\pi\left(\overline{\alpha}_1 + \overline{\alpha}_2 + 2\overline{\alpha}_3\right)}\right], \qquad a_{43} = \frac{2k_P\alpha}{\pi},$$
$$a_{34} = k_D\left[\frac{\overline{\alpha}_2 + \overline{\alpha}_3}{\overline{\alpha}_1 + \overline{\alpha}_2 + 2\overline{\alpha}_3}\right], \qquad a_{44} = -k_D.$$

The linearised system about the FPEP is associated with a classification of stability, which can be determined through the derivation of the characteristic equation using the formula

$$\lambda(s) = \det\left(sI - \mathbf{A}\right).$$

The characteristic equation

$$\lambda(s) = \overline{a}_0 s^4 + \overline{a}_1 s^3 + \overline{a}_2 s^2 + \overline{a}_1 s + \overline{a}_0 = 0 \tag{A.78}$$

was thus derived using $\mathbf{A}$ from eq. (A.77), where

$$\begin{aligned}
\overline{a}_0 &= \pi\left[\overline{\alpha}_1 + \overline{\alpha}_2 + 2\overline{\alpha}_3\right],\\
\overline{a}_1 &= k_D\pi\left[\overline{\alpha}_1 + \overline{\alpha}_2 + 2\overline{\alpha}_3\right] + 2k_P\alpha\left[\overline{\alpha}_2 + \overline{\alpha}_3\right],\\
\overline{a}_2 &= \pi\left[\overline{\beta}_1 + \overline{\beta}_2 + k_P\left[\overline{\alpha}_1 + \overline{\alpha}_2 + 2\overline{\alpha}_3\right]\right],\\
\overline{a}_3 &= k_D\pi\left[\overline{\beta}_1 + \overline{\beta}_2\right] + 2k_P\alpha\overline{\beta}_2,\\
\overline{a}_4 &= k_P\pi\left[\overline{\beta}_1 + \overline{\beta}_2\right].
\end{aligned}$$

It is apparent from the characteristic equation that the local stability of the undamped TC-ROPA$_{n-1}$ robot is indeed dependent on the gains k_P and k_D. We must now choose appropriate values of k_P and k_D to ensure that the FPEP is unstable. We will now derive an analytical solution using the Routh-Hurwitz stability criterion implemented in the form of the Routh array

s^4	$\overline{a}_0$	$\overline{a}_2$	$\overline{a}_4$
s^3	$\overline{a}_1$	$\overline{a}_3$	0
s^2	$\overline{b}_1$	$\overline{b}_2$	0
s^1	$\overline{c}_1$	0	0
s^0	$\overline{d}_1$	0	0

where the table has been populated with the coefficients of the characteristic equation shown in eq. (A.78). The FPEP will be defined as unstable if there are any sign changes that occur between the coefficients on the far left-hand column of the Routh array, termed the *critical Routh coefficients* (every sign change corresponds to one pole in the right-hand side of the complex plane). We shall thus calculate the remaining Routh array coefficients and evaluate the possibility of a sign change with respect to the magnitudes of k_P and k_D, with the critical coefficients being $\overline{a}_0$, $\overline{a}_1$, $\overline{b}_1$, $\overline{c}_1$, and $\overline{d}_1$.

It is evident that the critical coefficients $\overline{a}_0 > 0$ and $\overline{a}_1 > 0$ since

$$\overline{\alpha}_1 > 0, \qquad \overline{\alpha}_2 > 0, \qquad \overline{\alpha}_3 > 0, \tag{A.79a}$$

$$k_P > 0, \qquad k_D \geq 0, \qquad \alpha > 0. \tag{A.79b}$$

The critical coefficient $\overline{b}_1$ is calculated as

$$\overline{b}_1 = \frac{\overline{a}_1\overline{a}_2 - \overline{a}_0\overline{a}_3}{\overline{a}_1}.$$

This simplifies to

$$\overline{b}_1 = \frac{2k_P\pi\alpha\overbrace{\left(\overline{\alpha}_2\overline{\beta}_1 + \overline{\alpha}_3\overline{\beta}_1 - \overline{\alpha}_1\overline{\beta}_2 - \overline{\alpha}_3\overline{\beta}_2\right)}^{>0}}{k_D\pi\left(\overline{\alpha}_1 + \overline{\alpha}_2 + 2\overline{\alpha}_3\right) + 2k_P\alpha\left(\overline{\alpha}_2 + \overline{\alpha}_3\right)} + k_P\pi\left(\overline{\alpha}_1 + \overline{\alpha}_2 + 2\overline{\alpha}_3\right).$$

It is apparent, therefore, that $\overline{b}_1 > 0$ regardless of the magnitudes of k_P and k_D since the conditions shown in eqs. (A.79a) and (A.79b) must hold, and because of the condition shown in eq. (A.42), which represents a modification of Lemma 2.1 found in [5]. Additionally, $\overline{b}_2$ is described as

$$\overline{b}_2 = \overline{a}_4$$

which results in $\overline{b}_2 > 0$ because of the conditions in eqs. (A.79a) and (A.79b) and because

$$\overline{\beta}_1 > 0, \qquad \overline{\beta}_2 > 0. \tag{A.80}$$

We also find, by inspection of the Routh array, that

$$\overline{d}_1 = \overline{\beta}_2 = \overline{a}_4 > 0.$$

It is conclusive, therefore, that the only coefficient whose sign could still possibly change due to the magnitudes of the gains k_P and k_D is $\overline{c}_1$. We find that if $\overline{c}_1 < 0$, then there will be two poles in both the left-hand and right-hand halves of the pole-zero plane. This is formally described in the following criterion:

Criterion A.1. ***Critical Routh Coefficient Condition for the undamped TC-ROPA$_{n-1}$ robot:*** The FPEP of the undamped TC-ROPA$_{n-1}$ robot is guaranteed to be locally unstable if the critical Routh coefficient $\overline{c}_1 < 0$, causing the allocation of two poles in both the left-hand and right-hand halves of the complex plane.

We thus express $\overline{c}_1$ analytically as

$$\overline{c}_1 = \frac{\overline{b}_1\overline{a}_3 - \overline{a}_1\overline{b}_2}{\overline{b}_1}$$

which simplifies to

$$\overline{c}_1 = \frac{\overline{w}_2\left(-\overline{n}_0 {k_p}^2 - \overline{n}_1 k_D k_P + \overline{n}_2 k_D + \overline{n}_3 k_P\right)}{\overline{w}_0 k_P + \overline{w}_1 k_D + \overline{w}_2}$$

where

$$\begin{aligned}
\overline{w}_0 &= 2\alpha\left[\overline{\alpha}_1 + \overline{\alpha}_2 + 2\overline{\alpha}_3\right]^2, \\
\overline{w}_1 &= \pi\left[\overline{\alpha}_2 + \overline{\alpha}_3\right]\left[\overline{\alpha}_1 + \overline{\alpha}_2 + 2\overline{\alpha}_3\right], \\
\overline{w}_2 &= 2\alpha\left[\overline{\alpha}_2\overline{\beta}_1 + \overline{\alpha}_3\overline{\beta}_1 - \overline{\alpha}_1\overline{\beta}_2 - \overline{\alpha}_3\overline{\beta}_2\right]
\end{aligned}$$

and

$$\begin{aligned}
\overline{n}_0 &= 2\alpha\left[\overline{\alpha}_2 + \overline{\alpha}_3\right], & \overline{n}_1 &= \pi\left[\overline{\alpha}_1 + \overline{\alpha}_2 + 2\overline{\alpha}_3\right], \\
\overline{n}_2 &= \pi\left[\overline{\beta}_1 + \overline{\beta}_2\right], & \overline{n}_3 &= 2\overline{\beta}_2\alpha.
\end{aligned}$$

The denominator of this expression is positive $\forall t$ since

$$\overline{w}_0 > 0, \qquad \overline{w}_1 > 0$$

as a direct result of the conditions shown in eqs. (A.79a) and (A.79b), and $w_2 > 0$ as dictated by the modified Lemma shown in eq. (A.42). Therefore, to ensure that the FPEP of the undamped TC-ROPA$_{n-1}$ robot is unstable, we must guarantee that

$$\begin{aligned}
\overline{c}_{1_n} &= \overline{n}_0 {k_P}^2 + \overline{n}_1 k_D k_P + \overline{n}_2 k_D + \overline{n}_3 k_P \\
&= -2\alpha\left[\overline{\alpha}_2 + \overline{\alpha}_3\right]{k_P}^2 - \pi\left[\overline{\alpha}_1 + \overline{\alpha}_2 + 2\overline{\alpha}_3\right]k_D k_P + \pi\left[\overline{\beta}_1 + \overline{\beta}_2\right]k_D + 2\alpha\overline{\beta}_2 k_P < 0.
\end{aligned} \tag{A.81}$$

This is a convoluted expression, but we can represent this expression as a constraint on k_D with respect to k_P, resulting in

$$k_D < \overline{k}_P = \frac{2\alpha k_P}{\pi}\left[\frac{\left[\overline{\alpha}_2 + \overline{\alpha}_3\right]k_P - \overline{\beta}_2}{\overline{\beta}_1 + \overline{\beta}_2 - k_P\left[\overline{\alpha}_1 + \overline{\alpha}_2 + \overline{\alpha}_3\right]}\right]. \tag{A.82}$$

Therefore, if $k_D < \overline{k}_P$, then $\overline{c}_1 < 0$. It is evident that this constraint is only valid between the bounds

$$\frac{\overline{\beta}_2}{\overline{\alpha}_2 + \overline{\alpha}_3} < k_P < \frac{\overline{\beta}_1 + \overline{\beta}_2}{\overline{\alpha}_1 + \overline{\alpha}_2 + 2\overline{\alpha}_3} \tag{A.83}$$

since for $k_P < \dfrac{\overline{\beta}_2}{\overline{\alpha}_2 + \overline{\alpha}_3}$ and $k_P > \dfrac{\overline{\beta}_1 + \overline{\beta}_2}{\overline{\alpha}_1 + \overline{\alpha}_2 + 2\overline{\alpha}_3}$, $\overline{k}_P < 0$. This is invalid since $k_D \geq 0$ and therefore $k_D \not< \overline{k}_P$. We prove this as follows:

Proof A.5.1. *We shall begin this proof by showing that*

$$\frac{\overline{\beta}_2}{\overline{\alpha}_2+\overline{\alpha}_3} < \frac{\overline{\beta}_1+\overline{\beta}_2}{\overline{\alpha}_1+\overline{\alpha}_2+\overline{\alpha}_3}. \tag{A.84}$$

This is done by taking the difference between the aforementioned expressions, resulting in

$$\delta\hat{k}_p = \frac{\overline{\beta}_1+\overline{\beta}_2}{\overline{\alpha}_1+\overline{\alpha}_2+\overline{\alpha}_3} - \frac{\overline{\beta}_2}{\overline{\alpha}_2+\overline{\alpha}_3}.$$

This simplifies to

$$\delta\hat{k}_p = \frac{\overline{\beta}_1\overline{\alpha}_2+\overline{\beta}_1\overline{\alpha}_3-\overline{\beta}_2\overline{\alpha}_1-\overline{\beta}_2\overline{\alpha}_3}{\left[\overline{\alpha}_1+\overline{\alpha}_2+2\overline{\alpha}_3\right]\left[\overline{\alpha}_2+\overline{\alpha}_3\right]}.$$

The modification on Lemma 2.1 of [5] seen in eq. (A.42) thus leads to the conclusion that $\delta\hat{k}_p > 0$. *The statement in eq. (A.84) is thus proven.*

Next, we shall prove that the condition $k_D < \overline{k}_P$ *is only valid within the boundaries*

$$\frac{\overline{\beta}_2}{\overline{\alpha}_2+\overline{\alpha}_3} < k_P < \frac{\overline{\beta}_1+\overline{\beta}_2}{\overline{\alpha}_1+\overline{\alpha}_2+2\overline{\alpha}_3}$$

by completing the following steps:

(i) Prove the lower boundary of this condition is $k_P = \dfrac{\overline{\beta}_2}{\overline{\alpha}_2+\overline{\alpha}_3}$ *by proving that* $\overline{k}_P < 0$ *when* $k_P < \dfrac{\overline{\beta}_2}{\overline{\alpha}_2+\overline{\alpha}_3}$.

(ii) Prove the upper boundary of this condition is $k_P = \dfrac{\overline{\beta}_1+\overline{\beta}_2}{\overline{\alpha}_1+\overline{\alpha}_2+2\overline{\alpha}_3}$ *by proving that* $\overline{k}_P < 0$ *when* $k_P < \dfrac{\overline{\beta}_1+\overline{\beta}_2}{\overline{\alpha}_1+\overline{\alpha}_2+2\overline{\alpha}_3}$.

(iii) Show that $\overline{k}_P > 0$ *between these boundaries.*

This process is executed below:

(i) We shall now evaluate the lower boundary of the condition highlighted in eq. (A.82) by choosing

$$k_P = \frac{\overline{\beta}_2}{\overline{\alpha}_2+\overline{\alpha}_3} - \epsilon$$

where ϵ *is a positive infinitesimally small number. Substituting this* k_P *into eq. (A.82) produces*

$$\overline{k}_P = -\frac{2\alpha k_P}{\pi}\left[\frac{\epsilon\left[\overline{\alpha}_2+\overline{\alpha}_3\right]^2}{\left[\overline{\beta}_1\overline{\alpha}_2+\overline{\beta}_1\overline{\alpha}_3-\overline{\beta}_2\overline{\alpha}_1-\overline{\beta}_2\overline{\alpha}_3\right]+\epsilon\left[\overline{\alpha}_1+\overline{\alpha}_2+2\overline{\alpha}_3\right]\left[\overline{\alpha}_2+\overline{\alpha}_3\right]}\right].$$

It is, therefore, evident that $\overline{k}_P < 0$ *when* $k_P < \dfrac{\overline{\beta}_2}{\overline{\alpha}_2 + \overline{\alpha}_3}$ *according to the condition in eq. (A.42).*

(ii) *The upper boundary of the condition highlighted in eq. (A.82) is evaluated by choosing*

$$k_P = \frac{\overline{\beta}_1 + \overline{\beta}_2}{\overline{\alpha}_1 + \overline{\alpha}_2 + 2\overline{\alpha}_3} + \epsilon$$

where, as before, ϵ *is chosen as a positive and infinitesimally small number. Substituting this* k_P *into eq. (A.82) produces the simplified result*

$$\overline{k}_P = -\frac{2\alpha k_P}{\pi}\left[\frac{\left[\overline{\beta}_1\overline{\alpha}_2 + \overline{\beta}_1\overline{\alpha}_3 - \overline{\beta}_2\overline{\alpha}_1 - \overline{\beta}_2\overline{\alpha}_3\right] + \epsilon\left[\overline{\alpha}_2 + \overline{\alpha}_3\right]\left[\overline{\alpha}_1 + \overline{\alpha}_2 + 2\overline{\alpha}_3\right]}{\epsilon\left[\overline{\alpha}_1 + \overline{\alpha}_2 + 2\overline{\alpha}_3\right]^2}\right].$$

We can again conclude in this instance that where $k_P > \dfrac{\overline{\beta}_1 + \overline{\beta}_2}{\overline{\alpha}_1 + \overline{\alpha}_2 + 2\overline{\alpha}_3}$, $\overline{k}_P < 0$ *as suggested by the modified version of Lemma 2.1 shown in eq. (A.42).*

(iii) *We shall now explore the validity of the condition shown in eq. (A.82) with a gain selection for* k_P *that falls between the boundaries as shown in eq. (A.83). We begin by choosing a gain that falls below the upper boundary, whereby*

$$k_P = \frac{\overline{\beta}_1 + \overline{\beta}_2}{\overline{\alpha}_1 + \overline{\alpha}_2 + 2\overline{\alpha}_3} - \epsilon$$

and where $\epsilon > 0$ *and is no longer necessarily an infinitesimally small number. The substitution of this expression for* k_P *into eq. (A.82) produces*

$$\overline{k}_P = \frac{2\alpha k_P}{\pi}\left[\frac{\left[\overline{\beta}_1\overline{\alpha}_2 + \overline{\beta}_1\overline{\alpha}_3 - \overline{\beta}_2\overline{\alpha}_1 - \overline{\beta}_2\overline{\alpha}_3\right] - \epsilon\left[\overline{\alpha}_2 + \overline{\alpha}_3\right]\left[\overline{\alpha}_1 + \overline{\alpha}_2 + 2\overline{\alpha}_3\right]}{\epsilon\left[\overline{\alpha}_1 + \overline{\alpha}_2 + 2\overline{\alpha}_3\right]^2}\right].$$

Therefore, $\overline{k}_P > 0$ *if*

$$0 < \epsilon < \epsilon_{\max} = \frac{\overline{\beta}_1\overline{\alpha}_2 + \overline{\beta}_1\overline{\alpha}_3 - \overline{\beta}_2\overline{\alpha}_1 - \overline{\beta}_2\overline{\alpha}_3}{\left[\overline{\alpha}_2 + \overline{\alpha}_3\right]\left[\overline{\alpha}_1 + \overline{\alpha}_2 + 2\overline{\alpha}_3\right]}.$$

Therefore

$$k_P > \frac{\overline{\beta}_1 + \overline{\beta}_2}{\overline{\alpha}_1 + \overline{\alpha}_2 + 2\overline{\alpha}_3} - \epsilon_{\max}.$$

This simplifies to

$$k_P > \frac{\overline{\beta}_2}{\overline{\alpha}_2 + \overline{\alpha}_3}.$$

This proves that $\overline{k}_P > 0$ so long as

$$\frac{\overline{\beta}_2}{\overline{\alpha}_2 + \overline{\alpha}_3} < k_P < \frac{\overline{\beta}_1 + \overline{\beta}_2}{\overline{\alpha}_1 + \overline{\alpha}_2 + 2\overline{\alpha}_3}.$$

We now understand that the inequality shown in eq. (A.82) is only valid when k_P is chosen between the boundaries demonstrated in eq. (A.83). We shall now demonstrate two other gain selection conditions that ensures $\overline{c}_1 < 0$ whilst the value of k_P falls outside this range.

Beginning with the lower boundary, we chose

$$k_P = \frac{\overline{\beta}_2}{\overline{\alpha}_2 + \overline{\alpha}_3} - \epsilon$$

to describe k_P, where

$$0 < \epsilon < \frac{\overline{\beta}_2}{\overline{\alpha}_2 + \overline{\alpha}_3}.$$

This k_P, when substituted into eq. (A.81), produces

$$\begin{aligned}\overline{c}_{1_n} = 2\alpha\epsilon\left[\overline{\alpha}_2 + \overline{\alpha}_3\right]\left[\frac{\overline{\beta}_2}{\overline{\alpha}_2 + \overline{\alpha}_3}\right] + \frac{k_D\pi}{\overline{\alpha}_2 + \overline{\alpha}_3}\big[\overline{\beta}_1\overline{\alpha}_2 + \overline{\beta}_1\overline{\alpha}_3 - \overline{\beta}_2\overline{\alpha}_1 - \overline{\beta}_2\overline{\alpha}_3 \\ + \epsilon\left[\overline{\alpha}_1 + \overline{\alpha}_2 + 2\overline{\alpha}_3\right]\left[\overline{\alpha}_2 + \overline{\alpha}_3\right]\big]\end{aligned}$$

which is evidently guaranteed to satisfy $\overline{c}_{1_n} \geq 0$ so long as $k_D \geq 0$. Additionally, if $\epsilon = \dfrac{\overline{\beta}_2}{\overline{\alpha}_2 + \overline{\alpha}_3}$ (which results in $k_P = 0$) we find that

$$\overline{c}_{1_n} = k_D\pi\left[\overline{\beta}_1\overline{\alpha}_2 + \overline{\beta}_1\overline{\alpha}_3 - \overline{\beta}_2\overline{\alpha}_1 - \overline{\beta}_2\overline{\alpha}_3\right]$$

which also results in $\overline{c}_{1_n} \geq 0$ so long as $k_D \geq 0$. Therefore, $\overline{c}_{1_n} \geq 0$ when

$$0 < k_P \leq \frac{\overline{\beta}_2}{\overline{\alpha}_2 + \overline{\alpha}_3}, \qquad k_D \geq 0.$$

Looking at the upper boundary, we chose the gain expression

$$k_P = \frac{\overline{\beta}_1 + \overline{\beta}_2}{\overline{\alpha}_1 + \overline{\alpha}_2 + 2\overline{\alpha}_3} + \epsilon$$

where $\epsilon > 0$ and is not necessarily an infinitesimally small number. The substitution of the expression for k_P into eq. (A.81) produces

$$\begin{aligned}\overline{c}_{1_n} = &-2\alpha\left[\frac{\overline{\beta}_1+\overline{\beta}_2}{\overline{\alpha}_1+\overline{\alpha}_2+2\overline{\alpha}_3}+\epsilon\right]\left[\frac{\overline{\beta}_1\overline{\alpha}_2+\overline{\beta}_1\overline{\alpha}_3-\overline{\beta}_2\overline{\alpha}_1-\overline{\beta}_2\overline{\alpha}_3}{\overline{\alpha}_1+\overline{\alpha}_2+2\overline{\alpha}_3}+\epsilon\left[\overline{\alpha}_2+\overline{\alpha}_3\right]\right]\\ &-k_D\pi\epsilon\left[\overline{\alpha}_1+\overline{\alpha}_2+2\overline{\alpha}_3\right]\end{aligned}$$

which guarantees that $\overline{c}_{1_n} < 0$ so long as $k_D \geq 0$. This is also true if $\epsilon = 0$ in this case, which corresponds to

$$k_P = \frac{\overline{\beta}_1+\overline{\beta}_2}{\overline{\alpha}_1+\overline{\alpha}_2+2\overline{\alpha}_3}.$$

Considering the results derived above, we will now summarise the gain selection criterion that is necessary to ensure that the FPEP of the undamped TC-ROPA$_{n-1}$ robot is locally unstable (i.e. guarantee that the critical Routh coefficient $\overline{c}_1 < 0$)

The FPEP of the undamped TC-ROPA$_{n-1}$ robot is guaranteed to be locally unstable so long as the following selection conditions for the gains k_P and k_D are satisfied:

(1) For $\dfrac{\overline{\beta}_2}{\overline{\alpha}_2+\overline{\alpha}_3} < k_P < \dfrac{\overline{\beta}_1+\overline{\beta}_2}{\overline{\alpha}_1+\overline{\alpha}_2+2\overline{\alpha}_3}$:

$$0 \leq k_D < \frac{2\alpha k_P}{\pi}\left[\frac{\left[\overline{\alpha}_2+\overline{\alpha}_3\right]k_P-\overline{\beta}_2}{\overline{\beta}_1+\overline{\beta}_2-k_P\left[\overline{\alpha}_1+\overline{\alpha}_2+\overline{\alpha}_3\right]}\right];$$

(2) For $k_P \geq \dfrac{\overline{\beta}_1+\overline{\beta}_2}{\overline{\alpha}_1+\overline{\alpha}_2+2\overline{\alpha}_3}$; $\quad k_D \geq 0$:

This set of conditions is formalised as criterion 9.1 in section 9.4.1. □

A.6 The Gain Selection Criterion for the Passively Damped TC-ROPA$_{n-1}$ Robot

Choosing the state-space variables

$$q_1 = \mathbf{x}_1, \qquad q_2 = \mathbf{x}_2,$$
$$\dot{q}_1 = \mathbf{x}_3, \qquad \dot{q}_2 = \mathbf{x}_4$$

to represent the angular displacements and velocities of the TC-ROPA$_{n-1}$ robot, we can describe the equations of motion shown in eqs. (9.18) and (9.19) as

$$\mathbf{f}(\mathbf{x}) = \begin{bmatrix} \mathbf{x}_3 \\ \mathbf{x}_4 \\ f_1(\mathbf{x}) \\ f_2(\mathbf{x}) \end{bmatrix} \tag{A.85}$$

where

$$f_1(\mathbf{x}) = \Bigg[-\overline{M}_{12}(\mathbf{x}) \left(k_P \left[\left(\frac{2\alpha}{\pi} \right) \arctan \mathbf{x}_3 - \mathbf{x}_2 \right] - k_D \mathbf{x}_4 \right) + \overline{\alpha}_3 \left(2\mathbf{x}_3\mathbf{x}_4 + {\mathbf{x}_4}^2 \right) \sin \mathbf{x}_2$$
$$- b_1 \dot{q}_1 + \overline{\beta}_1 \sin \mathbf{x}_1 + \overline{\beta}_2 \sin \left(\mathbf{x}_1 + \mathbf{x}_2 \right) \Bigg] \Big/ \left[\overline{M}_{11}(\mathbf{x}) \right],$$
$$f_2(\mathbf{x}) = k_P \left[\left(\frac{2\alpha}{\pi} \right) \arctan \mathbf{x}_3 - \mathbf{x}_2 \right] - k_D \mathbf{x}_4$$

and where b_1 represents the passive damping condition. The model of the TC-ROPA$_{n-1}$ robot linearised about the FPEP is represented as

$$\mathbf{f}(\tilde{\mathbf{x}}) \approx \mathbf{A}\tilde{\mathbf{x}}$$

where

$$\mathbf{A} = \left(\frac{\partial \mathbf{f}(\mathbf{x})}{\partial \tilde{\mathbf{x}}} \right) \Bigg|_{\mathbf{x}=\mathbf{x}^*}$$

and where $\mathbf{x}^* = (\pi, 0, 0, 0)$. Applying this linearisation on the system shown in eq. (A.85) produces

$$\mathbf{A} = \begin{bmatrix} 0 & 0 & 1 & 0 \\ 0 & 0 & 0 & 1 \\ a_{31} & a_{32} & a_{33} & a_{34} \\ a_{41} & a_{42} & a_{43} & a_{44} \end{bmatrix} \tag{A.86}$$

where the entries are described as

$$a_{31} = \frac{-\overline{\beta}_1 - \overline{\beta}_2}{\overline{\alpha}_1 + \overline{\alpha}_2 + 2\overline{\alpha}_3}, \qquad a_{41} = 0,$$

$$a_{32} = \frac{k_P\left(\overline{\alpha}_2 + \overline{\alpha}_3\right) - \overline{\beta}_2}{\overline{\alpha}_1 + \overline{\alpha}_2 + 2\overline{\alpha}_3}, \qquad a_{42} = -k_P,$$
$$a_{33} = -\left[\frac{2k_P\alpha\left[\overline{\alpha}_2 + \overline{\alpha}_3\right] + \pi b_1}{\pi\left(\overline{\alpha}_1 + \overline{\alpha}_2 + 2\overline{\alpha}_3\right)}\right], \qquad a_{43} = \frac{2k_P\alpha}{\pi},$$
$$a_{34} = k_D\left[\frac{\overline{\alpha}_2 + \overline{\alpha}_3}{\overline{\alpha}_1 + \overline{\alpha}_2 + 2\overline{\alpha}_3}\right], \qquad a_{44} = -k_D.$$

The characteristic equation of the system is found through the implementation of

$$\lambda(s) = \det\left(sI - \mathbf{A}\right)$$

which, with the substitution of the $\mathbf{A}$ matrix found in eq. (A.86) results in the characteristic equation

$$\lambda(s) = \overline{a}_0 s^4 + \overline{a}_1 s^3 + \overline{a}_2 s^2 + \overline{a}_1 s + \overline{a}_0 = 0$$

where

$$\begin{aligned}
\overline{a}_0 &= \pi\left[\overline{\alpha}_1 + \overline{\alpha}_2 + 2\overline{\alpha}_3\right],\\
\overline{a}_1 &= \pi\left[b_1 + k_D\left[\overline{\alpha}_1 + \overline{\alpha}_2 + 2\overline{\alpha}_3\right]\right] + 2k_P\alpha\left[\overline{\alpha}_2 + \overline{\alpha}_3\right],\\
\overline{a}_2 &= \pi\left[\overline{\beta}_1 + \overline{\beta}_2 + k_P\left[\overline{\alpha}_1 + \overline{\alpha}_2 + 2\overline{\alpha}_3\right] + b_1 k_D\right],\\
\overline{a}_3 &= \pi\left[k_D\left[\overline{\beta}_1 + \overline{\beta}_2\right] + b_1 k_p\right] + 2k_P\alpha\overline{\beta}_2,\\
\overline{a}_4 &= k_P\pi\left[\overline{\beta}_1 + \overline{\beta}_2\right].
\end{aligned}$$

The stability of the linearised system about the FPEP can be determined analytically through the implementation of the Routh-Hurwitz criterion in the form

$$\begin{array}{c|ccc}
s^4 & \overline{a}_0 & \overline{a}_2 & \overline{a}_4\\
s^3 & \overline{a}_1 & \overline{a}_3 & 0\\
s^2 & \overline{b}_1 & \overline{b}_2 & 0\\
s^1 & \overline{c}_1 & 0 & 0\\
s^0 & \overline{d}_1 & 0 & 0
\end{array}.$$

The characteristic equation of the TC-ROPA$_{n-1}$ model linearised about the FPEP will contain a pole on the right-hand half of the complex plane for every sign change that is seen in the coefficients that are found on the far-left column of the Routh array (i.e. this concerns the critical coefficients $\overline{a}_0$, $\overline{a}_1$, $\overline{b}_1$, $\overline{c}_1$, and $\overline{d}_1$). As seen with the undamped case, it is evident that the critical Routh coefficients $\overline{\alpha}_0 > 0$ and $\overline{\alpha}_1 > 0$ since

$$\overline{\alpha}_1 > 0, \qquad \overline{\alpha}_2 > 0, \qquad \overline{\alpha}_3 > 0, \tag{A.87a}$$
$$k_P > 0, \qquad k_D \geq 0, \qquad \alpha > 0. \tag{A.87b}$$

The next critical Routh coefficient is $\overline{b}_1$, which is calculated as

$$\overline{b}_1 = \frac{\overline{a}_1\overline{a}_2 - \overline{a}_0\overline{a}_3}{\overline{a}_1}$$

which simplifies to

$$\overline{b}_1 = \pi\left[\frac{b_1{k_D}^2\overline{n}_1 + {k_P}^2\overline{w}_0 + k_P k_D\left(\overline{w}_1 + b_1\overline{n}_0\right) + k_P\overline{w}_2 + k_D\pi{b_1}^2 + b_1\overline{n}_2}{b_1\pi + k_D\overline{n}_1 + k_P\overline{n}_0}\right]$$

where

$$\begin{aligned}
\overline{w}_0 &= 2\alpha\left[\overline{\alpha}_1 + \overline{\alpha}_2 + 2\overline{\alpha}_3\right]^2,\\
\overline{w}_1 &= \pi\left[\overline{\alpha}_2 + \overline{\alpha}_3\right]\left[\overline{\alpha}_1 + \overline{\alpha}_2 + 2\overline{\alpha}_3\right],\\
\overline{w}_2 &= 2\alpha\left[\overline{\alpha}_2\overline{\beta}_1 + \overline{\alpha}_3\overline{\beta}_1 - \overline{\alpha}_1\overline{\beta}_2 - \overline{\alpha}_3\overline{\beta}_2\right]
\end{aligned}$$

and

$$\begin{aligned}
\overline{n}_0 &= 2\alpha\left[\overline{\alpha}_2 + \overline{\alpha}_3\right], & \overline{n}_1 &= \pi\left[\overline{\alpha}_1 + \overline{\alpha}_2 + 2\overline{\alpha}_3\right],\\
\overline{n}_2 &= \pi\left[\overline{\beta}_1 + \overline{\beta}_2\right], & \overline{n}_3 &= 2\overline{\beta}_2\alpha.
\end{aligned}$$

It is evident that, since the conditions in eqs. (A.87a) and (A.87b) must hold, the conditions

$$\overline{w}_0 > 0, \qquad \overline{w}_1 > 0, \tag{A.88}$$

$$\overline{n}_0 > 0, \qquad \overline{n}_1 > 0 \tag{A.89}$$

must also hold. The modification on Lemma 2.1 found in [5] (see eq. (A.42)) leads to $\overline{w}_2 > 0$, and knowing that

$$\overline{\beta}_1 > 0, \qquad \overline{\beta}_2 > 0$$

we are certain that

$$\overline{n}_2 > 0, \qquad \overline{n}_3 > 0.$$

It is evident, therefore, that the critical coefficient $\overline{b}_1$ cannot under any permissible circumstances exit the positive real space (i.e. $\overline{b}_1 > 0\ \forall t$ so long as the aforementioned conditions hold). Additionally,

$$\overline{d}_1 = \overline{b}_2 = \overline{a}_4 > 0.$$

We can thus conclude that the only coefficient that has an influence on the stability of the passively damped TC-ROPA$_{n-1}$ robot about the FPEP is $\overline{c}_1$, as seen in the undamped case, which results in the following criterion:

Criterion A.2. ***Critical Routh Coefficient condition for passively damped***

TC-ROPA$_{n-1}$ robot: The FPEP of the passively damped TC-ROPA$_{n-1}$ robot is guaranteed to be locally unstable if the critical Routh coefficient $\overline{c}_1 < 0$, causing the allocation of two poles in both the left-hand and right-hand halves of the complex plane.

This critical Routh coefficient is calculated using

$$\overline{c}_1 = \frac{\overline{b}_1\overline{a}_3 - \overline{a}_1\overline{b}_1}{\overline{b}_1}.$$

Substituting the necessary expressions leads to

$$\overline{c}_1 = \frac{p_1 k_D^3 + p_2 {k_D}^2 k_P + p_3 k_D^2 + p_4 k_D k_P + p_5 k_D + p_6 {k_P}^3 + p_7 k_D {k_P}^2 + p_8 {k_P}^2 + p_9 k_P}{\pi\left[z_1 {k_D}^2 + z_2 k_D k_P + z_3 k_D + z_4 {k_P}^2 + z_5 k_P + z_6\right]}$$

where

$$\begin{aligned}
p_1 &= \pi b_1 \overline{n}_1 \overline{n}_2, \\
p_2 &= \pi^2 {b_1}^2 \overline{n}_1 + \left(\overline{w}_1 \pi - {\overline{n}_1}^2\right)\overline{n}_2 + \pi b_1\left(\overline{n}_0\overline{n}_2 + \overline{n}_1\overline{n}_3\right), \\
p_3 &= \pi^2 {b_1}^2 \overline{n}_2, \\
p_4 &= \pi\left(\pi^2 {b_1}^3 + \pi\overline{n}_3 {b_1}^2 - 2b_1\overline{n}_1\overline{n}_2 + \overline{w}_2\overline{n}_2\right), \\
p_5 &= \pi b_1 {\overline{n}_2}^2, \\
p_6 &= \pi\overline{w}_0\left[\overline{n}_3 + \pi b_1\right] - {\overline{n}_0}^2\overline{n}_2, \\
p_7 &= \pi\left[\overline{n}_0\overline{n}_3 + \overline{w}_1\pi\right] b_1 + \pi^2 {b_1}^2\overline{n}_0 + \left[\overline{w}_0\pi - 2\overline{n}_0\overline{n}_1\right]\overline{n}_2 + \pi\overline{w}_1\overline{n}_3, \\
p_8 &= \pi\left[\left[\pi\overline{w}_2 - 2\overline{n}_0\overline{n}_2\right] b_1 + \overline{w}_2\overline{n}_3\right], \\
p_9 &= \pi b_1\overline{n}_2\overline{n}_3
\end{aligned}$$

and

$$\begin{aligned}
z_1 &= b_1\overline{n}_1, & z_2 &= \overline{n}_0 b_1 + \overline{w}_1, \\
z_3 &= \pi {b_1}^2, & z_4 &= \overline{w}_0, \\
z_5 &= \overline{w}_2, & \overline{z}_6 &= b_1\overline{n}_2.
\end{aligned}$$

This problem is difficult to solve analytically since there are three unknowns that may all effect the stability of the system (b_1, k_D, and k_P). To simplify this problem, and in the interest of completing this derivation, we chose $k_D = 0$. The implications of this decision on the final swing-up control is unknown at this point of the derivation, but sacrificing the feedback of the distal pendulum's angular velocity is deemed necessary for the successful completion of the *gain selection criterion* for the passively damped TC-ROPA$_{n-1}$ robot.

Substituting $k_D = 0$ into the expression for $\overline{c}_1$ produces

$$\overline{c}_1\Big|_{k_D=0} = \frac{k_P}{\pi}\left[\frac{r_1 {k_P}^2 + r_2 k_P + r_3}{\overline{w}_0 {k_P}^2 + \overline{w}_2 k_P + b_1 \overline{n}_2}\right] \tag{A.90}$$

where

$$\begin{aligned} r_1 &= \pi^2 b_1 \overline{w}_0 + \pi \overline{w}_0 \overline{n}_3 - {\overline{n}_0}^2 \overline{n}_2, \\ r_2 &= \pi\left[\pi b_1 \overline{w}_2 + \overline{w}_2 \overline{n}_3 - 2 b_1 \overline{n}_0 \overline{n}_2\right], \\ r_3 &= \pi b_1 \overline{n}_2 \overline{n}_3. \end{aligned}$$

With the conditions set out in eqs. (A.88) and (A.89), it is evident that the denominator of the expression in eq. (A.90) will have no effect on the sign of $\overline{c}_1$ (along with the term k_P/π since $k_P > 0$). The sign change of $\overline{c}_1$ can thus be determined solely through the analysis of the expression

$$\overline{c}_{1_D} = r_1 {k_P}^2 + r_2 k_P + r_3. \tag{A.91}$$

We can thus solve for the intercepts of $\overline{c}_1$ by evaluating $\overline{c}_{1_D}$. We shall subsequently determine what gain k_P will produce a negative valued $\overline{c}_{1_D}$ with respect to the passive damping coefficient b_1. The results of the intercept values of k_P are represented as

$$\overline{c}_1 = 0; \begin{cases} k_P = k_{P_1} = 0; \\ k_P = k_{P_2} = \dfrac{\overline{\beta}_2}{\overline{\alpha}_2 + \overline{\alpha}_3}; \\ k_P = k_{P_3}(b_1) = \dfrac{\pi b_1\left(\overline{\beta}_1 + \overline{\beta}_2\right)}{\pi b_1\left(\overline{\alpha}_1 + \overline{\alpha}_2 + 2\overline{\alpha}_3\right) - 2\alpha\left(\overline{\beta}_1\overline{\alpha}_2 + \overline{\beta}_1\overline{\alpha}_3 - \overline{\beta}_2\overline{\alpha}_1 - \overline{\beta}_2\overline{\alpha}_3\right)} \end{cases}$$

which results in

$$r_1 {k_P}^2 + r_2 k_P + r_3 = 0 \begin{cases} k_P = k_{P_2}; \\ k_P = k_{P_3}. \end{cases} . \tag{A.92}$$

The gain $k_{P_3}(b_1)$ may also be represented as

$$k_{P_3}(b_1) = \frac{\overline{n}_2 b_1}{\overline{n}_1 b_1 - \overline{w}_2}.$$

We shall now identify the orientation of each of these gains with respect to each other on the real number axis with the following lemma:

Lemma A.2. It is evident that $k_{P_3}(b_1)$ is described by the asymptote

$$b_{1_{\text{lim}}} = \frac{2\alpha\left(\overline{\beta}_1\overline{\alpha}_2 + \overline{\beta}_1\overline{\alpha}_3 - \overline{\beta}_2\overline{\alpha}_1 - \overline{\beta}_2\overline{\alpha}_3\right)}{\pi\left(\overline{\alpha}_1 + \overline{\alpha}_2 + 2\overline{\alpha}_3\right)}$$

where $b_1 = b_{1_{\text{lim}}}$. This results in

$$b_1 < b_{1_{\text{lim}}} \leftrightarrow k_{P_3}(b_1) < 0,$$
$$b_1 > b_{1_{\text{lim}}} \leftrightarrow k_{P_3}(b_1) > 0.$$

Choosing $b_1 = b_{1_{\text{lim}}} + \epsilon$ where ϵ is an infinitesimally small number, we find that

$$k_{P_3}(b_1) = \frac{(b_{1_{\text{lim}}} + \epsilon)\left(\overline{\beta}_1 + \overline{\beta}_2\right)}{\epsilon\left(\overline{\alpha}_1 + \overline{\alpha}_2 + 2\overline{\alpha}_3\right)}.$$

Therefore, taking $\epsilon \to \infty_+$ results in

$$b_1 \to_+ b_{1_{\text{lim}}} \leftrightarrow k_{P_3} \to \infty_+.$$

Additionally, it is evident that

$$b_1 \to \infty_+ \leftrightarrow k_{P_3} \to \frac{\overline{\beta}_1 + \overline{\beta}_2}{\overline{\alpha}_1 + \overline{\alpha}_2 + 2\overline{\alpha}_3}.$$

From Proof A.5.1 we know that

$$\frac{\overline{\beta}_1 + \overline{\beta}_2}{\overline{\alpha}_1 + \overline{\alpha}_2 + 2\overline{\alpha}_3} > \frac{\overline{\beta}_2}{\overline{\alpha}_2 + \overline{\alpha}_3}.$$

Therefore, we conclude that so long as $b_1 > b_{1_{\text{lim}}}$

$$k_{P_1} < k_{P_2} < k_{P_3}(b_1) \quad \forall t.$$

If, however, $b_1 < b_{1_{\text{lim}}}$ then

$$k_{P_3} < k_{P_1} < k_{P_2}.$$

The sign of the coefficient $\overline{c}_{1_D}$ between each of the intercepts will now be determined considering the cases where $b_1 > b_{1_{\text{lim}}}$ and $0 < b_1 < b_{1_{\text{lim}}}$ respectively.

Case 1: With $b_1 > b_{1_{\text{lim}}}$, we begin by evaluating the sign of $\overline{c}_{1_D}$ when $k_{P_1} < k_P < k_{P_2}$. We therefore choose $k_P = \epsilon$, where ϵ is a positive and infinitesimally small number. Substituting this k_P into eq. (A.91) results in

$$\overline{c}_{1_D} = r_1\epsilon^2 + r_2\epsilon + r_3$$

and since $\epsilon \approx 0$, then

$$\overline{c}_1 = \epsilon\left[\frac{r_3}{b_1\overline{n}_2}\right]$$

with

$$r_3 > 0, \qquad \overline{n}_2 > 0, \qquad b_1 > 0.$$

It is evident that $\overline{c}_1 > 0$ in this case. We know that the next intercept occurs when $k_P = k_{P_2}$ according to Lemma A.2. Therefore

$$\overline{c}_1 > 0, \quad \text{for} \quad 0 < k_P < k_{P_2}.$$

Next we must find the sign of $\overline{c}_{1_D}$ when

$$k_{P_2} < k_P < k_{P_3}(b_1).$$

First, a gain $k_P = k_{P_2} + \epsilon$ is chosen since $k_{P_3}(b_1) > k_{P_2}$. Substituting this gain into eq. (A.91) produces

$$\begin{aligned}\overline{c}_{1_D} &= r_1 \left(k_{P_2} + \epsilon\right)^2 + r_2 \left(k_{P_2} + \epsilon\right) + r_3 \\ &= r_1 {k_{P_2}}^2 + 2\epsilon r_1 k_{P_2} + \epsilon^2 r_1 + r_2 k_{P_2} + \epsilon r_2 + r_3.\end{aligned}$$

Using the intercept condition expressed in eq. (A.92), the expression for $\overline{c}_{1_D}$ simplifies as

$$\overline{c}_{1_D} = 2\epsilon k_{P_2} r_1 + \epsilon^2 k_{P_2} + \epsilon r_2$$

with $\epsilon^2 <<< \epsilon$, resulting in

$$\overline{c}_{1_D} = \epsilon \left(2k_{P_2} r_1 + r_2\right).$$

Expanding and solving the expression for $\overline{c}_{1_D}$ produces

$$\overline{c}_{1_D} = -\pi \overline{w}_2 \epsilon \left(2\overline{\beta}_2 \alpha + \pi b_1\right).$$

Therefore, it is evident that

$$\overline{c}_{1_D} < 0 \quad \text{for } k_{P_2} < k_P < k_{P_3}.$$

Therefore, choosing a gain k_P between k_{P_2} and k_{P_3} will ensure that the FPEP is an unstable equilibrium point.

Lastly, we will evaluate the gain selection $k_P > k_{P_3}$ and its effect on the coefficient $\overline{c}_{1_D}$. We thus select $k_P = k_{P_3} + \epsilon$, where, once again, ϵ is an infinitesimally small positive number. Substituting this gain selection into eq. (A.91) produces

$$\begin{aligned}\overline{c}_{1_D} &= r_1 \left(k_{P_3} + \epsilon\right)^2 + r_2 \left(k_{P_3} + \epsilon\right) + r_3 \\ &= r_1 {k_{P_3}}^2 + r_2 k_{P_3} + r_3 + 2\epsilon r_1 k_{P_3} + \epsilon^2 r_1 + \epsilon r_2.\end{aligned}$$

Implementing the intercept condition shown in eq. (A.92) allows for the simplification

$$\overline{c}_{1_D} = 2\epsilon r_1 k_{P_3} + \epsilon^2 r_1 + \epsilon r_2$$

and since $\epsilon^2 <<< \epsilon$, then

$$\overline{c}_{1_D} = \epsilon \left[2r_1 k_{P_3} + r_2\right].$$

Upon further simplification, we find that

$$\overline{c}_{1_D} = \pi \overline{w}_2 \epsilon \left(2\overline{\beta}_2 \alpha + \pi b_1\right)$$

which shows that if the gain k_P is chosen to be larger than k_{P_3}, then this would result in a stable response about the FPEP, since $\overline{c}_{1_D} > 0$, as shown above. We can, therefore, describe the *gain selection criterion* of the passively damped TC-ROPA$_{n-1}$ robot with $k_D = 0$ and $b_1 > b_{1_{\text{lim}}}$ as follows.

The FPEP of the passively damped TC-ROPA$_{n-1}$ robot when $b_1 > b_{1_{\text{lim}}}$ is guaranteed to be locally unstable so long as the conditions

$$\frac{\overline{\beta}_2}{\overline{\alpha}_2 + \overline{\alpha}_3} < k_P < \frac{\overline{n}_2 b_1}{\overline{n}_1 b_1 - \overline{w}_2}, \quad k_D = 0$$

are satisfied. We now move onto case 2.

Case 2: For the case where $0 < b_1 < b_{1_{\text{lim}}}$, it is apparent from Lemma A.2 that

$$k_{P_3} < k_{P_1} < k_{P_2}.$$

Therefore, there are only two intercepts that occur on the positive semi-definite real axis, since $k_{P_3} < 0$. Therefore, using the results from the last case, we can define the *gain selection criterion* for the case when $b_1 < b_{1_{\text{lim}}}$.

The FPEP of the passively damped TC-ROPA$_{n-1}$ robot when $0 < b_1 < b_{1_{\text{lim}}}$ is guaranteed to be locally unstable so long as the conditions

$$k_P > \frac{\overline{\beta}_2}{\overline{\alpha}_2 + \overline{\alpha}_3}, \quad k_D = 0$$

are satisfied. The results of each of these cases are formalised in criterion 9.2 of chapter 9. The position of the intercepts on the real-axis for each case of damping is demonstrated in figure A.6.

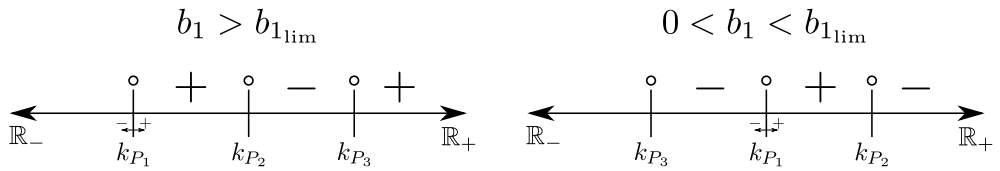

FIGURE A.6: The signs of $\overline{c}_{1_D}$ with reference to its intercepts, for $b_1 > b_{1_{\lim}}$ (left) and $0 < b_1 < b_{1_{\lim}}$ (right).

The positive sign represents a region of gain selections for k_P that results in a positively valued $\overline{c}_1$ (which corresponds to a stable system response about the FPEP). The negative sign represents a region of gain selections for k_P that results in a negatively valued $\overline{c}_1$ (which corresponds to an unstable system response about the FPEP).

Appendix B

Examples

This appendix contains a number of application examples of the certain techniques that were mentioned in the main body of the dissertation. These examples are included to provide the reader with a practical reference to assist them with particular modelling or control problems they may encounter. This appendix contains five sections which provide detailed examples of the following applications:

1. LDM-related control using the mechanical energy of a simple mass-spring-damper system.
2. Implementation of Krakovskii's method.
3. Exact feedback linearisation of the fully-actuated undamped DIP.
4. IOFBL of the fully-actuated undamped DIP.
5. PA_{n-1} robot VCL iteration procedure for $k = 1 : 3$.

B.1 LDM-related control using the mechanical energy of a simple mass-spring-damper system.

The Lyapunov candidate function is used in this example to determine the behaviour of the simple mass-spring-damper, and to prove that the mass block will always tend towards $x = 0$ if the damper is associated with some non-zero viscous damping coefficient. This example follows the procedure highlighted in chapter 5.

(1) Consider the classic model of the unactuated nonlinear mass-spring-damper system. If the mass in figure B.1 is displaced in such a manner that the length of the spring exceeds or falls short of its natural length, will the mass asymptotically tend towards the position of natural spring length after a finite amount of time? It would be possible to determine the local stability of the system around the vicinity of the equilibrium point using the Jacobian linearisation technique, but this technique cannot be employed if the mass is moved a large distance off the initial equilibrium point [2]. LDM is, therefore, well suited to solve this particular stability problem.

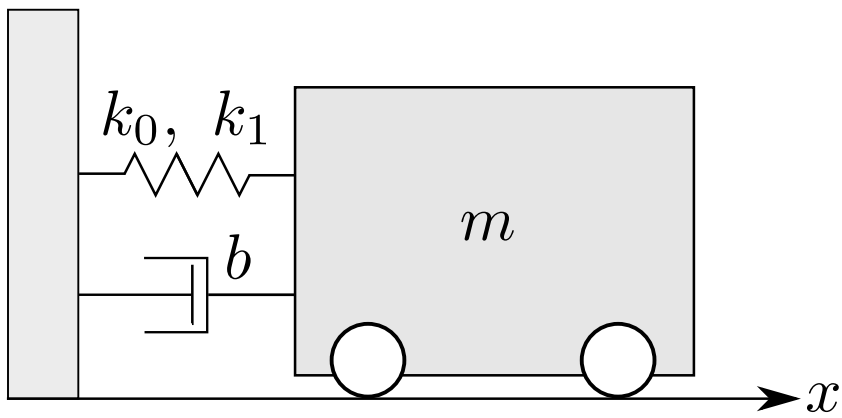

FIGURE B.1: Non-linear mass-spring-damper model. Adapted from [2].

The mass' movement is translational, moving only in a one-dimensional plane. The equation of motion dictating the behaviour of this block can be found through the implementation of Newtonian physics. This results in

$$m\ddot{x} + b\dot{x} + k_0 x + k_1 x^3 = 0 \tag{B.1}$$

where

$x =$ the translational displacement of mass off origin (m),
$m =$ the mass of block (kg),
$b =$ the linear damping coefficient (kg.m^{-1}.s^{-2}),
$k_0 =$ the linear spring constant (kg.s^{-2}), and
$k_1 =$ the nonlinear spring constant (kg.m^{-2}.s^{-2}).

A state-space is formed by choosing

$$\mathbf{x}_1 = x, \qquad \mathbf{x}_2 = \dot{x}.$$

Therefore, the state-space of this mass-spring-damper system is represented as

$$\dot{\mathbf{x}}_1 = \mathbf{x}_2, \tag{B.2}$$

$$\dot{\mathbf{x}}_2 = -\frac{b}{m}\mathbf{x}_2 - \frac{k_0}{m}\mathbf{x}_1 - \frac{k_1}{m}\mathbf{x}_1^3 \tag{B.3}$$

where $\dot{\mathbf{x}} = f(\mathbf{x})$. All the spring constants and damping coefficients are non-zero. The system, therefore, has only one equilibrium point, the origin. Therefore

$$\begin{bmatrix} \mathbf{x}_1^* \\ \mathbf{x}_2^* \end{bmatrix} = \mathbf{0}.$$

(2) The system is nonlinear. A trivial quadratic function cannot, therefore, be used as a candidate Lyapunov function. It seems appropriate to make use of the most accessible positive definite function for mechanical systems, its mechanical energy. Therefore, we chose

$$\begin{aligned} V(\mathbf{x}) &= \frac{1}{2}m\dot{x}^2 + \int_0^x \left(k_0 x + k_1 x^3\right)\mathrm{d}x \\ &= \frac{1}{2}m\dot{x}^2 + \frac{1}{2}k_0 x^2 + \frac{1}{4}k_1 x^4 \\ &= \frac{1}{2}m\mathbf{x}_2{}^2 + \frac{1}{2}k_0\mathbf{x}_1{}^2 + \frac{1}{4}k_1\mathbf{x}_1{}^4. \end{aligned} \tag{B.4}$$

This Lyapunov function has the following properties:

(a) The mechanical energy is zero when $\mathbf{x} = \mathbf{x}^*$.

(b) Increasing the magnitude of either $\mathbf{x}_1$ (corresponding to an increase in potential energy) or $\mathbf{x}_2$ (corresponding to an increase in kinetic energy) results in an increase in mechanical energy whilst moving the states away from the equilibrium point. Instability is, therefore, related to an increase in the mechanical energy.

(c) Conversely, moving the states closer to the equilibrium point ($\mathbf{x} \to \mathbf{x}^*$) reduces the mechanical energy of the system. Therefore, asymptotic stability of the equilibrium point is accompanied by the convergence of mechanical energy to zero.

It is evident that the mechanical energy scalar provides sufficient information about the stability of the equilibrium for it to be considered as a candidate Lyapunov function for this system.

(3) The candidate Lyapunov function is clearly positive definite for $\mathbf{x} \in \mathbb{R}$. The neighbourhood Ω_l is therefore boundless. Proving asymptotic stability in this region for the equilibrium point will, therefore, prove that the equilibrium point is globally asymptotically stable [2].

(4) The time differential of the candidate Lyapunov function $\dot{V}(\mathbf{x})$ needs to be expressed explicitly to determine if it is negative semi-definite, thus satisfying the Lyapunov function necessary conditions [2]. This time differential of the candidate Lyapunov function will effectively represent the change of mechanical energy in the system with respect to time. Taking the time differential of the mechanical energy and considering a substitution of the equation of motion in eq. (B.1), the rate of the mechanical energy is expressed as

$$\dot{V}(\mathbf{x}) = \mathbf{x}_2\left(m\dot{\mathbf{x}}_2 + k_0\mathbf{x}_1 + k_1\mathbf{x}_1{}^3\right) = -b\mathbf{x}_2{}^2 \tag{B.5}$$

[2]. It is apparent that $\dot{V}(\mathbf{x})$ is negative semi-definite, falling within the set $\mathbf{R}$ when the velocity of the mass $\mathbf{x}_2 = 0$ (see section 5.2.2). The candidate function

shown in eq. (B.4) can, therefore, be classified as a Lyapunov function, which will asymptotically tend toward the invariant set $\mathbf{M}$, which is a subset of $\mathbf{R}$ [2]. The equilibrium point has not, however, been proven to be asymptotically stable, as there could be many states in $\mathbf{M}$ which the trajectory could converge to (i.e. there could be other points in the system where an equilibrium is reached where $\mathbf{x}_2 = 0$ and $\mathbf{x}_1 = \mathbf{x}_1^*$). Asymptotic stability of this equilibrium point can be proven, however, by demonstrating that the equilibrium point found at $\mathbf{x} = \mathbb{0}$ is the point found in $\mathbf{M}$ [2].

Assume that a possible equilibrium point exists in the system, with $\mathbf{x}_2 = 0$ existing at a particular value of $\mathbf{x}_1$. If this is the case, these values should produce a zero rate matrix ($\dot{\mathbf{x}} = \mathbb{0}$). Instead, substituting these values into eq. (B.3) produces

$$\begin{aligned}\dot{\mathbf{x}}_1 &= 0,\\ \dot{\mathbf{x}}_2 &= -\frac{k_0}{m}\mathbf{x}_1 - \frac{k_1}{m}\mathbf{x}_1^3 \neq 0\end{aligned}$$

[2]. This is clearly a contradiction; The acceleration of the mass is non-zero, which will cause the block to move off the candidate equilibrium point. The only state found within the set $\mathbf{M}$, therefore, is the equilibrium point found at the origin (i.e. $\mathbf{x} = \mathbb{0}$). The equilibrium point at the origin is, as proved by contradiction, asymptotically stable due to the negative semi-definite $\dot{V}(\mathbf{x})$, which guarantees that the trajectory will converge in the set $\mathbf{M}$, a set that conveniently contains only one equilibrium point, namely the equilibrium point at the origin [2].

B.2 Implementation of Krakovskii's Method

In this example, Krakovskii's method is used to identify an appropriate Lyapunov candidate function for the mass-spring-damper shown in the previous example. We have shown that the using the mechanical energy is sufficient as a Lyapunov candidate function, but a system's behaviour may be described by multiple candidate functions, as we shall now prove.

The identification of this asymptotically stable equilibrium point may also be successfully preformed using Krakovskii's method:

Using the system described in eqs. (eq. B.2) and (B.3), the Jacobian matrix $\mathbf{A}$ is represented as

$$\mathbf{A} = \frac{\partial f(\mathbf{x})}{\partial \mathbf{x}} = \begin{bmatrix} \dfrac{\partial f_1(\mathbf{x})}{\partial \mathbf{x}_1} & \dfrac{\partial f_1(\mathbf{x})}{\partial \mathbf{x}_2} \\ \dfrac{\partial f_2(\mathbf{x})}{\partial \mathbf{x}_1} & \dfrac{\partial f_2(\mathbf{x})}{\partial \mathbf{x}_2} \end{bmatrix}$$

$$= \begin{bmatrix} 0 & 1 \\ -\dfrac{k_0}{m} - \dfrac{3k_1}{m}{\mathbf{x}_1}^2 & -\dfrac{b}{m} \end{bmatrix}.$$

Choosing $\mathbf{P} = \mathbf{I}$, we find that

$$\mathbf{F}(\mathbf{x}) = \mathbf{A}^{\mathrm{T}}\mathbf{P} + \mathbf{P}\mathbf{A} = \mathbf{A}^{\mathrm{T}} + \mathbf{A} = -\mathbf{Q}$$

$$= \begin{bmatrix} 0 & -\dfrac{k_0}{m} - \dfrac{3k_1}{m}{\mathbf{x}_1}^2 + 1 \\ -\dfrac{k_0}{m} - \dfrac{3k_1}{m}{\mathbf{x}_1}^2 + 1 & -\dfrac{2b}{m} \end{bmatrix}.$$

$\mathbf{Q}$ must be positive definite to conclude that $\dot{V}(\mathbf{x})$ is negative definite. A negative definite $\dot{V}(\mathbf{x})$, therefore, corresponds to the requirement that $\mathbf{F}(\mathbf{x})$ must be negative definite. One way to prove this is to identify the eigenvalues of the resultant matrix, whereby a negative definite matrix will only have negative eigenvalues [2]. Taking the determinant of $\mathbf{F}(\mathbf{x}) - \mathbf{I}\lambda$ we find that

$$|\mathbf{F}(\mathbf{x}) - \mathbf{I}\lambda| = \det \begin{bmatrix} -\lambda & -\dfrac{k_0}{m} - \dfrac{3k_1}{m}{\mathbf{x}_1}^2 + 1 \\ -\dfrac{k_0}{m} - \dfrac{3k_1}{m}{\mathbf{x}_1}^2 + 1 & -\dfrac{2b}{m} - \lambda \end{bmatrix}$$

$$
\begin{aligned}
&= -\lambda\Big(-\frac{2b}{m}-\lambda\Big)-\Big(-\frac{k_0}{m}-\frac{3k_1}{m}\mathbf{x}_1{}^2+1\Big)^2 \\
&= \lambda^2+\frac{2b}{m}\lambda-\frac{1}{m^2}\Big(-k_0-3k_1\mathbf{x}_1{}^2+m\Big)^2.
\end{aligned}
$$

The quadratic equation is used to solve for these eigenvalues, where

$$
\begin{aligned}
\lambda &= -\frac{b}{m}\pm\frac{\sqrt{\Big(\frac{2b}{m}\Big)^2-\frac{4}{m^2}\Big(-k_0-3m\mathbf{x}_1{}^2+m\Big)}}{2} \\
&= -\frac{b}{m}\pm\frac{\sqrt{b^2-\Big(-k_0-3m\mathbf{x}_1{}^2+m\Big)^2}}{m}.
\end{aligned}
$$

There are three different results that can be obtained from the quadratic formula which are dependent on the values of the physical parameters of the system.

(i) In the case where $|b| \geq |-k_0-3m\mathbf{x}_1{}^2+m|$, the eigenvalues will always be real and negative definite. This is because the term $\sqrt{b^2-\Big(-k_0-3m\mathbf{x}_1{}^2+m\Big)^2}$ will be equal to γ, a real valued number that will never be larger in magnitude than b. Therefore,

$$
\lambda_1 = \frac{-\gamma-b}{m} < 0, \qquad\qquad \lambda_2 = \frac{\gamma-b}{m} < 0.
$$

The equilibrium point at the origin is globally asymptotically stable in this case.

(ii) In the case where $|b| < |-k_0-3m\mathbf{x}_1{}^2+m|$, the eigenvalues will be complex in nature with negative real values. The term $b^2-\Big(-k_0-3m\mathbf{x}_1{}^2+m\Big)^2$ will be negative in magnitude, with $\sqrt{b^2-\Big(-k_0-3m\mathbf{x}_1{}^2+m\Big)^2}$ resulting in an imaginary number of magnitude $j\gamma$. Therefore,

$$
\lambda_1 = \frac{-j\gamma-b}{m},\ \frac{-b}{m} < 0 \qquad \text{and} \qquad \lambda_2 = \frac{j\gamma-b}{m},\ \frac{-b}{m} < 0.
$$

The equilibrium point at the origin is also globally asymptotically stable in this case, but will exhibit oscillatory behaviour introduced by the imaginary poles.

(iii) The most complex case involves the condition $(-k_0 - 3m\mathbf{x}_1{}^2 + m) = 0$. In this case, the eigenvalues are negative semi-definite, with

$$\lambda_1 = \frac{-2b}{m} < 0, \qquad \lambda_2 = 0.$$

The equilibrium point can only be labelled as marginally stable as the trajectory is guaranteed to converge to a state in the set $\mathbf{M}$, but it is not certain which set it will converge to. The asymptotic stability of this equilibrium point can be proven using invariant set theorem, as seen with the previous Lyapunov function.

According to the invariant set theorem, the equilibrium point is asymptotically stable if $\dot{V}(\mathbf{x}) \leq 0$ and it can be proven that the equilibrium point in question is the only state located in $\mathbf{M}$. Therefore

$$\dot{V}(\mathbf{x}) = -\mathbf{x}^{\mathrm{T}}\mathbf{Q}\mathbf{x} = -\mathbf{x}^{\mathrm{T}}\mathbf{F}(\mathbf{x})\mathbf{x}$$

$$= \begin{bmatrix}\mathbf{x}_1 & \mathbf{x}_2\end{bmatrix} \begin{bmatrix} 0 & -\dfrac{k_0}{m} - \dfrac{3k_1}{m}\mathbf{x}_1{}^2 + 1 \\ -\dfrac{k_0}{m} - \dfrac{3k_1}{m}\mathbf{x}_1{}^2 + 1 & -\dfrac{2b}{m} \end{bmatrix} \begin{bmatrix}\mathbf{x}_1 \\ \mathbf{x}_2\end{bmatrix}.$$

Substituting the condition $(-k_0 - 3m\mathbf{x}_1{}^2 + m) = 0$ into the matrix $\mathbf{F}(\mathbf{x})$ we find that

$$\dot{V}(\mathbf{x}) = \begin{bmatrix}\mathbf{x}_1 & \mathbf{x}_2\end{bmatrix} \begin{bmatrix} 0 & 0 \\ 0 & -\dfrac{2b}{m} \end{bmatrix} \begin{bmatrix}\mathbf{x}_1 \\ \mathbf{x}_2\end{bmatrix}$$

$$= -\frac{2b}{m}\mathbf{x}_2{}^2.$$

$\dot{V}(\mathbf{x})$ is clearly negative semi-definite in this case. The system equations are also altered, where

$$\dot{\mathbf{x}}_1 = \mathbf{x}_2,$$
$$\dot{\mathbf{x}}_2 = -\mathbf{x}_1 + \left(3 - \frac{k_1}{m}\right)\mathbf{x}_1{}^3 - \frac{b}{m}\mathbf{x}_2.$$

If one were to imagine that the set $\mathbf{M}$ contained all invariant states, let us assume, once again, that there are multiple states that exist in the set $\mathbf{M}$ where $\mathbf{x}_2 = 0$ and with $\mathbf{x}_1 \neq 0$. If the states truly existed, the rates of these states will be zero (i.e. $\dot{\mathbf{x}} = \mathbf{0}$). Substituting these values of states into the system

equations, however, produces

$$\dot{\mathbf{x}}_1 = 0,$$
$$\dot{\mathbf{x}}_2 = -\mathbf{x}_1 + \left(3 - \frac{k_1}{m}\right)\mathbf{x}_1{}^3 \neq 0.$$

This is, once again, a contradiction. The rates cannot cause the states to accelerate away from an equilibrium point. It is, therefore, proved by contradiction that the only state found in the set $\mathbf{M}$ is the equilibrium point found at the origin. The equilibrium point is, therefore, proven to be asymptotically stable.

The equilibrium point is proven to be asymptotically stable in all cases, thus proving that the equilibrium point at the origin is globally asymptotically stable. This means that, no matter how the block is displaced from the origin, the block will eventually return to the origin over some finite time.

B.3 Exact Feedback Linearisation of the Fully-Actuated Undamped DIP

The feedback linearisation of a UMS cannot be demonstrated using ELFBL since the total relative degree $r < n$. We shall, therefore, demonstrate the technique on a fully-actuated undamped DIP system (checking the relative degree of the system along the way).

The system dynamics of the undamped DIP is derived using Lagrangian mechanics in [6], [34], and [64]. These dynamics are represented using the prototypical form described by

$$\mathbf{M}(\mathbf{q})\ddot{\mathbf{q}} + \mathbf{D}(\mathbf{q},\dot{\mathbf{q}}) + \mathbf{K}(\mathbf{q}) = \mathbf{G}(\mathbf{q})\mathbf{u}$$

with

$$\mathbf{M}(\mathbf{q}) = \begin{bmatrix} M_{11} & M_{12} \\ M_{21} & M_{22} \end{bmatrix} = \begin{bmatrix} \alpha_1 + \alpha_2 + \alpha_3\cos(q_2) & \alpha_2 + \alpha_3\cos(q_2) \\ \alpha_2 + \alpha_3\cos(q_2) & \alpha_2 \end{bmatrix},$$

$$\mathbf{D}(\mathbf{q},\dot{\mathbf{q}}) = \begin{bmatrix} D_1 \\ D_2 \end{bmatrix} = \alpha_3 \begin{bmatrix} -2\dot{q}_1\dot{q}_2 - \dot{q}_2^2 \\ \dot{q}_1^2 \end{bmatrix} \sin q_2,$$

$$\mathbf{K}(\mathbf{q}) = \begin{bmatrix} K_1 \\ K_2 \end{bmatrix} = \begin{bmatrix} -\beta_1 \sin q_1 - \beta_2 \sin(q_1 + q_2) \\ -\beta_2 \sin(q_1 + q_2) \end{bmatrix}, \text{ and}$$

$$\mathbf{G}(\mathbf{q})\mathbf{u} = \begin{bmatrix} \tau_1 \\ \tau_2 \end{bmatrix}$$

where

$$\begin{aligned} \alpha_1 &= m_1 {l_1}^2 + m_2 {L_1}^2 + I_1, & \alpha_2 &= m_2 {l_2}^2 + I_2, \\ \alpha_3 &= m_2 L_1 l_2, & \beta_1 &= g L_1 (m_1 + m_2), \\ \beta_2 &= g m_2 l_2. \end{aligned}$$

The equations of motion of the system are therefore defined as

$$\ddot{\mathbf{q}} = \mathbf{M}^{-1}(\mathbf{q})\Big[\mathbf{G}(\mathbf{q})\mathbf{u} - \mathbf{D}(\mathbf{q},\dot{\mathbf{q}}) - \mathbf{K}(\mathbf{q})\Big]$$

where

$$\mathbf{M}^{-1}(\mathbf{q}) = \begin{bmatrix} M_{11}^* & M_{12}^* \\ M_{21}^* & M_{22}^* \end{bmatrix}.$$

The equations of motion are now transformed into the state-space using

$$\begin{aligned} q_1 &= \mathbf{x}_1, & \dot{q}_1 &= \mathbf{x}_2, \\ q_2 &= \mathbf{x}_3, & \dot{q}_2 &= \mathbf{x}_4. \end{aligned}$$

Therefore

$$\begin{aligned} \dot{\mathbf{x}}_1 &= \mathbf{x}_2, \\ \dot{\mathbf{x}}_2 &= M_{11}^*\big[\tau_1 - D_1 - K_1\big] + M_{12}^*\big[\tau_2 - D_2 - K_2\big], \\ \dot{\mathbf{x}}_3 &= \mathbf{x}_4, \\ \dot{\mathbf{x}}_4 &= M_{21}^*\big[\tau_1 - D_1 - K_1\big] + M_{22}^*\big[\tau_2 - D_2 - K_2\big] \end{aligned}$$

which can be represented in the companion form as

$$\dot{\mathbf{x}} = f(\mathbf{x}) + g(\mathbf{x})\mathbf{u}$$

where

$$f(\mathbf{x}) = \begin{bmatrix} f_1(\mathbf{x}) \\ f_2(\mathbf{x}) \\ f_3(\mathbf{x}) \\ f_4(\mathbf{x}) \end{bmatrix} = \begin{bmatrix} \mathbf{x}_2 \\ -M_{11}^*\big[D_1 + K_1\big] - M_{12}^*\big[D_2 + K_2\big] \\ \mathbf{x}_4 \\ -M_{21}^*\big[D_1 + K_1\big] - M_{22}^*\big[D_2 + K_2\big] \end{bmatrix},$$

$$g(\mathbf{x}) = \begin{bmatrix} g_1(\mathbf{x}) & g_2(\mathbf{x}) \end{bmatrix} = \begin{bmatrix} 0 & 0 \\ M_{11}^* & M_{21}^* \\ 0 & 0 \\ M_{12}^* & M_{22}^* \end{bmatrix}$$

with the order of the system $n = 4$. The system is square, having the $m = 2$ inputs matched by the $m = 2$ outputs defined by

$$\mathbf{y}(t) = \begin{bmatrix} q_1 \\ q_2 \end{bmatrix} = \begin{bmatrix} \mathbf{x}_1 \\ \mathbf{x}_3 \end{bmatrix}.$$

With the outputs defined, we shall now check the relative degree of the system, knowing that

$$\begin{aligned} &L_{g_i} L_f^j h_i(\mathbf{x}) = 0 \qquad \text{for } 0 \le j \le r_i - 1, \\ &L_{g_i} L_f^{r_i - 1} h_i(\mathbf{x}) = 0 \end{aligned}$$

where in this case, $1 \le i \le 2$. Therefore, the process is initiated with $j = 0$ for the first output, which results in

$$L_{g_1} L_f^0 h_1(\mathbf{x}) = L_{g_1} h_1(\mathbf{x}) = \frac{\partial h_1(\mathbf{x})}{\partial \mathbf{x}} g_1(\mathbf{x})$$

$$
\begin{aligned}
&= \begin{bmatrix} 1 & 0 & 0 & 0 \end{bmatrix} \begin{bmatrix} 0 \\ M_{11}^* \\ 0 \\ M_{12}^* \end{bmatrix} \\
&= 0.
\end{aligned}
$$

This result is inconclusive. Iterating the process for $j = 1$ produces

$$
\begin{aligned}
L_{g_1} L_f^1 h_1(\mathbf{x}) &= L_{g_1} \left[\frac{\partial h_1(\mathbf{x})}{\partial \mathbf{x}} f(\mathbf{x}) \right] \\
&= L_{g_1} \begin{bmatrix} 1 & 0 & 0 & 0 \end{bmatrix} \begin{bmatrix} \mathbf{x}_2 \\ f_2(\mathbf{x}) \\ \mathbf{x}_4 \\ f_4(\mathbf{x}) \end{bmatrix} \\
&= L_{g_1} \mathbf{x}_2 = \frac{\partial \mathbf{x}_2}{\partial \mathbf{x}} g_1(\mathbf{x}) \\
&= \begin{bmatrix} 0 & 1 & 0 & 0 \end{bmatrix} \begin{bmatrix} 0 \\ M_{11}^* \\ 0 \\ M_{12}^* \end{bmatrix} \\
&= M_{11}^* \neq 0.
\end{aligned}
$$

Therefore $r_1 = 2$. This process is repeated for the second output, where

$$
\begin{aligned}
L_{g_2} L_f^0 h_2(\mathbf{x}) &= L_{g_2} h_2(\mathbf{x}) = \frac{\partial h_2(\mathbf{x})}{\partial \mathbf{x}} g_2(\mathbf{x}) \\
&= \begin{bmatrix} 0 & 0 & 1 & 0 \end{bmatrix} \begin{bmatrix} 0 \\ M_{21}^* \\ 0 \\ M_{22}^* \end{bmatrix} \\
&= 0.
\end{aligned}
$$

This result is, once again, inconclusive. The procedure must be iterating once more with $j = 1$. Therefore

$$
\begin{aligned}
L_{g_2} L_f^1 h_2(\mathbf{x}) &= L_{g_2} \left[\frac{\partial h_2(\mathbf{x})}{\partial \mathbf{x}} f(\mathbf{x}) \right] \\
&= L_{g_2} \begin{bmatrix} 0 & 0 & 1 & 0 \end{bmatrix} \begin{bmatrix} \mathbf{x}_2 \\ f_2(\mathbf{x}) \\ \mathbf{x}_4 \\ f_4(\mathbf{x}) \end{bmatrix} \\
&= L_{g_2} \mathbf{x}_4 = \frac{\partial \mathbf{x}_4}{\partial \mathbf{x}} g_2(\mathbf{x})
\end{aligned}
$$

$$
\begin{aligned}
&= \begin{bmatrix} 0 & 0 & 0 & 1 \end{bmatrix} \begin{bmatrix} 0 \\ M_{21}^* \\ 0 \\ M_{22}^* \end{bmatrix} \\
&= M_{22}^* \neq 0
\end{aligned}
$$

which shows that $r_2 = 2$. It can be concluded that the system is indeed fully-actuated, having $r = r_1 + r_2 = n$. We can now continue with the ELFBL procedure knowing that it is appropriate to this application.

The first objective of the procedure involves the establishment of a coordinate transformation $z = \Phi(\mathbf{x})$, where

$$
\begin{aligned}
\Phi(\mathbf{x}) &= \begin{bmatrix} \phi^1(\mathbf{x}) & \phi^2(\mathbf{x}) \end{bmatrix}^{\mathbf{T}} \\
&= \begin{bmatrix} \phi_1^1(\mathbf{x}) & \phi_2^1(\mathbf{x}) & \phi_1^2(\mathbf{x}) & \phi_2^2(\mathbf{x}) \end{bmatrix}^{\mathbf{T}} \\
&= \begin{bmatrix} \mathbf{x}_1 & \mathbf{x}_2 & \mathbf{x}_3 & \mathbf{x}_4 \end{bmatrix}.
\end{aligned}
$$

The new state-space can, therefore, be defined as

$$
\begin{aligned}
\dot{\mathbf{z}} = \dot{\Phi}(\mathbf{x}) &= \frac{\partial \Phi(\mathbf{x})}{\partial \mathbf{x}} \dot{\mathbf{x}} \\
&= I_n \dot{\mathbf{x}} \\
&= \dot{\mathbf{x}} \left(\Phi^{-1}(\mathbf{z}) \right).
\end{aligned}
$$

It turns out that the coordinate transformation led to the definition of a new state-space $\mathbf{z}$ that is identical to that of the original state-space. This is caused by the configuration of the original system, which is evidently in the controllability canonical form. Therefore

$$
\begin{aligned}
\dot{\mathbf{z}}_1 &= \mathbf{z}_2, \\
\dot{\mathbf{z}}_2 &= M_{11}^* \left(\Phi^{-1}(\mathbf{z}) \right) \left[\tau_1 - D_1 \left(\Phi^{-1}(\mathbf{z}) \right) - K_1 \left(\Phi^{-1}(\mathbf{z}) \right) \right] + M_{12}^* \left(\Phi^{-1}(\mathbf{z}) \right) [\tau_2 - \\
&\quad D_2 \left(\Phi^{-1}(\mathbf{z}) \right) - K_2 \left(\Phi^{-1}(\mathbf{z}) \right)], \\
\dot{\mathbf{z}}_3 &= \mathbf{z}_4, \\
\dot{\mathbf{z}}_4 &= M_{21}^* \left(\Phi^{-1}(\mathbf{z}) \right) \left[\tau_1 - D_1 \left(\Phi^{-1}(\mathbf{z}) \right) - K_1 \left(\Phi^{-1}(\mathbf{z}) \right) \right] + M_{22}^* \left(\Phi^{-1}(\mathbf{z}) \right) [\tau_2 - \\
&\quad D_2 \left(\Phi^{-1}(\mathbf{z}) \right) - K_2 \left(\Phi^{-1}(\mathbf{z}) \right)]
\end{aligned}
$$

which can, once again, be written in the companion form

$$
\dot{\mathbf{z}}(t) = f(\Phi^{-1}(\mathbf{z})) + g(\Phi^{-1}(\mathbf{z}))\mathbf{u}(t)
$$

where

$$f\left(\Phi^{-1}(\mathbf{z})\right) = \begin{bmatrix} f_1\left(\Phi^{-1}(\mathbf{z})\right) \\ f_2\left(\Phi^{-1}(\mathbf{z})\right) \\ f_3\left(\Phi^{-1}(\mathbf{z})\right) \\ f_4\left(\Phi^{-1}(\mathbf{z})\right) \end{bmatrix} = \begin{bmatrix} \mathbf{z}_2 \\ -M_{11}^*\left[D_1 + K_1\right] - M_{12}^*\left[D_2 + K_2\right] \\ \mathbf{z}_4 \\ -M_{21}^*\left[D_1 + K_1\right] - M_{22}^*\left[D_2 + K_2\right] \end{bmatrix},$$

$$g\left(\Phi^{-1}(\mathbf{z})\right) = \left[g_1\left(\Phi^{-1}(\mathbf{z})\right) \quad g_2\left(\Phi^{-1}(\mathbf{z})\right)\right] = \begin{bmatrix} 0 & 0 \\ M_{11}^* & M_{12}^* \\ 0 & 0 \\ M_{21}^* & M_{22}^* \end{bmatrix}.$$

We shall now design a static-state feedback controller of the form

$$\mathbf{u}(t) = \alpha(\mathbf{z}) + \beta(\mathbf{z})\mathbf{v}(t)$$

to introduce a linearising feedback into the system, which results in

$$\dot{\mathbf{z}}_2 = v_1, \tag{B.6a}$$

$$\dot{\mathbf{z}}_4 = v_2. \tag{B.6b}$$

We find, however, that the control inputs are present in both $\dot{\mathbf{z}}_2$ and $\dot{\mathbf{z}}_4$. We will have to solve for each of the control inputs (τ_1 and τ_2) separately. We, therefore, define

$$v_1 = M_{11}^*\left[\tau_1 - D_1 - K_1\right] + M_{12}^*\left[\tau_2 - D_2 - K_2\right], \tag{B.7a}$$

$$v_2 = M_{21}^*\left[\tau_1 - D_1 - K_1\right] + M_{22}^*\left[\tau_2 - D_2 - K_2\right] \tag{B.7b}$$

which are a consequence of eq. (B.6a) and (B.6b) (all of the expressions above are dependent on $\Phi^{-1}(\mathbf{x})$, but this is omitted for sake of brevity). To solve these simultaneous equations, we first solve for τ_2 in eq. (B.7a), where

$$\tau_2 = \frac{M_{21}^*}{M_{22}^*}\left[D_1 + K_1 - \tau_1\right] + \frac{v_2}{M_{22}^*} + D_2 + K_2. \tag{B.8}$$

Substituting eq. (B.8) into eq. (B.6a) produces

$$v_1 = \left[M_{11}^* - \frac{M_{12}^* M_{21}^*}{M_{22}^*}\right]\tau_1 + \left[\frac{M_{12}^* M_{21}^*}{M_{22}^*} - M_{11}^*\right]\left(D_1 + K_1\right) + \frac{M_{12}^*}{M_{22}^*}v_2. \tag{B.9}$$

We now solve for τ_1 in eq. (B.9), where

$$\tau_1 = \left[\frac{M_{22}^*}{M_{11}^* M_{22}^* - M_{12}^* M_{21}^*}\right]v_1 - \left[\frac{M_{12}^*}{M_{11}^* M_{22}^* - M_{12}^* M_{21}^*}\right]v_2 + D_1 + K_1. \tag{B.10}$$

This is the finalised torque expression for τ_1. Substituting eq. (B.10) into eq. (B.6b) produces

$$v_2 = \left[\frac{M_{21}^* M_{22}^*}{M_{11}^* M_{22}^* - M_{12}^* M_{21}^*}\right] v_1 - \left[\frac{M_{12}^* M_{21}^*}{M_{11}^* M_{22}^* - M_{12}^* M_{21}^*}\right] v_2 + M_{22}^* \tau_2 - M_{22}^* \big(D_2 + K_2\big). \tag{B.11}$$

Taking eq. (B.11) and solving for τ_2 produces the finalised expression for τ_2, with

$$\tau_2 = \left[\frac{M_{11}^*}{M_{11}^* M_{22}^* - M_{12}^* M_{21}^*}\right] v_2 - \left[\frac{M_{21}^*}{M_{11}^* M_{22}^* - M_{12}^* M_{21}^*}\right] v_1 + D_2 + K_2 \tag{B.12}$$

we can now construct the linear state-space using these linearising feedback control inputs by substituting eqs. (B.10) and (B.12) into eqs. (B.6a) and (B.6b), which results in

$$\dot{\mathbf{z}}(t) = A\mathbf{z}(t) + B\mathbf{v}(t)$$

where

$$A = \begin{bmatrix} 0 & 1 & 0 & 0 \\ 0 & 0 & 0 & 0 \\ 0 & 0 & 0 & 1 \\ 0 & 0 & 0 & 0 \end{bmatrix}, \qquad B = \begin{bmatrix} 0 & 0 \\ 1 & 0 \\ 0 & 0 \\ 0 & 1 \end{bmatrix}.$$

The stabilising input $\mathbf{v}$ can now be designed for using pole-placement. This results in the linear state-feedback controller

$$\mathbf{v} = -\mathbf{k}^{\mathbf{T}} \tilde{\mathbf{z}}$$

where

$$\mathbf{K} = \begin{bmatrix} k_1^1 & k_2^1 & k_3^1 & k_4^1 \\ k_1^2 & k_2^2 & k_3^2 & k_4^2 \end{bmatrix}, \qquad \tilde{\mathbf{z}} = \begin{bmatrix} \mathbf{z}_1 - \mathbf{z}_1^d \\ \mathbf{z}_2 - \mathbf{z}_2^d \\ \mathbf{z}_3 - \mathbf{z}_3^d \\ \mathbf{z}_4 - \mathbf{z}_4^d \end{bmatrix}$$

and where $\mathbf{z}_i^d$ for $1 \leq i \leq 4$ represents the desired final condition of each state.

B.4 IOFBL of the Fully-Actuated Undamped DIP

The state-space equations of the fully-actuated undamped DIP have already been derived in example B.3, whereby

$$\begin{aligned}
\dot{\mathbf{x}}_1 &= \mathbf{x}_2, \\
\dot{\mathbf{x}}_2 &= M_{11}^*\big[\tau_1 - D_1 - K_1\big] + M_{12}^*\big[\tau_2 - D_2 - K_2\big], \\
\dot{\mathbf{x}}_3 &= \mathbf{x}_4, \\
\dot{\mathbf{x}}_4 &= M_{21}^*\big[\tau_1 - D_1 - K_1\big] + M_{22}^*\big[\tau_2 - D_2 - K_2\big]
\end{aligned}$$

which may be represented in companion form

$$\dot{\mathbf{x}}(t) = f(\mathbf{x}) + g(\mathbf{x})\mathbf{u}(t)$$

where

$$f(\mathbf{x}) = \begin{bmatrix} f_1(\mathbf{x}) \\ f_2(\mathbf{x}) \\ f_3(\mathbf{x}) \\ f_4(\mathbf{x}) \end{bmatrix} = \begin{bmatrix} \mathbf{x}_2 \\ -M_{11}^*\big[D_1 + K_1\big] - M_{12}^*\big[D_2 + K_2\big] \\ \mathbf{x}_4 \\ -M_{21}^*\big[D_1 + K_1\big] - M_{22}^*\big[D_2 + K_2\big] \end{bmatrix},$$

$$g(\mathbf{x}) = \begin{bmatrix} g_1(\mathbf{x}) & g_2(\mathbf{x}) \end{bmatrix} = \begin{bmatrix} 0 & 0 \\ 1 & 0 \\ 0 & 0 \\ 0 & 1 \end{bmatrix}.$$

The outputs of the system are defined as

$$\mathbf{y}(\mathbf{x}) = \begin{bmatrix} h_1(\mathbf{x}) \\ h_2(\mathbf{x}) \end{bmatrix} = \begin{bmatrix} \mathbf{x}_1 \\ \mathbf{x}_3 \end{bmatrix}.$$

As seen in section 5.3.3, we define the static-state feedback control torque as

$$\mathbf{u}(t) = \begin{bmatrix} \tau_1 \\ \tau_2 \end{bmatrix} = C^{-1}(\mathbf{x})\big[\mathbf{v}(t) - b(\mathbf{x})\big] \tag{B.13}$$

where

$$C(\mathbf{x}) = \begin{bmatrix} L_{g_1}L_f h_1(\mathbf{x}) & L_{g_2}L_f h_1(\mathbf{x}) \\ L_{g_1}L_f h_2(\mathbf{x}) & L_{g_2}L_f h_2(\mathbf{x}) \end{bmatrix}$$

and

$$b(\mathbf{x}) = \begin{bmatrix} L_f^2 h_1(\mathbf{x}) \\ L_f^2 h_2(\mathbf{x}) \end{bmatrix}.$$

We already know from example B.3 that

$$L_{g_1} L_f h_1(\mathbf{x}) = M_{11}^*, \qquad\qquad L_{g_2} L_f h_2(\mathbf{x}) = M_{22}^*.$$

The remaining entries of $C(\mathbf{x})$ and $b(\mathbf{x})$ are calculated by defining

$$\begin{aligned}
L_{g_2} L_f h_1(\mathbf{x}) &= L_{g_2}\big[\mathbf{x}_2\big] \\
&= \frac{\partial \mathbf{x}_2}{\partial \mathbf{x}} g_2(\mathbf{x}) \\
&= \begin{bmatrix} 0 & 1 & 0 & 0 \end{bmatrix} \begin{bmatrix} 0 \\ M_{12}^* \\ 0 \\ M_{22}^* \end{bmatrix} \\
&= M_{12}^*,
\end{aligned}$$

$$\begin{aligned}
L_{g_1} L_f h_2(\mathbf{x}) &= L_{g_1}\big[\mathbf{x}_4\big] \\
&= \frac{\partial \mathbf{x}_4}{\partial \mathbf{x}} g_1(\mathbf{x}) \\
&= \begin{bmatrix} 0 & 0 & 0 & 1 \end{bmatrix} \begin{bmatrix} 0 \\ M_{11}^* \\ 0 \\ M_{21}^* \end{bmatrix} \\
&= M_{21}^*,
\end{aligned}$$

$$\begin{aligned}
L_f^2 h_1(\mathbf{x}) &= L_f\big[L_f h_1(\mathbf{x})\big] \\
&= L_f\big[\mathbf{x}_2\big] \\
&= \frac{\partial \mathbf{x}_2}{\partial \mathbf{x}} f(\mathbf{x}) \\
&= \begin{bmatrix} 0 & 1 & 0 & 0 \end{bmatrix} \begin{bmatrix} \mathbf{x}_2 \\ f_2(\mathbf{x}) \\ \mathbf{x}_4 \\ f_4(\mathbf{x}) \end{bmatrix} \\
&= f_2(\mathbf{x}),
\end{aligned}$$

$$\begin{aligned}
L_f^2 h_2(\mathbf{x}) &= L_f\big[L_f h_2(\mathbf{x})\big] \\
&= L_f\big[\mathbf{x}_4\big] \\
&= \frac{\partial \mathbf{x}_4}{\partial \mathbf{x}} f(\mathbf{x})
\end{aligned}$$

$$
\begin{aligned}
&= \begin{bmatrix} 0 & 0 & 0 & 1 \end{bmatrix} \begin{bmatrix} \mathbf{x}_2 \\ f_2(\mathbf{x}) \\ \mathbf{x}_4 \\ f_4(\mathbf{x}) \end{bmatrix} \\
&= f_4(\mathbf{x}).
\end{aligned}
$$

Therefore

$$
C(\mathbf{x}) = \begin{bmatrix} M_{11}^* & M_{12}^* \\ M_{21}^* & M_{22}^* \end{bmatrix},
$$

$$
b(\mathbf{x}) = \begin{bmatrix} f_2(\mathbf{x}) \\ f_4(\mathbf{x}) \end{bmatrix}.
$$

Additionally

$$
C^{-1}(\mathbf{x}) = \frac{1}{M_{11}^* M_{22}^* - M_{12}^* M_{21}^*} \begin{bmatrix} M_{22}^* & -M_{12}^* \\ -M_{21}^* & M_{11}^* \end{bmatrix}.
$$

Using eq. (B.13) we find that

$$
\begin{aligned}
\tau_1 &= \frac{1}{M_{11}^* M_{22}^* - M_{12}^* M_{21}^*} \Big[M_{22}^* \big(v_1 - f_2(\mathbf{x})\big) - M_{12}^* \big(v_2 - f_4(\mathbf{x})\big) \Big] \\
&= \left[\frac{M_{22}^*}{M_{11}^* M_{22}^* - M_{12}^* M_{21}^*} \right] v_1 - \left[\frac{M_{12}^*}{M_{11}^* M_{22}^* - M_{12}^* M_{21}^*} \right] v_2 + \\
&\quad \frac{M_{22}^* \Big[M_{11}^* \big(D_1 + K_1\big) + M_{12}^* \big(D_2 + K_2\big) \Big]}{M_{11}^* M_{22}^* - M_{12}^* M_{21}^*} - \frac{M_{12}^* \Big[M_{21}^* \big(D_1 + K_1\big) + M_{22}^* \big(D_2 + K_2\big) \Big]}{M_{11}^* M_{22}^* - M_{12}^* M_{21}^*} \\
&= \left[\frac{M_{22}^*}{M_{11}^* M_{22}^* - M_{12}^* M_{21}^*} \right] v_1 - \left[\frac{M_{12}^*}{M_{11}^* M_{22}^* - M_{12}^* M_{21}^*} \right] v_2 + D_1 + K_1
\end{aligned}
$$

and

$$
\begin{aligned}
\tau_2 &= \frac{1}{M_{11}^* M_{22}^* - M_{12}^* M_{21}^*} \Big[M_{21}^* \big(v_1 - f_2(\mathbf{x})\big) - M_{11}^* \big(v_2 - f_4(\mathbf{x})\big) \Big] \\
&= \left[\frac{M_{11}^*}{M_{11}^* M_{22}^* - M_{12}^* M_{21}^*} \right] v_2 - \left[\frac{M_{21}^*}{M_{11}^* M_{22}^* - M_{12}^* M_{21}^*} \right] v_1 + \\
&\quad \frac{M_{21}^* \Big[M_{11}^* \big(D_1 + K_1\big) + M_{12}^* \big(D_2 + K_2\big) \Big]}{M_{11}^* M_{22}^* - M_{12}^* M_{21}^*} - \frac{M_{11}^* \Big[M_{21}^* \big(D_1 + K_1\big) + M_{22}^* \big(D_2 + K_2\big) \Big]}{M_{11}^* M_{22}^* - M_{12}^* M_{21}^*} \\
&= \left[\frac{M_{11}^*}{M_{11}^* M_{22}^* - M_{12}^* M_{21}^*} \right] v_2 - \left[\frac{M_{21}^*}{M_{11}^* M_{22}^* - M_{12}^* M_{21}^*} \right] v_1 + D_2 + K_2.
\end{aligned}
$$

Substituting these torques back into the original system equations produces

$$\begin{aligned}\dot{\mathbf{x}}_1 &= \mathbf{x}_2,\\ \dot{\mathbf{x}}_2 &= v_1,\\ \dot{\mathbf{x}}_3 &= \mathbf{x}_4,\\ \dot{\mathbf{x}}_4 &= v_2.\end{aligned}$$

Choosing a diffeomorphism $\mathbf{z} = \Phi(\mathbf{x})$ such that

$$\begin{aligned}\mathbf{z}_1 &= \mathbf{x}_1,\\ \mathbf{z}_2 &= \mathbf{x}_2,\\ \mathbf{z}_3 &= \mathbf{x}_3,\\ \mathbf{z}_4 &= \mathbf{x}_4\end{aligned}$$

and substituting these transforms into the newly derived system equations results in

$$\begin{aligned}\dot{\mathbf{z}}_1 &= \mathbf{z}_2,\\ \dot{\mathbf{z}}_2 &= v_1,\\ \dot{\mathbf{z}}_3 &= \mathbf{z}_4,\\ \dot{\mathbf{z}}_4 &= v_2\end{aligned}$$

which can be represented by the linear state-space

$$\dot{\mathbf{z}}(t) = A\mathbf{z}(t) + B\mathbf{v}(t)$$

where

$$A = \begin{bmatrix} 0 & 1 & 0 & 0\\ 0 & 0 & 0 & 0\\ 0 & 0 & 0 & 1\\ 0 & 0 & 0 & 0 \end{bmatrix}, \qquad B = \begin{bmatrix} 0 & 0\\ 1 & 0\\ 0 & 0\\ 0 & 1 \end{bmatrix}.$$

The transformation and the control input are identical to the results produced in example B.3, thereby demonstrating that the IOFBL technique does indeed produce the same result as the ELFBL technique when $r = n$.

Once again, a linear-sate feedback controller may now be designed using the control law

$$\mathbf{v}(t) = -\mathbf{k}^{\mathbf{T}}\tilde{\mathbf{z}}$$

where

$$\mathbf{K} = \begin{bmatrix} k_1^1 & k_2^1 & k_3^1 & k_4^1 \\ k_1^2 & k_2^2 & k_3^2 & k_4^2 \end{bmatrix} \qquad \tilde{\mathbf{z}} = \begin{bmatrix} \mathbf{z}_1 - \mathbf{z}_1^d \\ \mathbf{z}_2 - \mathbf{z}_2^d \\ \mathbf{z}_3 - \mathbf{z}_3^d \\ \mathbf{z}_4 - \mathbf{z}_4^d \end{bmatrix}$$

and where $\mathbf{z}_i^d$ for $1 \leq i \leq 4$ represents the desired final condition of each state.

B.5 $\mathbf{PA}_{n-1}$ Robot VCL Iteration Procedure for $k = 1:3$

$\mathbf{k = 1}$

(i) $i = n - 1$.

(ii) Substituting the expressions for $\dot{\bar{q}}_n$ and $\dot{\bar{\beta}}_n$ (seen in eqs. (7.27) and (7.28)) into eq. (7.25) produces

$$\begin{aligned}\dot{\bar{q}}_{n-1} &= \dot{q}_{n-1} + w_n\dot{\bar{q}}_n + v_n\dot{\bar{\beta}}_n \\ &= \dot{q}_{n-1} + w_n\dot{q}_n \\ &= \dot{q}_{n-1} + \psi_{(n-1)n}\dot{q}_n. \end{aligned} \tag{B.14}$$

The coefficient w_n is relabelled as $\psi_{(n-1)n}$ to prevent confusion later on in the derivation [5]. The index of ψ is an amalgamation of the index of the evaluated joint and the index of the associated angular velocity respectively [5].

(iii) Substituting the expressions for $\dot{\bar{q}}_i$ and $\dot{\bar{\beta}}_{i+1}$ (seen in eqs. (7.27) and (7.28)) into eq. (7.26) produces

$$\begin{aligned}\dot{\bar{\beta}}_{n-1} &= p_n\dot{\bar{q}}_n + f_n\dot{\bar{\beta}}_n \\ &= p_n\dot{q}_n \\ &= \rho_{(n-1)n}\dot{q}_n \end{aligned} \tag{B.15}$$

[5]. Once again, the coefficient p_n is relabelled as $\rho_{(n-1)n}$ to prevent confusion later on in the derivation, with the index of ρ being an amalgamation of the index of the evaluated joint and the index of the associated angular velocity respectively [5].

$\mathbf{k = 2}$

(i) $i = n - 2$.

(ii) Substituting the expressions for $\dot{\bar{q}}_{n-1}$ and $\dot{\bar{\beta}}_{n-1}$ (seen in eqs. (B.14) and (B.15)) into eq. (7.25) produces

$$\begin{aligned}\dot{\bar{q}}_{n-2} &= \dot{q}_{n-1} + w_{n-1}\dot{\bar{q}}_{n-1} + v_{n-1}\dot{\bar{\beta}}_{n-1} \\ &= \dot{q}_{n-2} + w_{n-1}\dot{q}_{n-1} + \Big[w_{n-1}\psi_{(n-1)n} + v_{n-1}\rho_{(n-1)n}\Big]\dot{q}_n \\ &= \dot{q}_{n-2} + \psi_{(n-2)(n-1)}\dot{q}_{n-1} + \psi_{(n-2)n}\dot{q}_n \end{aligned} \tag{B.16}$$

where

$$\begin{aligned}\psi_{(n-2)(n-1)} &= w_{n-1}, \\ \psi_{(n-2)n} &= w_{n-1}\psi_{(n-1)n} + v_{n-1}\rho_{(n-1)n}\end{aligned}$$

[5].

(iii) Substituting the expressions for $\dot{\bar{q}}_{n-1}$ and $\dot{\bar{\beta}}_{n-1}$ (seen in eqs. (B.14) and (B.15)) into eq. (7.26) produces

$$\begin{aligned}\dot{\bar{\beta}}_{n-2} &= p_{n-1}\dot{\bar{q}}_{n-1} + f_{n-1}\dot{\bar{\beta}}_{n-1} \\ &= p_{n-1}\dot{q}_{n-1} + \Big[p_{n-1}\psi_{(n-1)n} + f_{n-1}\rho_{(n-1)n}\Big]\dot{q}_n \\ &= \rho_{(n-2)(n-1)}\dot{q}_{n-1} + \rho_{(n-2)n}\dot{q}_n \end{aligned} \tag{B.17}$$

where

$$\begin{aligned}\rho_{(n-2)(n-1)} &= p_{n-1}, \\ \rho_{(n-2)n} &= p_{n-1}\psi_{(n-1)n} + f_{n-1}\rho_{(n-1)n}\end{aligned}$$

[5].

$\mathbf{k = 3}$

(i) $i = n - 3$.

(ii) Substituting the expressions for $\dot{\bar{q}}_{n-2}$ and $\dot{\bar{\beta}}_{n-2}$ (seen in eqs. (B.16) and (B.17)) into eq. (7.25) produces

$$\begin{aligned}\dot{\bar{q}}_{n-3} &= \dot{q}_{n-3} + w_{n-2}\dot{\bar{q}}_{n-1} + v_{n-2}\dot{\bar{\beta}}_{n-1} \\ &= \dot{q}_{n-3} + w_{n-2}\dot{q}_{n-2} + \Big[w_{n-2}\psi_{(n-2)(n-1)} + v_{n-2}\rho_{(n-2)(n-1)}\Big]\dot{q}_{n-1} + \\ &\quad \Big[w_{n-2}\psi_{(n-2)(n)} + v_{n-2}\rho_{(n-2)(n)}\Big]\dot{q}_n \\ &= \dot{q}_{n-3} + \psi_{(n-3)(n-2)}\dot{q}_{n-2} + \psi_{(n-3)(n-1)}\dot{q}_{n-1}\psi_{(n-3)n}\dot{q}_n \end{aligned} \tag{B.18}$$

where

$$\begin{aligned}\psi_{(n-3)(n-2)} &= w_{n-2}, \\ \psi_{(n-3)(n-1)} &= w_{n-2}\psi_{(n-2)(n-1)} + v_{n-2}\rho_{(n-2)(n-1)}, \\ \psi_{(n-3)(n)} &= w_{n-2}\psi_{(n-2)n} + v_{n-2}\rho_{(n-2)n}\end{aligned}$$

[5].

(iii) Substituting the expressions for $\dot{\bar{q}}_{n-2}$ and $\dot{\bar{\beta}}_{n-2}$ (seen in eqs. (B.16) and (B.17)) into eq. (7.26) produces

$$\begin{aligned}\dot{\bar{\beta}}_{n-3} &= p_{n-2}\dot{\bar{q}}_{n-2} + f_{n-2}\dot{\bar{\beta}}_{n-2} \\ &= p_{n-2}\dot{q}_{n-2} + \Big[p_{n-2}\psi_{(n-2)(n-1)} + f_{n-2}\rho_{(n-2)(n-1)}\Big]\dot{q}_{n-1} + \qquad \text{(B.19)} \\ &\quad \Big[p_{n-2}\psi_{(n-2)n} + f_{n-2}\rho_{(n-2)n}\Big]\dot{q}_n \\ &= \rho_{(n-3)(n-2)}\dot{q}_{n-2} + \rho_{(n-3)(n-1)}\dot{q}_{n-1} + \rho_{(n-3)n}\dot{q}_n \qquad \text{(B.20)}\end{aligned}$$

where

$$\begin{aligned}
\rho_{(n-3)(n-2)} &= p_{n-2}, \\
\rho_{(n-3)(n-1)} &= p_{n-2}\psi_{(n-2)(n-1)} + f_{n-2}\rho_{(n-2)(n-1)}, \\
\rho_{(n-2)n} &= p_{n-2}\psi_{(n-2)n} + f_{n-2}\rho_{(n-3)n}.
\end{aligned}$$

Appendix C

Supplementary Reading

This appendix contains background information on the phenomenon of viscous damping friction to supplement the information included in the main body of the dissertation.

C.1 Viscous Damping Friction

The term "damping" has been coined to describe a phenomenon commonly seen in non-ideal oscillatory systems, whereby a nonconservative analogous force causes the decrease of a system's mechanical energy over time [82]. This principle may be quickly illustrated with a simple mechanical oscillatory system. The block-mass in figure C.1 (inertial component of the system) has a set-point found on the x-axis at x_s, and is attached to a fixed spring (accumulates potential energy) with a spring constant k_0. The system is frictionless, which implies that energy that enters the system can only be removed through the use of an external force (energy dissipation is not an intrinsic property of the system itself). This type of system is expected to oscillate for all time when influenced by an impulse force [82]. This is an expected result, since no energy is dissipated from this system at any point, but this is proven for convenience.

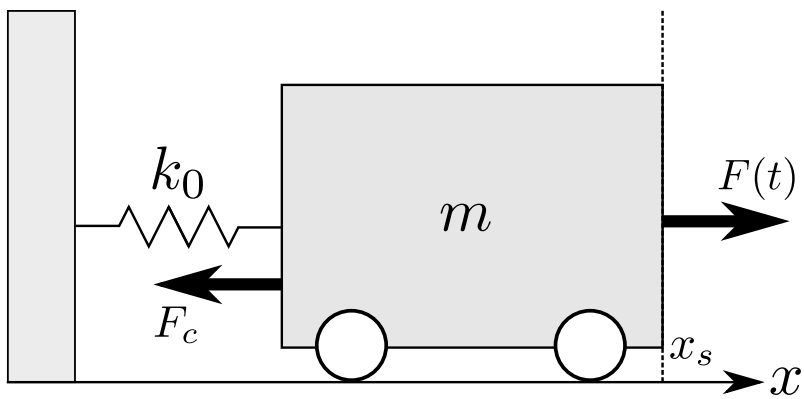

FIGURE C.1: A simple mechanical system. Figure adapted from [2, pg. 57]

The movement of the block-mass about the set-point is ascertainable through the implementation of Newton's laws of motion [82]. The sum of all the forces acting on the block-mass is generalised as

$$\sum F_i = m\frac{\mathrm{d}^2\tilde{x}(t)}{\mathrm{dt}^2} = F(t) - F_c \tag{C.1}$$

where

$F_c =$ the force applied by the spring on the block-mass,
$F(t) =$ an input force, and
$\tilde{x} = x(t) - x_s$.

The spring applies a force on the block proportionally to the displacement away from the set-point x_s, where

$$\begin{aligned} F_c &= k_0\Big(x(t) - x_s\Big) \\ &= k_0\tilde{x}(t) \end{aligned} \tag{C.2}$$

[82]. Substituting eq. (C.2) into eq. (C.1) produces a second-order differential equation described as

$$m\frac{\mathrm{d}^2\tilde{x}(t)}{\mathrm{dt}^2} + k_0\tilde{x}(t) = F(t). \tag{C.3}$$

Using the Laplace transform, the complex transformation of $x(t)$ is described as

$$\tilde{X}(s) = \frac{F(s) + ms\left(x(0) - x_s\right) + mv(0)}{ms^2 + k_0} \tag{C.4}$$

where

$x(0) =$ the initial position of block-mass, and
$v(0) =$ the initial velocity of block-mass.

The denominator of this expression represents the *characteristic equation* of the system, a concept introduced in chapter 4. The poles of the system are thus described as

$$s = \pm j\frac{k_0}{m}$$

and is calculated using the quadratic formula. This result suggests that the system will oscillate indefinitely if an impulse is introduced into the system. This can be shown through the application of the inverse Laplace transform on eq. (C.4), assuming that $F(t) = \delta(t)$, $x(0) = x_s$ and $v(0) = 0$. This results in

$$x(t) = \frac{1}{\sqrt{k_0 m}}\sin\left(\sqrt{\frac{k_0}{m}}t\right) + x_s. \tag{C.5}$$

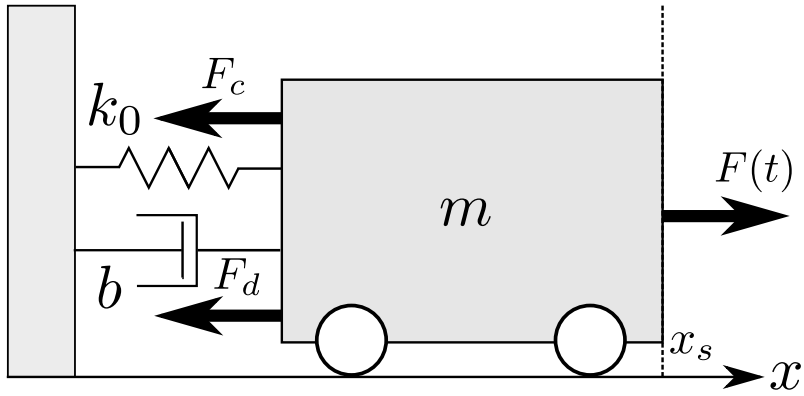

FIGURE C.2: The mass-spring-damper. Figure adapted from [2, pg. 57]

The block-mass evidently oscillates about the set-point with this configuration, but the energy contained in the system does not dissipate, allowing this oscillation to occur without attenuation indefinitely.

As stated before, this effect is a result of the ideal case; the model in figure C.1 does not take nonconservative forces that act on typical systems into account. The model is thus adjusted with the inclusion of a damper, as shown in figure C.2.

In this case, the damper applies a force against the motion of the block proportionally to the block-mass' velocity. This type of friction is known as **viscous damping friction** and is typically used to model friction experienced by an object moving through a fluid, such as air friction ([81] and [82, pg. 471]). Once again, Newton's law of motion describes the summation of the forces in the system as

$$\sum F_i = m\frac{\mathrm{d}^2\tilde{x}(t)}{\mathrm{dt}^2} = F(t) - F_c - F_d \tag{C.6}$$

where

$$F_d = bv(t) = b\frac{\mathrm{d}x(t)}{\mathrm{dt}} = b\frac{\mathrm{d}\tilde{x}(t)}{\mathrm{dt}} \tag{C.7}$$

which represents the damping force. Substituting the expression for F_c found in eq. (C.2), and eq. (C.7) into eq. (C.6) produces

$$m\frac{\mathrm{d}^2\tilde{x}(t)}{\mathrm{dt}^2} + b\frac{\mathrm{d}\tilde{x}(t)}{\mathrm{dt}} + k_0\tilde{x}(t) = F(t).$$

The effect of the viscous damping on the system can only be clearly observed once the poles of the system are determined. The differential equation is modified using the Laplace transform, with the complex plane transformation of $\tilde{x}(t)$ represented

as $\tilde{X}(s)$ as

$$\tilde{X}(s) = \frac{F(s) + \tilde{x}(0)(b + ms) + mv(0)}{ms^2 + bs + k_0}. \tag{C.8}$$

The poles of the system are determined through the evaluation of the characteristic equation of this transfer function. Again, the quadratic function is implemented here, producing

$$s = \frac{-b \pm \sqrt{b^2 - 4mk_0}}{2m}. \tag{C.9}$$

The equation provides two fundamentally different results depending on which condition below is satisfied (provided that $b \neq 0$).

(1) If $b^2 \geq 4mk_0$, then the poles will be found explicitly on the real axis, with the time-dependent response containing no oscillating components. Additionally, the poles will be found explicitly in the left-hand plane of the pole-zero plot, simply because $-b + \sqrt{b^2 - 4mk_0} \not> 0$. The time-dependent impulse response will therefore be represented by an **exponentially decaying signal with no oscillating components**.

(2) if $0 < b^2 < 4mk_0$, then the function $\sqrt{b^2 - 4mk_0}$ is explicitly imaginary. In this case, the poles will contain a real and imaginary component, with the real component being found on the left-hand plane of the pole-zero plot. This results in an **exponentially decaying and oscillating time-dependent impulse response**.

Regardless of whether the time-dependent impulse response contains oscillating components, the response of a viscously damped linear system is predicted to always decay toward an equilibrium point. The time-dependent responses of the system in each case is shown to validate these predictions. This system response is solved through the implementation of the inverse Laplace transform as before, with $F(t) = \delta(t)$, $x(0) = x_s$, and $v(0) = 0$. The result of this procedure for the first and second cases are proven to be

$$x_1(t) = \frac{1}{2k_1}\left[e^{\alpha_0} - e^{\alpha_1}\right] + x_s, \tag{C.10}$$

$$x_2(t) = \frac{e^{-bt}}{|k_1|}\sin\left(\frac{|k_1|}{2m}t\right) + x_s \tag{C.11}$$

where

$$\alpha_0 = \frac{(-b + k_1)t}{2m},$$
$$\alpha_1 = \frac{(-b - k_1)t}{2m},$$
$$k_1 = \sqrt{b^2 - 4mk_0}.$$

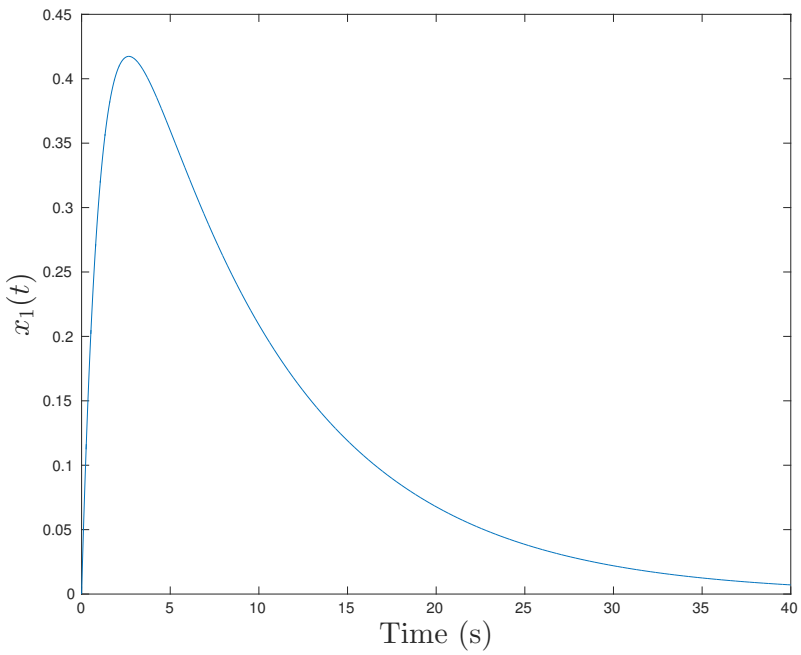

FIGURE C.3: The typical behaviour of a damped second-order system, mathematically described by eq. (C.10).

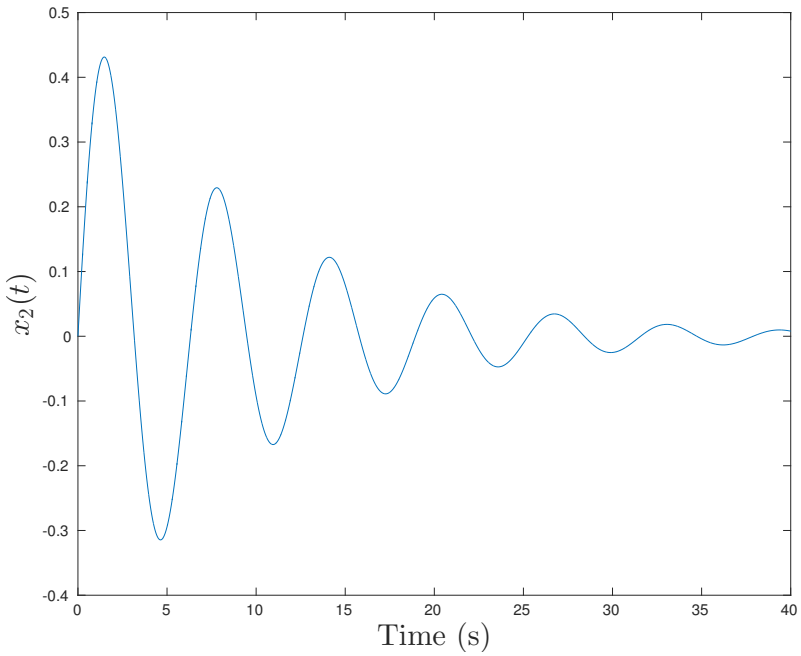

FIGURE C.4: The typical behaviour of an underdamped second-order system, mathematically described by eq. (C.11).

Examples of both of these signals are provided in figures C.3 and C.4. The decay towards the set-point is evident in both cases, with the presence of oscillation in the underdamped signal being the only differing factor. It can be concluded, from this evaluation of linear oscillatory systems, that the introduction of damping forces (specifically viscous damping friction in this case) leads to the eventual dissipation of the system's mechanical energy until the system reaches a stable equilibrium point (the set-point x_s for the case of the mass-spring-damper).

Appendix D

Partial Feedback Linearisation Techniques for the PA$_{n-1}$ Robot

The derivations of the partial feedback linearisation techniques used in this research project are included in this chapter for supplementation purposes. There are three sections that are dedicated to the discussion of the three available techniques, namely *Traditional Collocated Partial Feedback Linearisation*, *Modified Collocated Partial Feedback Linearisation*, and *Noncollocated Partial Feedback Linearisation*.

D.1 Traditional Collocated Partial Feedback Linearisation

The linear state feedback controllers for the ith pendulum (where $3 \leq i \leq n$) is defined as

$$v_i = -k_{D_i}\dot{q}_i + k_{P_i}(q_i^d - q_i).$$

The linear state feedback controller for v_2 can be designed for according to the specific control objective. We shall now derive the FBL torques that are required to linearise the $n-1$ distal pendulums using TCPFL technique.

Consider the dynamical equations of the PA$_{n-1}$ robot, described by

$$\begin{aligned}
&M_{11}(\mathbf{q})\ddot{q}_1 + M_{12}(\mathbf{q})\ddot{q}_2 + \cdots + M_{1n}(\mathbf{q})\ddot{q}_n + D_1(\mathbf{q},\dot{\mathbf{q}}) + K_1(\mathbf{q}) = 0,\\
&M_{21}(\mathbf{q})\ddot{q}_1 + M_{22}(\mathbf{q})\ddot{q}_2 + \cdots + M_{2n}(\mathbf{q})\ddot{q}_n + D_2(\mathbf{q},\dot{\mathbf{q}}) + K_2(\mathbf{q}) = \tau_2,\\
&M_{31}(\mathbf{q})\ddot{q}_1 + M_{32}(\mathbf{q})\ddot{q}_2 + \cdots + M_{3n}(\mathbf{q})\ddot{q}_n + D_3(\mathbf{q},\dot{\mathbf{q}}) + K_3(\mathbf{q}) = \tau_3,\\
&\quad\vdots\\
&M_{n1}(\mathbf{q})\ddot{q}_1 + M_{n2}(\mathbf{q})\ddot{q}_2 + \cdots + M_{nn}(\mathbf{q})\ddot{q}_n + D_n(\mathbf{q},\dot{\mathbf{q}}) + K_n(\mathbf{q}) = \tau_n.
\end{aligned}$$

The objective of this technique is to negate the nonlinear dynamics of the $n-1$ most distal pendulums and have to have each of these accelerations assigned to a newly defined input. Therefore

$$\begin{aligned}
\ddot{q}_2 &= v_2,\\
\ddot{q}_3 &= v_3,
\end{aligned}$$

$$\vdots$$
$$\ddot{q}_n = v_n.$$

A new input v_1 cannot be assigned to $\ddot{q}_1$ since the system only contains $n-1$ actuators. Substituting these expressions into the dynamical equations of the PA$_{n-1}$ robot produces

$$M_{11}(\mathbf{q})\ddot{q}_1 + M_{12}(\mathbf{q})v_2 + \cdots + M_{1n}(\mathbf{q})v_n + D_1(\mathbf{q},\dot{\mathbf{q}}) + K_1(\mathbf{q}) = 0, \tag{D.2a}$$
$$M_{21}(\mathbf{q})\ddot{q}_1 + M_{22}(\mathbf{q})v_2 + \cdots + M_{2n}(\mathbf{q})v_n + D_2(\mathbf{q},\dot{\mathbf{q}}) + K_2(\mathbf{q}) = \tau_2, \tag{D.2b}$$
$$M_{31}(\mathbf{q})\ddot{q}_1 + M_{32}(\mathbf{q})v_2 + \cdots + M_{3n}(\mathbf{q})v_n + D_3(\mathbf{q},\dot{\mathbf{q}}) + K_3(\mathbf{q}) = \tau_3, \tag{D.2c}$$
$$\vdots$$
$$M_{n1}(\mathbf{q})\ddot{q}_1 + M_{n2}(\mathbf{q})v_2 + \cdots + M_{nn}(\mathbf{q})v_n + D_n(\mathbf{q},\dot{\mathbf{q}}) + K_n(\mathbf{q}) = \tau_n. \tag{D.2d}$$

We will now solve for $\ddot{q}_1$ since it is the only unknown in this set of equations. Therefore, rearranging eq. (D.2a) results in

$$\ddot{q}_1 = \frac{-M_{12}(\mathbf{q})v_2 - M_{13}(\mathbf{q})v_3 - \cdots - M_{1n}(\mathbf{q})v_n - D_1(\mathbf{q},\dot{\mathbf{q}}) - K_1(\mathbf{q})}{M_{11}(\mathbf{q})}. \tag{D.3}$$

The substitution of eq. (D.3) into eq. (D.2b) results in the torque expression

$$\tau_2 = \hat{M}_{22}(\mathbf{q})v_2 + \hat{M}_{23}(\mathbf{q})v_3 + \cdots + \hat{M}_{2n}(\mathbf{q})v_n + \hat{D}_2(\mathbf{q},\dot{\mathbf{q}}) + \hat{K}_2(\mathbf{q})$$

where, for $2 \leq j \leq n$,

$$\hat{M}_{2j}(\mathbf{q}) = M_{2j}(\mathbf{q}) - \frac{M_{21}(\mathbf{q})M_{1j}(\mathbf{q})}{M_{11}(\mathbf{q})},$$
$$\hat{D}_2(\mathbf{q},\dot{\mathbf{q}}) = D_2(\mathbf{q},\dot{\mathbf{q}}) - \frac{M_{21}(\mathbf{q})}{M_{11}(\mathbf{q})}D_1(\mathbf{q},\dot{\mathbf{q}}),$$
$$\hat{K}_2(\mathbf{q}) = K_2(\mathbf{q}) - \frac{M_{21}(\mathbf{q})}{M_{11}(\mathbf{q})}K_1(\mathbf{q}).$$

We repeat this process with the next entry of the prototypical form. Therefore, the substitution of the expression for $\ddot{q}_1$ found in eq. (D.3) into eq. (D.2c) produces the expression that accommodates the solving of the FBL torque τ_3, whereby

$$\tau_3 = \hat{M}_{32}(\mathbf{q})v_2 + \hat{M}_{33}(\mathbf{q})v_3 + \cdots + \hat{M}_{3n}(\mathbf{q})v_n + \hat{D}_3(\mathbf{q},\dot{\mathbf{q}}) + \hat{K}_3(\mathbf{q})$$

where, for $2 \leq j \leq n$,

$$\hat{M}_{3j}(\mathbf{q}) = M_{3j}(\mathbf{q}) - \frac{M_{31}(\mathbf{q})M_{1j}(\mathbf{q})}{M_{11}(\mathbf{q})},$$
$$\hat{D}_3(\mathbf{q},\dot{\mathbf{q}}) = D_3(\mathbf{q},\dot{\mathbf{q}}) - \frac{M_{31}(\mathbf{q})}{M_{11}(\mathbf{q})}D_1(\mathbf{q},\dot{\mathbf{q}}),$$

$$\hat{K}_3(\mathbf{q}) = K_3(\mathbf{q}) - \frac{M_{31}(\mathbf{q})}{M_{11}(\mathbf{q})} K_1(\mathbf{q}).$$

A similar result can be seen with the substitution of eq. (D.3) into eq. (D.2d), whereby

$$\tau_n = \hat{M}_{n2}(\mathbf{q})v_2 + \hat{M}_{n3}(\mathbf{q})v_3 + \cdots + \hat{M}_{nn}(\mathbf{q})v_n + \hat{D}_n(\mathbf{q}, \dot{\mathbf{q}}) + \hat{K}_n(\mathbf{q})$$

and where, for $2 \leq j \leq n$,

$$\begin{aligned}
\hat{M}_{nj}(\mathbf{q}) &= M_{nj}(\mathbf{q}) - \frac{M_{n1}(\mathbf{q})M_{1j}(\mathbf{q})}{M_{11}(\mathbf{q})}, \\
\hat{D}_n(\mathbf{q}, \dot{\mathbf{q}}) &= D_n(\mathbf{q}, \dot{\mathbf{q}}) - \frac{M_{n1}(\mathbf{q})}{M_{11}(\mathbf{q})} D_1(\mathbf{q}, \dot{\mathbf{q}}), \\
\hat{K}_n(\mathbf{q}) &= K_n(\mathbf{q}) - \frac{M_{n1}(\mathbf{q})}{M_{11}(\mathbf{q})} K_1(\mathbf{q}).
\end{aligned}$$

Therefore, by induction, we can conclude that the FBL torques that are required to implement TCPFL on the PA$_{n-1}$ robot must be described by

$$\tau_i = \hat{M}_{i2}(\mathbf{q})v_2 + \hat{M}_{i3}(\mathbf{q})v_3 + \cdots + \hat{M}_{in}(\mathbf{q})v_n + \hat{D}_i(\mathbf{q}, \dot{\mathbf{q}}) + \hat{K}_i(\mathbf{q}) \tag{D.4}$$

for $2 \leq i \leq n$ and where, for $2 \leq j \leq n$,

$$\begin{aligned}
\hat{M}_{ij}(\mathbf{q}) &= M_{ij}(\mathbf{q}) - \frac{M_{i1}(\mathbf{q})M_{1j}(\mathbf{q})}{M_{11}(\mathbf{q})}, \\
\hat{D}_i(\mathbf{q}, \dot{\mathbf{q}}) &= D_i(\mathbf{q}, \dot{\mathbf{q}}) - \frac{M_{i1}(\mathbf{q})}{M_{11}(\mathbf{q})} D_1(\mathbf{q}, \dot{\mathbf{q}}), \\
\hat{K}_i(\mathbf{q}) &= K_i(\mathbf{q}) - \frac{M_{i1}(\mathbf{q})}{M_{11}(\mathbf{q})} K_1(\mathbf{q}).
\end{aligned}$$

Choosing $v_m = -k_{D_m}\dot{q}_m - k_{P_m}q_m$ for $2 \leq m \leq n$, the application of these FBL torques on the PA$_{n-1}$ robot results in a set of equations described by

$$\ddot{q}_1 = \frac{-M_{12}(\mathbf{q})v_2 - M_{13}(\mathbf{q})v_3 - \cdots - M_{1n}(\mathbf{q})v_n - D_1(\mathbf{q}, \dot{\mathbf{q}}) - K_1(\mathbf{q})}{M_{11}(\mathbf{q})}, \tag{D.5a}$$

$$\ddot{q}_2 = -k_{D_2}\dot{q}_2 - k_{P_2}q_2, \tag{D.5b}$$

$$\ddot{q}_3 = -k_{D_3}\dot{q}_3 - k_{P_3}q_3, \tag{D.5c}$$

$$\vdots$$

$$\ddot{q}_n = -k_{D_n}\dot{q}_n - k_{P_n}q_n \tag{D.5d}$$

where we must ensure that

$$M_{11}(\mathbf{q}) \neq 0 \; \forall \mathbf{q}. \tag{D.6}$$

D.2 Modified Collocated Partial Feedback Linearisation

This inductive derivation begins with the definition of the equations of motion for a PA$_{n-1}$ robot, which are defined as

$$\begin{aligned}
&M_{11}(\mathbf{q})\ddot{q}_1 + M_{12}(\mathbf{q})\ddot{q}_2 + \cdots + M_{1n}(\mathbf{q})\ddot{q}_n + D_1(\mathbf{q},\dot{\mathbf{q}}) + K_1(\mathbf{q}) = 0,\\
&M_{21}(\mathbf{q})\ddot{q}_1 + M_{22}(\mathbf{q})\ddot{q}_2 + \cdots + M_{2n}(\mathbf{q})\ddot{q}_n + D_2(\mathbf{q},\dot{\mathbf{q}}) + K_2(\mathbf{q}) = \tau_2,\\
&M_{31}(\mathbf{q})\ddot{q}_1 + M_{32}(\mathbf{q})\ddot{q}_2 + \cdots + M_{3n}(\mathbf{q})\ddot{q}_n + D_3(\mathbf{q},\dot{\mathbf{q}}) + K_3(\mathbf{q}) = \tau_3,\\
&\quad\vdots\\
&M_{n1}(\mathbf{q})\ddot{q}_1 + M_{n2}(\mathbf{q})\ddot{q}_2 + \cdots + M_{nn}(\mathbf{q})\ddot{q}_n + D_n(\mathbf{q},\dot{\mathbf{q}}) + K_n(\mathbf{q}) = \tau_n.
\end{aligned}$$

The torque τ_2 will be used for the Lyapunov swing-up control, and will thus not be assigned a FBL torque expression. This means that both $\ddot{q}_1$ and $\ddot{q}_2$ will be unknowns in this case. The other equations of motion, however, will be assigned as a new input v that results from the linearisation of its corresponding dynamics. Therefore

$$\begin{aligned}
\ddot{q}_3 &= v_3,\\
\ddot{q}_4 &= v_4,\\
&\vdots\\
\ddot{q}_n &= v_n.
\end{aligned}$$

Linear state feedback controllers will be designed for each new input v_i, thus ensuring that the associated angular displacement $q_i \approx 0$. The equations of motion are thus described as

$$M_{11}(\mathbf{q})\ddot{q}_1 + M_{12}(\mathbf{q})\ddot{q}_2 + \cdots + M_{1n}(\mathbf{q})v_n + D_1(\mathbf{q},\dot{\mathbf{q}}) + K_1(\mathbf{q}) = 0, \tag{D.7a}$$
$$M_{21}(\mathbf{q})\ddot{q}_1 + M_{22}(\mathbf{q})\ddot{q}_2 + \cdots + M_{2n}(\mathbf{q})v_n + D_2(\mathbf{q},\dot{\mathbf{q}}) + K_2(\mathbf{q}) = \tau_2, \tag{D.7b}$$
$$M_{31}(\mathbf{q})\ddot{q}_1 + M_{32}(\mathbf{q})\ddot{q}_2 + \cdots + M_{3n}(\mathbf{q})v_n + D_3(\mathbf{q},\dot{\mathbf{q}}) + K_3(\mathbf{q}) = \tau_3, \tag{D.7c}$$
$$\vdots$$
$$M_{n1}(\mathbf{q})\ddot{q}_1 + M_{n2}(\mathbf{q})\ddot{q}_2 + \cdots + M_{nn}(\mathbf{q})v_n + D_n(\mathbf{q},\dot{\mathbf{q}}) + K_n(\mathbf{q}) = \tau_n. \tag{D.7d}$$

The objective is to describe the FBL torques (τ_3, τ_4, ..., τ_n) solely in terms of the desired inputs v, the system's inertial, centrifugal and potential properties and the Lyapunov torque τ_2. To do this, we first solve for $\ddot{q}_1$ in eq. (D.7a), which results in

$$\ddot{q}_1 = \frac{-M_{12}(\mathbf{q})\ddot{q}_2 - M_{13}(\mathbf{q})v_3 - \cdots - M_{1n}(\mathbf{q})v_n - D_1(\mathbf{q},\dot{\mathbf{q}}) - K_1(\mathbf{q})}{M_{11}(\mathbf{q})}. \tag{D.8}$$

Substituting eq. (D.8) into eq. (D.7b) produces

$$\tau_2 = \tilde{M}_{22}(\mathbf{q})\ddot{q}_2 + \tilde{M}_{23}(\mathbf{q})v_3 + \cdots + \tilde{M}_{2n}(\mathbf{q})v_n + \tilde{D}_2(\mathbf{q},\dot{\mathbf{q}}) + \tilde{K}_2(\mathbf{q})$$

where, for $2 \leq k \leq n$,

$$\tilde{M}_{2k}(\mathbf{q}) = M_{2k}(\mathbf{q}) - \frac{M_{1k}(\mathbf{q})M_{21}(\mathbf{q})}{M_{11}(\mathbf{q})}$$

and

$$\tilde{D}_2(\mathbf{q}, \dot{\mathbf{q}}) = D_2(\mathbf{q}, \dot{\mathbf{q}}) - \frac{M_{21}(\mathbf{q})}{M_{11}(\mathbf{q})} D_1(\mathbf{q}, \dot{\mathbf{q}}),$$

$$\tilde{K}_2(\mathbf{q}) = K_2(\mathbf{q}) - \frac{M_{21}(\mathbf{q})}{M_{11}(\mathbf{q})} K_1(\mathbf{q}).$$

Therefore

$$\ddot{q}_2 = \frac{\tau_2 - \tilde{M}_{23}(\mathbf{q})v_3 - \cdots - \tilde{M}_{2n}(\mathbf{q})v_n - \tilde{D}_2(\mathbf{q}, \dot{\mathbf{q}}) - \tilde{K}_2(\mathbf{q})}{\tilde{M}_{22}(\mathbf{q})}. \tag{D.9}$$

We note that $\ddot{q}_2$ is completely independent of $\ddot{q}_1$, but the converse instance is not true. Thus, we substitute eq. (D.9) into eq. (D.8) to produce

$$\ddot{q}_2 = \frac{-\tilde{M}_{13}(\mathbf{q})v_3 - \cdots - \tilde{M}_{1n}(\mathbf{q})v_n - \tilde{D}_1(\mathbf{q}, \dot{\mathbf{q}}) - \tilde{K}_1(\mathbf{q}) - \tilde{\tau}_2}{\tilde{M}_{11}(\mathbf{q})} \tag{D.10}$$

where, for $3 \leq i \leq n$,

$$\tilde{M}_{1i}(\mathbf{q}) = M_{1i}(\mathbf{q}) - \frac{M_{12}(\mathbf{q})\tilde{M}_{2i}(\mathbf{q})}{\tilde{M}_{22}(\mathbf{q})},$$

$$\tilde{D}_1(\mathbf{q}, \dot{\mathbf{q}}) = D_1(\mathbf{q}, \dot{\mathbf{q}}) - \frac{M_{12}(\mathbf{q})}{\tilde{M}_{22}(\mathbf{q})} \tilde{D}_2(\mathbf{q}, \dot{\mathbf{q}}),$$

$$\tilde{K}_1(\mathbf{q}) = K_1(\mathbf{q}) - \frac{M_{12}(\mathbf{q})}{\tilde{M}_{22}(\mathbf{q})} \tilde{K}_2(\mathbf{q}),$$

$$\tilde{\tau}_2 = \frac{M_{12}(\mathbf{q})}{\tilde{M}_{22}(\mathbf{q})} \tau_2.$$

We now begin with the iterative part of the proof, whereby the expressions seen in eqs. (D.9) and (D.10) are substituted into the remaining equations of motion. Upon performing this on the first two equations, however, we find a pattern in the torque expressions, allowing for this proof to be completed by induction.

Substituting eqs. (D.9) and (D.10) into eq. (D.7c) produces

$$\tau_3 = \hat{M}_{33}(\mathbf{q})v_3 + \cdots + \hat{M}_{3n}(\mathbf{q})v_n + \hat{D}_3(\mathbf{q}, \dot{\mathbf{q}}) + \hat{K}_3(\mathbf{q}) + \hat{\tau}_3$$

where, for $3 \leq j \leq n$,

$$\hat{M}_{3j}(\mathbf{q}) = M_{3j}(\mathbf{q}) - \frac{\tilde{M}_{1j}(\mathbf{q})M_{31}(\mathbf{q})}{M_{11}(\mathbf{q})} - \frac{\tilde{M}_{2j}(\mathbf{q})M_{32}(\mathbf{q})}{\tilde{M}_{22}(\mathbf{q})}$$

and

$$\hat{D}_3(\mathbf{q}, \dot{\mathbf{q}}) = D_3(\mathbf{q}, \dot{\mathbf{q}}) - \frac{M_{31}(\mathbf{q})}{M_{11}(\mathbf{q})}\tilde{D}_1(\mathbf{q}, \dot{\mathbf{q}}) - \frac{M_{32}(\mathbf{q})}{\tilde{M}_{22}(\mathbf{q})}\tilde{D}_2(\mathbf{q}, \dot{\mathbf{q}}),$$

$$\hat{K}_3(\mathbf{q}) = K_3(\mathbf{q}) - \frac{M_{31}(\mathbf{q})}{M_{11}(\mathbf{q})}\tilde{K}_1(\mathbf{q}) - \frac{M_{32}(\mathbf{q})}{\tilde{M}_{22}(\mathbf{q})}\tilde{K}_2(\mathbf{q}),$$

$$\hat{\tau}_3 = \frac{M_{32}(\mathbf{q})}{\tilde{M}_{22}(\mathbf{q})}\tau_2 - \frac{M_{31}(\mathbf{q})}{M_{11}(\mathbf{q})}\tilde{\tau}_2.$$

Similarly, if we were to substitute eqs. (D.9) and (D.10) into eq. (D.7c) we find that

$$\tau_n = \hat{M}_{n3}(\mathbf{q})v_3 + \cdots + \hat{M}_{nn}(\mathbf{q})v_n + \hat{D}_n(\mathbf{q}, \dot{\mathbf{q}}) + \hat{K}_n(\mathbf{q}) + \hat{\tau}_n$$

where, for $3 \leq j \leq n$,

$$\hat{M}_{nj}(\mathbf{q}) = M_{nj}(\mathbf{q}) - \frac{\tilde{M}_{1j}(\mathbf{q})M_{n1}(\mathbf{q})}{M_{11}(\mathbf{q})} - \frac{\tilde{M}_{2j}(\mathbf{q})M_{n2}(\mathbf{q})}{\tilde{M}_{22}(\mathbf{q})}$$

and

$$\hat{D}_n(\mathbf{q}, \dot{\mathbf{q}}) = D_n(\mathbf{q}, \dot{\mathbf{q}}) - \frac{M_{n1}(\mathbf{q})}{M_{11}(\mathbf{q})}\tilde{D}_1(\mathbf{q}) - \frac{M_{n2}(\mathbf{q})}{\tilde{M}_{22}(\mathbf{q})}\tilde{D}_2(\mathbf{q}),$$

$$\hat{K}_n(\mathbf{q}) = K_n(\mathbf{q}) - \frac{M_{n1}(\mathbf{q})}{M_{11}(\mathbf{q})}\tilde{K}_1(\mathbf{q}) - \frac{M_{n2}(\mathbf{q})}{\tilde{M}_{22}(\mathbf{q})}\tilde{K}_n(\mathbf{q}),$$

$$\hat{\tau}_n = \frac{M_{n2}(\mathbf{q})}{\tilde{M}_{22}(\mathbf{q})}\tau_2 - \frac{M_{n1}(\mathbf{q})}{M_{11}(\mathbf{q})}\tilde{\tau}_2.$$

Therefore, we prove by induction that

$$\tau_i = \hat{M}_{i3}(\mathbf{q})v_3 + \hat{M}_{i4}(\mathbf{q})v_4 + \cdots + \hat{M}_{in}(\mathbf{q})v_n + \hat{D}_i(\mathbf{q}, \dot{\mathbf{q}}) + \hat{K}_i(\mathbf{q}) + \hat{\tau}_i \qquad \text{(D.11)}$$

represents the FBL torques required to implement MCPFL on a PA$_{n-1}$ robot, where, for $3 \leq i \leq n$, $3 \leq j \leq n$ and $2 \leq k \leq n$,

$$\hat{M}_{ij}(\mathbf{q}) = M_{ij}(\mathbf{q}) - \frac{\tilde{M}_{1j}(\mathbf{q})M_{i1}(\mathbf{q})}{M_{11}(\mathbf{q})} - \frac{\tilde{M}_{2j}(\mathbf{q})M_{i2}(\mathbf{q})}{\tilde{M}_{22}(\mathbf{q})},$$

$$\hat{D}_i(\mathbf{q}, \dot{\mathbf{q}}) = D_i(\mathbf{q}, \dot{\mathbf{q}}) - \frac{M_{i1}(\mathbf{q})}{M_{11}(\mathbf{q})}\tilde{D}_1(\mathbf{q}, \dot{\mathbf{q}}) - \frac{M_{i2}(\mathbf{q})}{\tilde{M}_{22}(\mathbf{q})}\tilde{D}_2(\mathbf{q}, \dot{\mathbf{q}}),$$

$$\hat{K}_i(\mathbf{q}) = K_i(\mathbf{q}) - \frac{M_{i1}(\mathbf{q})}{M_{11}(\mathbf{q})}\tilde{K}_1(\mathbf{q}) - \frac{M_{i2}(\mathbf{q})}{\tilde{M}_{22}(\mathbf{q})}\tilde{K}_2(\mathbf{q}),$$

$$\hat{\tau}_i = \frac{M_{i2}(\mathbf{q})}{\tilde{M}_{22}(\mathbf{q})}\tau_2 - \frac{M_{i1}(\mathbf{q})}{M_{11}(\mathbf{q})}\tilde{\tau}_2,$$

$$\tilde{\tau}_2 = \frac{M_{12}(\mathbf{q})}{\tilde{M}_{22}(\mathbf{q})}\tau_2$$

and

$$\tilde{M}_{2k}(\mathbf{q}) = M_{2k}(\mathbf{q}) - \frac{M_{1k}(\mathbf{q})M_{21}(\mathbf{q})}{M_{11}(\mathbf{q})}, \qquad \tilde{M}_{1j}(\mathbf{q}) = M_{1j}(\mathbf{q}) - \frac{M_{12}(\mathbf{q})\tilde{M}_{2i}(\mathbf{q})}{\tilde{M}_{22}(\mathbf{q})},$$

$$\tilde{D}_2(\mathbf{q}, \dot{\mathbf{q}}) = D_2(\mathbf{q}, \dot{\mathbf{q}}) - \frac{M_{21}(\mathbf{q})}{M_{11}(\mathbf{q})}D_1(\mathbf{q}, \dot{\mathbf{q}}), \quad \tilde{D}_1(\mathbf{q}, \dot{\mathbf{q}}) = D_1(\mathbf{q}, \dot{\mathbf{q}}) - \frac{M_{12}(\mathbf{q})}{\tilde{M}_{22}(\mathbf{q})}\tilde{D}_2(\mathbf{q}, \dot{\mathbf{q}}),$$

$$\tilde{K}_2(\mathbf{q}) = K_2(\mathbf{q}) - \frac{M_{21}(\mathbf{q})}{M_{11}(\mathbf{q})}K_1(\mathbf{q}), \qquad \tilde{K}_1(\mathbf{q}) = K_1(\mathbf{q}) - \frac{M_{12}(\mathbf{q})}{\tilde{M}_{22}(\mathbf{q})}\tilde{K}_2(\mathbf{q}).$$

This form of linearisation results in a set of equations of motion for the MC-ROPA$_{n-1}$ robot described by

$$\ddot{q}_1 = \frac{-\tilde{M}_{13}(\mathbf{q})v_3 - \tilde{M}_{14}(\mathbf{q})v_4 - \cdots - \tilde{M}_{1n}(\mathbf{q})v_n - \tilde{D}_1(\mathbf{q}, \dot{\mathbf{q}}) - \tilde{K}_1(\mathbf{q})}{M_{11}(\mathbf{q})},$$
$$\ddot{q}_2 = \frac{\tau_2 - \tilde{M}_{23}(\mathbf{q})v_3 - \tilde{M}_{24}(\mathbf{q})v_4 - \cdots - \tilde{M}_{2n}(\mathbf{q})v_n - \tilde{D}_2(\mathbf{q}, \dot{\mathbf{q}}) - \tilde{K}_2(\mathbf{q})}{M_{11}(\mathbf{q})}.$$

Additionally, we must select a set of physical parameters that will ensure that

$$M_{11}(\mathbf{q}) \neq 0 \; \forall \mathbf{q}. \tag{D.12}$$

D.3 Noncollocated Partial Feedback Linearisation

We have included the already derived dynamical equations of the PA_{n-1} robot, whereby

$$\begin{aligned}
&M_{11}(\mathbf{q})\ddot{q}_1 + M_{12}(\mathbf{q})\ddot{q}_2 + \cdots + M_{1n}(\mathbf{q})\ddot{q}_n + D_1(\mathbf{q},\dot{\mathbf{q}}) + K_1(\mathbf{q}) = 0,\\
&M_{21}(\mathbf{q})\ddot{q}_1 + M_{22}(\mathbf{q})\ddot{q}_2 + \cdots + M_{2n}(\mathbf{q})\ddot{q}_n + D_2(\mathbf{q},\dot{\mathbf{q}}) + K_2(\mathbf{q}) = \tau_2,\\
&M_{31}(\mathbf{q})\ddot{q}_1 + M_{32}(\mathbf{q})\ddot{q}_2 + \cdots + M_{3n}(\mathbf{q})\ddot{q}_n + D_3(\mathbf{q},\dot{\mathbf{q}}) + K_3(\mathbf{q}) = \tau_3,\\
&\quad\vdots\\
&M_{n1}(\mathbf{q})\ddot{q}_1 + M_{n2}(\mathbf{q})\ddot{q}_2 + \cdots + M_{nn}(\mathbf{q})\ddot{q}_n + D_n(\mathbf{q},\dot{\mathbf{q}}) + K_n(\mathbf{q}) = \tau_n.
\end{aligned}$$

Conversely to the CPFL technique, the objective of the NCPFL technique is to negate the nonlinear dynamics of the $n-1$ most proximal pendulums and have it assigned to a newly defined input, where

$$\begin{aligned}
\ddot{q}_1 &= v_1,\\
\ddot{q}_2 &= v_2,\\
&\vdots\\
\ddot{q}_{n-1} &= v_{n-1}.
\end{aligned}$$

The new input v_n cannot be assigned to $\ddot{q}_n$ despite the fact that the most distal joint is actuated since the system only contains $n-1$ actuators. The linearisation responsibilities of the actuator found on the nth joint are, in this case, transferred to the most proximal joint, thus resulting in the internal dynamics represented by $\ddot{q}_n$. We now need to solve for the FBL torques that will realise the newly defined system dynamics. Substituting these new inputs into the dynamical equations of the PA$_{n-1}$ robot produces

$$M_{11}(\mathbf{q})v_1 + \cdots + M_{1n-1}(\mathbf{q})v_{n-1} + M_{1n}(\mathbf{q})\ddot{q}_n + D_1(\mathbf{q},\dot{\mathbf{q}}) + K_1(\mathbf{q}) = 0, \tag{D.13a}$$
$$M_{21}(\mathbf{q})v_1 + \cdots + M_{2n-1}(\mathbf{q})v_{n-1} + M_{2n}(\mathbf{q})\ddot{q}_n + D_2(\mathbf{q},\dot{\mathbf{q}}) + K_2(\mathbf{q}) = \tau_2, \tag{D.13b}$$
$$M_{31}(\mathbf{q})v_1 + \cdots + M_{3n-1}(\mathbf{q})v_{n-1} + M_{3n}(\mathbf{q})\ddot{q}_n + D_3(\mathbf{q},\dot{\mathbf{q}}) + K_3(\mathbf{q}) = \tau_3, \tag{D.13c}$$
$$\vdots$$
$$M_{n1}(\mathbf{q})v_1 + \cdots + M_{nn-1}(\mathbf{q})v_{n-1} + M_{nn}(\mathbf{q})\ddot{q}_n + D_n(\mathbf{q},\dot{\mathbf{q}}) + K_n(\mathbf{q}) = \tau_n. \tag{D.13d}$$

We will now solve for $\ddot{q}_n$ since it represents the internal dynamics of the linearised system. Therefore, rearranging eq. (D.2a) results in

$$\ddot{q}_n = \frac{-M_{11}(\mathbf{q})v_1 - M_{12}(\mathbf{q})v_2 - \cdots - M_{1n-1}(\mathbf{q})v_{n-1} - D_1(\mathbf{q},\dot{\mathbf{q}}) - K_1(\mathbf{q})}{M_{1n}(\mathbf{q})}. \tag{D.14}$$

Solving for necessary FBL torque τ_2 requires the substitution of eq. (D.14) into eq. (D.13b), which produces

$$\tau_2 = \hat{M}_{21}(\mathbf{q})v_1 + \hat{M}_{22}(\mathbf{q})v_2 + \cdots + \hat{M}_{2n-1}(\mathbf{q})v_{n-1} + \hat{D}_2(\mathbf{q}, \dot{\mathbf{q}}) + \hat{K}_2(\mathbf{q})$$

where, in the NCPFL case and for $1 \leq j \leq n-1$,

$$\begin{aligned}
\hat{M}_{2j}(\mathbf{q}) &= M_{2j}(\mathbf{q}) - \frac{M_{21}(\mathbf{q})M_{1j}(\mathbf{q})}{M_{1n}(\mathbf{q})}, \\
\hat{D}_2(\mathbf{q}, \dot{\mathbf{q}}) &= D_2(\mathbf{q}, \dot{\mathbf{q}}) - \frac{M_{2n}(\mathbf{q})}{M_{1n}(\mathbf{q})} D_1(\mathbf{q}, \dot{\mathbf{q}}), \\
\hat{K}_2(\mathbf{q}) &= K_2(\mathbf{q}) - \frac{M_{2n}(\mathbf{q})}{M_{1n}(\mathbf{q})} K_1(\mathbf{q}).
\end{aligned}$$

The solving of each FBL thus becomes an iterative process, occurring next for the FBL torque τ_3. The expression for $\ddot{q}_n$ found in eq. (D.14) is thus substituted into eq. (D.13c), which produces

$$\tau_3 = \hat{M}_{31}(\mathbf{q})v_1 + \hat{M}_{32}(\mathbf{q})v_2 + \cdots + \hat{M}_{3n-1}(\mathbf{q})v_{n-1} + \hat{D}_3(\mathbf{q}, \dot{\mathbf{q}}) + \hat{K}_3(\mathbf{q})$$

where, for $1 \leq j \leq n-1$,

$$\begin{aligned}
\hat{M}_{3j}(\mathbf{q}) &= M_{3j}(\mathbf{q}) - \frac{M_{3n}(\mathbf{q})M_{1j}(\mathbf{q})}{M_{1n}(\mathbf{q})}, \\
\hat{D}_3(\mathbf{q}, \dot{\mathbf{q}}) &= D_3(\mathbf{q}, \dot{\mathbf{q}}) - \frac{M_{3n}(\mathbf{q})}{M_{1n}(\mathbf{q})} D_1(\mathbf{q}, \dot{\mathbf{q}}), \\
\hat{K}_3(\mathbf{q}) &= K_3(\mathbf{q}) - \frac{M_{3n}(\mathbf{q})}{M_{1n}(\mathbf{q})} K_1(\mathbf{q}).
\end{aligned}$$

A similar result can be seen with the substitution of eq. (D.14) into eq. (D.13d), whereby

$$\tau_n = \hat{M}_{n1}(\mathbf{q})v_1 + \hat{M}_{n2}(\mathbf{q})v_2 + \cdots + \hat{M}_{nn-1}(\mathbf{q})v_{n-1} + \hat{D}_n(\mathbf{q}, \dot{\mathbf{q}}) + \hat{K}_n(\mathbf{q})$$

and where, for $1 \leq j \leq n-1$,

$$\begin{aligned}
\hat{M}_{nj}(\mathbf{q}) &= M_{nj}(\mathbf{q}) - \frac{M_{nn}(\mathbf{q})M_{1j}(\mathbf{q})}{M_{1n}(\mathbf{q})}, \\
\hat{D}_n(\mathbf{q}, \dot{\mathbf{q}}) &= D_n(\mathbf{q}, \dot{\mathbf{q}}) - \frac{M_{nn}(\mathbf{q})}{M_{1n}(\mathbf{q})} D_1(\mathbf{q}, \dot{\mathbf{q}}), \\
\hat{K}_n(\mathbf{q}) &= K_n(\mathbf{q}) - \frac{M_{nn}(\mathbf{q})}{M_{1n}(\mathbf{q})} K_1(\mathbf{q}).
\end{aligned}$$

There is a pattern that is evident in these expressions. We can thus conclude, by induction, that the FBL torques that are required to implement NCPFL on the PA$_{n-1}$

robot must have the following form

$$\tau_i = \hat{M}_{i1}(\mathbf{q})v_1 + \hat{M}_{i2}(\mathbf{q})v_2 + \cdots + \hat{M}_{in-1}(\mathbf{q})v_{n-1} + \hat{D}_i(\mathbf{q}, \dot{\mathbf{q}}) + \hat{K}_i(\mathbf{q})$$

for $1 \leq i \leq n-1$, where

$$\begin{aligned}
\hat{M}_{ij}(\mathbf{q}) &= M_{ij}(\mathbf{q}) - \frac{M_{in}(\mathbf{q})M_{1j}(\mathbf{q})}{M_{1n}(\mathbf{q})}, \\
\hat{D}_i(\mathbf{q}, \dot{\mathbf{q}}) &= D_i(\mathbf{q}, \dot{\mathbf{q}}) - \frac{M_{in}(\mathbf{q})}{M_{1n}(\mathbf{q})} D_1(\mathbf{q}, \dot{\mathbf{q}}), \\
\hat{K}_i(\mathbf{q}) &= K_i(\mathbf{q}) - \frac{M_{in}(\mathbf{q})}{M_{1n}(\mathbf{q})} K_1(\mathbf{q})
\end{aligned}$$

for $1 \leq j \leq n-1$. Choosing $v_m = -k_{D_m}\dot{q}_m - k_{P_m}q_m$ for $1 \leq m \leq n-1$, the application of these FBL torques on the PA$_{n-1}$ robot results in a set of equations for the NC-ROPA$_{n-1}$ robot described by

$$\ddot{q}_1 = -k_{D_1}\dot{q}_1 - k_{P_1}q_1, \tag{D.15a}$$

$$\ddot{q}_2 = -k_{D_2}\dot{q}_2 - k_{P_2}q_2, \tag{D.15b}$$

$$\vdots$$

$$\ddot{q}_{n-1} = -k_{D_{n-1}}\dot{q}_{n-1} - k_{P_{n-1}}q_{n-1}, \tag{D.15c}$$

$$\ddot{q}_n = \frac{-M_{11}(\mathbf{q})v_1 - \cdots - M_{1n-1}(\mathbf{q})v_{n-1} - D_1(\mathbf{q}, \dot{\mathbf{q}}) - K_1(\mathbf{q})}{M_{1n}(\mathbf{q})}. \tag{D.15d}$$

Additionally, a specific set of physical parameters must be selected to guarantee that

$$M_{1n}(\mathbf{q}) \neq 0 \; \forall \mathbf{q}. \tag{D.16}$$

Appendix E

Convergence Algorithm Simulink Models

This appendix serves to demonstrate the structure of the Simulink models used in the *convergence algorithm*. The general Simulink model layout for the Acrobot that is used for both the *swing-up* and *balance test* segments of the *convergence algorithm* is demonstrated in figure E.1.

Each system contains four subsystems, namely the *Natural dynamics*, *Friction* (R_1), *Friction* (R_2), and the *Controller* subsystems. The natural dynamics subsystem is demonstrated in figure E.2. This subsystem houses the state-space of the simulated

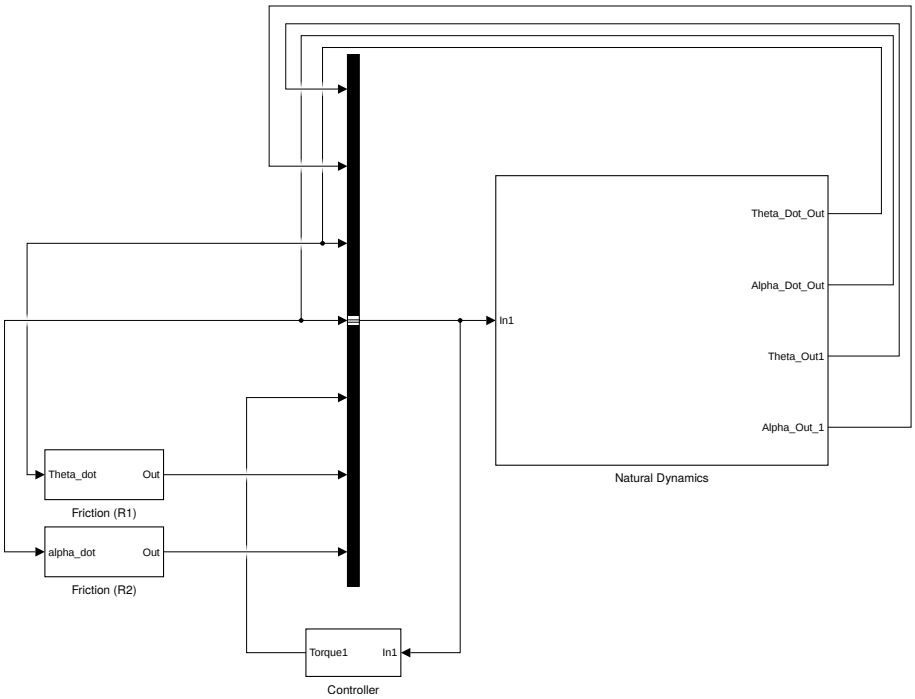

FIGURE E.1: The high-level overview of the Simulink model of the Acrobot used in the *convergence algorithm*.

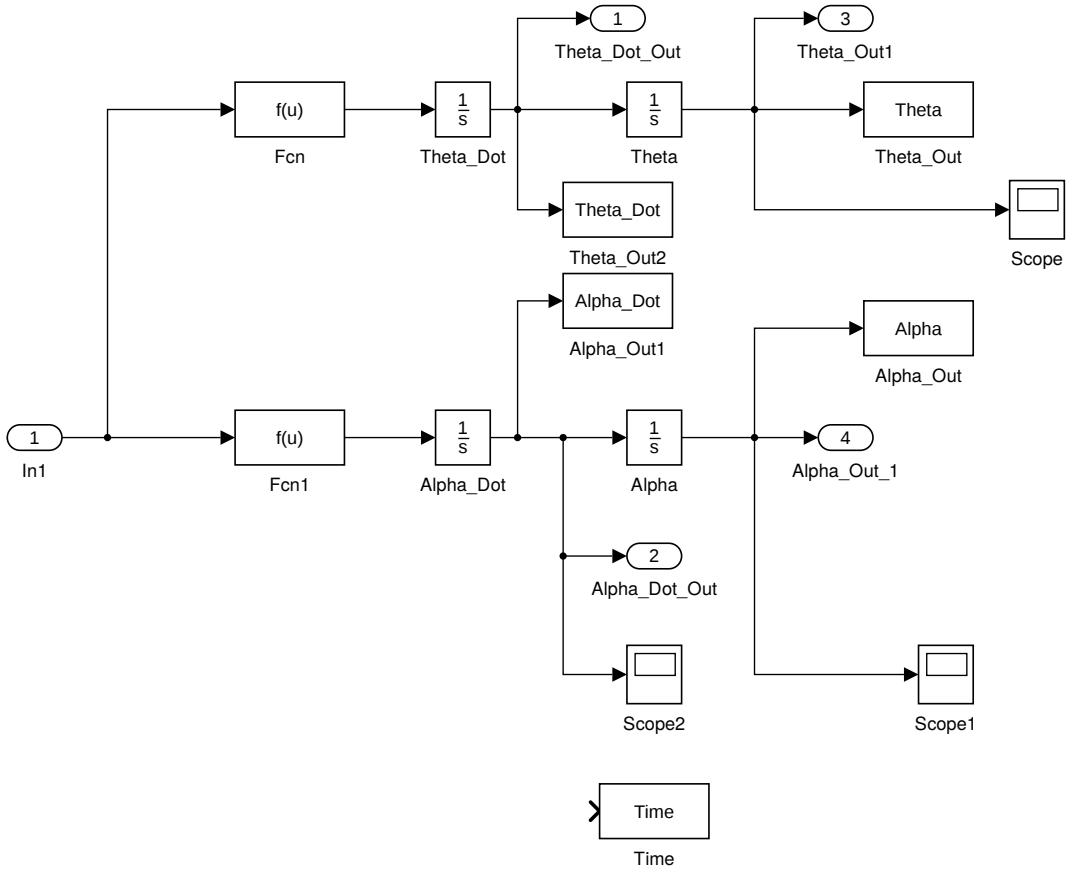

FIGURE E.2: The *Natural Dynamics* subsystem of the Simulink model of the Acrobot used in the *convergence algorithm*.

pendulum systems, which include the equations of motion and respective integrators. This subsystem produces the states q_1 (Theta), q_2 (Alpha), $\dot{q}_1$ (Theta_Dot), and $\dot{q}_2$ (Alpha_Dot) of the NC-ROPA$_{n-1}$ model as outputs.

The *Friction* subsystems are demonstrated in figures E.3 and E.4. These systems encompass the viscous damping torque function for the passive joint (R1) and the active joint (R2).

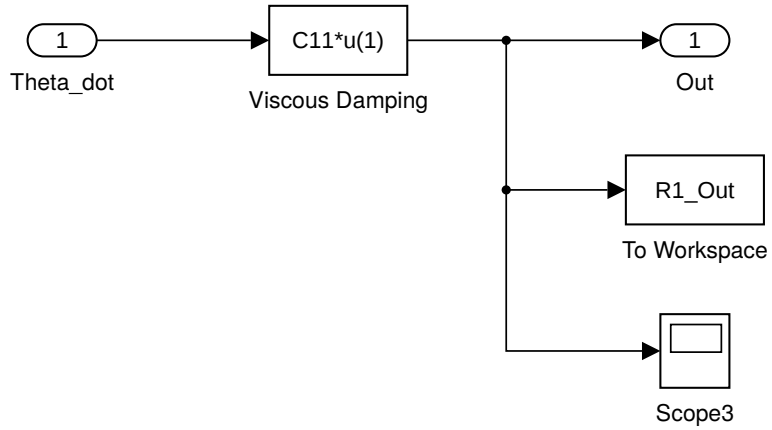

FIGURE E.3: The *Friction (R1)* subsystem of the Simulink model of the Acrobot used in the *convergence algorithm*.

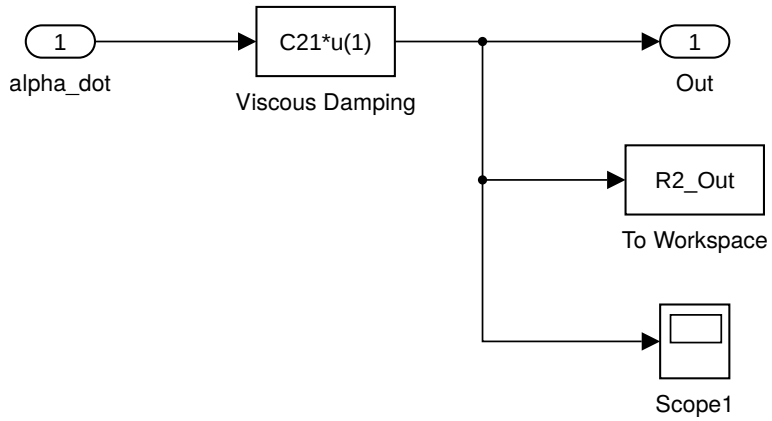

FIGURE E.4: The *Friction (R2)* subsystem of the Simulink model of the Acrobot used in the *convergence algorithm*.

The *Controller* subsystem is demonstrated in figure E.5. This subsystem houses the relevant torque expression for the operation. The Simulink systems for the Swing-up and LQR simulations are identical in structure, with the only fundamental difference being the torque expression that is stored in the *Torque* block. The *Energy* block calculates the mechanical energy of the system at any time.

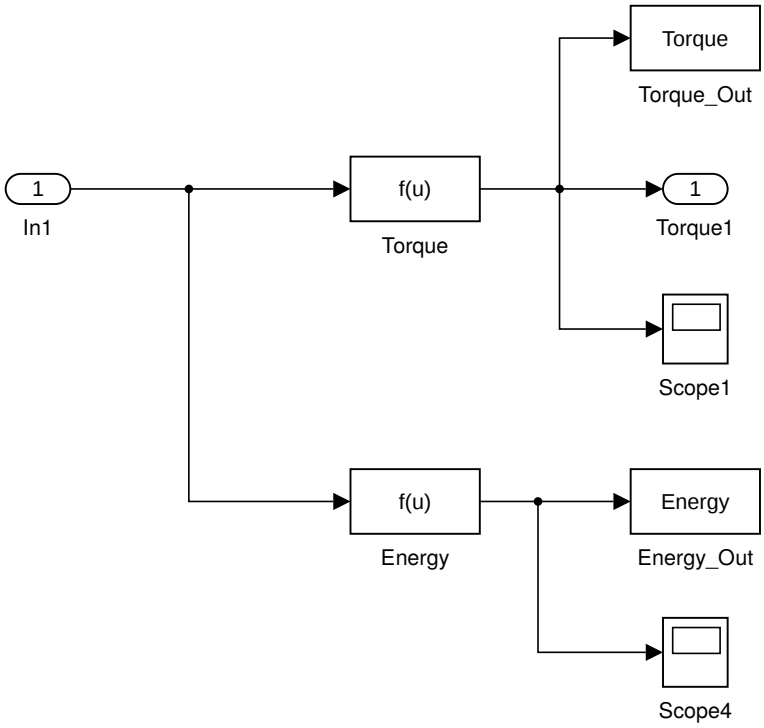

FIGURE E.5: The *Controller* subsystem of the Simulink model of the Acrobot used in the *convergence algorithm*.

Appendix F

Publications

Two papers, which contain work produced during this research project, have been submitted and accepted for inclusion in the *IEEE AFRICON17* conference and the *IFAC Control Conference Africa* respectively. These papers, which have the titles:

1. *Gain selection criteria for the swing-up control of the Acrobot using collocated partial feedback linearisation* [110].
2. *Swing-up control of the Acrobot using noncollocated partial feedback linearisation: an iterative approach* [111].

have been appended to this dissertation.

Gain selection criterion for the swing-up control of the Acrobot using collocated partial feedback linearisation

Ricardo De Almeida*, Otis Nyandoro*

* Department of Electrical and Information Engineering, University of the Witwatersrand
1 Jan Smut Avenue, Braamfontein, Johannesburg, 2000
Ricardo.DeAlmeida@students.wits.ac.za and Otis.Nyandoro@wits.ac.za

***Abstract*—A novel set of feedback gain selection conditions pertaining to the swing-up control of the Acrobot using collocated partial feedback linearisation is derived and presented in this research. This set of conditions, collectively known as the *gain selection criterion*, highlights a region of possible feedback gain combinations, known as the *region of appropriate gains* (RAG), that will guarantee the unstable response of the Acrobot when initialised approximately near the fully-pendant equilibrium point. The criterion is derived using the Routh-Hurwitz stability criterion applied on the characteristic equation of the system linearised about the fully-pendant equilibrium point. Only one left-column coefficient, known as the *critical Routh coefficient*, demonstrates the potential of influencing the stability of the system. The boundaries of the RAG are defined from the analysis of the critical Routh coefficient. The gain selection criterion will prevent the unintended selection of a combination of feedback gains that will cause a stable response about the fully-pendant equilibrium point, preventing the satisfactory execution of swing-up control on the Acrobot from the fully-pendant equilibrium point. This criterion may, more conveniently, be applied to specific types of multi-link pendulum system that approximate the behaviour of the partially linearised Acrobot.**

***Keywords*—Mechatronic systems, Mechatronics and Robotics, Nonlinear Systems**

I. Introduction

The Acrobot is a double-pendulum system that is commonly used as a simplified modelling tool for robotic manipulators [1]. The Acrobot is underactuated, having only one actuator in the second joint that is responsible for controlling the two angular degrees of freedom [1]. A common objective for the Acrobot is swing-up control, whereby the Acrobot is *swung* from its conventional fully-pendant equilibrium point into a complete upright orientation, i.e. stabilising the Acrobot about the upper equilibrium point (UEP) [2]–[6]. A number of contributions in the field of swing-up controlled Robotics were presented by Spong, who introduced the concept of partial feedback linearisation (a variation of feedback linearisation) [7], [8].

Feedback linearisation involves the transformation of non-linear systems into equivalent linear representations [9]. The most notable feature of the feedback linearisation technique is its ability to simplify system dynamics [9]. This presents an opportunity for the application of conventional linear control techniques on a previously nonlinear system [9]. The implementation of full-state feedback linearisation produces a fully transformed set of dynamical equations, but this is only realisable if the number of actuators equal the number of degrees of freedom of the system [1]. An underactuated system does not satisfy this condition, and therefore full-state linearisation is not feasible for the Acrobot [1]. There is, however, an opportunity to reduce the complexity of the system through the linearisation of only a portion of the system's dynamics where possible [1]. This is known as Partial Feedback Linearisation (PFL), where the linearisation of the pendulum associated with the active joint is known as Collocated PFL (CPFL) with the converse procedure known as Noncollocated PFL (NCPFL) [1], [7]. An appropriate swing-up controller can thus be designed to control the linearised pendulum whilst indirectly influencing the other [1]. The resulting internal and zero dynamics of the system can then be analysed to determine the behaviour of the system [7], [9]. This has been performed with notable success in [7], [8].

Despite the success of this technique, the necessary internal and zero dynamics are generally difficult to evaluate analytically, and can only, therefore, be evaluated through simulation. These dynamics are directly influenced by the magnitude of the linear feedback gains k_p and k_d. These gains can only be chosen through trial-and-error, which is evidently time consuming and laborious. In this paper, we derive an analytical proof of the *gain selection criterion* for the CPFL related swing-up control of the Acrobot. This criterion specifies a set of boundaries that enclose a region of possible feedback gain combinations (referred to as the *the region of appropriate gains*, or RAG) that are guaranteed to produce a locally unstable response of the Acrobot when its states are initialised approximately near the fully-pendant equilibrium point (FPEP). This criterion eliminates a set of gain combinations that are guaranteed to produce a stable response when the system is approximately near the FPEP,

which is undesirable in the case of the swing-up objective. This criterion thus provides a general guideline for feedback gain selection.

The remainder of the paper is structured as follows. A model of the Acrobot is explicitly defined for the purpose of the linearisation and control law formulation. The CPFL technique is performed on the Acrobot, followed by the formulation of the swing-up control law using the energy-pump method demonstrated in [7]. The *gain selection criterion* is derived analytically using the Routh-Hurwitz stability criterion. Certain gain combinations are tested to demonstrate the concurrence between the predicted and simulated results. The swing-up control of the Acrobot is also demonstrated with the implementation of a gain combination found within the RAG. A short discussion on the limitations of the criterion, and implications of the gain selection criterion on multi-body pendulum systems is included along with concluding comments.

II. Model

A. Physical Model

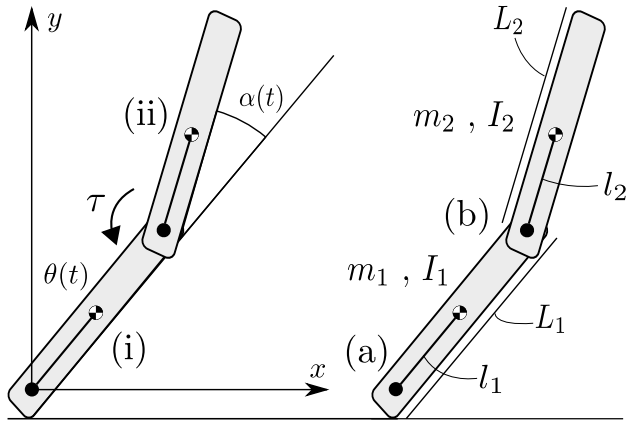

Fig. 1. The Acrobot model.

The Acrobot model depicted in Figure 1 is adapted from [2], [7], [8]. The model is constrained to a 2-D plane with the position of the pendulums being described at any time t by the angular degrees of freedom $q_1(t)$ (for the proximal pendulum (i)) and $q_2(t)$ (for the distal pendulum (ii)). The masses of the pendulums m_1 and m_2 are point masses that represent each pendulum's centre-of-mass (COM). The pendulums are assumed to be stiff rods with lengths L_1 and L_2, COM lengths l_1 and l_2, and moments of inertia I_1 and I_2. The torque τ is exerted by an actuator that is fixed to the distal actuated joint (b). The proximal joint (a) remains unactuated.

B. Mathematical Model

The generalised equation of motion for an undamped rotational mechanical system can be collectively represented by the prototypical

$$M(q)\ddot{q} + C(q,\dot{q}) + K(q) = G(q)u \tag{1}$$

where $M(q)$ represents the mass matrix, $C(q,\dot{q})$ collectively represents the Coriolis and Centrifugal forces, $K(q)$ represents the gravitational torques, and $G(q)u$ represents the system actuation [10]. The motion vectors for the Acrobot are derived from the generalised coordinates

$$q = \begin{bmatrix} q_1 \\ q_2 \end{bmatrix}, \qquad \dot{q} = \begin{bmatrix} \dot{q}_1 \\ \dot{q}_2 \end{bmatrix}, \qquad \ddot{q} = \begin{bmatrix} \ddot{q}_1 \\ \ddot{q}_2 \end{bmatrix}.$$

The matrices included in the prototypical form are structured as

$$\begin{aligned} M(q) &= \begin{bmatrix} M_{11}(q) & M_{12}(q) \\ M_{21}(q) & M_{22}(q) \end{bmatrix} \\ &= \begin{bmatrix} \alpha_1 + \alpha_2 + 2\alpha_3\cos(q_2) & \alpha_2 + \alpha_3\cos(q_2) \\ \alpha_2 + \alpha_3\cos(q_2) & \alpha_2 \end{bmatrix}, \\ C(q,\dot{q}) &= \begin{bmatrix} C_1(q,\dot{q}) \\ C_2(q,\dot{q}) \end{bmatrix} = \alpha_3 \begin{bmatrix} -2\dot{q}_1\dot{q}_2 - {\dot{q}_2}^2 \\ {\dot{q}_1}^2 \end{bmatrix} \sin q_2, \\ K(q) &= \begin{bmatrix} K_1(q) \\ K_2(q) \end{bmatrix} = \begin{bmatrix} -\beta_1 \sin q_1 - \beta_2 \sin(q_1+q_2) \\ -\beta_2 \sin(q_1+q_2) \end{bmatrix} \end{aligned}$$

where

$$\begin{aligned} &\alpha_1 = m_1 {l_1}^2 + m_2 {L_1}^2 + I_1, && \alpha_2 = m_2 {l_2}^2 + I_2, \\ &\alpha_3 = m_2 L_1 l_2, && \beta_1 = g(m_1 l_1 + m_2 L_1), \\ &\beta_2 = g m_2 l_2 \end{aligned}$$

and where g represents the gravitational acceleration constant. As previously mentioned, the Acrobot model is an underactuated mechanical system, with actuation occurring only at the distal joint [7]. It is evident, therefore, that

$$G(q)u = \begin{bmatrix} 0 \\ \tau \end{bmatrix}$$

III. Collocated Partial feedback Linearisation

The objective of the application of this technique is to reduce the complexity of the system by linearising the dynamics of one of the pendulums to accommodate the swing-up control of the Acrobot. The results in this investigation are generated with the form of PFL that involves the linearisation of the distal pendulum (CPFL). More information on NCPFL can be found in [7]. The consequence of this technique is the lack of direct control of the first pendulum. A control method must be carefully designed to accommodate this limitation, allowing for the transfer of mechanical energy from the distal pendulum into the proximal pendulum. The details of the CPFL technique included in this section are compiled according to the work presented in [7].

The input-output feedback linearisation technique is applied to the output equation

$$y_2 = q_2.$$

This output is found on the actuated joint. The dynamical equations of the Acrobot, derived from the prototypical form seen in eq. (1), are described as

$$M_{11}\ddot{q}_1 + M_{12}\ddot{q}_2 + C_1 + K_1 = 0 \tag{2}$$

$$M_{21}\ddot{q}_1 + M_{22}\ddot{q}_2 + C_2 + K_2 = \tau \tag{3}$$

The term M_{11} in eq. (2) is a single entry, and can therefore be divided through in the equation, which produces

$$\ddot{q}_1 = {M_{11}}^{-1}(-M_{12}\ddot{q}_2 - C_1 - K_1). \tag{4}$$

Substituting eq. (4) into eq. (3) produces

$$\overline{M}_{22}\ddot{q}_2 + \overline{C}_2 + \overline{K}_2 = \tau \tag{5}$$

where

$$\overline{M}_{22} = M_{22} - {M_{11}}^{-1}M_{21}M_{12} \quad \overline{C}_2 = C_2 - {M_{11}}^{-1}M_{21}C_1$$
$$\overline{K}_2 = K_2 - {M_{11}}^{-1}M_{21}K_1.$$

The control input τ may now be used to produce a linearising controller. This is done through the substitution of a new control input v_2, whereby

$$\tau = \overline{M}_{22}v_2 + \overline{C}_2 + \overline{K}_2 \tag{6}$$

Enforcing this input produces newly defined system dynamics represented by

$$M_{11}\ddot{q}_1 + C_1 + K_1 = -M_{12}v_2, \tag{7}$$
$$\ddot{q}_2 = v_2, \tag{8}$$
$$y_2 = q_2. \tag{9}$$

The nonlinear dynamics of the second pendulum have been replaced with the desired input v_2. A linear feedback controller may now be designed for this desired input as seen in [7], whereby

$$v_2 = k_p(q_2^d - q_2) - k_d\dot{q}_2 \tag{10}$$

with k_p and k_d representing positive feedback gains. The desired distal angle q_2^d is defined as

$$q_2^d = \left[\frac{2a}{\pi}\right]\arctan(\dot{q}_1). \tag{11}$$

This input will cause the controller to *swing* the distal pendulum towards the set point angle found at the bounds $\pm a$. The pendulums will be swung in phase as dictated by the arctan function, thus generating an unstable response, contingent on the values of the gains k_d and k_p and on the initial conditions of the system [7].

The most extreme case of swing-up control would involve swinging the Acrobot up from a position that is approximately near the fully-pendant position (where $q_1 = \pi \pm 2k\pi$, $q_2 = 0$, $\dot{q}_1 = 0$ and $\dot{q}_2 = 0$, $k \in \mathbb{Z}$). Substituting the values of these states into eqs. (7) and (8) reveals that this position is an equilibrium point. This equilibrium point cannot, therefore, be asymptotically stable if swing-up control is to be performed when the Acrobot is initialised within an approximate neighbourhood of this position.

IV. Linearisation about Fully-Pendant Equilibrium Point

The Acrobot is linearised according to Lyapunov's linearisation method highlighted in [9]. The linear representation of a system's dynamics, when converted to state-space linearly approximated form, may be represented as

$$\dot{\mathbf{x}} \approx \left(\frac{\partial \mathbf{f}}{\partial \mathbf{x}}\bigg|_{\mathbf{x}=\mathbf{x}^*}\right)\mathbf{x} = \mathbf{A}\mathbf{x}.$$

The system dynamics of the partially linearised Acrobot may be represented in state space form through the transformation

$$\begin{bmatrix} q_1 & \dot{q}_1 & q_2 & \dot{q}_2 \end{bmatrix}^{\mathbf{T}} = \begin{bmatrix} \mathbf{x}_1 & \mathbf{x}_2 & \mathbf{x}_3 & \mathbf{x}_4 \end{bmatrix}^{\mathbf{T}}.$$

Therefore

$$\begin{bmatrix} \dot{\mathbf{x}}_1 & \dot{\mathbf{x}}_2 & \dot{\mathbf{x}}_3 & \dot{\mathbf{x}}_4 \end{bmatrix}^{\mathbf{T}} = \begin{bmatrix} \mathbf{x}_2 & \mathbf{f}_1(\mathbf{x}) & \mathbf{x}_4 & \mathbf{f}_2(\mathbf{x}) \end{bmatrix}^{\mathbf{T}},$$
$$\begin{bmatrix} \mathbf{x}_1^* & \mathbf{x}_2^* & \mathbf{x}_3^* & \mathbf{x}_4^* \end{bmatrix}^{\mathbf{T}} = \begin{bmatrix} \pi \pm 2k\pi & 0 & 0 & 0 \end{bmatrix}^{\mathbf{T}}$$

where

$$\mathbf{f}_1(\mathbf{x}) = M_{11}^{-1}(\mathbf{x})\Big[-M_{12}(\mathbf{x})v_2(\mathbf{x}) - C_1(\mathbf{x}) - K_1(\mathbf{x})\Big],$$
$$\mathbf{f}_2(\mathbf{x}) = v_2(\mathbf{x}).$$

The $\mathbf{A}$ matrix may now be represented as

$$\mathbf{A}\bigg|_{\mathbf{x}=\mathbf{x}^*} = \begin{bmatrix} 0 & 1 & 0 & 0 \\ a_{21} & a_{22} & a_{23} & a_{24} \\ 0 & 0 & 0 & 1 \\ 0 & \frac{2k_p a}{\pi} & -k_p & -k_d \end{bmatrix} \tag{12}$$

where

$$a_{21} = \frac{\beta_1 + \beta_2}{\alpha_1 + \alpha_2 + 2\alpha_3}, \qquad a_{22} = \frac{2ak_p(\alpha_2 + \alpha_3)}{\pi(\alpha_1 + \alpha_2 + 2\alpha_3)},$$
$$a_{23} = \frac{k_p(\alpha_2 + \alpha_3 - \beta_2)}{\alpha_1 + \alpha_2 + 2\alpha_3}, \quad a_{24} = \frac{k_d(\alpha_2 + \alpha_3)}{\alpha_1 + \alpha_2 + 2\alpha_3}.$$

V. Gain Selection Criterion

The feedback gains k_p and k_d, used to enforce the newly designed input v_2, must now be selected to complete the swing-up control formulation. As mentioned before, these gains are typically selected through a process of trial-and-error, which is evidently not ideal (see [7]). The key contribution of this paper, the *Gain selection criterion*, is derived in this section through the implementation of the Routh-Hurwitz stability criterion, which requires the completion of the following steps:

(i) Derivation of the characteristic equation about the FPEP.
(ii) Definition of the Routh-Array coefficients.
(iii) Analysis of first-column Routh-Array coefficients.
(iv) Derivation of the boundaries of the region of appropriate gains.

Steps (i)-(iii) are typically followed when executing the Routh-Array stability algorithm, but these seemingly trivial steps lead to the novel contribution of this research, which is derived in step (iv).

A. Derivation of characteristic equation

The characteristic equation of the partially linearised Acrobot approximated about the FPEP is calculated with

$$\begin{aligned}\lambda(s) &= \det(s\mathbf{I}_2 - \mathbf{A}) = 0\\ &= a_0 s^4 + a_1 s^3 + a_2 s^2 + a_3 s + a_4\end{aligned}$$

using the $\mathbf{A}$ matrix found in eq. (12), where

$$\begin{aligned}a_0 &= \pi(\alpha_1 + \alpha_2 + 2\alpha_3),\\ a_1 &= \pi k_d(\alpha_1 + \alpha_2 + 2\alpha_3) + 2k_p a(\alpha_2 + \alpha_3),\\ a_2 &= \pi\big[\beta_1 + \beta_2 + k_p(\alpha_1 + \alpha_2 + 2\alpha_3)\big],\\ a_3 &= \pi\big[k_d(\beta_1 + \beta_2) + 2k_p a\beta_2\big],\\ a_4 &= \pi k_p(\beta_1 + \beta_2)\end{aligned}$$

B. Defining the Routh-Array coefficients

The poles of the characteristic equation, which dictate the stability of the Acrobot when found approximately near the FPEP, are determined with the use of the Routh-Hurwitz stability criterion [11]. The coefficients of the characteristic equation are populated in a Routh-Hurwitz array, which is structured as

s^4	a_0	a_2	a_4
s^3	a_1	a_3	0
s^2	b_1	b_2	0
s^1	c_1	0	0
s^0	d_1	0	0

The new Routh coefficients that are introduced in the Routh array are calculated using

$$\begin{aligned}b_i &= \frac{a_1 a_{2i} - a_0 a_{2i+1}}{a_1} \qquad \text{with } i = 1, 2;\\ c_1 &= \frac{b_1 a_3 - a_1 b_2}{b_1},\\ d_1 &= b_2.\end{aligned}$$

The implementation of these equations results in

$$\begin{aligned}b_1 &= \frac{\pi k_p(w_0 k_p + w_1 k_d + w_2)}{\pi k_d(\alpha_1 + \alpha_2 + 2\alpha_3) + 2ak_p(\alpha_2 + \alpha_3)},\\ b_2 &= d_1 = \pi k_p(\beta_1 + \beta_2),\\ c_1 &= \frac{w_2(m_0 k_p^2 + m_1 k_d k_p + m_2 k_d + m_3 k_p)}{w_0 k_p + w_1 k_d + w_2}\end{aligned}$$

where

$$\begin{aligned}w_0 &= 2a(\alpha_2^2 + 2\alpha_3^2 + \alpha_1\alpha_2 + \alpha_1\alpha_3 + 3\alpha_2\alpha_3),\\ w_1 &= \pi(\alpha_1^2 + \alpha_2^2 + 2\alpha_1\alpha_2 + 4(\alpha_3^2 + \alpha_1\alpha_3 + \alpha_2\alpha_3)),\\ w_2 &= 2a(\alpha_2\beta_1 - \alpha_1\beta_2 + \alpha_3\beta_1 - \alpha_3\beta_2)\end{aligned}$$

and

$$\begin{aligned}m_0 &= -2a(\alpha_2 + \alpha_3), \qquad m_1 = -\pi(\alpha_1 + \alpha_2 + 2\alpha_3),\\ m_2 &= \pi(\beta_1 + \beta_2), \qquad m_3 = 2\beta_2 a.\end{aligned}$$

C. Analysis of first-column Routh-Array coefficients

According to the Routh-Hurwitz stability criterion, the system will have all of its poles found in the left-hand half of the complex pole-zero plane if the first-column Routh-Array coefficients are found to be either all negative or all positive [11]. Any sign change between the coefficients represents the presence of a pole in the right-hand half of the complex pole-zero plane [11]. It is evident that the coefficients a_0 and a_1, and the newly formed coefficients b_1, b_2, and d_1 are all found to be positive and non-zero for the following reasons:

(1) $k_p > 0$ and $k_d \geq 0$.
(2) The physical parameters of the system (the masses, lengths and moments of inertia) must also be positive and non-zero.
(3) The coefficient w_2 is positive and non-zero due to the findings of Lemma 2.1 seen in [2].

For this reason, the unstable poles of the system can only be introduced into the system through the Routh coefficient c_1, referred to as the *critical Routh coefficient*. The boundaries of the RAG are thus constructed through the evaluation of the critical Routh coefficient.

D. The region of acceptable gains: Evaluation of critical Routh coefficient

The system will have two poles in the right-hand plane if $c_1 < 0$. It is evident that the above listed properties cause the denominator of c_1 to be positive and non-zero. Therefore, $c_1 < 0$ when

$$c_{1_n} = m_0 k_p^2 + m_1 k_d k_p + m_2 k_d + m_3 k_p < 0. \tag{13}$$

Once evaluated, the inequality shown in eq. (13) can be summarised with the following conditions:

(1) For $\dfrac{\overline{\beta}_2}{\overline{\alpha}_2 + \overline{\alpha}_3} < k_P < \dfrac{\overline{\beta}_1 + \overline{\beta}_2}{\overline{\alpha}_1 + \overline{\alpha}_2 + 2\overline{\alpha}_3}$,

$$0 \leq k_D < \frac{2\alpha k_P}{\pi}\left[\frac{[\overline{\alpha}_2 + \overline{\alpha}_3]\, k_P - \overline{\beta}_2}{\overline{\beta}_1 + \overline{\beta}_2 - k_P\,[\overline{\alpha}_1 + \overline{\alpha}_2 + \overline{\alpha}_3]}\right].$$

(2) For $k_P \geq \dfrac{\overline{\beta}_1 + \overline{\beta}_2}{\overline{\alpha}_1 + \overline{\alpha}_2 + 2\overline{\alpha}_3}$, $\qquad k_D \geq 0$.

These conditions represent the Gain selection criteria for any particularly configured Acrobot. These constraints are demonstrated in Figure 2 for an Acrobot described by the parameters seen in the next section, where the shaded area represents the RAG, a collection of gain selection options that will induce an unstable response when the states of the Acrobot are initialised within an approximate neighbourhood of the FPEP.

VI. Results

The gain selection criteria was tested on the Acrobot containing the dimensions

$$\begin{aligned}&m_1 = 1 \text{ kg}, \quad L_1 = 1 \text{ m}, \quad m_2 = 1 \text{ kg},\\ &L_2 = 2 \text{ m}, \quad l_1 = 0.5 \text{ m}, \quad I_1 = 0.083 \text{ kg.m}^2,\\ &l_2 = 1 \text{ m}, \quad I_2 = 0.33 \text{ kg.m}^2.\end{aligned}$$

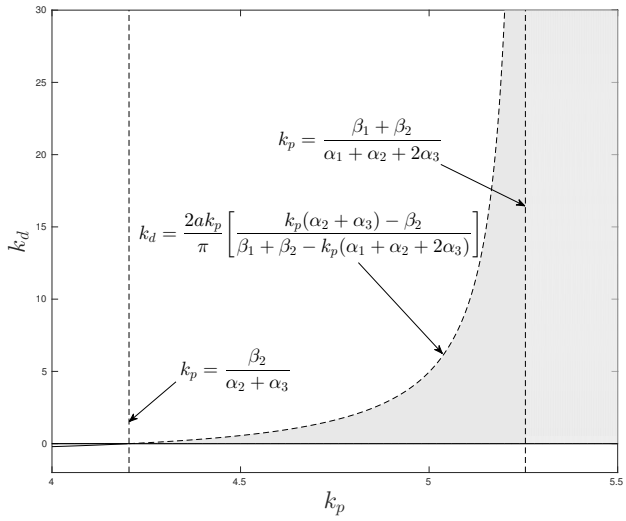

Fig. 2. The Gain selection criteria for the Acrobot, whose parameters are described in section VI.

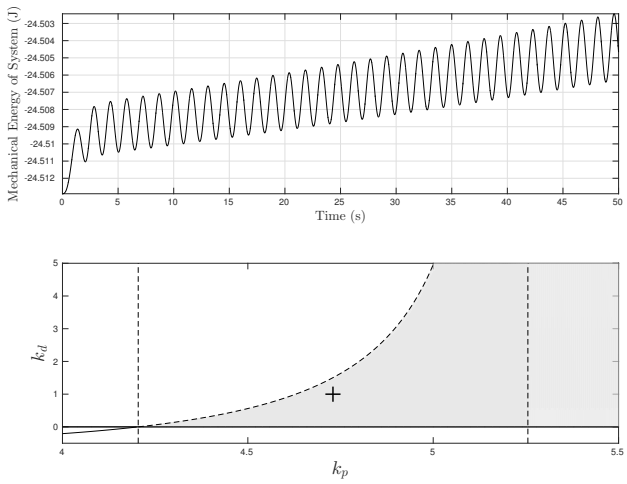

Fig. 3. Unstable mechanical energy response (Top) when gains are chosen within region of appropriate gains (Bottom).

as seen in [7] and [2]. A number of gain selections, both inside and outside the RAG, were chosen and their effect on the Acrobot's mechanical energy was simulated using the Dormand-Price (ode8) fixed-step solver with a resolution of 0.001s. The Acrobot was initialised with the conditions

$$q_1(0) = -\frac{101}{100}\pi, \quad q_2(0) = 0, \quad \dot{q}_1(0) = 0, \quad \dot{q}_2(0) = 0.$$

in each experiment. Each result produced the expected behaviour, with an increasing mechanical energy seen when gains found within the RAG were chosen and vice-versa. Examples of these tests are demonstrated in Figures 3 and 4. The swing-up of the Acrobot with a gain combination found within the RAG ($k_p = 100$, $k_d = 7.55482$, and $a = \pi/40$) is demonstrated in Figure 5. The CPFL controller is subsequently switched for an LQR controller once the Acrobot is found

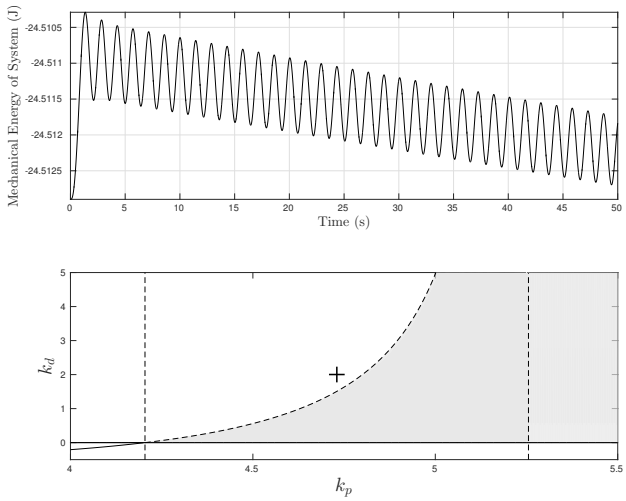

Fig. 4. Stable mechanical energy response (Top) when gains are chosen outside of the region of appropriate gains (Bottom).

approximately near the UEP. The gains for the LQR controller are found using the MATLAB LQR designer, where

$$K_1 = -246.2160, \qquad K_2 = -98.5841, \tag{14}$$
$$K_3 = -106.3313, \qquad K_4 = -50.0957. \tag{15}$$

Details on the formulation of the LQR controller can be found in [8]. The swing-up demonstrated in Figure 6 is performed in the instance where the gains k_p and k_d are constrained to fall within the region described by condition (1) of the gain selection criteria, whereby

$$k_d = 1.128022, \qquad k_p = \frac{\beta_1 + \beta_2}{\alpha_1 + \alpha_2 + 2\alpha_3} = 5.2554.$$

It is apparent that such a constraint will result in a significantly slower swing-up time, but we demonstrate that successful swing-up control from the FPEP can be performed despite this constraint using the gain selection criteria.

VII. Discussion

The gain selection criterion provides a useful guideline to gain selection, which can guarantee swing-up control of

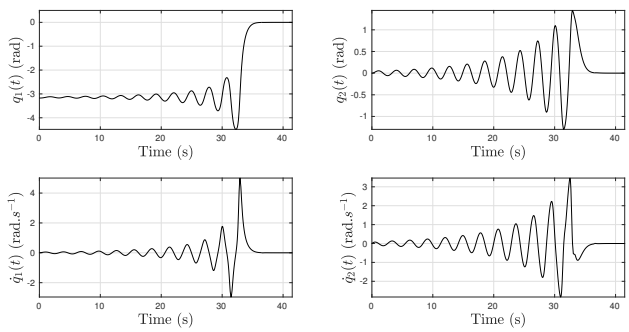

Fig. 5. The Swing-up and Balancing control of the Acrobot from the FPEP.

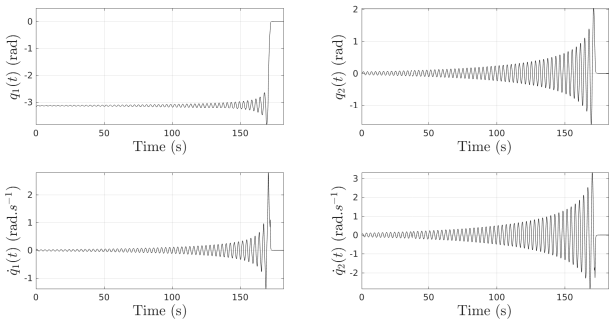

Fig. 6. The Swing-up and Balancing control of the Acrobot from the FPEP using a more gentle swing-up approach.

the Acrobot. It is, however, apparent that faster swing-up control can be achieved when a larger gain value for k_p is implemented. Additionally, the gain selection criteria may be analytically true for Acrobots with any combination of physical parameters (so long as the values of these parameters are positive, non-zero, and the values of the moments of inertia comply with the necessary and sufficient condition outlined in eq. (2.76) of [2]), but the performance of the swing-up control may vary greatly between Acrobots with different physical parameter values. One may imagine, for example, that an Acrobot whose proximal pendulum is much longer and heavier than its distal counterpart will require more effort to swing-up. This occurs intuitively because the physical parameters of the proximal pendulum will influence the dynamics of the system to a greater degree as compared to the distal pendulum. These limitations may affect the performance of the swing-up control, but, at the very least, the gain selection criterion will exclude a range of gain selections that will enforce a stable response in the region that is approximately near the FPEP, which is not compatible with swing-up control. Additionally, if one is presented with a n-link pendulum system with $n-1$ number of actuators (with the first joint being unactuated), the application of partial feedback linearisation to the n-link pendulum system will effectively negate the nonlinear dynamics of the actuated pendulums. The n-link pendulum system's behaviour will, therefore, approximate the behaviour of the Acrobot. In this case, the gain selection criteria can not only theoretically predict what feedback gains are required to produce unstable behaviour of the Acrobot about the FPEP, but may also be used to determine this region of appropriate gains for the n-link pendulum system. This result is not proven in this paper and is left for future research, but the implications are clear since the criterion may also be valid not only for the Acrobot, but also when considering the swing-up control of multi-body systems.

VIII. Conclusion

In this paper, we analytically introduced a novel design principle relating to the swing-up control of the Acrobot using collocated partial feedback linearisation known as the *gain selection criterion*. This criterion was derived using the Routh-Hurwitz stability criterion, which was applied on a linear approximation of the system about the fully-pendant equilibrium point. The criterion highlights a region of possible feedback gain selections (for gains k_p and k_d) that will guarantee the unstable response of the Acrobot when it is initialised approximately near the fully-pendant equilibrium point. The contribution is seen as significant because the inadvertent selection of a gain combination outside the region of appropriate gains will guarantee a stable response about the fully-pendant equilibrium point, which predictably will not accommodate the swing-up control objective. The swing-up control of the Acrobot using gain selections from within the region of appropriate gains is demonstrated in this paper to support the analytical results. The performance of the swing-up controller is, however, dependent on the dimensions of the Acrobot itself, as it will intuitively experience greater difficulty when the dimensions of the unactuated pendulum have a greater influence over system dynamics as compared to the actuated pendulum. The authors propose that the gain selection criterion may be applied to partially linearised multi-link pendulum systems, which are described by an unactuated most proximal joint (the only joint that is unactuated in the system). Hypothetically, if the linear feedback gains implemented in the swing-up control are sufficiently large and non-oscillatory, the behaviour of the partially linearised n-link pendulum system will approximate the behaviour of an Acrobot, thus falling within the applicable realm of the gain selection criteria derived in this paper. These results must, however, be confirmed in future research.

References

[1] R. Tedrake, *Underactuated Robotics: Learning, Planning and Control for Efficient and Agile Machines*. Massachussetts Inistitute of Technology, 2009.

[2] X. Xin and Y. Liu, *Control Design and Analysis for Underactuated Robotic Systems*. Springer-Verlag London, 2014.

[3] A. D. Mahindrakar and R. N. Ranavar, "A swing-up of the acrobot based on a simple pendulum strategy," *International Journal of Control*, vol. 78, no. 6, pp. 424–429, Dec. 2005.

[4] S. Lee, M. Eom, and D. Chwa, "Robust swing up and balancing control of the acrobot based on a disturbance observer," in *15th International Conference on Control, Automation and Systems (ICCAS 2015)*. IEEE, Oct. 2015, pp. 48–53.

[5] B. D. Nichols, "Continuous action-space reinforcement learning methods applied to the minimum-time swing-up of the acrobot," in *Int. Conference on Systems, Man, and Cybernetics*. IEEE, 2015, pp. 2084–2089.

[6] A. Chaudhari and I. Kar, "Adaptive control of underactuated systems using neural networks," in *Indian Control Conference (ICC)*. IEEE, Jan. 2017, pp. 22–27.

[7] M. W. Spong, "Partial feedback linearisation of underactuated mechanical systems," *Proceedings of the IEEE/RSJ/GI International conference on Intelligent Robots and Systems '94 'Advanced Robotics and the Real World'*, vol. 1, pp. 314–321, Sep. 1994, munich.

[8] ——, "The swing-up control problem for the acrobot," in *Proceedings of the Conference of IEEE Control Systems*, vol. 15, no. 1. IEEE, Feb. 1995, pp. 45–55.

[9] J.-J. E. Slotine and W. Li, *Applied Nonlinear Control*. New Jersey: Prentice-Hall Inc., 1991.

[10] J. Naude, "Control design using energy-shaping methods," Masters of Science in Engineering (MSc. Eng.), University of the Witwatersrand, Braamfontein, Johannesburg, South Africa, 2012.

[11] R. C. Dorf and R. H. Bishop, *Modern Control Systems*, 11st ed. Pearson Education International, 2008, ch. 6: The Stability of Linear Feedback Systems: The Routh-Hurwitz Stability Criterion, pp. 360–368.

Swing-up Control of the Acrobot using Noncollocated Partial Feedback Linearisation: An Iterative Approach

Ricardo De Almeida * **Otis Nyandoro** *

* *The School of Electrical and Information Engineering, The University of the Witwatersrand, Johannesburg, 1 Jan Smuts Avenue, Braamfontein, 2000, South Africa (e-mail: ricardo.dealmeida@students.wits.ac.za, otis.nyandoro@ee.wits.ac.za)*

Abstract: The swing-up control of the Acrobot using noncollocated partial feedback linearisation (NCPFL) has been demonstrated extensively in existing literature, whereby a linear state feedback control law which tracks the upright equilibrium point is designed for the linearised proximal pendulum. This control law cannot be designed for the distal pendulum since the Acrobot is underactuated. The distal pendulum will, however, follow a desirable trajectory towards the upright state so long as the initial angular condition of the distal pendulum ($q_2(0)$) and the frequency response of the existing actuator (ω_n) are finely tuned. There is currently no formalised method of tuning these properties for any specifically configured Acrobot. We thus present a novel approach of determining these properties using an adapted binary search algorithm designed to converge on an appropriate set of angular initial conditions for a specified range of ω_n. We demonstrate that selecting a sufficiently large ω_n accommodates a full range of swing-up for the proximal pendulum. The relationship between $q_1(0)$ and $q_2(0)$ becomes nonlinear towards the acceptable limits of $q_1(0)$. Satisfactory NCPFL-related swing-up control is thus demonstrated on an Acrobot described by one specific set of parameters.

Keywords: Robotic systems, Novel control theory and techniques

1. INTRODUCTION

The field of underactuated robotics involves the control of mechanical systems that are characterised by n degrees of freedom using $< n$ actuators (Spong, 1998). The Acrobot is a two degree of freedom (DOF) underactuated robotic model that has been explored significantly in existing literature, especially in the topic of swing-up control (Xin and Liu, 2014; Chaudhari and Kar, 2017; Akiyama et al., 2017; Horibe and Sakamoto, 2016). The earliest contributions were presented by Spong, who demonstrated the successful swing-up control of underactuated robotic systems through the implementation of partial feedback linearisation (PFL), an adaptation of the traditional feedback linearisation technique (Spong, 1994, 1995).

Feedback linearisation is a technique used to linearise the dynamics of complex systems, transforming the nonlinear state-space into an equivalent linear representation (Slotine and Li, 1991). This is advantageous since the implementation of complicated nonlinear control techniques are no longer necessary (Slotine and Li, 1991). This can only be done, however, if the entire state-space is linearised, thus preventing the execution of the exact feedback linearisation technique on underactuated systems (Slotine and Li, 1991). Despite this constraint, the actuators that are present in the system can be used to linearise a portion of the system's dynamics using PFL (Spong, 1998). In the case of a two DOF system, the linearisation of the dynamics of the active joint is known as Collocated PFL (CPFL), and the linearisation of the dynamics of the passive joint is referred to as Noncollocated PFL (NCPFL) (Spong, 1998, 1994). Once the system has been partially linearise, a linear feedback controller can be designed for the newly derived input, allowing the controller to track a desirable objective for the controllable dynamics (Spong, 1998). Spong also demonstrated that the behaviour of the system can be observed through the analysis of the system's internal and zero dynamics (Spong, 1994, 1995).

It has been shown in Spong (1994, 1995) that the CPFL-related swing-up control of the Acrobot can only be performed by choosing an angular trajectory that steadily introduces energy into the system. This results in the *gentle* swing-up of the Acrobot, the behaviour of which can be compared to that of a playground swing being swung-up from a resting position. The control may be switched to a LQR controller when the Acrobot is found to be approximately upright. Whilst the objective can be achieved in this manner, this *gentle* swing-up method is time consuming, with many repetitions required to approximately reach an upright position. The implementation of a less-gentle swing-up approach may cause the Acrobot to overshoot the equilibrium point, making it difficult for the LQR controller to regulate its behaviour around the desired trajectory. This is explained by the balancing fitness function seen in Xue et al. (2011); Brown and Passino (1997). Noncollocated feedback linearisation provides a work-around solution for this limitation. Linearising the dynamics of the proximal pendulum allows

for the implementation of linear control techniques which will cause the proximal pendulum to track the desired trajectory in a stable and exponential manner regardless of the proximal pendulum's initial angular condition, thus eliminating the presence of the necessary swing-up cycles seen in the CPFL control. The solution is limited, however, by the lack of observed feedback of the distal pendulum's dynamics. The desired swing-up of the distal pendulum thus requires fine-tuning of the outer-loop gains used to control the proximal pendulum as well as the angular initial conditions of both pendulums (Spong, 1994, 1995). Successful NCPFL-related swing-up control of the Acrobot has been demonstrated in Spong (1994, 1995), although Spong does not sufficiently explain how he managed to choose appropriate initial conditions and outer-loop gains to ensure satisfactory control. We thus present a novel algorithmic approach to iteratively determine these appropriate outer-loop gains and the distal pendulum's angular initial condition, referred to as the Convergence Algorithm (CA).

The remainder of the paper is structured as follows. A model of the Acrobot is explicitly defined is section 2 for the purpose of the linearisation and control law formulation. The NCPFL technique is subsequently performed on the Acrobot using the Lie derivative method in section 3, followed by the formulation of the NCPFL tracking swing-up control law in section 4. The structure of the CA is described in section 5, which is subsequently executed on an Acrobot described by a specific set of parameters, the results of which are described in section 6. Concluding remarks are included in section 7.

2. MODEL

2.1 Physical Model

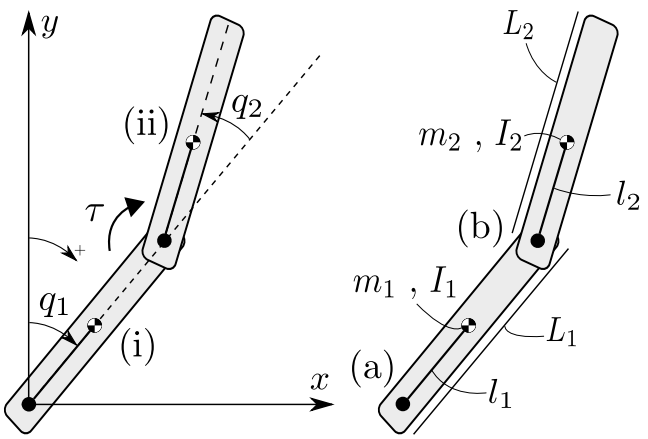

Fig. 1. The Acrobot model.

The Acrobot model depicted in fig. 1 is adapted from Spong (1994, 1995); Xin and Liu (2014). The model is constrained to a 2-D plane with the position of the pendulums being described at any time t by the angular degrees of freedom $q_1(t)$ (for the proximal pendulum (i)) and $q_2(t)$ (for the distal pendulum (ii)). The masses of the pendulums m_1 and m_2 are point masses that represent each pendulum's centre-of-mass (COM). The pendulums are assumed to be stiff rods with lengths L_1 and L_2, COM lengths l_1 and l_2, and moments of inertia I_1 and I_2. The torque τ is exerted by an actuator that is fixed to the distal actuated joint (b). The proximal joint (a) remains unactuated.

2.2 Mathematical Model

The generalised equation of motion for an undamped rotational mechanical system can be collectively represented by the prototypical form seen in eq. (1) (Naude, 2012), where

$$M(q)\ddot{q} + C(q,\dot{q}) + K(q) = G(q)u \tag{1}$$

and where $M(q)$ represents the mass matrix, $C(q,\dot{q})$ collectively represents the Coriolis and Centrifugal forces, $K(q)$ represents the gravitational torques, and $G(q)u$ represents the system actuation (Naude, 2012). The motion vectors for the Acrobot are comprised of the generalised coordinates, where

$$q = \begin{bmatrix} q_1 \\ q_2 \end{bmatrix}, \qquad \dot{q} = \begin{bmatrix} \dot{q}_1 \\ \dot{q}_2 \end{bmatrix}, \qquad \ddot{q} = \begin{bmatrix} \ddot{q}_1 \\ \ddot{q}_2 \end{bmatrix}.$$

The matrices included in the prototypical form are structured as

$$\begin{aligned} M(q) &= \begin{bmatrix} M_{11}(q) & M_{12}(q) \\ M_{21}(q) & M_{22}(q) \end{bmatrix} \\ &= \begin{bmatrix} \alpha_1 + \alpha_2 + 2\alpha_3\cos(q_2) & \alpha_2 + \alpha_3\cos(q_2) \\ \alpha_2 + \alpha_3\cos(q_2) & \alpha_2 \end{bmatrix}, \\ C(q,\dot{q}) &= \begin{bmatrix} C_1(q,\dot{q}) \\ C_2(q,\dot{q}) \end{bmatrix} = \alpha_3 \begin{bmatrix} -2\dot{q}_1\dot{q}_2 - \dot{q}_2{}^2 \\ \dot{q}_1{}^2 \end{bmatrix} \sin q_2, \\ K(q) &= \begin{bmatrix} K_1(q) \\ K_2(q) \end{bmatrix} = \begin{bmatrix} -\beta_1 \sin q_1 - \beta_2 \sin(q_1+q_2) \\ -\beta_2 \sin(q_1+q_2) \end{bmatrix} \end{aligned}$$

where

$$\begin{aligned} &\alpha_1 = m_1 l_1{}^2 + m_2 L_1{}^2 + I_1, && \alpha_2 = m_2 l_2{}^2 + I_2, \\ &\alpha_3 = m_2 L_1 l_2, && \beta_1 = g(m_1 l_1 + m_2 L_1), \\ &\beta_2 = g m_2 l_2 \end{aligned}$$

and where g represents the gravitational acceleration constant. As previously mentioned, the Acrobot model is an underactuated mechanical system, with actuation occurring only at the distal joint (Spong, 1994). It is evident, therefore, that

$$G(q)u = \begin{bmatrix} 0 \\ \tau \end{bmatrix} \tag{2}$$

The angular displacement of the most proximal pendulum

$$y = q_1$$

was chosen as the output of interest in this application.

3. NONCOLLOCATED PARTIAL FEEDBACK LINEARISATION

The states of the Acrobot are chosen as

$$\mathbf{x} = [\mathrm{x}_1\ \mathrm{x}_2\ \mathrm{x}_3\ \mathrm{x}_4]^T = [q_1\ \dot{q}_1\ q_2\ \dot{q}_2]^T. \tag{3}$$

Portions of the state-space companion form representation of the Acrobot's nonlinear dynamics are produced by inverting the $M(q)$ matrix in eq. (1), resulting in

$$\dot{\mathbf{x}} = \mathbf{f}(\mathbf{x}) + \mathbf{g}(\mathbf{x})u \tag{4}$$

where

$$\mathbf{f}(\mathbf{x}) = \begin{bmatrix} \mathrm{x}_2 \\ \dfrac{1}{\triangle}[-M_{22}(C_1+K_1) + M_{12}(C_2+K_2)] \\ \mathrm{x}_4 \\ \dfrac{1}{\triangle}[M_{21}(C_1+K_1) - M_{11}(C_2+K_2)] \end{bmatrix} \tag{5}$$

and where

$$\triangle = M_{11}M_{22} - M_{12}M_{21}. \tag{6}$$

The input coupling matrix is represented by

$$\mathbf{g(x)} = \begin{bmatrix} 0 & \frac{-M_{12}}{\triangle} & 0 & \frac{M_{11}}{\triangle} \end{bmatrix}^T. \tag{7}$$

The output of the system is selected as

$$\mathbf{h(x)} = h_1 = x_1 = q_1(t). \tag{8}$$

The NCPFL procedure is executed using the input-output feedback linearisation (IOFBL) method, which is represented with

$$y_i^{(r_i)} = L_{\mathbf{f}}{}^{r_i} h_i + \sum_{j=1}^{m} L_{\mathbf{g}_j} L_{\mathbf{f}}{}^{r_i - 1} h_i u_j \tag{9}$$

where $m = 1$ and $i = 1$ for the Single-Input Single-Output (SISO) Acrobot (Slotine and Li, 1991). Additionally, r_i represents the relative degree of the ith output. The equation provides a means of determining the behaviour of each particular output through the use of repeated Lie derivatives. The Lie derivative is repeatedly applied until an input appears in the resultant expression (Slotine and Li, 1991). We thus simplify eq. (9) as

$$y_1^{(r_1)} = L_{\mathbf{f}}{}^{r_1} h_1 + L_{\mathbf{g}} L_{\mathbf{f}}{}^{r_1 - 1} h_1 u. \tag{10}$$

If $r_1 = 1$, equation (10) is represented as

$$y_1^{(1)} = L_{\mathbf{f}} h_1 + L_{\mathbf{g(x)}} h_1 u. \tag{11}$$

This is equivalent to

$$y_1^{(1)} = L_{\mathbf{f}} \mathrm{x}_1 + L_{\mathbf{g(x)}} \mathrm{x}_1 u. \tag{12}$$

Solving for each term in (12) results in

$$\begin{aligned} L_{\mathbf{f}} x_1 &= \nabla \mathrm{x}_1 \mathbf{f(x)} \\ &= \mathrm{x}_2, \end{aligned} \tag{13}$$

$$\begin{aligned} L_{\mathbf{g}} x_1 &= \nabla \mathrm{x}_1 \mathbf{g(x)} \\ &= 0. \end{aligned}$$

Therefore

$$y_1^{(1)} = \mathrm{x}_2. \tag{14}$$

No control input is found in equation (14). The procedure must, therefore, be repeated with an increased value of r_i.

Choosing $r_1 = 2$ results in

$$y_1^{(2)} = L_{\mathbf{f}}{}^2 \mathrm{x}_1 + L_{\mathbf{g}} L_{\mathbf{f}} \mathrm{x}_1 u. \tag{15}$$

This expression is adjusted to reveal the expanded format of the repeated Lie derivative, whereby

$$y_1^{(2)} = L_{\mathbf{f}}[L_{\mathbf{f}} \mathrm{x}_1] + L_{\mathbf{g}}[L_{\mathbf{f}} \mathrm{x}_1] u. \tag{16}$$

Substituting eq. (13) into eq. (16) results in

$$y_1^{(2)} = L_{\mathbf{f}} \mathrm{x}_2 + L_{\mathbf{g}} \mathrm{x}_2 u. \tag{17}$$

We thus solve each term separately, whereby

$$\begin{aligned} L_{\mathbf{f}} x_2 &= \nabla \mathrm{x}_2 \mathbf{f(x)} \\ &= \frac{1}{\triangle}[-M_{22}(C_1 + K_1) + M_{12}(C_2 + K_2)], \end{aligned} \tag{18}$$

$$\begin{aligned} L_{\mathbf{g}} x_2 &= \nabla \mathrm{x}_2 \mathbf{g(x)} \\ &= \frac{-M_{12}}{\triangle}. \end{aligned} \tag{19}$$

Substituting these newly calculated terms into eq. (17) produces the result seen in eq. (20), with

$$\begin{aligned} y_1^{(2)} = \frac{1}{\triangle}[-M_{22}(C_1 + K_1) + M_{12}(C_2 + K_2)] - \\ \frac{M_{12}}{\triangle} u. \end{aligned} \tag{20}$$

The newly derived expression $y_1^{(2)}$ may now be equated to a desired control input v. The actuated torque required to achieve this linear result is represented by u when chosen as the subject of the formula, as shown in eq. (20), whereby

$$u = \frac{1}{M_{12}}[-M_{22}(C_1 + K_1) + M_{12}(C_2 + K_2) - \triangle v]. \tag{21}$$

Substituting this expression back into eq. (20) produces

$$y_1^{(2)} = \ddot{\mathrm{x}}_1 = v. \tag{22}$$

The dynamics of the proximal pendulum may now be specifically defined to accommodate a linear feedback control law as shown in (Slotine and Li, 1991), whereby

$$v = \dot{\mathrm{x}}_2^d + k_d \left(\mathrm{x}_2^d - \mathrm{x}_2\right) + k_p \left(\mathrm{x}_1^d - \mathrm{x}_1\right). \tag{23}$$

The transformation of the system may be illustrated through the definition of new state variables, described by

$$\begin{aligned} \eta_1 &= \mathrm{x}_1 - \mathrm{x}_1^d & \eta_2 &= \mathrm{x}_2 - \mathrm{x}_2^d, \\ z_1 &= \mathrm{x}_3 & z_2 &= \mathrm{x}_4 \end{aligned}$$

with the output error defined as $\tilde{y}_1 = \mathrm{x}_1 - \mathrm{x}_1^d$. The resulting transformed state space equations are represented as

$$\dot{\eta}_1 = \eta_2, \qquad \dot{\eta}_2 = -k_p \eta_1 - k_d \eta_2, \tag{24}$$

$$\dot{z}_1 = z_2, \qquad \dot{z}_2 = -\frac{1}{M_{12}}(C_1 + K_1), \tag{25}$$

$$\tilde{y}_1 = \eta_1. \tag{26}$$

The aformentioned expressions may be represented in matrix form as

$$\dot{\eta} = A\eta, \qquad \dot{z} = \zeta(\eta, z, t), \qquad \tilde{y}_1 = C\eta. \tag{27}$$

The system is partially linearised as made evident by the system's internal dynamics (represented by $\dot{z}$). Full-state feedback linearisation only occurs when the total relative degree of the procedure $\sum_{i=1}^{n} r_i = r = n$ (Slotine and Li, 1991). This condition is obviously not satisfied in this case, where $r = 2$ and $n = 4$ ($r < n$).

4. SWING-UP CONTROL FORMULATION

The newly transformed NCPFL-related state-space dynamics seen in eqs. (24) and (25) represent the behaviour of the linearised proximal pendulum and the nonlinear internal dynamics of the distal pendulum respectively. The time-domain response of $q_1(t)$ is determined by taking the Laplace transform and, subsequently, the inverse Laplace transformations of the state-related dynamics in eq. (24). Applying the Laplace transformation on this equation produces

$$\tilde{n_1}(s)(s^2 + k_d s + k_p) = \tilde{n_1}(0)(s + k_d) + \tilde{\dot{n_1}}(0). \tag{28}$$

The expression simplifies when enforcing the condition $\dot{q}(0) = 0$, with

$$\tilde{n_1}(s) = \tilde{n}_1(0) \frac{s + k_d}{s^2 + k_d s + k_p}. \tag{29}$$

Choosing $k_p = {k_d}^2/4$ and applying the inverse Laplace transform results in

$$\tilde{n_1}(t) = \tilde{n_1}(0) e^{0.5 k_d t}(1 + 0.5 k_d t) \tag{30}$$

where $0.5k_d = \omega_n$, the natural frequency of the actuator. This damped response is thus guaranteed when

$$k_d = 2\omega_n \qquad\qquad k_p = {\omega_n}^2$$

provided that $\omega_n \neq 0$. The response of the proximal pendulum is damped and will tend exponentially towards the desired trajectory as time tends towards infinity. Choosing a greater value for ω_n will increase the rate at which the trajectory of the proximal pendulum converges within a sufficiently close neighbourhood of the desired trajectory. It is uncertain, however, if the dynamics of the distal pendulum will converge within a sufficiently close neighbourhood of its desired trajectory (ie. $x_3 = 0$, $x_4 = 0$) since the internal dynamics of the system is not directly observable and controllable. It is evident in Spong (1994), however, that choosing a perfectly tuned set of initial conditions and feedback gains (k_p and k_d) will ensure this convergence, since the distal pendulum will coincidently approach the desired trajectory through the indirect influence of the feedback control on the proximal pendulum. There is currently no solution present in existing literature that assists in determining the necessary initial conditions and feedback gains that will result in the satisfactory NCPFL-related swing-up control of the Acrobot. We therefore present the following contribution, referred to as the Convergence Algorithm (CA), to address the following concerns:

(i) If the linear state feedback control law for the proximal pendulum is swung-up with a response frequency ω_n and an initial angular condition $q_1(0)$, what angular position $q_2(0)$ must the distal pendulum be initialised with to accommodate the satisfactory swing-up control of the Acrobot?
(ii) What is the minimum response frequency ω_n that must be used to produce satisfactory swing-up control if the proximal pendulum is initialised at any angular position $q_1(0)$ within the range $q_1 \in [-\pi, \pi]$?

5. CONVERGENCE ALGORITHM

5.1 Preliminaries

Despite there being no known analytical method that addresses the concerns highlighted in (i) and (ii), it is possible to perform an iterative series of purposely configured simulations that will converge upon a desirable solution, thus preventing the need for guesswork. The basic premise of this algorithm is highlighted as follows:

(1) Choose an actuator response frequency ω_n that will dictate the behaviour of the linear control law described in eq. (23). Additionally, select a value for $q_1(0)$ from which you wish to swing the Acrobot from. It is assumed that the initial angular velocities $\dot{q}_1(0) = \dot{q}_2(0) = 0$.
(2) Select a value for $q_2(0)$.
(3) Perform the swing-up control simulation and determine what changes to the initial condition of the distal pendulum need to occur to accommodate the conditions $q_2 \approx 0$ and $\dot{q}_2 \approx 0$. This can be intuitively derived by determining:
   (i) The sign of the region the pendulum was initialised in ($\text{sgn}\{q_2(0)\}$).
   (ii) Whether the distal pendulum undershot or overshot the UEP ($\text{sgn}\{q_2(T)\}\text{sgn}\{q_2(0)\} = \pm 1$ respectively).

   The sign of the next iteration change (δ) is determined by

$$\begin{aligned}\text{sgn}\{\delta\} &= -\text{sgn}\{q_2(0)\}\text{sgn}\{q_2(T)\}\text{sgn}\{q_2(0)\} \\ &= -\text{sgn}\{q_2(T)\}.\end{aligned}$$

(4) Alter the value of $q_2(0)$ according to this result ($q_{2_{i+1}} = q_{2_i} \pm \delta$).
(5) Repeat the simulation until an adequately tuned value of $q_2(0)$ is determined.

The alteration to the value of $q_2(0)$ is based on the idea of convergence, as shown by the convergent series

$$2\pi \left(\lim_{n\to\infty} \sum_{i=1}^{n} \left(\frac{1}{2}\right)^i \right) = 2\pi \tag{31}$$

where i represents the number of iterations performed. Therefore, using an infinite number of iterations will allow us, in one extreme, to circle around the entire range of $q_2(0)$, where $q_2(0) \in [-\pi, \pi]$. The difference is halved with each iteration. It is evidently impossible to iterate an infinite number of times to determine the exact value of $q_2(0)$, but one can expect the system to converge within an approximate neighbourhood of the most appropriate value of $q_2(0)$. This error is represented as

$$\epsilon = \pm 2\pi \left(\sum_{i=1}^{n} \left(\frac{1}{2}\right)^i \right) \text{ rads}$$

where $n = k_{\max}$, the total number of iterations that are performed (also referred to as the *maximum convergence index*). The result of this algorithm is thus represented by the

$$q_{2_d}(0) = \pi \left(\pm\frac{1}{2} \pm \frac{1}{4} \pm \cdots \pm \left(\frac{1}{2}\right)^{k_{\max}} \right) \tag{32}$$

which either subtracts or adds a difference depending on whether the distal pendulum undershoots or overshoots. This algorithm effectively represents an adaptation of the binary search algorithm.

5.2 Algorithm Structure

The flow-chart demonstrated in Figure 2 represents a high-level interpretation of the Convergence Algorithm. An explanation for each step in the algorithm (which is numerically ordered in the flow-chart) is provided in this section.

1 Declare the necessary input variables, ie. system parameters (A), actuator response frequency maximum index (B), gain multiplication factor (C), resolution of q_1 within the range $[-\pi, \pi]$ (D), maximum convergence index (E), filename prefix of output file (F), and filename of the appropriate Simulink model (S).
2 Initialise the relevant input parameters to the system parameters (SP), the actuator response frequency maximum index K_D, and the gain multiplication factor (GM).
3 Iterate through each possible actuator response index from 1 to K_D.
4 Set the actuator response frequency Wn.

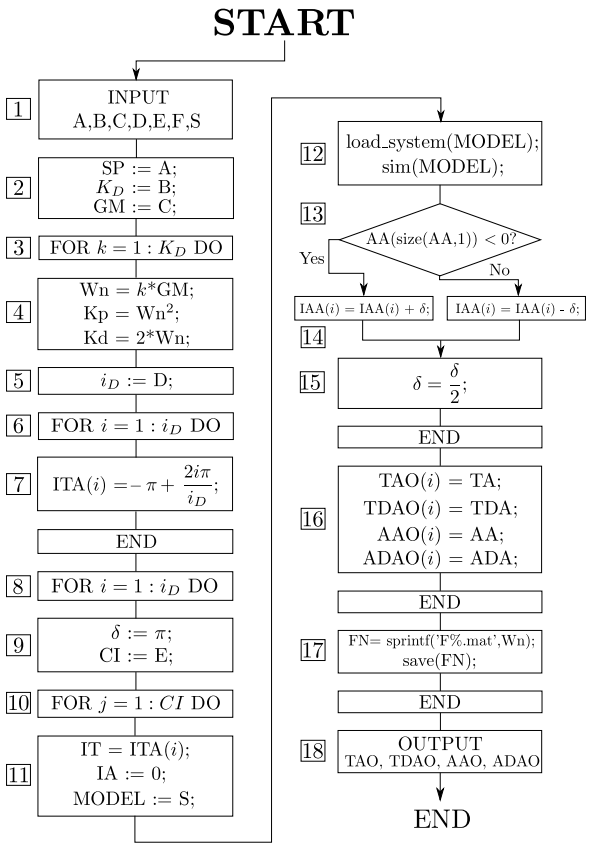

Fig. 2. A high-level flow chart of the Convergence algorithm.

5 Initialise the number of divisions of $q_1(0)$ that will be iterated through within the range $[-\pi, \pi]$ (i_D) using the appropriate input variable D. The angular resolution of this procedure is thus $^{2\pi}/_{i_D}$.

6 Iterate through each possible index between 1 and i_D so that each possible configuration of $q_1(0)$ may be populated in an array.

7 Populate the Initial Theta Array (ITA) with all possible values of $q_1(0) \in [-\pi, \pi]$ using i_D (Theta represents q_1 in this instance).

8 Iterate through each possible index between 1 and i_D so that each of the possible configurations of $q_1(0)$ within ITA may be tested with respect to Wn.

9 Initialise the angular difference value δ to π. Initialise the maximum convergence index CI to the variable E.

10 Iterate through each index between 1 and CI to generate a converged solution for $q_n(0)$.

11 Configure the Acrobot by initialising the Initial Theta (IT, which represents $q_1(0)$) to the ith entry of ITA and the Initial Alpha (represents $q_2(0)$) to 0. Initialise the MODEL variable to the appropriate filename of the Simulink model that will be simulated (S).

12 Load the appropriate Simulink model into MATLAB and simulate. This generates the results of the swing-up control using the currently selected $q_1(0)$, $q_2(0)$, and Wn. These results are stored in the form of the following arrays: Theta Array (TA, which represents the time-dependent values of q_1), Alpha Array (AA, representing q_2), Theta Dot Array (TDA, representing $\dot{q}_1$), and Alpha Dot Array (ADA, representing $\dot{q}_2$).

13 Check the end-state value of AA (the last value in the array). Is the end-state of AA > 0 or is the end-state of AA < 0? The success of this step is contingent on the selection of appropriate values for the simulation end-time (T) and the fixed-time resolution $\triangle t$.

14 Alter the value of $q_2(0)$ by δ according to whether the distal pendulum had overshot or undershot the UEP.

15 Half δ for the next iteration so that a solution may be converged upon, as highlighted by the convergence series in eq. (31).

16 Populate the output arrays TAO (Theta Array Output), TDAO (Theta Dot Array Output), Alpha Array Output (AAO), and Alpha Dot Array Output (ADAO) with the resultant outputs of the simulation, namely TA, TDA, AA, and ADA respectively.

17 Create a file with the chosen filename prefix F and merge it with the suffix Wn to give the file a unique identification. Save the file.

18 The outputs of this procedure are thus TAO, TDAO, AAO, and ADAO.

6. RESULTS & DISCUSSION

The following parameters are selected for the Acrobot (referred to as SP in the algorithm):

Table 1. Parameter Values

m_1	m_2	L_1	L_2	l_1	l_2	I_1	I_2	g
1	1	1	2	0.5	1	0.083	0.333	9.81

Table 2. Parameter Values

K_D	GM	i_D	CI	$\triangle t$ (s)	T (s)
50	0.5	128	25	$\frac{\pi}{500k}$	$\frac{12\pi}{k}$

The results of the convergence algorithm executed on an Acrobot described by the parameters found in table 1 using the algorithmic parameters seen in table 2 are demonstrated in Figures 3 and 4, with k representing the counter used in the algorithm. Successful swing-up, as defined in this research, occurs when

$$|q_2(t^*)| \leq |q_1^* \pm \epsilon_1|, \qquad |\dot{q}_2(t^*)| \leq |\dot{q}_2^* \pm \epsilon_1|$$

whereby $\epsilon_1 = 1 \times 10^{-4}$ rads of the UEP (described by $q_1^* = q_2^* = 0$), and when $\dot{q}_2(t^*)$ is found within $\epsilon_2 = 0.1$ rad.s^{-1} of $\dot{q}_1^* = 0$ (time t^* refers to the instances where $|q_1(t)| < \epsilon_1$). The maximum angular displacement of $q_1(0)$ is demonstrated in Figure 3 whereby the Acrobot can be swung-up satisfactorily using NCPFL with varying values of actuator response frequency ω_n. It is evident that actuators that have a sufficiently large response frequency will accommodate the NCPFL-related swing-up control of Acrobots with a larger range of proximal pendulum displacements (ie. as $q_1(0) \to \pm\pi$, a larger ω_n must be selected). Therefore, actuators that are constrained with $\omega_n < 33$ rad.s^{-1} in this particular instance will not be able to accommodate a full-range of NCPFL-related swing-up control. This is demonstrated in Figure 4. It is also evident that the relationship between the appropriate values of $q_1(0)$ and $q_2(0)$ is linear when a sufficiently large value

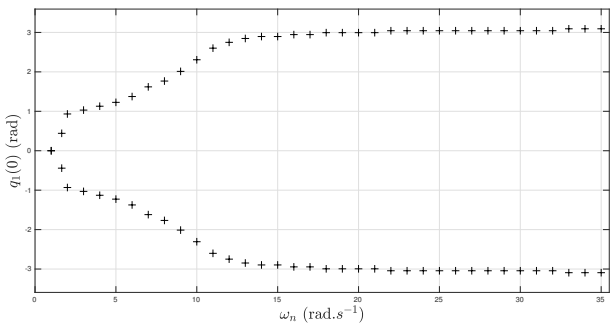

Fig. 3. The minimum gain requirements for satisfactory swing-up control when considering $q_1(0)$.

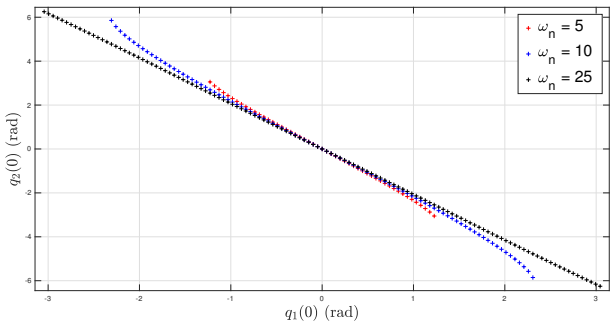

Fig. 4. The initial condition requirements for satisfactory swing-up demonstrated for $\omega_n = 5$rad.s^{-1} (red), $\omega_n = 10$rad.s^{-1} (blue), and $\omega_n = 25$rad.s^{-1} (black).

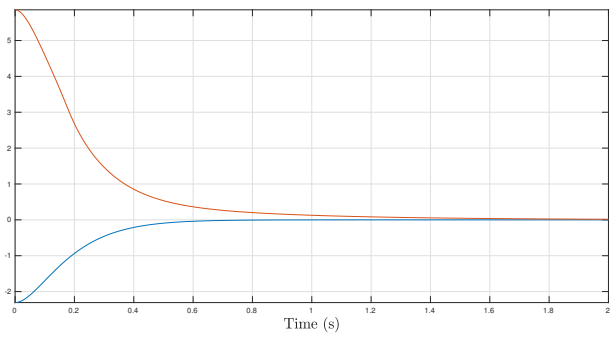

Fig. 5. The NCPFL swing-up control of the proximal pendulum (blue) and the distal pendulum (red) of the Acrobot. Angles represented in radians.

of ω_n is selected. This relationship becomes nonlinear towards the limits of acceptable values of $q_1(0)$. This curvature in the relationship between $q_1(0)$ and $q_2(0)$ is evident when selecting $\omega_n = 5$ rad.s^{-1} or $\omega_n = 10$ rad.s^{-1}, as shown in Figure 4. We thus demonstrate the satisfactory swing-up control of the Acrobot initialised with $\omega_n = 10$ rad.$^{-1}$, $q_1(0) = -2.3071$ rad, and $q_2(0) = 5.8562$ rad (Figure 5). These values were selected according to the results shown in the previous figures. A regulating controller can be designed to ensure that the Acrobot remains at this equilibrium point as $t \to \infty$.

7. CONCLUSION

In this paper, a novel method of determining the most appropriate values for the angular initial conditions of the Acrobot to ensure satisfactory NCPFL-related swing-up control for a range of actuator response frequencies through the implementation of an adapted binary search algorithm was described. A linear feedback control law is designed to ensure that the proximal pendulum tracks the upright position. The distal pendulum will thus follow a trajectory toward its own upright state if an appropriate value for $q_2(0)$ is selected. We found that satisfactory swing-up control can be achieved for $q_1(0) \in [-\pi : \pi]$ if a sufficiently large actuator response frequency is chosen. The relationship between $q_1(0)$ and $q_2(0)$ will be linear throughout this region in this case. If a sufficiently large value for ω_n cannot be selected, then the possible range of satisfactory values of $q_1(0)$ will tend to 0 as $\omega_n \to 0$. Additionally, the relationship between $q_1(0)$ and $q_2(0)$ becomes evidently nonlinear towards the limits of the possible range of $q_1(0)$. Satisfactory swing-up control for one particular configuration of the Acrobot using the algorithm was demonstrated, but it is suggested that the robustness of this algorithm must be tested on Acrobots with varying parameters in future research. Additionally, the use of other established algorithm structures, such as Newton's method, must also be explored.

REFERENCES

Akiyama, M., Henmi, T., and Yamamoto, T. (2017). Verification of the relationship between desired angle ratio and control performance in the links of a gymnastic based controller for an underactuated robot. In *Advanced Control of Industrial Processes (AdCONIP), 2017 6th International Symposium on*, 172–177. IEEE.

Brown, S.C. and Passino, K.M. (1997). Intelligent control for an acrobot. *Journal of Intelligent and Robotic Systems*, 18, 209–248.

Chaudhari, A. and Kar, I. (2017). Adaptive control of underactuated systems using neural networks. In *Control Conference (ICC), 2017 Indian*, 22–27. IEEE.

Horibe, T. and Sakamoto, N. (2016). Swing up and stabilization of the acrobot via nonlinear optimal control based on stable manifold method. *IFAC-PapersOnLine*, 49(18), 374–379.

Naude, J. (2012). *Control Design using Energy-Shaping methods*. Masters of science in engineering (msc. eng.), University of the Witwatersrand, Braamfontein, Johannesburg, South Africa.

Slotine, J.J.E. and Li, W. (1991). *Applied Nonlinear Control*. Prentice-Hall Inc., New Jersey.

Spong, M. (1998). *Control Problem in Robotics and Automation*, volume 230, chapter 9: Underactuated Mechanical Systems, 135–150. Springer-Verlag London Ltd.

Spong, M.W. (1994). Partial feedback linearisation of underactuated mechanical systems. *Proceedings of the IEEE/RSJ/GI International conference on Intelligent Robots and Systems '94 'Advanced Robotics and the Real World'*, 1, 314–321. Munich.

Spong, M.W. (1995). The swing-up control problem for the acrobot. In *Proceedings of the Conference of IEEE Control Systems*, number 1 in 15, 45–55. IEEE.

Xin, X. and Liu, Y. (2014). *Control Design and Analysis for Underactuated Robotic Systems*. Springer-Verlag London.

Xue, F., Hou, Z., and Deng, H. (2011). Balance control for an acrobot. In *Chinese Control and Decision Conference (CCDC)*, 3426 – 3429. IEEE, Mianyang.